DAYLIGHT ILLUMINANCE MODELLING FOR THE UNITED KINGDOM AND EUROPE

by

Roderick Charles Angus, BEng(Hons)

A thesis presented in partial fulfilment of the requirements for the degree of

Doctor of Philosophy of Napier University

SPONSORS:

Department of Mechanical Manufacturing and Software Engineering
Napier University
EDINBURGH

ETSU
Department of Trade and Industry
Harwell, Didcot
Oxfordshire
OX11 0RA

Department of Building & Surveying
Heriot Watt University
Riccarton
EDINBURGH

COLLABORATING ESTABLISHMENT

Building Research Establishment
Garston
Watford

November 1995

TABLE OF CONTENTS

ACKNOWLEDGEMENTS

The successful completion of this work has been made possible through the contributions of several individuals. Dr Tariq Muneer has been an inspiration throughout the course of this thesis and has provided assistance where and when required, I take this opportunity to thank him for his supervision. Dr Paul Littlefair acting as an advisor has gone to great lengths to provide essential data and information required to carry out the modelling work and the time he has given to read chapters of the thesis is much appreciated. Many thanks are due to Professor Alex Young, the Head of Department of the Mechanical Manufacturing and Software Engineering Department for providing an extension to my funding in order to complete this thesis. The contributions of the Energy Technology Support Unit and in particular Mr Phil Dolley, Dr Ian McCubbin and Mr Joe Lynes are gratefully acknowledged. Dr Bob Stafford of Edinburgh University is thanked for his assistance in reading and commenting on several chapters of this thesis as is Professor Sam Allwinkle of the Building and Surveying Department at Napier University.

Many of the staff and technicians of the Mechanical Manufacturing and Software Engineering Department have helped provide technical support and guidance throughout the duration of this project. Mr George Pringle, the chief technician is thanked for his organisation of technician support and for the production of the computer drafted drawings used in the thesis. Mr Ken Russell, Mr Kevin McCann, Mr Ian Campbell and Mr Andrew Kerr were a tremendous help with the installation and commissioning of the Daylight station as were Mr Peter Reid and his technician staff at Heriot Watt University, their assistance is most appreciated.

For the provision of data from which much of the thesis depended I would like to thank Dr Paul Littlefair at BRE, Mr Basil Psiloglou and Dr Harry Kambezidis at the National Observatory of Athens in Greece, Professor Nakamura at Kyushu University Japan and Dr Michael Wright at Sheffield University.

On a more personal note there are many individuals who although they may not be aware of their contribution to this thesis have helped produce an ideal working environment. All the members of the Mechanical Manufacturing and Software Engineering Department, in particular the researchers, Donald and his network, Mark and Di,

Jonathan, Alec and his repartee, Neil, Louise, Forrest, Bao Lie, Steve and his no-hand-deals and from Heriot Watt, Lucy, Grant, Sean, Kitty and Mike. I would like to thank them all for their enthusiastic pursuit of excellent nights of indulgence. Bob Stafford who made a career out of such events and who's motto reads 'a bad days fishing is better than any day's working' is once again thanked for his ability to keep things in perspective. The support and patience of my parents have been instrumental towards the completion of this work and I am extremely grateful to them both. The past 18 months have been made considerably easier through the love and support of my girlfriend Lindsey who will be only slightly more relieved to see the back of this thesis than me.

ABSTRACT

This thesis highlights the benefits to occupants and owners of buildings who utilise daylight effectively. Many cases of absence are related to depression or Seasonal Adjustment Disorder(SAD) which results from inadequate exposure to daylight in the work place. The use of artificial lights has been linked to minor as well as more serious ailments such as cancer and increases in cases of miscarriage.

The use of daylight in buildings from economic and environmental perspectives is the main concern of the thesis. The work and analysis of this thesis have produced two new illuminance models. In addition detailed illuminance and irradiance data for Central Scotland were recorded which has previously not been available.

A comprehensive study of luminous efficacy research was undertaken in Chapter 3 which evaluated a complete range of models. Furthermore the luminous efficacy of various UK and international sites were compared to examine climatic differences. The development of a new slope illuminance model which more accurately predicts external illuminance for all sky conditions was shown to perform consistently better than previous models. This was due to the new model's treatment of the sky background diffuse component utilising an anisotropic form as opposed to the traditional assumption of an isotropic sky background diffuse component.

The availability of sky luminance distribution data from introduction of sky scanners enabled innovative daylight illuminance factors to be developed. These factors model the distribution of the sky's hemisphere under all levels of cloud cover and calculate the internal illuminance taking into account window size, glazing type, orientation and time of the day. The development of the daylight illuminance factors has been shown to significantly improve the energy efficient design of buildings in comparison to the current practice of employing the sky factor method.

The daylight illuminance factors were used in a modelled building design scenario to assess their performance and to examine energy efficient design. Lighting controls and various glazing types were analysed to study their impact on a buildings energy consumption. This study also incorporated an embodied energy analysis which considered the energy consumption of windows in manufacture and operation.

INTRODUCTION

The sun's energy is essential to the existence of the earth, it dictates our seasons, weather patterns and influences our whole way of life. Daylight is necessary for the production of all our agricultural produce and sustains the food chain through the process of photosynthesis. Photosynthesis is a biological phenomena which describes the ability of plant life to convert light into chemical energy for growth. Daylight is one of the most important part of the solar spectrum, it is the band of the sun's energy that we associate with day and night and has been the centre of much attention in recent years for a variety of reasons. These reasons shall be introduced and discussed in some detail because of their impact on daily routines.

In the United Kingdom and the world as a whole there is a severe lack of data detailing levels of daylight to the extent that daylight was not recorded on a continuous basis by the Meteorological Office until the 1950's and up to 1970 only 7 sites across the UK measured global horizontal illuminance, these included only two locations in Scotland, Eskdalemuir (55.3^{o}N) and Lerwick (60.2^{o}N). Furthermore, until 1992 there were no records of vertical illuminance for any location in the UK north of Watford (51.7^{o}N) leaving the majority of the country without these measurements. At present vertical illuminance measurements exist for only 4 sites across the country- BRE Watford, Manchester, Sheffield and Edinburgh. Appendix 1 contains a list of world-wide daylight stations.

The conservation of energy from an economical view point is obvious but reducing the countries annual energy consumption is a matter which should concern all of us. The reason for this lies with the increase in concern over 'global warming' and the 'greenhouse effect'. Global warming results from what is commonly known as the greenhouse effect, where a build up in green house gases in the earth's atmosphere prevents the radiating of energy from the earth back out of the troposphere, hence trapping the energy and causing the heating of the earth. The main greenhouse gases are CO_2, CFC's(Chlorofluorocarbons), methane and nitrous oxide. The largest contributor from these gases is CO_2 which accounts for approximately 50% of the total green house gas production[1.1]. The levels of CO_2 in the atmosphere can be altered in two main ways:

(i) Absorption from vegetation, e.g. rain forests which leads to another environmental issue.

(ii) Production, which is primarily a consequence of the combustion of fossil fuels, coal oil and gas, for the generation of electricity.

$$CH_4 + 2O_2 = CO_2 + 2H_2O + \text{heat energy} \qquad (1.1)$$

Electricity production accounts for 39% of the UK's total CO_2 production[1.1]. Since 1765 levels of green house gases have increased substantially, CO_2 by 25%, CH_4 by 112.5% and Nitrous oxides by 8.8%[1.1]. The use of computers in the analysis and prediction of global warming has given scientists a better insight into the likely outcomes of these increases in green house gases. Computer models predict that the change in the global radiation balance will be roughly equivalent to a 1% increase in the luminosity of the sun[1.1]. The main repercussions for the planet concern agriculture. It is estimated that the European Community and North America will suffer falls in crop yields of 20% with rises in the USSR of approximately 10%, the overall effect will be a reduction in output. The second effect would be a 2% reduction in land which would be a direct result of the rise in sea levels caused by melting of the polar ice caps[1.1]. Overall the global temperature is eventually expected to increase from between 0.8^{o}C and 2.6^{o}C due to the current changes in green house gas levels.

Electrical generation of CO_2 can be reduced in two ways:

(i) Changing the fossil fuel type which is combusted, oil emits 20% less CO_2 than coal.

(ii) Reduce the primary demand for electricity through conservation methods.

Market forces and government policy tend to dictate fuel type and the natural resources of fossil fuels the country possesses mean that for the foreseeable future little will change with respect to fossil fuel consumption for electricity generation. It is therefore concluded that conservation is the most accessible vehicle to use on the road to reduce annual CO_2 production.

Electrical lighting in the UK accounts for an estimated 5% of the total primary energy consumed per annum, this figure rises to between 30% and 60% for buildings such as office blocks and light industry, often larger that heating costs[1.2]. It is in building

types such as the ones described where, through the exploitation of the natural resource of daylight significant savings can achieved. It has been estimated that the savings of between 20% and 40% are attainable for office buildings which utilise daylight effectively[1.3]. The energy potential of daylight in the UK was calculated at between 0.66 and 1.31 mtce (million tonnes of coal equivalent, one tonne of coal amounts to 8000 kWh of energy) per annum by 2020[1.3].

The benefits and savings associated with daylight design are several fold, with the reduction of electrical lighting due to the increased contribution of daylight resulting in the reduction of sensible heat gains. This has the knock on effect of lowering the cooling requirements of the buildings air conditioning units, another high cost centre of a building's annual energy budget. As cooling plants are high consumers of electricity the costs associated with their operation can be as much as four times greater than that of heating. Furthermore the overall efficiency of a cooling plant is only 5% due to the energy conversions associated with refrigeration, with losses accumulating form electricity generation, transmission and final consumption.

Buildings in the UK have traditionally been designed using daylight data recorded from the National Physical Laboratory in Teddington between 1933 and 1939. More recently new building constructions have employed illuminance data from Kew. The age of the data may not create any serious concern, although the clean air acts passed in major towns and cities across the country could possibly influence present daylight levels. There is however great concern centering around the lack of illuminance data for the majority of the country, with Kew and Teddington lying at approximately 51.5^{o} N. The data recorded at these locations is only representative of their latitudes as the latitude dependency of daylight is well recognised, and it is highly possible that the data is site specific[1.4]. The gap in measured daylight data spans some 8 degrees of latitude and includes the majority of the UK's' urban and industrial belt, containing a large percentage of the population. The limited data sets that does exist confirms with out exception the effect of latitude on daylight levels. In a relevant study it was shown that values of average daily global horizontal illuminance varied greatly from that of the reference site, Kew. The percentage differences were found to be as much as 32% different from the measurements for Kew[1.4]. These differences have far reaching consequences for a building's performance.

The qualities of daylight when considered in a building environment go far beyond its potential for saving energy. Much research has focused on investigating the social benefits associated with its inclusion into the work place. From a medical standpoint

the admission of daylight has far reaching consequences for the recovery of patients. In a study[1.5] carried out on surgical patients to evaluate the benefits of exposure to natural daylight during recuperation, it was revealed that the number of cases of organic delirium were reduced by more than half. It was also discovered that in recovery rooms which incorporated natural daylight the patients responded better, consuming less analgesics, and that the presence of daylight was highly advantageous in the prevention of sensory deprivation.

What is of greater interest to building designers and owners/occupants are the affects and advantages gained from working under a daylit environment. A study was carried out to assess and compare the behaviour of children which identified changes in amounts of a hormone, cortisol with exposure to natural daylight[1.5]. The implications of these findings suggest that work carried out in windowless environments, or rooms which lack adequate illumination, may cause a severe disturbance in chronobiological system regulating the production of hormones. Personnel seated near to windows displayed higher levels of morning cortisol as opposed to those who worked far from windows. The significance of this finding is that high levels of morning cortisol are an indication of sociability, while low values tend to favour individual concentration. It was also discovered that the production of cortisol particularly during winter influenced the levels of sick leave, high levels of cortisol during this period correlated with low rates of sick leave. This is due to the nature of cortisol which acts as a mobiliser of the bodies defence mechanism. It is clear then that if the illuminance level in rooms is raised through the inclusion of daylight then the most susceptible children may increase their resistance to colds and mild infections. These conclusions have been substantiated by a similar study[1.6] which revealed that children who spent at least two hours outside during winter became more resistant to disease.

Occupants' performance in offices is of prime importance to building owners and the correlation between workers' satisfaction and performance and the lighting of the work space has been well proven[1.7]. Furthermore associations have been made between light and the decision process as a result of the mood of the occupants, and there is a strong evidence that mood influences the problem-solving process in humans.

Whilst the medical benefits of daylight are not disputed, the health risks to building occupants as a consequence of working in an artificially illuminated office are not as

well recognised. Fluorescent lamps are the most common lighting element used in non-domestic buildings, they are relatively cheap to operate and replace. However fluorescent tubes have been identified as being responsible for a number of ailments and health complaints[1.8].

Some of the recognised side-affects associated with fluorescent lamps include, headache, eyestrain, fatigue, reductions in levels of concentration and an increase in accidents. Other symptoms diagnosed in occupants working in an artificially illuminated environment include stress which can lead to heart disease and skin disorders such as dermatitis. Furthermore fluorescent lamps are suspected to be responsible for more serious health issues, increased risk of seizure in epilepsy sufferers and higher incidence of miscarriage[1.9]. The eyes and skin suffer badly with an increase in the ageing of the retina and an increased risk of skin cancer to the extent that exposure to fluorescent lighting at work may double the chances of developing melanomas compared to naturally illuminated work spaces[1.10].

Another potentially lethal hazard that arises from the use of fluorescent lamps comes from the capacitor used in the switching of the lights. These capacitors were typically made from polychlorinated biphenyl (PCB) and when burned they discharge poisonous fumes which may contain dioxin and dibenzofurans which are some of the most toxic chemicals known to man. PCB's are carcinogenic causing particular damage to the skin, lungs, pancreas, liver and responsible for damage to the nervous system. This hazard still exists in fittings that are pre 1986. A Life Cycle Analysis(LCA) performed on the above lamps and lamp fittings is thus highly desirable.

Clearly the avoidance of problems identified through the use of natural daylight and the undisputed benefits for occupants health as a result, highlights the importance of implementing better daylight design in new and retrofit buildings. Also considering the large cost of artificial lighting in buildings and the potential savings resulting from the effective use of daylight in building design, it is essential that daylight is adopted by architects and building designers in their design strategy. To achieve these objectives it is fundamental to have daylight data for the buildings location.

Daylight is an extremely dynamic quantity, which unlike solar radiation cannot be defined in simple terms such as hourly or daily dosage for most building applications. The exception being museums and galleries which have to consider the damaging

effects of daylight to art work, even so precise estimates of the amount of daylight the building is exposed to is essential. The variations in daylight levels are not restricted to time of day but also on geographical location and season. Simple correlations can be established to allow an estimate of daylight levels using a linear interpolation relating it to the geographical latitude, but this approach is both crude and unrepresentative as it cannot possibly account for the microclimate differences. Clearly there is no substitute for actual measurements. In the absence of measurements, however, is to use a precise method for predicting daylight levels for any location, time of day, season and orientation of the recipient plane.

As a direct result of the absence of measured illuminance data throughout the country, building designers have to rely on predictive tools and models. These models should be capable of accurately predicting illuminance values from meteorological parameters such as solar radiation in an effort to provide as large a network of generated illuminance data as possible. Currently, global horizontal radiation records are available for 57 sites across the UK[1.11] which makes it an ideal parameter for daylight modelling purposes.

With one minute instantaneous, hourly or daily values of horizontal global irradiation it is possible to estimate horizontal diffuse irradiation through the use of established correlations. Furthermore much work has been carried out on the conversion of horizontal global and diffuse irradiance to their illuminance counterparts. This is a well established modelling process as daylight and solar radiation are very similar quantities as one would logically expect- daylight encapsulates the visible part of the solar radiation spectrum (0.39 to 0.78 μm) hence it is likely to posses similar characteristics.

To design buildings to their full daylight potential it is necessary to have slope illuminance data, of which vertical surface data is most useful. The best scenario for building design, however, would be information detailing the luminance distribution of the sky as the amount of daylight a window will receive depends on the luminance of the patch of sky that the window faces. Unfortunately measurements of slope illuminance are scarce and sky luminance distributions even more so. To date only two locations in the UK possess the necessary equipment to carry out this research, BRE Watford and Sheffield. The luminance distribution of the sky is a complex characteristic to model and predict due to the two dimensional nature of the sky luminance distribution.

The complexities of implementing sky luminance distributions into building design, mean that it cannot as yet be readily used to its advantage. Specialist software such as RADIANCE, a product of the Lawrence Berkeley Laboratory offer such a facility. However, implementation of particular sky luminance distribution in a facility such as RADIANCE is a highly specialised task and may be undertaken by only a handful of professionals. One example is the implementation of Frieburg's(Germany) sky luminance distribution functions carried out at the Fraunhofer Institute for Solar Energy Systems in Frieburg. The alternative is therefore to employ vertical illuminances, which are a more manageable quantity and one that can be incorporated into building design. The estimation of slope illuminance has been attempted by several authors using a variety of approaches and limited success. The total illuminance on a sloped surface can be divided into individual components, traditionally these have been beam or direct component, which is the main contributor under clear skies, and background diffuse component, which is the contribution from the sky itself. Other authors have employed additional components to cope with more realistic sky types due to the poor performance of the simpler models. These parameters include circumsolar components, which is the intense luminous region that surrounds the sun. This is best observed on lightly overcast skies where the halo can be seen. Horizon and zenith brightening are components that are included to compensate for the complex form of the sky, these are allowed to change depending on cloud cover to model the variation in the luminance of the sky as one traverses from the horizon to the zenith.

These approaches at best consider the background diffuse component to be isotropic, uniform from the zenith to horizon and artificially apply additional components to cater for the nature of the sky's luminance distribution. However the nature of the sky's background component is anisotropic, varying in luminance gradually from horizon to zenith. This effect is most obvious in clear skies where the horizon appears brighter than the zenith. This is a phenomenon that is quite simple to explain; as one observes a clear sky looking along the horizon the eye's line of sight intercepts a higher density of light scattering dust particles and air molecules compared to a vertical direction of sight. This gradual variation reverses in the case of an overcast sky with higher luminances coming form the zenith and less from the horizon. The reversal effect is a most important phenomenon it being a function of sky clarity.

The most common daylight design tool used by architects and building designers to predict internal illuminances are daylight factors. Its basis comprises of the sky factor, which is a value dependent on glazing size only, using an overcast sky as its reference. The disadvantage of using this method of design is that is unrepresentative of the majority of real sky conditions and fails to consider the orientation of the building. Overall the daylight factor is a rather inadequate design tool that can under and over-estimate internal illuminances quite considerably. Its is therefore an unsuitable tool to be used in design for energy savings through use of daylight. There exists a requirement for a design tool that pays due consideration to the factors discussed to enable the benefits of natural daylight to be realised.

The aims of this work are to evaluate luminous efficacy models and sloped surfaces models with a view to producing a comprehensive sloped surface model that addresses the shortcomings of previous approaches. In addition current design tools are examined and an innovative daylight illuminance factor shall be presented herein.

Luminous efficacy modelling enables daylight levels to be derived from solar radiation measurements. This is a vital stage for the design procedure as global and diffuse illuminance values are essential for further model development. A semi-empirical approach has been adopted by most authors which considers the altitude of the sun and the cloud cover of the sky, although alternative approaches are much more involved, requiring several additional meteorological parameters in their computation. Both methods perform very satisfactorily and have been evaluated against a large database of measured data. The results of this analysis are reported in some detail both graphically and statistically.

REFERENCES

1.1 Ingham A and Ulph A, Economics of Global Warming The Economic Review Vol.10 pp2-6 Nov(1991)

1.2 British Standards Institute BS:8206 Lighting for Buildings: Part 2 Code of practice for daylighting buildings(1992)

1.3 Crisp V H C, Littlefair P J, Cooper I and McKennan G, Daylight as a passive solar energy option Crown Copyright 1987 Building Research Establishment

1.4 Secker S, Regional variations of daylight availability: a review LR&T 15(3)(1983)

1.5 Kuller R and Lindsten C, Health and Behaviour of children in classrooms with and without windows Journal of Environmental Psychology 12, pp305-317, (1992)

1.6 Lykken K B, Outdoor daylight and resistance to respiratory infections Environmental Psychology monographs N0.2 Lund: School of Arch. Lund Inst. of Technol. pp23-27,(1982)

1.7 Boubekri M, Hulliv R B and Boyer L L, Impact of window size and sunlight penetration on office workers' mood and satisfaction: A novel way of assesing sunlight Environment and Behaviour 23(4) pp474-493 (1991)

1.8 London Hazards Centre Flourescent Lighting: A health hazard overhead London Hazards Centre Booklet London (Gray's Inn Road WC1X 8DS)

1.9 Cox D S, Is flourescent lighting a problem for health Health and safety at work pp28-29, May(1985)

1.10 Beral V, Malignant melanoma and exposure to flourescent lighting at work The Lancet pp290-293 Aug(1972)

1.11 Muneer T, Solar irradiation database for the United Kingdom Building Serv. Eng. Res. Technol. 10(1) pp41-45 (1989)

2 EQUIPMENT

Notation

ψ = the angle an obstruction subtends from edge to edge (°)
θ = the elevation angle of an obstruction above the horizon (°)
DEC = solar declination angle (°)

2.1 INTRODUCTION

To aid the development of new illuminance models and the evaluation of current estimation methods it is essential to have an extensive database of daylight measurements. With the CIE (Commission International de'Eclairage) declaring 1991 International Daylight Measurement Year ETSU (Energy Technology Support Unit Harwell) awarded a 3 year contract to Napier and Heriot Watt Universities in a joint venture to measure daylight in Central Scotland. The measurements were carried out in accordance with the CIE guide to recommended practice for the operation of a general class station[2.1]. The introduction of this project would provide much needed daylight data for Central Scotland and the wider International Daylight Measuring Programme (IDMP) shall produce a wealth of measured data for analysis in this present research. The equipment used were purchased from a German company PRC Krochmann in Berlin. A description of the equipment and measurement methods is given along with additional information on another recording programme run in parallel to the main project. The commissioning of the station is described and the faults and errors associated with the operation of the station are reported herein.

The general class station consists of 12 measurement sensors, 6 dedicated to illuminance and 6 to irradiance. Illuminance and irradiance equipment measured in 4 vertical and 2 horizontal positions, with the horizontal sensors recording global and diffuse illuminance and irradiance. Schematic diagrams and pictures of the equipment used are shown in Figs. 2.1.1 to 2.1.7. The illuminance sensors are termed either photometers or daylight sensors and the irradiance sensors are referred to either as pyranometers or solarimeters.

The station consists of,

one 910 GV horizontal global and 4 vertical illuminance sensors (Fig.2.1.1)
one 910 S horizontal diffuse illuminance sensor (Fig.2.1.2)
one CM11 GV horizontal global and 4 vertical irradiance sensors (Fig.2.1.3)
one CM11/121 horizontal diffuse illuminance sensor (Fig.2.1.4)

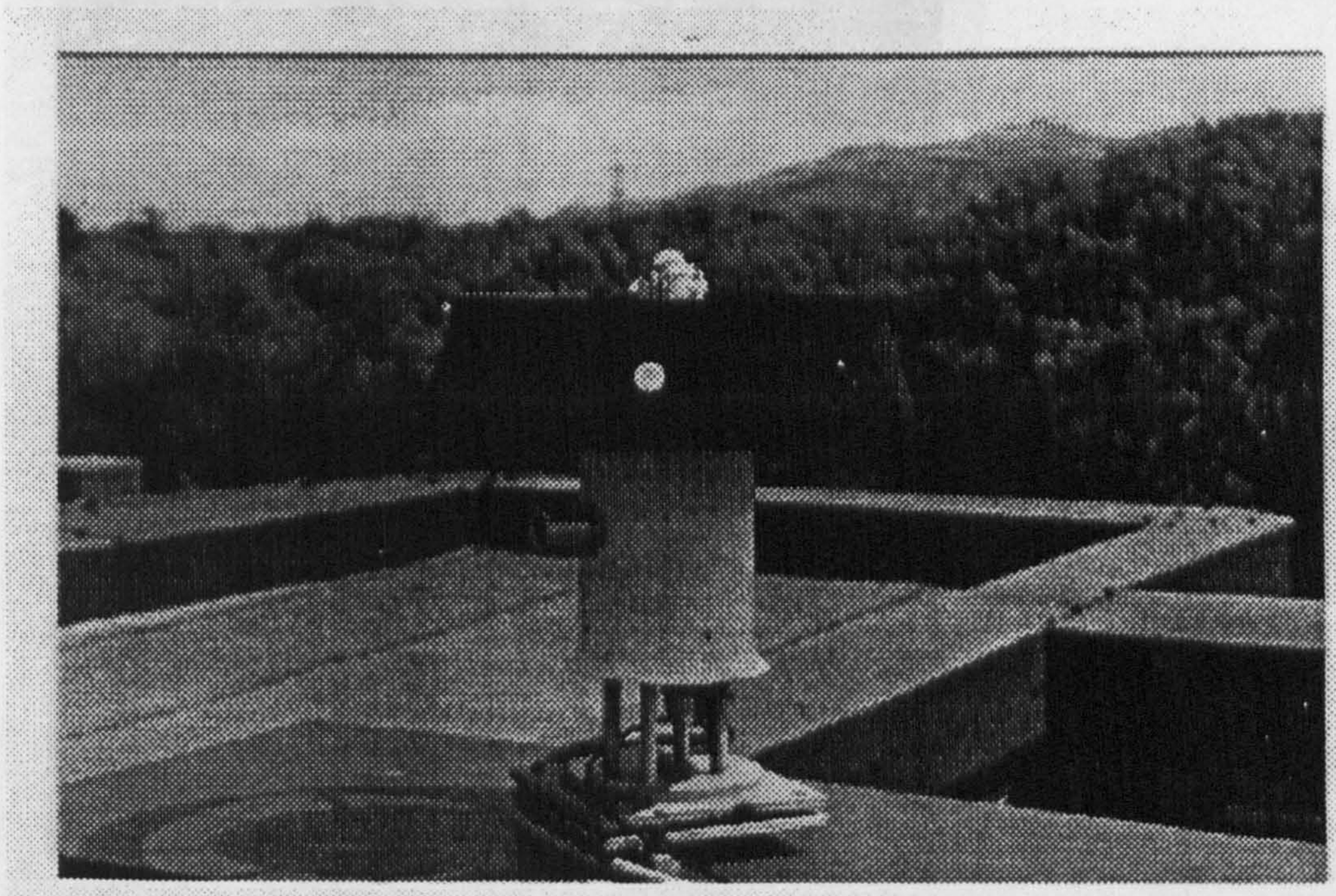

Figure 2.1.1 910 GV horizontal global and 4 vertical illuminance sensors

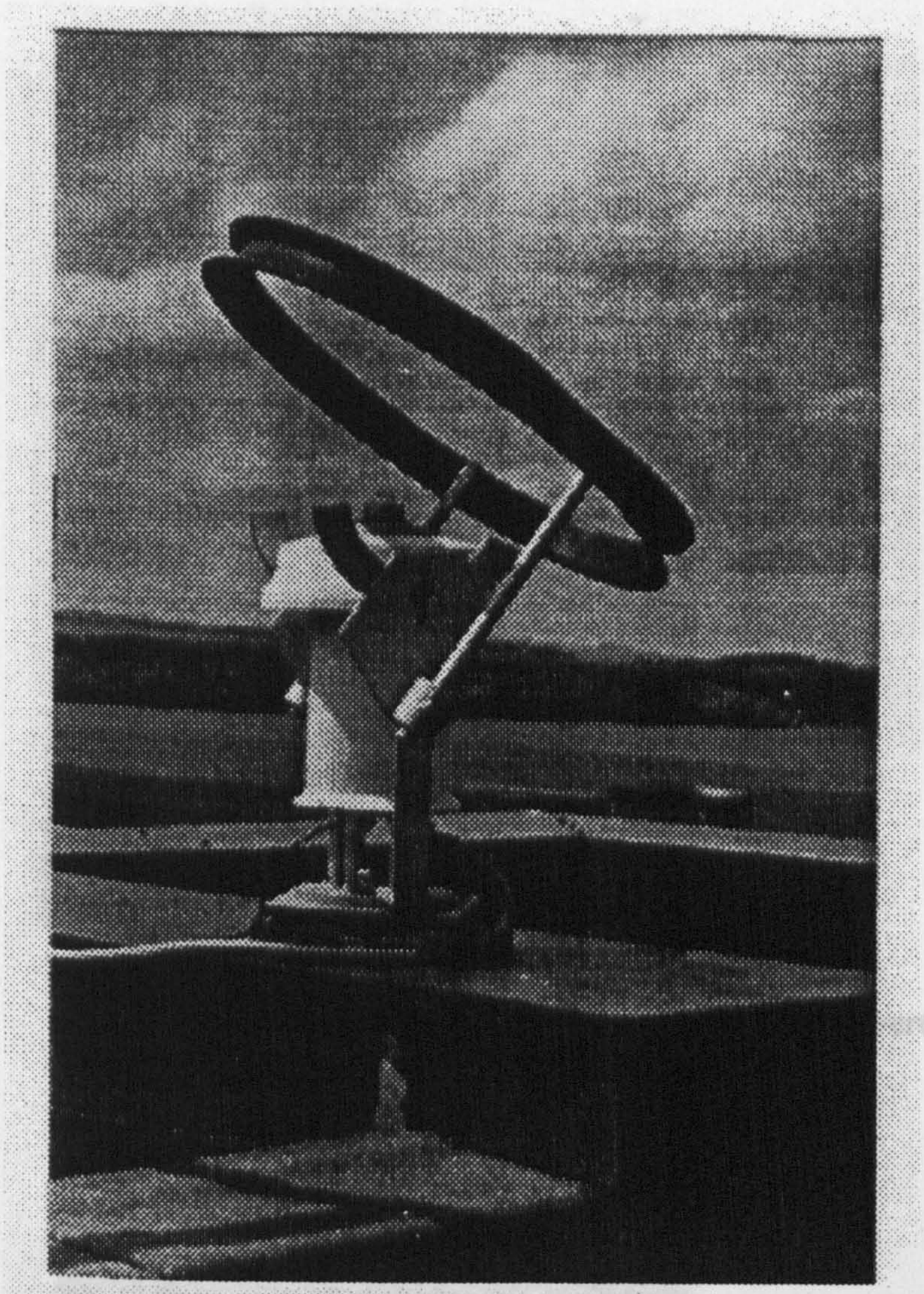

Figure 2.1.2. 910 S horizontal diffuse illuminance sensor (Fig.2.1.2)

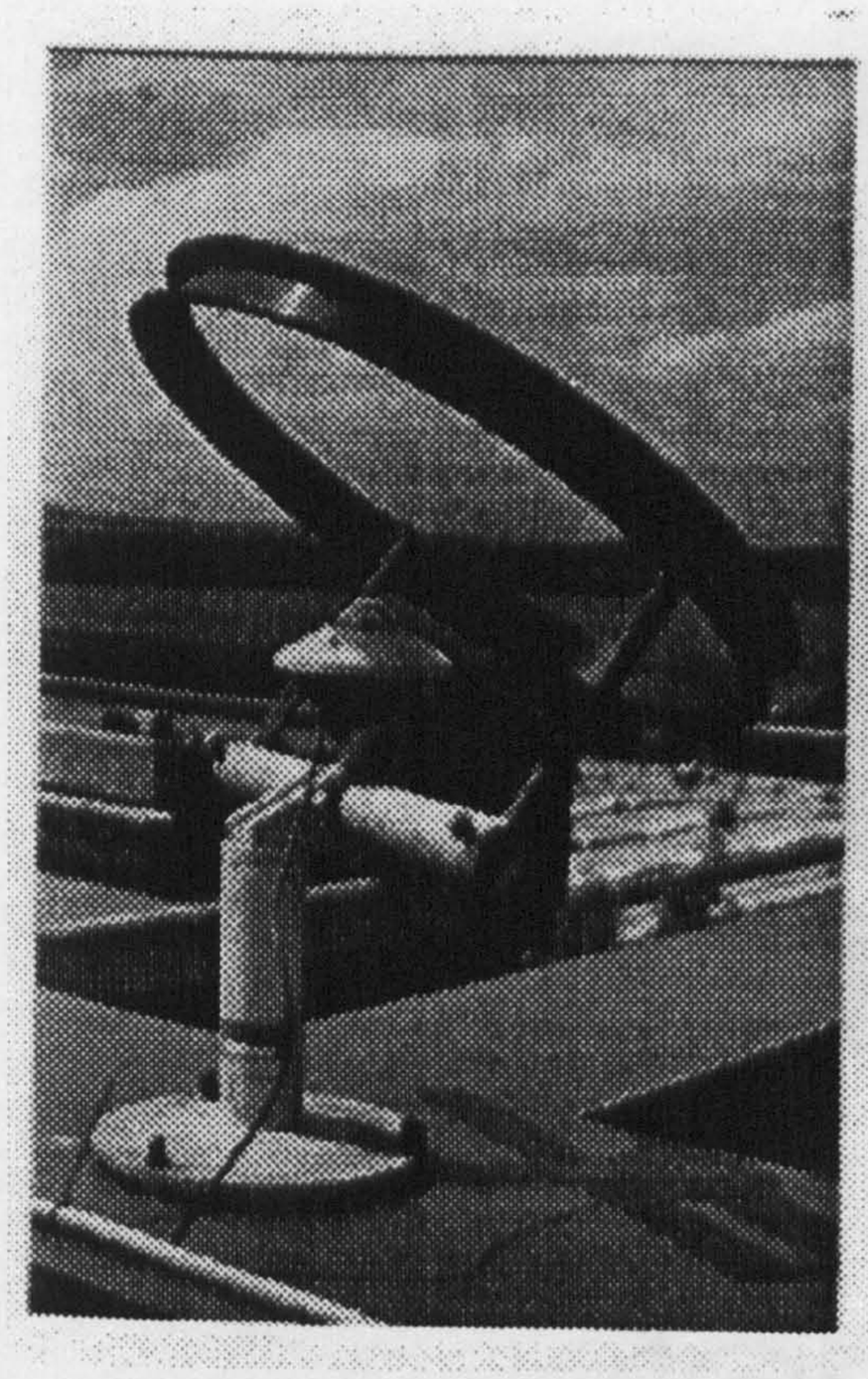

Figure 2.1.3. CM11 GV horizontal global and 4 vertical irradiance sensors

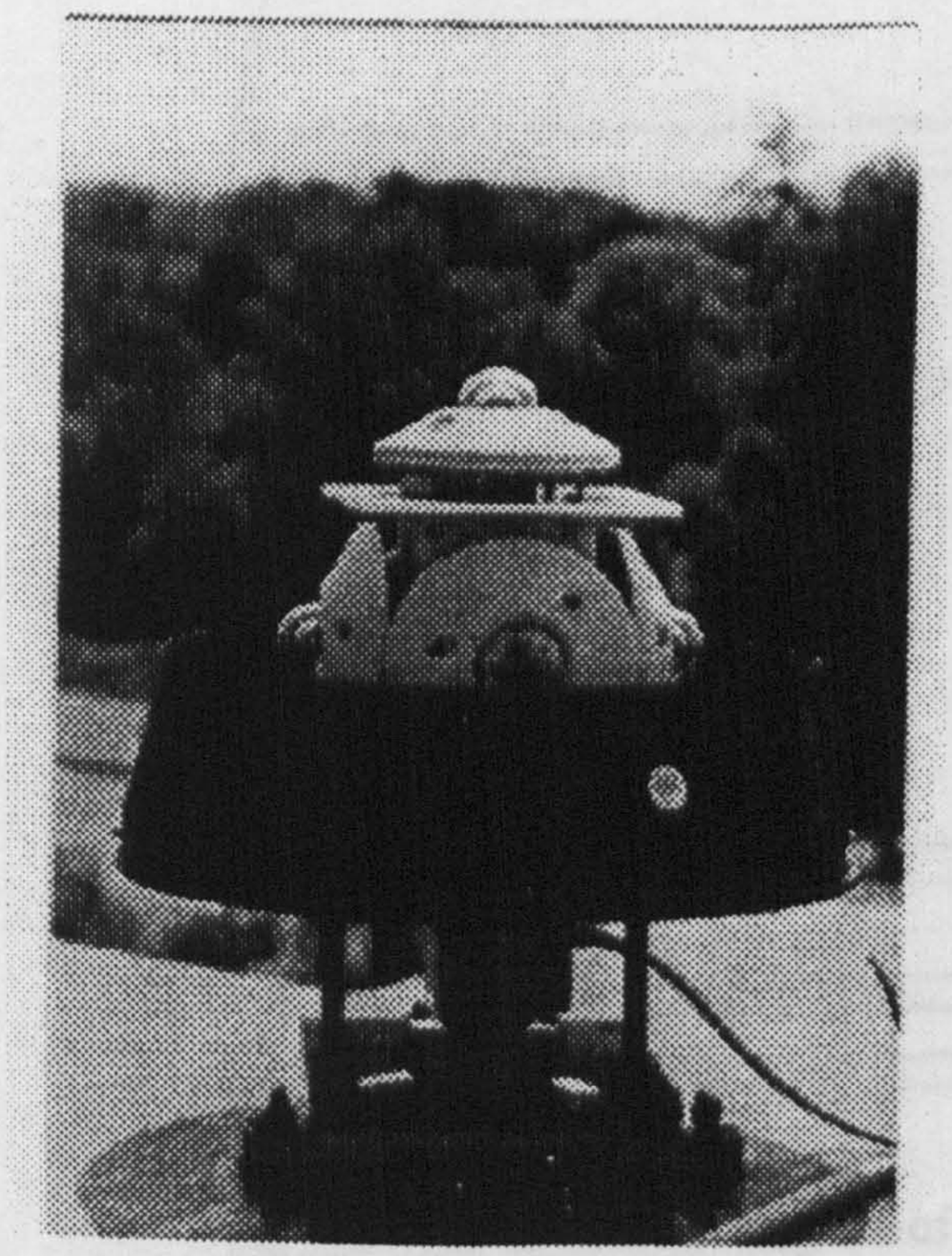

Figure 2.1.4. CM11/121 horizontal diffuse illuminance sensor

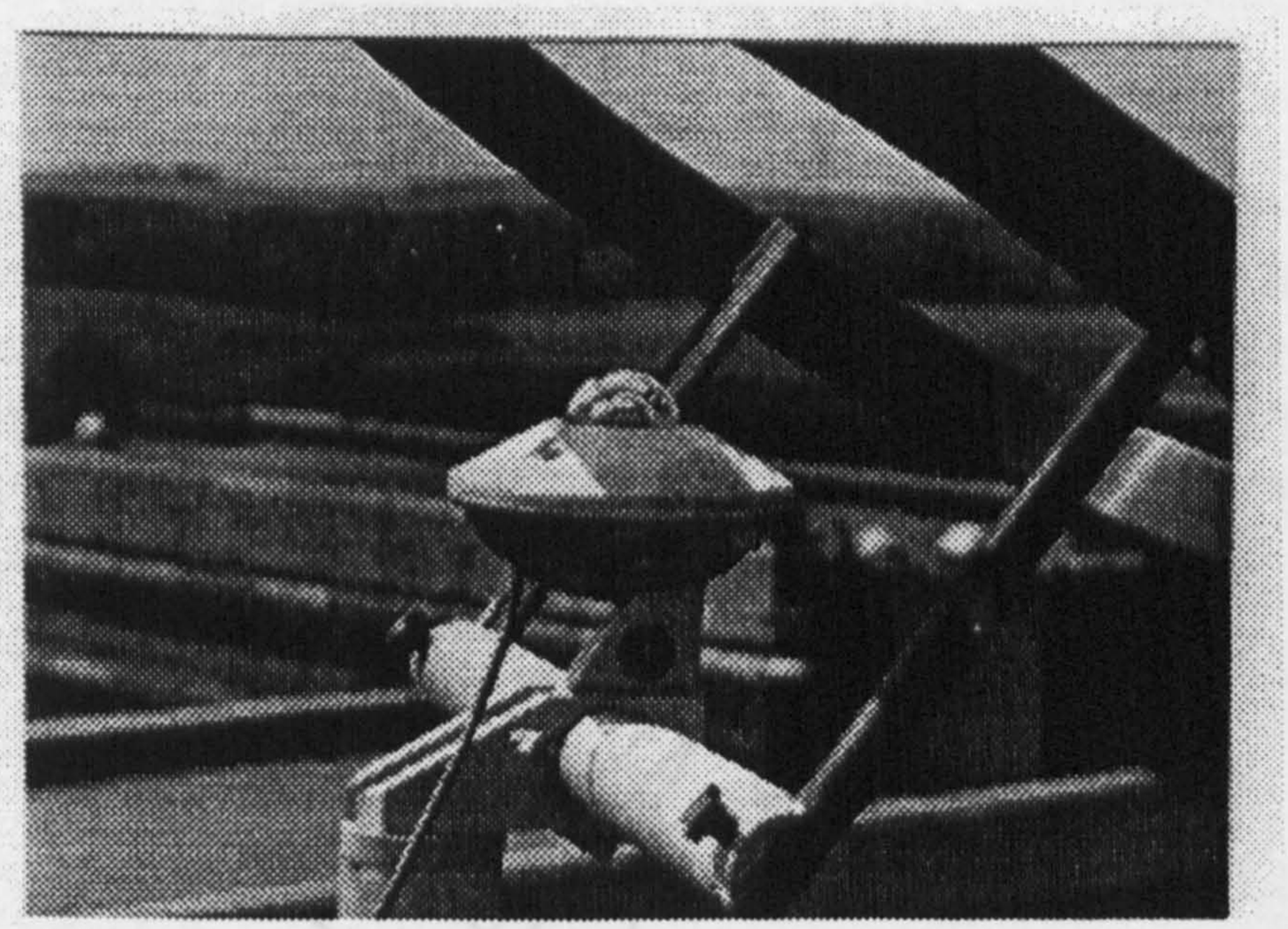

Figure 2.1.5 Solarimeter

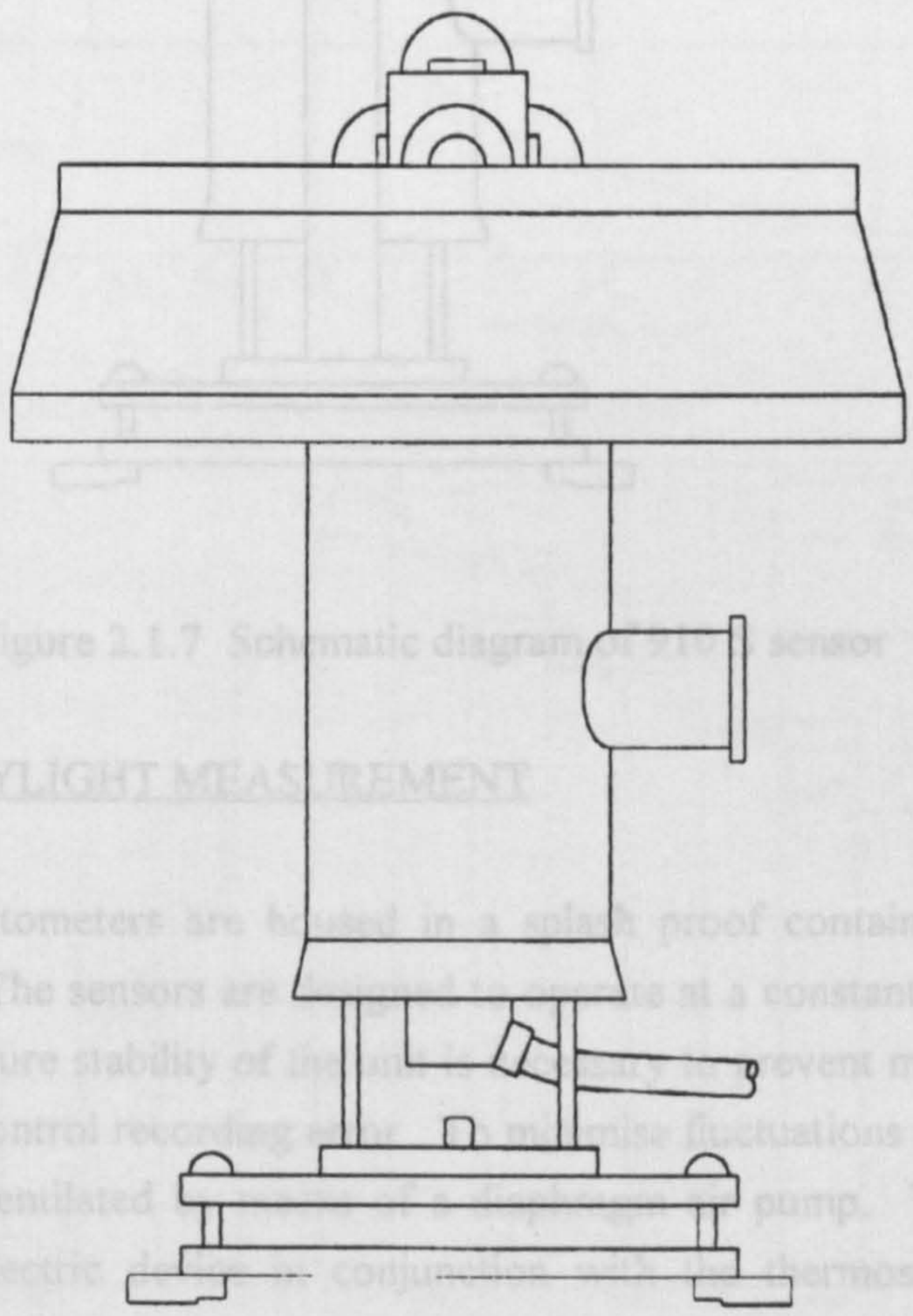

Figure 2.1.6 Schematic diagram of 910 GV sensor

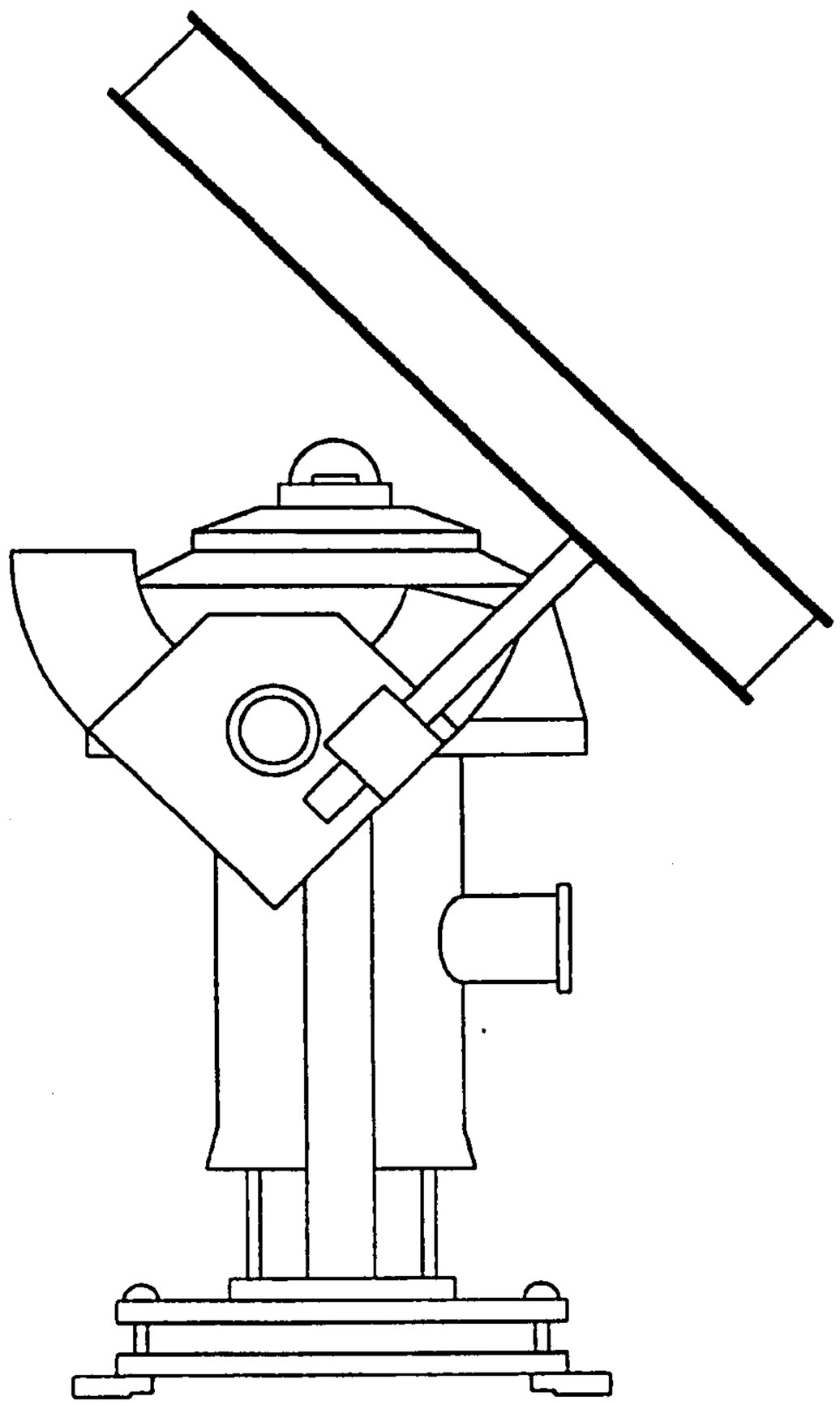

Figure 2.1.7 Schematic diagram of 910 S sensor

2.2 DAYLIGHT MEASUREMENT

The photometers are housed in a splash proof container covered by a fibreglass shield. The sensors are designed to operate at a constant temperature of 35°C. The temperature stability of the unit is necessary to prevent moisture build up in the cells and to control recording error. To minimise fluctuations in temperatures the housing unit is ventilated by means of a diaphragm air pump. When heating is required a thermoelectric device in conjunction with the thermostatic unit's microprocessor supplies the correct current through a PID (Proportional Integral Derivative) algorithm to the heating element[2.2]. This method of control reduces response time to changes in external temperature. The ventilation of the glass domes along with the

use of silica gel cartridges prevents the formation of condensation on the inside of the glass domes.

The photometers measure the visible spectrum and are tuned to the relative spectral response V(λ) of the human eye. Fig. 2.2.1 demonstrates the solar spectrum with the main spectral bands shown and Fig. 2.2.2 the relative sensitivity against wavelength for the human eye. The visible spectrum covers wavelengths between 0.39 to 0.77 μm, this bandwidth accounts for 46.41% [2.3], of the total extraterrestrial irradiance and is the largest percentage of any of the spectral bands.

Figure 2.2.1 Solar radiation spectrum

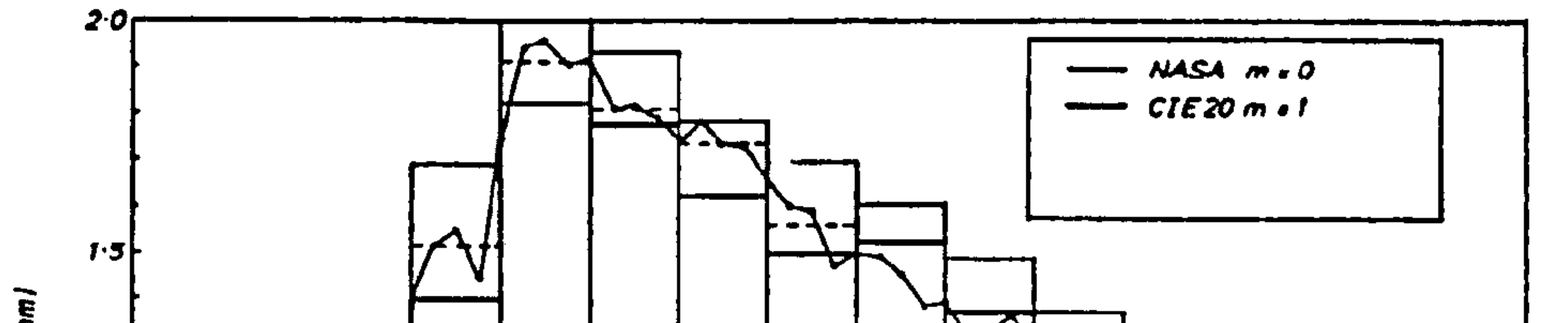

Figure 2.2.2 Visible radiation spectrum

The 910 GV apparatus as shown schematically by Fig. 2.1.6 demonstrates the shading ring, this eliminates any contribution from ground reflectance which would affect the measurement of vertical illuminance, especially in cases where the surface possessed a high value of albedo.

The diffuse illuminance sensor type 910 S is similar in construction to the 910 GV as seen from Fig. 2.1.7 with the single photocell mounted horizontally. The main difference between the diffuse and global sensors is the addition of a shadowband or ring whose purpose is to remove the contribution of the suns' direct light. The shadowband adjusts to allow the suns' rays to be obscured all year to account for the changing declination of the sun. The adjustment of the shadowband is of great importance as incorrect adjustment will result in poor quality data. Adjustment can be carried out in two ways. Firstly through the use of the following equation;

$$\text{Height of sliding bar} = 297^{*} \tan(\text{DEC}) \qquad (2.1)$$

the value calculated from this formula gives the height the sliding bar to be set for correct shading of the cell. The sliding bar is marked on both arms with numbers to aid in the adjustment. This formula is applicable for the whole year, the values calculated are employed to the lower arms of the sliding bar between 21st March to 23rd September and upper figures for the remaining months. Secondly, by the observation of the shadow cast over the cell. This task is best executed while the sensor is under a clear sky where correct setting of the shadowband will produce adequate shading for the sensor.

Adjustment should take place every 2 to 3 days on average. However more frequent maintenance of the shadowband is necessary during the approach of the vernal and autumnal equinoxes where the declination angle of the sun changes rapidly. Daily setting of the shadowband is recommended during these periods. Furthermore shadowband adjustment should, cloud cover permitting, follow the second method described calling on the use of Eq. 2.1 as a guide. This is because the values obtained have a tendency to be crude, occasionally providing unsatisfactory shading of the sensor.

As a result of the omission of direct sunlight through the implementation of the shadowband there is a corresponding loss of skylight recorded by the sensor. If this cannot be avoided, however, the loss can be compensated for by employing

correction factors or algorithms. This process shall be dealt with in the database chapter.

The actual cells are of selenium construction and act as a photovoltaic cell which produce a photocurrent under exposure to visible light. This photocurrent is converted to a voltage and read into the data acquisition system. The signals from the 6 sensors are then transmitted to a dedicated 386 computer via a standard IEEE 488 interface cable. These voltages can be converted to illuminances by applying the appropriate calibration constants to each signal. These are then stored through the daylight software, provided as an integral part of the station. The daylight software is tailored to data acquisition with timetabling, data storage and quality control checking facilities. To this end the station is automatic in its daily operation once the users specific data recording requirements have been programmed. In the present research programme, both the Napier and Heriot Watt sites recorded data instantaneously at one minute intervals and stored on hard disk. Periodically the stored data are backed up onto miniature tape using a tape streamer and the manufacturer's software, compressing the data for downloading and analysis. The raw data are in an unsuitable format for processing and have to be converted to ASCII format. This is yet another task completed through the 'daylight' software. Figure 2.2.3 demonstrates the schematic arrangement of the main station.

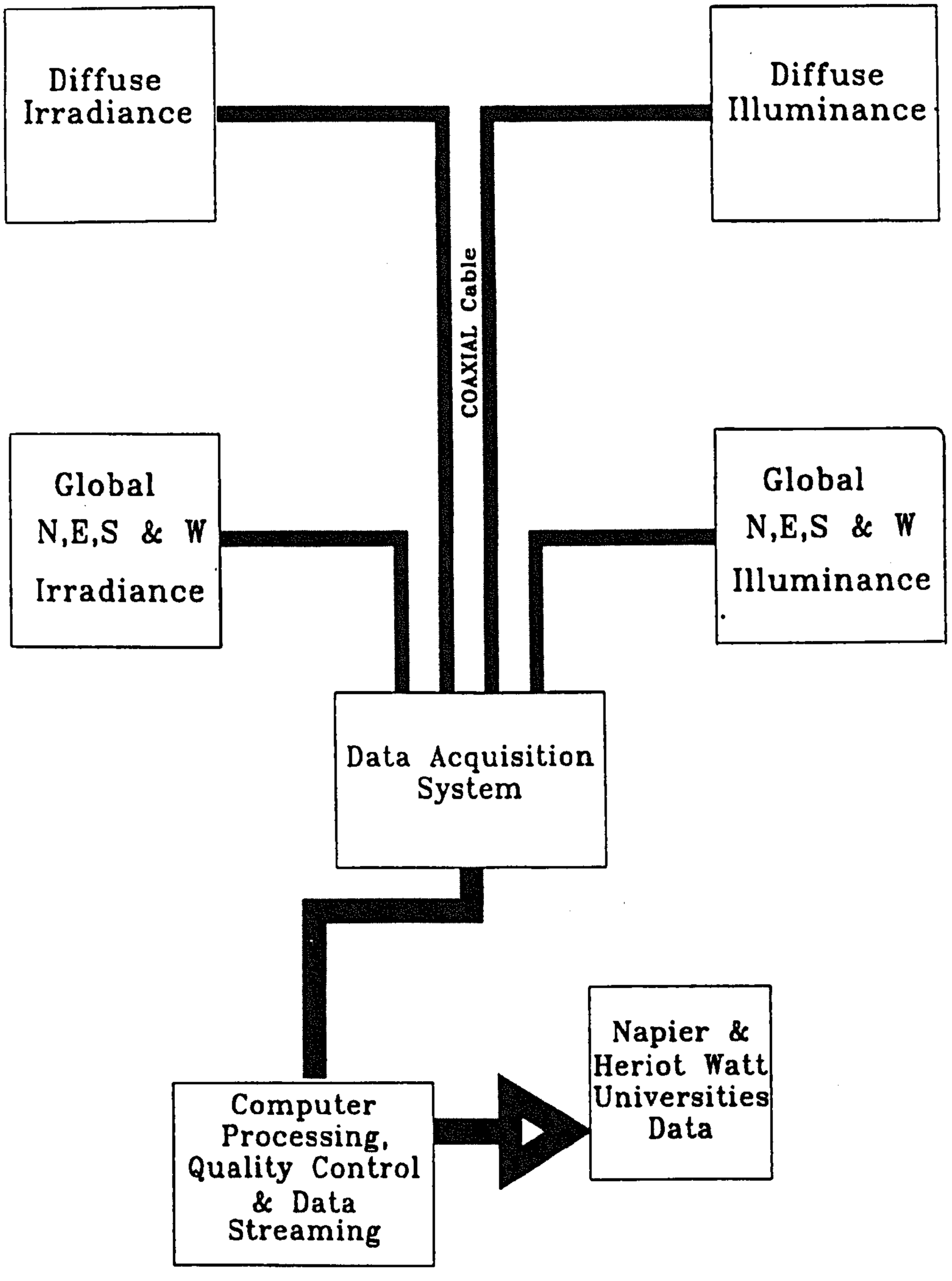

Figure 2.2.3 Main station schematic diagram

2.3 SOLAR RADIATION MEASUREMENTS

All of the pyranometers supplied by PRC Krochmann for irradiance measurement are manufactured by Kipp and Zonen. The CM 11 is regarded as the standard reference pyranometer type due to its accuracy, stability and quality of construction and reliability as a sensor. The sensing element shown in close up in Fig. 2.1.5 is a thermal detector which responds to the total power absorbed without being selective to the spectral distribution of the radiation. The heat energy which is generated by the absorption of radiation on the black disk flows through a thermal resistance to the heat sink. The resultant temperature difference across the thermal resistance of the disk is converted into a voltage which can be read by computer. The double glass construction minimises temperature fluctuations from the natural elements, wind, rain and the like and reduces thermal radiation losses to the atmosphere. Moisture is prevented from forming inside the domes through the presence of silica gel crystals in the body of the CM 11. The pyranometers have a spectral response of between 335 to 2200 nm of the solar spectrum which includes the visible wavelengths measured by the photometers. Output from the sensors go directly to the acquisition equipment via 30 metres of screened cable and then to the computer, where the individual sensitivities of the sensors converts the voltages to irradiance values. A copy of the calibration certificates for all the stations sensors are given in Appendix 2.1.

The adjustment of the diffuse irradiance sensors' shadowband follows the same method as the 910 S illuminance sensor, although more frequent attention is often required as the sensing area is somewhat larger than the diffuse illuminance sensor.

Asides the regular adjustment of the shadowband, the station requires minimum maintenance. The glass domes can collect debris overtime and through weekly cleaning this is controlled. Any irregularities in measurements are identified by the daylight software and equipment faults can be detected through the quality control checks carried out on line at 10 minute intervals. The results of the quality control checks are stored on hard disk for further scrutiny as well as being displayed on screen. The quality control aspects shall be dealt with by the database chapter.

2.4 EQUIPMENT ERROR AND UNCERTAINTY

With any measurement there exist errors some of which are systematic and others inherent of the equipment employed. With daylight and solar radiation measurements the most common sources of error arise from the sensors and their construction. These are broken down into the most general types of errors and described.

1) Cosine response
2) Azimuth response
3) Temperature response
4) Spectral selectivity
5) Stability
6) Non-linearity

To be classed as a secondary standard instrument (such as the CM 11) pyranometers have to meet the specifications set out by the WMO (World Meteorological Organisation) given in Appendix 2.2.

Of all the aforementioned errors the cosine effect is the most apparent and widely recognised, this is the sensors response to the angle at which radiation strikes the sensing area. The more acute the angle of the sun, i.e. at sunrise and sunset the greater the source of this error. This effect is more pronounced for highly reflective surfaces such as snow or water covered. The correction of this error is not entirely satisfactory although authors have produced algorithms to compensate this error[2.4]. Appendix 2.3 highlights the cosine effect with the results from the calibration tests carried out on the 910 S illuminance cell. Cosine error is typically dealt with through the exclusion of the recorded data at sun rise and sunset times in calculations or modelling.

The azimuth error is a result of imperfections of the glass domes and in the case of solarimeters the angular reflection properties of the black paint. This is an inherent manufacturing error which yield a similar percentage error as the cosine effect.

Like the azimuth error the temperature response of the sensor is an individual fault for each cell. The photometers are thermostatically temperature controlled hence the percentage error due to fluctuations in the sensor's temperature are reduced. However the CM 11 pyranometers have a much less elaborate temperature control

system. The pyranometers rely on the two glass domes to prevent large temperature swings.

The spectral selectivity of the CM 11 is dependant on the spectral absorbency of the black paint and the spectral transmission of the glass. The overall effect contributes only a small percentage error to the measurements. Each sensor possesses a high level of stability with the deterioration of the cells resulting in approximately ±1% change in the full scale measurement per year. Finally the non-linearity of the sensors is a concern especially with photometers. It is a function of variation with illuminance or irradiance, which tends to contribute only a small percentage error to the measurements.

2.5 EQUIPMENT FAILURE

Besides the fundamental errors that exist with the measurement of daylight and solar radiation there have been several instances of unavoidable equipment failure. It is important to detail the problems encountered with sensitive equipment like the photometers and pyranometers to disseminate the experience gained during the operation of a general class station. It is foreseen that the experience obtained and problems encountered will aid in the prevention of future data loss and interruption. In order to achieve these aims the malfunctions and difficulties which confronted the measurement station are documented along with the measures taken to resolve them.

The first and most persistent fault which developed from the station concerned the 910 S diffuse illuminance sensor and its thermostatic unit. An intermittent fault arose which began with the thermostatic units failure to maintain the sensor at 35°C. This was identified via the error message displayed on the thermostatic unit, code 03. The station was under guarantee and both the illuminance sensor and thermostatic unit were returned to the manufacturers for repair, with a resultant loss of 2 months diffuse illuminance data.

Approximately a year later, while calibration tests were carried out on the station the 910 S diffuse illuminance sensor was found to have drifted from its original calibration factor by a considerable margin. The shadowband was removed so that the diffuse sensor could be compared with the horizontal global illuminance cell. The results of this test are shown in Appendix 2.4. The manufacturers were notified of this problem and after consultation with other daylighting experts and the subsequent

investigation of the possible sources of error, the diffuse illuminance sensor was returned once more to PRC Krochmann.

The 910 S diffuse illuminance sensor was returned two months later, an amplification fault having been diagnosed as the offender. Due to the uncertainty of this fault, some six months of diffuse illuminance data was removed to ensure the quality of the dataset.

Once the sensor was installed a further set of independent tests were carried out to ascertain the level of confidence that could be placed on its measurements. The shadowband was removed and the 910 S diffuse illuminance sensor was again compared to the horizontal global illuminance cell. The results of this experiment were quite alarming. Appendix 2.5 shows the extent of the error found between the two sensors. The results indicate that the 910 S diffuse illuminance sensor continues to measure on average 12% higher than the global sensor. Another possibility was the reliability of the global sensor. To this end a further set of tests were run on the horizontal global illuminance sensor using a first class LMT horizontal global illuminance cell on loan form the BRE (Building Research Establishment). Appendix 2.6 proves beyond doubt that the horizontal global illuminance sensor is not a source of error with an overall percentage difference of 2.3% when compared with the LMT cell. One significant error was identified as the reflection problem with the 910GV sensor. This is highlighted in appendix 2.11

Other sources of data loss include an occasional time-out error with the IEEE 488 cable which occurred 3 to 4 times a year. This was resolved by resetting the computer. The solarimeters however, have operated faithfully throughout the recording period and showed no significant variation in their original calibration constants when re-calibrated.

2.6 CONTROL STATIONS

With an ever-increasing number of buildings being constructed on the outskirts of towns and cities and in green belt sites it is important to investigate any differences between the microclimate of the city centre and its suburbs. Changes in microclimate can be attributed to several factors: pollutions and surrounding landscape, i.e. hills and coasts. These variations can effect temperatures, wind direction snow cover and levels of radiation and daylight. This has a direct consequence for the daylight design

of buildings. The use of the most appropriate daylight database for a city can lead to a better designed building in terms of occupant comfort and energy savings. A need therefore exists to investigate potential microclimate differences for not only design but for environmental issues.

To analyse the extent of variations in microclimate in the Edinburgh area solar radiation and daylight levels were monitored at two locations in the city in a separate study to the overall collection of illuminance data in Central Scotland. The two sites investigated were at Napier University and Heriot Watt University located in the city centre and outskirts of town respectively. The Napier site(urban) is surrounded by residential housing 1.5 km form the city centre, whilst the Heriot Watt site(suburban) is 7.5 km West-South-West from Napier surrounded by farmland with the Pentland hills to the south. The prevailing wind is westerly from Heriot Watt University to Napier University.

Each site was equipped with one horizontal global illuminance sensor and one horizontal global irradiance sensor. The sensors' signals were amplified and transmitted along screened cabling to an analogue to digital converter (ADC) attached to the back of a dedicated host computer, where in-house software collated the data and stored it on hard disk. The majority of the components were commissioned on site along with the development of the data acquisition software. The complete apparatus arrangements are known as the control stations. Fig.2.6.1 shows the configuration of the control stations. Kipp and Zonen CM 11 pyranometers, on loan from the Robert Gordon's University, Aberdeen were used in solar radiation measurements whilst for a short time Megatron illuminance cells were employed at both sites to measure daylight. The Megatron cells were soon replaced with first class LMT illuminance sensors (on loan from the BRE) due to the unsuitability of the Megatron sensors for this task. Problems encountered include the ingress of water into the cells and non-linearity.

The solarimeter signals were amplified at source prior to the transmission of their output voltage to the ADC in an effort to minimise signal loss. The amplifier circuit used at both stations are given in Appendix 2.7. They were constructed along with the ±12 volt supply required to power the amplifiers from base components. The calibration of the amplifiers were carried out in the Mechanical, Manufacturing and Software Engineering Department of Napier University using a variable voltage supply and high sensitivity digital voltmeter. The amplifiers' gain were derived from the individual sensitivity of the sensors and could easily be adjusted for replacement

cells. The calibration certificates for the control station sensors are given in Appendix 2.8. The calibration of the LMT photometers took place at the BRE using a photometric bench under the supervision of Dr P J Littlefair in November 1992. The MET Office calibrated the solarimeters in the April of 1992. In addition the LMT photocells required ±30 volt supply packs to power the heating element inside the body of the sensors in a similar arrangement to the main stations photometers.

The ADC inside the computer handled both signals using a multiplexer. The digital signals were then read by the computer software and simultaneously displayed on screen and hard disk for further analysis. The software read 6 instantaneous values from each sensor and reported a one minute average of those readings. This method aided in reducing the spikes associated with instantaneous measurements. Both stations were synchronised with each other and the main station to allow a cross comparison and to provide additional confidence in measurements. Every 5 days the recorded data were transferred to disk at both sites and compared. Details of the control station data and results are dealt with in future chapters.

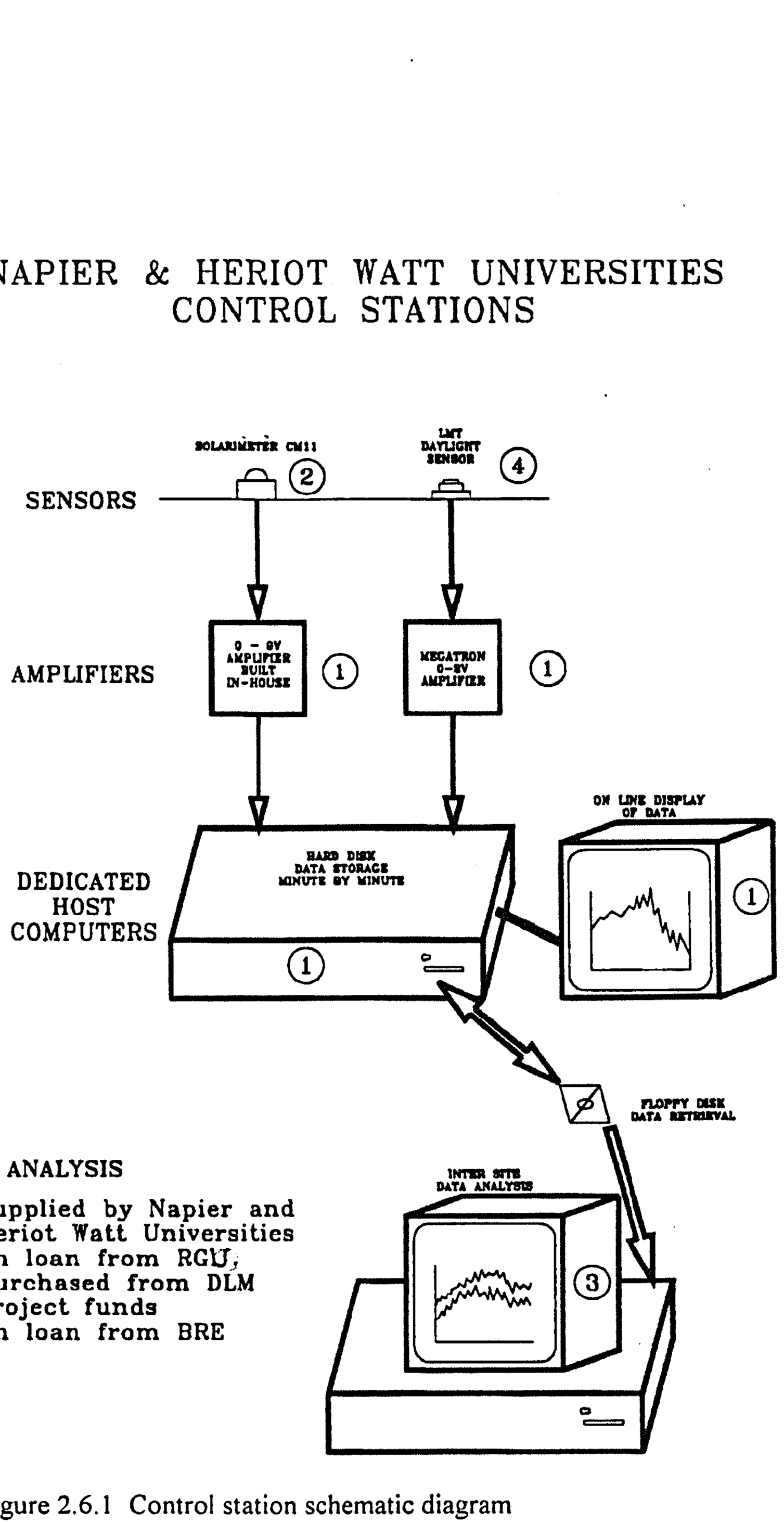

Figure 2.6.1 Control station schematic diagram

2.6.1 Equipment failure

The simplistic arrangement of the control stations has resulted in a great deal of down time for the first 18 months of the project. Asides the replacement of the Megatron illuminance cells, the actual solar and daylight sensors proved reliable. The majority of faults centred around the ADC card, amplifiers and cables. The ADC cards purchased for both sites were basic in architecture and ultimately proved unreliable in operation. The station recorded continuously 24 hours a day a task it was apparent that these cards were not capable of. The replacement ADC cards type PC 26AT were of a greater quality supplied by Amplicon[2.5].

An inherent fault with amplifiers was their capability for burning microchips. This was a regular occurrence with the components requiring replacement every few months. This problem was overcome through the employment of a slightly different chip, type CA 3140E supplied by RS Components[2.6].

The exclusion of water from the amplifiers and sensors was a major concern. The sensors themselves were sealed units and the solarimeter amplifiers had weatherproof cases to protect them from the elements. The daylight sensors were located inside the laboratory beside the computer. However the photometers' cable connectors were susceptible to the ingress of water. This is a design fault of the connectors, whilst being quick release they failed to be water tight. Water would enter the connector plugs and over time dust and debris would accumulate and cause a short circuit. This anomaly was exclusive to the Heriot Watt control station as construction work which was taking place a few hundred metres away would create plumes of dust. Once this fault had been diagnosed the connectors were securely wrapped in self amalgamating tape preventing any further incidents of this sort.

2.7 COMMISSIONING OF THE IDMP STATION

With the introduction of the IDMP the CIE proposed a code of practice to be implemented for all participants in the programme to adhere to. The CIE proposed a Guide to recommended practice[2.1] which laid out standards and methods to be employed in the commissioning, measuring and presentation of daylight data. This would ensure world-wide conformity in data collection and allow the maximum benefits of the programme to be achieved. The main recommendations relate to the selection of the measurement site, for which there are two main requirements. The first requires that the proposed location of the sensors has an extensive view of the

hemisphere, with obstructions such as buildings and trees to meet the following guidelines:

1) Continuous obstructions should not be higher than 0.08 radians (4.6 degrees)above the horizon.

2) In any quarter of the sky the total solid angle subtended by obstructions should not exceed 0.13 steradians but should be significantly less.

The second requirement is of particular importance when the orientation of an obstruction is in an easterly or westerly direction as this may obscure the sun for substantial periods of the day at certain times of the year. The calculation of an obstruction can be made by using Eq. 2.2.

$$\int_{\varphi}^{\theta} d\theta d\varphi \cos\theta \qquad 2.2$$

where θ is the elevation angle of the obstruction above the horizon and ψ is the angle the obstruction subtends from edge to edge. An example of this calculation is given for the assessment of one of the Heriot Watt sites in Appendix 2.9.

The other requirement states that personnel must be made available for the daily operation of the station and maintenance including the setting of the shadowbands. The commissioning of the station requires consideration to several additional factors, these include the detailed planning of the site and sensors location to minimise individual interference. The site must allow reasonable access to each sensor for maintenance purposes but be remote enough to avoid external human interference. Lightning protection is essential, not only to prevent damage to the equipment but to avoid personnel injury. The site should also pay due consideration to possible sources of electrical interference such as lifting gear or transformers which generate electrical fields and may affect the sensors output. Attention should also be paid to the restriction in cable length in the initial stages of design.

A requirement of each station operator is the production of a site description, detailing a comprehensive breakdown of the stations' location, surrounding landscape, climate and equipment. A copy of this form is given in Appendix 2.10.

On completion of the CIE guidelines the station requires fine tuning in the form of aligning and levelling before data can be recorded. Each piece of apparatus has to be aligned with north, this can be carried out in several ways. The most straight forward approach is to use a good quality compass and an ordnance survey map of the area. Magnetic north can be found and marked on the map and adjusted to obtain true north through the application of the appropriate adjustment angle to compensate for the earth's magnetism. This value should be available on request from the Royal Observatory. However if the given site has a large concentration of iron creating magnetic distortions this method is unsuitable. An alternative approach is to align the sensors with the sun at solar noon where the sun will have reached its maximum altitude. This occurs around 12 noon GMT with the exact time found by approaching the observatory or by looking up an astronomical almanac[2.7]. Once the time of solar noon has been established the most straight forward method is to use the compass alignment apparatus included with the diffuse irradiance sensor. This device allows the sun to be sighted through a viewing mount while the sensor is set aligned to south. This can then act as a reference for the remaining sensors.

Once alignment has been completed the equipment has to be levelled to the horizontal. Each sensor either has a spirit level or attachment facility. Through the careful adjustment of the levelling screws on the base plate the bubble in the spirit level can be located in the centre ring ensuring the sensing element is horizontal to within 0.1°. A tilt of only 1/8 th of a degree is enough to displace the bubble half way out of the centre ring.

As part of the DTI contract the main station was transferred to Heriot Watt University to complete a years' measurements, with the same commissioning procedures being followed. Several difficulties were encountered as a result of this move. A complete set of instrument cables had to be purchased as the removal of the cables at Napier was adjudged to be too difficult and may have caused damage. Once the new cabling had arrived the station was set-up in the laboratory to ensure that no damage to the equipment had occurred. To this end it was discovered that the CM 11 GV was measuring incorrect values. After consultation with the manufacturer and some investigation, a cabling fault was diagnosed and resolved before the installation of the equipment.

Establishing a suitable site for the station proved to be far from straight forward due to the restrictions imposed by cable length and in adequate flat roof space.

Eventually two sites on the same building were identified as potential locations, the first on the main roof of the physics department which had the advantage of easy access and was within close proximity of a suitable room to house the acquisition equipment. However the obstructions to the sensors from adjacent plant rooms would prove to be a drawback. The second location benefited from having a better unobstructed view of the hemisphere and was close to the same room. The main obstacle to using this site was the lack of adequate platforms on which to mount the sensors and the difficulty in accessing the site. Despite these difficulties the second location was chosen with beams erected to mount the sensors and scaffolding brought in to allow access, hence overcoming the initial problems.

REFERENCES

2.1 Tregenza P R Guide to recommended practice of daylight measurement Supplement to CIE journal 6(2) (1987)

2.2 PRC Krochmann GMBH Instruction manuals for operation of daylight station D-1000 Berlin (1991)

2.3 Iqbal M An introduction to solar radiation (Academic press, Toronto) (1983)

2.4 Coulson K L Solar and terrestrial radiation (Academic press, New York)(1975)

2.5 Amplicon Liveline Ltd Purchasing catalogue Brighton (1993)

2.6 RS Components Electronic and Electrical Components catalogue July-October Corby (1994)

2.7 HM Nautical Almanac Office Astronomical Phenomena (London: HMSO) (1994)

3 DATABASE

3.1 INTRODUCTION

To evaluate and aid the development of daylight models it was essential to have access to weather databases for a variety of locations across the UK and Europe. As many of the daylight models presented and derived for this research have been developed from only one location and dataset, it was necessary to provide as much alternative data in order to complete a comprehensive evaluation of the models. This chapter details the data used, additional parameters required and the processing, quality control checks and formatting needed to ensure high quality datasets.

3.2 DATABASES

The datasets used in both evaluation and development are given in Table 3.2.1.

Table 3.2.1 Daylight and solar radiation data for various measurement stations.

Station	Period of measurement	Latitude	Longitude	Type of measurement	Data used
BRE Watford	1984,1990-2	51.71 N	0.32 W	One minute instantaneous	5 Min- avg.
Edinburgh Napier	1992-93 16 months	55.95 N	3.2 W	One minute instantaneous	5 Min- avg.
Edinburgh Heriot Watt	1993-94 10 months	55.83 N	3.3 W	One minute instantaneous	5 Min- avg.
Sheffield	1992 4 months	53.37 N	1.5 W	One minute instantaneous	1 min
Athens	1993 12 months	37.97 N	23.72 E	One minute instantaneous	5 Min- avg.
Japan	1993 7 days*	33.52 N	130.48 E	One minute instantaneous	1 min

* Randomly chosen through the period of one year.

The BRE 1984 data were used in the evaluation of luminous efficacy models and the initial development of the proposed sloped surface model. The data were in a

magnetic tape format produced for main frame analysis on VAX systems. This was not compatible with the PRIME mainframe installed at Napier University. As a result of the problems associated with using the mainframe, it was preferable to use a more universal medium for data analysis, namely a personal computer. A dedicated 486 PC was employed along with the latest software packages, Microsoft Fortran™, Lotus 123™ spreadsheet and BDMP™ statistical software. These packages enabled data in almost any format to be imported and manipulated for modelling purposes.

The BRE 1990-1991 data were used in the evaluation of the proposed slope illuminance model as were the Edinburgh, Sheffield, Athens and Japanese data. Despite the limited amount of Japanese data that was acquired it remains important to use as comprehensive a database as possible. There remains a high possibility that this is not enough data on which to make a fair assessment of any models performance. However, it may provide an indication of the performance of a model's. A specimen copy of the UK IDMP standard format for daylight and solar radiation data adopted by the majority of the aforementioned locations is given in Appendix 3.1.

The BRE 1992 data contains sky scanner data used to examine the luminance distribution of the hemisphere. The sky scanner is a very specialised piece of equipment which houses a photometric measurement head which is mounted in the body of a rotating case. At 15 minute intervals the scanner records illuminance and luminance values at several altitudes as it rotates through 360 degrees from North. A complete scan contains some 149 measurements. The format of the sky scanners output is given in Appendix 3.2. The purpose of using this data was to aid the development of sky luminance distributions for various sky conditions which could then be implemented into sky factor and internal illuminance calculations.

3.3 QUALITY CONTROL

All daylight and solar radiation data produced were quality controlled to remove data of doubtful quality and hence improve confidence in the measurements. The quality control checks were mainly concerned with ensuring each measurement falling within acceptable limits in accordance with the CIE IDMP[3.1]. In addition any data recorded at solar altitudes below 6 degrees were discarded from further analysis due to the cosine response of the instruments used. A full program listing of the quality control tests is given by Appendix 3.3.

In the case of the control stations at Heriot Watt and Napier Universities, the instantaneous one-minute recorded values of horizontal global illuminance and irradiance, were used to produce hourly average values. All the relevant quality control tests the main stations data were subjected to(Appendix 3.3) were also carried out on the control station data. This was of particular importance as the control station was examining small changes in microclimate, which demanded reliable data for its analysis.

3.4 DATA LOSS

Through the course of the 25 months of measurements at Edinburgh there have been several instances of data loss resulting from routine and unavoidable closure of the station. The main causes of the complete shutdown of the station were,

1) Power failure
2) Transfer of main station
3) Computer failure
4) Down loading of data

1) Power failure in the laboratory which housed the computer and data acquisition equipment resulted in the loss of approximately 10 days of data over a period of 4 months of 1992 whilst essential maintenance work was being carried out in the building.

2) A relatively large amount of data were lost due to the planned transfer of the main station from Napier University to Heriot Watt University in November 1993. Additional data loss occurred as a result of the supply by the manufacturer of faulty replacement cabling. From completion of recording at Napier to the commissioning of the main station at Heriot Watt, a total of approximately 30 days were lost.

3) A random fault concerning the data storage computer occurred from time to time which accounted for the disruption of the station on approximately 6 occasions throughout the recording period at Napier University. The fault message displayed by the data acquisition program attributed the error to an IEEE-488 interface cable fault. The cable was tested and found to be in perfect working order

and no other explanation like a spell of unusual weather could be found for the fault, hence the error was considered to be random.

4) The downloading of recorded data from the main station was responsible for several weeks of data loss. The reason for this stems from the method used to store the recorded data. Once the daylight and solar radiation measurements have been stored on the hard-disk of the computer the data were periodically copied onto miniature magnetic tape using a tape streamer in order to release computer memory for future measurements. The format of the recorded data was such that analysis was not possible until it had been converted by the daylight software. This meant that while previous recorded data were being converted into a usable format the station could not measure illuminance and irradiance. The task of data conversion consumed a large amount of time as around 120 days consisting of separate illuminance and irradiance files were produced at a time.

Asides the complete shutdown of the main station due to faults, only one piece of equipment gave rise to significant data loss. The horizontal diffuse illuminance sensor whose failure has been documented in section 2.4 was of great concern as its measurements were crucial for analysis and model development purposes. It was most undesirable for modelling purposes to have this absence of diffuse illuminance data and for this reason the missing data were replaced with estimated values. The diffuse illuminance model employed to produce the estimated data was the modified Littlefair model presented in detail in section 4.3. This model has the advantage of having been evaluated for Edinburgh data and as Table 4.3 shows the model performs very well. All the diffuse illuminance data recorded at Napier University between March 1993 and November 1993 has been replaced with modelled data, this is stated in the file header of the final 5 minute average data files. The horizontal diffuse illuminance data were corrected using Littlefair's shade-ring correction algorithms[3.2]. A copy of the actual extrapolated equations for the Napier site are given in Appendix 3.4.

This chapter intended to present the databases used in the course of the research. It also highlighted some of the possible sources of dataloss. It is foreseen that this information will benefit researchers embarking on a similar measurement project.

REFERENCES

3.1 Tregenza P R Guide to recommended practice of daylight measurement Supplement to CIE journal 6(2) (1987)

3.2 Littlefair P J Correcting for the shade ring used in diffuse daylight and radiation measurements Proc. 'Daylight and solar radiation measurements' CIE symposium Berlin (1989)

4 LUMINOUS EFFICACY

Notation

Δ = sky brightness coefficient

ε = sky clearness index

σ = sunshine probability

β = the Ångström turbidity coefficient

α = the wavelength exponent

λ = wavelength (nm)

α_{IL} = illuminance extinction coefficient

α_r = irradiance extinction coefficient

γ_S = solar altitude (°)

ρ = albedo or ground reflectivity

a_i, b_i, c_i and d_i = empirical coefficients

B = Schuepp coefficient

C = fractional cloud cover

$C_{a\lambda}$ = the attenuation coefficient for aerosols,

$C_{d\lambda}$ = dust particle scattering coefficient

$C_{ws\lambda}$ = water vapour scattering coefficient

Ed = horizontal diffuse illuminance(lux) (by shadowband and corrected)

Eed = horizontal diffuse irradiance (by shadowband and corrected)

Eeg = horizontal global irradiance(W/m^2)

E_{EO} = extraterrestrial irradiance (W/m^2)

Ees = direct or beam irradiation(W/m^2)

Eg = horizontal global illuminance(lux)

E_{LO} = horizontal extraterrestrial illuminance (lux)

Es = direct or beam illuminance(lux)

F = clearness function

f,g and h = analytical functions

i = inclination angle of the sun's beam on a vertical surface (°)

$I(\lambda)$ = solar spectral irradiance (W/m^2)

I_d = horizontal diffuse irradiance (W/m^2)

I_D = direct or beam irradiation (W/m^2)

IE = extraterrestrial irradiance (W/m^2)

I_G = horizontal global irradiance (W/m^2)

k = a constant equal to 1.041

K = luminous efficacy (lumens/Watt)

Kcl = the clear sky luminous efficacy (lumens/Watt)

K_D = sky diffuse luminous efficacy (lumens/Watt)

Kg = horizontal global luminous efficacy (lumens/Watt)

Kgr = ground reflected luminous efficacy (lm/W)

Koc = overcast sky luminous efficacy (=115 lm/W)

Ks = direct luminous efficacy (lumens/Watt)

L_β= illuminance on a slope inclined at an angle β° from the horizontal (lux)

L_D = horizontal diffuse illuminance(lux)

LG = horizontal global illuminance(lux)

m = absolute air mass

R_D = direct fraction of the global irradiance

R_G = ground-reflected fraction of the global irradiance

RS = sky diffuse fraction of the global irradiance

td = dew-point temperature (°C),

Td = three-hourly surface dewpoint temperature (°C)

T_{IL} = illuminance turbidity coefficient

T_L = Linke turbidity factor

V(λ) = CIE spectral sensitivity of the human eye

Vis = the visibility in a horizontal direction (km)

w = water vapour content (cm)

WSA = azimuth angle of vertical surface from 0° to 360° from North.

y = coefficient as reported by Iqbal (dimensionless)

z = solar zenith angle (radians)

4.1 INTRODUCTION

The development of inclined surface illuminance models requires measured values of horizontal global and diffuse illuminance. In the absence of measurements it is necessary to resort to luminous efficacy models in order to obtain these values from other atmospheric parameters. Luminous efficacy models produce luminous efficacy values which when multiplied by measurements of global, direct or diffuse irradiance produce their respective illuminance counterparts. Several approaches have been adopted by researchers to achieve this conversion including the use of solar altitude, water vapour content, Linke turbidity factor and many other atmospheric parameters.

The luminous efficacy of daylight is expressed as the ratio of illuminance (lux) to irradiance (W/m^2) which can be found through the integration of the whole spectrum as shown in Eq.4.1.

$$K = \frac{680\int_{400}^{700} V(\lambda)Ee(\lambda)d\lambda}{\int_{0}^{\infty} Ee(\lambda)d\lambda} \qquad 4.1$$

where K = luminous efficacy (lumens/watt)

$V(\lambda)$ = the CIE spectral sensitivity of the human eye

λ = wavelength (nm)

$Ee(\lambda)$ = solar spectral irradiance (W/m^2)

This chapter is concerned with the various methods and approaches adopted by researchers. Several models shall be investigated and two models in particular will be evaluated in greater detail. Further, a novel approach to estimating direct illuminance is examined and two luminous efficacy models are presented herein. The analysis is divided into the luminous efficacy of direct, global and diffuse irradiance. As this is a subject area that has undergone extensive investigation by several authors e.g.[4.1- 4.6] the focus of this work shall be the evaluation of various models for Central Scotland and their applicability to a more northerly latitude. In addition a brief description of the most common atmospheric parameters incorporated in daylight models is presented.

4.1.1 ATMOSPHERIC PARAMETERS AND COEFFICIENTS

Luminous efficacy values enable daylight values to be derived from solar radiation measurements. As we have seen, this modelling problem has been tackled in many different ways by authors. The variation in methods is as a result of the differing approaches to compensate for the absorption and scattering processes that radiation encounters as it passes through the atmosphere. The following sections describe the terms and processes occurring in the atmosphere and their effect on luminous efficacy.

4.1.2 The Atmosphere

The composition of the earth's atmosphere is regarded as 78% nitrogen, 21% oxygen, 1% argon and 0.33% carbon dioxide by volume. Other constituents present include, water vapour, ice crystals, dust and soot particles. The quantity of daylight which a surface receives will depend on the transmittance of the atmosphere which in turn is a function of the quantity of the additional water vapour and aerosol particulates. In the case of dust and soot particles these are present as a result of man-made pollution and from naturally occurring disasters, a significant contributor are volcanic eruptions which expel millions of tonnes of soot high into the atmosphere where jet streams disperse the particles across the earth. Another common cause of particulate pollution are forest fires, like the forest clearing in Central and South America.

4.1.3 Aerosols

Particles such as soot and dust are defined as aerosols. The density of dust particles varies from location and season with higher densities located over land in drier seasons. A turbid atmosphere is renowned for possessing high levels of aerosols resulting in the attenuation or scattering of solar radiation from its path. Fig 4.1.1 demonstrates the role of aerosols in the scattering of solar radiation.

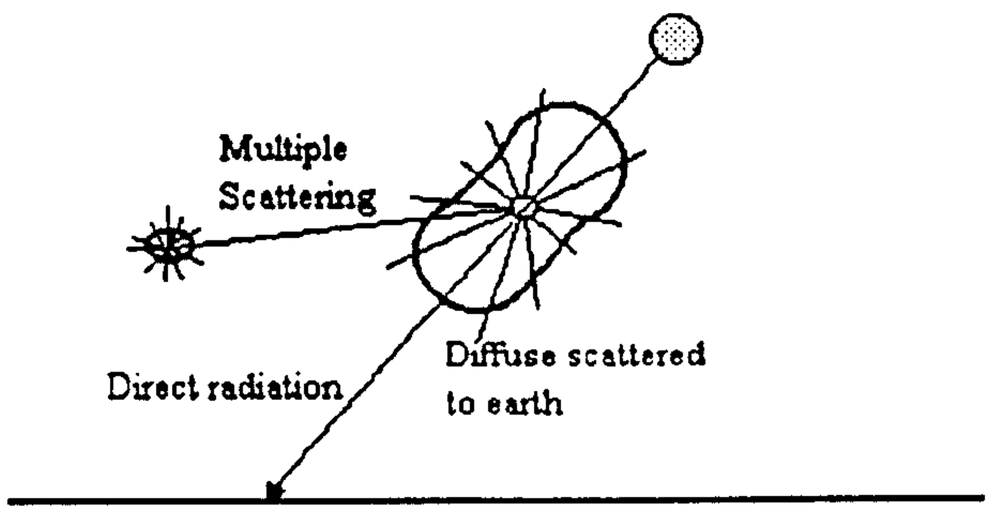

Figure 4.1.1 Atmospheric scattering

The scattering process and its effects are discussed in two sections which detail the different scattering phenomenon.

4.1.4 Rayleigh scattering

When the suns beam strikes a particle energy is scattered in all directions creating what is known as diffuse radiation. Lord Rayleigh derived a theory for calculating the amount of energy scattered for a specific case where the particle involved is spherical and smaller than the wavelength of the radiation. This theory is commonly used to examine scattering by air molecules. An example of Rayleigh scattering is shown in Fig. 4.1.2 where the level of scattering is equal in forward and backward directions, and perpendicular to the incident radiation. A chain reaction can occur with the scattered radiation striking other particles. It has been estimated that in a clean dry atmosphere, about half of the scattered energy returns to space while the remainder reaches earth as diffuse radiation[4.7]. Rayleigh scattering is wavelength dependent and is confined to shortwave radiation having the result of reducing the luminous efficacy of direct solar radiation. This can be seen by comparing the luminous efficacy value for direct and global radiation. As much of the direct incident radiation is scattered in the visible waveband this reduces the ratio of visible to infra-red solar radiation.

4.1.5 Mie scattering

Mie scattering as presented by Gustav Mie is a similar process to Rayleigh scattering with the particle size now of the same order if not larger than the wavelength of the incident radiation. In this case the majority of the scattering occurs in the same direction of the incident beam radiation with the effect being more pronounced for larger particles as seen in Fig.4.1.3. Much work has been undertaken by several authors, Van de Hulst, Moon and Ångstrom[4.8], to develop scattering coefficients that accounted for scattering by water vapour and dust particles given by equations 4.2 and 4.3 respectively. These coefficients represent both scattering and absorption processes with scattering the greater of the two with respect to the effect on solar radiation.

$$C_{ws\lambda} = 0.008635\lambda^{-2} \qquad 4.2$$

$$C_{d\lambda} = 0.008128\lambda^{-0.75} \qquad 4.3$$

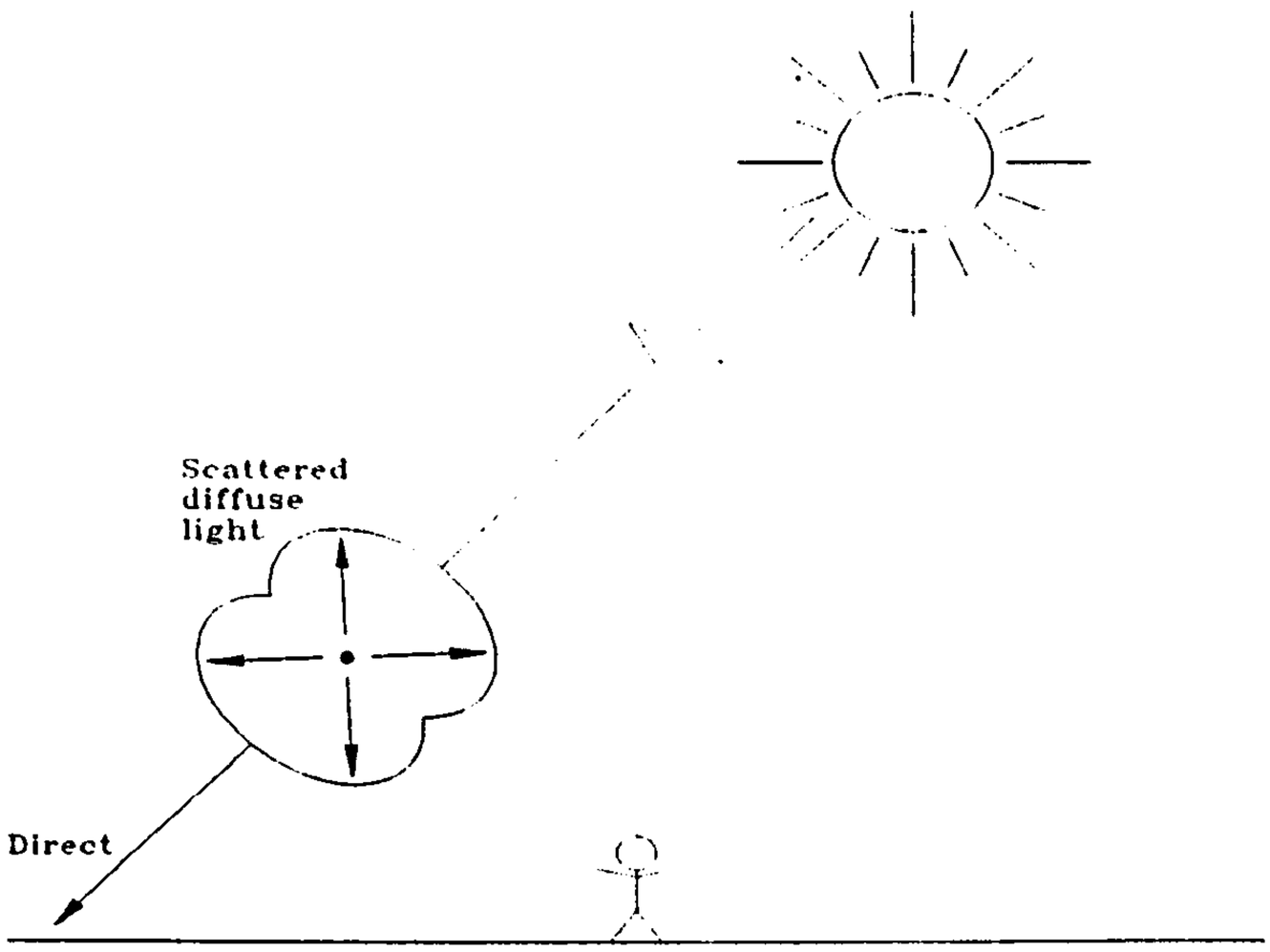

Figure 4.1.2

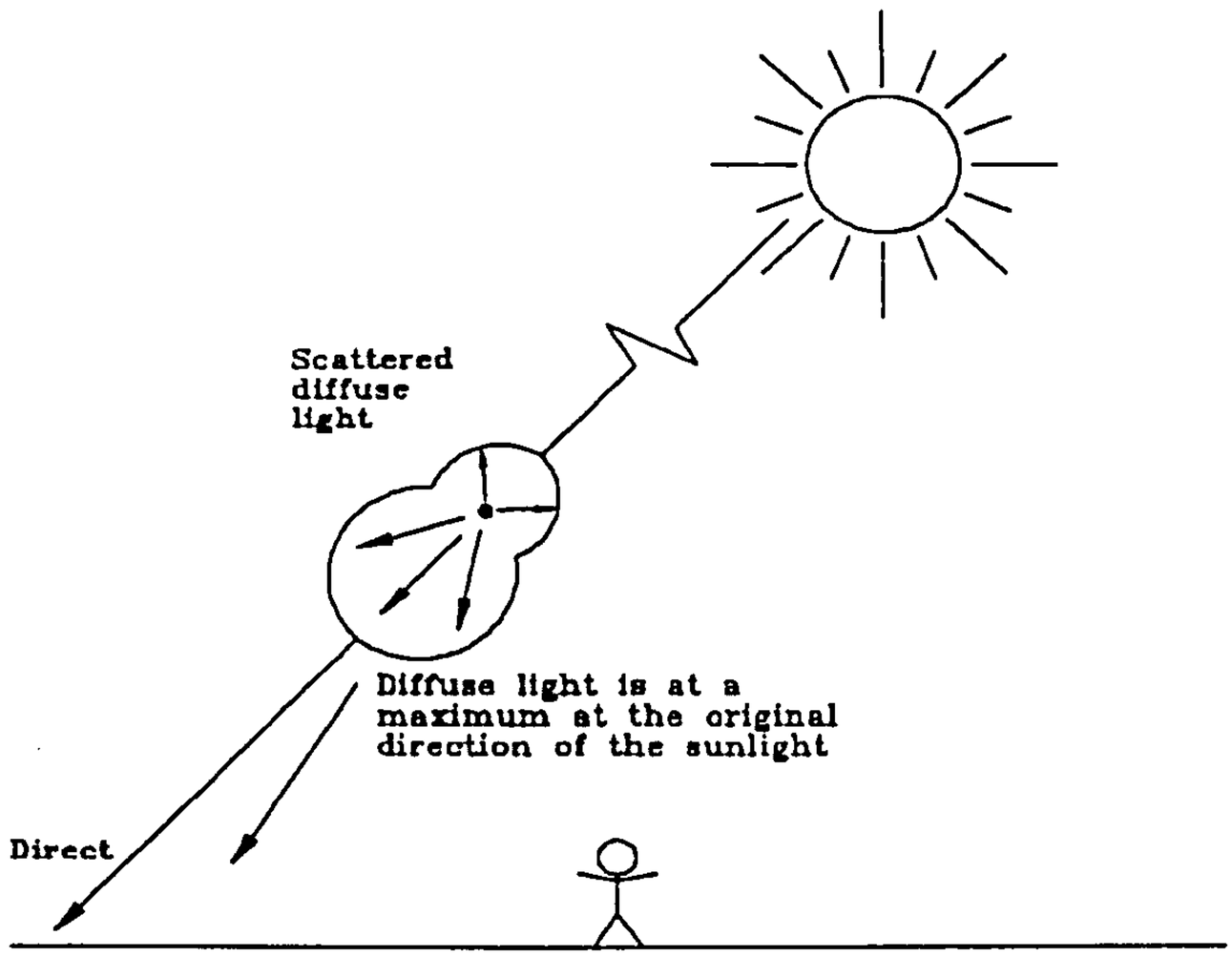

Figure 4.1.3

4.1.6 Ångström turbidity coefficient

Following the work of Moon[4.8] on the attenuation coefficients for particles, Ångström developed a formula that accounted for particle size and in doing so introduced the Ångström turbidity coefficient, the formulae is given by Eq.4.4.

$$C_a\lambda = \beta\lambda^{-\alpha} \qquad 4.4$$

where $C_a\lambda$ is the attenuation due to all aerosols,
β is the Ångström turbidity coefficient,
λ is the wavelength and
α is the wavelength exponent

β is an index representing the turbidity or optical clarity of the atmosphere, a low value of β represents a clear atmosphere and a high value indicates a turbid or polluted atmosphere as demonstrated in Table 4.2.1. α represents the ratio of small aerosols to large aerosols with a high value indicating a large number of small aerosols, although a constant value of 1.3 is usually taken as the norm. Measurements of α and β are possible at specific wavelengths [4.9], although values of β can be estimated from Eq.4.17 assuming a value of α =1.3 and using visibility measurements from a local Meteorological Office.

4.1.7 Linke turbidity factor

The Linke turbidity factor T_L allows the estimation of irradiance as seen by Eq.4.14 with the illuminance values Es and E_{LO} replaced by Ees and Eeo their irradiance counterparts, with T_{IL} and α_{IL} replaced by T_L and α_r. The theory states that the turbidity of the atmosphere could be described by the number of Rayleigh atmospheres required to produce the correct amount of attenuation. Several authors have developed formulas to estimate T_L including Dogniaux and Valko[4.6].

$$\text{Dogniaux} \quad T_L = \left[\frac{\gamma s + 85}{39.5e^{-w} + 47.4} + 0.1\right] + (16 + 0.22w)\beta \qquad 4.5$$

$$\text{Valko} \quad T_L = (B + 0.54)[1.75\log(w/m + 0.1) + 14.5] - 5.4 \qquad 4.6$$

where γ_s is solar altitude (degrees)

w is water vapour content

β is Ångström turbidity coefficient

and B as given by Schuepp[4.6] is $1.07\times\beta$.

The problem with using Linke turbidity as a sky clarity indicator for daylight calculations is that the formulae incorporate the contributions of water vapour and aerosols which have opposite effects on daylight, i.e. water vapour absorbs radiation in the infra-red region whilst aerosol scattering is responsible for the reduction in solar radiation in the visible waveband.

4.1.8 Illuminance turbidity factor

Due to the shortcomings of the Linke turbidity factor Navvab et al[4.6] developed an illuminance turbidity coefficient T_{IL} which is expressed by Eq. 4.16 which utilises Ångstrom turbidity coefficient β. The advantage of using this formula alongwith Eq. 4.14 in the calculation of direct illuminance is the removal of compounded errors as a result of the elimination of luminous efficacy values. Navvab concluded that the illuminance turbidity factor may be more sensitive to atmospheric conditions than T_L as during a comparative test turbidity peaks corresponding to rush-hour traffic were noticed with the illuminance turbidity factor.

4.1.9 Water Vapour

Water vapour content is utilised in several daylight and solar radiation models to assist in accounting for absorption processes. It is usually calculated in cm and is termed as the height of water that would result if all the vapour in a vertical column were condensed. The amount of precipitable water in the air changes with seasons and location. Many authors have correlated its calculation with partial pressures of water vapour, humidity and dew-point temperature. The formula due to Perez[4.10] was derived from Reitan[4.10] and is similar to that by Atwater and Ball[4.8].

$$w = \exp(0.07074td + y) \qquad 4.7$$

where w is the water vapour content (cm),

td is dew-point temperature (°C),

and y = -0.0229 from April to June and 0.02023 for the remaining months.

4.1.10 Air mass

Another commonly used atmospheric parameter is the air mass, m. A comprehensive formula is presented for its calculation in Eq 4.15. It represents the relative amount of air a beam of radiation passes through to reach the earth. Eq 4.15 is often simplified to a correlation with solar altitude as shown in Eq. 4.8.

$$m \approx 1/(\sin\gamma_s) \qquad 4.8$$

4.1.11 Clouds

The effect of cloud cover for daylight calculations are complex and yet important. Clouds are good attenuators of solar radiation with multiple scattering processes taking place. It is fair to assume that all the energy removed by the clouds water droplet is in turn scattered. This scattering is not wavelength selective. The treatment of clouds and their transmission by Perez et al[4.10] resulted in the use of a sky brightness coefficient given by Eq. 4.29. This characterises the thickness of the clouds or their opacity. Tregenza[4.11] developed an approach to estimate illuminances from clouds for use in daylight factors. This method involved the geometry of clouds amongst other considerations. Preliminary results proved encouraging and of particular use for the UK with its predominantly cloudy skies.

As scattering due to cloud cover will increase the path length of rays of light whilst water vapour absorption takes place in the infra-red waveband, the luminous efficacy of an overcast sky will be slightly higher than that of a clear sky with values averaging around 110-120 lm/W[4.1].

4.2 DIRECT LUMINOUS EFFICACY

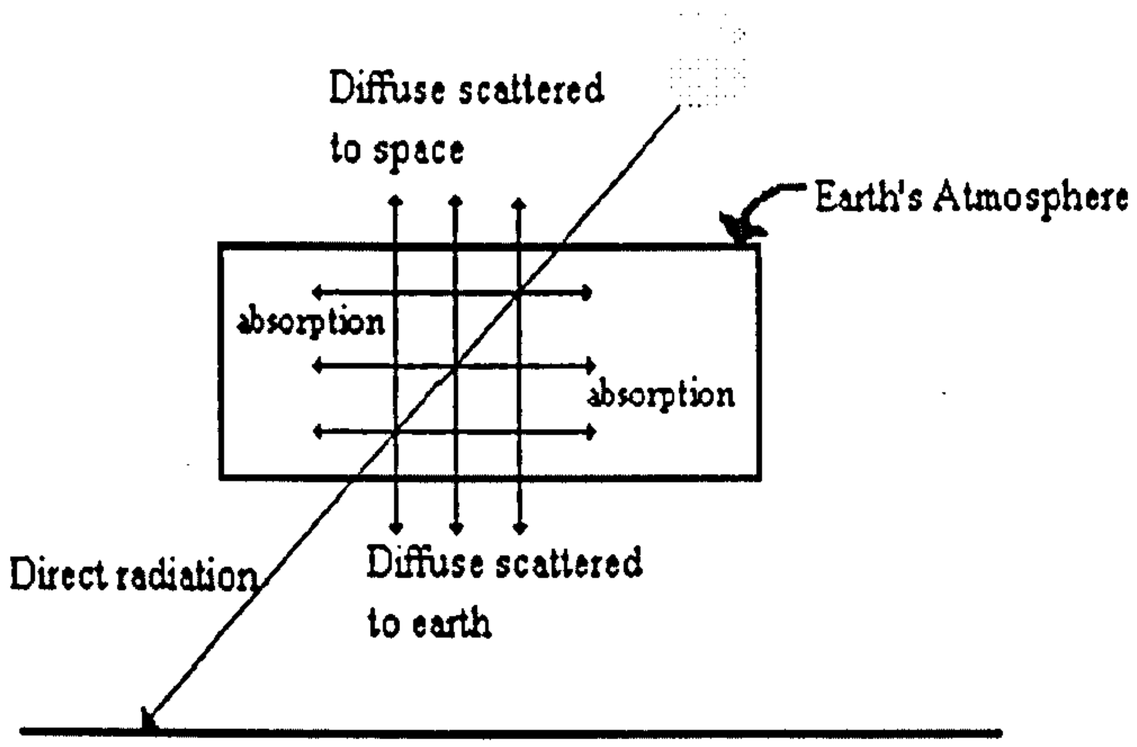

Figure 4.2.1 Scattering and absorption processes in the earth's atmosphere

Figure 4.2.1 demonstrates the scattering and absorption processes the beam radiation from the sun encounters as it passes through the earth's atmosphere. Beam radiation undergoes strong attenuation under a process known as Rayleigh scattering which is most prevalent at low solar altitudes. Rayleigh scattering by air molecules tends to be wavelength dependent, in particular effecting the visible spectrum. It is estimated that between 10 and 15% of the beam radiation is removed as a result of Rayleigh scattering[4.1]. Another process responsible for the reduction of beam radiation is the effect of Ångströms aerosol turbidity coefficient which is an indication of the levels of dust and particulate matter

suspended in the atmosphere. Again this is most sensitive in the visible waveband. Another attenuator of beam radiation comes as a result of water vapour absorption. This absorption process is mainly confined to the infrared region of the solar spectrum as shown in Fig. 4.2.1. The overall effect of these processes is the reduction in beam radiation reaching the earth and of more significance is the reduction in luminous efficacy by Rayleigh scattering and aerosol attenuation along with an increase through water vapour absorption. Some authors have utilised these processes in the development of luminous efficacy models and produced good correlations with measured data[4.2].

Navvab et al[4.6] developed a semi-empirical formula for a range of turbidities and produced a relationship for the estimation of direct luminous efficacy given by Eq.4.9.

$$Ks = 104.59(1 - e^{-9.39\gamma s}) \qquad 4.9$$

where γ_S is solar altitude in radians

This is a basic formula exploiting the solar altitude variation of direct luminous efficacy through the use of an exponential term, γ_S. The values of Ks were multiplied by the direct irradiance values from the station at Napier University. The results are presented in graphical form in Fig. 4.2.1. All of the models presented herein were evaluated using over 4000 measurements of five-minute averaged radiation and daylight incorporating all types of sky conditions from clear through to overcast. The models were computed and their results interpreted through the help of spreadsheet and statistical software packages. The measurements were 5 minute averages of one minute instantaneous measurements with the direct components of illuminance and irradiance calculated by Eq.4.10.

$$Ees = Eeg - Eed \qquad 4.10$$

where Ees = direct or beam irradiation
Eeg = horizontal global irradiance
Eed = horizontal diffuse irradiance (by shadowband and corrected)

Direct illuminance is obtained by replacing Ees, Eeg and Eed by the illuminance terms Es, Eg and Ed.

Navvabs' model performs with a reasonable level of accuracy although some scatter is noticable. This formulae was developed for clear skies and to this end clear skies were identified and the model evaluated again so as to correctly evaluate this approach. The results from this analysis proved to be almost identical to those for all sky conditions indicating that Navvab's models' application may be more universal. Details of similar analysis that account for clear and all sky conditions are presented later in this chapter for other authors work. Navvab's model was developed from San Francisco data exclusively and this may well explain the scatter produced with the evaluation for Edinburgh data. The San Francisco climate has a tendency to be turbid with high levels of traffic pollution combining with solar radiation to create the common problem of smog.

Graphical analysis is useful as an initial medium for conveying modelling results. However for cross comparison purposes with other models it is essential to employ a more sophisticated method of analysis. This was done using statistical tests. The most useful and commonly used indicators in the examination of a models performance are the Mean Bias error (MBE), Root Mean Square error (RMSE) and r^2. MBE provides an indication of the trend of the model, whether it has a tendency to underpredict or overpredict its modelled values. It can be expressed as a percentage or absolute value, in this case lux.

$$MBE = \frac{\Sigma(\text{estimated value - observed value})}{\text{No. of observations}} \quad \text{(lux)} \qquad 4.11$$

RMSE gives a value to the level of scatter that the model produces. This is an important statistical test as it highlights the reliability and repeatability of the model. This can be seen in the majority of the graphs, Figs. 4.2.1 and 4.2.2 in particular. RMSE is given by Eq 4.12.

$$RMSE = \frac{(\Sigma(\text{estimated value - observed value})^2)}{\text{No. of observations}} \quad \text{(lux)} \qquad 4.12$$

r^2 is a common statistical test used to place a level of confidence on the models results. It is usually presented as a percentage, for example an r^2 value of 94% signify that 94% of the doubt over the correlation has been removed or explained by the model.

Table 4.2.3 displays the statistical results of all the luminous efficacy models presented in this chapter.

Aydinli[4.4] developed an algorithm which related direct solar luminous efficacy to solar altitude in a polynomial structure as shown by Eq. 4.13:

$$Ks = 17.72 + 4.4585\gamma_S - 8.7563x10^{-2}\gamma_S^2 + 7.3948x10^{-4}\gamma_S^3 - 2.167x10^{-6}\gamma_S^4 - 8.4132x10^{-10}\gamma_S^5 \qquad 4.13$$

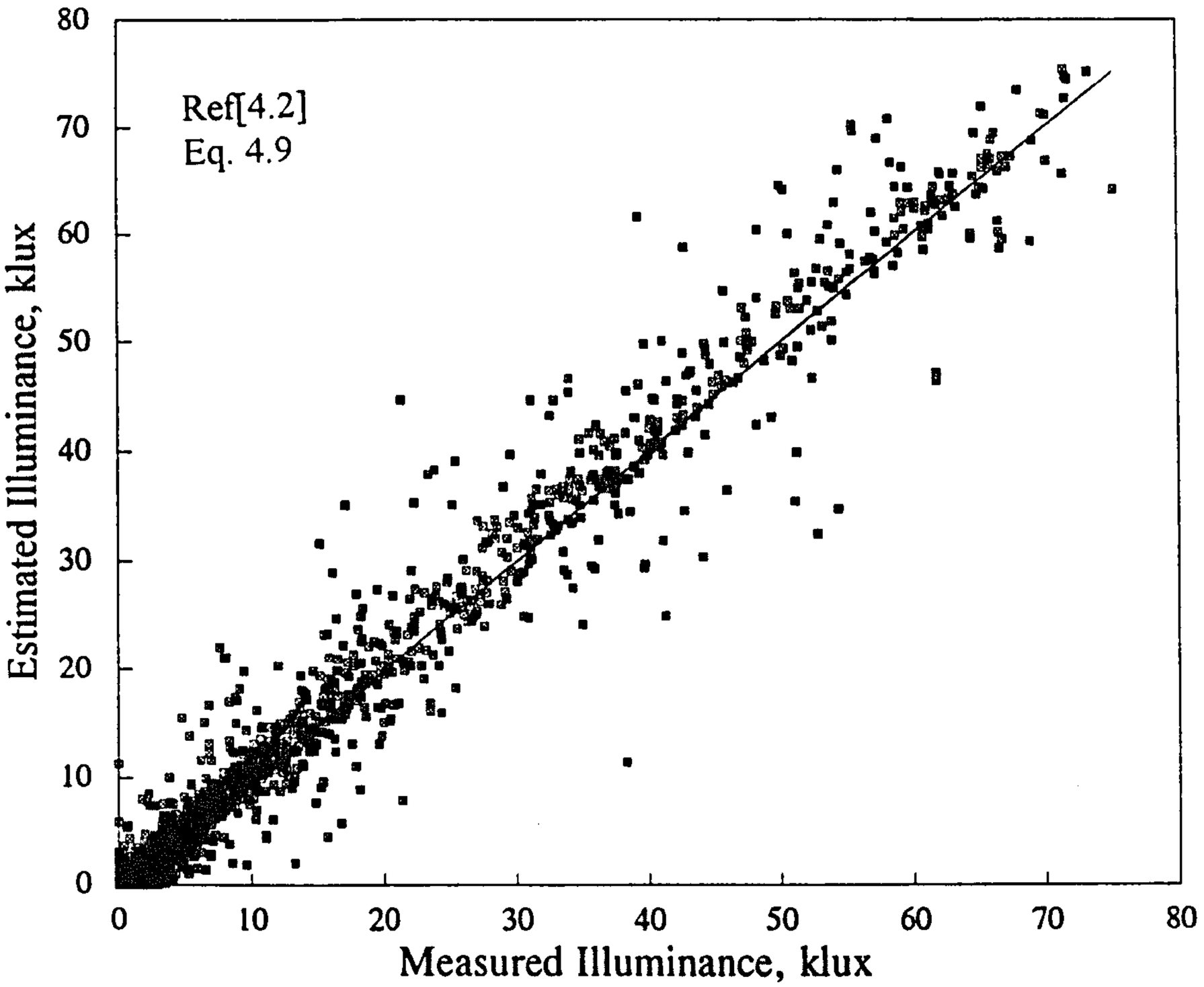

Figure 4.2.1 Navvab's direct luminous efficacy model

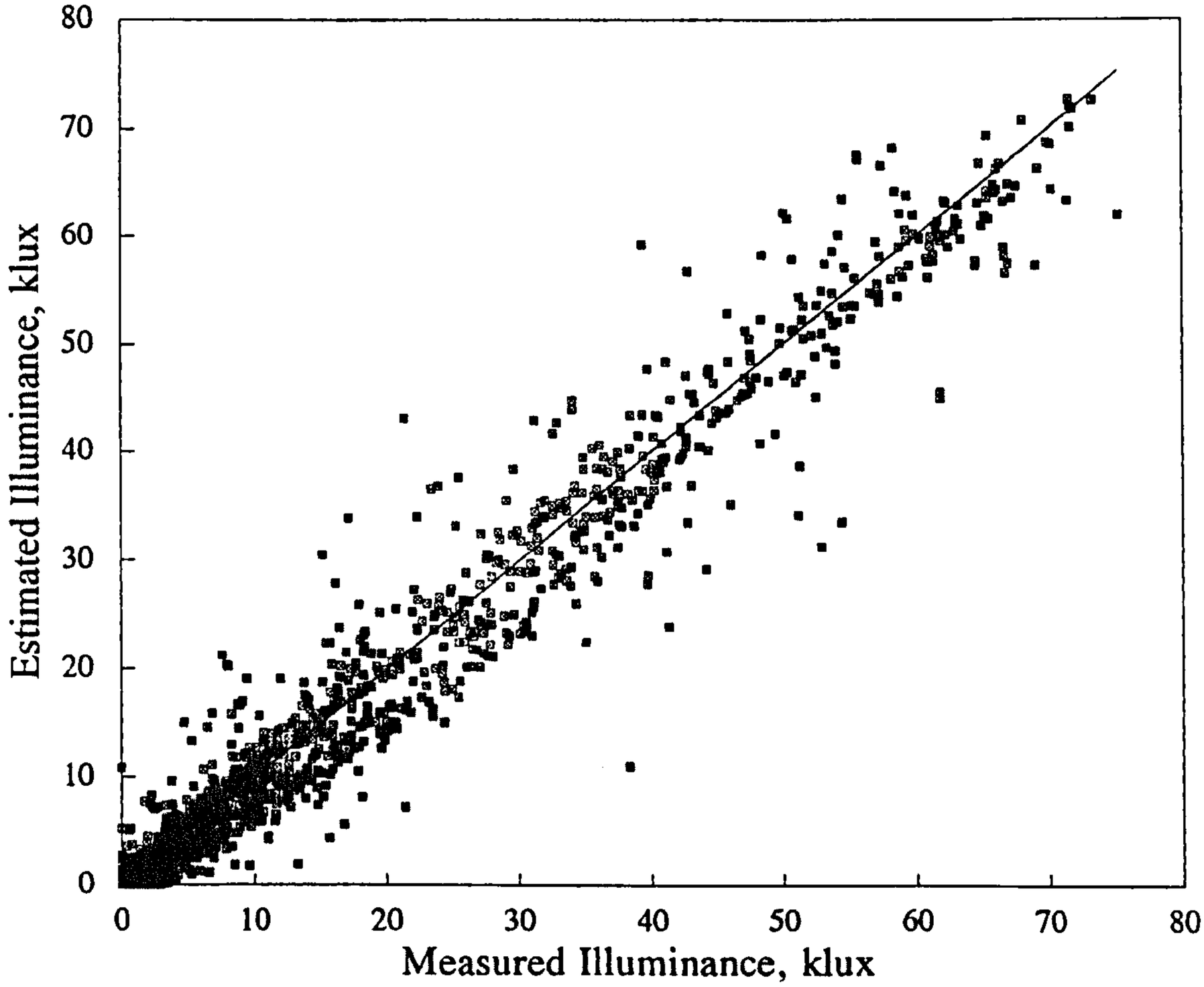

Figure 4.2.2 Aydinli direct luminous efficacy model

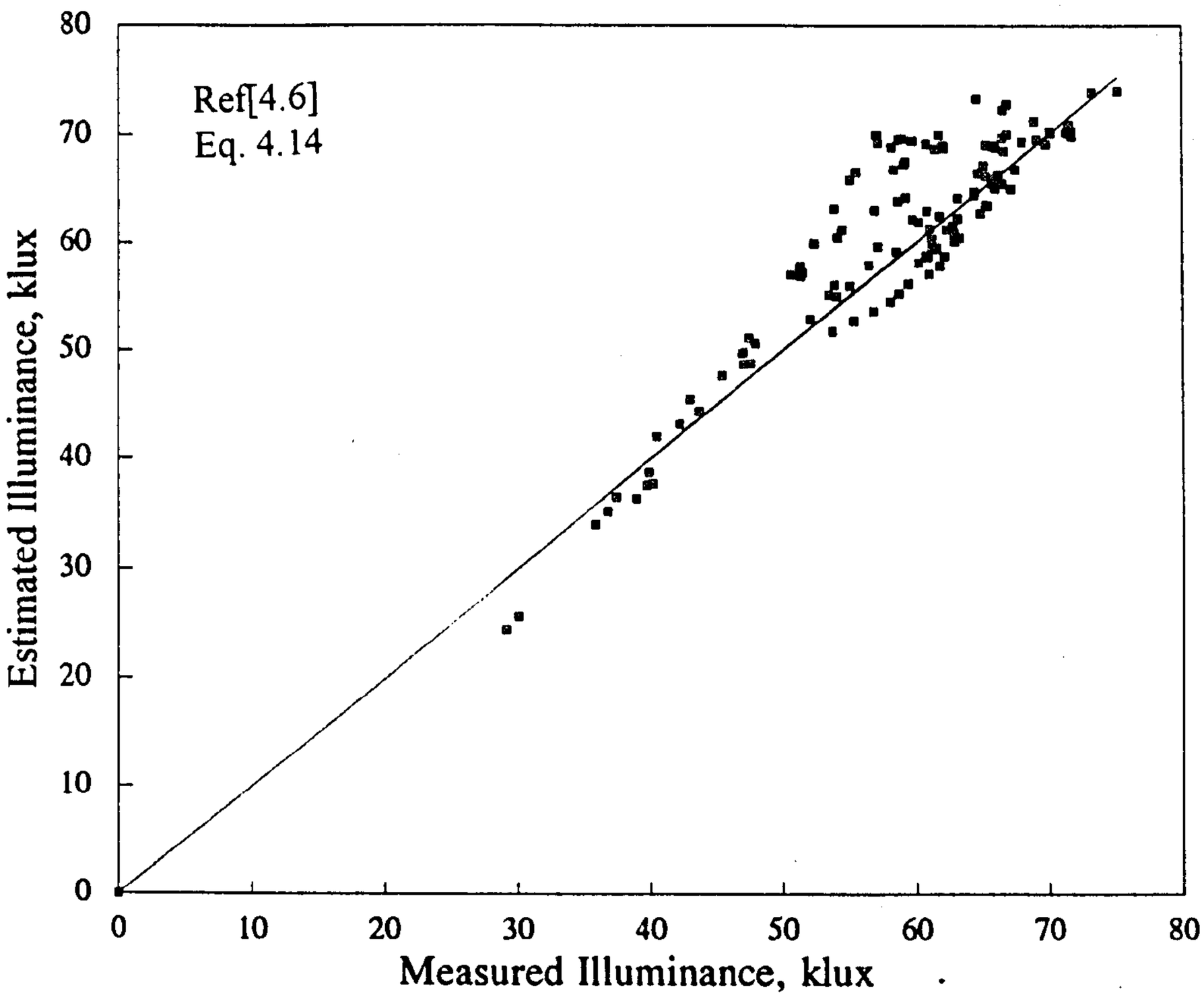

Figure 4.2.3 Navvab's direct luminous efficacy model

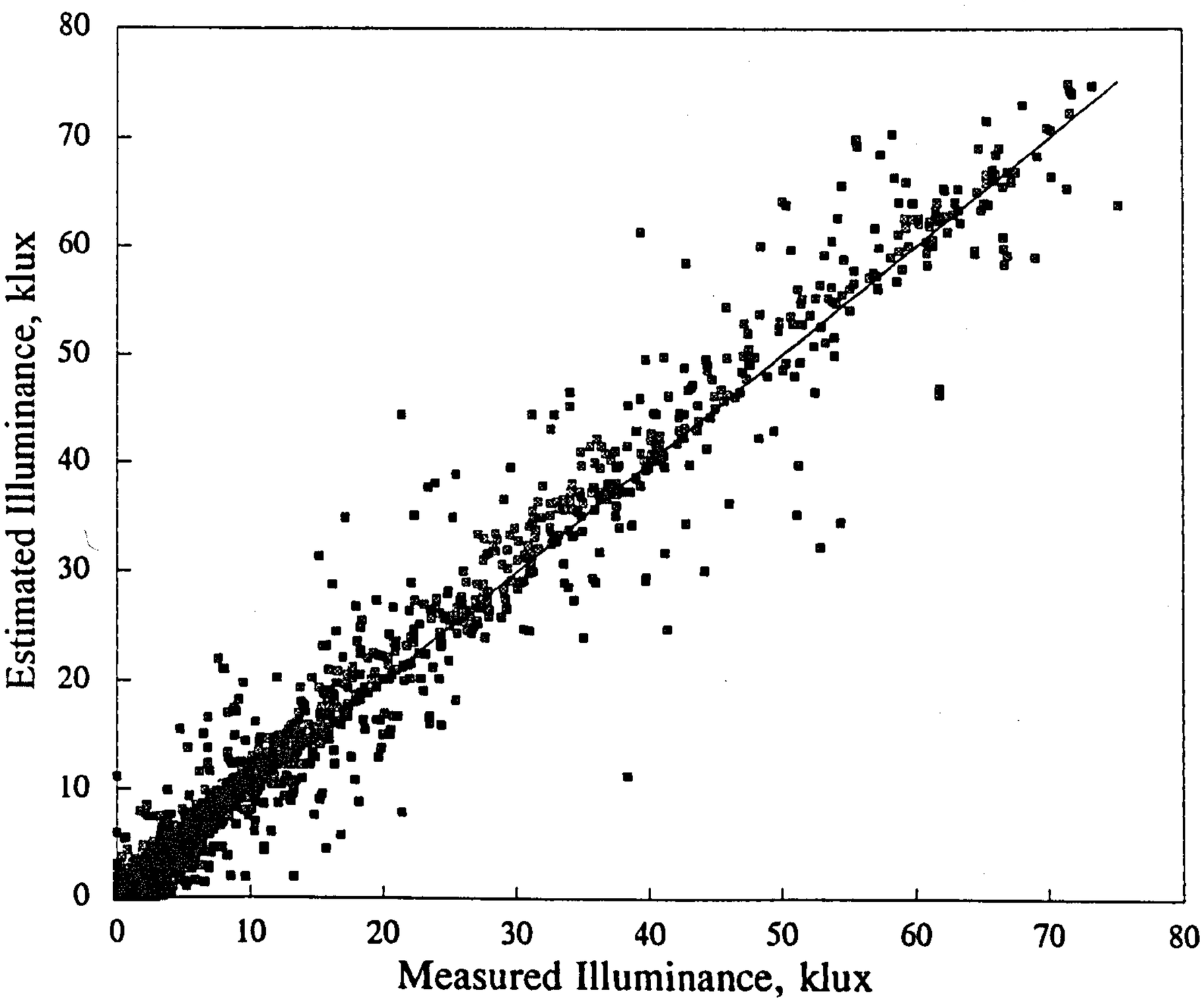

Figure 4.2.4 104 lm/W direct luminous efficacy model

Once again the results of the evaluation of this model with Edinburgh data are shown in Fig. 4.2.2 and Table 4.2.3. Aydinli's model has a tendency to underestimate direct illuminance. It would appear that like Navvab's work this model may be better suited to more turbid atmospheres. In addition to the luminous efficacy algorithm Aydinli also presented a set of tables of direct luminous efficacy related to solar altitude, water vapour content and aerosol turbidity[4.1]. As measurements of water vapour content and aerosol turbidity are uncommon in the UK this approach is not satisfactory for a comprehensive analysis. Aydinli's tabular values are presented in Appendix 4.1.

A more fundamental approach to the problem of estimating direct illuminance was adopted by Navvab et al[4.6], where the effects of atmospheric scattering and turbidity were considered. This research produced a new illuminance turbidity factor Til which is employed in place of the Linke turbidity factor, a coefficient which was derived primarily for radiation computation. The illuminance turbidity factor in conjunction with several additional atmospheric parameters can be utilised to estimate direct illuminance avoiding the involvement of a luminous efficacy value to convert irradiance values.

$$Es = E_{LO} \times \exp(-\alpha_{IL} \times m \times T_{IL}) \qquad 4.14$$

where E_{LO} is extraterrestrial illuminance taken as extraterrestrial irradiance multiplied by the luminous efficacy of extraterrestrial solar radiation (96.8 lm/W)[4.1]

α_{IL} extinction coefficient = $0.1/(1 + 0.0045m)$ or taken as $0.1 \pm 5\%$ for $\gamma_S > 5°$

$$\text{m absolute air mass} = \frac{-\sin\gamma_s + \left[\sin^2\gamma_s - 1 + (1.001572)^2\right]^{\frac{1}{2}}}{0.001572} \qquad 4.15$$

$$T_{IL} \text{ illuminance turbidity factor} = 1 + 21.6\beta \qquad 4.16$$

and β is the Angstrom turbidity coefficient (see Table 4.2.1), or estimated as

$$\beta = (0.55)^{\alpha}(3.912/\text{Vis} - 0.01162)[0.02472(\text{Vis} - 5) + 1.132] \qquad 4.17$$

α is the wavelength exponent given in Table 4.2.1 [4.8] and Vis is the visibility in a horizontal direction in km.

Table 4.2.1 Angstrom turbidity and wavelength values for various types of atmosphere

Atmosphere	β	α	**Visibility (km)**
Clean	0	1.3	340
Clear	0.1	1.3	28
Turbid	0.2	1.3	11
Very Turbid	0.4	1.3	<5

As this approach is different from the one's presented earlier an evaluation would be valuable. As measurements of β were not available for this site an average value of 0.1 was assumed from observations of the microclimate and consultation of Table 4.2.1 (this is close to the value used by the authors in their studies). The model estimates normal direct illuminance for clear or cloudless skies. For this reason clear skies had to be identified. The criteria on which clear skies are chosen is of some interest with each author having a preference towards a particular method. Of the measures used to identify clear skies the most common are either cloud cover observations or a variety of calculated methods. Cloud cover observations usually grade the cloud cover into eighths or tenths with a low value 1-2 representing clear skies. The calculated methods use a ratio of either direct normal irradiance to horizontal diffuse or global irradiance or more complex methods as presented later by Perez et al[4.10]. For this research the preferred method is to use a parameter known as the clearness function F where F is a ratio of horizontal beam to extraterrestrial illuminance given by Eq. 4.2.10. This accounts not only for cloud cover but turbidity as it includes the absorption and scattering beam illuminance encounters as it passes through the atmosphere. The higher the value of F the clearer the sky, with F described in cloud cover terms in Table 4.2.2.

$$F = \left(\frac{Eg - Ed}{E_{LO}\sin\gamma}\right) \qquad 4.18$$

Table 4.2.2 Sky classification with clearness function F

F	**Sky condition**
0.0 - 0.15	Overcast sky
0.16 - 0.30	Overcast → partly cloudy sky
0.31 - 0.50	Partly cloudy → Clear sky
0.51 - 0.75	Clear sky

The nature of Central Scotland's weather means that partly cloudy skies are predominant, and for this reason identifying clear skies was of particular importance to ensure reliability of results. To filter out any spurious sky conditions the lower limit of F was fixed at 0.55, unfortunately the database was reduced severely but this would at least provide an indication of the model's performance.

The model was used with the parameters α_{IL} and β taken as 0.1 respectively, corresponding to a clear atmosphere as defined in Table 4.2.1. Fig. 4.2.3 contains the results of this analysis which demonstrate the extremely good performance of the Navvab model despite the requirement to estimate values of α_{IL} and β for Edinburgh and the limited number of suitable clear sky observations. A more extensive study and evaluation is necessary in order to provide a more comprehensive insight into the performance of this model. It does present a refreshing alternative to the estimation of direct normal illuminance by removing the need for a luminous efficacy value. Its use may well prove applicable for sites of lower latitude with higher instances of clear skies.

An alternative to predictive models involving solar altitude or atmospheric parameters is the use of one single value of luminous efficacy, a method that has been adopted by several authors with Petersen and Treado & Gillette[4.1] assuming a constant value. An average value of between 93 and 115 lm/W is typical for direct luminous efficacy. Fig. 4.2.4 provides the results of employing an average direct luminous efficacy value of 104 lm/W to the irradiance data. The performance of the single value approach are at least on par with Navvab and Aydinli. This is quite interesting considering the simplicity of the model.

Table 4.2.3 Comparison of luminous efficacy models for Edinburgh data.

Direct luminous efficacy	r^2	**MBE (lux)**	**RMSE (lux)**	**Fig. No.**	**Ref. No.**
Navvab et al	.973	-258	2339	4.2.1	4.2
Aydinli	.970	-718	2381	4.2.2	4.4
Navvab et al	.861	-2010	4354	4.2.3	4.6
104 lm/W	.973	-247	2319	4.2.4	4.1

Global luminous efficacy					
Aydinli (all conditions)	.987	-3016	4351	4.3.1	4.4
Chroscicki (all conditions)	.985	-5378	6915	4.3.2	4.3
Perez	.990	-174	1805	4.3.3	4.8
Littlefair	.987	-767	2842	4.3.4	4.1,4.9
Proposed	.987	1014	3500	4.3.5	---
Aydinli (clear sky)	.870	-6242	6712	4.3.6	4.4
Chroscicki (clear sky)	.879	-13073	6258	4.3.7	4.3
110 lm/W	.987	-1667	3277	4.3.8	4.1
Diffuse luminous efficacy					
Perez	.994	29	737	4.4.1	4.8
Littlefair	.989	-945	1580	4.4.2	4.1,4.9
Proposed	.986	-69	1869	4.4.3	---
120 lm/W	.986	-82	1870	4.4.4	4.1

4.3 HORIZONTAL GLOBAL LUMINOUS EFFICACY

The determination of global luminous efficacy has been investigated by several authors with two main approaches being adopted. The most straight forward and simplistic models contain only a few empirically derived coefficients in conjunction with solar altitude, whilst alternate approaches involve the use of atmospheric parameters and measurements of horizontal global and diffuse irradiances.

Several models shall be evaluated using the dataset recorded at Napier University. This section shall present the models, their results and review their suitability for inclusion in daylight calculations and introduce a proposed global luminous efficacy model for the UK. The majority of the analysis will concentrate on graphical and statistical methods from which the individual performance of each model shall be compared and contrasted.

Traditionally researchers have modelled global luminous efficacy for clear and overcast skies separately Aydinli[4.4] and Chroscicki[4.3] developed formulae relating clear sky global luminous efficacy to solar altitude. Aydinli's model is given by Eq.4.19. To

complete a comprehensive examination of both evaluation were carried out for all sky conditions and also for clear skies as their use was intended.

$$Kg = 80.7 + 2.071\gamma_S - 7.4125\times10^{-2}\gamma_S^2 + 1.3482\times10^{-3}\gamma_S^3 - 1.2088\times10^{-5}\gamma_S^4 + 4.2206\times10^{-8}\gamma_S^5 \qquad 4.19$$

Fig. 4.3.1 shows the result of this formula when plotted with Edinburgh's measured global illuminance data. The graph (Fig.4.3.1) highlights the tendency of Aydinli's model to underestimate the majority of the illuminance range, although the order of scatter is kept to a minimum. Despite the underprediction, the trend is good as reflected in the MBE and r^2 values(see Table 4.2.3.).

Adopting a similar approach, Chroscicki[4.3] developed a simple algorithm to predict global luminous efficacy given by Eq.4.20

$$Kg = 59.2\gamma_S^{0.1252} \qquad 4.20$$

Fig. 4.3.2 once again shows the order of under-estimation that results from this approach. The trend is quite clear with a good r^2 value, however the model produces higher MBE and RMSE values compared to Aydinli's model.

The significant under-estimation resulting from these models is probably largely due to the site specificness or latitude dependency associated with their development and may also be a product of their simplistic nature. It is therefore likely that these models would perform more satisfactory if they were derived from the Edinburgh database. With this in mind a simple polynomial function was used as the base for an empirical derivation of a new proposed global luminous efficacy model. 4000 data points were used to produce a model given by Eq. 4.21.

$$Kg = A + B\gamma_S + C\gamma_S^2 \qquad 4.21$$

where A was found to be 131.4, B = -0.51 and C = 6.0×10^{-3}.

Fig. 4.3.5 demonstrates the improved performance of this model over those due to Aydinli and Chroscicki with the statistical evaluation given in Table 4.2.3. The model does have a

tendency towards over estimation at higher illuminances but overall the trend is greatly improved.

As mentioned previously both Aydinli's and Chroscicki's models were intended for use with clear skies, and an analysis using all sky conditions may be seen to bias the results in favour of a model developed from local data. Clear skies were therefore once again identified using the same procedure employed in the case of Navvab's direct illuminance model. The models were not altered in any fashion from their reported form in Eqs. 4.19 and 4.20 with the results presented graphically in Figs. 4.3.6 and 4.3.7. It is clear from these plots that under-estimation remains a feature of the models with Aydinli's model's performing slightly better than Chroscicki's. In a direct comparison against their respective all sky conditions it is clear that the poor results shown in Figs. 4.3.1 and 4.3.2 are not as a result of using non-clear sky data. This breakdown of the results leads to the possibility of both Aydinli's and Chroscicki's models being applied for more than one sky condition. This additional benefit may well go a long way to compensate for the relatively poor results the model's yield.

As with direct luminous efficacy additional authorssuch as Drummond, Petersen and Krochmann[4.1] have reported a single value of global luminous efficacy averaging around 110 lm/W, which like the direct luminous efficacy proved to be on a par with many of the models presented herein(Fig.4.3.8) and certainly performing better than Aydinli or Chroscicki models.

An extensive amount of research into the luminous efficacy of daylight has been carried out by Littlefair[4.1,4.12,4.13] in the UK and this has led to the development of global and diffuse luminous efficacy models. The estimation of global luminous efficacy by Littlefair involves a novel technique of weighing the diffuse and direct luminous efficacies using a cloud ratio factor. Diffuse luminous efficacy was found to be sensitive to fractional cloud cover C, which could be estimated from values of sunshine probability. The complete structure of Littlefair's model is given in equations 4.22 and 4.23.

$$Kg = RD(144-29C) + (1-RD)(51.8 + 1.646\gamma_S - 0.01513\gamma_S^2) \qquad 4.22$$

$$C = -.55\sigma + 1.22\sigma^2 - 1.68\sigma^3 + 1 \qquad 4.23$$

where RD is the ratio of horizontal diffuse to global irradiance and σ is sunshine probability. The first term on the right-hand-side of Eq.4.22 represent K_D, the diffuse luminous efficacy whilst the remainder represent direct luminous efficacy.

An absence of sunshine probability data meant that Littlefair's model couldn't be evaluated in its present form. A modified version of the original model which does not require sunshine probability values was analysed instead[4.14]. Replacing values of fractional cloud cover which are estimated from sunshine probability was a cloud ratio calculation. The modified version of Littlefairs model is presented below.

$$Kg = RS \times Ks + RD \times K_D + RG \times Kgr \qquad 4.24$$

where Kg, Ks, K_D and Kgr are respectively the global, direct, sky diffuse and ground reflected luminous efficacies (lm/W) and RS. RD and RG represent the direct, sky diffuse and ground-reflected fractions of the global irradiance.

Ks and K_D are given by

$$Ks = 51.8 + 1.646\gamma_S - 0.01513\gamma_S^2 \qquad 4.25$$

$$K_D = (1 - RD)Kcl + RDKoc \qquad 4.26$$

where Kcl is the clear sky luminous efficacy (=144 lm/W), Koc the overcast sky luminous efficacy (=115 lm/W) and Kgr is taken as 86 lm/W. The values of global and diffuse illuminance are then obtained by the multiplication of the appropriate efficacy by the respective irradiance measure. The performance of this modified model were first presented by Muneer and Angus[4.15]. However the current analysis was carried out using Edinburgh data which has not been reported to date. This is an important evaluation of Littlefair's modified model as there exists a large latitude difference between the Edinburgh and Garston sites from where the Littlefair model originated. Fig. 4.3.4 displays the results of this analysis and the good performance of this model showing its suitability to the climate and latitude of Central Scotland.

Perez et al[4.10] presents a comprehensive model which has a more involved structure and is therefore considered to be more sophisticated. The model's basic form is given by equation 4.27:

$$F(\varepsilon,\Delta,z,w) = a_i + b_i(\varepsilon)f(w) + c_i(\varepsilon)g(z) + d_i(\varepsilon)h(\Delta) \qquad 4.27$$

where f,g and h are analytical functions and a_i, b_i, c_i and d_i are the coefficients of a 4 x 8 matrix (Appendix 4.2). ε represents the sky clearness from overcast through partly cloudy to clear skies:

$$\varepsilon = [(Eed + Ees)/Eed + kz^3]/[1 + kz^3] \qquad 4.28$$

where z is the solar zenith angle (90°- solar altitude) and k is a constant equal to 1.041 for z in radians.

Perez et al.[4.10] regard the variations in ε as reflecting the changing atmospheric turbidity and cloud cover, and the sky brightness coefficient Δ as denoting the optical transparency of the cloud cover. The equation for sky brightness is

$$\Delta = Eed \times m/E_{EO} \qquad 4.29$$

m is the optical air mass which can be calculated from Eq. 4.15 or approximated by Eq.4.8 and as before E_{EO} is the extraterrestrial irradiance.

Littlefair[4.12] reported a distinct correlation between the parameter Δ and overcast sky luminous efficacy, noting that Δ was approximately proportional to the fraction of radiation that penetrates the clouds.

The last component in the model is the atmospheric precipitable water content w:

$$w = \exp(0.07\ Td - 0.075) \qquad 4.30$$

where Td is the three-hourly surface dewpoint temperature (°C). The final form of the model is then given by equation 4.31.

$$Eg = Eeg[a_i + b_i w + c_i\cos(z) + d_i\ln(\Delta)] \qquad 4.31$$

Perez model's results are for Garston data only due to the lack of surface dewpoint temperatures for the Edinburgh site, however the results shown in Fig. 4.3.3 are extremely good considering the model was derived from a mainly North American database.

In this work both Perez and Littlefairs modified models have been shown to produce reliable results across the full range of sky conditions and at low and high illuminances. The more complex nature of the Perez model along with the requirement for dewpoint temperatures and large matrices containing empirical coefficients tends to prejudice its use in daylight modelling. Of the two models the modified Littlefair algorithm is simpler to implement, a large advantage when the end user tend to prefer straight forward methods.

4.4 HORIZONTAL DIFFUSE LUMINOUS EFFICACY

In this section two well established diffuse luminous efficacy models shall be evaluated along with a new proposed model and an alternative single value approach to provide a cross-section of the methods available to estimate diffuse illuminance.

Perez[4.10] and Littlefair[4.12] both produce luminous efficacy models for estimation of diffuse illuminance. The Perez model for diffuse luminous efficacy has exactly the same structure as given by Eq. 4.31 where Eg and Eeg are replaced by Ed and Eed with the coefficients a_i, b_i, c_i and d_i taken from Appendix 4.3. Figure 4.4.1 shows the results of Perez diffuse illuminance model. Littlefair's diffuse luminous efficacy model is represented by Eq. 4.26 with the results given in Fig.4.4.2.

To complement the analysis undertaken against global luminous efficacy model a similar work was carried out to produce an empirical correlation relating solar altitude to diffuse luminous efficacy with the coefficients A, B and C 121.74, -0.192 and $3.3\text{x}10^{-3}$,respectively given by Eq. 4.32.

$$K_D = 121.74 - 0.192\gamma_S + 3.3\text{x}10^{-3}\gamma_S^2 \qquad 4.32$$

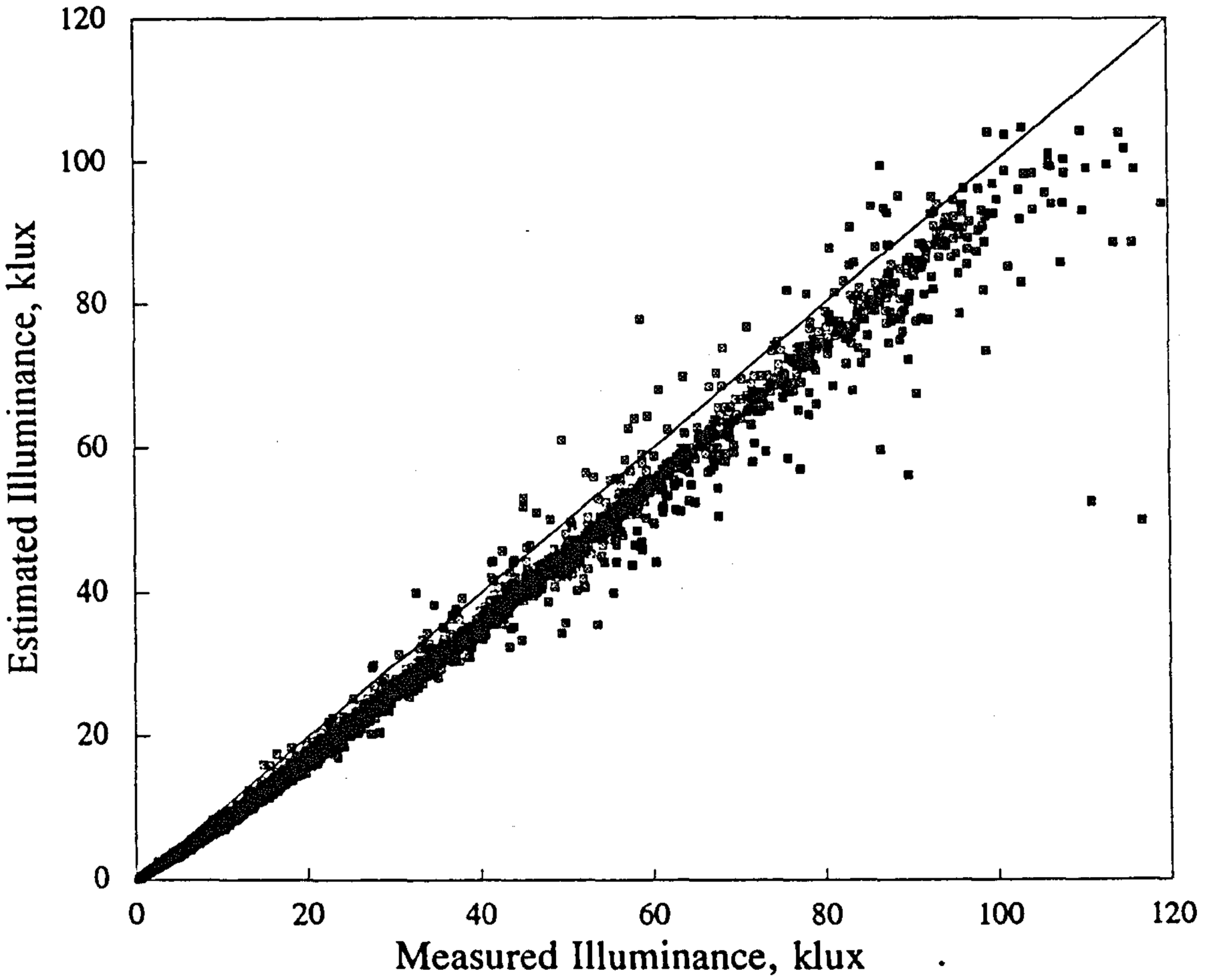

Figure 4.3.1 Aydinli Global luminous efficacy model

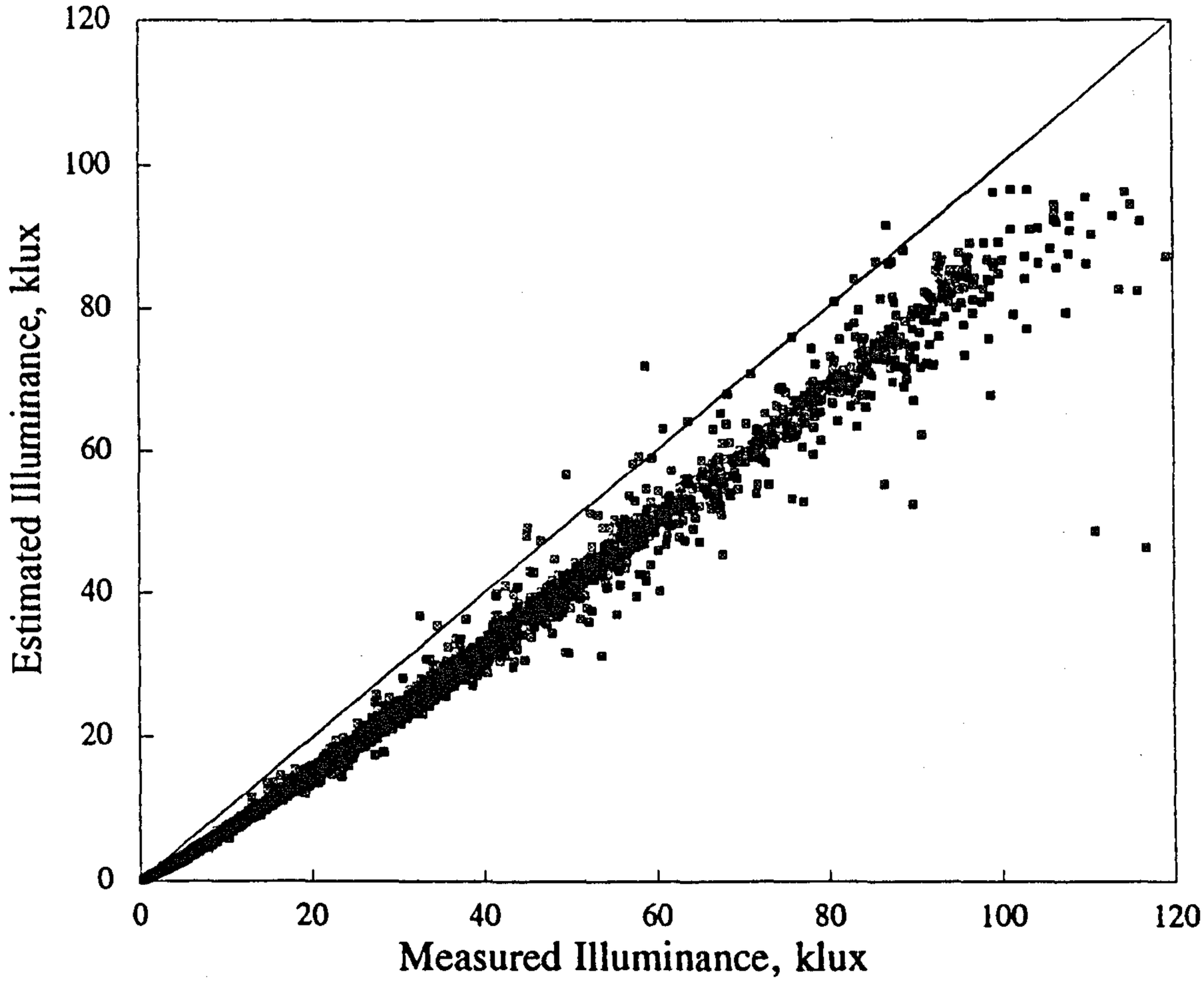

Figure 4.3.2 Chroscicki Global luminous efficacy model

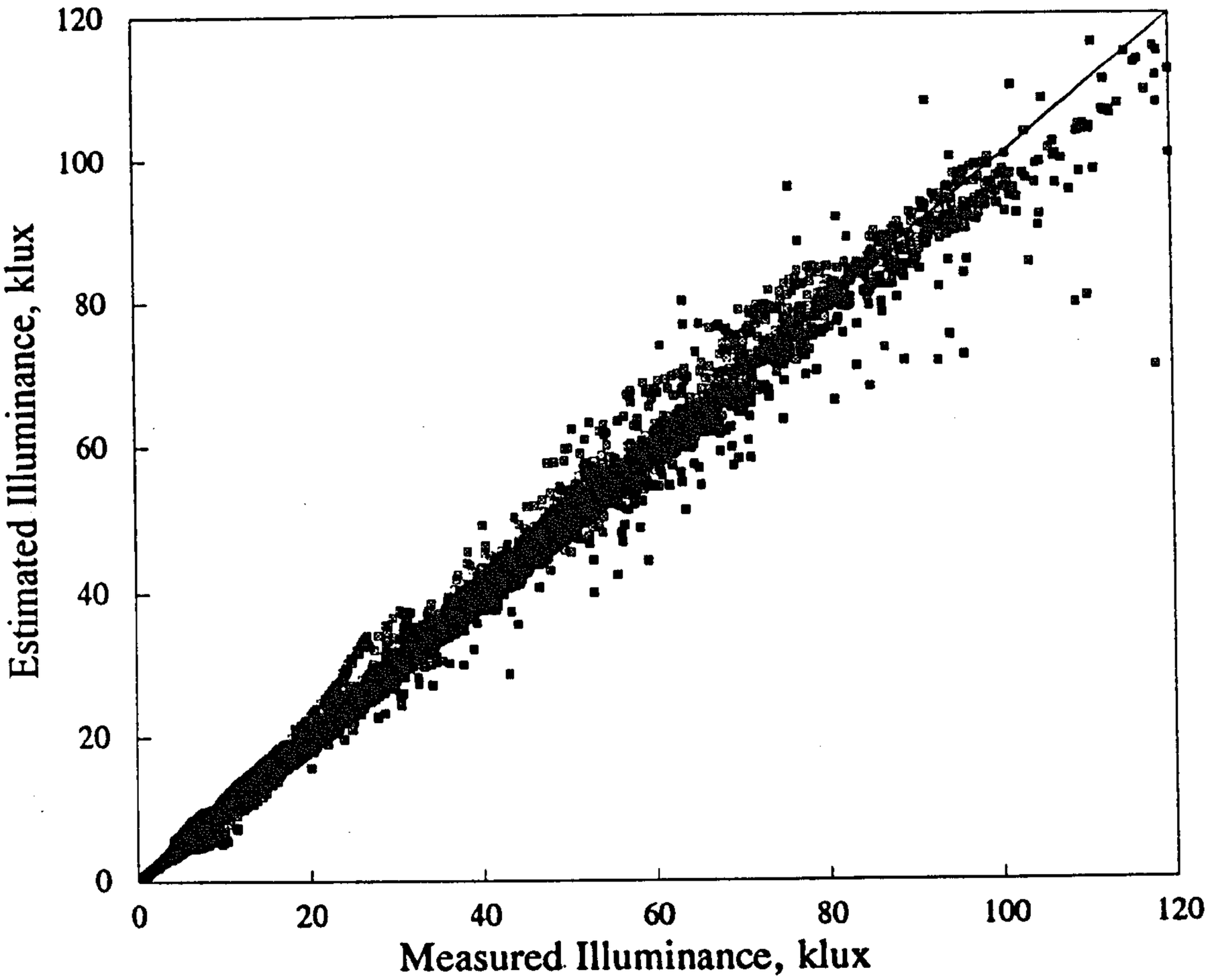

Figure 4.3.3 Perez Global luminous efficacy model

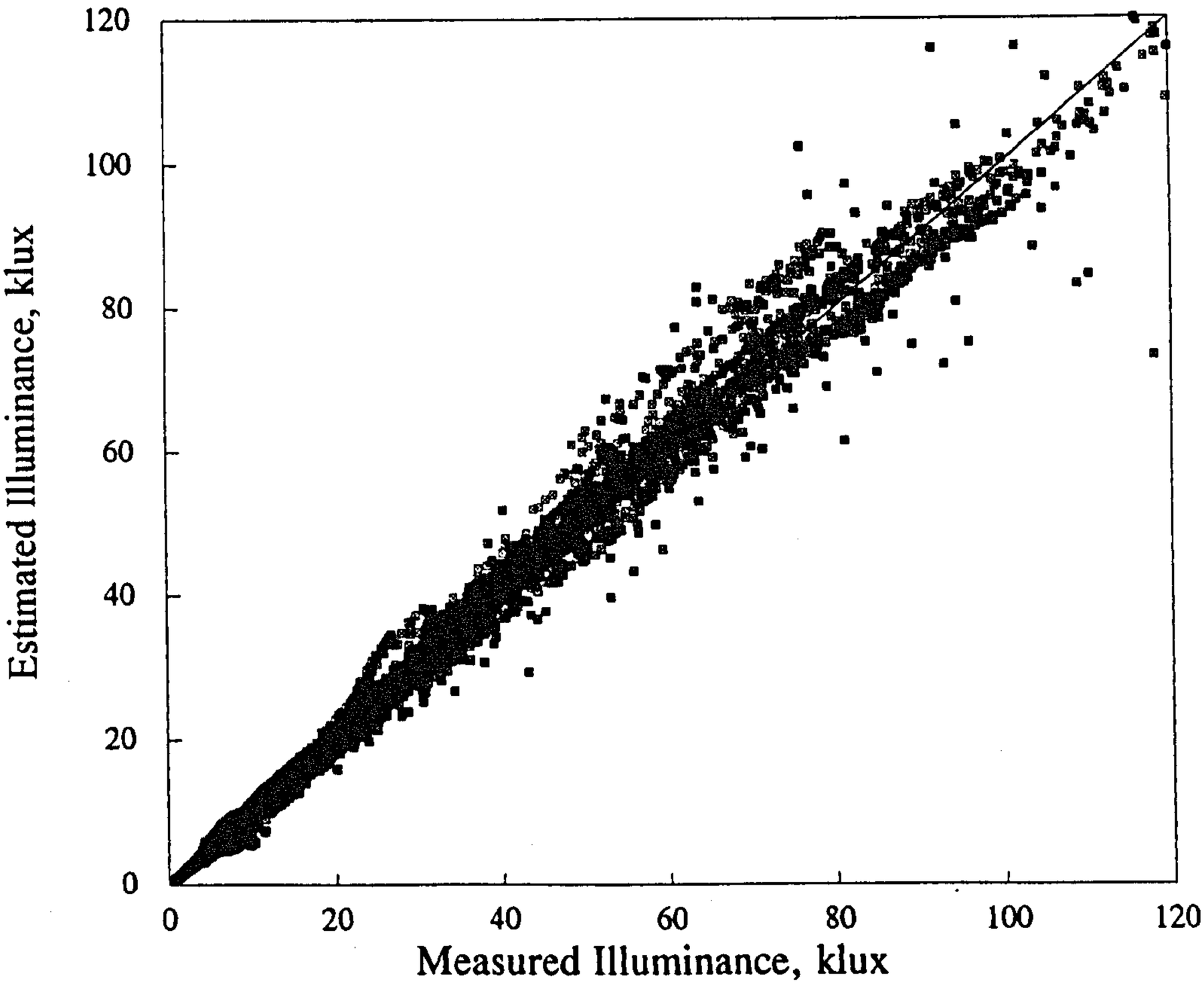

Figure 4.3.4 Littlefair Global luminous efficacy model

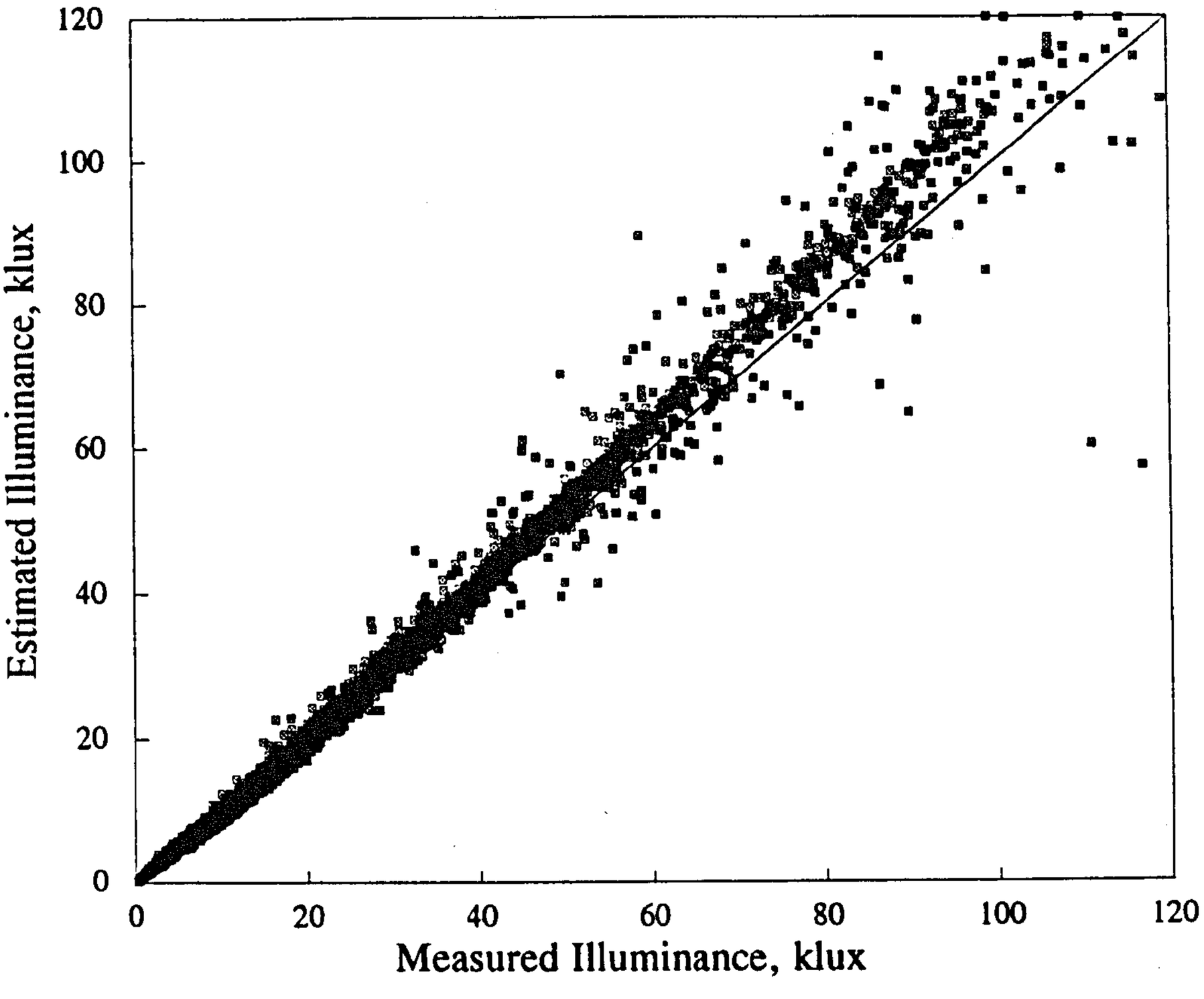

Figure 4.3.5 Proposed Global luminous efficacy model

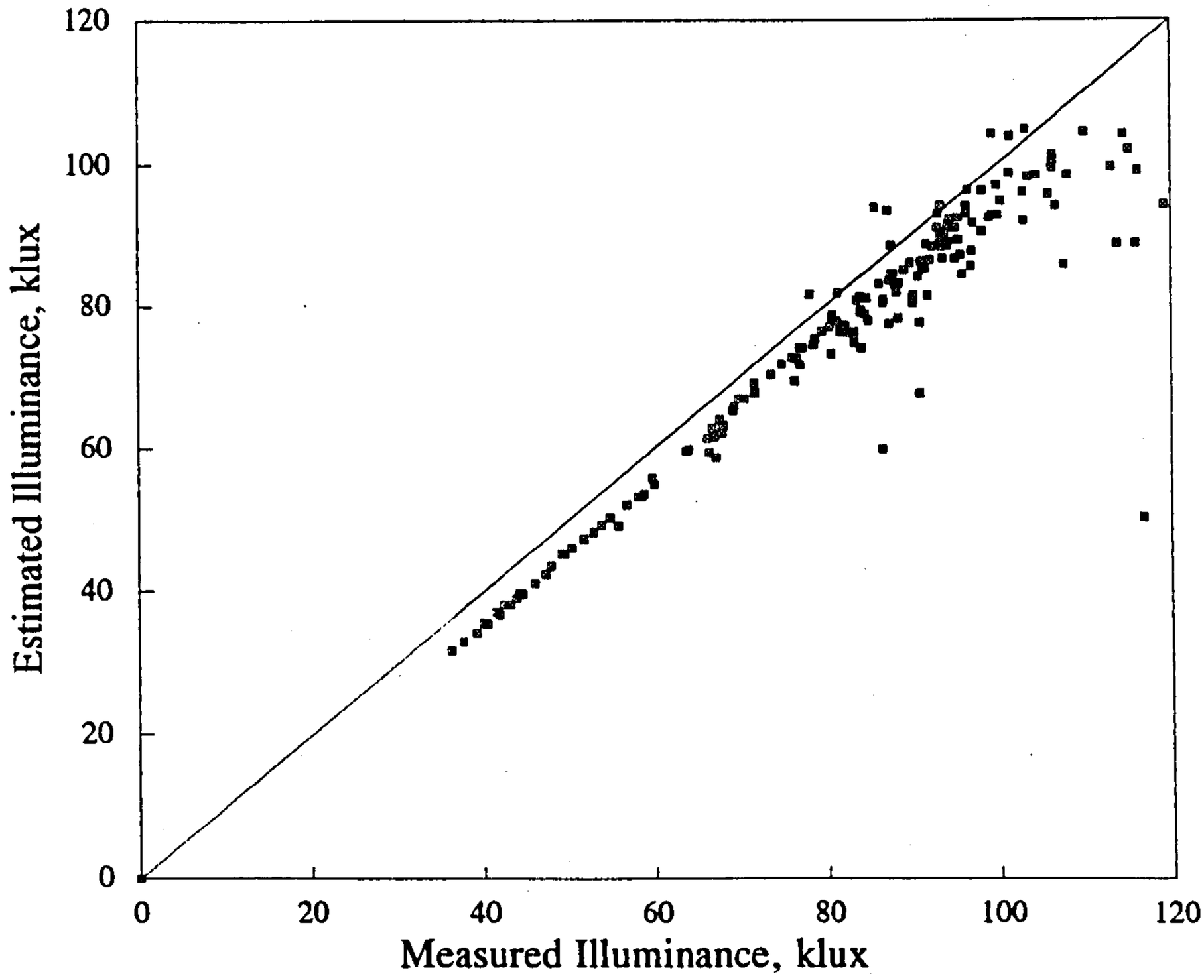

Figure 4.3.6 Aydinli Global luminous efficacy clear sky model

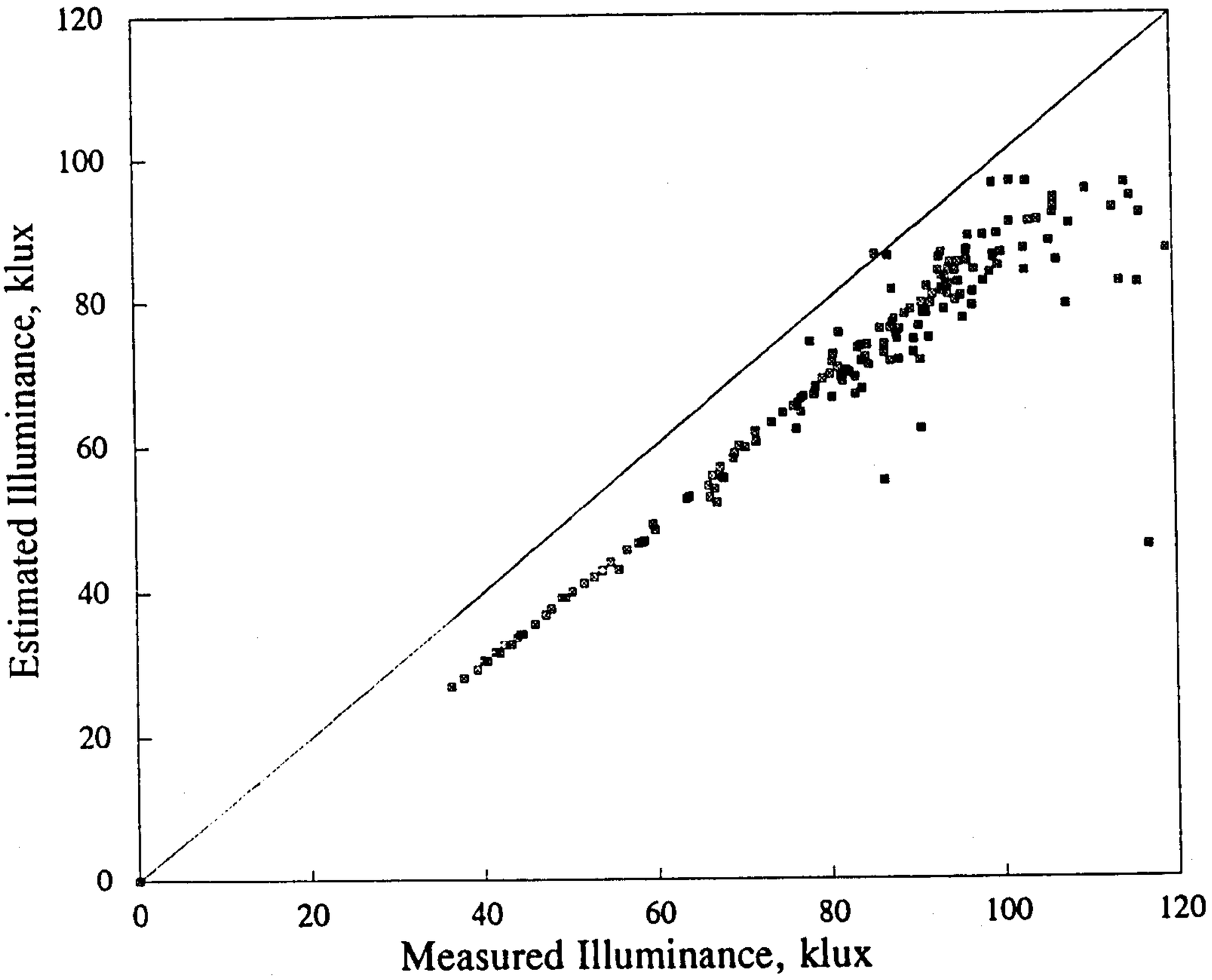

Figure 4.3.7 Chroscicki Global luminous efficacy clear sky model

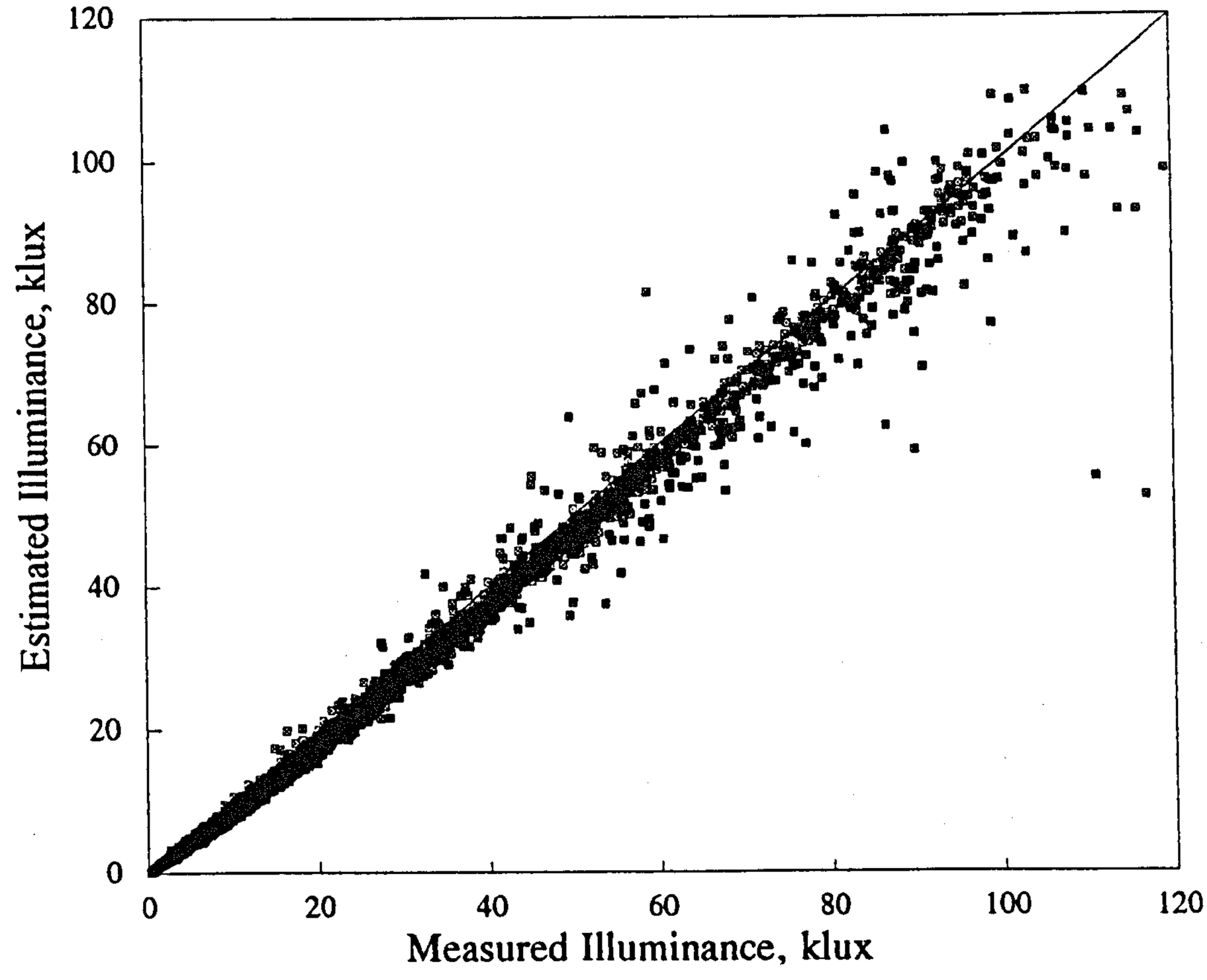

Figure 4.3.8 110 lm/W Global luminous efficacy model

The simplicity of this model is only surpassed by the quality of the results shown in Fig.4.4.3 where the MBE is only -69 lux.

Finally horizontal diffuse illuminance was estimated by the product of horizontal diffuse irradiance by an average luminous efficacy value of 120 lm/W as reported by Littlefair[4.1]. This value was employed to good effect as Fig. 4.4.4 shows, with the results comparable with any of the diffuse illuminance models presented herein. As the performance of the single value model proved to be so good the raw illuminance and irradiance data were used to derive the average diffuse luminous efficacy value for the database. A mean value of 120.5 lm/W was thus obtained.

This section presented several different approaches adopted by researchers to produce models for the prediction of global, diffuse and direct luminous efficacy. The analysis also presented two new diffuse and global luminous efficacy models primarily for use in the Central region of Scotland but with the potential of being suitable for a much larger area of the UK. It has to be mentioned that both of these new proposed models were derived from the local database. Hence it would be expected that they should perform well. However this does not mean to say that the models are site specific, as was demonstrated with Littlefair's models which performed well for the site they were originally developed for (Garston) and for the Edinburgh data. What is worthy of note is the form of the proposed models given in Eq.4.21 where the coefficients A, B and C can be derived for any location thereby increasing the chances of the model performing well. The most surprising and interesting findings are the performances of the constant-value models used to predict global, diffuse and illuminance. These models demonstrate performance similar to that of the more sophisticated approaches presented herein.

The data from the daylight stations were analysed to produce an average value of global and diffuse luminous efficacy which may be used in place of other more involved models. The results are shown in Table 4.4.1 where intersite differences are clearly visible. Global luminous efficacy tends to average around 115 lm/W with the main deviations arising for the Japanese and Greek data. The higher value of 123 lm/W reported for the Japanese data is a known characteristic[4.16]. The lower value of 108 lm/W for the Athens data can be apportioned to the higher incidence of clear skies which are a characteristic of the local climate. This would indicate that beam irradiation is prolific and hence a lower value of luminous efficacy is likely as found by Littlefair[4.1].

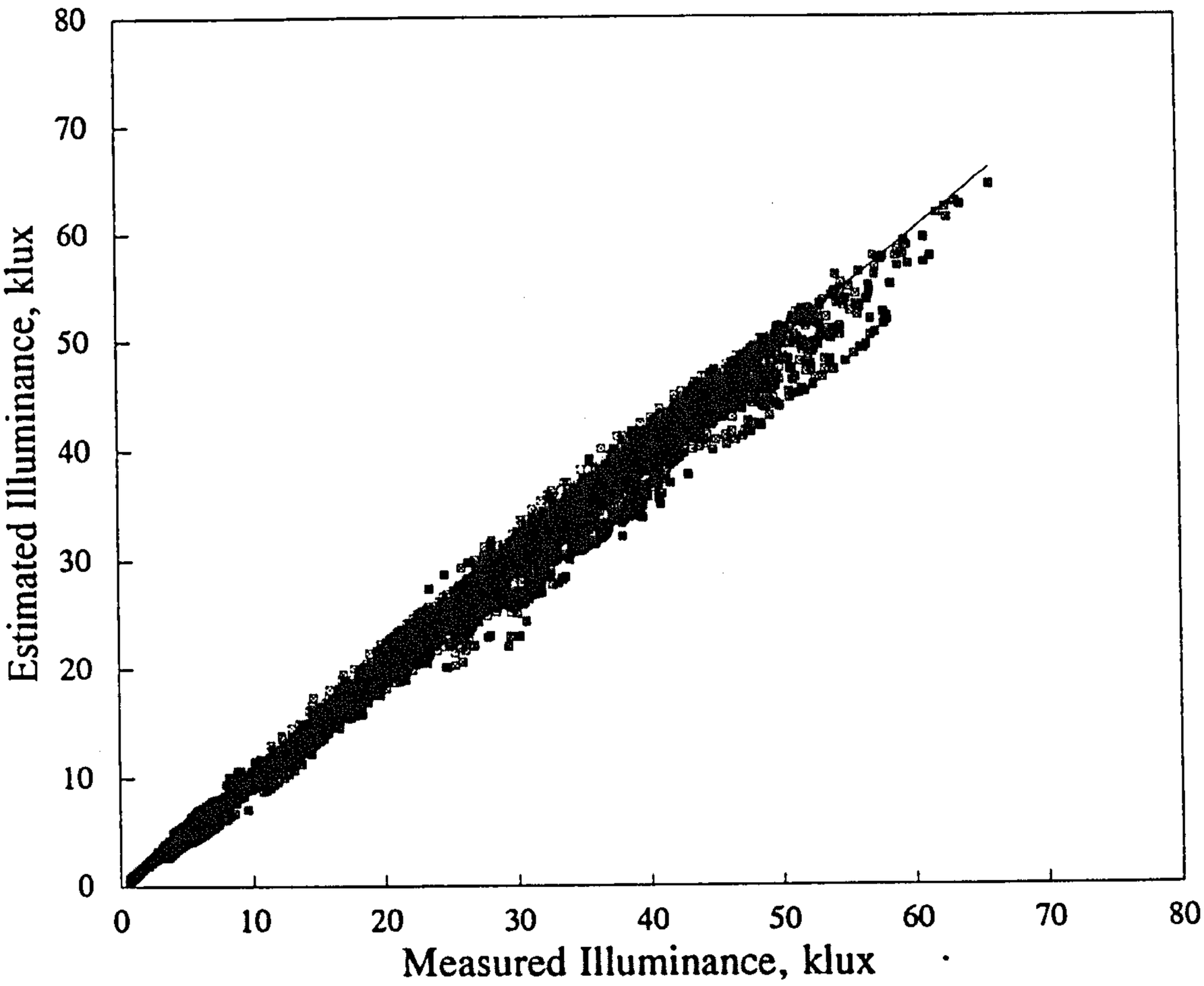

Figure 4.4.1 Perez Diffuse luminous efficacy model

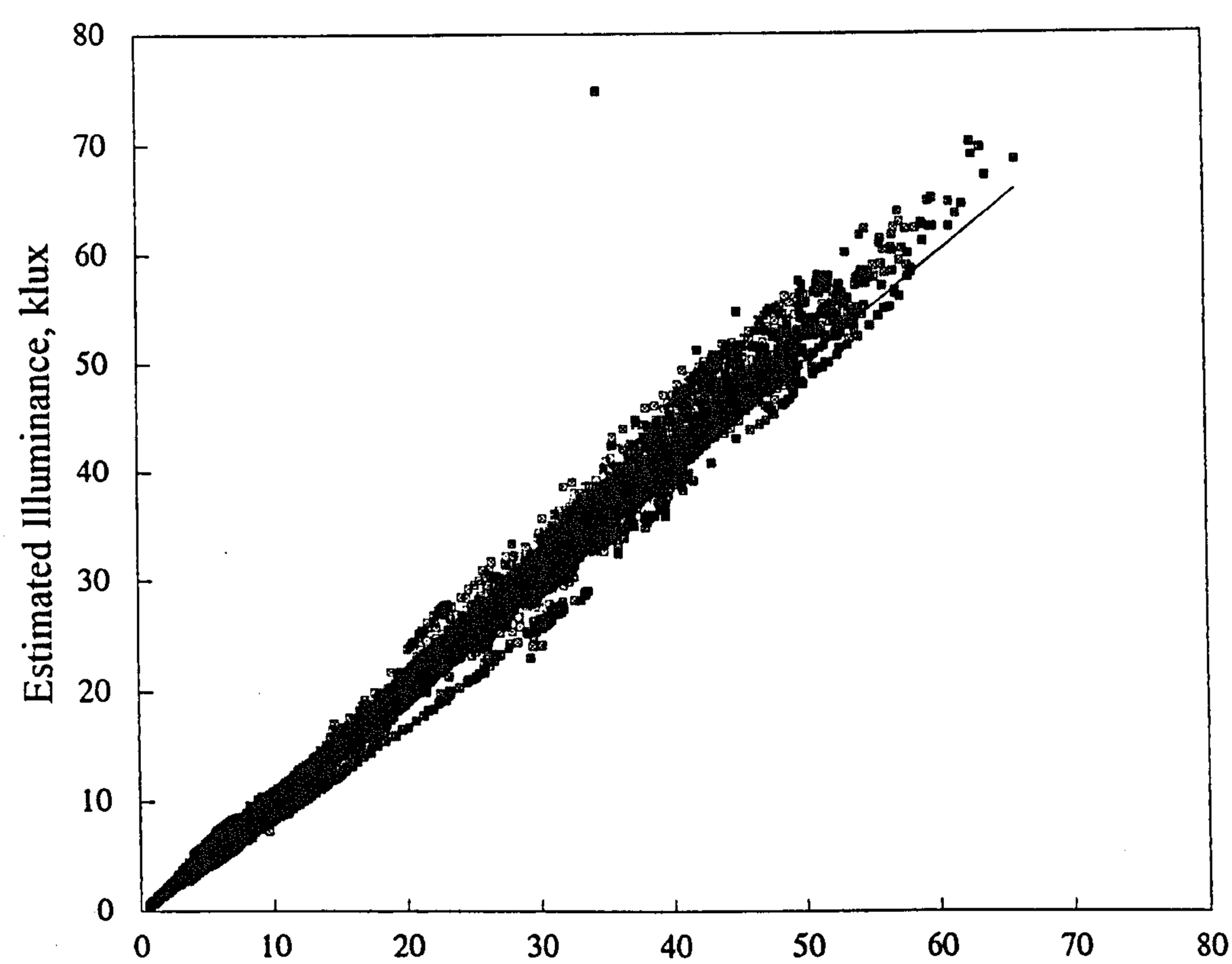

Figure 4.4.2 Littlefair Diffuse luminous efficacy model

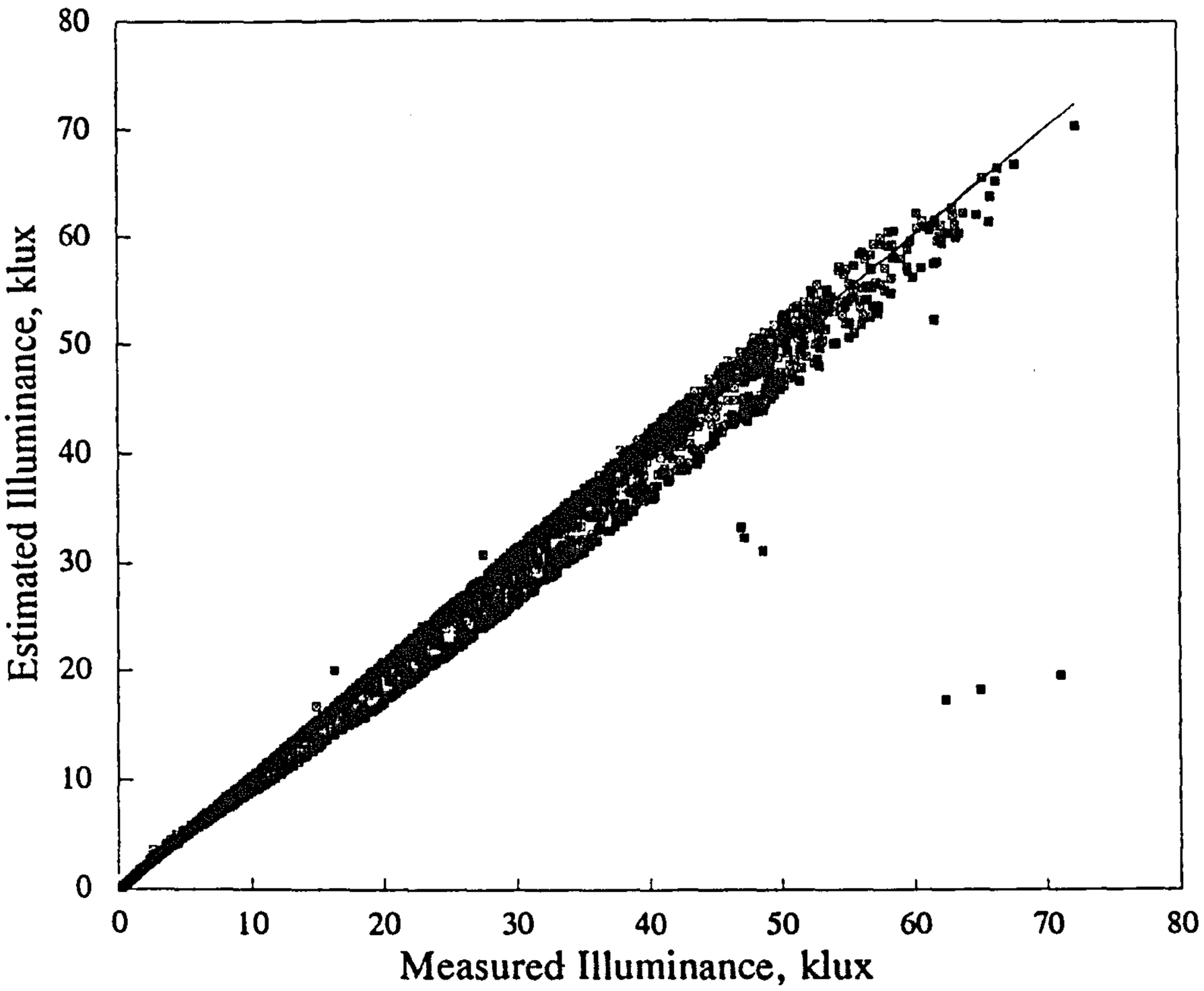

Figure 4.4.3 Proposed Diffuse luminous efficacy model

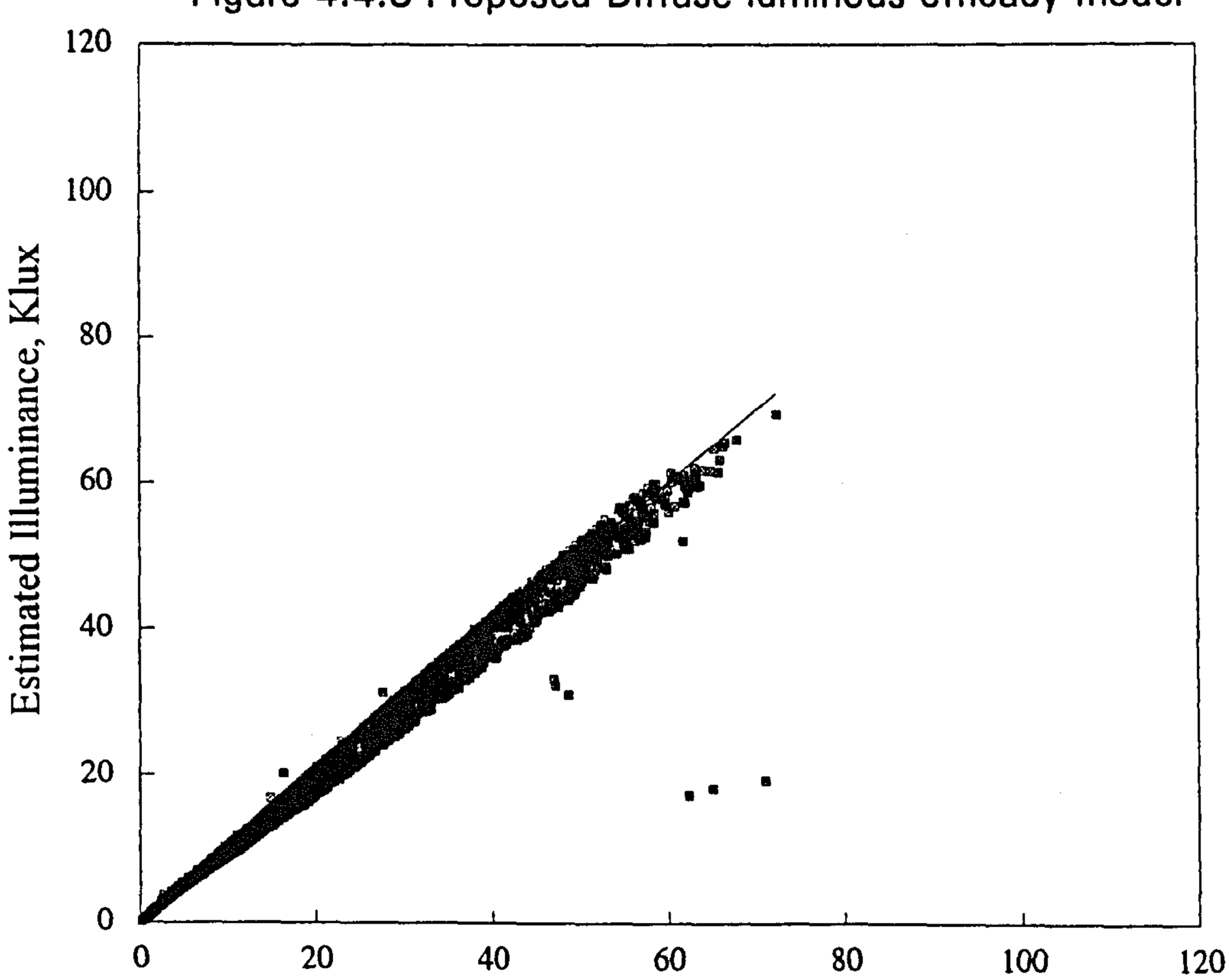

Figure 4.4.4 120 lm/W Diffuse luminous efficacy model

A small seasonal dependence was noted during the analysis of the data which demonstrated slightly higher global luminous efficacies in the summer months, this was also found to be the case in a study of regional luminous efficacy by Secker[4.17].

There appears to be a greater variation in the values of diffuse luminous efficacy particularly so for the Japanese and Greek sites. Both of these sites possess values around 150 lm/W and although diffuse luminous efficacy is expected to be higher than global luminous efficacy, differences such as the ones now illustrated are quite unexpected. The most probable explanation for this phenomenon in the case of Athens lies with the absorption of diffuse irradiance by aerosols and air pollutants created by traffic. In a recent study by Kambezidis et al[4.18] the ratio of background diffuse to horizontal diffuse irradiance dropped with increasing sky clearness. In a complementary piece of work by Muneer et al[4.19] this ratio for illuminance was found to increase with clearness index. This indicates that while diffuse irradiance is being absorbed diffuse illuminance is not affected and hence diffuse luminous efficacy will increase. This phenomenon is investigated in greater detail using a technique developed for slope illuminance modelling work with the results of this analysis discussed in chapter 5.4.

Table 4.4.1 Locational variations in global and diffuse luminous efficacy

Location	Global luminous efficacy (lumens/Watt)	Diffuse luminous efficacy (lumens/Watt)
Edinburgh(Heriot Watt)	**115**	**119**
Edinburgh(Napier)	**115**	**120**
BRE Watford	**111**	**120**
Sheffield	**116**	**129**
Japan	**123**	**150**
Athens	**108**	**155**

As climatic differences were under consideration it was of interest to examine the time scale effect of pollution and atmospheric change. To this end two sets of Edinburgh data were compared, one from the year 1937 [4.20]which is in a statistical format describing the number of days that a certain illuminance threshold is exceeded. The 1992 Edinburgh data were collated to produce a comparitive set of statistics with the results given in Tables 4.4.2 & 4.4.3.

Table 4.4.2 Edinburgh 1992/1993 data Frequency of horizontal global illumination throughout the year

	Lux	9 am	12 noon	3 pm
Below	**1076**	24	3	11
Below	**2152**	50	6	34
Below	**3228**	67	11	66
Below	**4304**	79	18	78
Below	**5380**	89	26	91
Below	**6456**	95	35	100
Below	**7532**	110	44	115
Below	**8608**	130	54	129
Below	**9684**	135	60	146
Below	**10760**	144	65	149
Above	**10760**	221	300	216

Table 4.4.3 Edinburgh old data Frequency of horizontal global illumination throughout the year

	Lux	9 am	12 noon	3 pm
Below	**1076**	19	1	12
Below	**2152**	47	4	37
Below	**3228**	72	11	63
Below	**4304**	88	17	81
Below	**5380**	104	26	94
Below	**6456**	118	33	109
Below	**7532**	130	44	120
Below	**8608**	139	53	132
Below	**9684**	149	66	141
Below	**10760**	158	80	149
Above	**10760**	207	285	216

Tables 4.4.2 and 4.4.3 show a remarkable amount of similarity indicating that pollution and climatic conditions over the past 50 years have not changed significantly.

The need for these design tools is unquestionable as the models provide the connection between solar radiation and daylight levels. As measurements of solar radiation are widespread[4.21] throughout the UK it is straightforward to obtain daylight values for many locations. This is the main vehicle for building designers to

predict accurately daylight values rather than relying on tables or diagrams for only one location in South East England.

REFERENCES

4.1 Littlefair P J The luminous efficacy of daylight: A review Lighting Res. Technol. 17(4) 162-182 (1985)

4.2 Navvab M, Karayel M, Ne'eman E, Selkowitz S Luminous efficacy of daylight CIBSE National Lighting Conference 409-420 (1988)

4.3 Chroscicki W Calculation methods of determining the value of daylight's intensity on the ground of photometric and actinometrical measurements Proc. CIE Barcelona p71.24 (1971)

4.4 Aydinli S and Krochmann J Data on daylight and solar radiation: Guide on Daylight Draft for CIE TC 4.2 (1983)

4.5 Dogniaux R Donnees Meteorologiques concernant l'Ensoliellement et L'Eclairage Naturel (Meteorological data on sunshine and natural light) Cahiers CSTB (44) Cahier 351 (1960)

4.6 Navvab M, Karayel M, Ne'eman E, Selkowitz S Analysis of Atmospheric turbidity for daylight calculations Energy and Buildings, 6 293-303 (1984)

4.7 Kondratyev K Ya Radiation in the atmosphere (Academic press, New York) (1969)

4.8 Iqbal M An introduction to solar radiation (Academic press, Toronto) (1983)

4.9 Coulson K L Solar and terrestrial radiation (Academic press, New York)(1975)

4.10 Perez R, Ineichen P and seals R Modeling daylight availability and irradiance components from direct and global irradiance Solar Energy 44(5) 271-289 (1990)

4.11 Tregenza P R A simple mathematical model of illumination from a cloudy sky Lighting Res. Technol. 12(3) 121-128 (1980)

4.12 Littlefair P J Measurement of the luminous efficacy of daylight Lighting Res. Technol. 20(4) 177-188 (1988)

4.13 Littlefair P J Daylight design and energy conservation PhD thesis (BRE/CNAA, Garston) (1984)

4.14 Muneer T Solar heated and daylight offices: Design study Building Serv. eng. Res. Technol. 11(4) 141-152 (1990)

4.15 Muneer T and Angus R C Daylight illuminance models for the United Kingdom, Lighting Res. and Technol. 25(3) 113-123 (1993)

4.16 Muneer T Solar radiation and daylight illuminance models for Japan: Part I &II Lighting. Res. & Technol. 27, 4 (1995)

4.17 Secker S M regional variations of daylight availability- a review of measured data and estimating methods Lighting Res. and Technol. 15(3) 151-156 (1983)

4.18 Kambezidis H D Psiloglou B E Muneer T Angus R C Comparison of solar irradiance models with measurements for two regions in Southern and Northern Europe North Sun Solar energy at high latitudes Conference 177-182 Glasgow (1994)

4.19 Muneer T Angus R C Kambezidis H Psiloglou Daylight illuminance models for the northerly and southerly latitudes North Sun Solar energy at high latitudes Conference 415-420 Glasgow (1994)

4.20 Lynes J A Principles of natural lighting (Elsevier Publishing Company Ltd: London)(1968)

4.21 Muneer T Solar irradiation database for the United Kingdom Building Serv. Eng. Res. Technol. 10(1) 41-42 (1989)

5 SLOPE ILLUMINANCE MODELS

Notation

ε = Obliquity of ecliptic (dimensionless)

α = Right ascension of body (°) measured 0° to 360°, increasing towards the East

β = angle of the sloped surface from the horizontal (°)

b = radiance distribution index (dimensionless)

Δ = sky brightness coefficient

ρ = albedo or ground reflectivity

C = Parameter (°)

D = Day of the month

DEC = Solar declination angle (°)

F_1, F_2 = coefficients (dimensionless)

F = sky clearness index (dimensionless)

G = Parameter (°)

GHA = Greenwich hour angle(°)

h = Hour

i = inclination angle of the sun's beam on a sloped surface (°)

L = Parameter (°)

$L\alpha$ = luminance of a patch of sky at angle α from the horizon(lux)

L_β= illuminance on a slope inclined at an angle β° from the horizontal (lux)

L_D = horizontal diffuse illuminance(lux)

LG = horizontal global illuminance(lux)

LAT = Latitude of observer(°) measured from 0° to ±90°

Lds = Slope background diffuse illuminance (lux)

LONG = Longitude of observer(°) measured from the Greenwich Meridian

Lz = Zenith luminance (lux)

M = Month of the year

m = Parameter(dimensionless)

min = minute

s = second

SAZ = Solar azimuth(°)

t = Parameter (dimensionless)

TF = Tilt factor (dimensionless)

UT = Universal time (h)

x, y = coefficients (dimensionless)

Y = Year

z = solar zenith angle (radians)

5.1 INTRODUCTION

As the first chapter has highlighted the benefits of reducing buildings' energy consumption through the replacement of electrical lighting by natural daylight are significant for economic, environmental and ergonomic reasons. This replacement can be achieved through acquiring the best knowledge of the availability of daylight for the building under consideration. The daylight information presently at the dispense of building designers and architects is either inaccurate or dated and on the whole inadequate for the type of daylight design that energy efficient building construction demands. To this end the development of a daylight estimation model that calculates slope illuminance for any location and under a complete year's weather pattern is essential if the potential energy savings and occupant benefits from using natural daylight are to be realised.

The development of an illuminance model must pay due consideration to the users of the models. There is little point in producing a highly accurate daylight prediction tool if its structure and operation are too complex or if the model requires information that is not readily available to the user. Generally, models which are simple in structure and require a limited amount of data input tend to be adopted more universally by building designers. This understanding directs modelling work to utilise data that is widely accessible to the building designer or can be easily derived. In addition the model must cater for all sky conditions and time of year, while remaining applicable for the whole of the United Kingdom.

Two of the most widely recorded meteorological parameters are horizontal global and diffuse irradiance whose measurements at metoerological offices and research establishments cover the length and breadth of the [5.1]. For this reason and considering the results of the luminous efficacy chapter, it is advantageous to utilise these irradiance measurements as conversion to illuminance can be achieved through the algorithms presented therein.

The model is structured to break down the modelling problem into sections with Fig. 5.1.1 showing the proposed configuration.

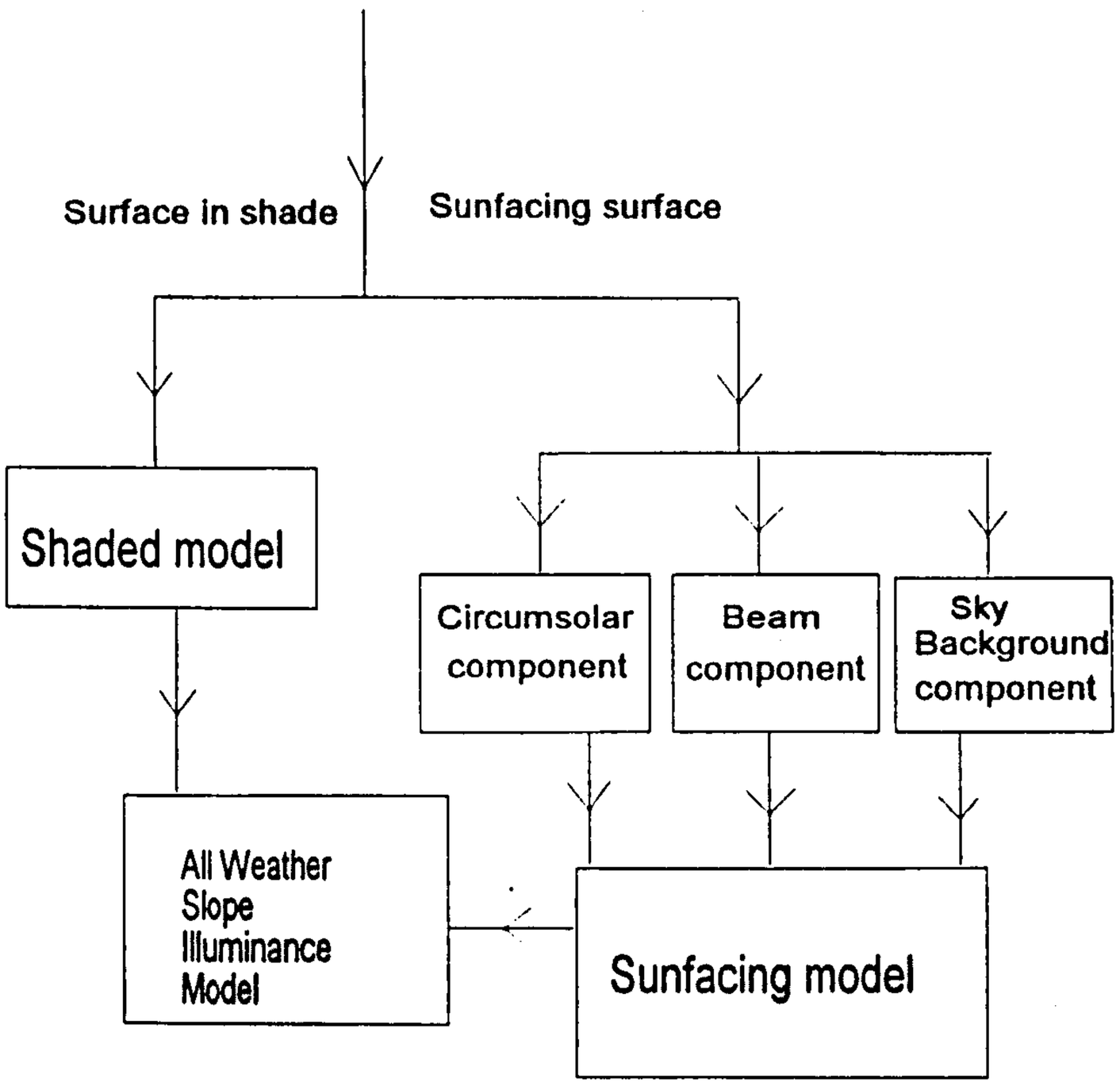

Figure 5.1.1 Proposed slope illuminance model flow diagram

5.2 SOLAR GEOMETRY

The proposed slope illuminance model has horizontal global and diffuse illuminance and solar geometry as its primary inputs. Solar geometry is concerned with the determination of angles necessary for the calculation of various illuminance values in this study and is used in solar irradiation studies for solar design purposes[5.2]. It is also of particular importance to the structure of the proposed model which relies on ascertaining a surface's orientation with respect to the sun. For these reasons the following section details the calculation of solar altitude, solar azimuth and inclination angle from inputs such as latitude, longitude and time.

The sun's position in the sky can be described in terms of two angles, γ_S the elevation angle above the horizon, and its azimuth- the angle from north of the sun's beam projection on the horizontal plane(SAZ). The co-ordinates (γ_S, SAZ) which describe the sun's position are dependent on the latitude(LAT) and longitude(LONG) of the location, the solar declination angle(DEC) and the Greenwich hour angle(GHA). Equations 5.1 and 5.2 detail the calculation of solar declination angle and GHA.

$$DEC = \tan^{-1}(\tan\varepsilon \sin\alpha) \qquad 5.1$$

$$GHA = 15UT - 180 - C + L - \alpha - LONG \qquad 5.2$$

where the obliquity of the ecliptic is given by

$$\varepsilon = 23.4393 - 0.013t \qquad 5.3$$

and

$$t = (UT/24 + D + [30.6m + 0.5] + [365.25(y-1976)] - 8707.5)/36525 \qquad 5.4$$

If M>2 then y =Y and m = M-3, otherwise y = Y-1 and m = M + 9. The terms in square brackets are integer values. Universal time UT is calculated from Eq. 5.5.

$$UT = h + min/60 + s/3600 \qquad 5.5$$

The remaining terms are given by the following equations.

$$\alpha = L - 2.466 \sin2L + 0.053 \sin4L \qquad 5.6$$

$$L = 280.460 + 36000.770t + C \qquad 5.7$$

$$C = 1.915 \sin G + 0.020 \sin 2G \qquad 5.8$$

$$G = 357.528 + 35999.05t \qquad 5.9$$

The solar co-ordinates may now be obtained from equations 5.10 and 5.11.

$$\sin \gamma_s = \sin LAT \sin DEC - \cos LAT \cos DEC \cos GHA \qquad 5.10$$

$$\cos SAZ = \frac{\cos DEC (\cos LAT \tan DEC + \sin LAT \cos GHA)}{\cos \gamma_s} \qquad 5.11$$

The angle of incidence that the sun's beam strikes a vertical surface can then be calculated from knowledge of the solar altitude and azimuth and the orientation of the surface itself(WSA). This angle is often termed the inclination angle and is given by Eq. 5.12.

$$i = \cos^{-1} (\cos\gamma_s \cos(SAZ-WSA)) \qquad 5.12$$

The algorithms used to determine declination angle and Greenwich hour angle were developed by Yallop[5.3] and have been presented by the author in detail[5.4], copies of the two articles on this topic are attached in Appendices 5.1 and 5.2.

5.3 SHADED SURFACE

Once the solar geometry calculations have identified surfaces in shade, the proposed model treats the estimation of illuminance on the surface differently to that of a surface which is exposed to a view of the sun. Several correlation's shall be evaluated with parameters such as solar geometry and measured illuminance investigated as potential modelling quantities.

5.3.1 Inclination angle

In any modelling problem it is essential to identify and eliminate all possible parameters which may or may not influence the value of the quantity being estimated, in this instance the illuminance received by a sloped surface. One such parameter is the inclination angle. The phenomenon of the anti-solar point and the possible dependence of slope illuminance on the angle of incidence merit some investigation. To this end measured values of slope illuminance were plotted against inclination angles using

Edinburgh data. The results are displayed in Fig.5.3.1. The graph(Fig.5.3.1) demonstrates tremendous scatter along with a distinct trend corresponding to an increase in inclination angle. Despite the trend, it is clear that a conclusive correlation between the two parameters is far from conclusive, furthermore there appeared to be no strong evidence to support the contribution of an anti-solar point from this analysis. As a result of these findings it was necessary to eliminate inclination angle and examine alternatives in the modelling solution.

5.3.2 Solar altitude

Shaded surfaces were identified and the measured illuminance of each surface were plotted against solar altitude calculated for the particular time of measurement using Eq.5.2.10. The outcome of this relationship proved to be more encouraging in comparison with the inclination angle model as can be seen form Fig.5.3.2. Once again a trend is clearly visible with the order of scatter increasing with solar altitude. Solar altitude has been used to good effect in luminous efficacy modelling but its use as a variable in the estimation of shaded surface illuminance is not satisfactory.

The overall poor performance of the two geometrical models used to predict illuminance on shaded sloped surfaces ultimately dismisses their implementation as estimation parameters. Despite this outcome it is worth considering the distinct relationship that exists between the two modelled quantities and the measured illuminance, especially in the case of the solar altitude angle.

5.3.3 Horizontal diffuse illuminance

By definition a surface in shade receives no direct sunlight, it follows that the light reaching the surface arrives solely from the sky's background which is diffuse illuminance. It is therefore extremely likely that a correlation exists between the measurements of shaded surface sloped illuminance and horizontal diffuse illuminance. To ascertain the extent of this correlation, measurements of shaded surface illuminance were plotted against the diffuse illuminance values as shown by Figs.5.3.3 to 5.3.8 for Napier, Heriot Watt, BRE, Sheffield, Fukuoka (Japan) and Athens data respectively. All of these graphs demonstrate a distinct relationship between the two quantities as was expected. The correlation between the two parameters is clearly linear and a

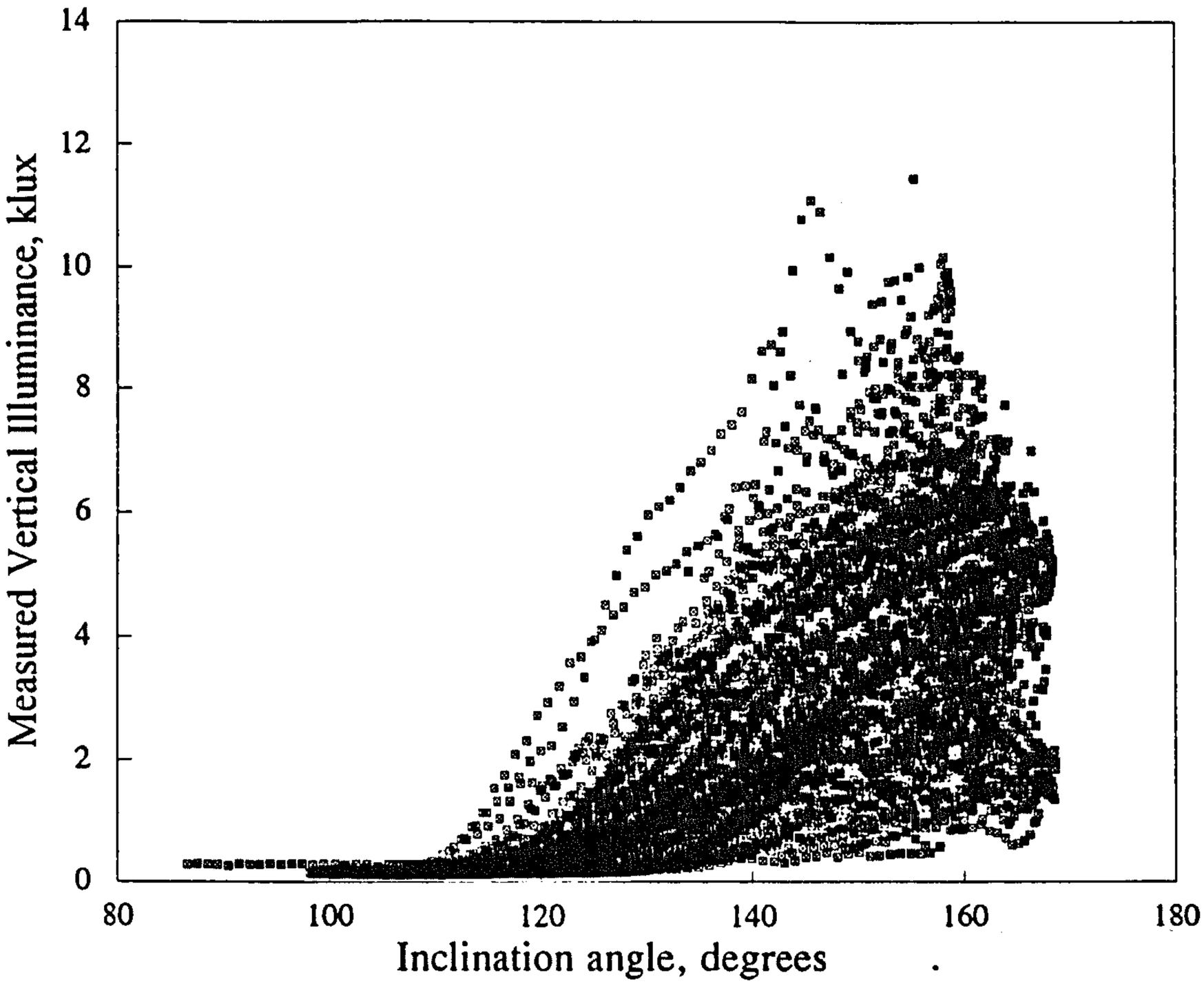

Figure 5.3.1 Shaded illuminance data versus inclination angle

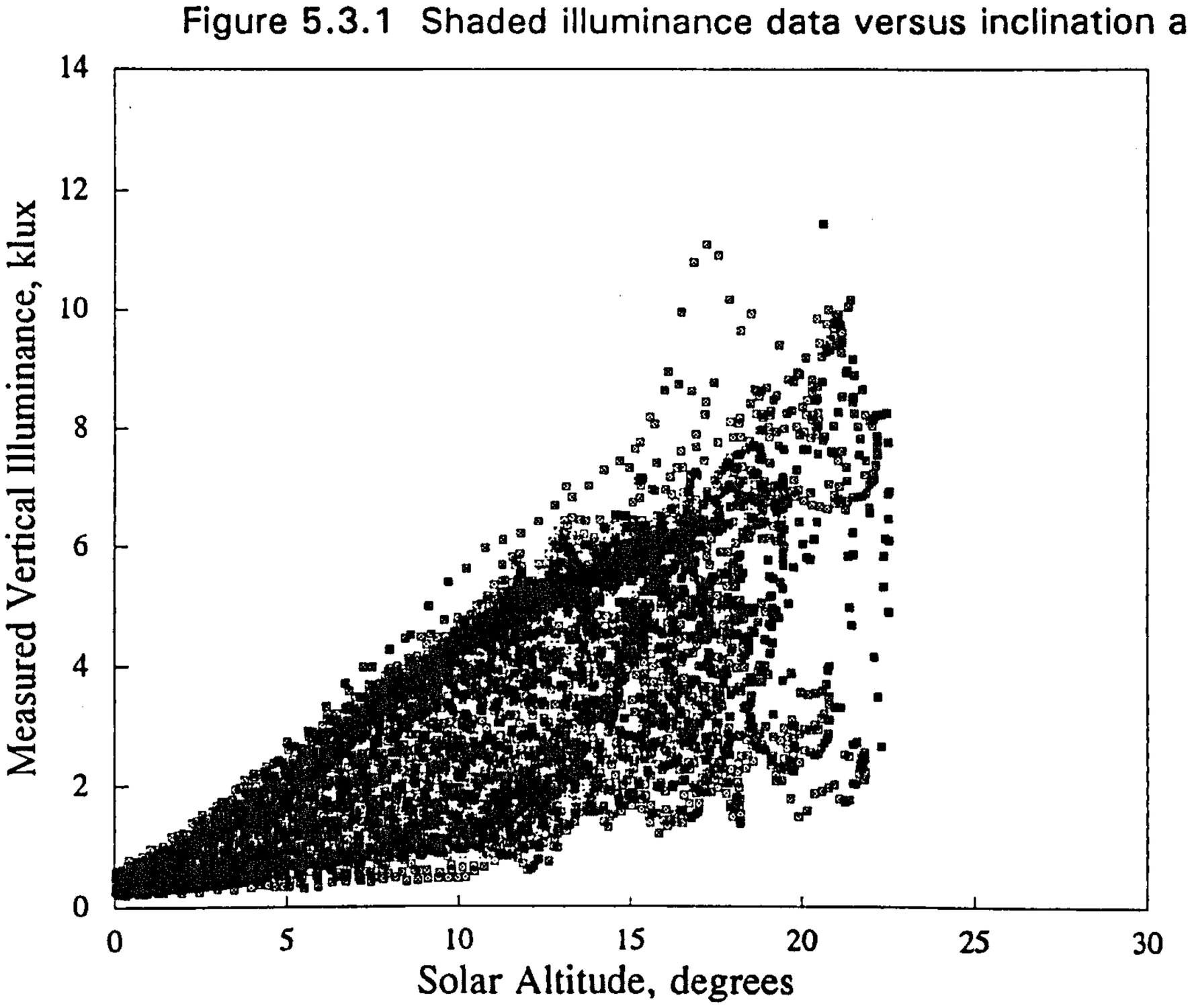

Figure 5.3.2 Shaded illuminance data versus solar altitude

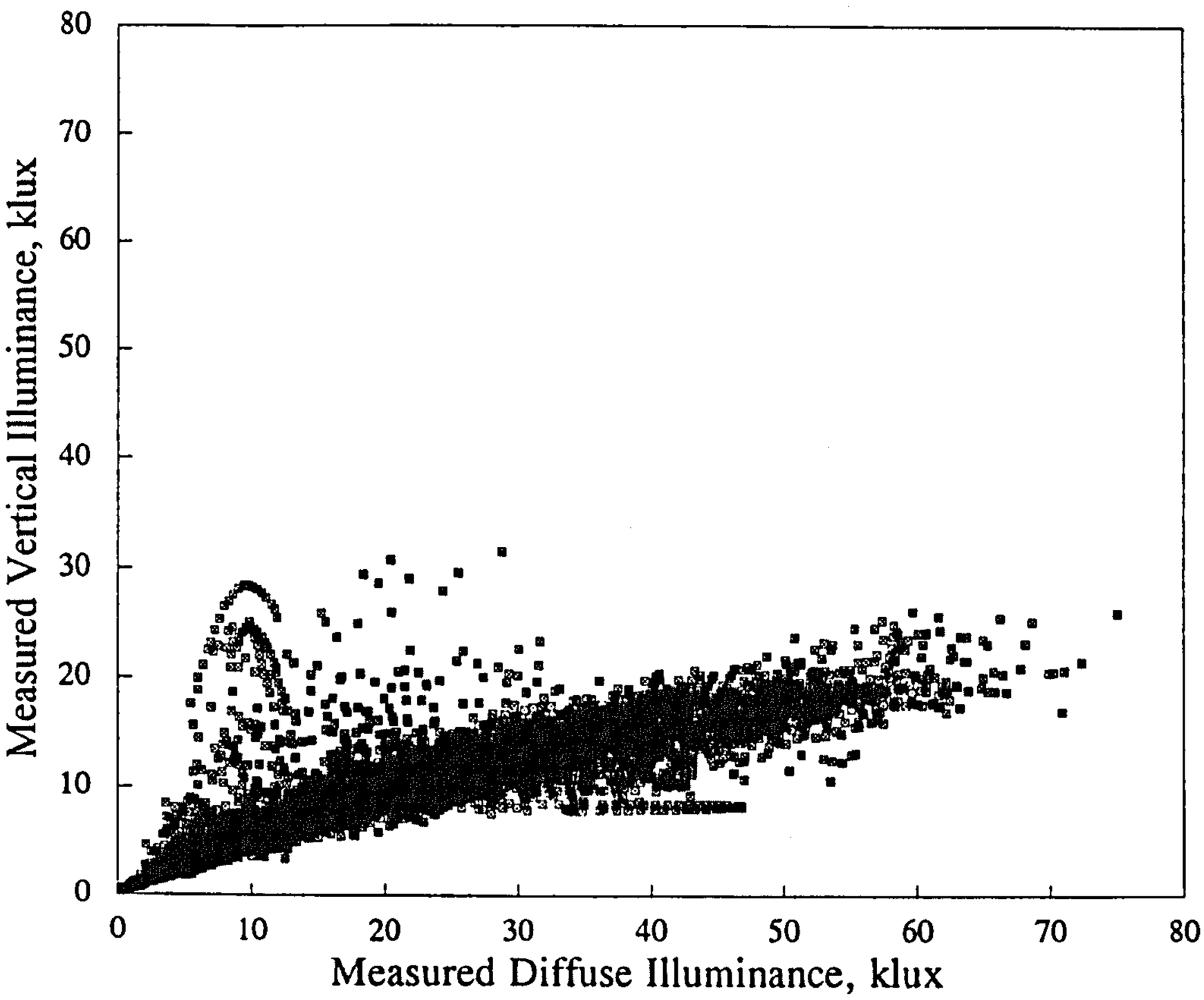

Figure 5.3.3 Napier: Shaded slope illuminance data

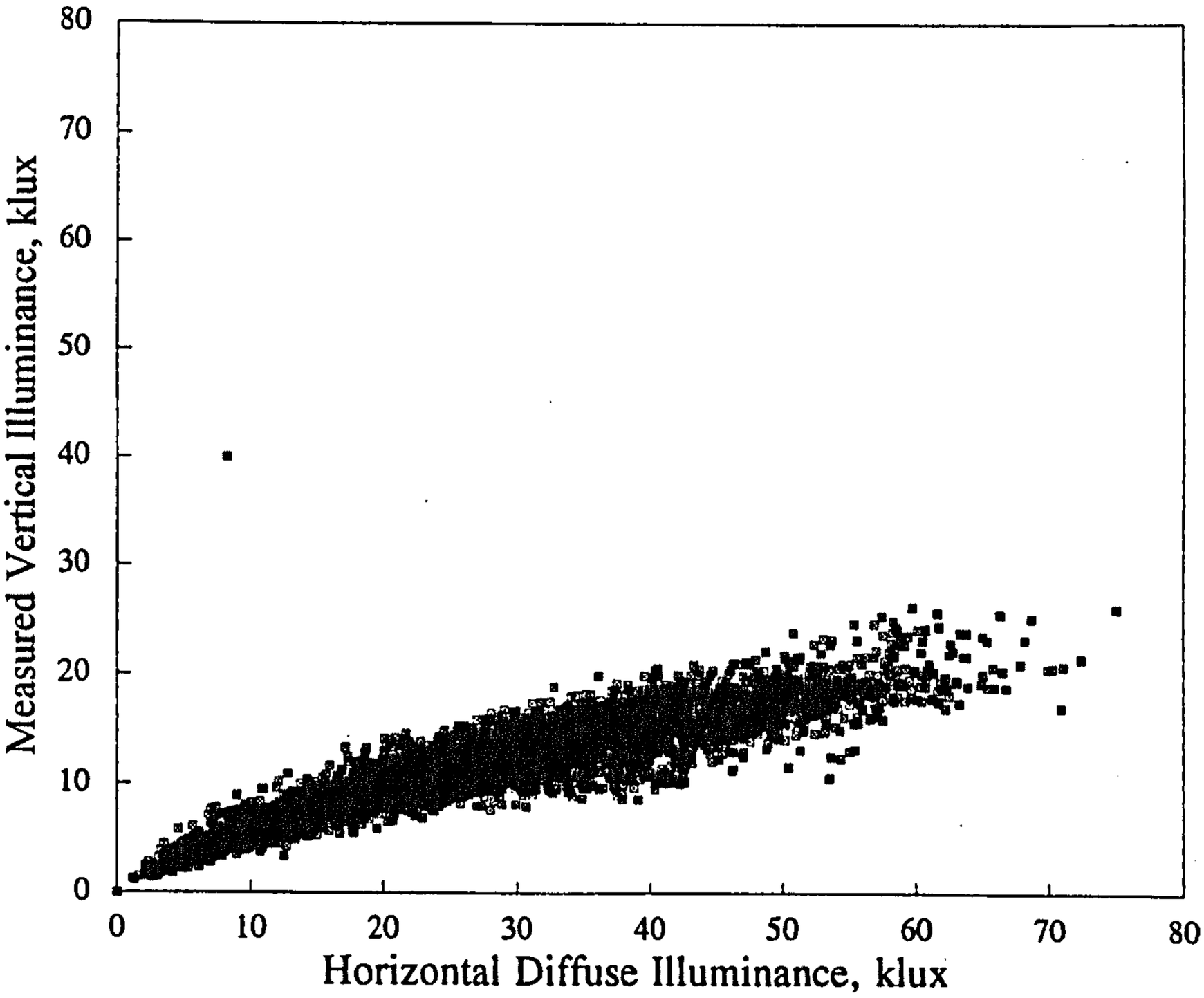

Figure 5.3.4 Heriot Watt: Shaded slope illuminance data

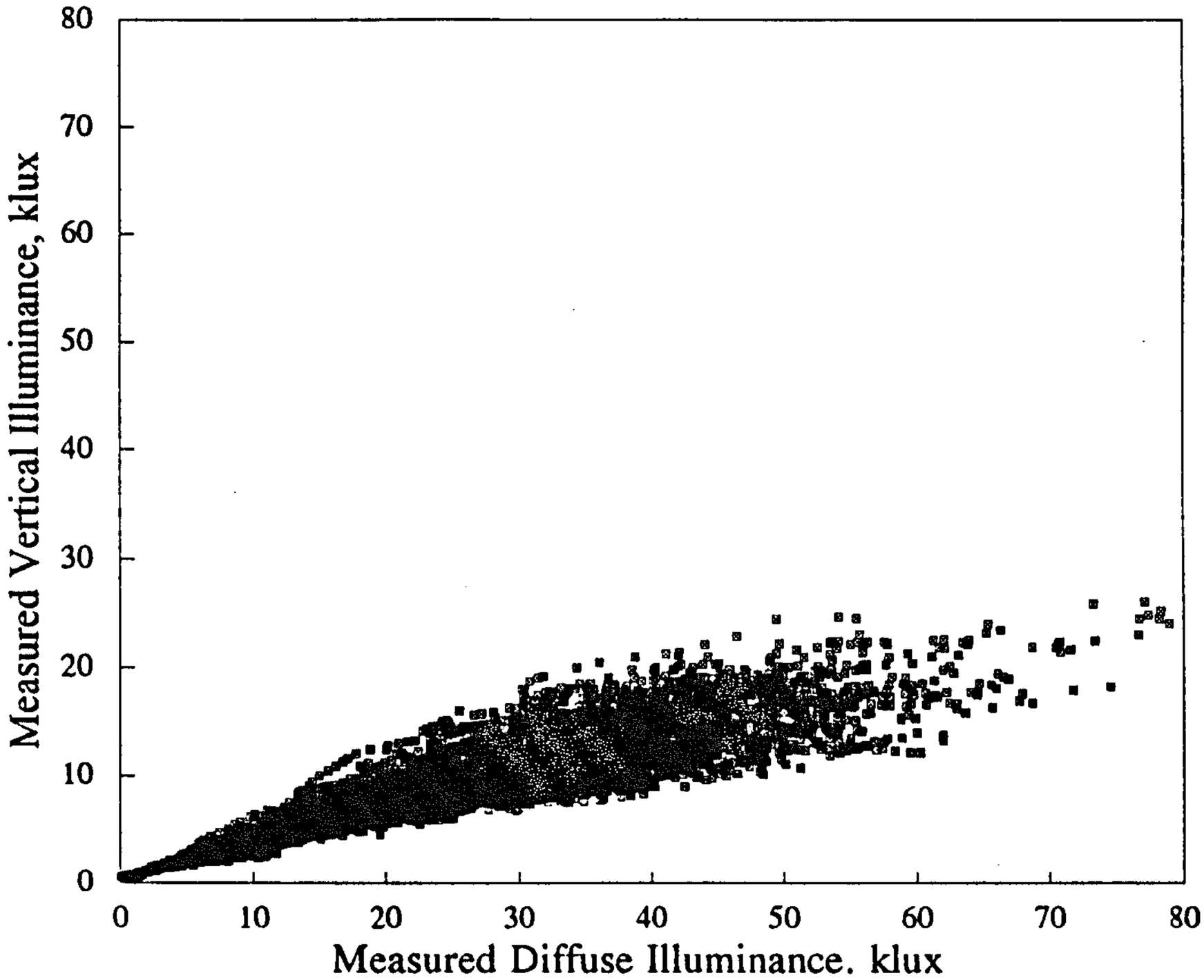

Figure 5.3.5 Sheffield: Shaded slope illuminance data

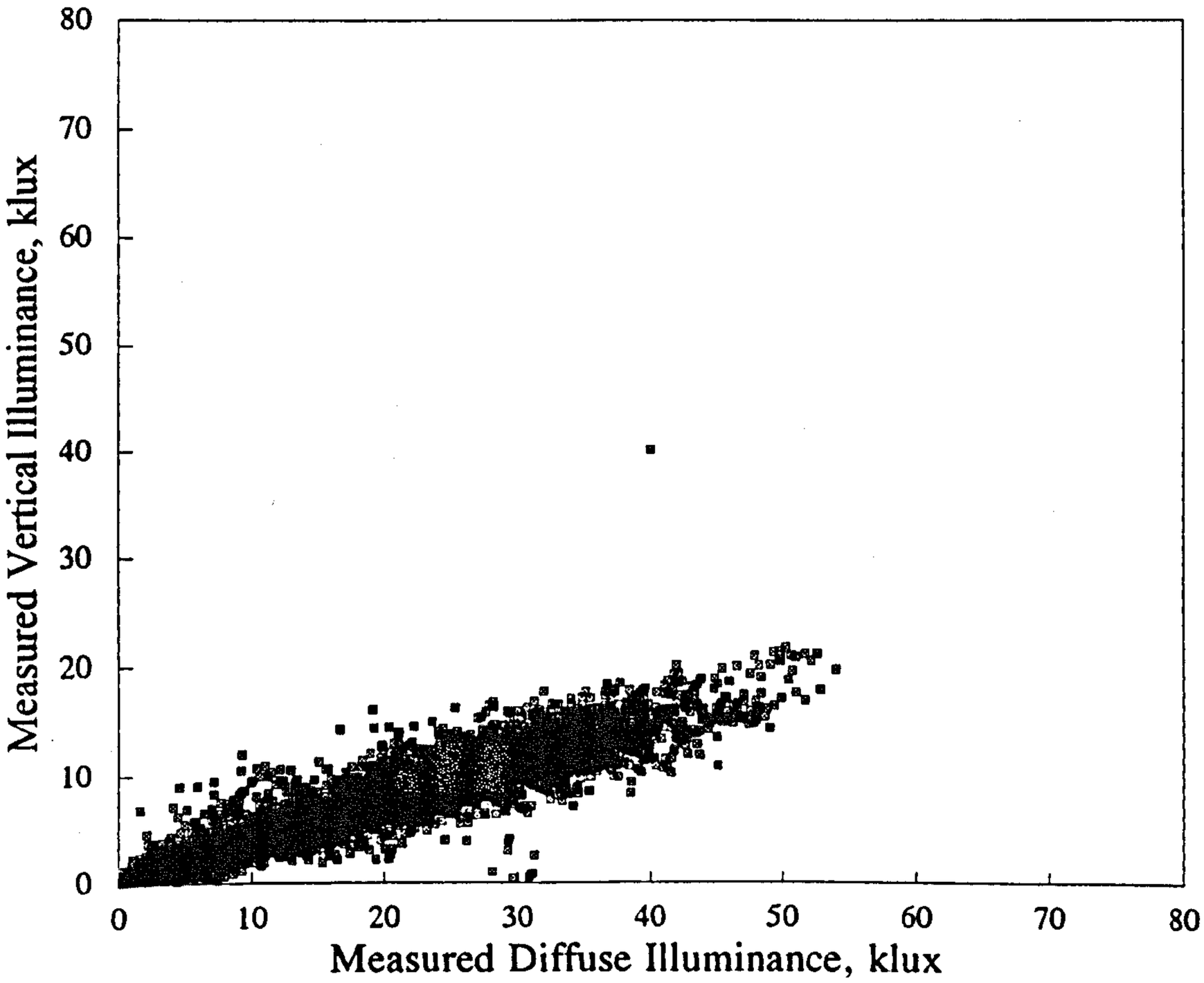

Figure 5.3.6 BRE: Shaded slope illuminance data

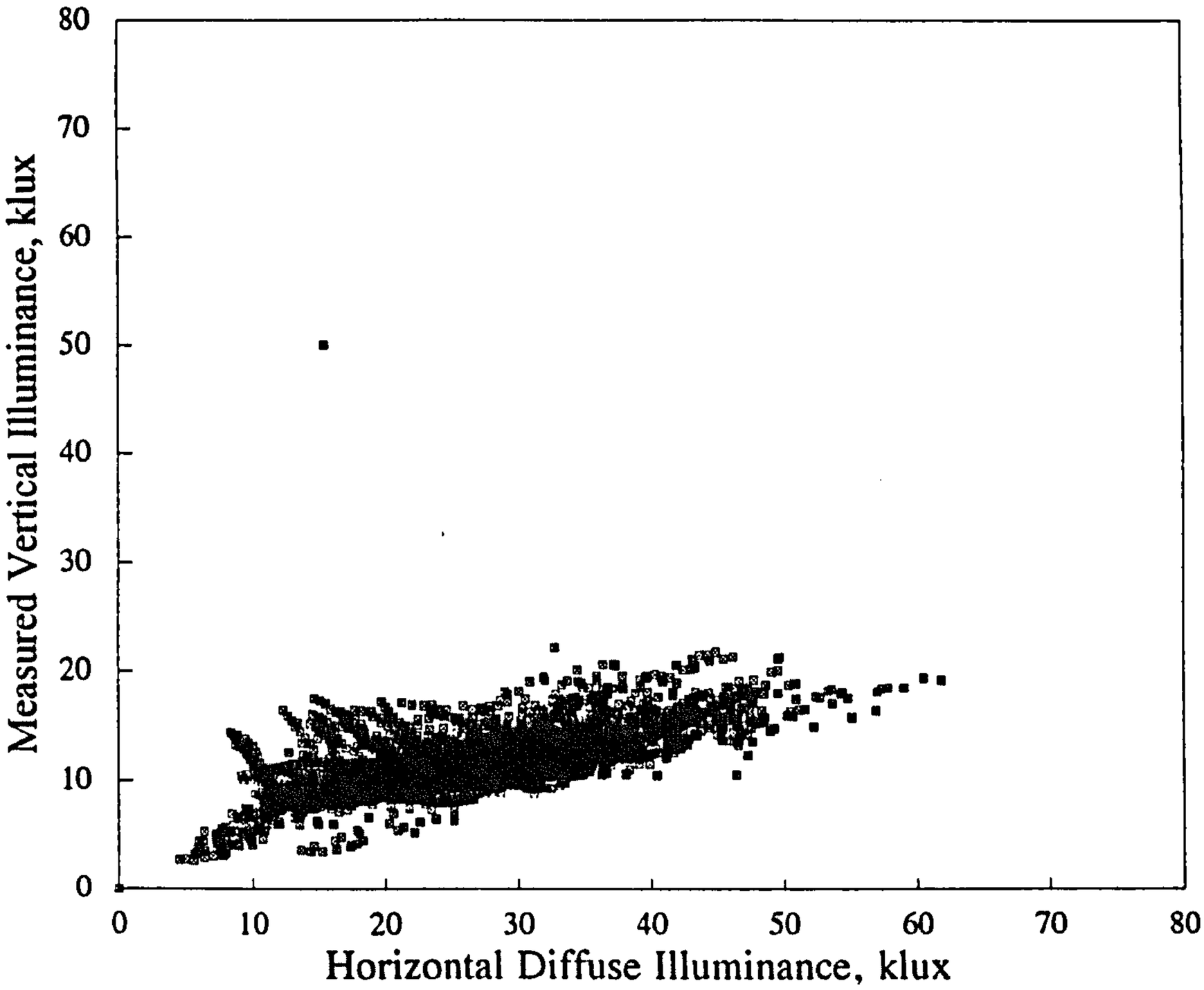

Figure 5.3.7 Athens: Shaded slope illuminance data

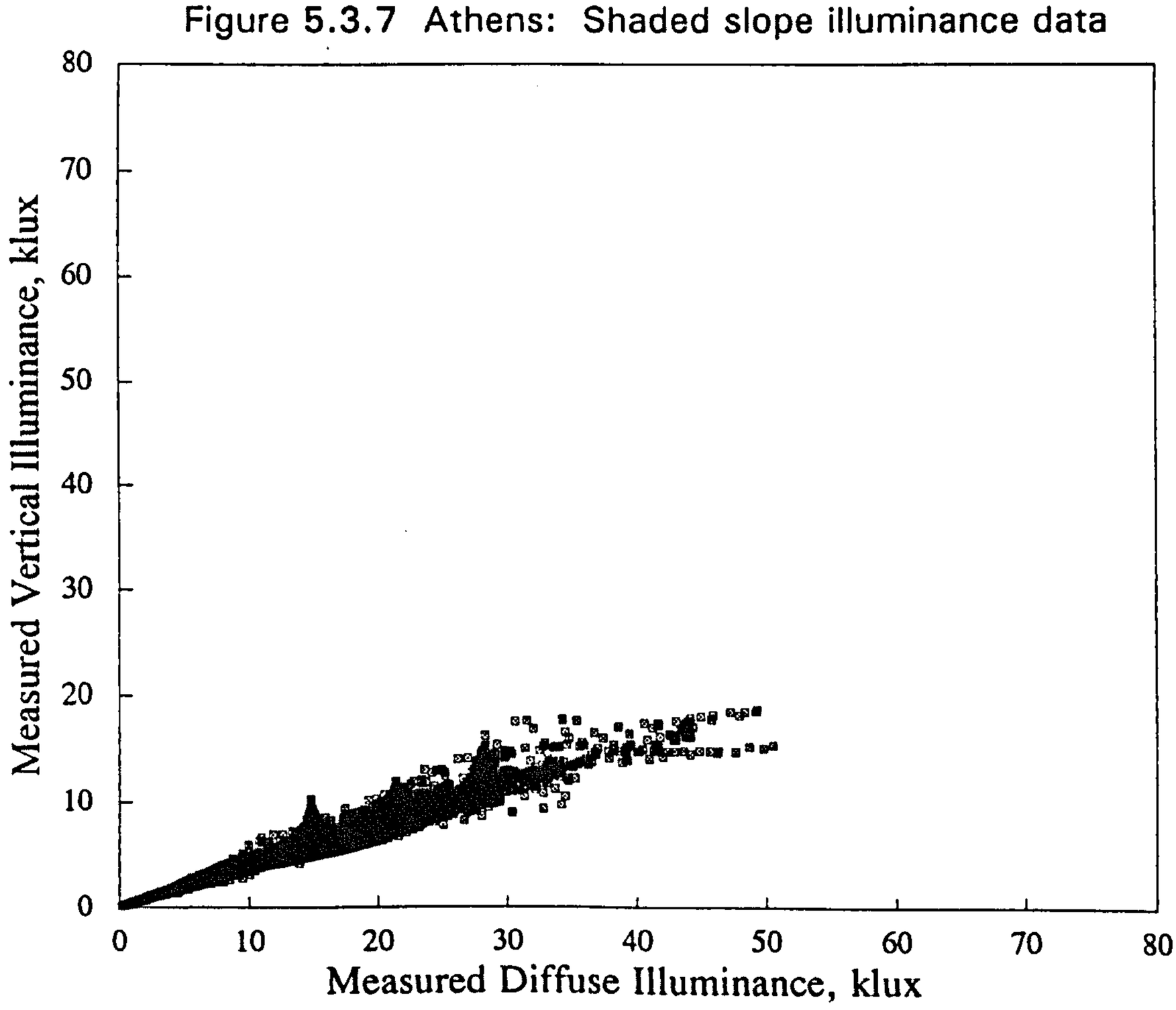

Figure 5.3.8 Japan: Shaded slope illuminance data

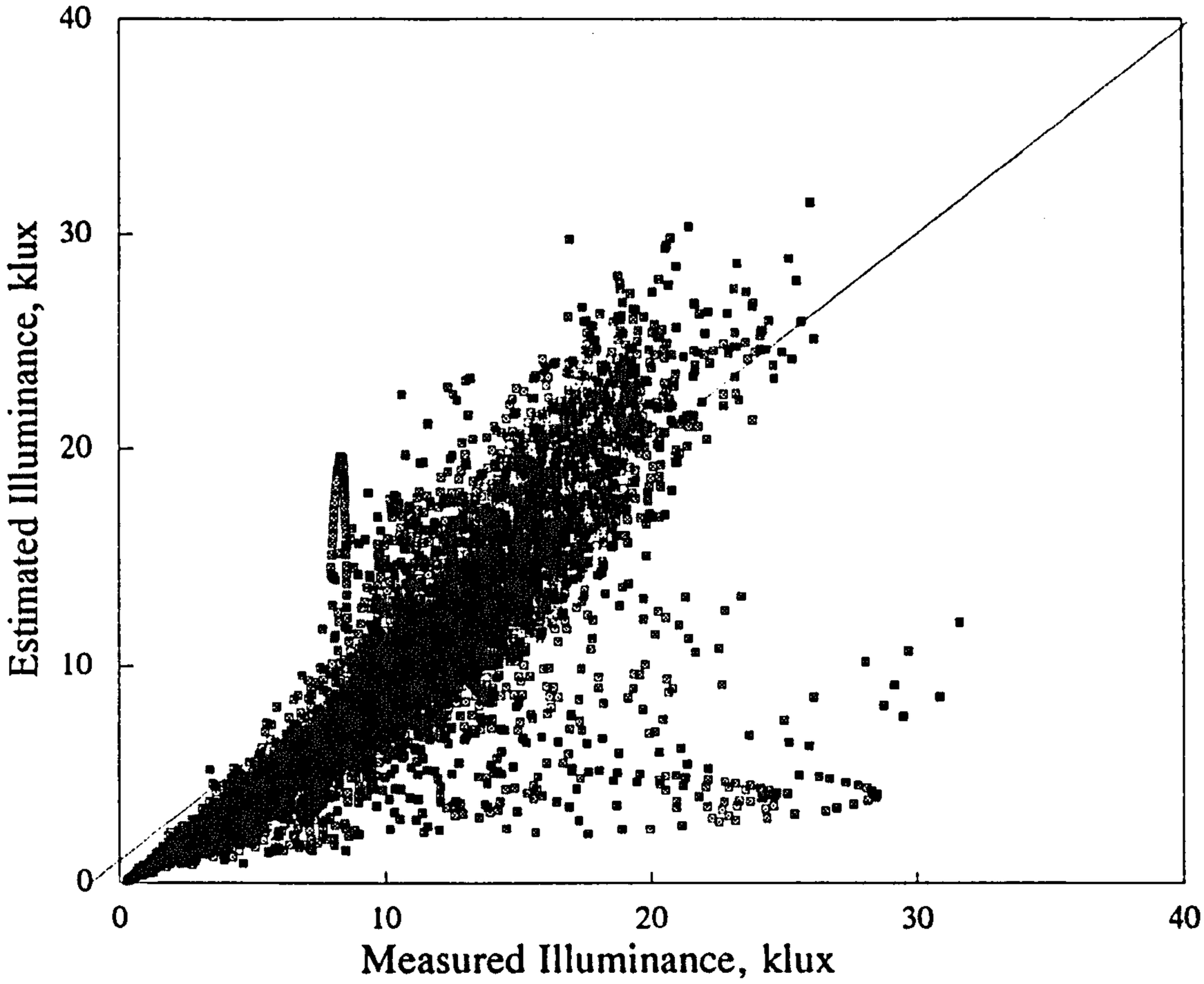

Figure 5.3.9 Napier: Shaded slope illuminance model

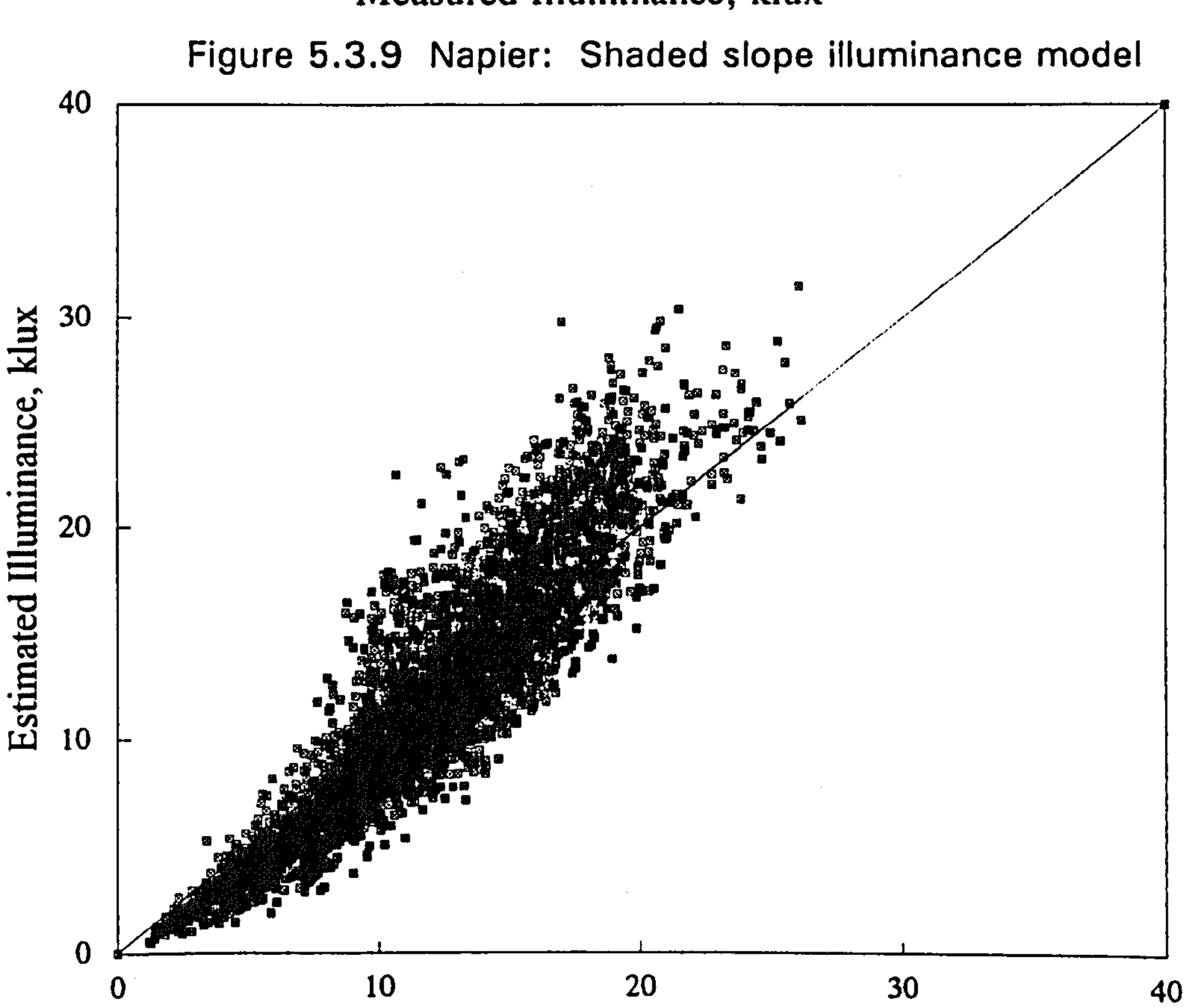

Figure 5.3.10 Heriot Watt: Shaded slope illuminance model

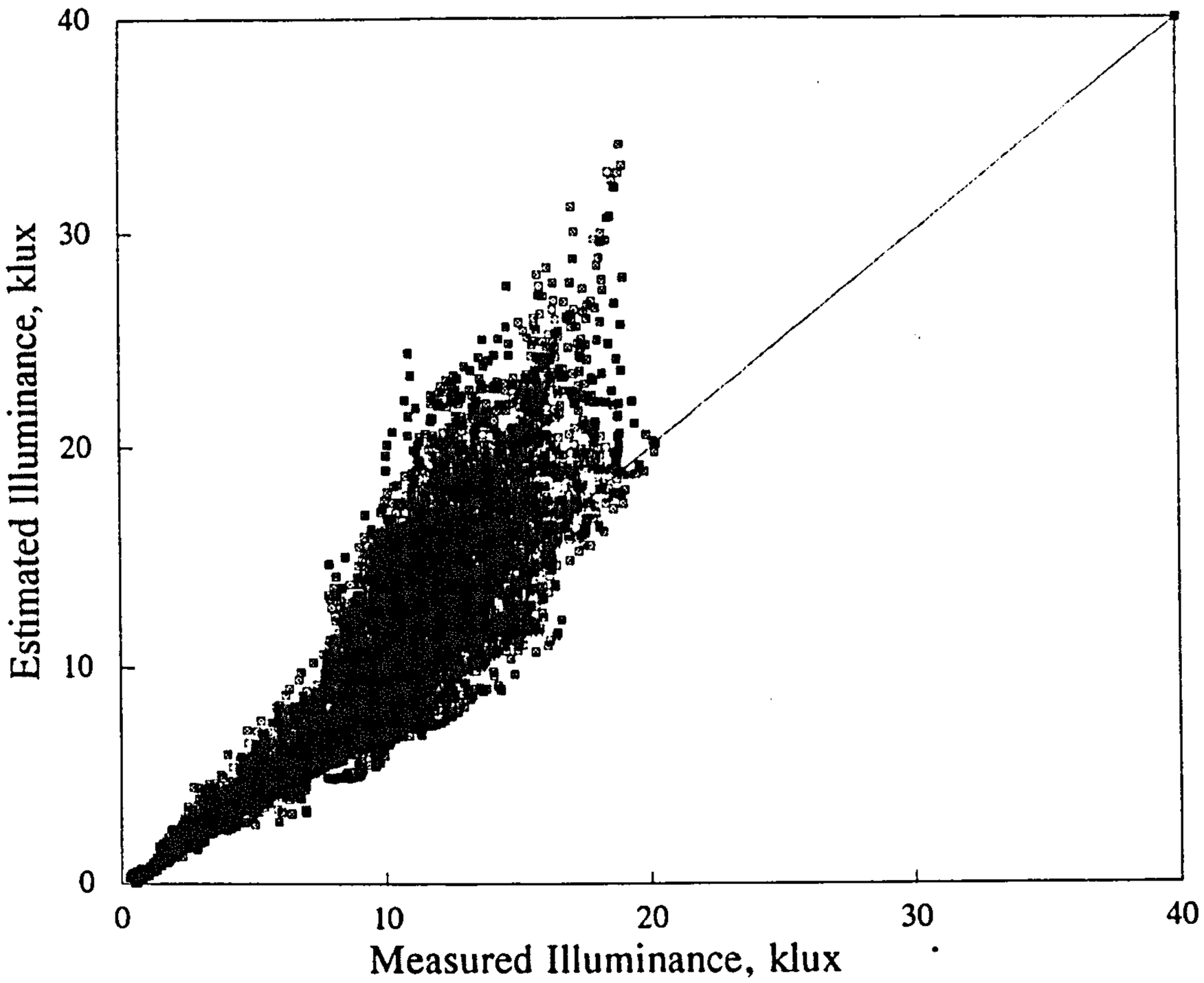

Figure 5.3.11 Sheffield: Shaded slope illuminance model

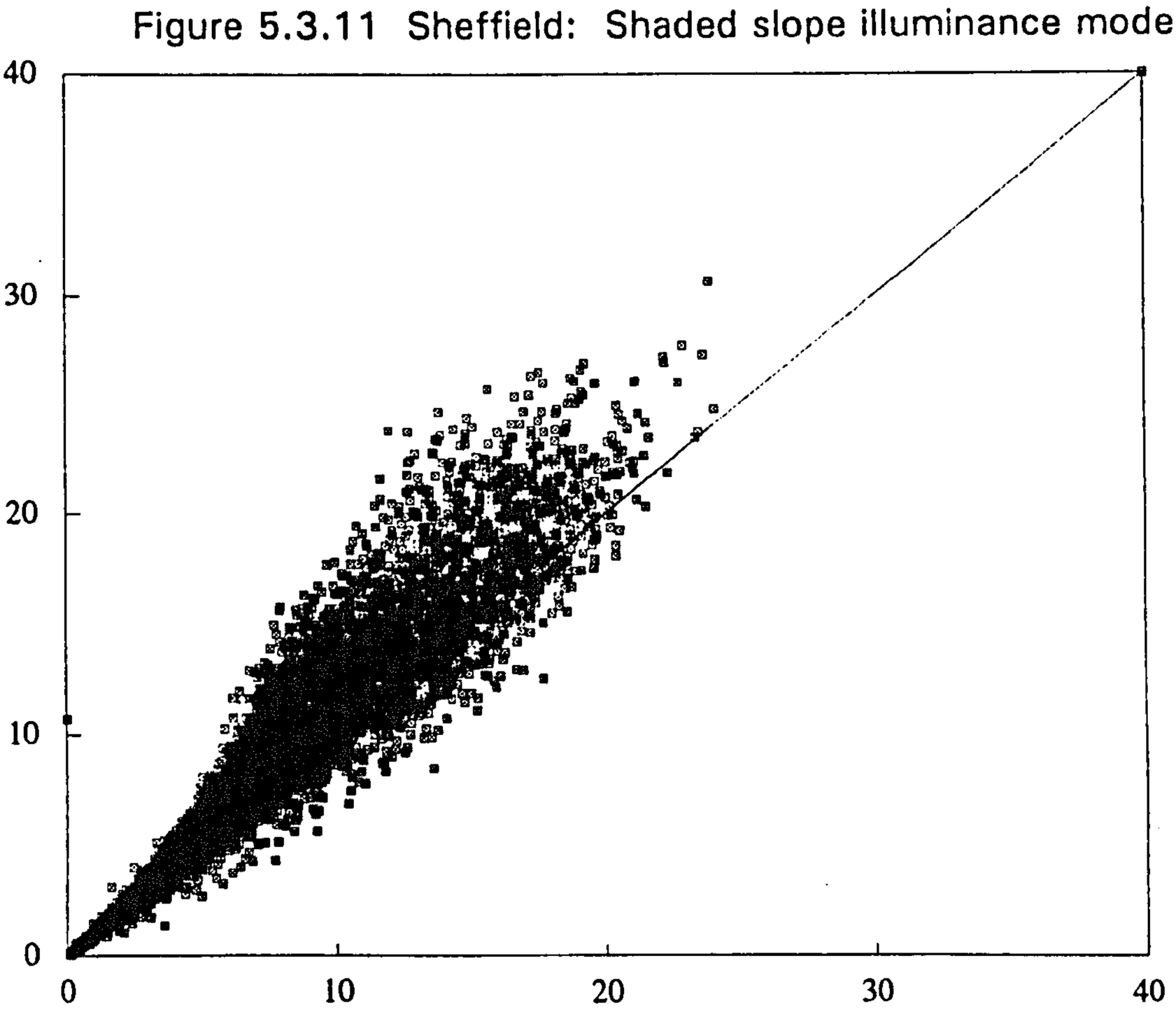

Figure 5.3.12 BRE: Shaded slope illuminance model

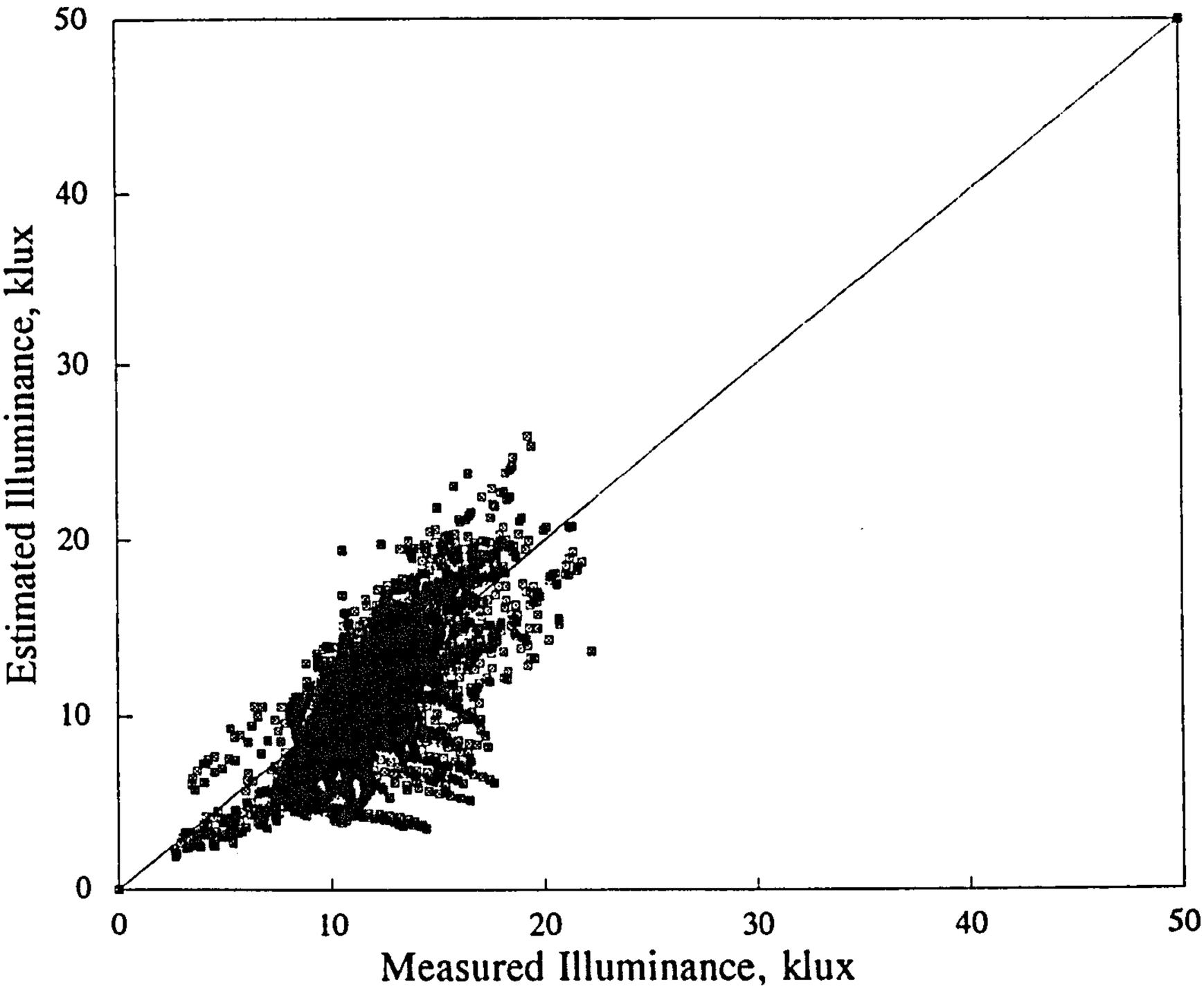

Figure 5.3.13 Athens: Shaded slope illuminance model

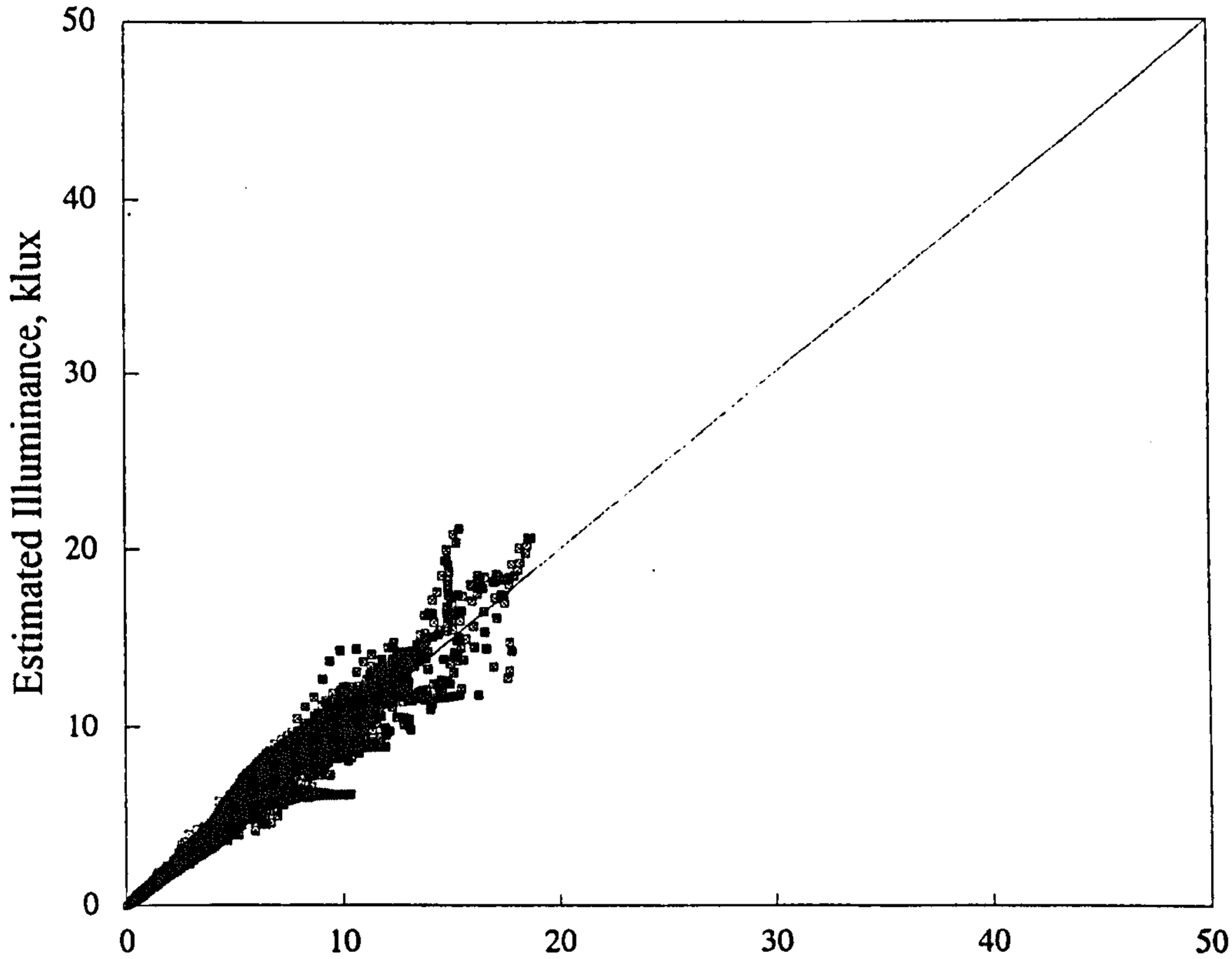

Figure 5.3.14 Japan: Shaded slope illuminance model

regression analysis was performed to produce a simple formula from which illuminance on a shaded sloped surface could be estimated from only horizontal diffuse illuminance values.

In order to produce this equation the ratio of measured vertical illuminance for a shaded surface to measured horizontal diffuse illuminance was calculated for each location and for each season which amounted to a total of over 200,000 data points. Table 5.3.1 shows the results of this comprehensive analysis.

Table 5.3.1 Locational and seasonal variations in the ratio of measured vertical shaded illuminance to measured horizontal diffuse illuminance

Location	Summer	Autumn/Spring	Winter	Annual Average
Edinburgh(Heriot Watt)	0.36	0.392	0.442	0.40
Edinburgh(Napier)	0.425	0.430	0.460	0.44
BRE Watford	0.365	0.395	0.398	0.39
Sheffield	0.40	-	-	0.40
Japan	0.420	0.418	0.443	0.43
Athens	0.479	0.400	0.400	0.43

The results for each location show some differences especially in the case of the summer results for the Watford database which reports a value some 14% lower than the seasonal average. The result for the Athens data is interesting with a large increase shown for the summer in the diffuse illuminance ratio. This may be explained by an increase in measured vertical illuminance for shaded surfaces, due to clear skies possessing a larger intensity of luminance from the horizon decreasing towards the zenith. Athens also has a high instance of clear skies throughout the year, this phenomenon shall be discussed in greater detail in later sections.

Despite the wide variation between sites it is interesting to note that annual averages are very similar with an overall average of 0.42. Hence the formula used to estimate vertical illuminance($\beta = 90°$) on a non sunfacing(shaded) surface is as follows;

$$L_\beta = 0.42\, L_D \qquad 5.13$$

The results for this shaded surface model for each location are given by Figs. 5.3.9 to 5.3.14.

5.4 NON-SHADED SURFACES

The inclination angle determines which category the surface in question falls into, an inclination angle of less than 90° indicates that the surface has a view of the sun. Once this has been established the contribution to the daylight received from the sun and sky quadrant has to be determined. One approach which was adopted by Muneer[5.5] subdivided non-shaded surfaces into 2 categories dependant on cloud cover. The categories were overcast skies and non-overcast skies, an overcast sky was selected by examination of horizontal global and diffuse radiation values such that for;

$$\text{Horizontal Global irradiance - Horizontal Diffuse irradiance} \leq 5\ \text{W/m}^2 \qquad 5.14$$

the sky was deemed to be completely overcast. If this criterion was not satisfied it is assumed that there was significant contribution from the circumsolar region of the sun. The overcast sky approach was investigated to evaluate its application for illuminance estimation purposes, this is dealt with in the following sections.

5.4.1 Overcast skies

On determining that the surface is not in shade it is necessary to ensure it meets with the overcast sky criterion. This was carried out using a similar approach to Muneer's with an overcast sky categorised as having a difference between horizontal global and diffuse illuminance of less than 1000 lux.

To develop a correlation that would allow the illuminance on a sloped surface to be estimated for overcast skies from readily available meteorological data, it was necessary to separate non-shade overcast sky surfaces from the dataset. Once these were identified the illuminance measured on the vertical surfaces were plotted against the horizontal diffuse illuminance for that point in time. Figures 5.4.1 to 5.4.3 demonstrate the correlation between the illuminance received on a sloped surface under overcast conditions and measured horizontal diffuse illuminance. These graphs show a clear dependence on horizontal diffuse illuminance from which a regression between the two quantities was calculated. The results of this regression analysis produced an algorithm given by equation 5.15.

$$L_\beta = 0.60\ L_D \qquad 5.15$$

This algorithm was then applied to the dataset to predict vertical surface illuminance with figures 5.4.4 - 5.4.6 showing the results, which proved to be most encouraging.

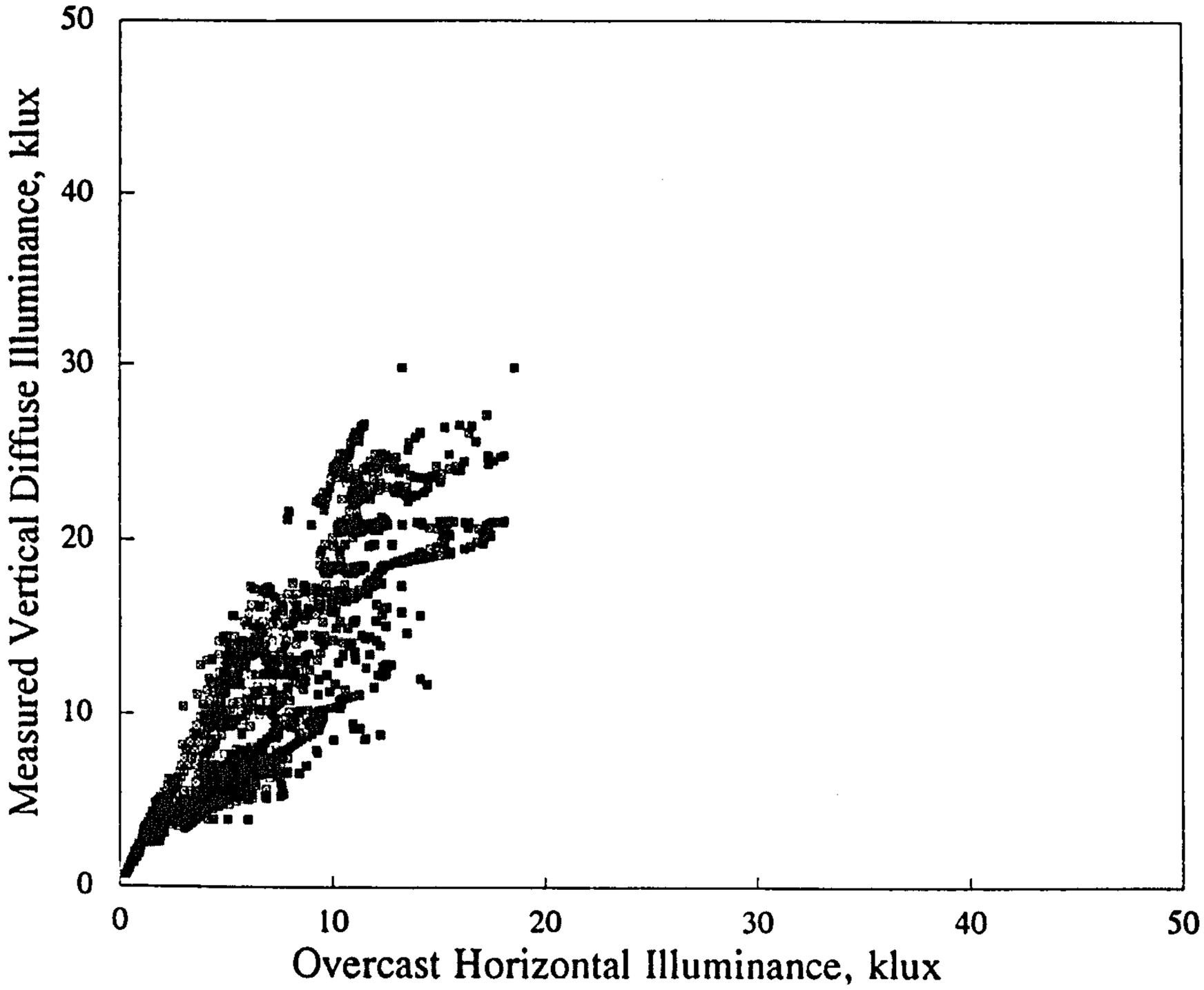

Figure 5.4.1 BRE: Overcast data

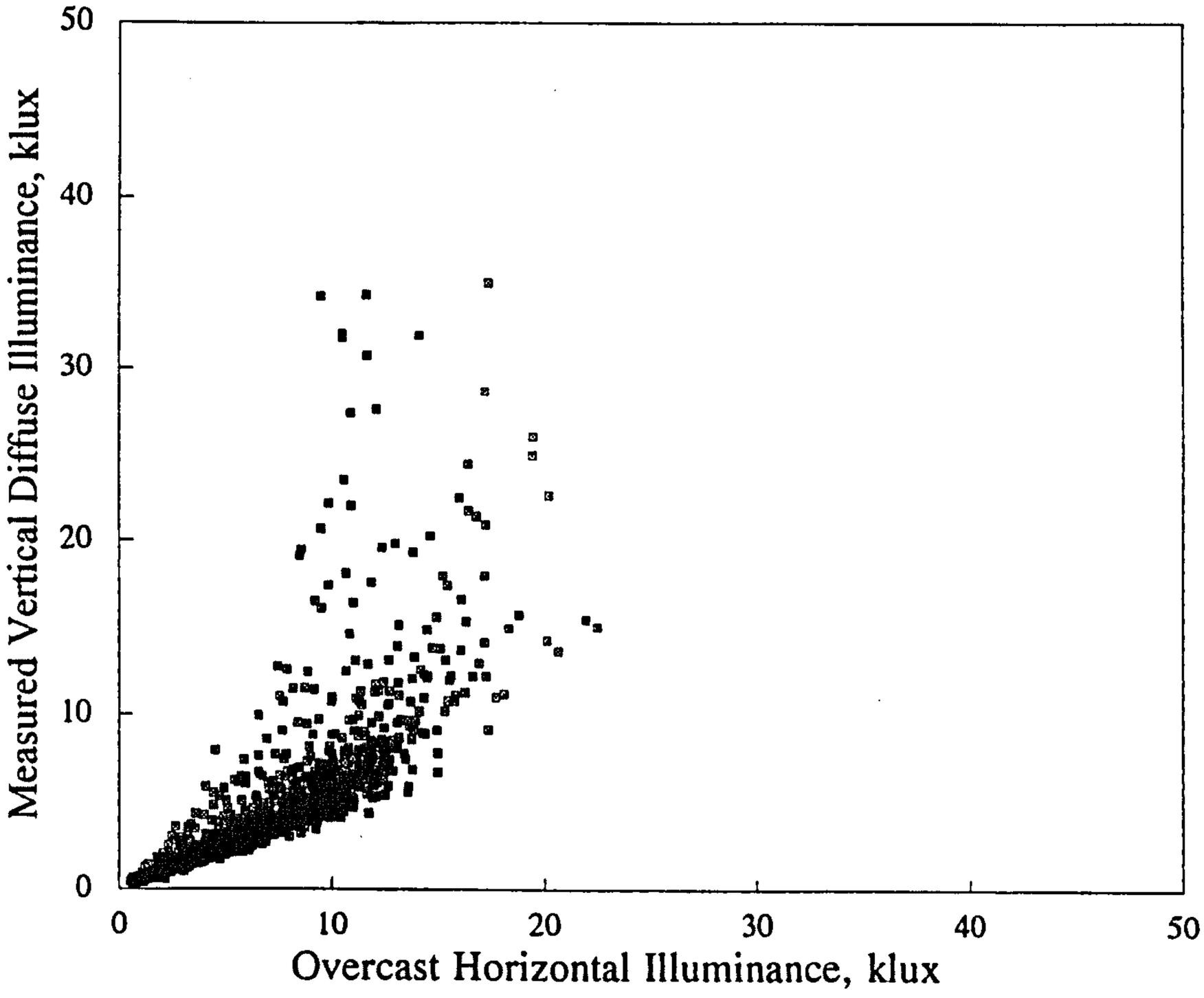

Figure 5.4.2 Heriot Watt: Overcast data

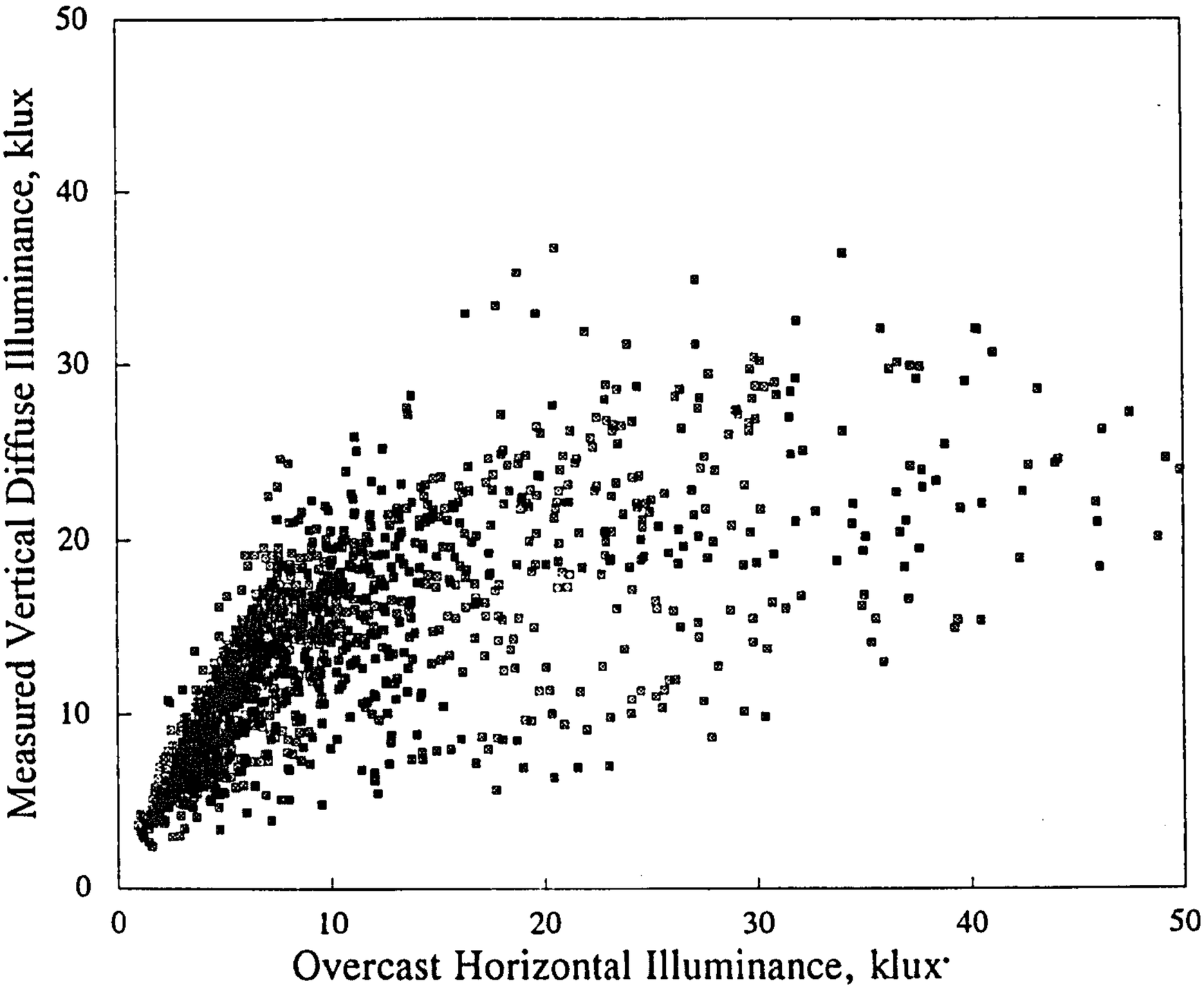

Figure 5.4.3 Athens: Overcast data

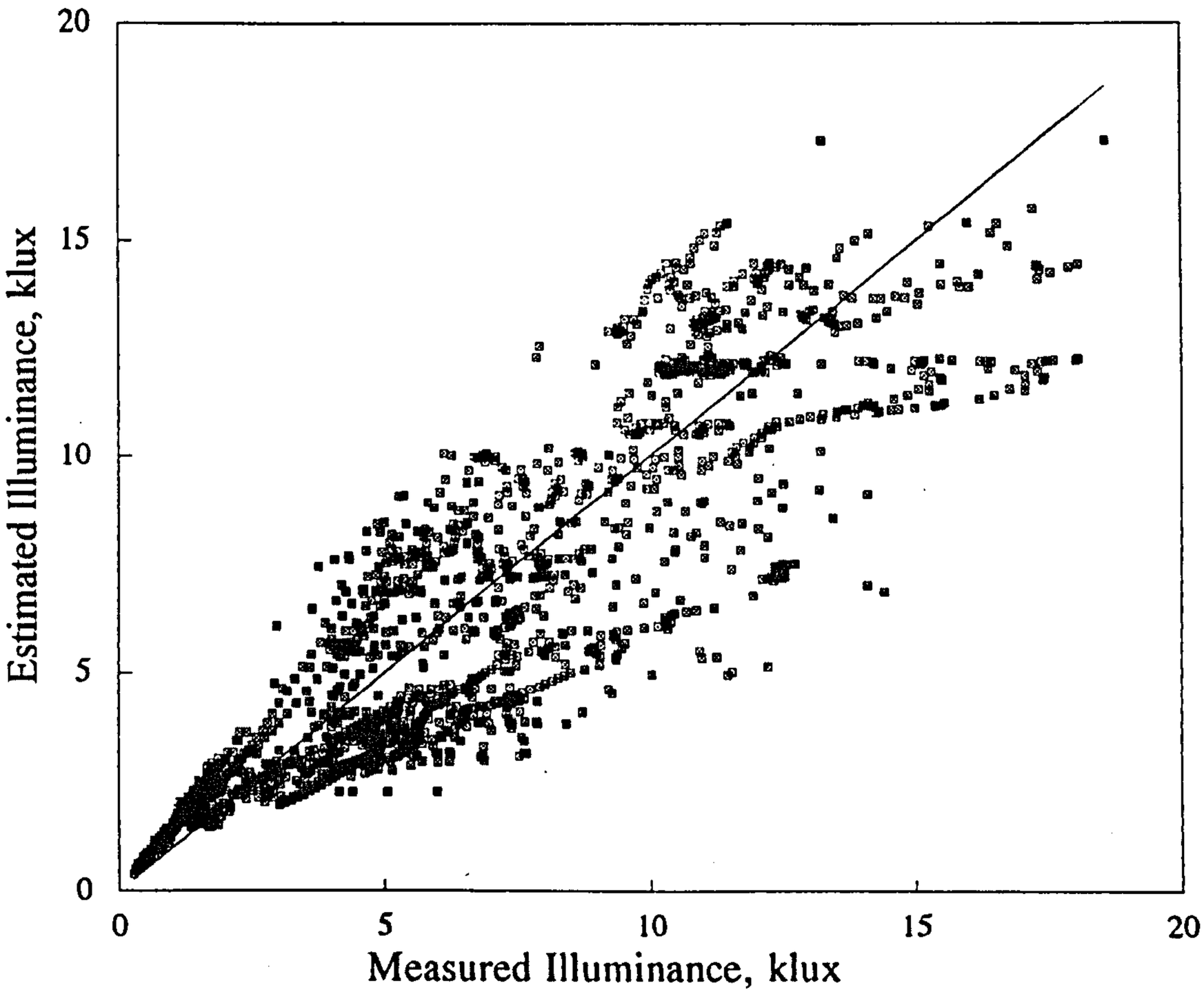

Figure 5.4.4 BRE: Overcast slope illuminance model

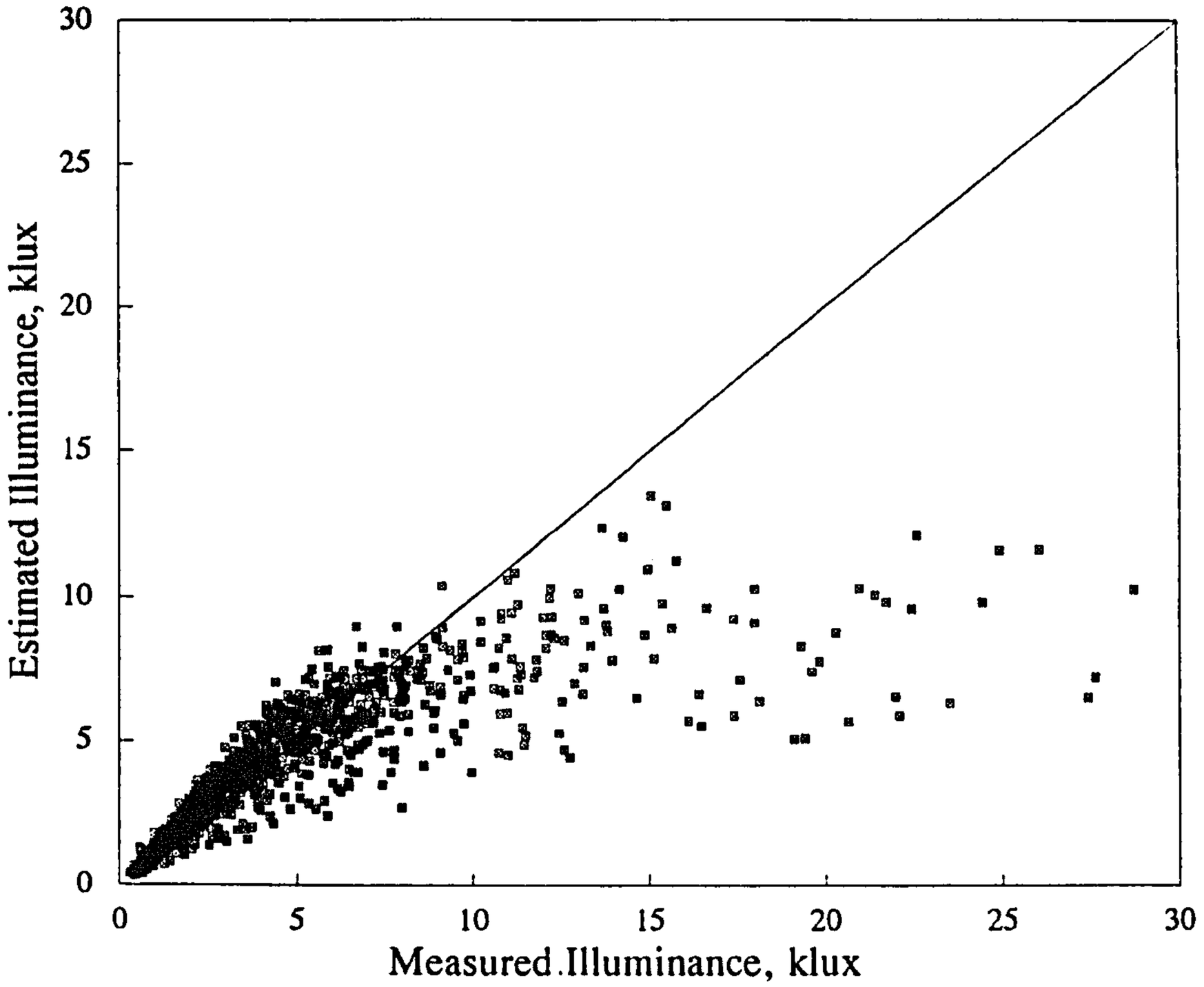

Figure 5.4.5 Heriot Watt: Overcast Illuminance model

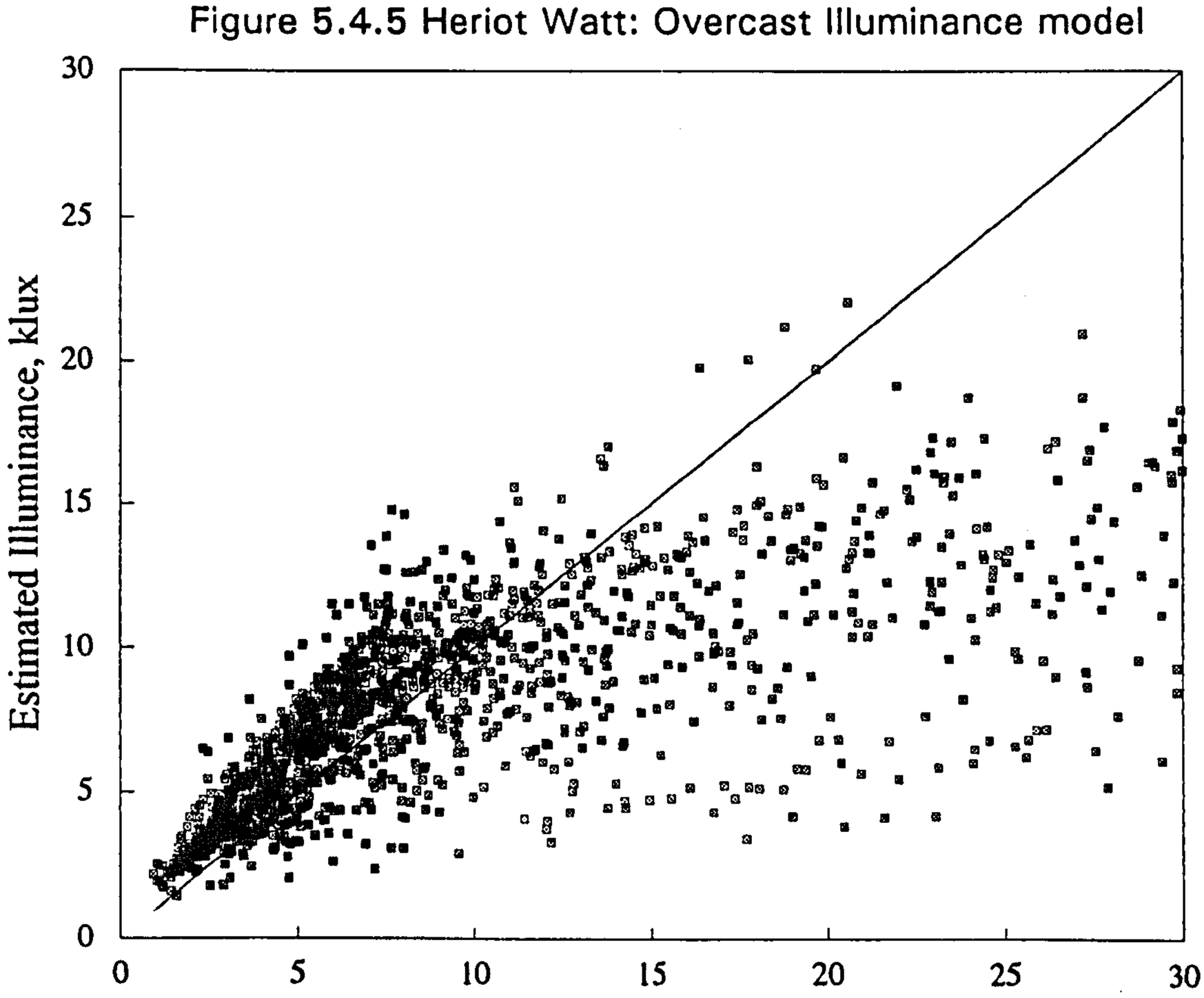

Figure 5.4.6 Athens: Overcast Illuminance model

5.4.2 Slope illuminance for all sky conditions

The total sky illuminance received by a sloped surface comprises of light from 3 sources. The contribution from these sources to the illuminance is dependent on the sky clearness index either directly or indirectly. These components combine to produce an overall estimation of slope illuminance. These components are, beam or direct illuminance, circumsolar illuminance and an anisotropic background diffuse component. The beam component which was introduced in chapter 4 is related indirectly to F (4.2.10) as the definition of beam illuminance makes reference to the difference between LG and L_D which also forms the basis of the sky clearness index. The circumsolar component is employed to account for the bright aura surrounding the sun which can best be seen during thin overcast conditions where the sun is obscured bar the bright disc surrounding its position.

The anisotropic background diffuse component accounts for the illuminance a surface receives from the sky quadrant it faces. This quantity is highly variable and is of prime importance to the proposed model's structure as shall be demonstrated in the following sections of this chapter. The use of a background diffuse component has been employed by several authors[5.6-5.10] in irradiance and illuminance work. However the approach adopted in this research uses for the first time an anisotropic background diffuse component which more accurately defines the changes in the illuminance of the sky quadrant for all sky conditions.

The proposed model's formulation as described earlier is divided into two cases, surfaces in shade and sunfacing. The shaded surface has been dealt with under section 5.3.3 where slope illuminance is defined solely as a function of horizontal diffuse illuminance by Eq. 5.13. In the case of sunfacing surfaces the total illuminance received on a sloped surface can be calculated from equation 5.16:

$$L_\beta = (LG - L_D)(\cos i/\sin \gamma s) + L_D[(1 - F)TF] + L_D[F(\cos i/\sin \gamma s)] \qquad 5.16$$

beam background diffuse circumsolar

The first term to the right of equality sign is the beam component, the second is the anisotropic background diffuse component with the circumsolar component being the last term. TF is defined as the tilt factor as given by equation 5.17:

$$TF = \{\cos^2(\beta/2) + [2b/\pi(3 + 2b)] \times (\sin(\beta) - \beta\cos(\beta) - \pi\sin^2(\beta/2))\} \qquad 5.17$$

where β is the angle of the slope from the horizontal. The term 'b' is known as the radiance distribution index, a term first introduced by Moon and Spencer[5.6] primarily to define the luminance distribution of overcast skies and has been used in radiation work since[5.5,5.7 & 5.11]. The Moon and Spencer model and the isotropic slope illuminance model shall be discussed and evaluated later in this chapter. As an indication of its application in the proposed model the value of 'b' varies with different sky conditions, Moon and Spencer reported a 'b' value of 2 for an overcast sky whilst a uniform sky would have a value of b equal to zero.

Equation 5.17 allows for the changes in sky luminance distribution through its ability to accommodate variable values of b. This variability is controlled by the clearness index F and is described as a function of F for the calculation of the background diffuse component.

This function is calculated from measured data through the use of Eqs. 5.16 and 5.17. The purpose is to separate TF from the proposed model;

$$Lds = L_\beta - (LG - L_D)(\cos i/\sin \gamma s) \qquad 5.18$$

$$L_D x TF\,(1 - F) = Lds - L_D x F(\cos i/\sin \gamma s) \qquad 5.19$$

$$TF = \frac{\frac{Lds}{L_D} - \frac{F\cos i}{\sin \gamma s}}{(1-F)} \qquad 5.20$$

TF as calculated from measured data by Eq.5.20 was then plotted against F to examine the relationship between the background diffuse illuminance and the clearness index.

To this end the BRE (1984) dataset were divided into the Summer, Winter and Autumn/Spring months and the raw data were plotted against F to produce figures 5.4.7a, b & c. The data for each season were averaged across the range of clearness index to produce the following equations;

Summer:

$$2b/\pi(3 + 2b) = 0.13F - 2.06F^2 \qquad 5.21$$

Autumn/Spring:

$$2b/\pi(3 + 2b) = 0 \qquad 5.22$$

Winter:

$$2b/\pi(3 + 2b) = -0.25F + 2.06F^2 \qquad 5.23$$

With one of the aims of this research being to produce a slope illuminance model for the United Kingdom and further afield it was necessary to examine this variation of background diffuse illuminance with clearness index for a variety of sites. Data from the 6 sites were collected and processed to produce the same graphs shown by figures 5.4.8 to 5.4.13. Appendix 5.3 details the proposed models development.

The first noteworthy point is that the curves are not susceptible to season variations as was observed with the BRE (1984) data. The seasonal approach adopted in the first instance was found to be of little benefit to the 6 sites and has been abandoned hereafter in favour of a single site curve. This discovery raised concern over the original processing of the BRE (1984) data as the 1992 data failed to exhibit the same seasonal trends. However, a second attempt with the given dataset produced identical results. One possible explanation may be that 1984 was a particularly freak year.
The background diffuse versus 'F' data were once again averaged to produce site equations given in Table 5.4.1.

Table 5.4.1 Background diffuse illuminance curves for various locations

Site Location	**Background curves** $[2b/\pi(3 + 2b)] =$	**Equation number**
Napier University	$0.75F - 6.75F^2$	5.24
Heriot Watt University	$0.125F - 4.356F^2$	5.25
Sheffield University	$-0.579F - 0.683F^2$	5.26
BRE Watford	$-2.245F + 1.112F^2$	5.27
NOA Athens	$-0.57F$	5.28
Japan (Kyushu University, Fukuoka)	$0.088F - 6.95F^2$	5.29

This information is extremely useful in looking for similarities and patterns between the 6 sites. The first and most obvious trend would be a latitude related variation. The table is listed in latitudinal order(with the actual latitudes given in Table 3.2.1) and to aid its interpretation the curves against F are presented graphically in figure 5.4.14.

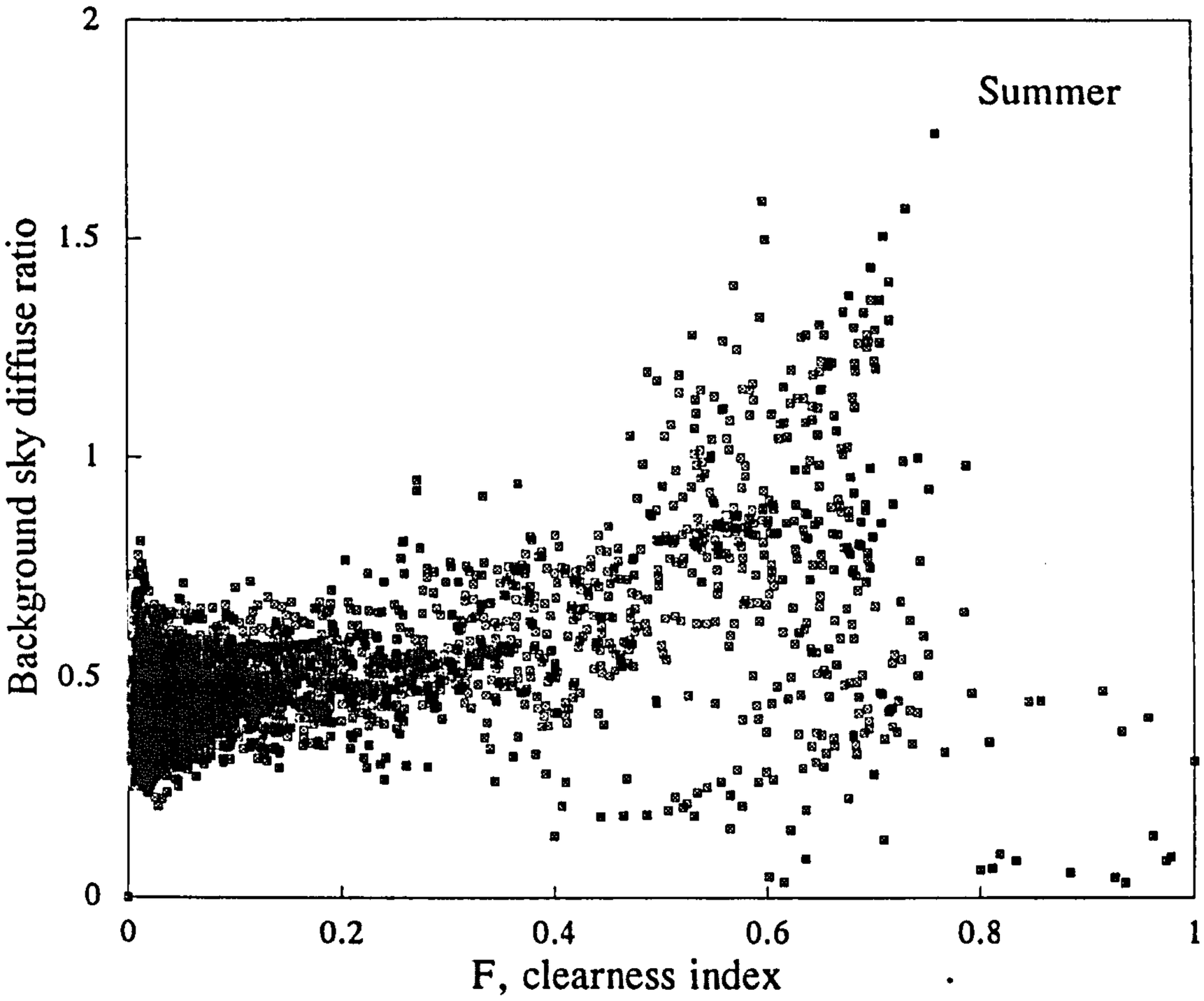

Figure 5.4.7a Summer background sky diffuse curves

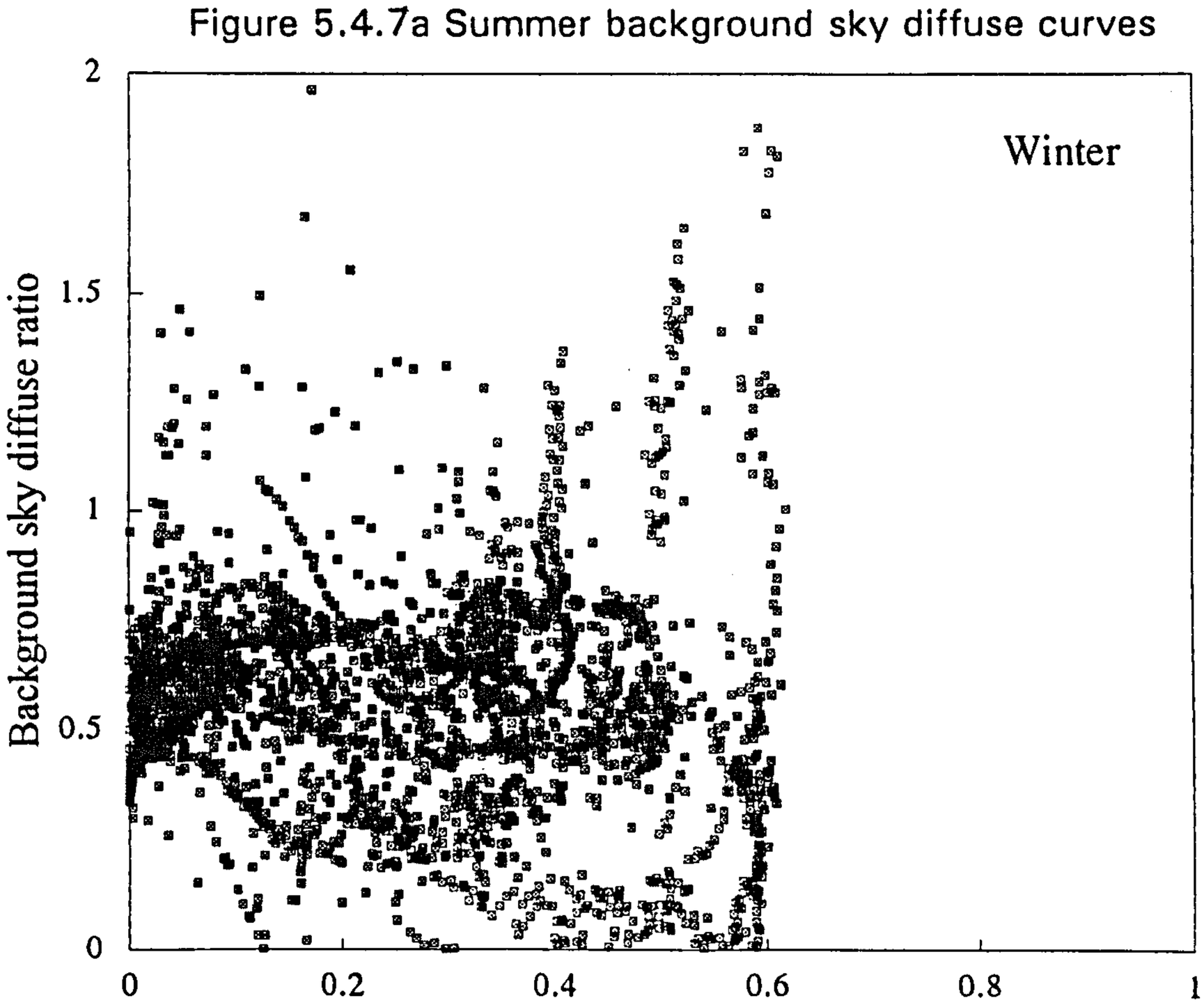

Figure 5.4.7b Winter background sky diffuse curves

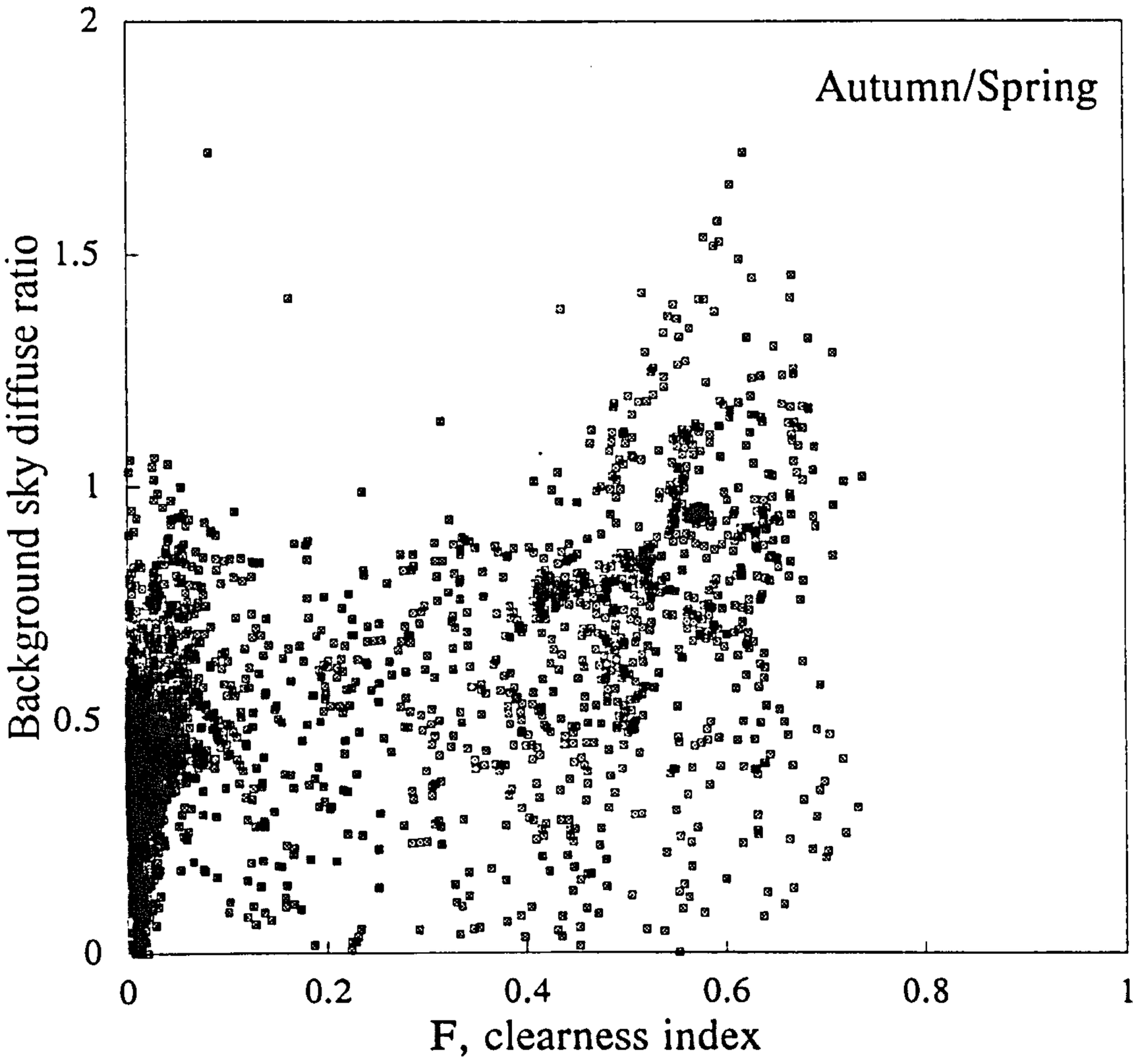

Figure 5.4.7c Autumn/spring background sky diffuse curves

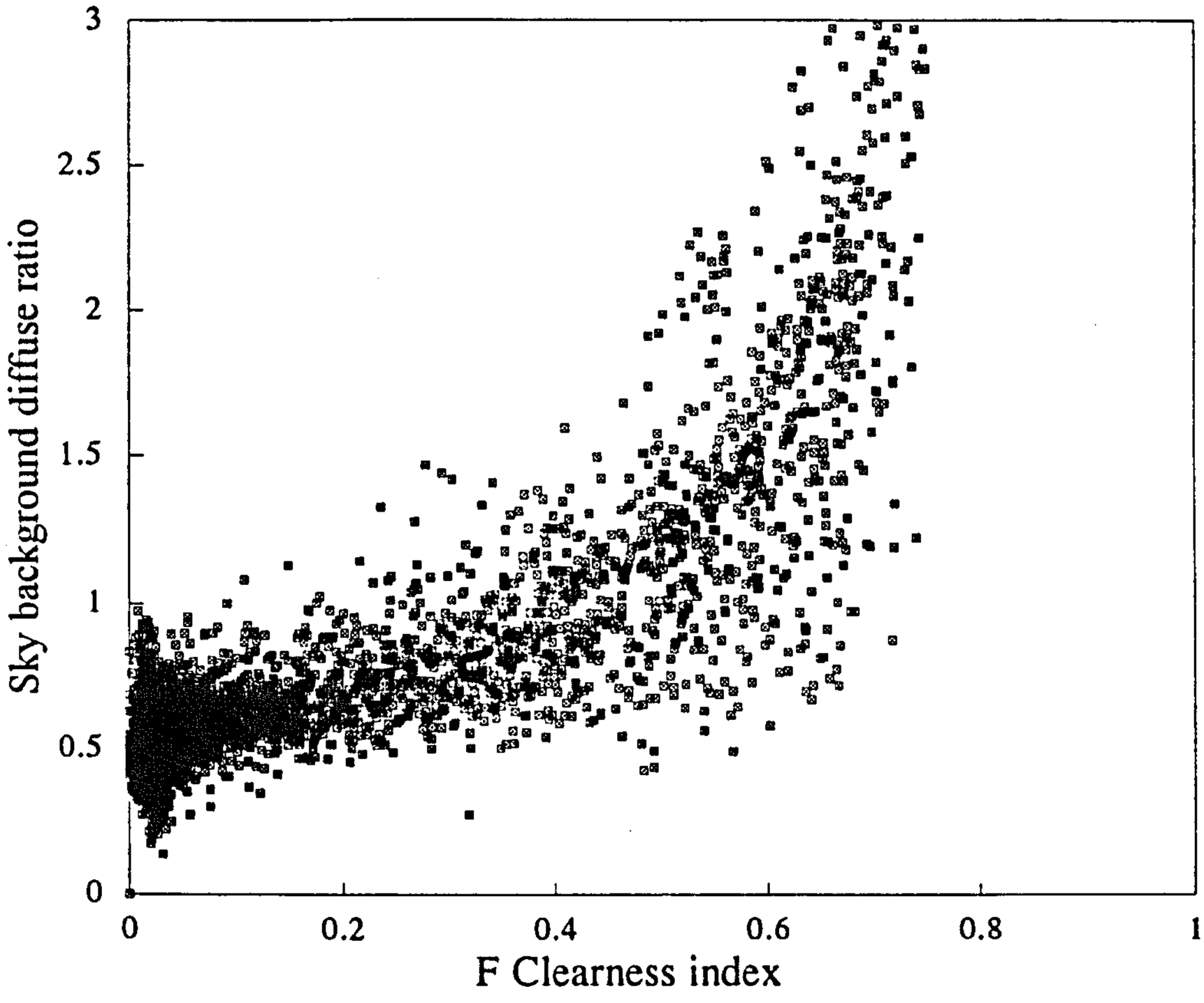

Figure 5.4.8 Napier: Sky background diffuse ratio against F

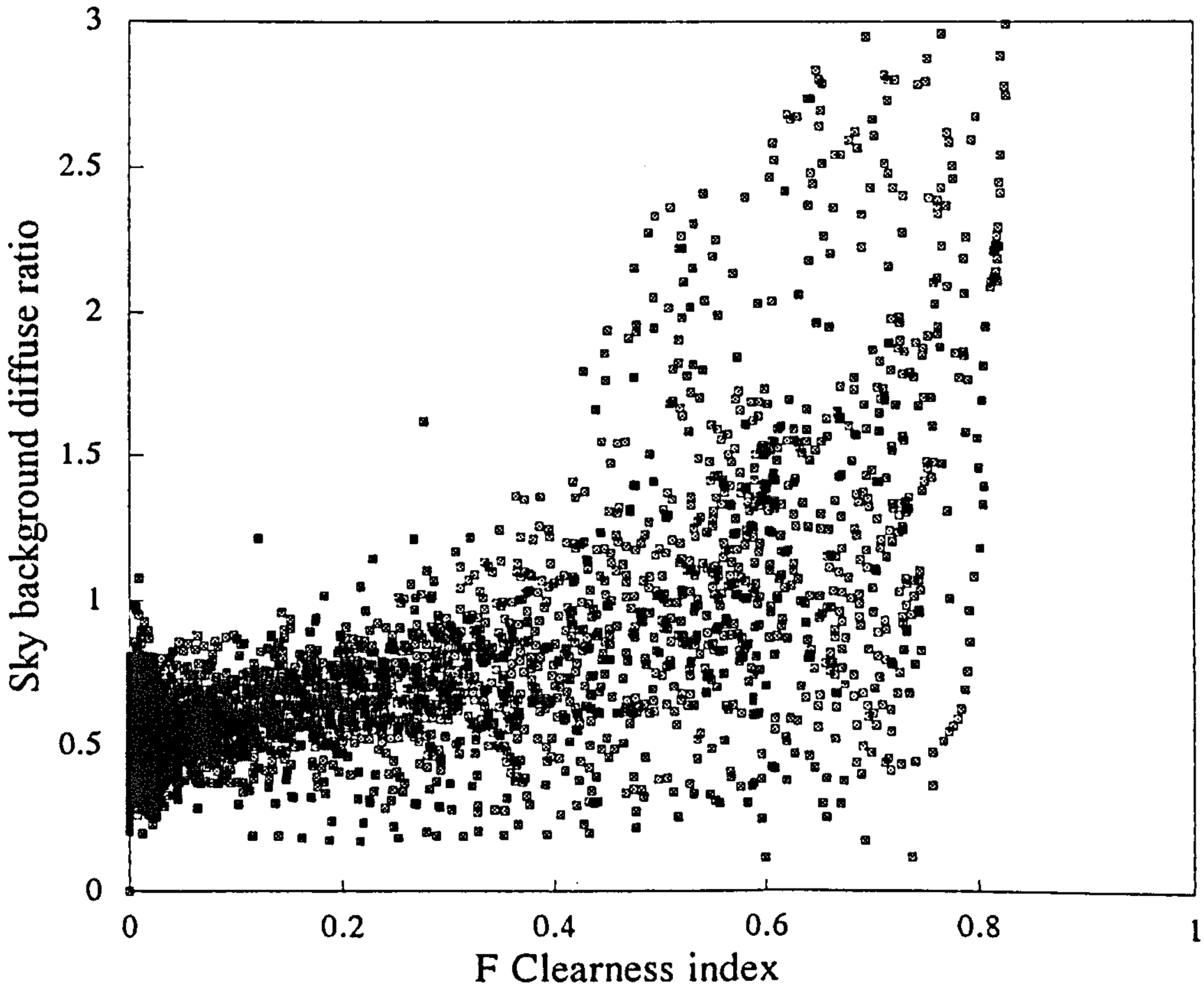

Figure 5.4.9 Heriot Watt: Sky background diffuse ratio against F

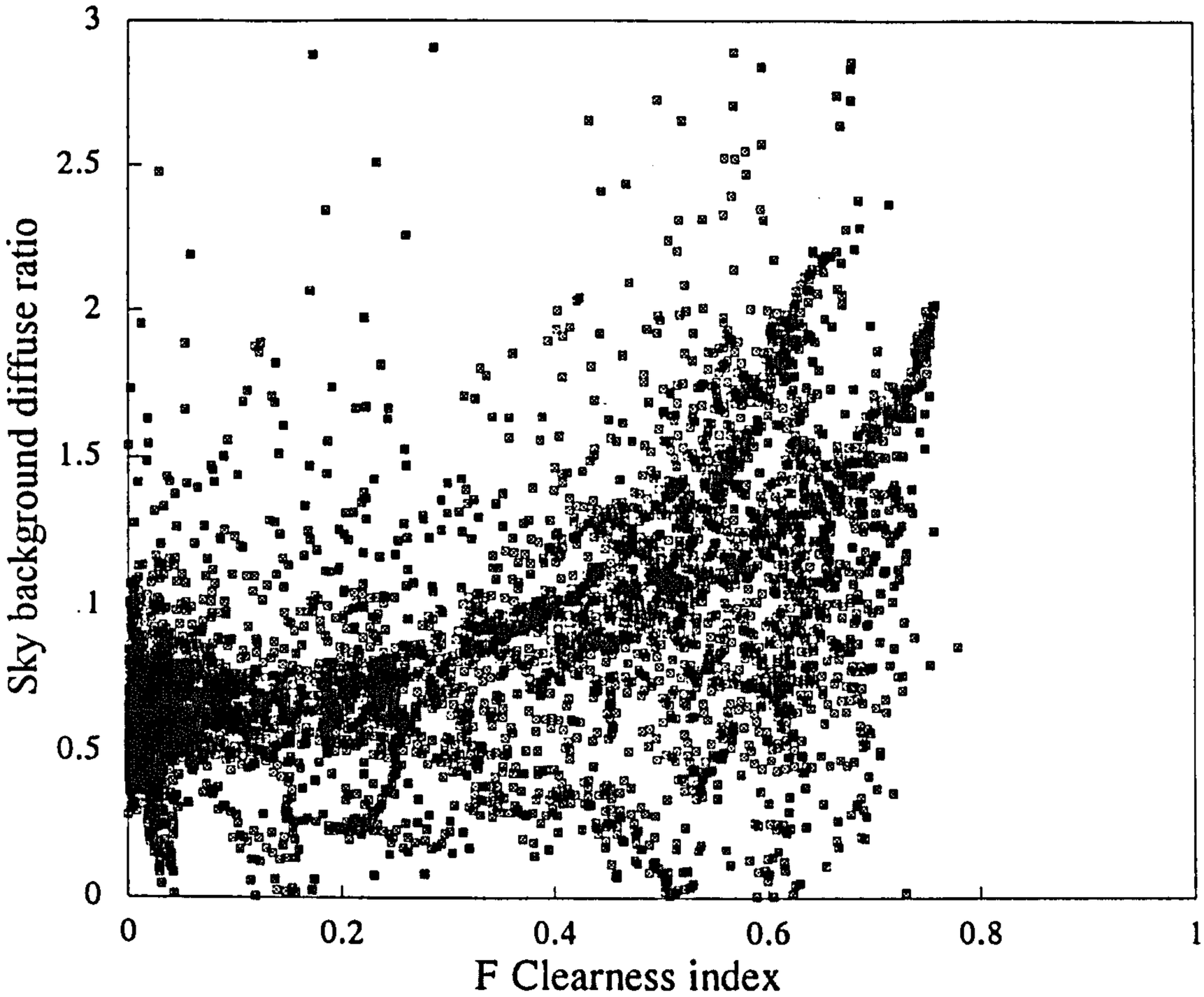

Figure 5.4.10 Sheffield: Sky background diffuse ratio against F

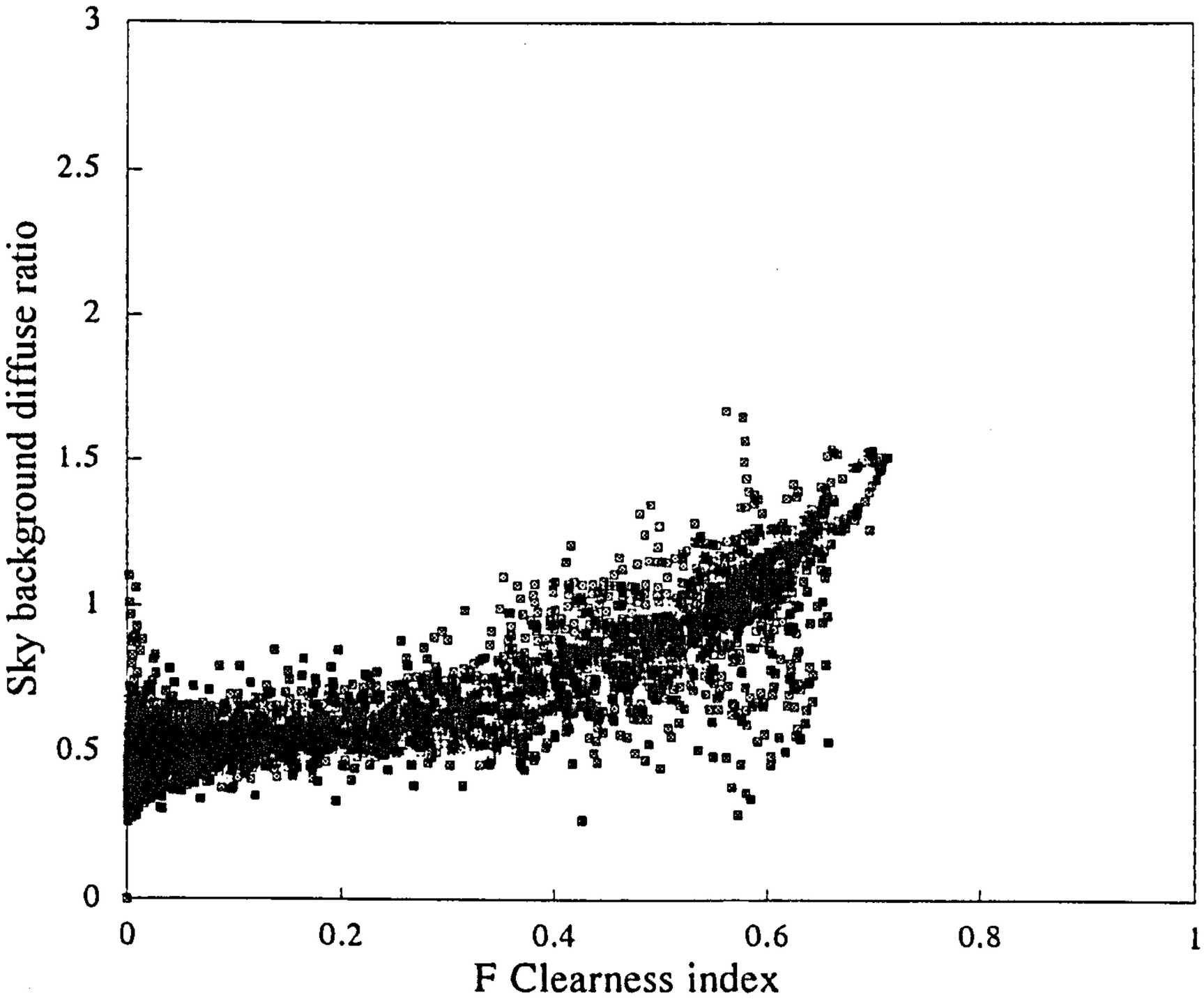

Figure 5.4.11 BRE: Sky background diffuse ratio against F

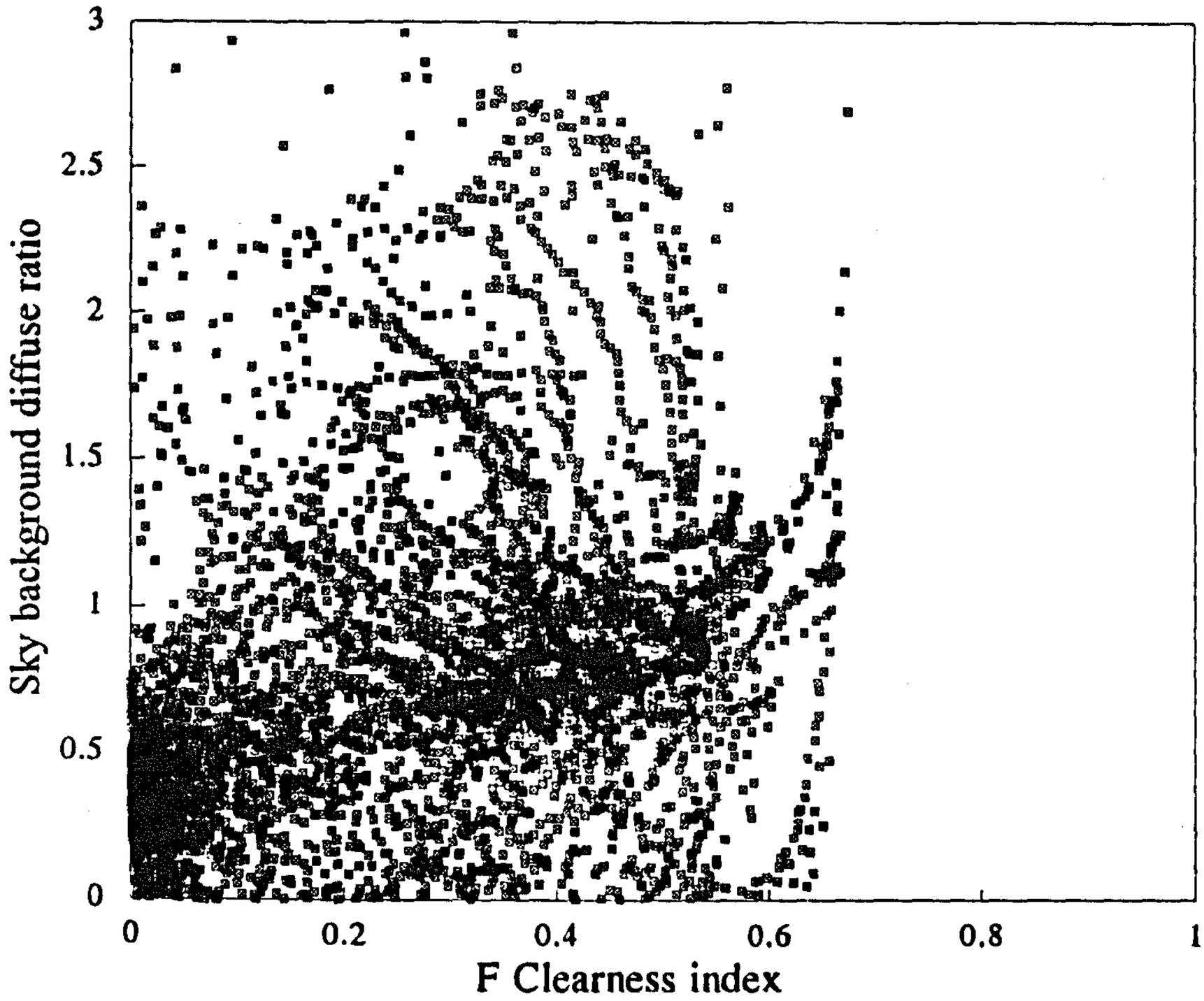

Figure 5.4.12 Athens: Sky background diffuse ratio against F

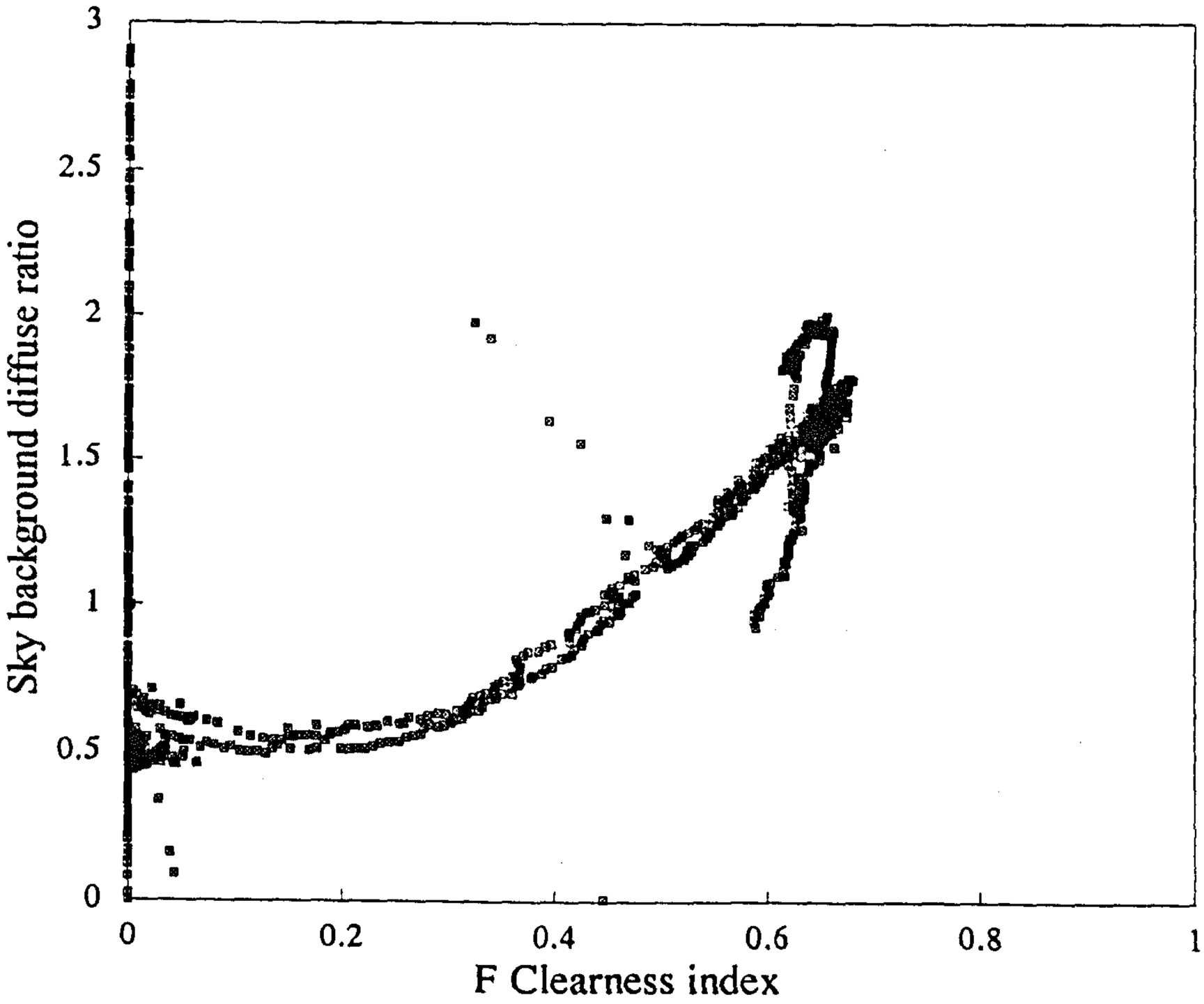

Figure 5.4.13 Japan: Sky background diffuse ratio against F

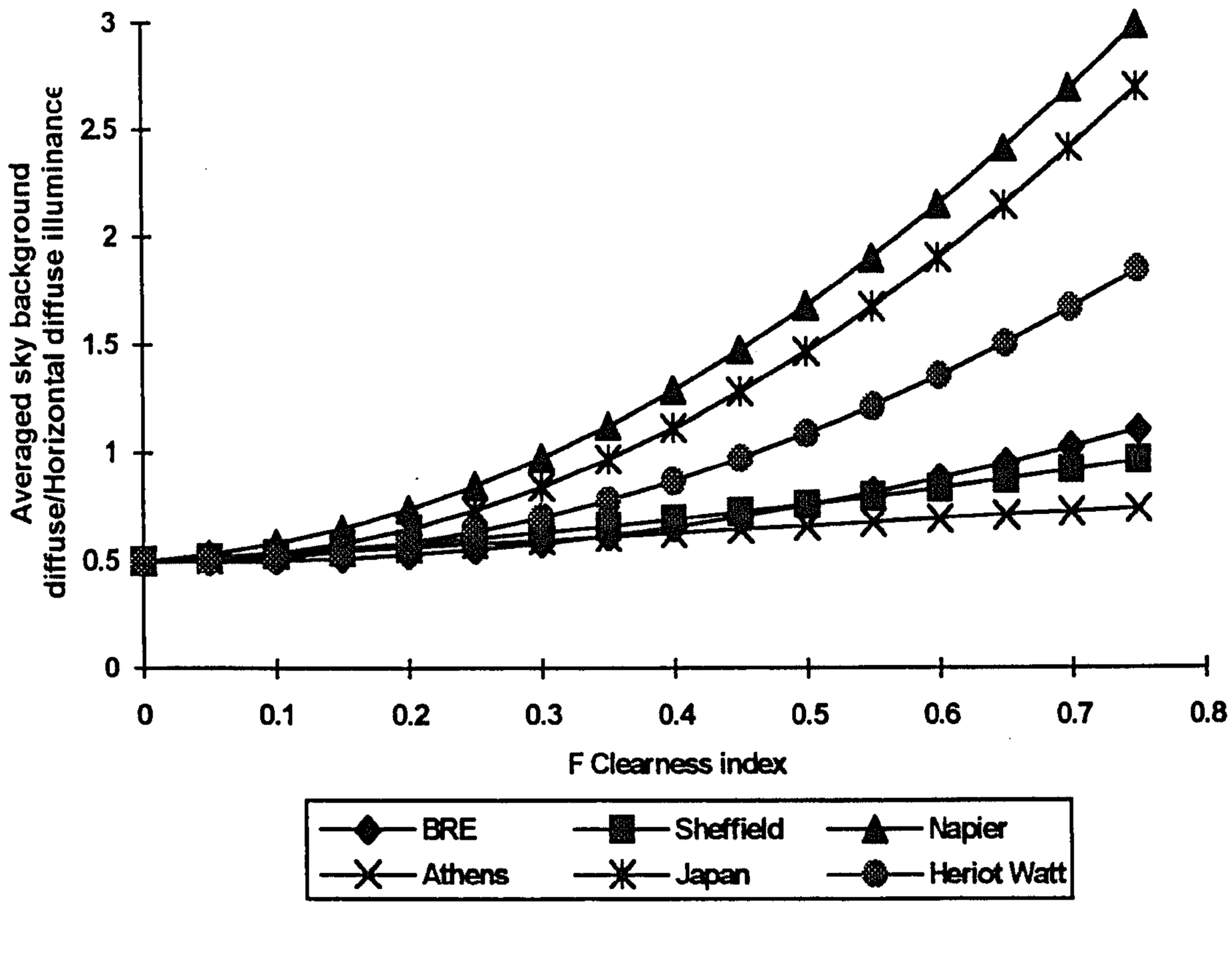

Figure 5.4.14 Background sky diffuse ratio versus F for various locations

To some extent there would appear to be a latitudinal dependence especially if the Japanese curve is ignored. However one could have expected the BRE and Sheffield curves to be separated by a greater margin, with the Sheffield curve above that of the BRE. It is also interesting to note the significant difference between the two Edinburgh sites. This leads to the likely explanation of atmospheric conditions influencing the luminance distribution.

If the atmospheres of the sites are considered then it is reasonable to assume that cleaner atmospheres would have higher curves indicating an increased contribution to slope illuminance from the sky background. Athens atmosphere is renowned for its turbidity and traffic generated air pollution, taking this into account it is understandable that its background curve has a flat linear profile.

At this stage it is possible to explain the high luminous efficacy values for the Athens site. A parallel study into the solar radiation climate of Athens[5.12] discovered that the sky background diffuse ratio fell rather than rose as with the illuminance curves.

This indicates that solar radiation is being absorbed by the atmosphere hence the luminous efficacy would be high especially on clear turbid days. Figure 5.4.15 shows the Athens irradiance data and its drooping trend.

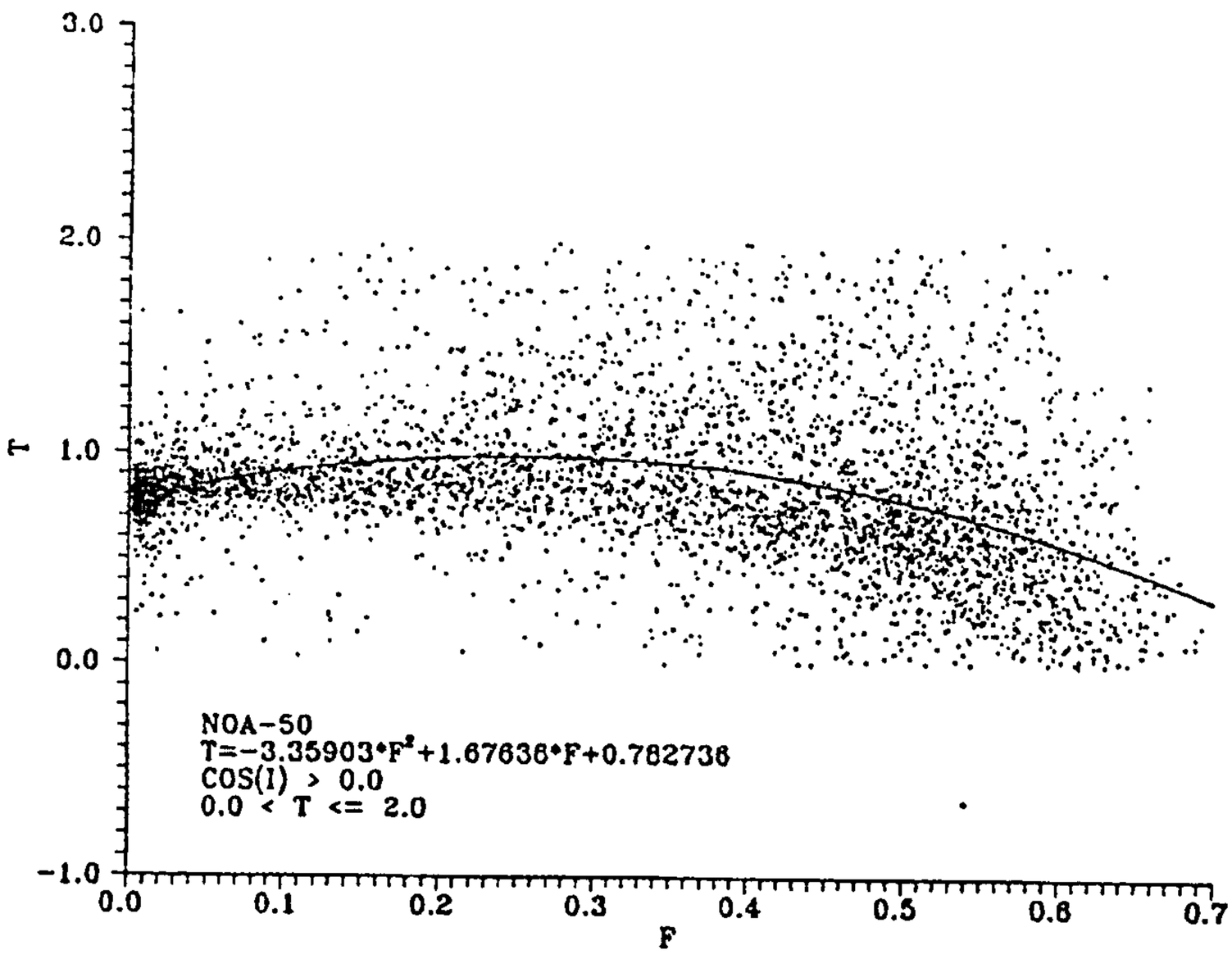

Figure 5.4.15 Background sky diffuse irradiance versus sky clearness[5.12]

The BRE site is situated only 400 metres east of the M1 motorway and encompassed by the M25, the largest ringroad in Europe. The Garston site is some 30 km Northwest of central London, this may also account for its low lying curve with traffic related pollution generating air borne particles.

Sheffield is situated in the central industrial belt of the UK where heavy industry has been traditionally located, this may well lead to higher instances of pollution and as with the BRE site, explain its similarly lower flat curve. It has to be noted that the 4 months of Sheffield data were all recorded in summer months but as seasonal variations in the remaining datasets have been deemed as negligible it is likely that this is a good reflection of the Sheffield areas microclimate.

The Japanese site has a constantly increasing curve very close to that of the Napier site, indicating a relatively clear clean atmosphere. The site itself is surrounded by hills and low mountains on one side and otherwise faces a suburban landscape.

The Napier and Heriot Watt sites themselves have been part of a more in-depth microclimate study with simultaneous measurements of solar radiation and illuminance being recorded at control stations operated separately. The background sky diffuse curves demonstrate some divergence suggesting each site has its own microclimate characteristics. The independent control stations show quite clearly via figure 5.4.16 a & b the differences in quantities of measured illuminance and irradiance. The Napier site receives on an average 9% more illuminance and 9.5% more irradiation compared to the Heriot Watt site. This is well above any differences that may be expected as a result of equipment sensitivity and error, furthermore the sensors employed were of 1st class WRO quality(see appendix 2.2). This would suggest that microclimate variations between the two sites are responsible for the illumination and irradiation differences experienced and the contrast between the background diffuse curves. Although the distances between the two sites is less than 5 miles, this microclimate difference has been observed elsewhere, specifically at a measurement site on the outskirts of Athens overlooking the city[5.13]. This conclusion is further qualified by earlier work carried out by Monteith[5.14] who discovered that local differences between two closely situated solar radiation stations in Wales resulted in considerable variations in short-wave energy measurements.

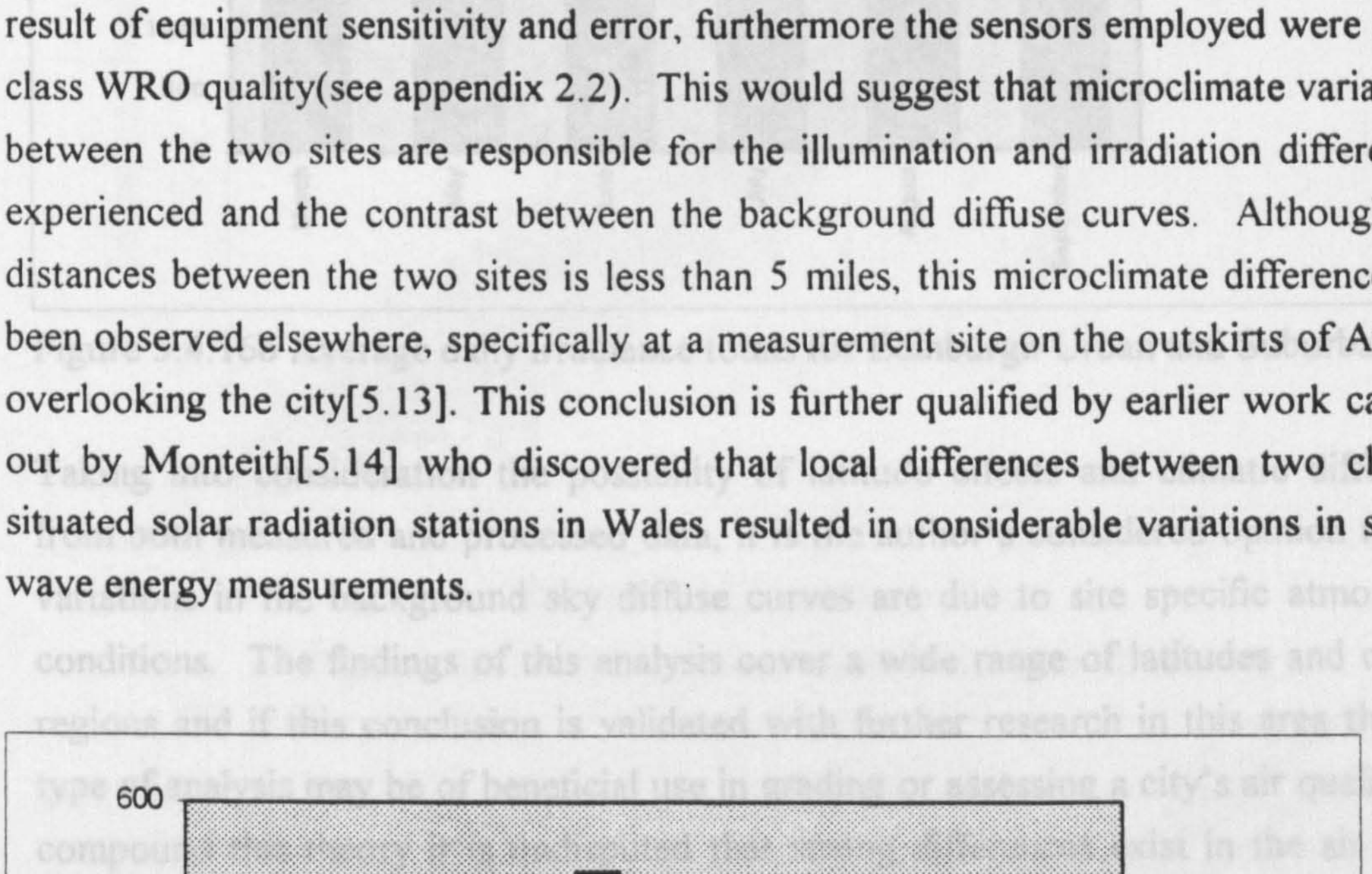

Figure 5.4.16a Average daily illumination totals for Edinburgh Urban and Suburban sites

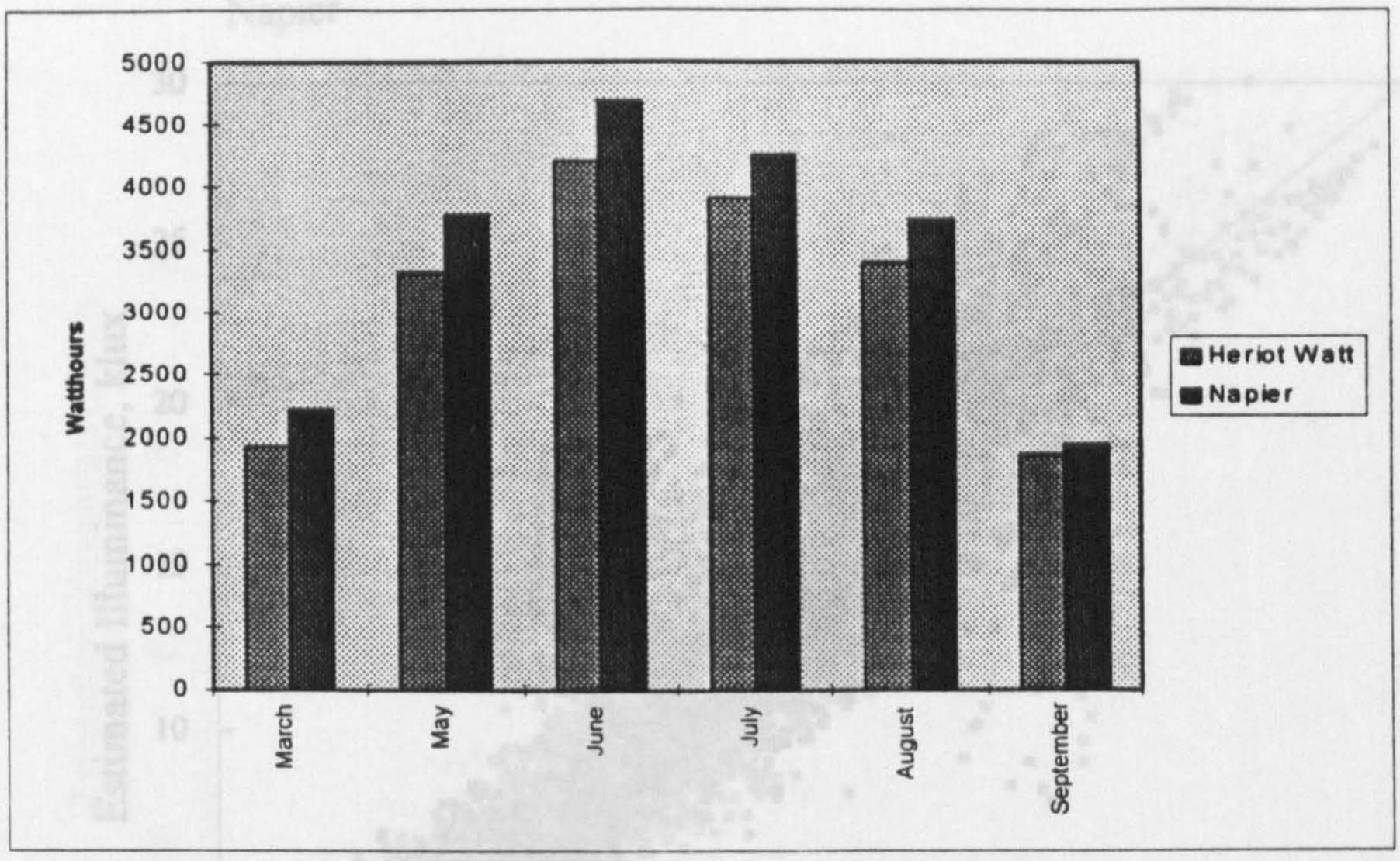

Figure 5.4.16b Average daily irradiance totals for Edinburgh Urban and Suburban sites

Taking into consideration the possibility of latitude effects and climatic differences from both measured and processed data, it is the author's considered opinion that the variations in the background sky diffuse curves are due to site specific atmospheric conditions. The findings of this analysis cover a wide range of latitudes and climatic regions and if this conclusion is validated with further research in this area then this type of analysis may be of beneficial use in grading or assessing a city's air quality. To compound this theory it is undisputed that strong differences exist in the air quality between Athens and Edinburgh. An examination of Fig.5.4.15 demonstrates this point to good effect.

The curves for each site were fitted using over 40,000 data points covering all seasons. The equations for these curves could then be placed into Eq.5.17 replacing as stated the terms in the square brackets. From this stage forth the measured horizontal global and diffuse illuminance values along with the solar geometry are applied to Eq.5.16 to predict the slope illuminance.

The proposed slope illuminance model has been presented for all sky conditions. The results for each of the sites are shown in Figs. 5.4.17 to 5.4.22 displaying one seasons results for four sloped surfaces. The remaining plots for the six sites are given in Appendix 5.4.

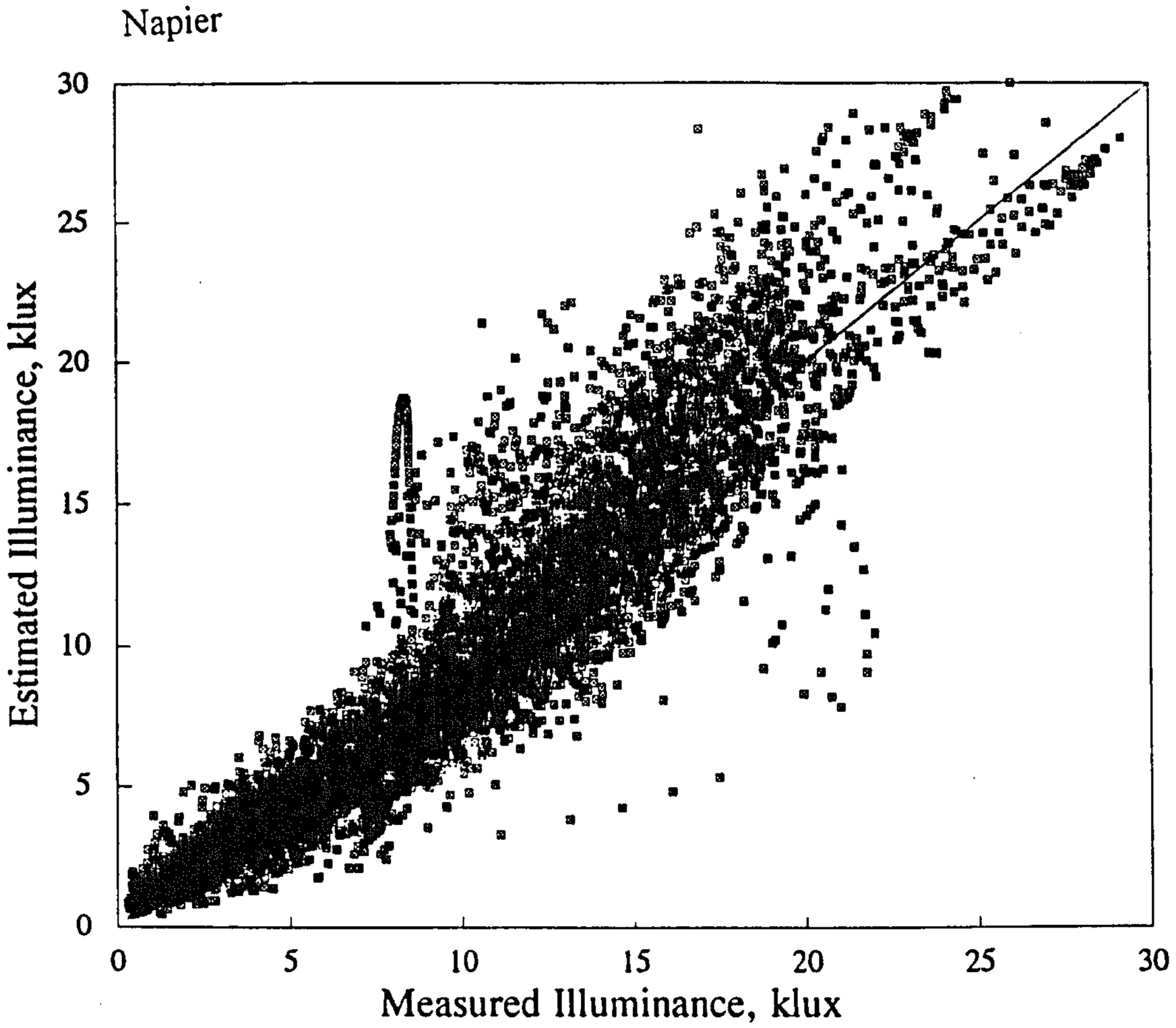

Figure 5.4.17a Summer: North surface illuminance

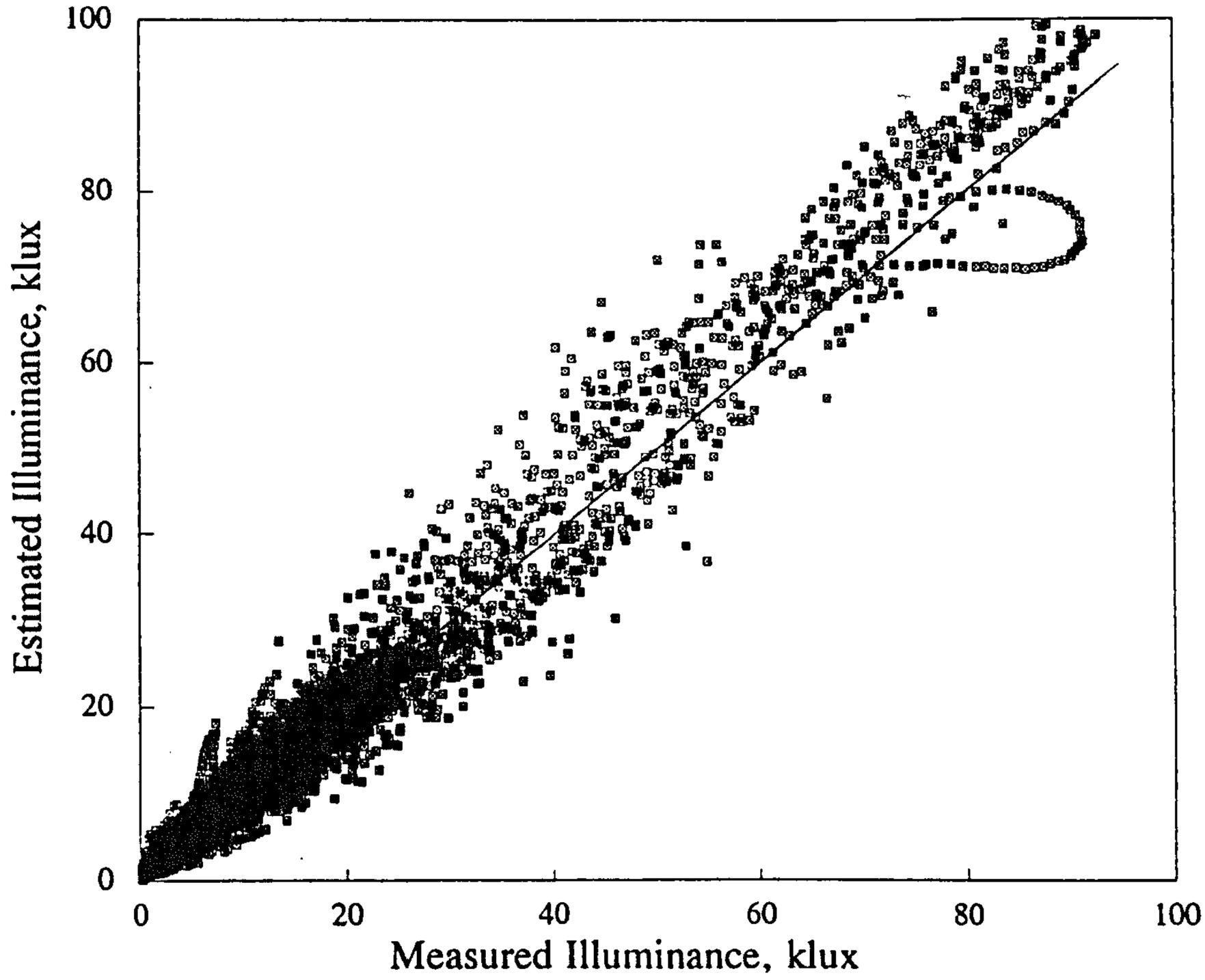

Figure 5.4.17b Summer: East surface illuminance

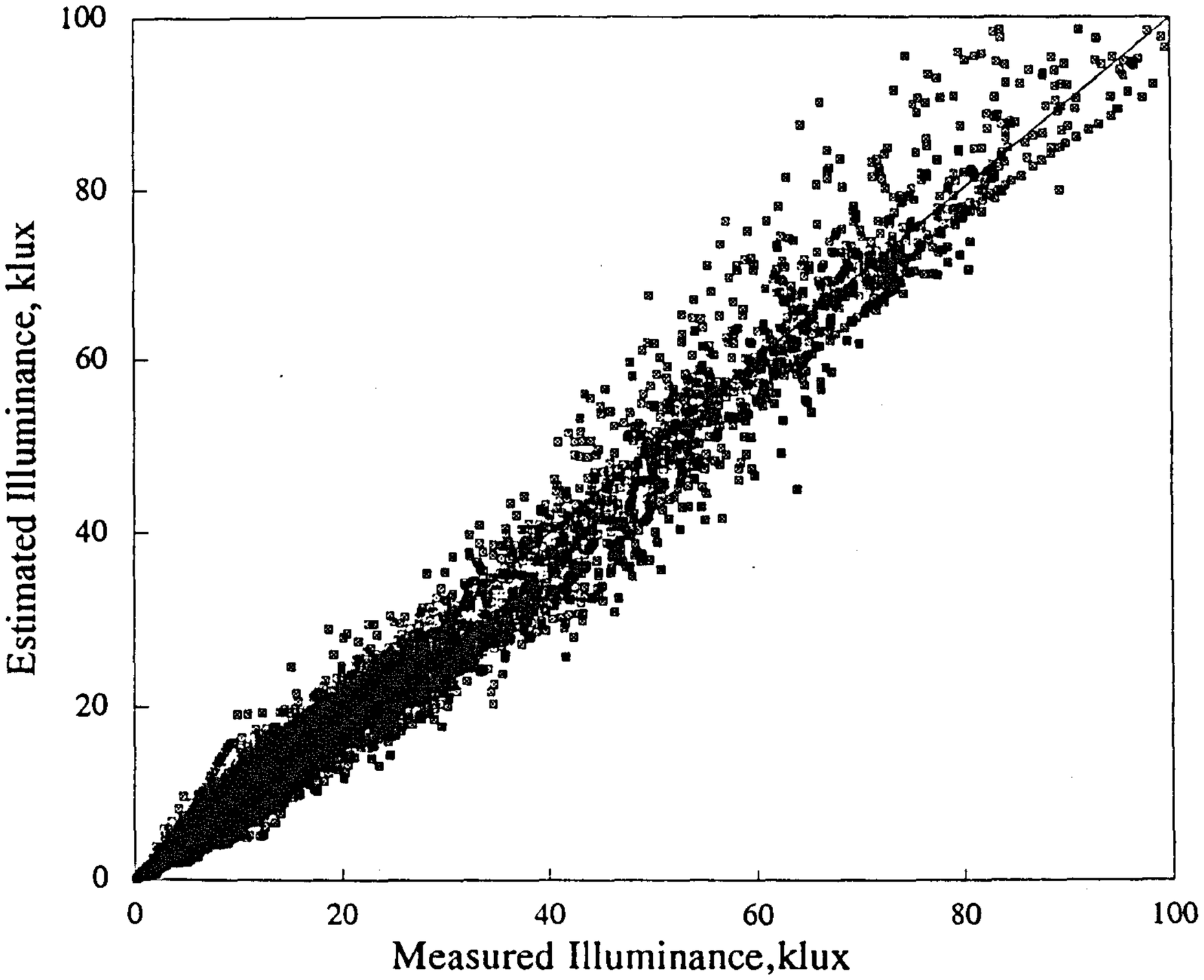

Figure 5.4.17c Summer: South surface illuminance

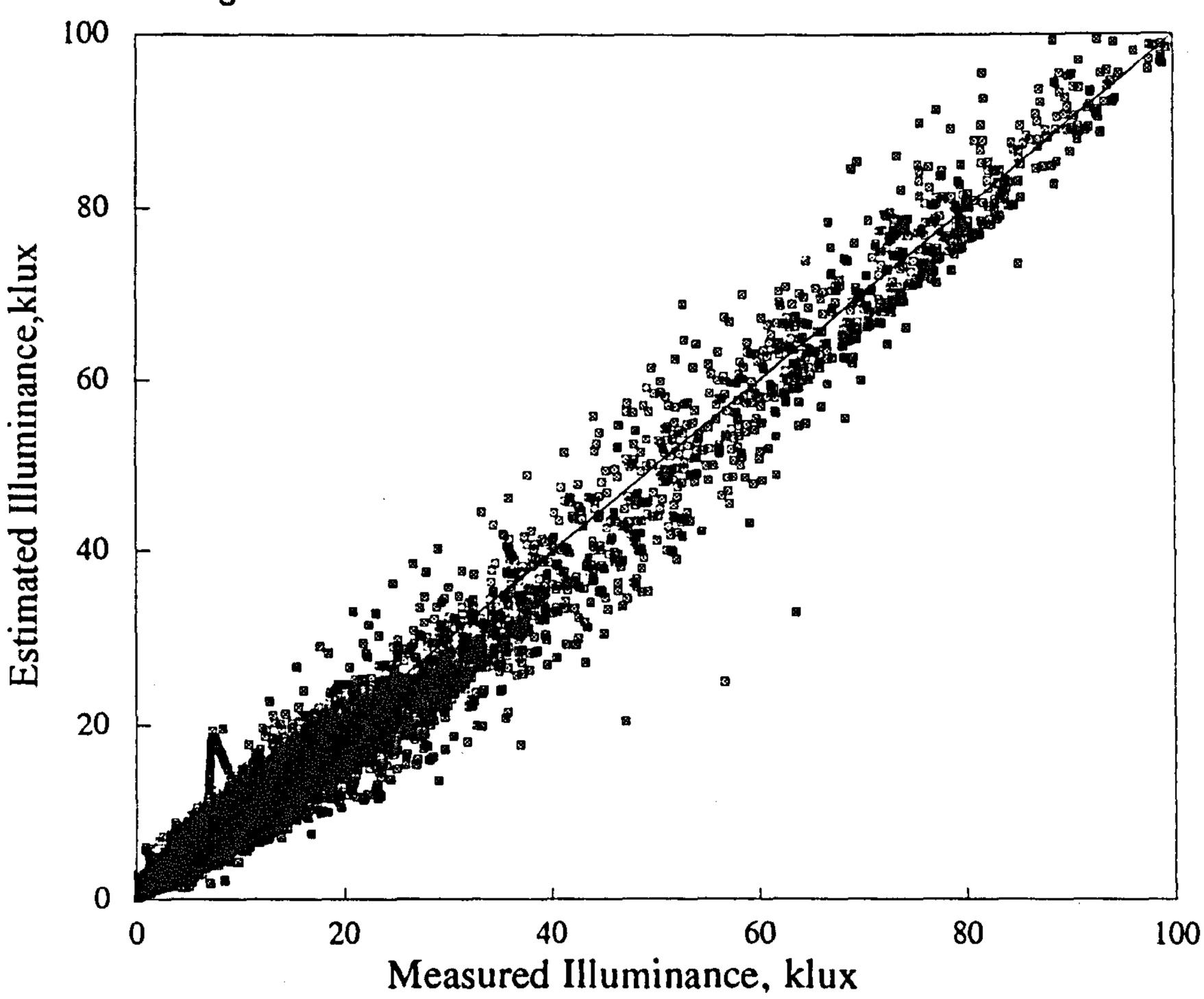

Figure 5.4.17d Summer: West surface illuminance

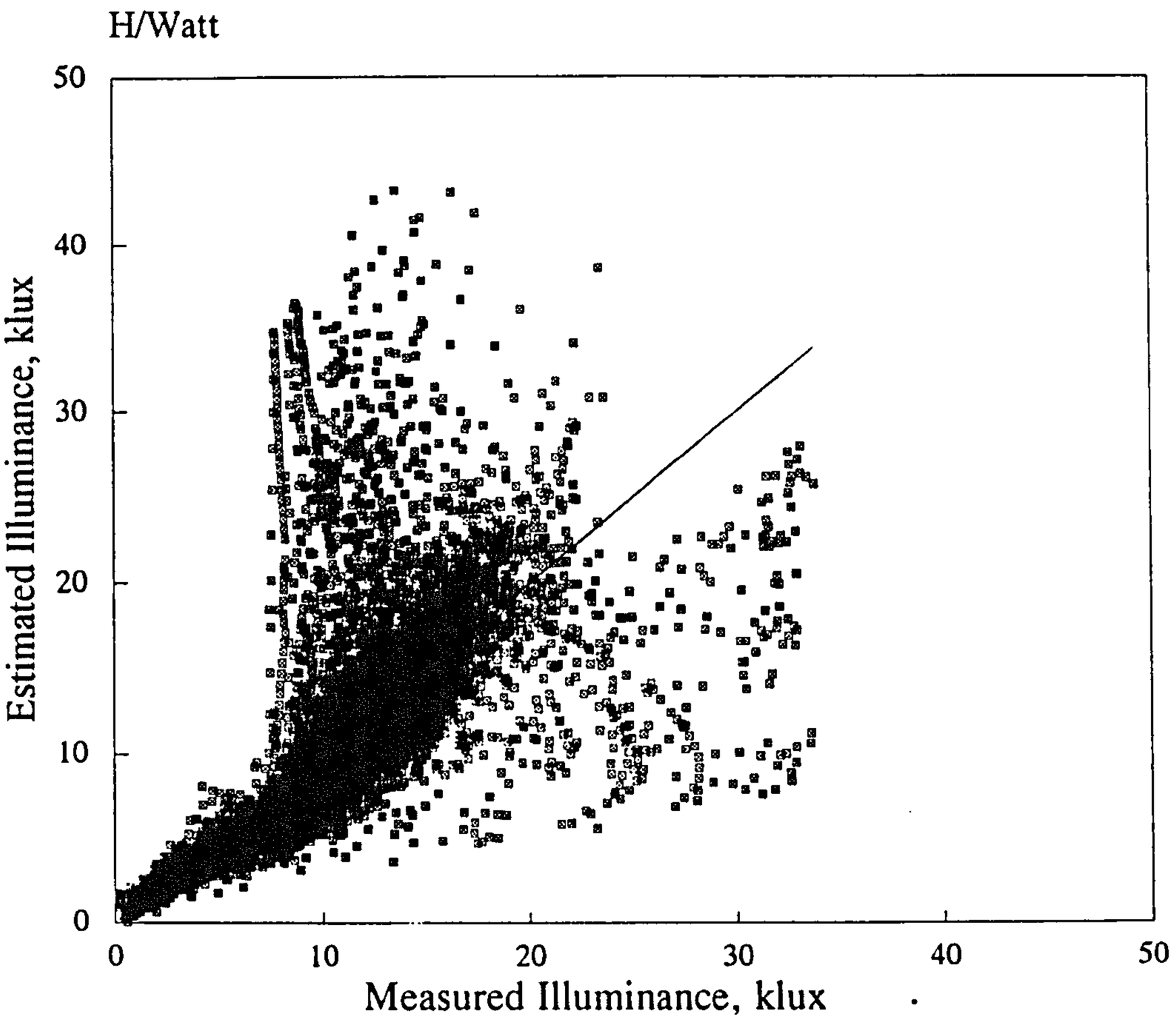

Figure 5.4.18a Summer: North surface illuminance

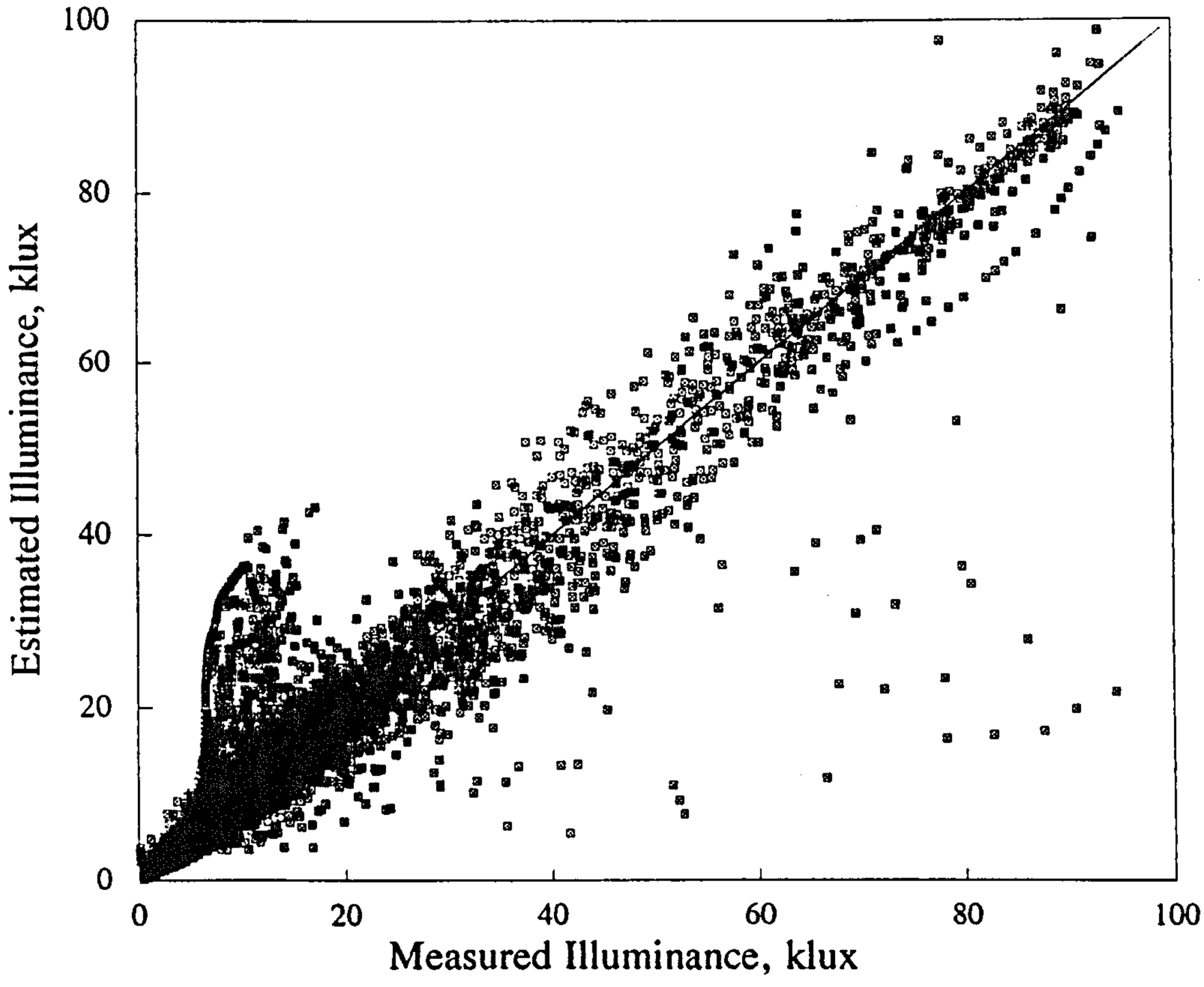

Figure 5.4.18b Summer: East surface illuminance

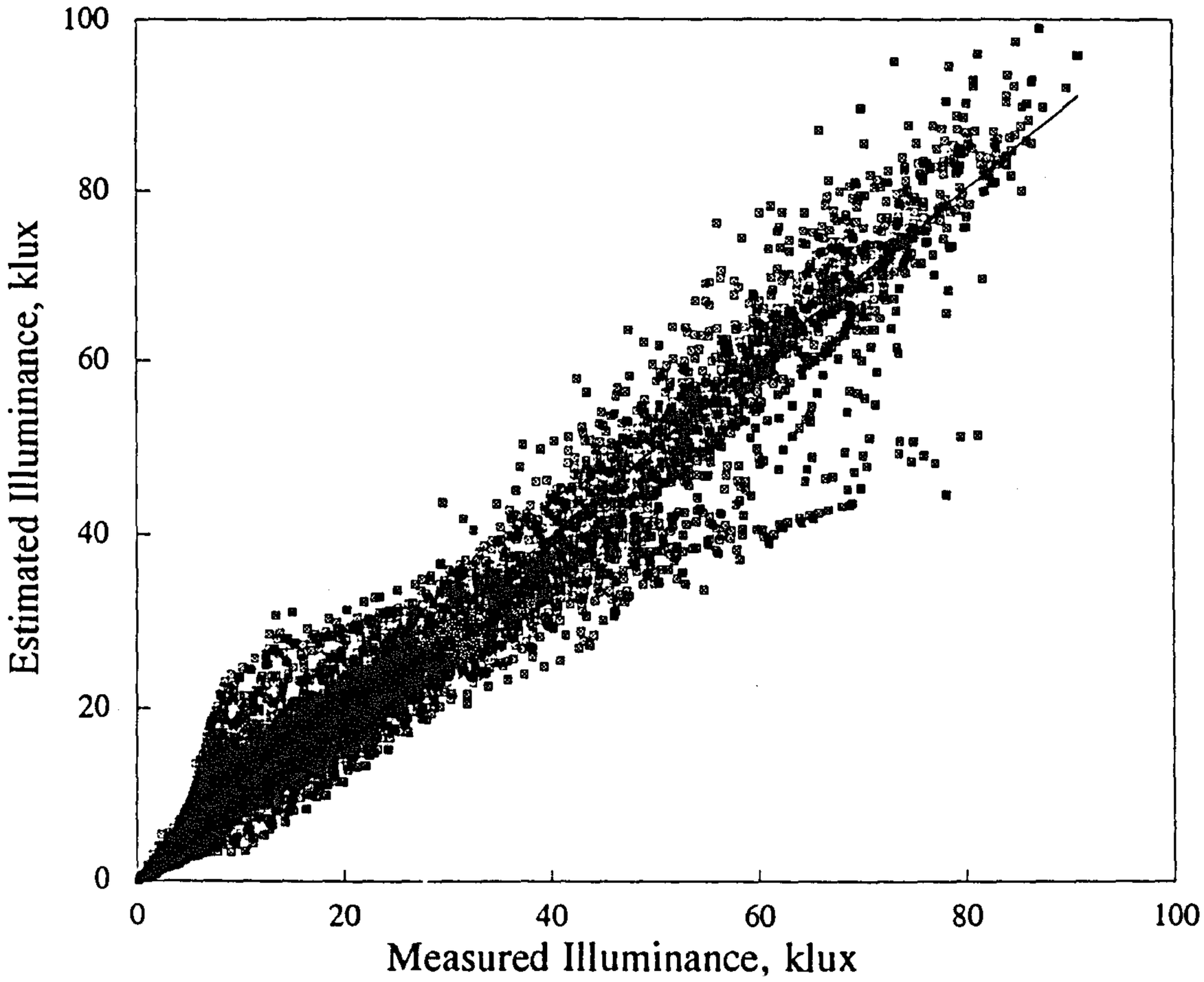

Figure 5.4.18c Summer: South surface illuminance

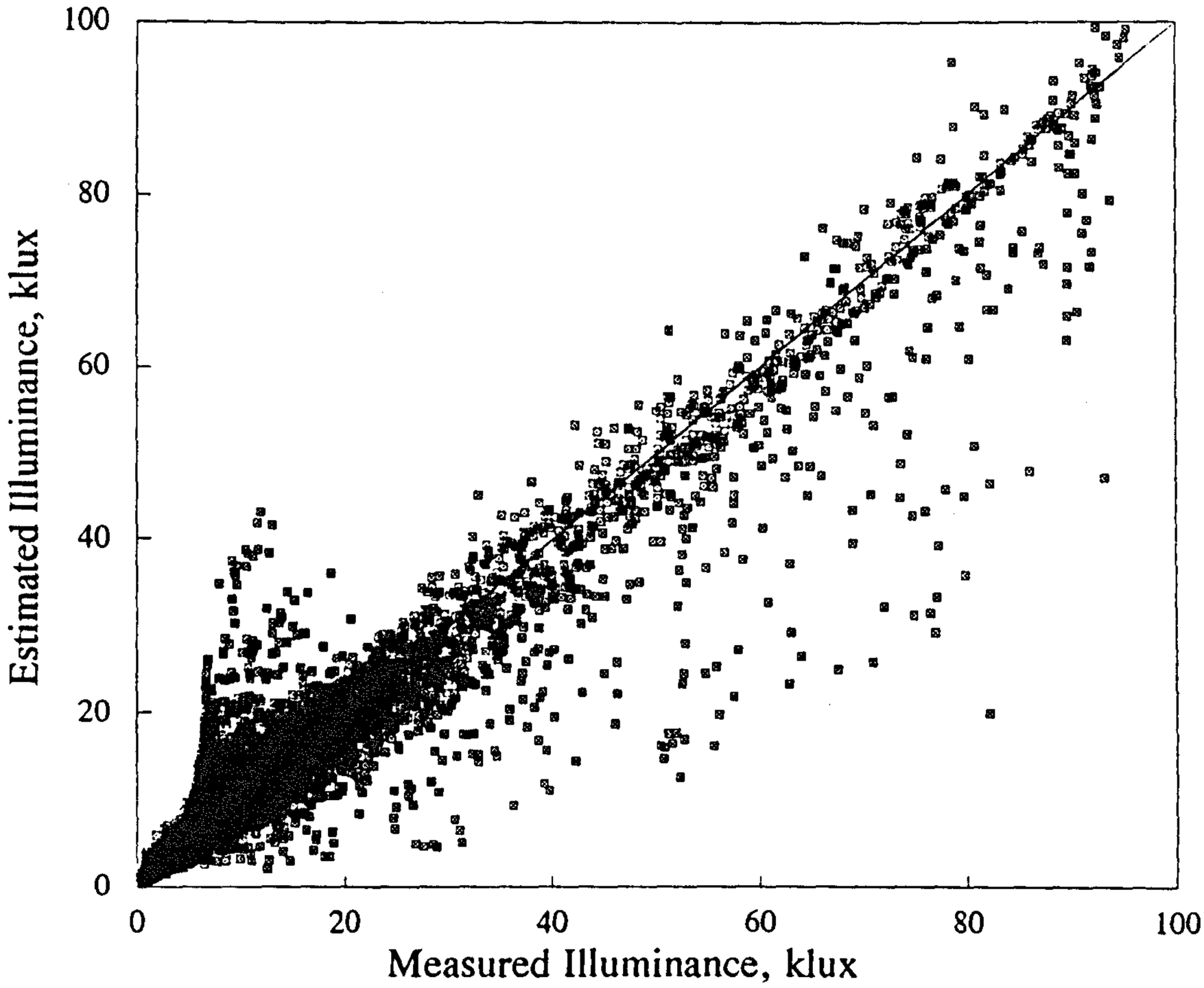

Figure 5.4.18d Summer: West surface illuminance

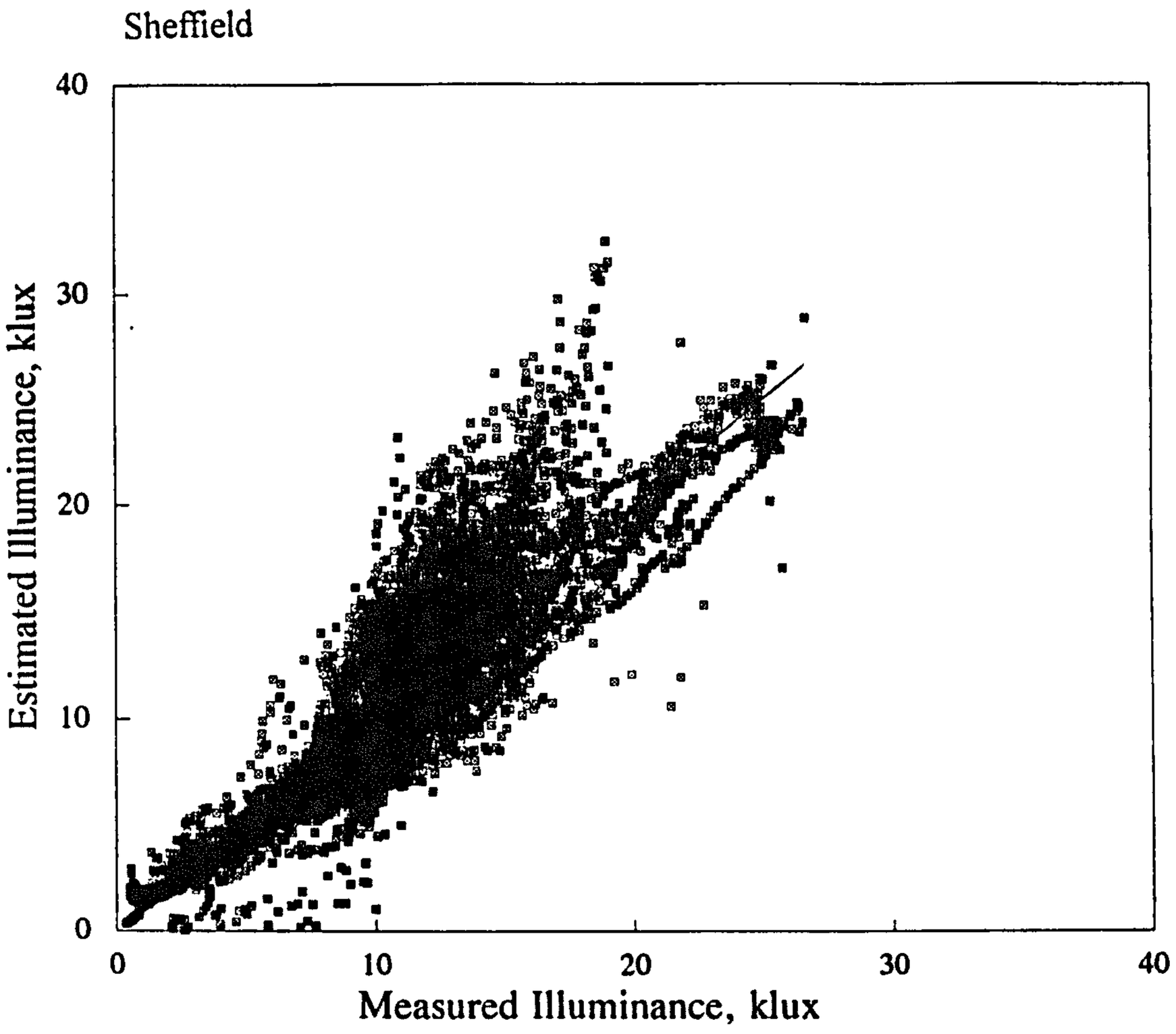

Figure 5.4.19a Summer: North surface illuminance

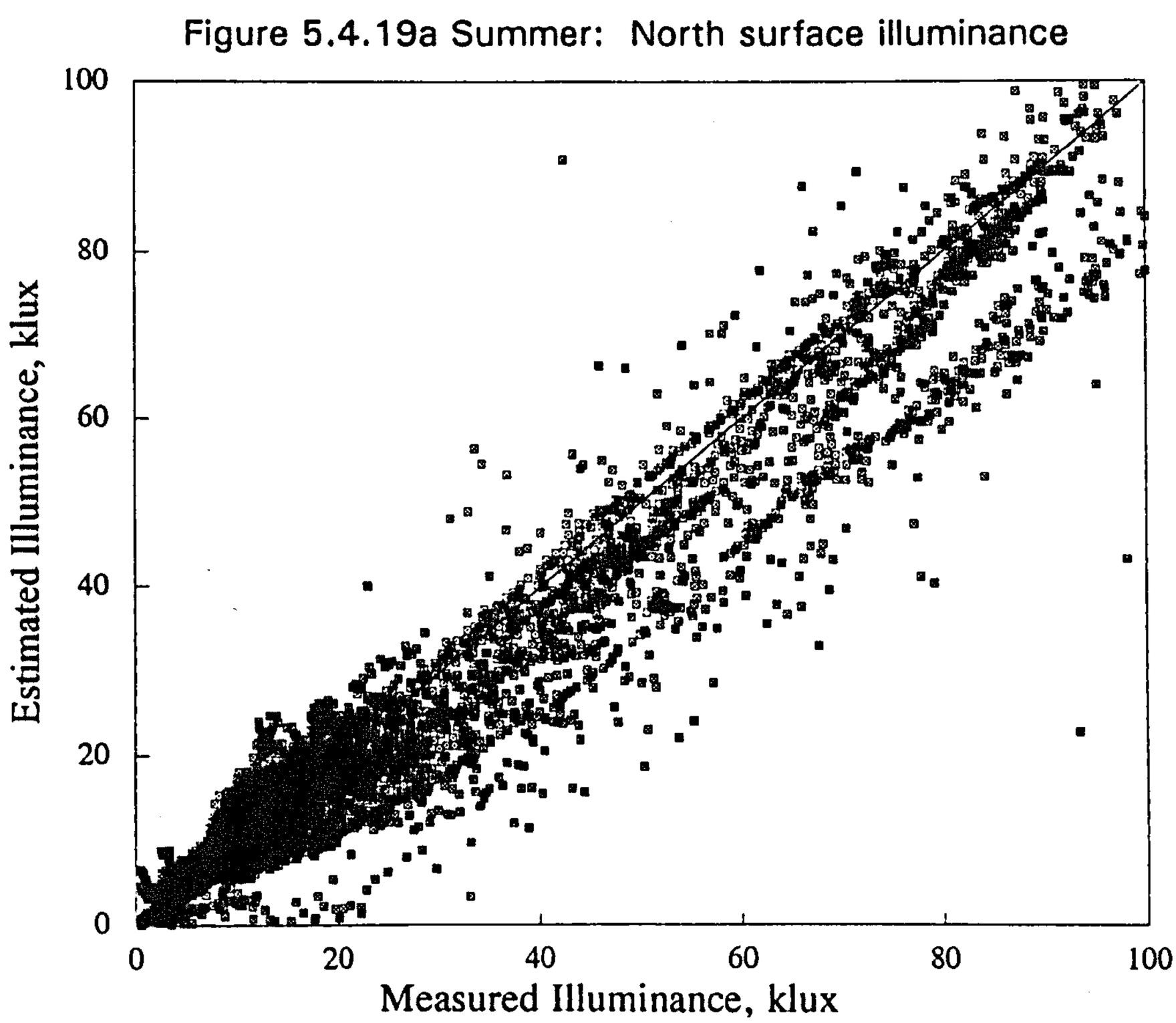

Figure 5.4.19b Summer: East surface illuminance

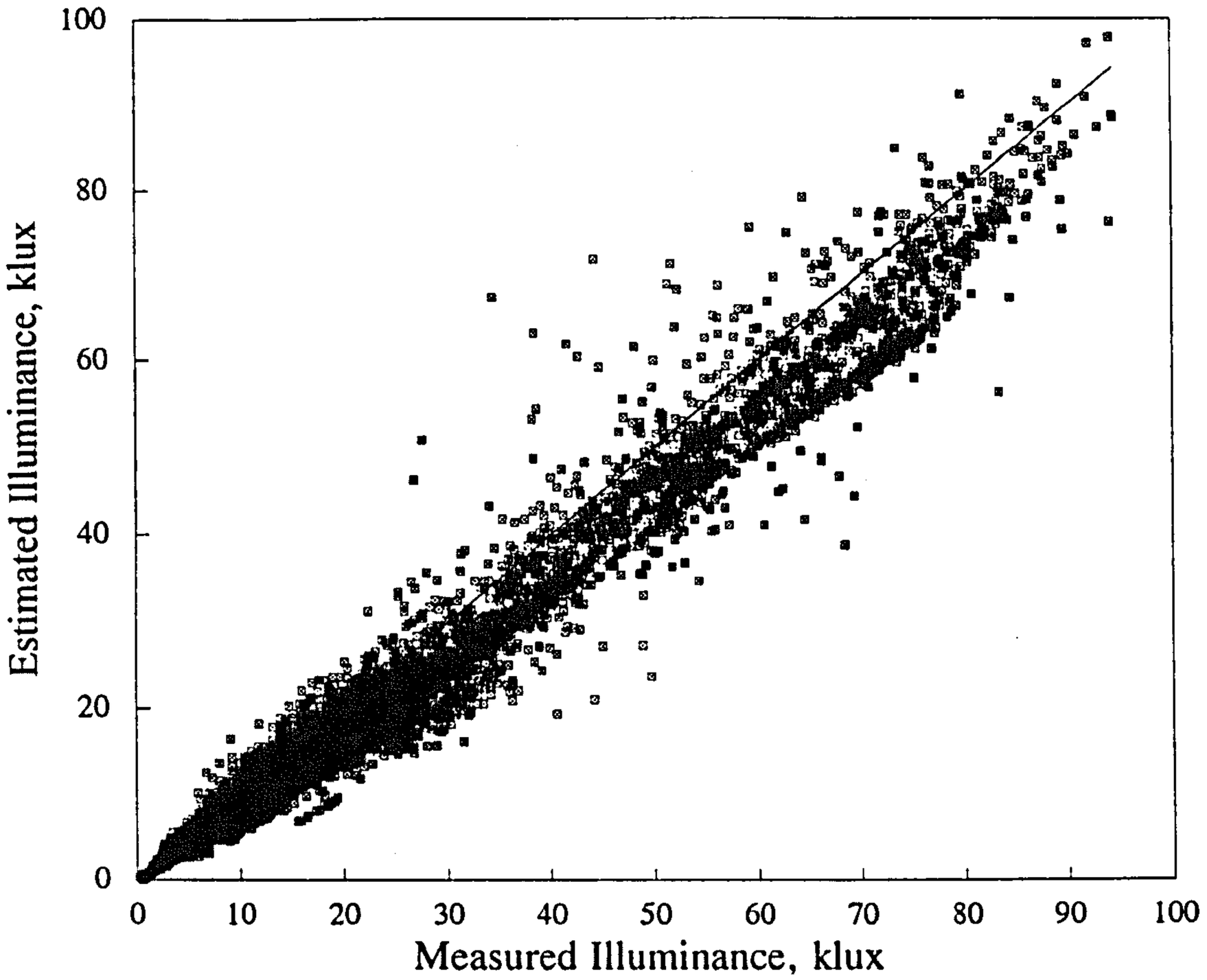

Figure 5.4.19c Summer: South surface illuminance

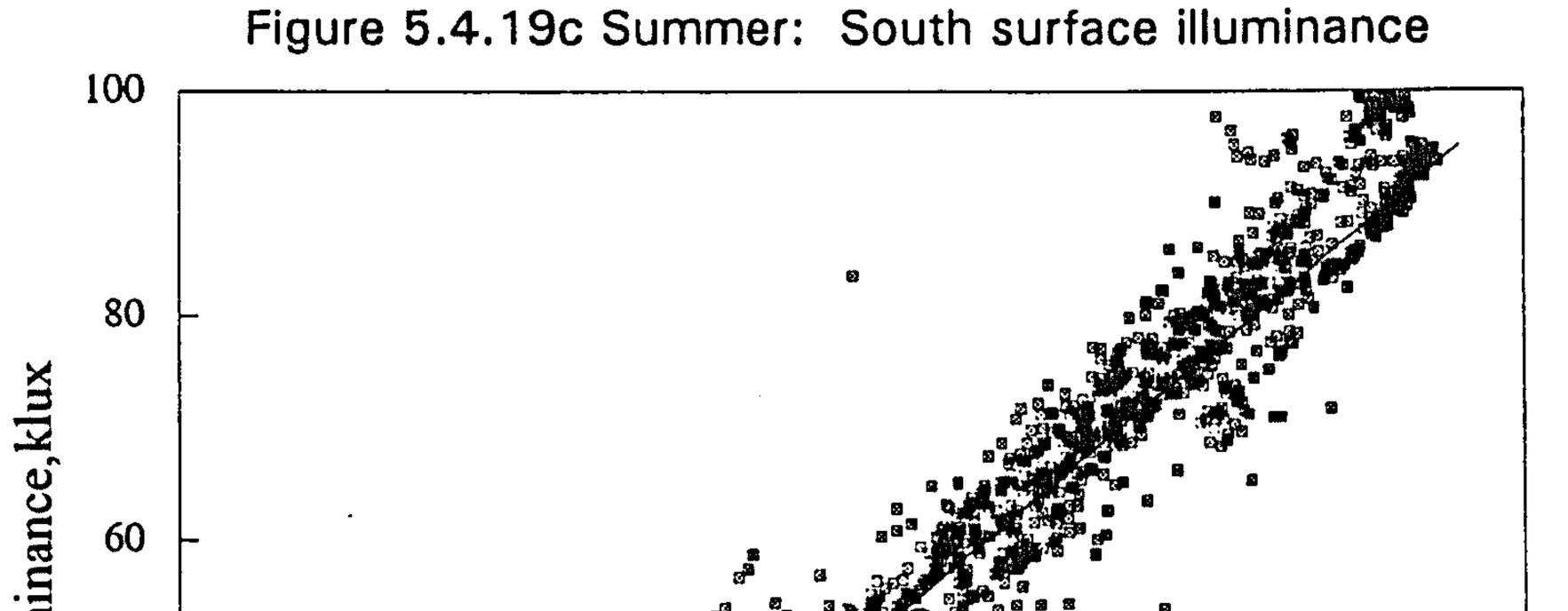

Figure 5.4.19d Summer: West surface illuminance

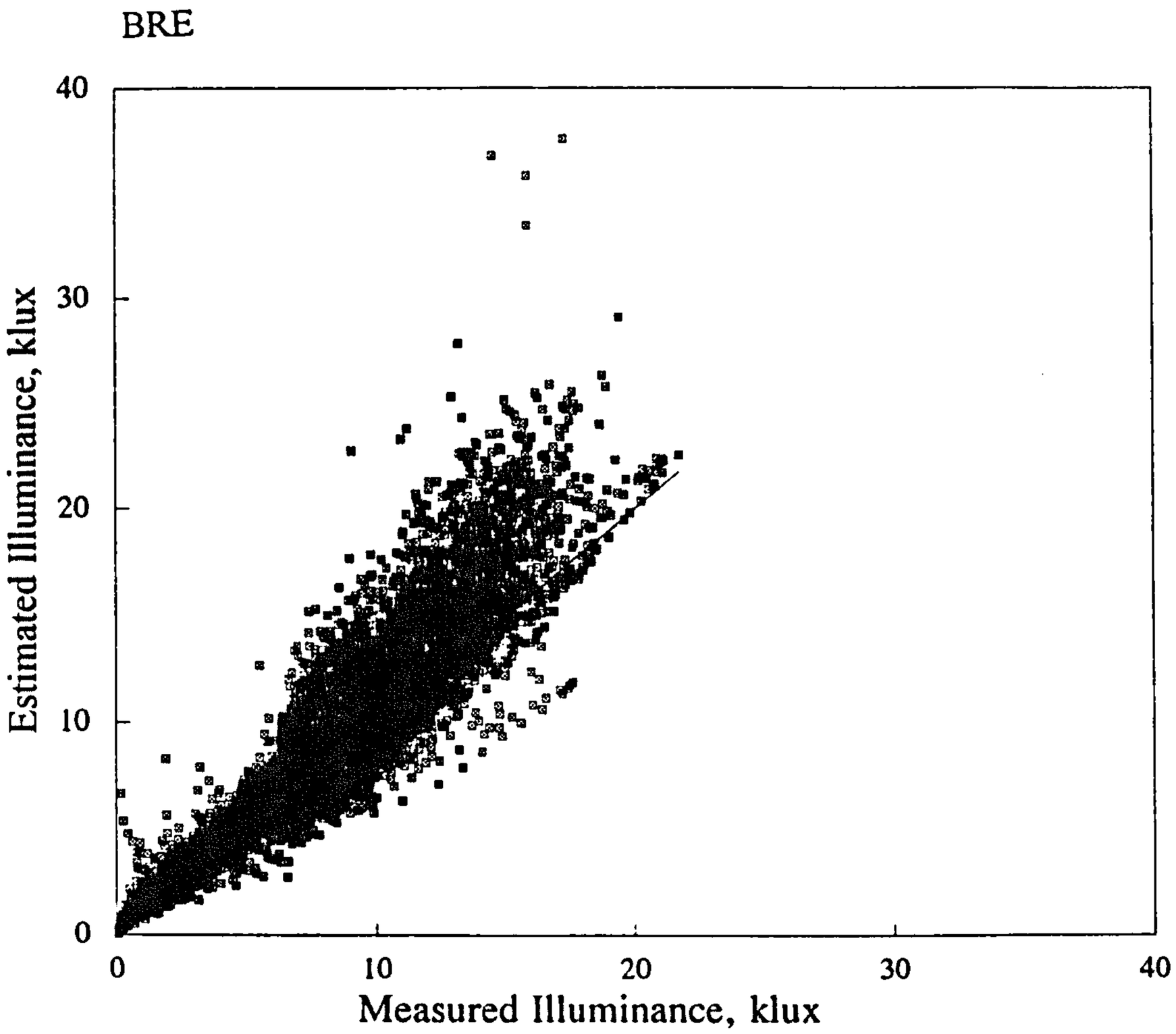

Figure 5.4.20a Summer: North surface illuminance

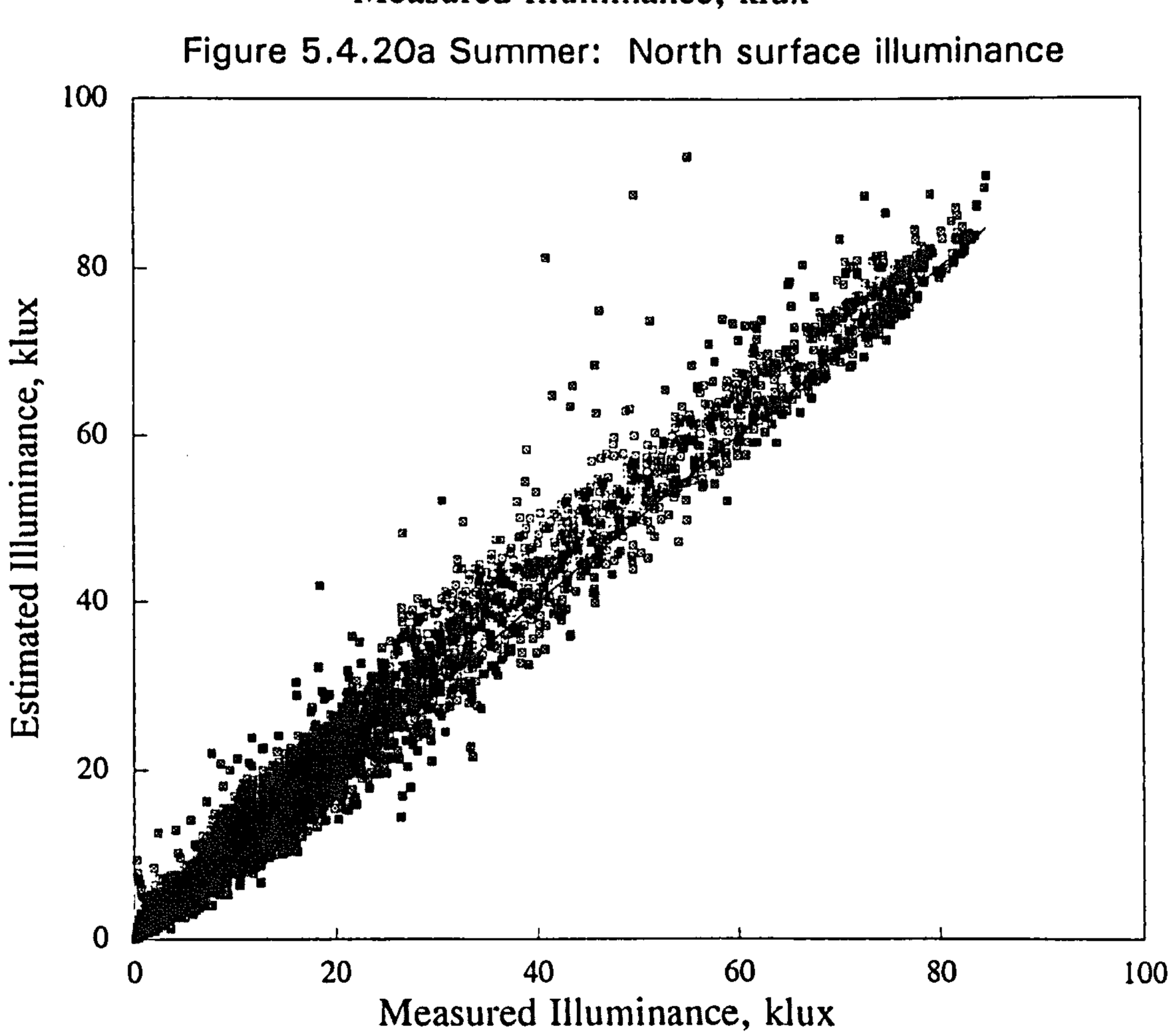

Figure 5.4.20b Summer: East surface illuminance

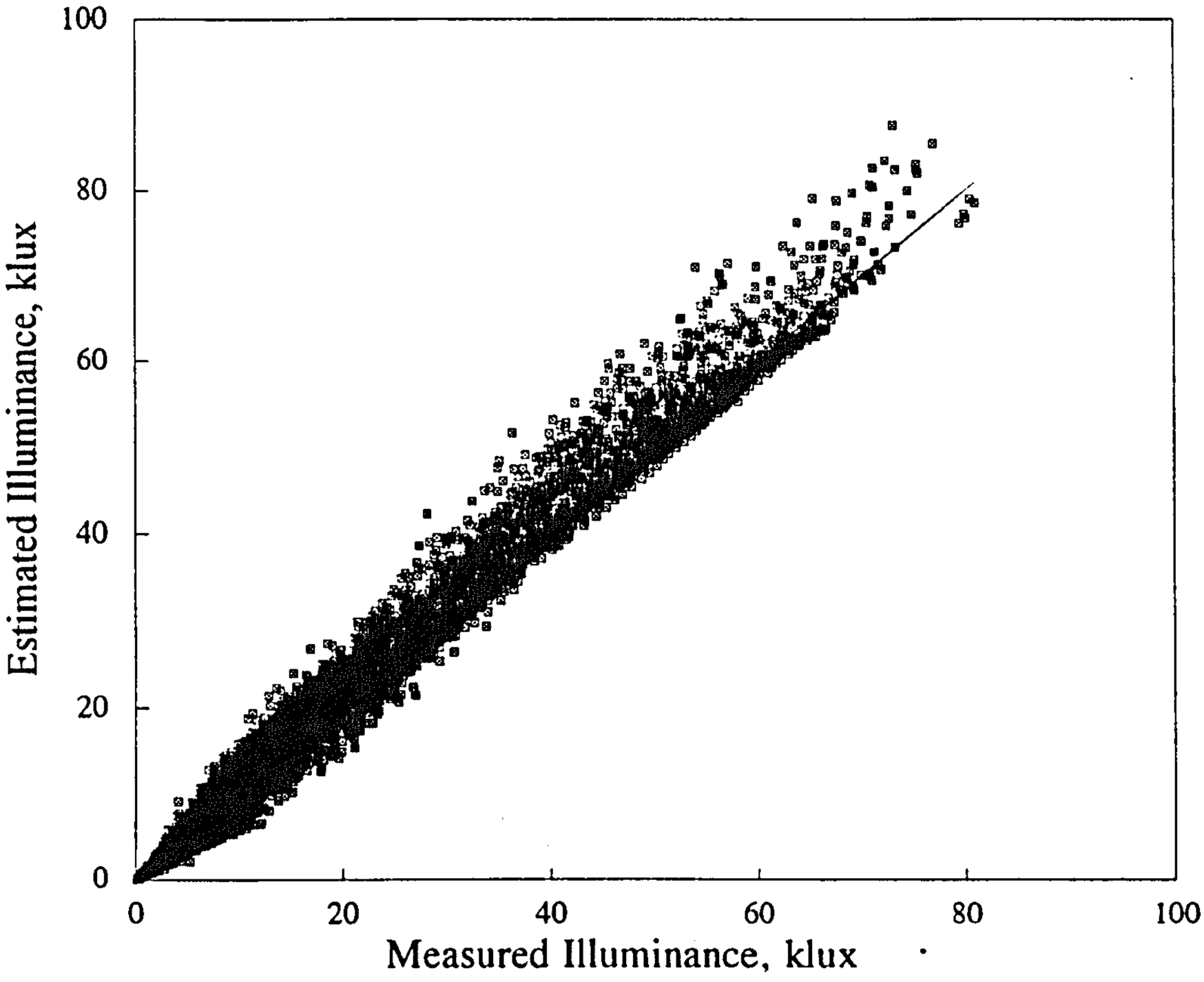

Figure 5.4.20c Summer: South surface illuminance

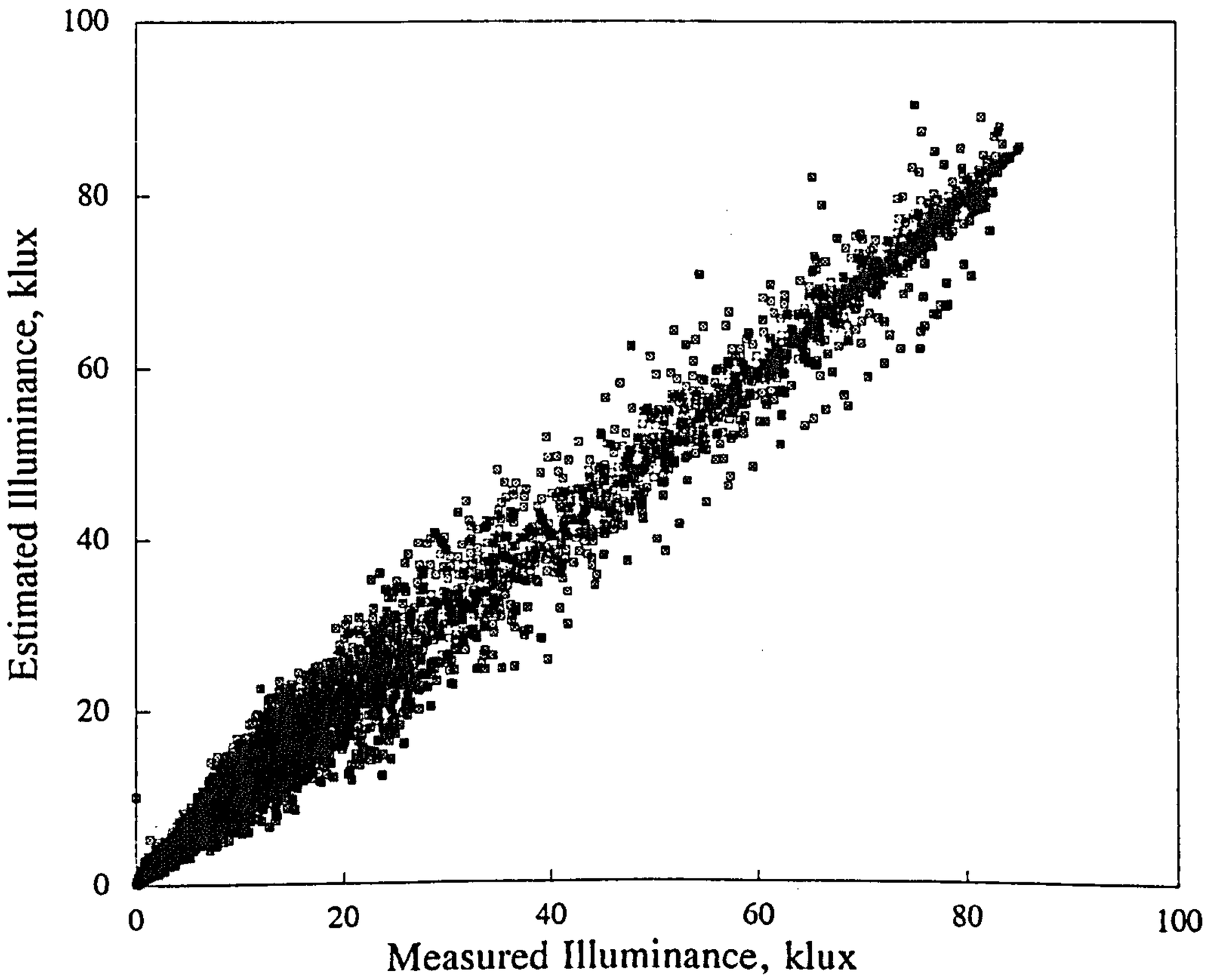

Figure 5.4.20d Summer: West surface illuminance

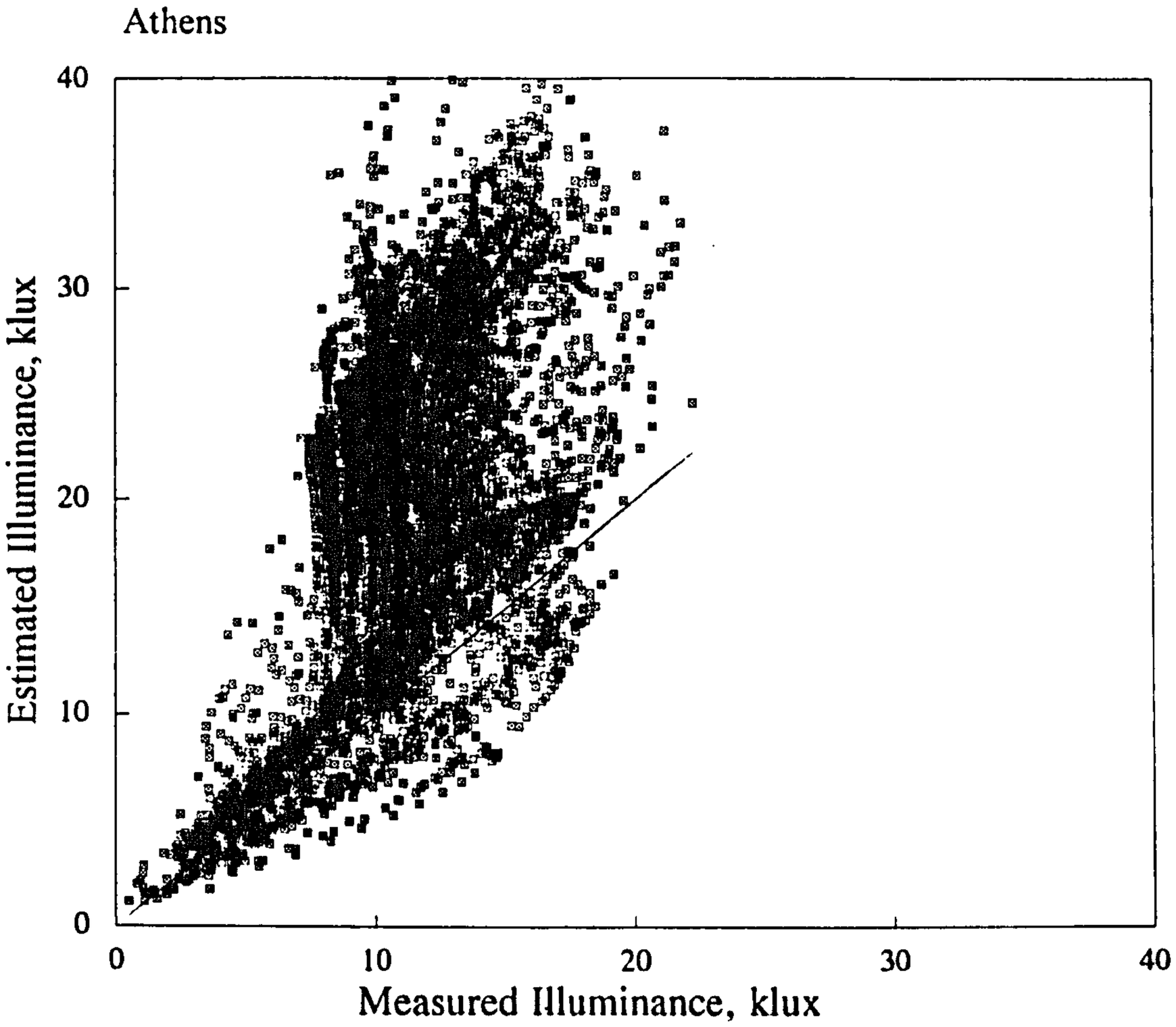

Figure 5.4.21a Summer: North surface illuminance

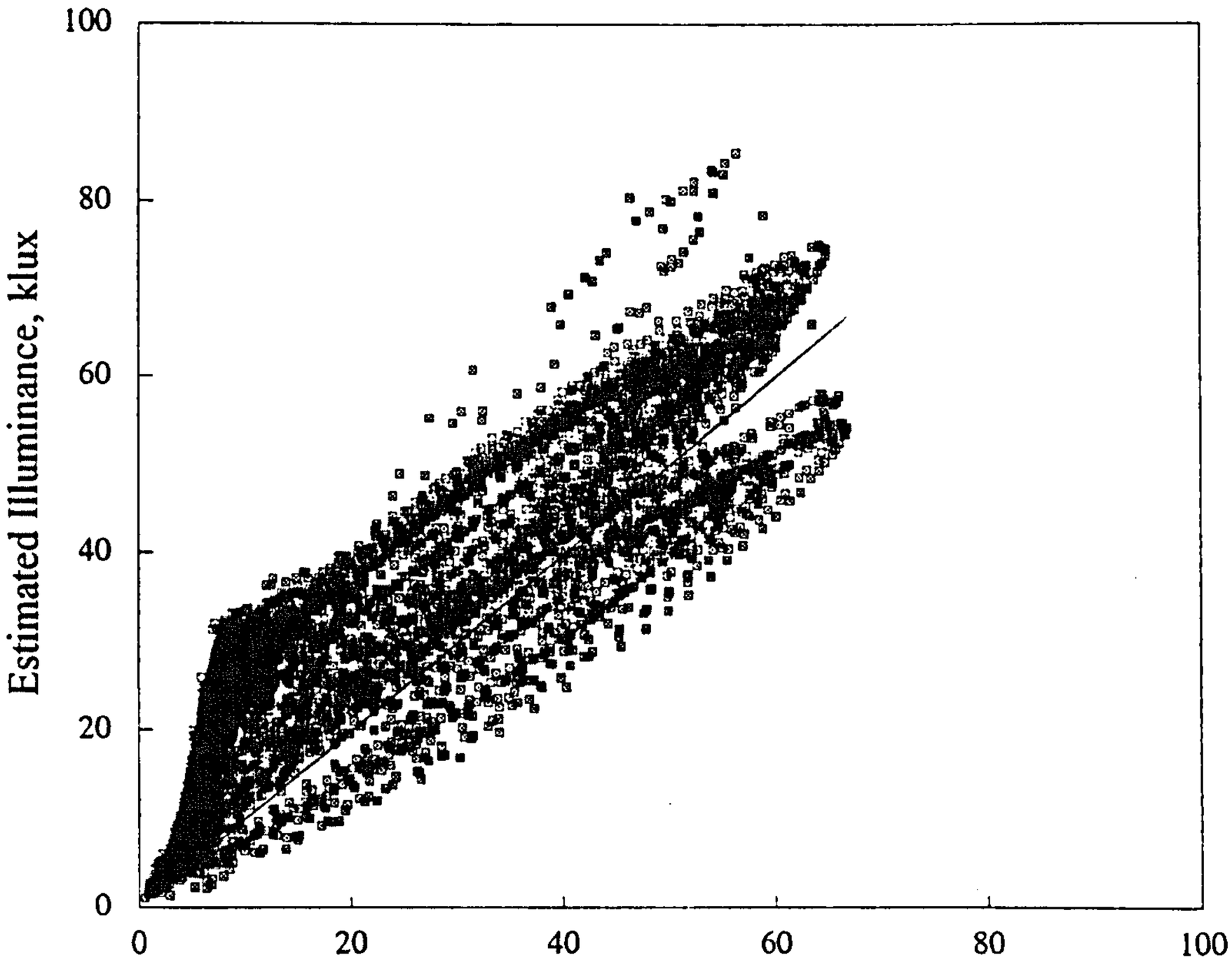

Figure 5.4.21b Summer: East surface illuminance

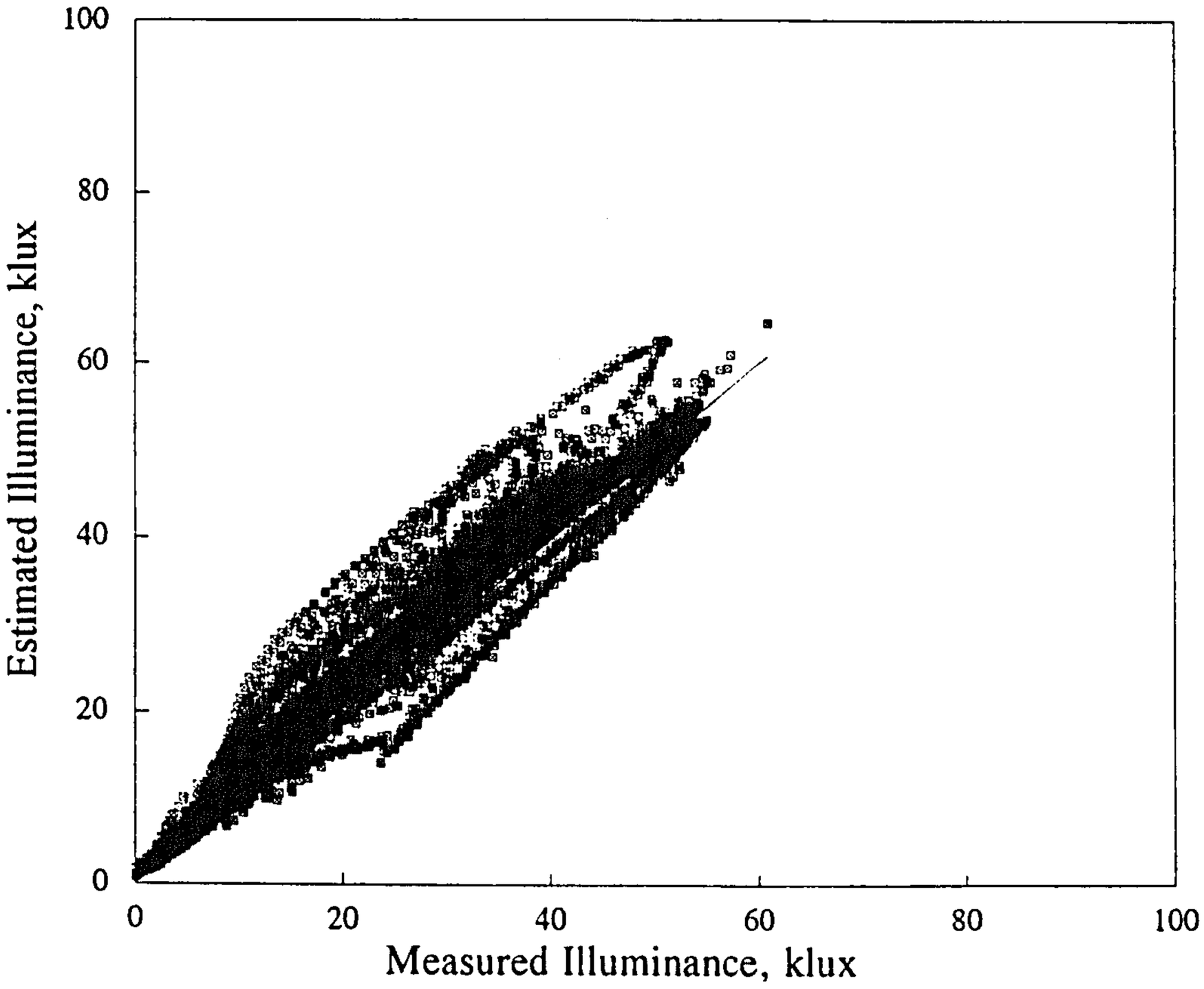

Figure 5.4.21c Summer: South surface illuminance

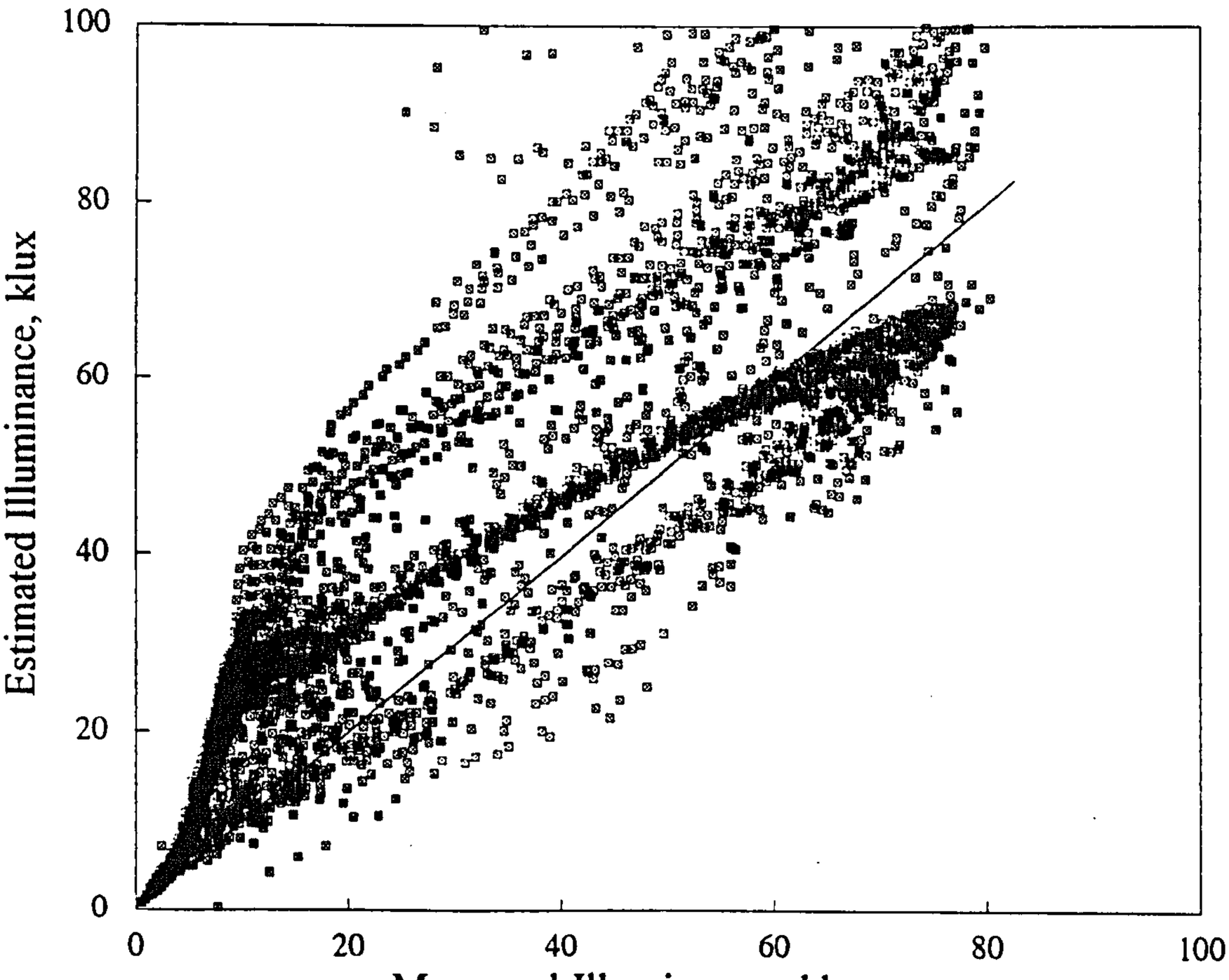

Figure 5.4.21d Summer: West surface illuminance

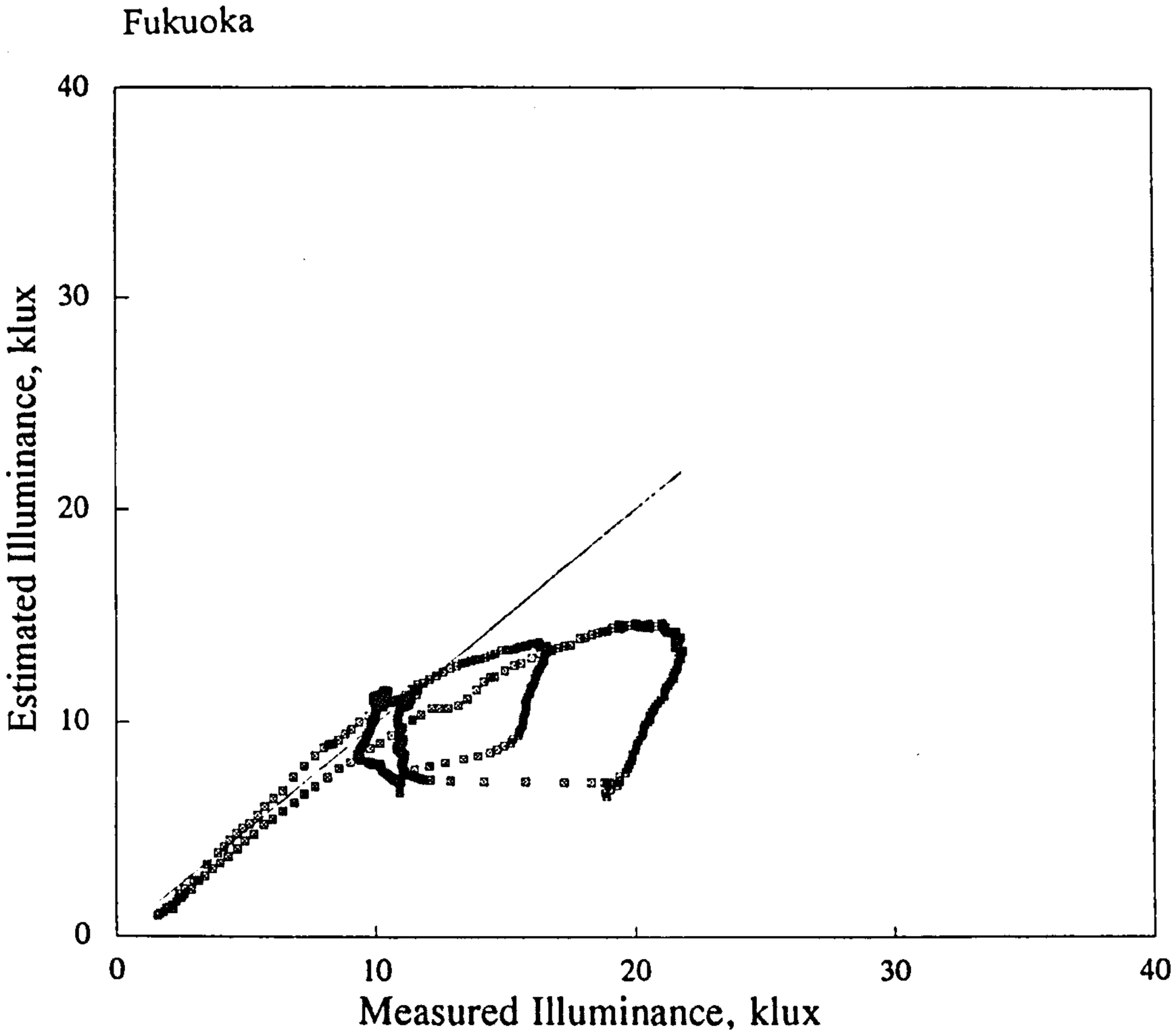

Figure 5.4.22a Summer: North surface illuminance

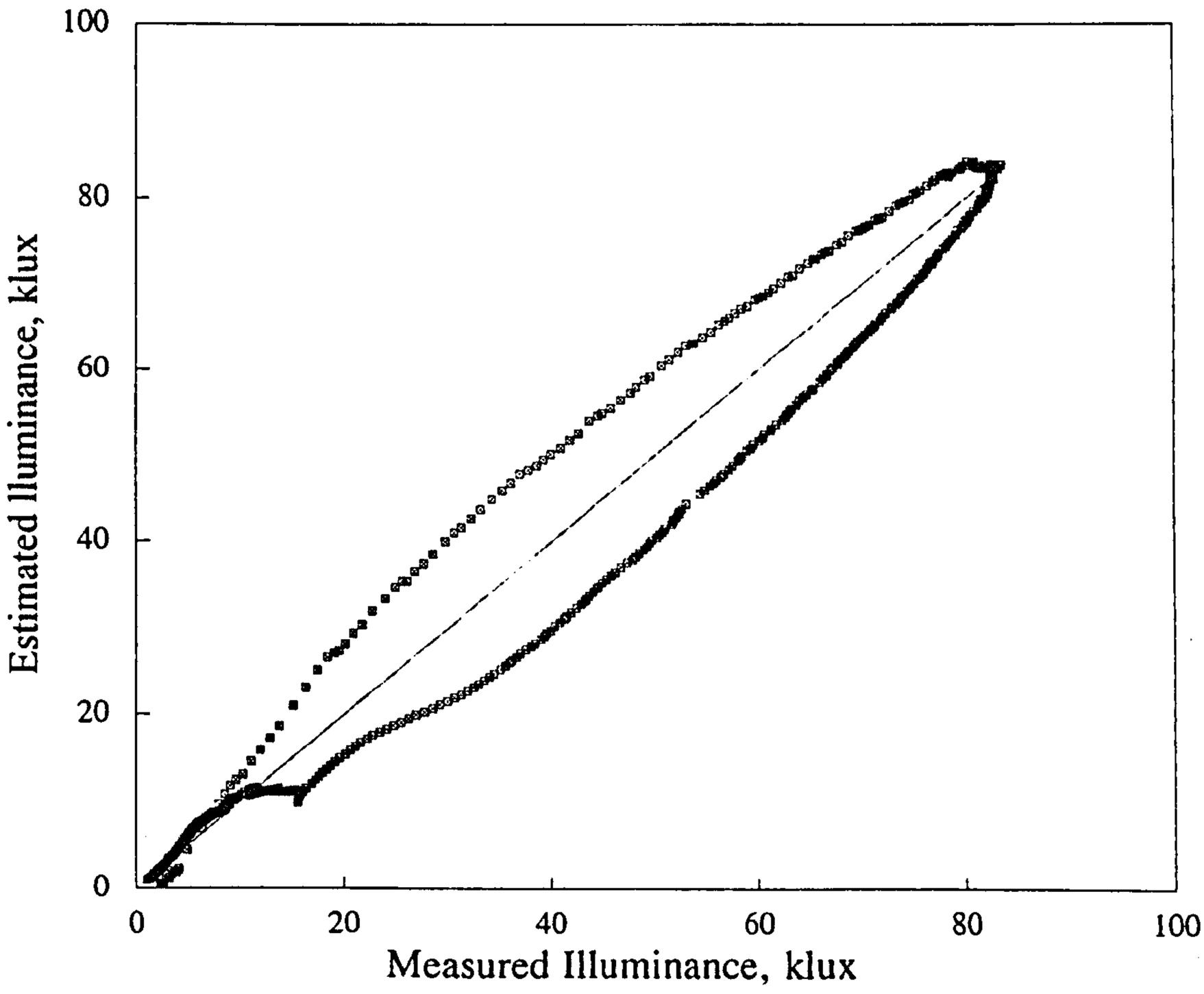

Figure 5.4.22b Summer: East surface illuminance

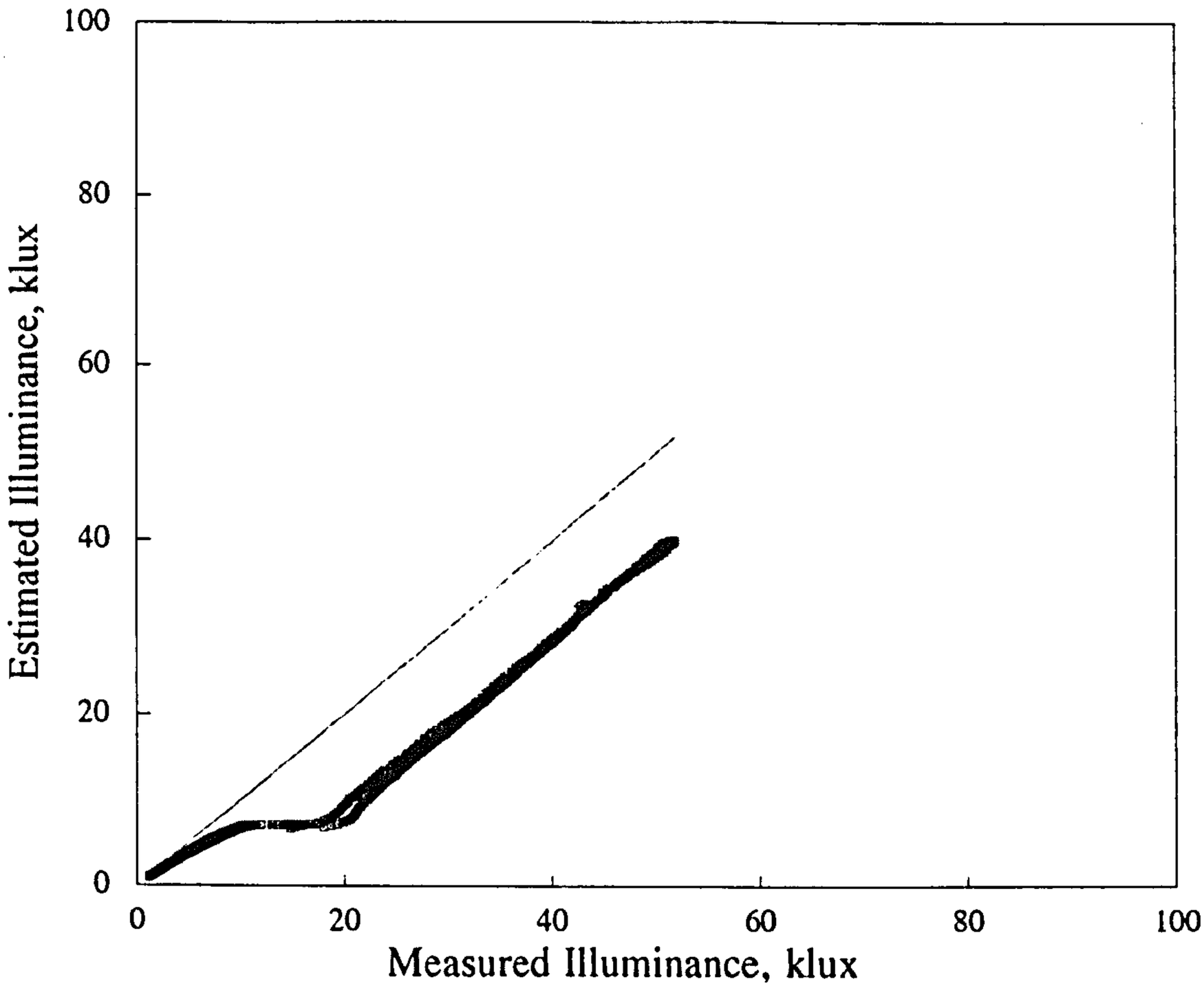

Figure 5.4.22c Summer: South surface illuminance

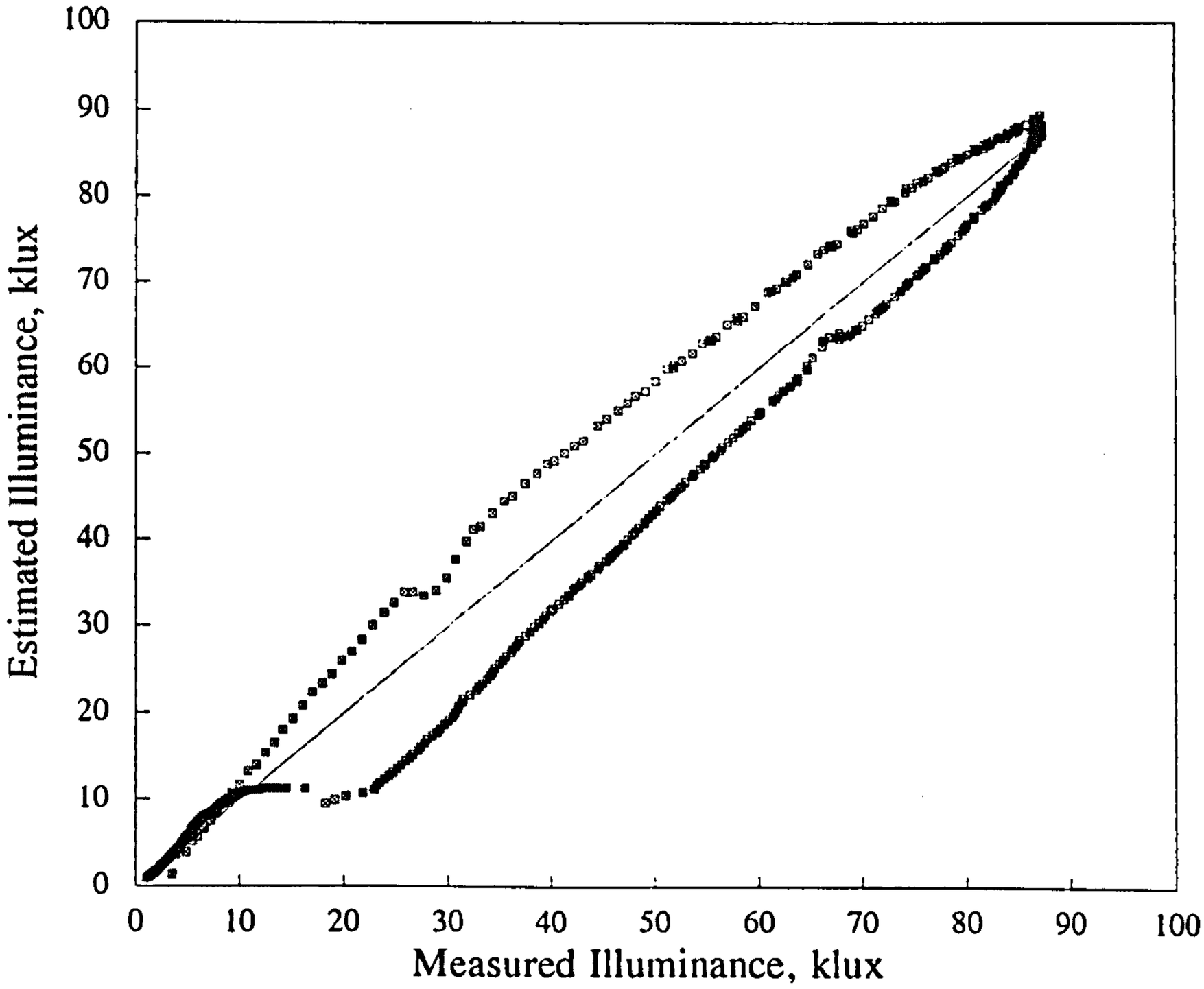

Figure 5.4.22d Summer: West surface illuminance

5.4.3 Proposed model: site performance

The Napier site shows the highest proportion of the sky-diffuse fraction. As shown in Figs 5.4.17a-d the proposed model produces extremely good results with the data points lying close to the one-to-one correspondence line. These results are reciprocated in all of the plots with the autumn/spring and winter graphs given in Appendix 5.4. Due to the number of plots produced for the 6 sites only the summer season data shall be attached herein. Plots for the remaining seasons can be found in Appendix 5.4. Table 5.4.3 includes a list of sites and associated figure and appendices numbers. The statistics for the Napier site highlight the accuracy of the model with a slight tendency to under-predict, this is most evident in the winter months.

The Heriot Watt results as demonstrated in figures 5.4.18a-d display the same level of accuracy as the Napier data with a slight increase in scatter which is backed up by higher RMSE values. The North surface is most interesting as it yields a MBE value of almost nil. However the high RMSE value of 4.93 is a sign of a large amount of scatter which can be seen from Fig 5.4.18a. Overall the model is neither biased towards underprediction or over-prediction and maintains low MBE values.

Only one season's data were available for the Sheffield site and plots 5.4.19a-d show the proposed model's results. The North and West surfaces are slightly better than the East and South with an increase in scatter evident once more. The data used were one minute instantaneous measurements as opposed to 5 minute averages for the other sites. It is therefore inferred that if this data were also averaged the level of scatter would be reduced, hence improving the RMSE values. Inspite of this the proposed model produces good results as the statistics prove.

The BRE results demonstrate clearly the excellent performance of the proposed model. The results of the graphs shown by figures 5.4.20a-d display a good trend throughout the illuminance range with no evidence of underprediction or over-prediction. These findings are borne out in the statistics with low MBE and RMSE values for all seasons and slopes. Earlier BRE data were used in the development and initial analysis of the proposed model are part of a comprehensive evaluation later in this chapter the results of which were first given in Ref.[5.15]. The latest BRE data(1991/92) employed the single curve given in table 5.4.1, where as the 1984 BRE data used the seasonal background curves.

The Athens site produces the poorest results of all 6 sites. Figures 5.4.21a-d for the autumn/spring months display a high level of scatter for all surfaces. The north surface in particular demonstrates an almost exponential correlation, with the estimated data rising steeply off the 45° line. The three pronged appearance of the data seem to relate to a particular months data which highlights the volatility of the atmosphere for each month. Atmospheric pollution may be one explanation for the relatively poor performance of the proposed model but some doubt has been raised over the quality of the data, in particular the west surface. As figure 5.4.4i in the appendix shows, on a clear day the west surface receives a fraction of the illuminance it should and in addition its data are well below that predicted by the shaded model. This problem was brought to the attention of the station operators who could give no explanation for the results. To this end it appears that the proposed model is less sensitive to this highly turbid atmosphere although data quality may also play an important role in its performance. A comparison of the data from Napier and Athens site can be found in Ref.[5.16].

The Japanese plots(Figs.5.4.22a-d) contain only a limited number of days and in no way represent a comprehensive evaluation of the proposed model's performance. However as stated in earlier chapters the data can be used to provide an indication of the models estimating ability. Excluding the south surface the model produces good results at least on a par with the Sheffield data. The MBEs on the whole are very good with a favourable level of scatter.

Table 5.4.3 Statistical analysis of proposed model performance for various sites

		NORTH	EAST	SOUTH	WEST	Figure No	Appendix No
NAPIER UNI.							
Summer	MBE	-0.36	0.71	-0.82	-0.67	5.4.17	
	RMSE	2.24	3.38	3.25	3.12		
Autumn/spring	MBE	-0.33	0.23	-1.64	-1.25		5.4.1
	RMSE	1.34	2.51	3.82	2.80		
Winter	MBE	0.28	-0.37	-2.39	-1.25		5.4.1
	RMSE	0.64	1.33	4.23	2.56		
HERIOT WATT							
Summer	MBE	0.01	0.73	-0.05	0.01	5.4.18	

Table 5.4.3 Statistical analysis of proposed model performance for various sites(cont'd)

		NORTH	EAST	SOUTH	WEST	Fig.No	App. No
	RMSE	4.93	5.66	4.30	5.25		
Autumn/spring	MBE	0.48	0.69	-0.75	-0.24		5.4.2
	RMSE	3.50	3.84	4.50	2.89		
Winter	MBE	-0.04	0.13	0.78	-0.35		5.4.2
	RMSE	1.27	2.03	4.64	1.94		
SHEFFIELD							
Summer	MBE	0.59	-1.68	-2.63	0.59	5.4.19	
	RMSE	2.74	6.10	4.62	3.92		
BRE. GARSTON							
Summer	MBE	1.05	1.51	1.15	0.75	5.4.20	
	RMSE	2.33	3.18	2.81	2.63		
Autumn/spring	MBE	0.71	1.12	1.27	0.50		5.4.3
	RMSE	1.81	2.80	2.94	2.05		
Winter	MBE	0.37	0.43	1.57	0.46		5.4.3
	RMSE	0.90	1.36	3.03	1.93		
ATHENS							
Summer	MBE	9.50	8.45	2.87	12.34	5.4.21	
	RMSE	11.88	11.82	4.60	19.15		
Autumn/spring	MBE	8.85	7.07	4.33	5.47		5.4.4
	RMSE	10.68	13.83	8.62	21.97		
Winter	MBE	8.68	4.99	4.10	8.93		5.4.4
	RMSE	16.48	7.34	10.32	16.72		
JAPAN							
Summer	MBE	-1.93	-0.54	-8.11	-0.17	5.4.22	
	RMSE	3.60	4.92	9.27	4.47		
Autumn/spring	MBE	-0.25	-0.25	-1.09	-0.61		5.4.5
	RMSE	0.87	3.58	3.44	3.13		
Winter	MBE	-0.09	0.89	4.01	-2.33		5.4.5
	RMSE	0.55	10.77	5.67	6.55		

As can be seen from each of the graphs the proposed model performs with a high level of accuracy with the data points following the line of equality. The North surface plots contain data mainly from shaded conditions using predictions from Eq.5.13, this clearly illustrates the good performance of this model. The model performs very well throughout the illuminance range from heavily overcast through partly cloudy to clear blue skies. It is an inherent feature of the proposed model that it predicts with accuracy slope illuminance for all sky conditions as opposed to traditionally adopted models that are specifically designed for a given atmospheric condition such as the CIE overcast sky and clear sky models.

5.5 TRADITIONAL SLOPE ILLUMINANCE MODELS

The proposed model has been evaluated successfully for a wide range of Scottish, UK, European and even Japanese data. It is essential to confirm the high level of performance of the proposed model through comparison with alternative slope illuminance models. Three such models shall be considered and evaluated using the BRE 1984 data.

5.5.1 Moon and Spencer model

Moon and Spencer's[5.6] model was developed in response to the use of a uniform sky model which was thought to be flawed in its assumptions. Moon and Spencer noted the change in the luminance of the sky vault from zenith to the horizon and developed a sinusoidal formula that accounted for this variation (Eq.5.24),

$$L\alpha = Lz((1 + b\sin\alpha)/(1 + b) \qquad 5.24$$

$L\alpha$ is the luminance of a patch of sky at an angle α from the horizon. This equation is integrated to form the slope illuminance formula given by Eq.5.25,

$$L_\beta = \frac{L_D}{14\pi}\{\pi(3+11\rho)+[11\pi(1-\rho)-8\beta]\cos\beta+8\sin\beta\} \qquad 5.25$$

in the case of a vertical surface where $\beta = 90°$ and ρ, the surface albedo, $= 0$;

$$\frac{L\theta}{L_D} = \frac{1}{14\pi}[3\pi+8] = 0.396 \qquad 5.26$$

As stated in section 5.4.2 the value of 0.396 relates to a 'b' value of 2 and can be calculated by applying this value to Eq.5.16 for the proposed model. The complete slope illuminance model would then take the form of Eq.5.27.

$$L_\beta = (LG - L_D)\frac{\cos i}{\sin \gamma s} + 0.396\, L_D \qquad 5.27$$

At the time of its inception this novel approach was highly commended and has been adopted as the CIE standard overcast sky model.

5.5.2 Uniform sky model

The model the Moon and Spencer's work superseded was the uniform sky model[5.2] which as its name implies assumes the sky hemisphere has a uniform luminance distribution and is often termed the isotropic sky model. The assumption of a uniform sky suggests that a slope surface would receive illumination from half of the hemisphere and to this end the parameter 'b' has a value equal to zero. Again applying this value of 'b' to Eq.5.16 yields a L_β/L_D ratio of 0.5, completing the uniform model as shown by Eq.5.28.

$$L_\beta = (LG - L_D)\frac{\cos i}{\sin \gamma s} + 0.5\, L_D \qquad 5.28$$

The Moon and Spencer and Isotropic models are both of a simple nature and cannot be expected to accurately predict slope illuminance for the large variety of sky conditions that are experienced in the UK. As stated above the Moon and Spencer model was developed only for overcast conditions. Partly cloudy skies are more common than the overcast scenario which have been the centre of much modelling work.

5.5.3 Perez model

It is well recognised that for building services and architectural designs a much more reliable method of predicting slope illuminance is required. Of recent illuminance modelling developments the work of Perez[5.7] is regarded as one of the most comprehensive in this area. The Perez slope illuminance model accounts for the variability of the sky background diffuse component through the use of circumsolar and horizon brightening components superimposed on an isotropic background;

$$L_\beta = L_D[(1 - F_1)(1 + \cos\beta)/2 + F_1\, x/y + F_2 \sin\beta] \qquad 5.29$$

β is in radians. F_1 is the circumsolar brightening coefficient, a function of sky brightness and zenith angle given by Eq.5.30. F_2, the horizon brightening coefficient is given by Eq.5.31.

$$F_1 = F_{11} + F_{12}\Delta + F_{13}z \qquad 5.30$$

$$F_2 = F_{21} + F_{22}\Delta + F_{23}z \qquad 5.31$$

The coefficients F_{ij} are given in table 1 of appendix 5.5. The parameters x and y can be calculated from equations 5.32 and 5.33 respectively.

$$x = \max(0,\cos i) \qquad 5.32$$

$$y = \max(0.087,\cos z) \qquad 5.33$$

The operation of the slope illuminance model like the luminous efficacy models relies on matrices bound by ε, the sky clearness parameter given by Eq.3.3.10. The calculation of ε in turn selects F_{ij} and Eq.3.3.11 calculates Δ, the sky brightness coefficient. The coefficients were derived from some 20,000 data points covering sites from North America and Central Europe.

5.6 SLOPE ILLUMINANCE MODELS EVALUATION

The analysis and evaluation of the models will primarily compare the Perez and proposed models and will include graphical and statistical examinations. North, east, south and west vertical surfaces were analysed for the summer, winter and autumn/spring periods. Both models were analysed statistically using the mean bias error (MBE), a measure of the underlying trend, and the root mean square error (RMSE), an indication of the scatter, for each surface and for each season(Table 5.6.1). As the graphs of each season are visually similar, only Autumn/spring plots are included in this chapter. The remaining seasons' graphs are shown in appendix 5.6. Figure 5.6.1 for the north surface shows both models producing similar results in all seasons; the Perez model gives consistent under-prediction. This can also be seen in Table 5.6.1 where the MBEs for the Perez model are several times greater than those for the proposed model(summer, autumn and spring). The proposed model has a more favourable trend. The plots for the east and west are presented in Figures 5.6.2. and 5.6.4 respectively. Once again the proposed model demonstrates a better performance. Table 5.6.1 highlights the improved MBEs for the proposed model as against that of Perez in four out of six cases the underlying trend is significantly better. The west surface demonstrates the particular strength of the model with Fig.5.6.4(and appendix 5.6 Fig.4) indicating that the Perez model, though producing a similar order of

scatter, displays a consistent over-prediction particularly in the higher illuminance band(part-cloudy to clear sky conditions). Figure 5.6.3 shows the plots for the south-facing surface. In conjunction with Table 5.6.1 the following points may be observed. The underlying trend (MBE) is significantly better for the proposed model for all seasons. This is also demonstrated in subplots (a) to (d), where the Perez model continues to over-predict. This may be explained by the fact that the large number of empirical coefficients used in the Perez model makes it site-specific. As stated earlier, the Perez model incorporates data only from the Central European sites (44°-46°N latitude) which are between 7° and 11° south of the major conurbation's in the United Kingdom.

A complimentary analysis was carried out between the Moon and Spencer and Uniform sky slope illuminance models. As one might expect, graphical examination display an extremely close similarity between the models with Figs.5.6.5-8 showing the results. The North surface shown in Fig.5.6.5 for the Autumn/spring months clearly demonstrates the better performance of the Moon and Spencer model. The Uniform sky model overestimates quite considerably and this is evident in the plots for the North surfaces for the remaining seasons, all of which are given in appendix 5.6 figures 9-16. The improved performance of the Moon and Spencer model is to be expected by its formulation. The North surface as it is generally in shade will receive 39.6% of the horizontal diffuse illuminance which is very close to the 42% value used by the proposed model for shaded surfaces. The remaining plots in particular highlight the unsuitability of both of these models for use in the estimation of slope illuminance. In these cases the under-estimation is quite apparent. In the majority of instances the Uniform sky model performs better than the Moon and Spencer model, a fact brought out by the statistics given in Table 5.6.2. This can be explained easily as the simple nature of both models neglect the combined contribution of the circumsolar component and anisotropic background diffuse component. This inevitably leads to under-estimation hence as the uniform sky model allows for 1/2 of the horizontal diffuse illuminance as its background diffuse component compared to only 0.396 for the Moon and Spencer model it will perform marginally better. Overall the MBEs are substantially higher when compared to that of the proposed model and demonstrate a clear tendency to under-predict slope illuminance.

Table 5.6.1 Statistical Analysis of Slope Illuminance models Proposed against Perez

		NORTH	EAST	SOUTH	WEST	Figure No	Appendix No
SUMMER							
PEREZ	MBE	-0.95	0.96	1.43	1.17		
	RMSE	1.99	3.84	4.03	4.05		5.6.1-
PROPOSED	MBE	0.19	0.84	-0.95	1.04		5.6.4
	RMSE	1.77	2.90	0.82	2.84		
WINTER							
PEREZ	MBE	-0.12	0.12	0.36	0.13		
	RMSE	0.80	1.39	2.72	1.40		5.6.5-
PROPOSED	MBE	-0.31	-1.10	-0.18	-0.71		5.6.8
	RMSE	1.13	2.07	3.25	1.75		
AUTUMN/SPRING							
PEREZ	MBE	-0.07	0.30	1.94	0.76		
	RMSE	0.92	2.09	3.39	2.47	5.6.1-	
PROPOSED	MBE	-0.02	-0.05	0.56	-0.39	5.6.4	
	RMSE	1.20	2.61	3.01	2.33		

Table 5.6.2 Statistical Analysis of Moon & Spencer against Uniform models

		NORTH	EAST	SOUTH	WEST	Figure No	Appendix No
SUMMER							
Moon & Spencer	MBE	-0.17	-1.23	-1.48	-1.23		
	RMSE	1.81	4.67	2.85	4.20		5.6.9-
UNIFORM	MBE	2.18	1.13	0.87	1.13		5.6.12
	RMSE	3.55	4.77	2.34	4.25		
WINTER							
Moon & Spencer	MBE	-0.33	-1.20	-7.32	-2.10		
	RMSE	1.13	3.45	8.69	2.81		5.6.13-
UNIFORM	MBE	0.86	-1.28	-6.13	-0.91		5.6.16
	RMSE	1.71	2.82	7.65	2.19		
AUTUMN/SPRING							
Moon & Spencer	MBE	0.04	-0.89	-2.91	-1.52		
	RMSE	1.15	2.56	5.53	3.34	5.6.5-	
UNIFORM	MBE	1.57	0.64	-1.39	-0.10	5.6.8	
	RMSE	2.42	2.49	4.59	2.91		

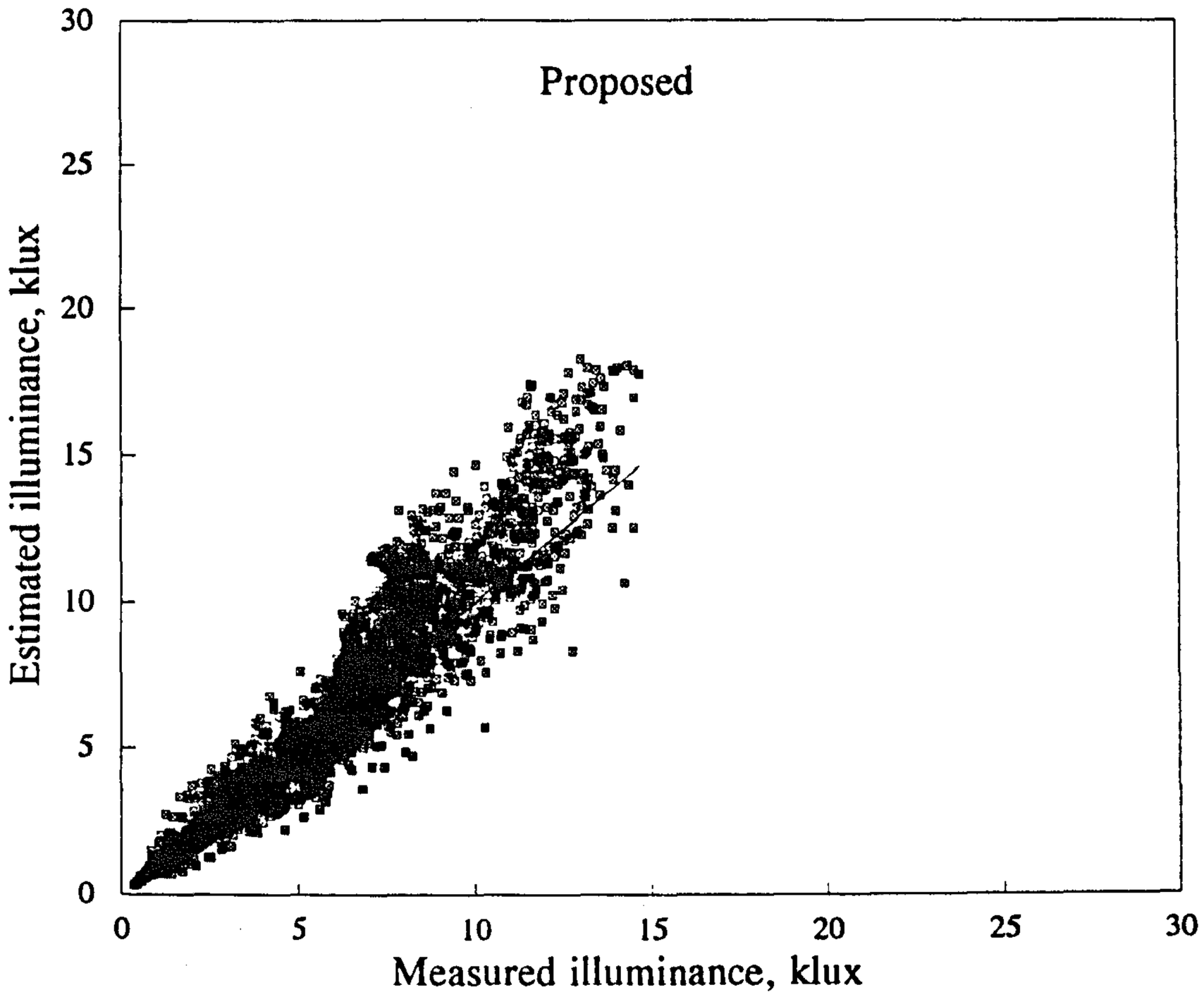

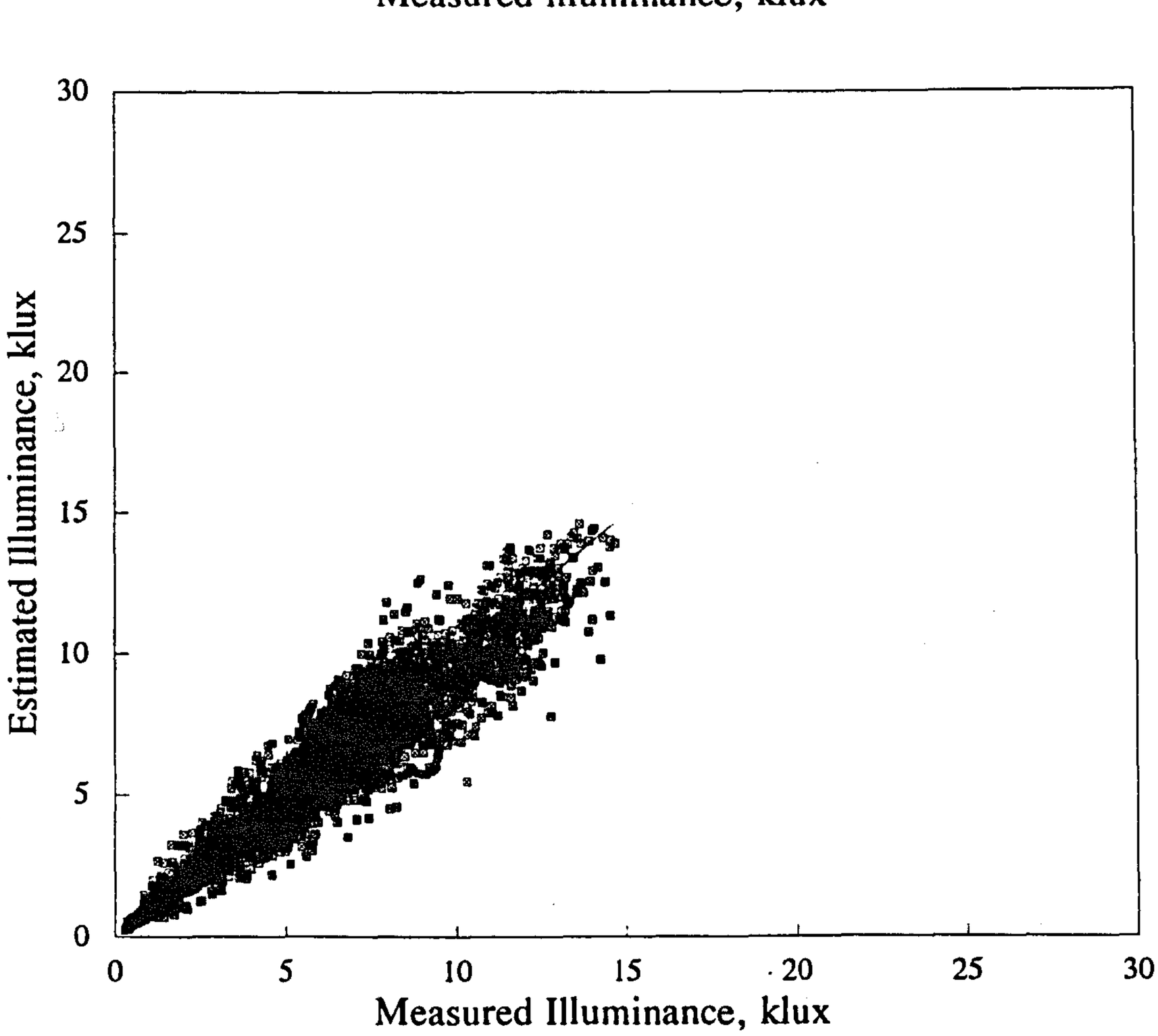

Figure 5.6.1 Autumn/spring: North surface Proposed against Perez model

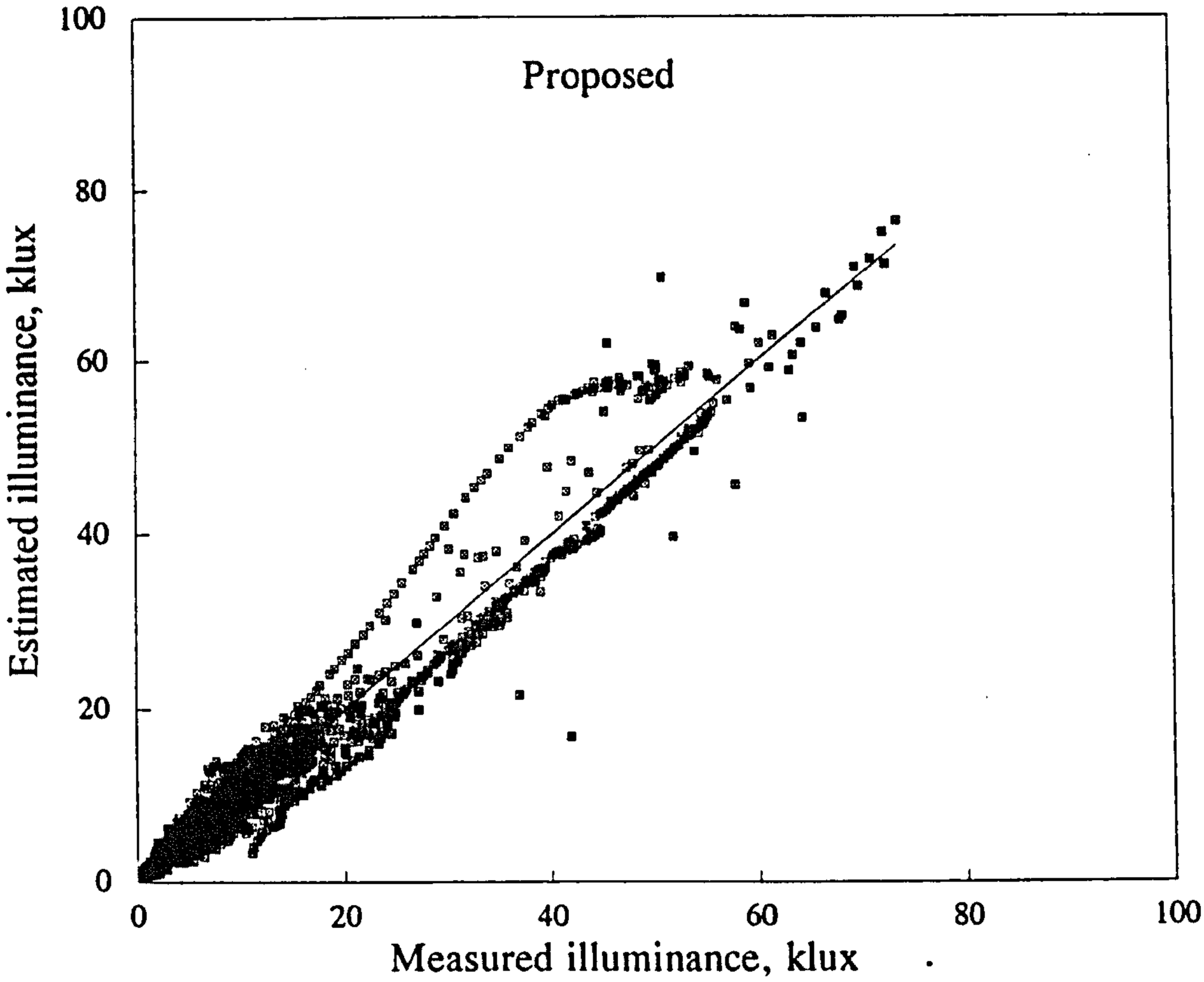

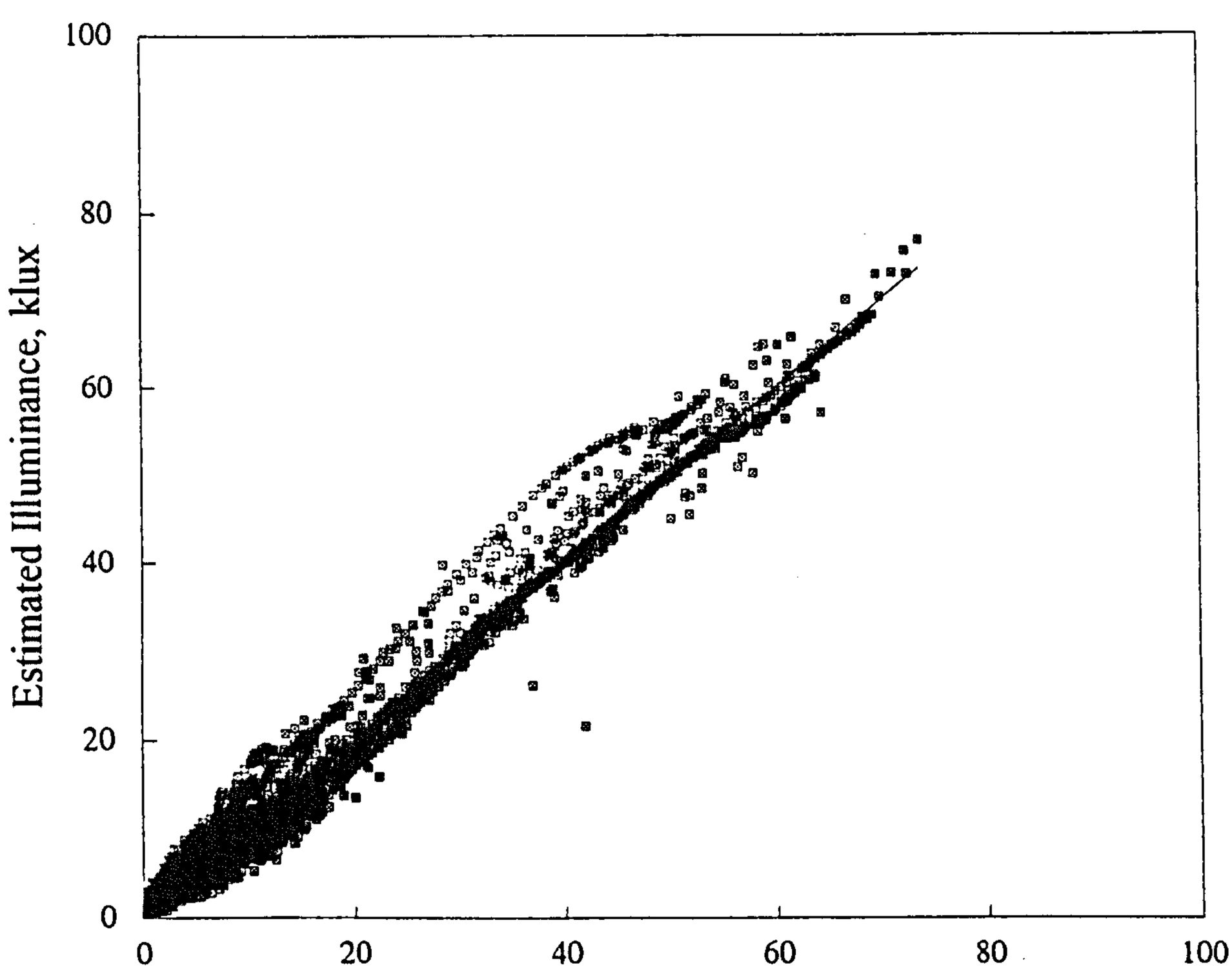

Figure 5.6.2 Autumn/spring: East surface Proposed against Perez mod

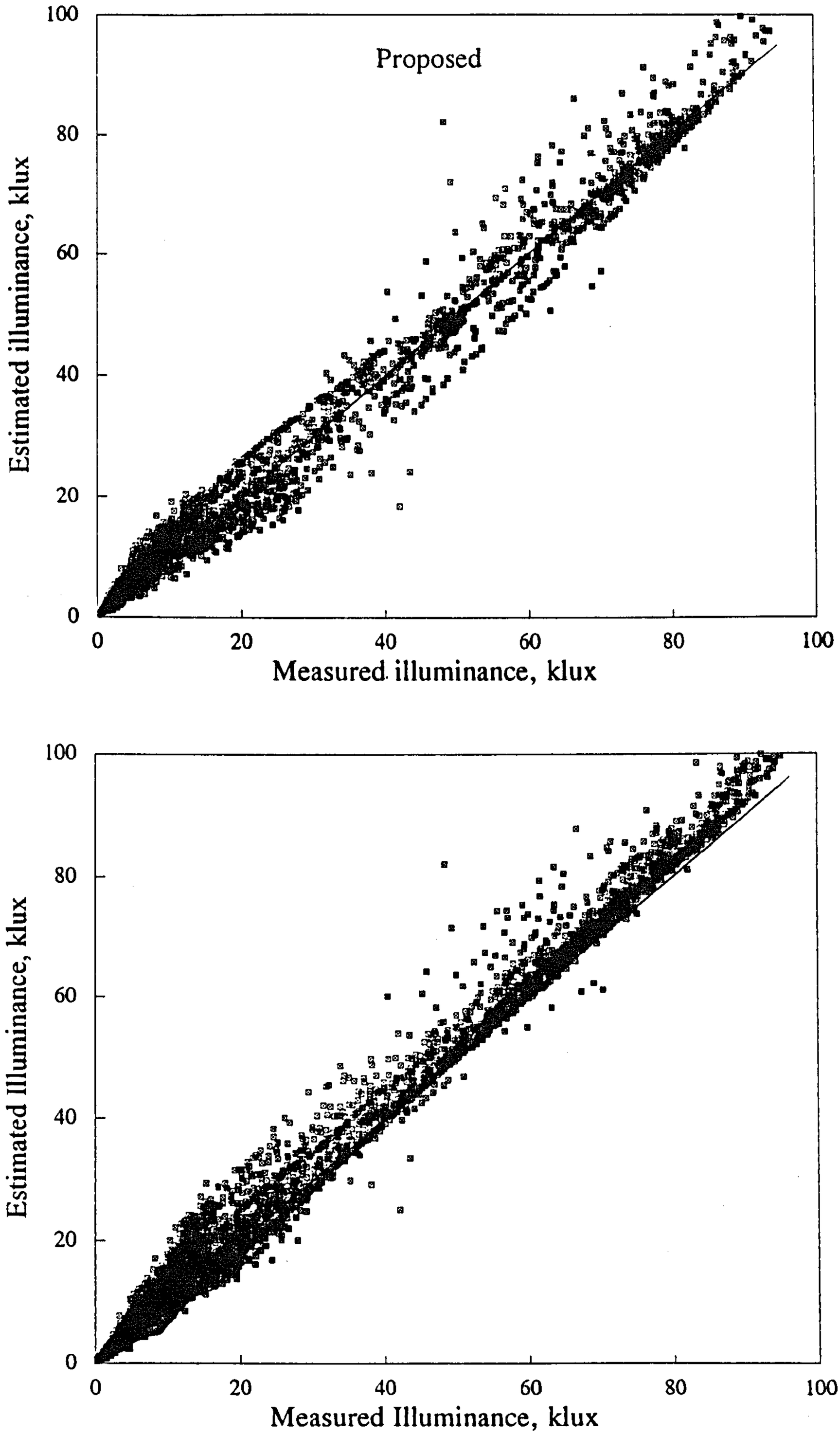

Figure 5.6.3 Autumn/spring: South surface Proposed against Perez model

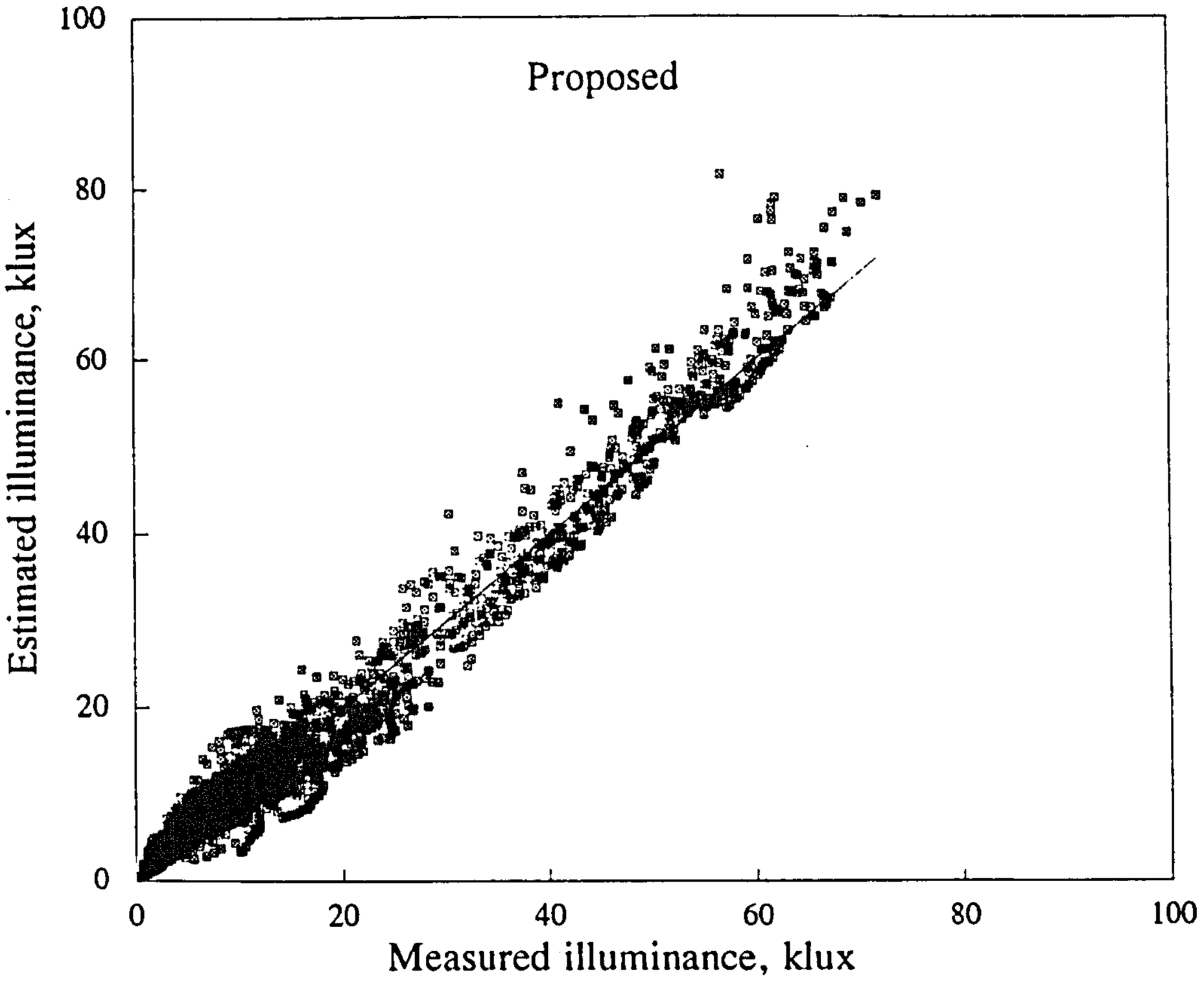

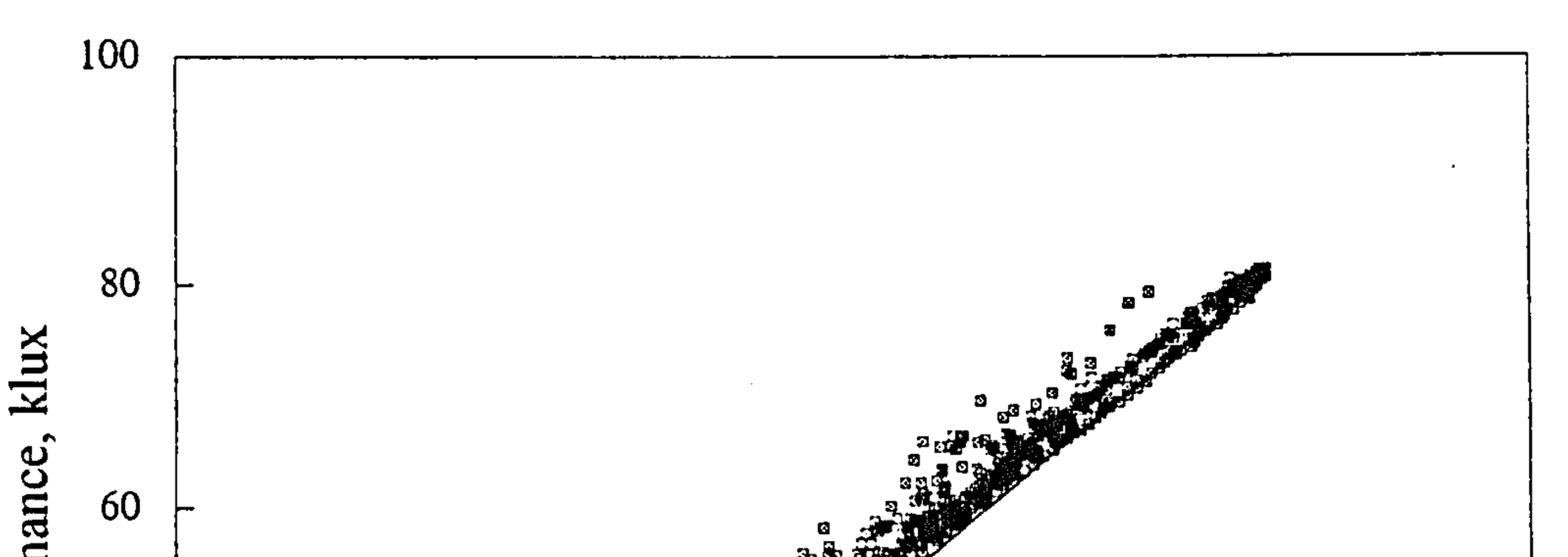

Figure 5.6.4 Autumn/spring: West surface Proposed against Perez mc

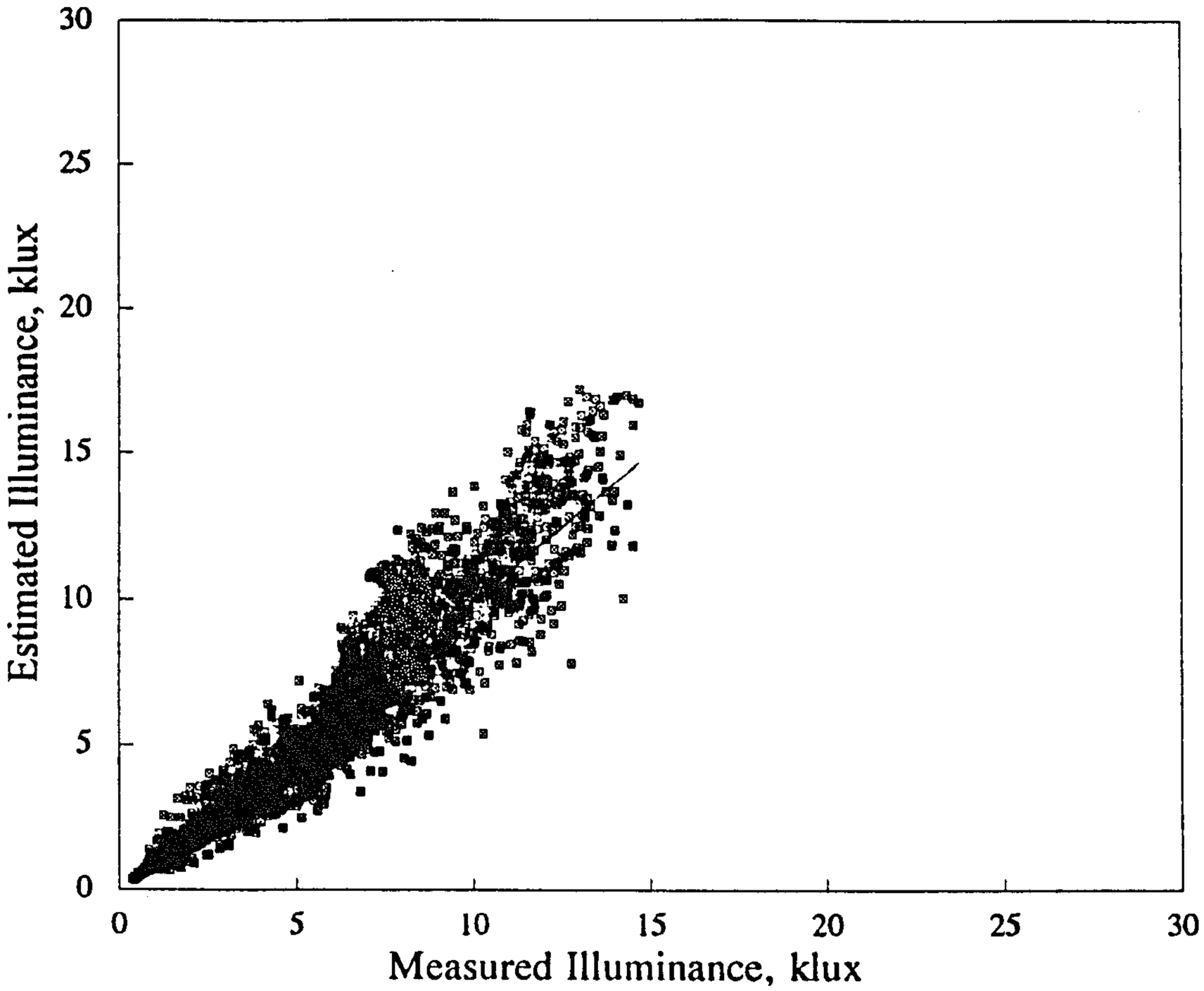

Figure 5.6.5 Autumn/spring:North slope illuminance Moon & Spencer

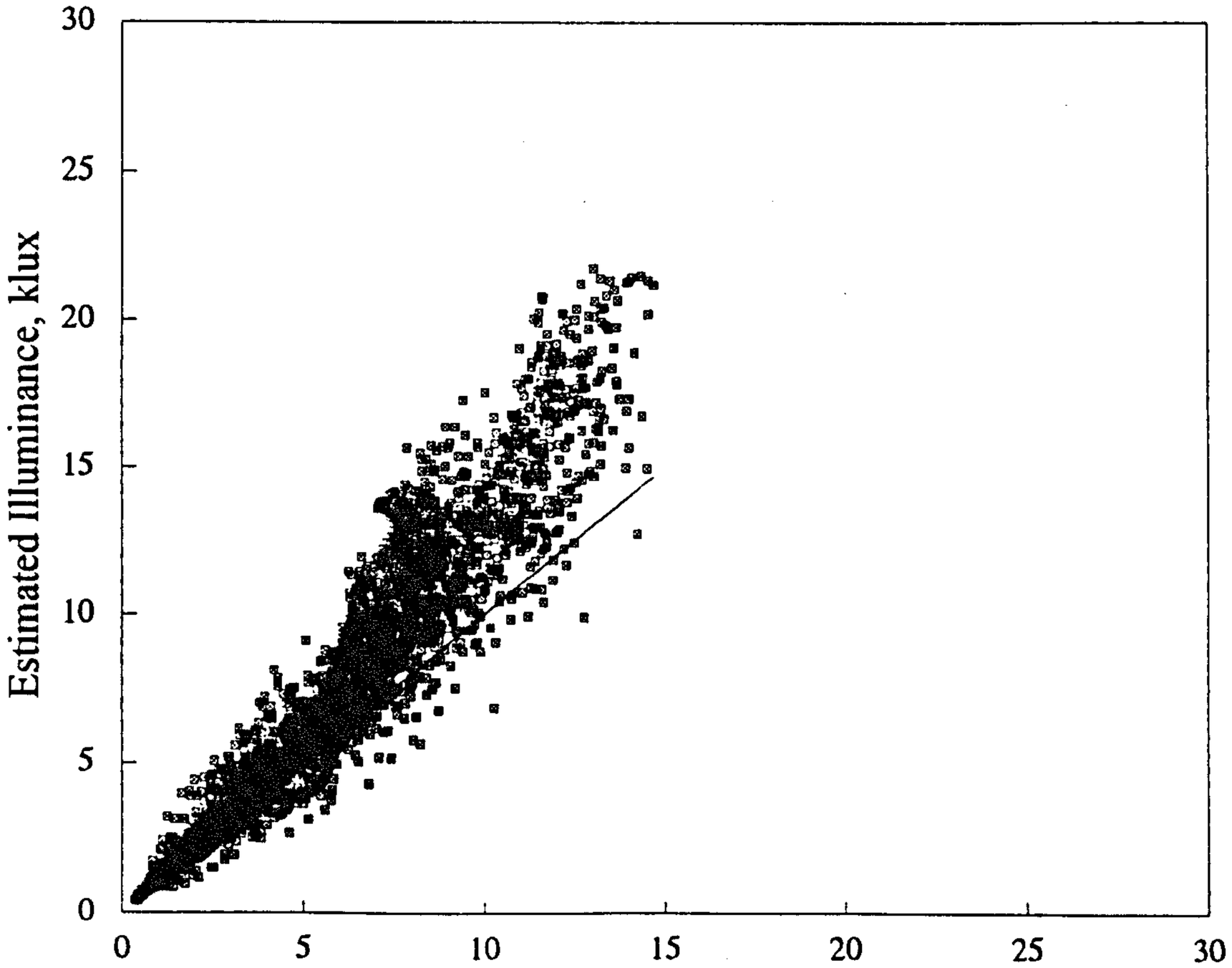

Figure 5.6.5 Autumn/spring: North slope illuminance Uniform

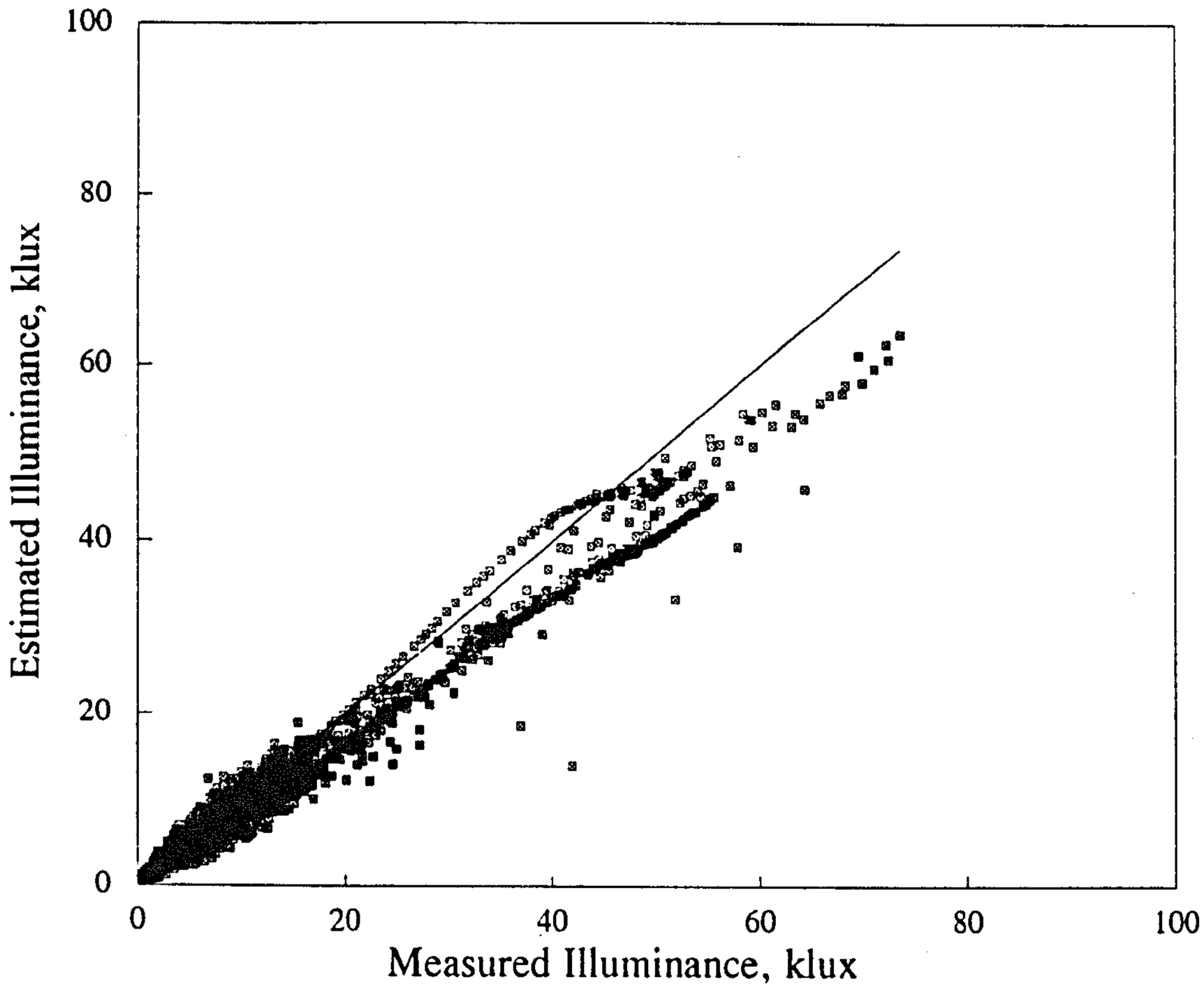

Figure 5.6.6 Autumn/spring:East slope illuminance Moon & Spencer

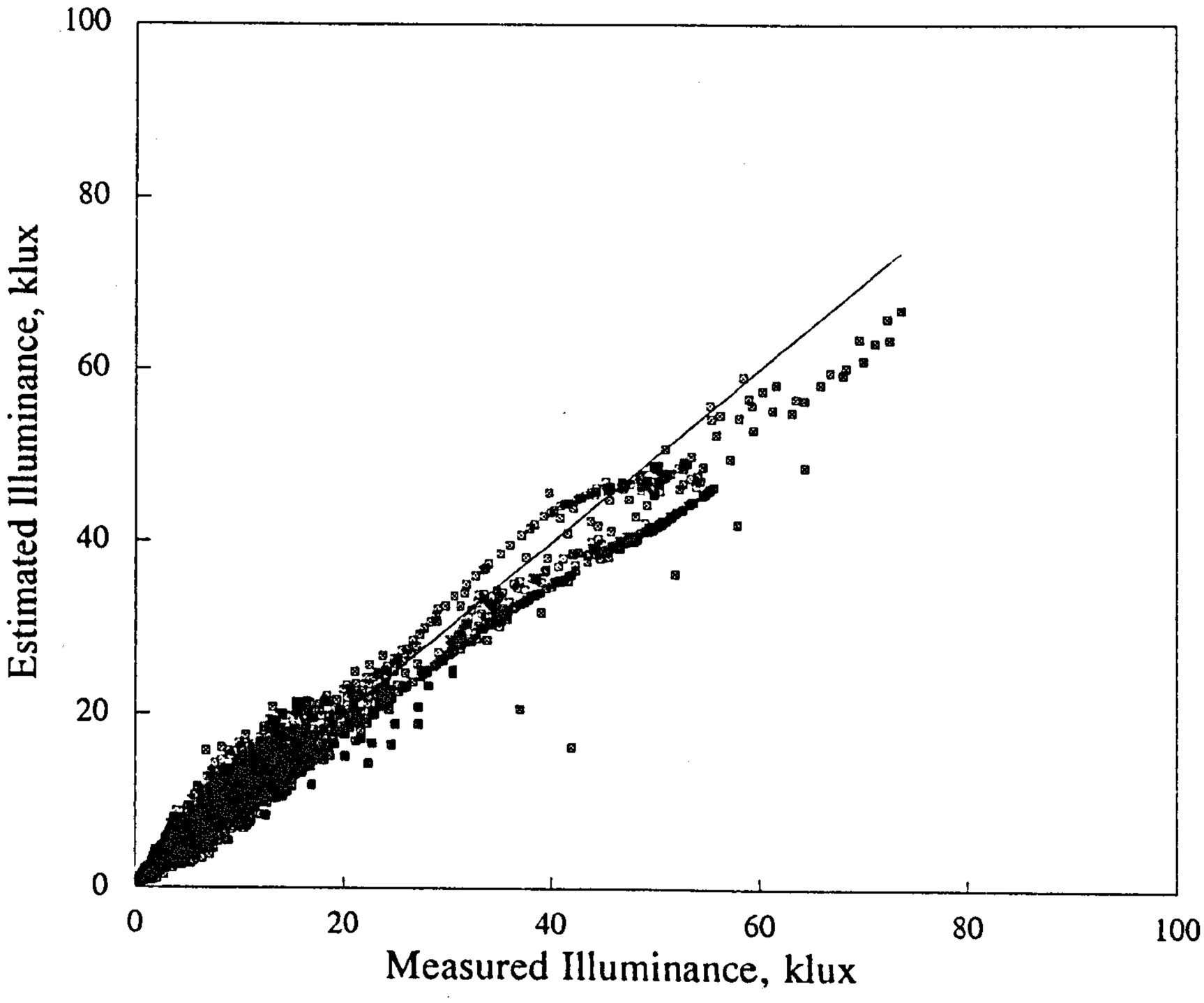

Figure 5.6.6 Autumn/spring: East slope illuminance Uniform

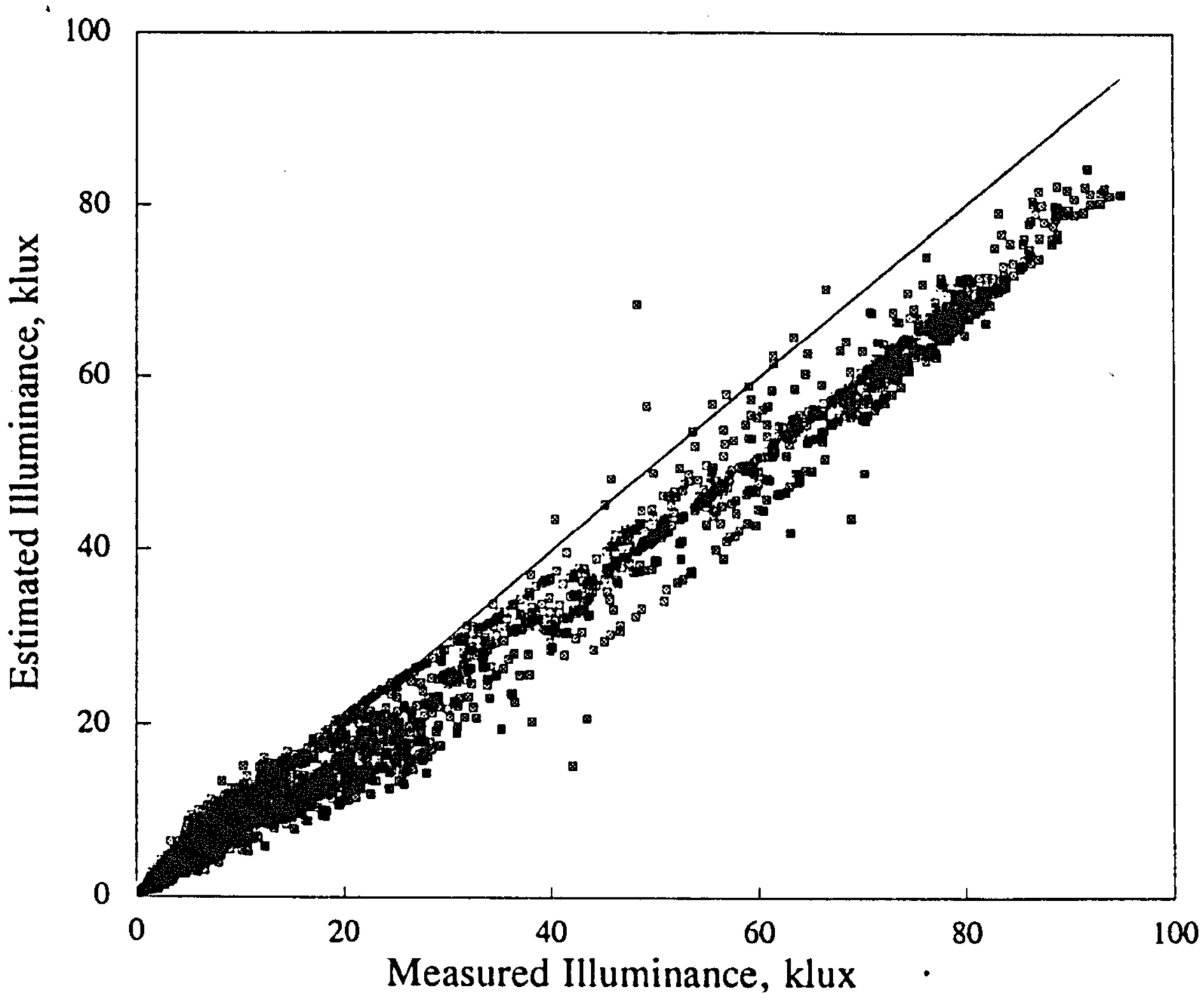

Figure 5.6.7 Autumn/spring:South slope illuminance Moon & Spence

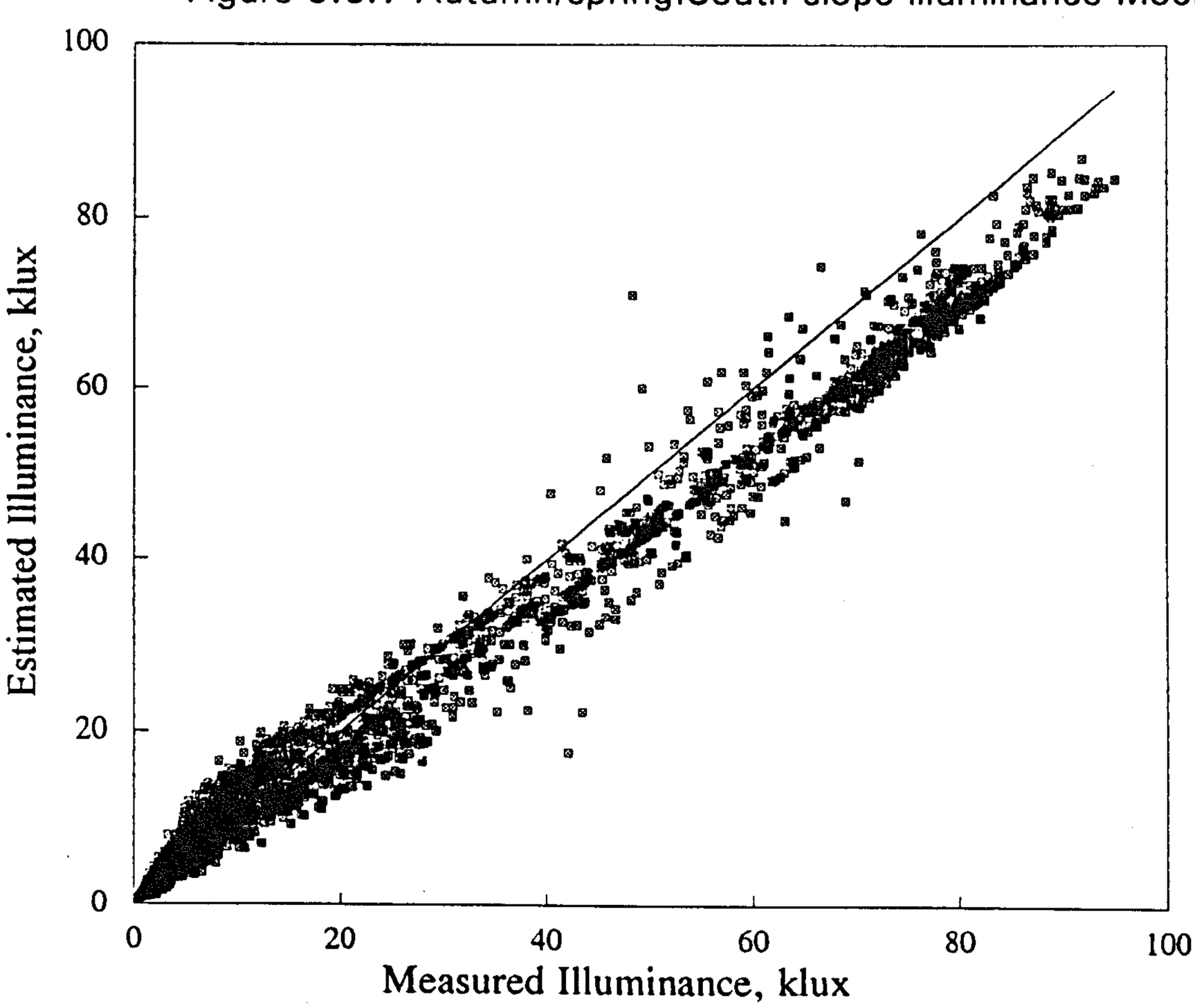

Figure 5.6.7 Autumn/spring: South slope illuminance Uniform

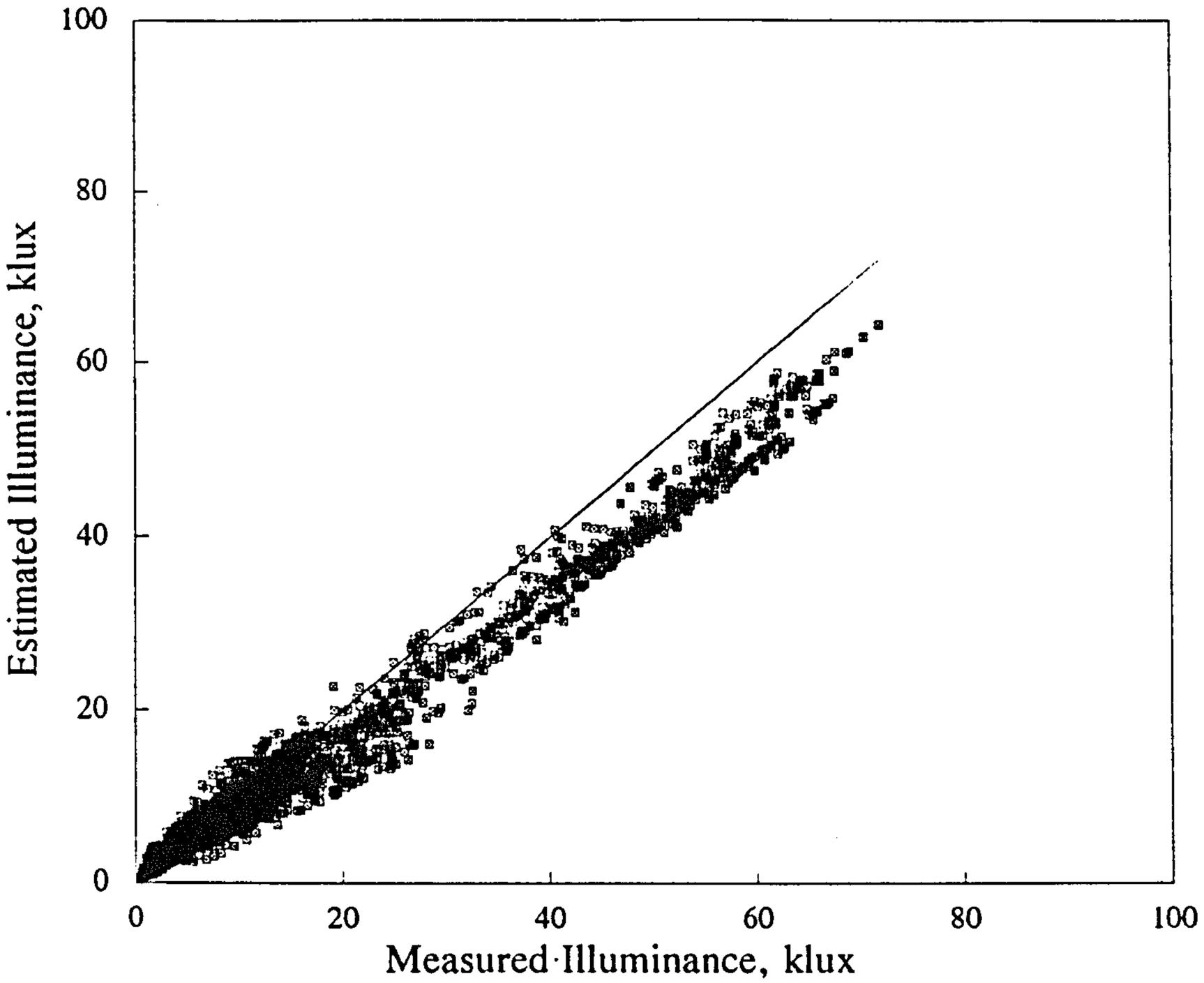

Figure 5.6.8 Autumn/spring:West slope illuminance Moon & Spencer

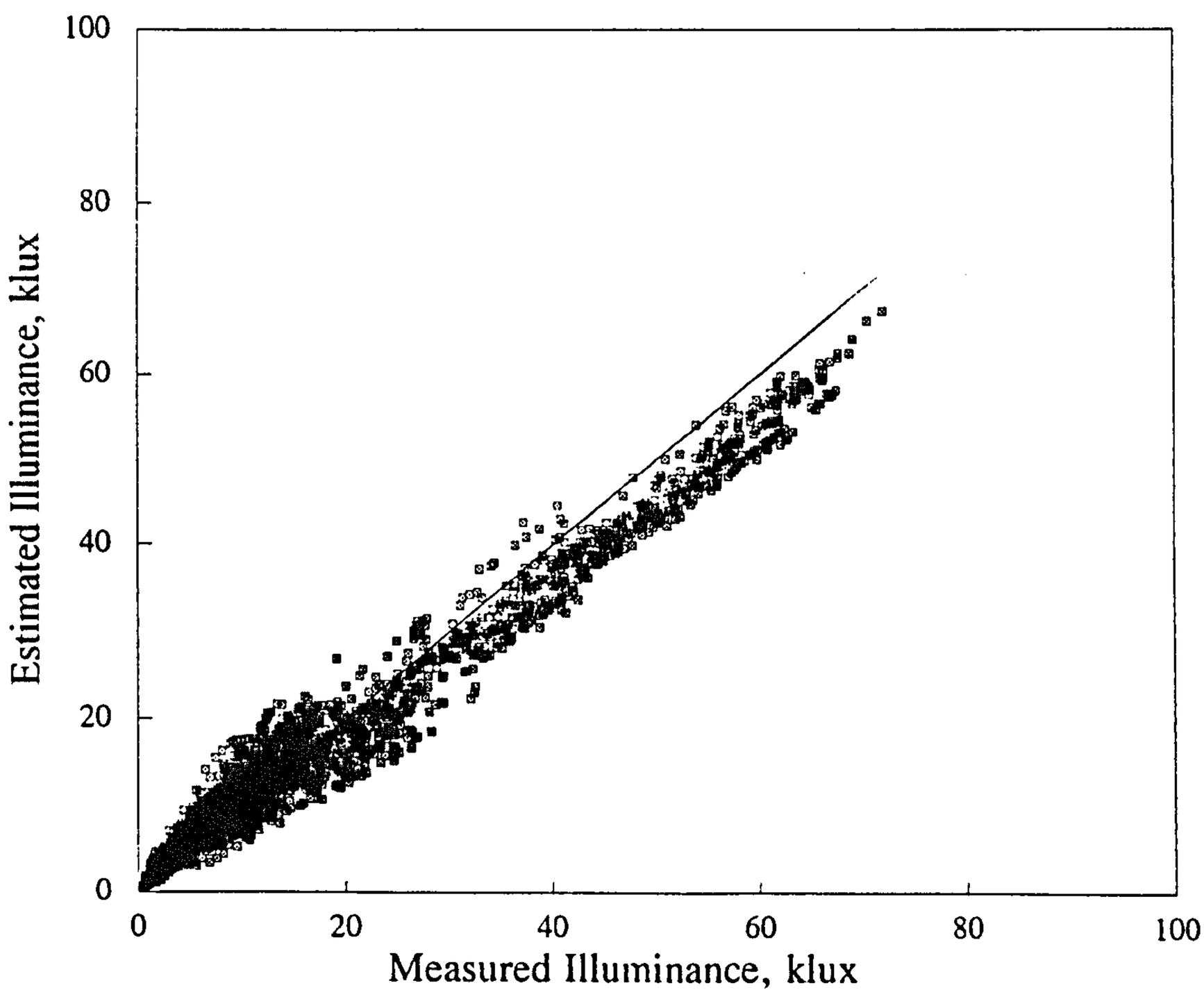

Figure 5.6.8 Autumn/spring: West slope illuminance Uniform

5.7 DISCUSSION

The proposed model for the estimation of vertical and slope illuminance is much simpler than Perez's model. Only three coefficients are required as opposed to forty-eight coefficients for Perez. Obviously it proved much easier to implement the proposed model on the computer using standard spreadsheet packages. The Perez model tends to over-predict the southern illuminances during the summer, autumn and spring seasons. The proposed model shows a better accuracy overall producing a better MBE in 9 out of 12 cases.

It must be emphasised that the simple nature of the proposed model makes it a good candidate for general applicability the as Perez model tends to be site-specific. The Moon and Spencer and uniform sky models perform best in overcast or shaded conditions with the Moon and Spencer model producing better results. Outwith these given criteria both models fail to replicate the same results. The results demonstrate the anisotropic nature of the sky background diffuse luminance for non-overcast conditions.

REFERENCES

5.1 Muneer T, Solar irradiation database for the United Kingdom Building Serv. Eng. Res. Technol. 10(1) 41-45 (1989)

5.2 Duffie J A and Beckmann W A Solar engineering of thermal processes (New York:Wiley) (1980)

5.3 Yallop B D Private communication (London: Royal Greenwich Observatory) (1992)

5.4 Angus R C and Muneer T Sun position for daylight models:Precise algorithms for determination Lighting Res. Technol. 25(2) 81-83 (1993)

5.5 Saluja G S and Muneer T An anisotropic model for inclined surface solar irradiation Proc. Inst. Mech. Engrs. 201 C1, 11-20 (1987)

5.6 Moon P and Spencer D E Illumination from a non-uniform sky Trans. Illum. Eng. Soc. (London) 37 707-725 (1942)

5.7 Perez R, Ineichen P and Seals R Modeling daylight availability and irradiance components from direct and global irradiance Solar Energy 44(5) 271-289 (1990)

5.8 Steven M D Standard distribution of clear sky radiance Q. J. R. Met. Soc. 103 457-465 (1977)

5.9 Kondratyev K J and Manolova M P The radiation balance of slopes Solar Energy 1 14-19 (1960)

5.10 Heywood H The computation of solar radiation intensities Part 2 Solar radiation on inclined surfaces Solar Energy 10 46-52 (1966)

5.11 Steven M D and Unsworth M H The angular distribution and interception of diffuse solar radiation below overcast skies Q. J. R. Met. Soc 106 57-61 (1980)

5.12 Kambezidis H D, Psiloglou B E, Muneer T and Angus R C, Comparison of solar irradiance models with measurements for two regions in Southern and Northern Europe NorthSun Int. Conf. Glasgow 177-182 (1994)

5.13 B E Psiloglou Private communication (Athens: National Observatory of Athens, GR-118 10 Athens)(1994)

5.14 Monteith J L Attenuation of solar radiation:a climatological study Q. J. R. Met. Soc. 88 508-521 (1962)

5.15 Muneer T and Angus R C Daylight illuminance models for the United Kingdom Lighting Res. Technol 25(3) 113-123 (1993)

5.16 Muneer T, Angus R C, Kambezidis H D and Psiloglou B E A comparison of daylight illuminance models for Edinburgh and Athens NorthSun Int. Conf. Glasgow 415-420 (1994)

6 METHODS AND MODELS FOR ESTIMATING INTERNAL ILLUMINANCE

Notation

γ = altitude of sky patch(°)
ε = angle between sky patch and zenith (°)
α = azimuth angle between sky patch and sun(°)
θ = scattering angle (°)
σ = sunshine probability (dimensionless)
τi = the transmissivity of the glass at incidence angle i (dimensionless)
γs = solar altitude(°)
εs = zenith angle (°)
A = total room area (m^2)
$D\gamma\alpha$ = daylight coefficient (dimensionless)
$Da\gamma\alpha$ = sky and externally reflected components (dimensionless)
$Db\gamma\alpha$ = internal reflection of upper room surfaces (dimensionless)
$Dc\gamma\alpha$ = internal reflection by lower parts of the room (dimensionless)
E = total daylight illuminance (lux)
L = Total luminance of all sky types (kCd/m^2)
$L\gamma$ = Luminance of sky at altitude γ (kCd/m^2)
$L\gamma\alpha$ = luminance of the sky patch (kCd/m^2)
L_{BV} = vertical beam illuminance (lux)
L_D = Horizontal diffuse illuminance (lux)
LG = Horizontal global illuminance (lux)
L_{INT} = internal illuminance (lux)
Lqcl = Luminance of quasi-clear sky (kCd/m^2)
Lqoc = Luminance of quasi-overcast sky (kCd/m^2)
Lz = zenith luminance (kCd/m^2)
$P_{1\text{-}4}$ = empirical parameters (dimensionless)
R = mean room reflectance (dimensionless)
Rcw = ceiling and upper wall surfaces reflectance (dimensionless)
Rfw = reflectance of the floor and lower walls (dimensionless)
Rg = Mean ground reflectance (dimensionless)
T = mean glass transmittance (dimensionless)
v = window azimuth (°)
W = window area (m^2)

6.1 INTRODUCTION

A commonly used method of estimating the natural daylight entering a building is the daylight factor calculation. This method provides architects and building designers with the necessary information to plan artificial lighting to supplement natural daylight. It is therefore important to evaluate the daylight factors precisely for a particular building at the design stage. To do this sky factors have to be calculated. Sky factors can be obtained either from CIE daylight tables or tables for Uniform Skies[6.1]. This simple and robust approach accounts for a small proportion of the varying sky conditions and generally does not represent the sky luminance distribution for real skies or take into account the building's orientation. This chapter shall review the current use of daylight design tools and investigate the area of sky luminance distribution models with a view to amalgamate the two topics to produce an innovative daylight design tool.

6.2 DAYLIGHT FACTORS AND SKY LUMINANCE DISTRIBUTIONS

Daylight factors have been employed by architects and building designers for many years. This approach expresses the amount of light inside a building as a percentage of the available exterior daylight. This percentage is calculated from the geometry of the glazed apertures and a knowledge of the sky's illumination. It is therefore vital for effective daylight design to have an accurate means of calculating external daylight as inappropriate methods can lead to occupancy discomfort and unnecessary artificial lighting consumption.

The daylight factor is in fact a combination of 3 components; sky component, externally reflected and internally reflected components shown in figure 6.2.1.

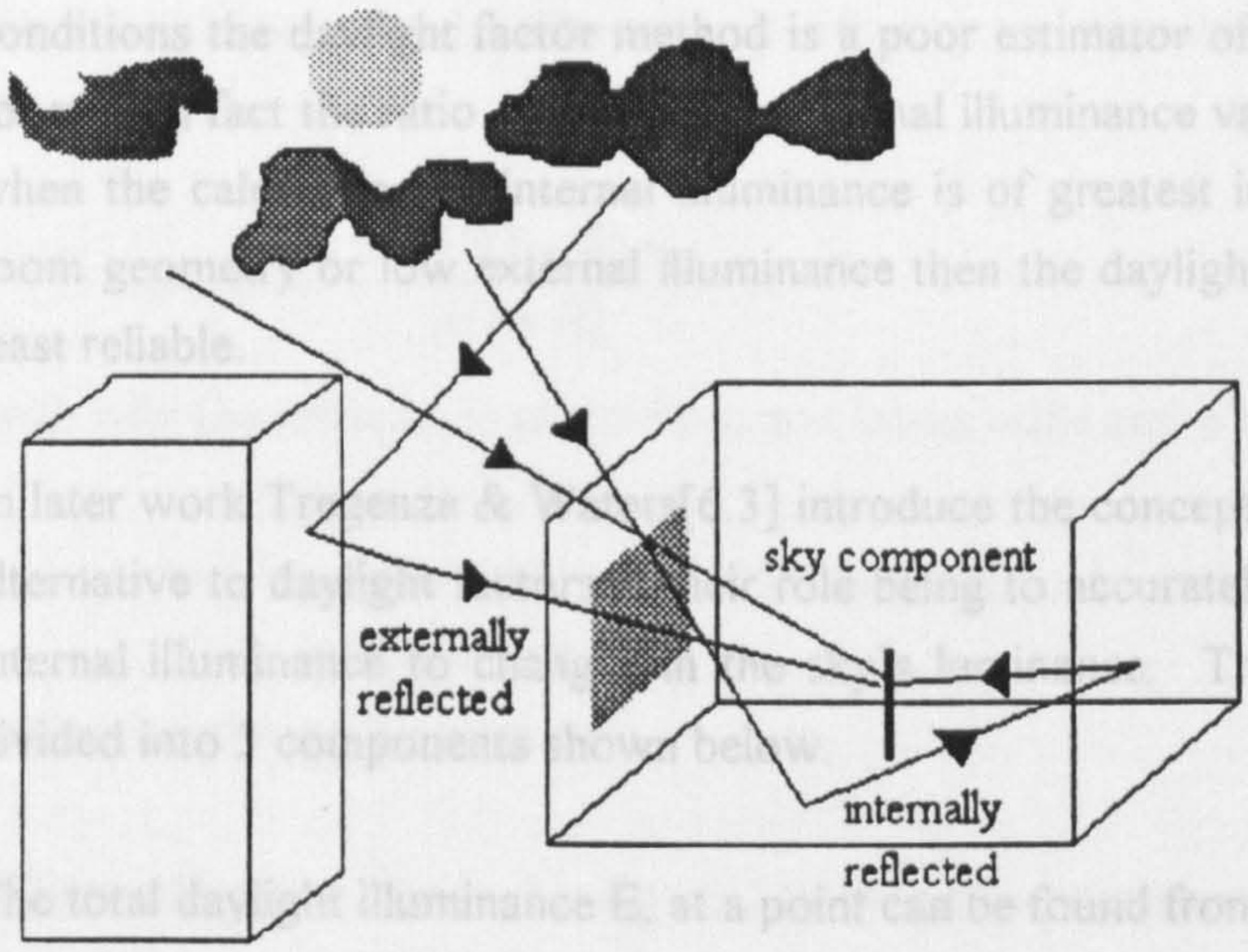

Figure 6.2.1 Illustration of daylight factor components

It is the sky component which is of most significance and in the case of a uniform sky and unglazed rectangular window is named the sky factor. As has been shown in chapter 5 the uniform sky is unsuitable for slope illuminance calculations and is unrepresentative of the majority of sky conditions and in light of this the CIE overcast sky is often employed as an alternative.

Much research has been centred around the use of daylight and sky factors with several authors questioning their applicability for daylight design purposes. Tregenza[6.2] examined daylight factors and investigated whether the ratio of internal illuminance to external horizontal illuminance was constant. This work was carried out using models of rooms erected externally on the roof of a building just outside Nottingham. Inside the model rooms 3 illuminance sensors were mounted to provide daylight factors of 5, 2 and 1%. Horizontal global and diffuse illuminance sensors measured external illumination. Measurements were carried out over several months for a whole range of sky conditions. This study revealed interesting results and raises doubt over the validity of the daylight factor method. The main observations arising from the study indicate that over all weather

conditions the daylight factor method is a poor estimator of the horizontal illuminance in rooms. In fact the ratio of internal to external illuminance varied considerably. Moreover when the calculation of internal illuminance is of greatest importance, i.e. as a result of room geometry or low external illuminance then the daylight factor method proved to be least reliable.

In later work Tregenza & Waters[6.3] introduce the concept of daylight coefficients as an alternative to daylight factors. Their role being to accurately define the sensitivity of the internal illuminance to changes in the sky's luminance. The daylight coefficient is sub-divided into 3 components shown below.

The total daylight illuminance E, at a point can be found from;

$$E = \int_0^{2\pi}\int_0^{\pi/2} D\gamma\alpha\, L\gamma\alpha \cos\gamma d\gamma d\alpha \qquad 6.1$$

where $D\gamma\alpha$ is the daylight coefficient, dependent on room geometry external and internal reflectance and transmittance of windows. $L\gamma\alpha$ is the luminance of the patch of sky being considered. γ is the altitude of the sky element and α is the azimuth. From this equation $D\gamma\alpha$ is split into 3 components where;

$$D\gamma\alpha = Da\gamma\alpha + Db\gamma\alpha + Dc\gamma\alpha \qquad 6.2$$

$Da\gamma\alpha$ consists of the sky and externally reflected components given below

$$Da\gamma\alpha = \sin\gamma\, \tau i \qquad 6.3$$

where τ is the transmissivity of the glass at incidence angle i.

$$Db\gamma\alpha = \frac{\sin\gamma\, Rg\, Rcw\, W\, T}{2A(1-R)} \qquad 6.4$$

$Db\gamma\alpha$ accounts for the internal reflection of upper room surfaces, where Rg, Rcw, W, A, T and R are respectively, mean ground reflectance, ceiling and upper wall surface reflectance, window area, total room area, mean glass transmittance and mean room reflectance.

The final component describes the contribution to internal reflection by lower parts of the room,

$$Dc\gamma\alpha = \frac{\cos i \; Rfw \; W \; \pi i}{A(1+R)} \qquad 6.5$$

with Rfw the reflectance of the floor and lower walls and where,

$$\cos i = \cos\gamma \cos(\alpha - v),\ 0 \le \gamma \le \pi/2,\ -\pi/2 \le \phi - v \le \pi/2,$$
$$= 0 \text{ otherwise} \qquad 6.6$$

where v is the window azimuth.

When added as shown by Eq. 6.2 they produce comprehensive daylight coefficients encompassing all interactive reflective components.

The second stage of this work was to transfer these coefficients into finite element matrices for computer application, allowing either measured sky luminance data or calculated values to be employed in order to calculate internal illuminances under clear and overcast skies. This approach allows such calculations to be made for all levels of cloud cover, solar position and turbidity making it a much more versatile alternative to the standard daylight factor method.

The prediction of internal illuminance in buildings has also been studied from a different view point by several authors[6.4,6.5,6.6] one of these studies is by Diasty et al[6.7]. Their research concentrated on the production of a more accurate sky or direct component for use in daylight factors. This involved a departure from the use of a uniformly luminous sky hemisphere and employs an adaptation of the CIE clear sky model developed by Kittler[6.8], acknowledging the horizon brightening effects present in clear skies.

The authors efforts produce a clear sky luminance distribution which is time dependent, i.e. incorporates variations in solar altitude as well as zenith luminance. Their work was evaluated using a variety of glazing geometry yielding interesting results. It was shown that the uniform blue sky model was on the whole unsuitable for daylight calculations as it failed to account for the dynamic nature of real, clear sky conditions. There are however some limitations to their model as it considers only clear skies which represent only a small percentage of typical UK and Northern European weather patterns. More significantly while they address the variance in the direct sky component the authors omit the

contribution to internal illuminance from direct sunlight which is synonymous with clear skies.

The underlying theme which is apparent in the majority of the research into internal illuminance is the modelling of the sky's luminance distribution. It is this specialised area that has attracted a great deal of attention over the past few years partly as a result of the IDMP programme expanding the database of measured sky luminance data. In the United Kingdom two research class stations at BRE, Watford and Sheffield University measure sky luminance via Krochmann sky scanners. Prior to these developments several authors[6.9-6.12] and in particular Kittler[6.8] and Gusev[6.12] have proposed sky luminance models that use atmospheric scattering phenomena through the diffusion indicatrix concept first development by Kittler and shown by Eq.6.7.

$$F(\varepsilon,\theta) = P_1(1 - e^{-P4\sec(\varepsilon)})\,(1 + P_2(e^{-3\theta} - 0.009) + P_3\cos^2\theta) \qquad 6.7$$

where P_1, P_2, P_3 and P_4 are empirical parameters calculated from measured data. The angles involved in sky luminance distribution work are illustrated in Figure 6.2.2. θ, the scattering angle is calculated by Eq.6.8.

$$\theta = \cos^{-1}(\sin\varepsilon \sin\varepsilon_s \cos\alpha + \cos\varepsilon \cos\varepsilon_s) \qquad 6.8$$

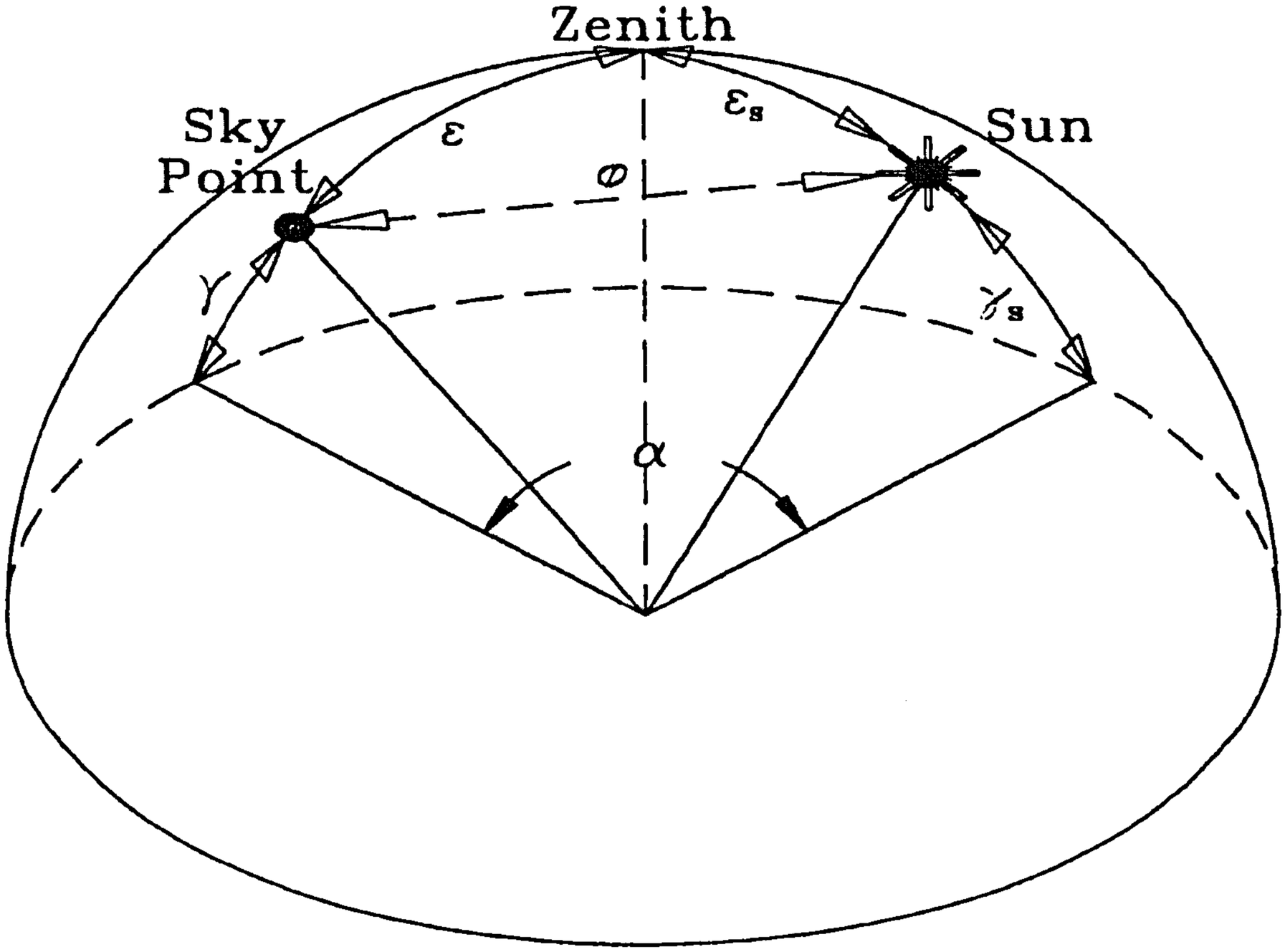

Figure 6.2.2 Solar geometry of sky hemisphere

Table 6.2.1 compares the values of P_{1-4} for Kittler, Gusev and a derived set of parameters from a dataset measured in San Fransisco in a project carried out by Karayel et al[6.13].

Table 6.2.1 Comparison of scattering indicatrix parameters by various authors

	Kittler	Gusev	Karayel et al
P_1	0.91	0.856	0.98
P_2	10	16	13
P_3	0.45	0.3	-0.28
P_4	0.32	0.32	0.38

The results were most encouraging with Karayel et al noting that model is suitable for the San Fransisco data. Karayel commented on the variances in the parameters and suggests a more in-depth analysis be carried out to relate the four coefficients to atmospheric properties. It is further suggested that atmospheric turbidity affects the shape of the diffusion indicatrix and hence the values of P_{1-4}, such that each location would possess its specific set of parameters, in a similar way to the proposed slope illuminance model with its background diffuse curves in chapter 5.

Kittler and Gusev's work has been the centre of analysis by other authors with Littlefair[6.14-6.16] evaluating their sky luminance models using a different approach. Both models were adapted to produce linear combinations of clear and overcast sky conditions weighted according to sunshine probability. The initial results indicated that the CIE clear sky was not anisotropic enough to adequately predict luminances opposite to the suns position in the sky.

The Gusev model on the whole performed better for the BRE data, the reason offered is that the cloudy and fairly turbid nature of the BRE site was better suited to the Gusev model which was intended for use in hazier clear skies with high Linke turbidity factors of 5 or greater.

As a result of these findings Littlefair[6.15] compared a variety of sky luminance models for differing atmospheric conditions, namely clear skies, quasi-clear skies and skies with Linke turbidities less and greater than 5 in an effort to find an optimum solution. In each case the sky dome was divided into 6 segments on which the analysis was based. The quasi-clear sky was introduced by Littlefair as an alternative to the clear sky scenario. The difference being that a sky is categorised quasi-clear if the sunshine probability was 1 even if clouds that didn't obscure the sun were present. The development of the quasi-clear sky allows for a higher frequency of clear skies as absolutely cloudless clear blue skies are rare in the UK and Northern Europe.

A result of some significance emerged from this analysis which involved the comparison of clear and quasi-clear skies. Examination showed the two types of skies produced very similar results in all the sky luminance models tested. This indicates that the average luminance distribution of quasi-clear and clear skies are very alike.

Littlefair developed a function that characterises the quasi-clear sky's luminance distribution using the BRE data. The function employs the scattering indicatrix approach of Kittler for which the coefficients P_{1-4} were derived to give the function below.

$$Lqcl = \frac{18200 \sin \gamma s}{(1 + 6\gamma s / \pi)}\left(1 + 21.5e^{-3\theta} + 0.28\cos^2 \theta\right)\left(1 - e^{-0.47 \sec \varepsilon}\right) \qquad 6.9$$

The first term in the brackets is the relative scattering indicatrix. The exponential term represents the effect of Mie scattering with high values of P_2 an indication of large levels of aerosols in the atmosphere. Rayleigh scattering is accounted for by the cos2θ term, this has less significance in hazy and turbid conditions. Under such conditions the value of P_4 will be large.

The newly developed quasi-clear sky luminance distribution produces the lowest RMSE values in comparison with the other models and very favourable MBE's which is as would be expected from a model evaluated by the same database that was the basis of its derivation. This model also produced good results when evaluated against the clear sky dataset which strengthens its broader application as a general clear sky model. The author suggests the model will be suitable for locations with similar climate and turbidity as southern England.

In a complementary analysis Littlefair also developed the quasi-overcast sky model using skies with a sunshine probability of zero;

$$Lqoc = (1 + \sin\gamma)(40 + 4078\gamma s + 1350e^{-2\theta}) \qquad 6.10$$

This model was combined with the quasi-clear sky model to produce a general sky luminance model using Eq.6.11.

$$L = \sigma Lqcl + (1 - \sigma)Lqoc \qquad 6.11$$

The model was evaluated against clear, intermediate and cloudy skies with indifferent results. It was demonstrated through statistics that this model performed poorly in the case of intermediate skies an area which has been investigated in some depth by Nakamura et al[6.17] and Matsuura[6.18].

Sky luminance models of a more complex nature such as the ASRC-CIE[6.19] model were also evaluated by Littlefair using the BRE data. The ASRC-CIE model incorporates 4 sky luminance models. These being Kittler's clear sky model, Gusev's clear sky model, Nakamura et al intermediate sky model and the Moon and Spencer CIE overcast model. The combined model selects two of the four models depending on values of ε, and sky clearness. The two models are combined in a weighted form depending on values of ε and Δ(see chapter 4.3). This technique reaps the benefits of the models while avoiding their individual weaknesses. A similar approach has been proposed by Kambezidis et al[6.20] for slope irradiance models using F clearness index as the dependent in selection of the most appropriate model. Overall the ASRC-CIE model yields extremely good results which have to be offset against the complexity of its structure and operation.

Perez et al[6.21] also developed an all weather model for sky luminance distribution which compared against the BRE data produces poorer results in comparison to the ASRC-CIE model. This may be as a result of the model being derived from the Berkeley dataset which possesses different climatic and atmospheric conditions than those of Southern England. This conclusion has also been borne out of the present slope illuminance modelling work.

6.3 ILLUMINANCE DATA

To evaluate the proposed sky luminance distributions, daylight data supplied from the Building Research Establishment (BRE) daylight monitoring station at Garston were used. This is a research class station in accordance with the International Daylight Measurement Programme[6.22]and uses data from a sky scanner in addition to the horizontal global and diffuse, and vertical measurements of illuminance and irradiance of the general class station. The sky scanner is a very specialised piece of equipment and is subject to measurement error as has found to be the case by many station supervisors. Faults have occurred in the sky scanners of Sheffield University and the BRE station. Littlefair[6.14] discusses a response time error with the scanner used by Ineichen who reported RMS errors of 10%.

As part of the analysis, clear and overcast days were selected from the BRE data to enable a study of sky conditions and allow a comparative analysis to take place. Clear days were selected first by visual inspection of global and diffuse illuminances. Overcast days were selected along similar lines with global and diffuse illuminance variation following each

other very closely. Once a visual inspection had identified potential clear and overcast days each day, had to satisfy a more stringent selection process which specified that on a clear day the ratio of diffuse to global illuminance was less than 0.4 and more than 0.95 for overcast skies. Further distinctions were made between a surface which faced towards the sky-quadrant containing the sun and away from it, such that for each sky condition there were two cases to be considered, i.e. sunfacing and shaded surface. The sky scanner data were separated into the clear and overcast sky conditions and orientations described. Circumsolar data were removed from the database as it showed extreme brightness in the vicinity of the sun even under overcast skies. It was found that the circumsolar component affected an area covering 15 degrees around the sun. Other measurements required were horizontal global and diffuse illuminance and zenith luminance (L'z), these were also obtained from the BRE. The data provided by the BRE were quality control checked using the CIE quality control programme[6.22].

6.4 DAYLIGHT ILLUMINANCE FACTORS

As has been shown in the previous sections much debate exists in the daylight fraternity as to which estimation method best calculates the internal illuminance in buildings. Doubts have been raised over the suitability of daylight factors by Tregenza and the use of standard sky luminance models is questioned by various authors. It appears that what's required is a model that uses real sky distributions and calculates internal illuminance for all possible scenarios. It is the aim of this section to produce such a design tool and evaluate its results in a comparison with currently employed CIE and Uniform sky factors. The concept of daylight factors shall be expanded to allow for variable and realistic sky conditions through the analysis of sky luminance distributions provided by the BRE. In addition this work will address the contribution to internal illuminance by the inclusion of direct sunlight. Several cases shall be considered which collectively characterise the actual conditions experienced in building design through the utilisation of building orientation and cloud cover. Five cases have been identified for analysis which are as follows;

Case 1: Overcast sky, window in shade

Case 2: Overcast sky, sunfacing window

Case 3: Clear sky, window in shade

Case 4: Clear sky, diffusely illuminated sunfacing window

Case 5: Clear sky, directly and diffusely illuminated sunfacing window

The extreme conditions of clear and overcast skies are examined initially with the remaining sky conditions catered for later in the section.

For each case the daylight illuminance factor is calculated by its definition introduced herein of the ratio of internal illuminance due to daylight component to the sky illuminance under the sky hemisphere,

$$\text{Daylight Illuminance Factor} = \frac{Lz\left[\frac{I_1}{1+b} + \frac{bI_2}{1+b}\right]}{\text{Illuminance under the sky hemisphere}} \qquad 6.12$$

Lz is the pseudo zenith luminance (kCd/m^2). This term (Lz) is employed to simplify the analysis and it is merely an estimated zenith luminance value which can be calculated from Eq 6.29. I_1 and I_2 are given by[6.1]

$$I_1 = \int_0^{\frac{H}{D}} \int_0^{\frac{W}{D}} \frac{Y}{\left(1+X^2+Y^2\right)} dX\, dY \qquad 6.13$$

$$I_2 = \int_0^{\frac{W}{D}} \int_0^{\frac{H}{D}} \frac{Y^2}{\left(1+X^2+Y^2\right)^{\frac{5}{2}}} dY\, dX \qquad 6.14$$

The geometry terms W/D and H/D referred herein are the ones shown in Fig.6.4.1. 'b' is the sky luminance distribution index first proposed by Moon and Spencer[6.9] and has the function of relating Lγ, the luminance of a patch of sky of altitude γ to the zenith luminance viz,

$$L\gamma = Lz\left(\frac{1+b\sin\alpha}{1+b}\right) \qquad 6.15$$

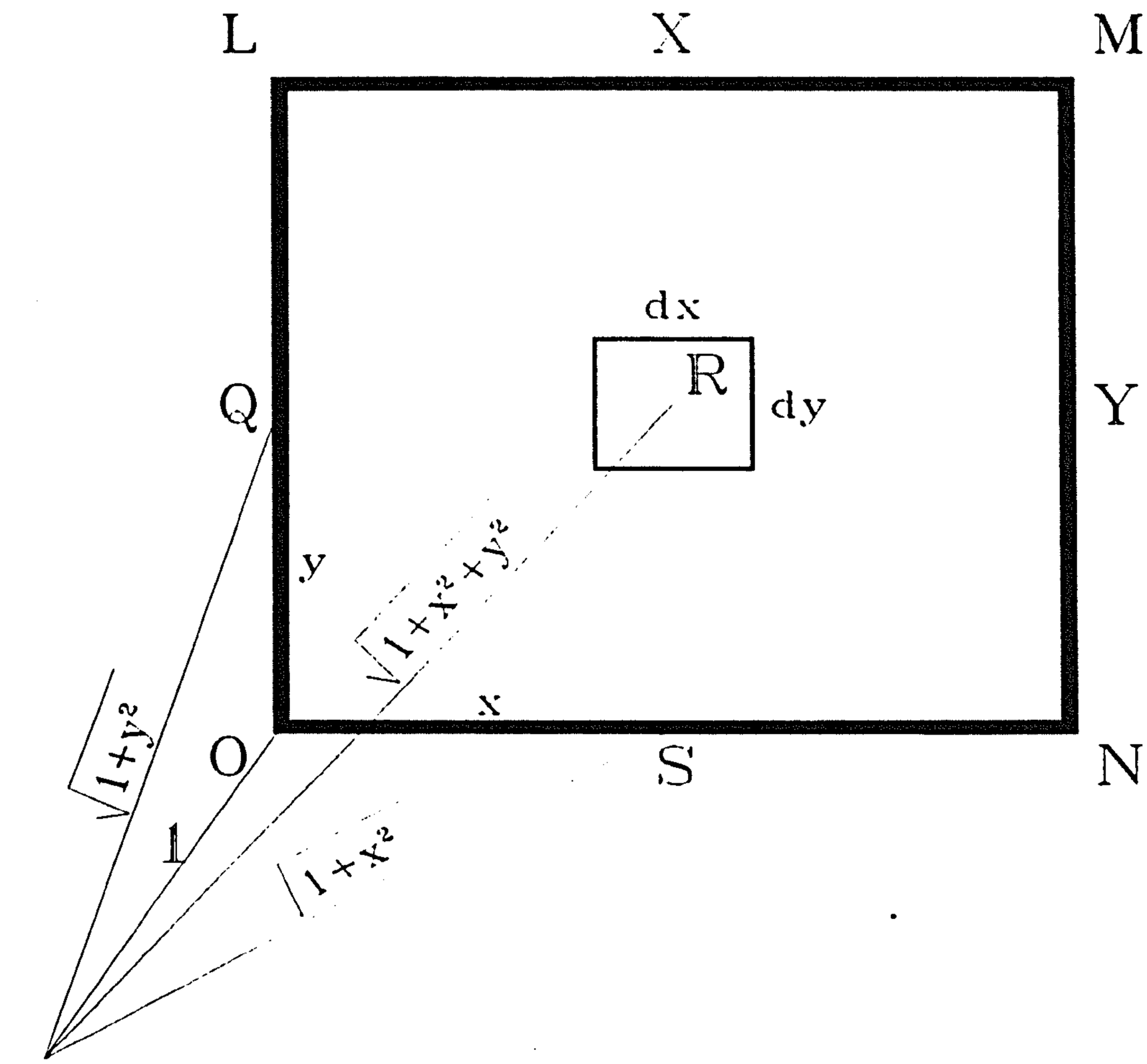

Figure 6.4.1a The illumination at a point on a horizontal plane from an element dxdy on a vertical rectangular window

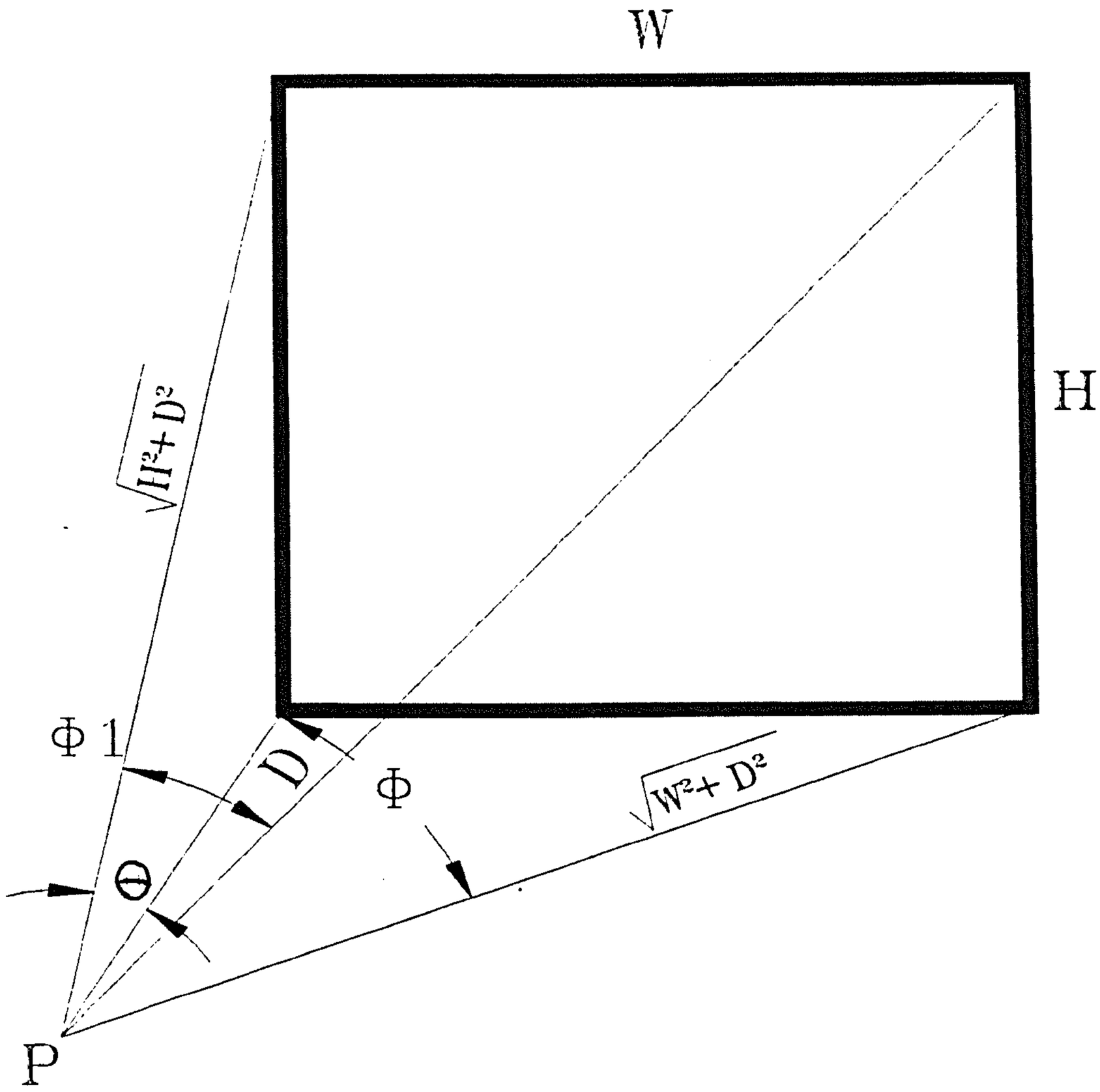

Figure 6.4.1b The illumination at a point on a horizontal plane from a vertical rectangular window

The calculation of 'b' is of importance in the proposed analysis for real sky conditions. The sky scanner data were formatted, averaged and plotted against α for each sky condition and orientation described above.

The sky component utilising the CIE overcast sky for a rectangular aperture in a vertical plane generalised to include a variable sky luminance distribution is derived below.

$$L_{INT} = \int_x \int_y \frac{Lz}{1+b}\left(1+\frac{by}{\sqrt{1+x^2+y^2}}\right)dxdy\frac{y}{\left(1+x^2+y^2\right)^2} \qquad 6.16$$

$$L_{INT} = \frac{Lz}{1+b}\int_x\int_y \frac{y\,dxdy}{\left(1+x^2+y^2\right)^2} + \frac{Lz\,b}{1+b}\int_x\int_y \frac{y^2\,dxdy}{\left(1+x^2+y^2\right)^{\frac{5}{2}}} \qquad 6.17$$

From Fig.6.4.1 the following angles are calculated;

$$L_{INT} = \frac{Lz}{1+b}\left[\phi - \phi_1\cos\theta\right] + I_2 \qquad 6.18$$

$$I_2 = I_{21} + I_{22} \qquad 6.19$$

$$I_{21} = \frac{-b}{2\pi(3+2b)}\left(\sin 2\theta \sin\phi_1\right) \qquad 6.20$$

$$I_{22} = \frac{b}{\pi(3+2b)}\sin^{-1}\left(\sin\phi\sin\theta\right) \qquad 6.21$$

Figure 6.4.4a shows the results of the two most distinct cases, clear sky sunfacing surface and overcast sky shaded surface. As expected a clear sky is brighter towards the horizon[(6.11,6.23-6.25)] and an overcast sky is brighter at the zenith[(6.9,6.24-6.26)]. Figure 6.4.2 illustrates the horizon brightening effect with an increase in scattering at the horizon taking place due to the large number of particles that light intercepts. As comprehensive proof of the non-uniformity of an overcast sky, Fig. 6.4.3 shows a plot of an overcast day with the horizontal global and diffuse and north and south measured illuminances. The graph shows quite clearly that although the sky is completely overcast the north and south surfaces receive different amounts of illumination.

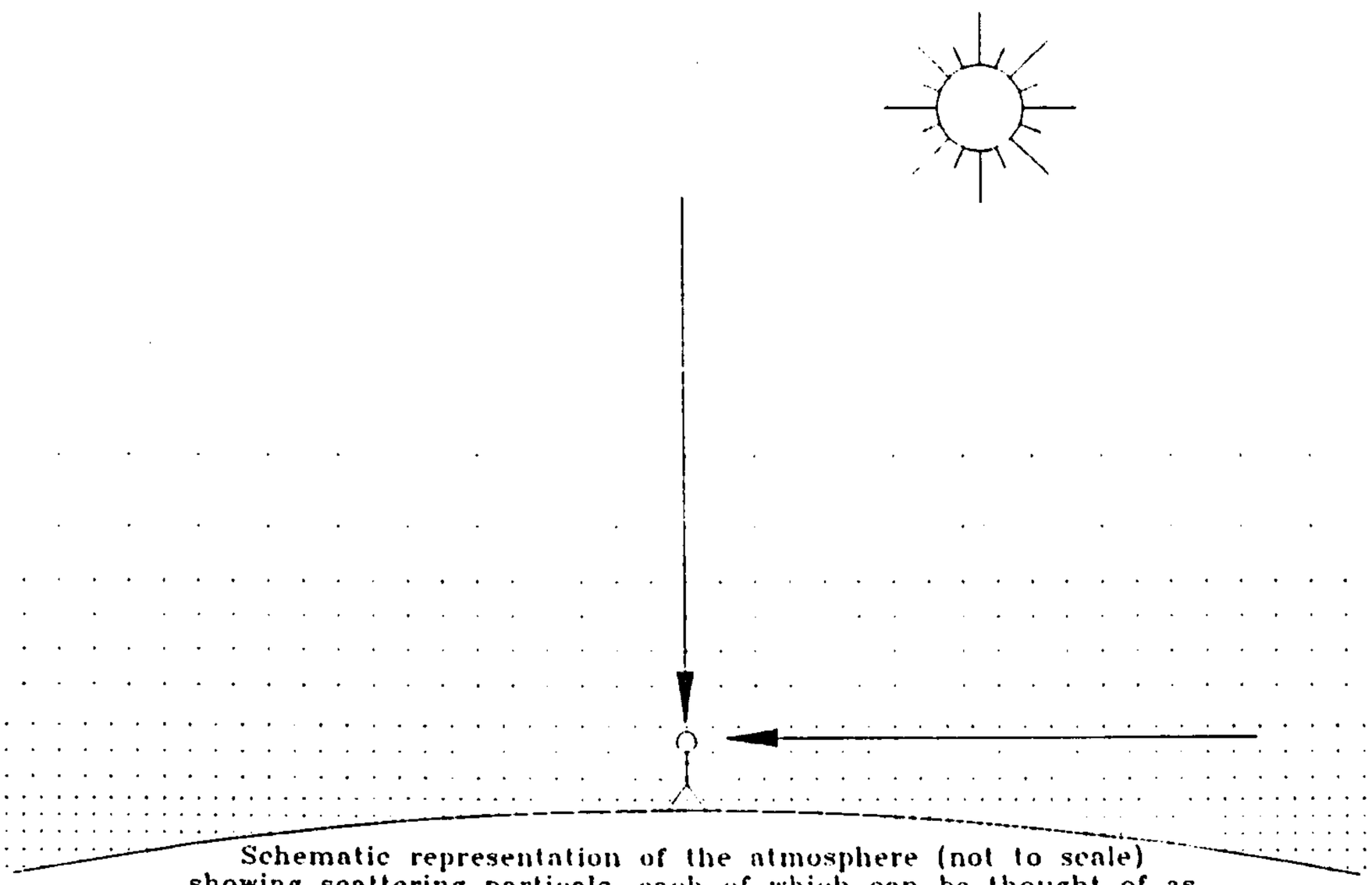

Figure 6.4.2 Horizontal brightening effects

The values of b for the clear sky sunfacing and overcast sky shaded surface were found to be -0.69 and 1.32 respectively. The two remaining cases displayed characteristics similar to a uniform sky distribution with b=0. The proposed functions are shown in Fig. 6.4.4b. Figure 6.4.5 demonstrates the proposed sky distributions for clear and overcast skies.

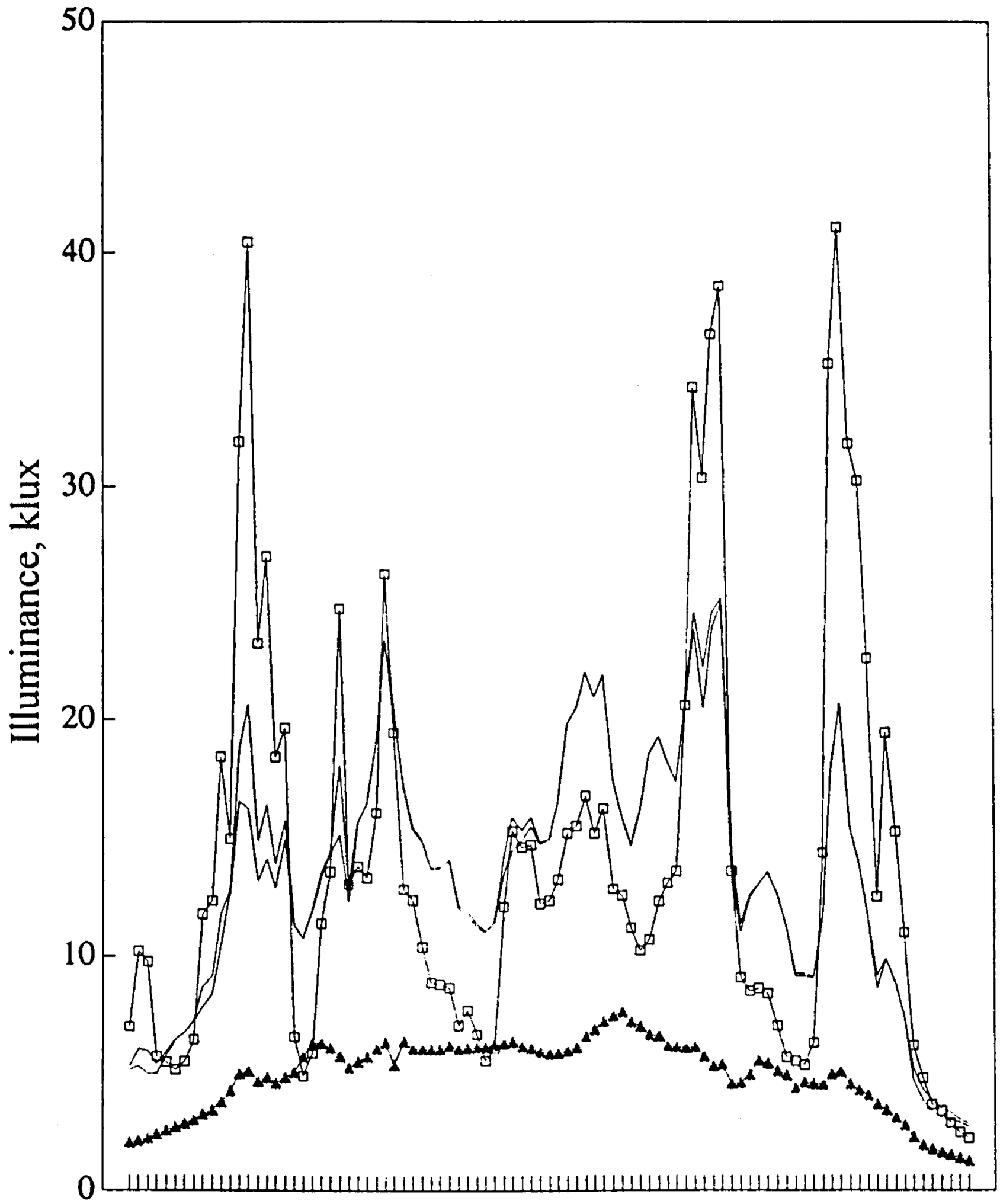

Figure 6.4.3 Overcast sky for sun and non-sunfacing surfaces

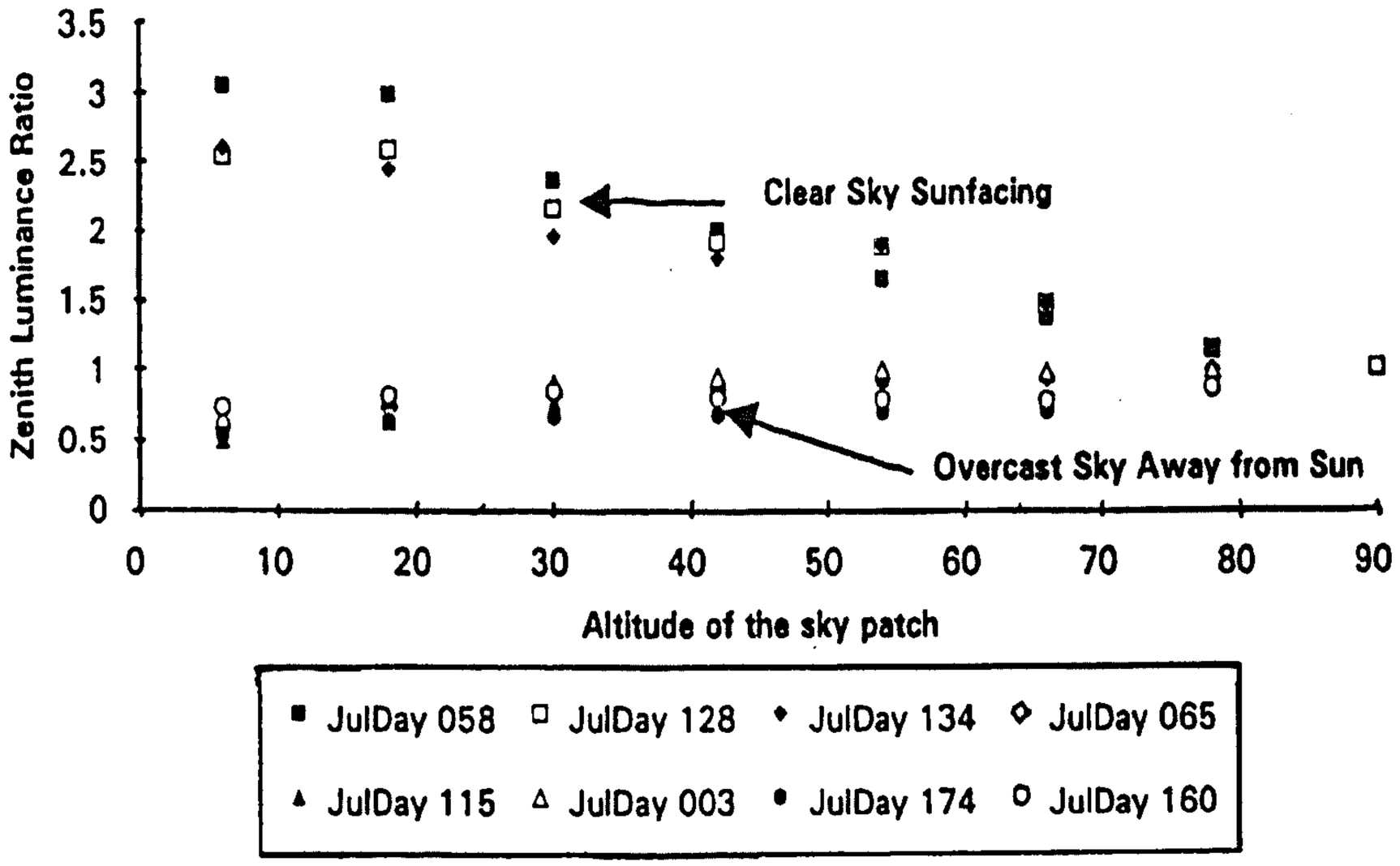

Figure 6.4.4a Sky Scanner data for clear and overcast sky conditions

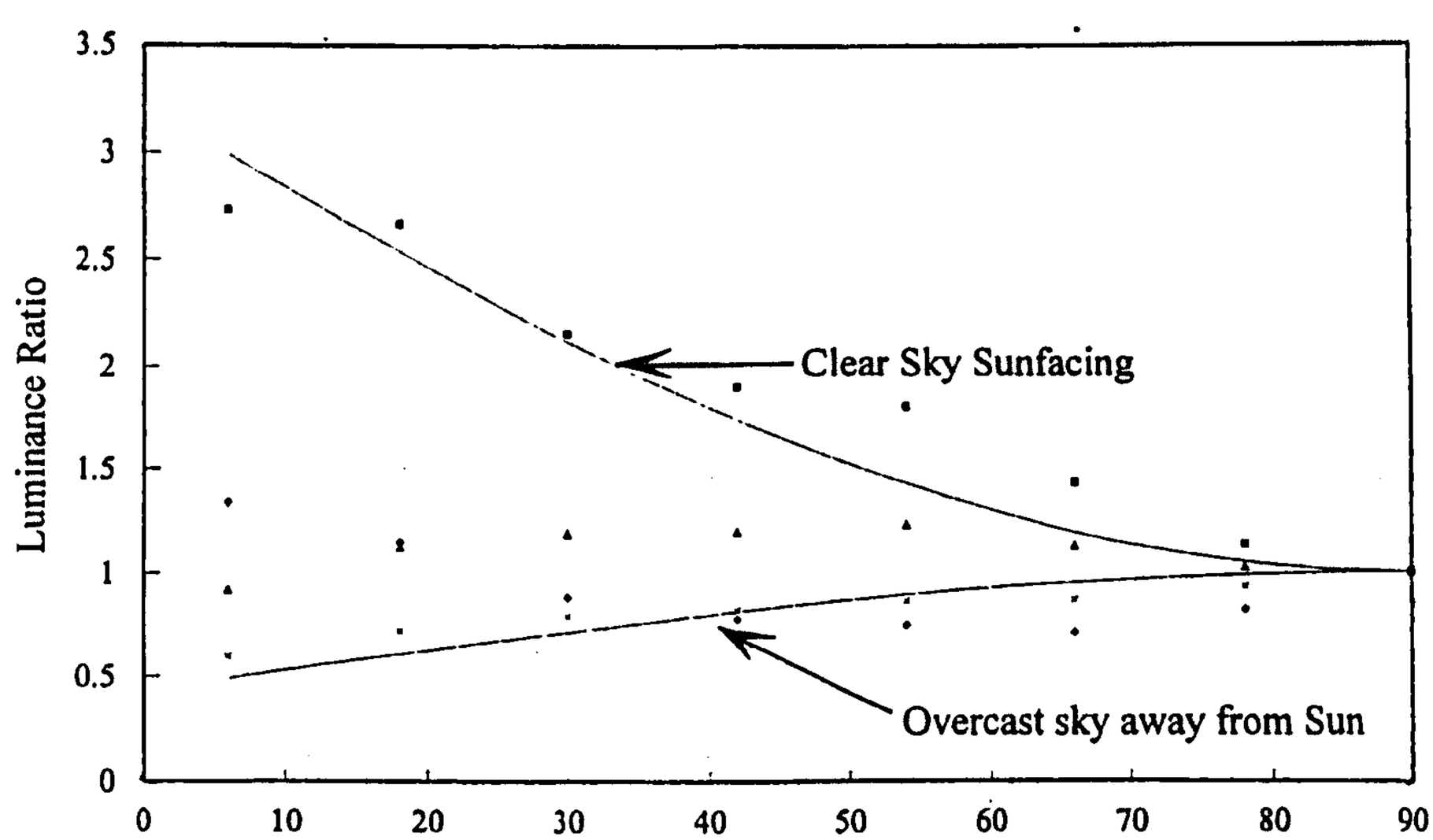

Figure 6.4.4b Averaged Sky Scanner data for clear and overcast sky conditions

Sunfacing Part : b = 0

Skyfacing Part : b = 1.32

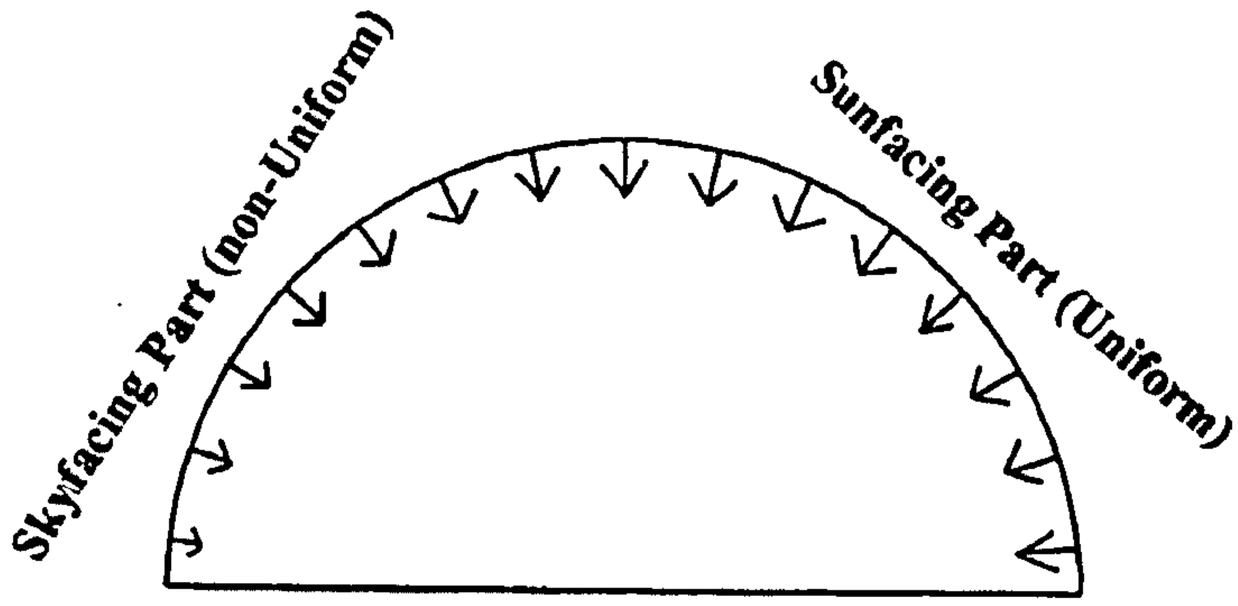

Overcast Sky

Figure 6.4.5a Schematic diagram of an overcast sky luminance distribution

Sunfacing Part : b = -0.69

Skyfacing Part : b = 0

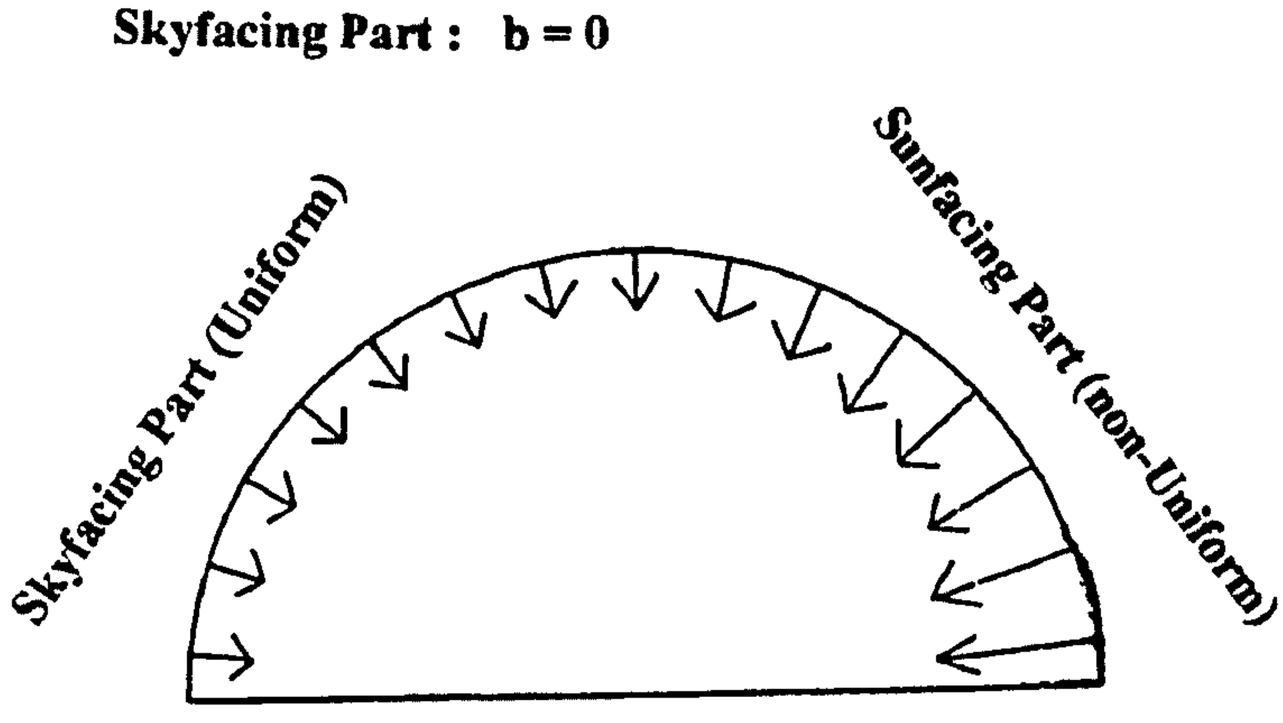

Clear Sky

Figure 6.4.5a Schematic diagram of clear sky luminance distribution

The daylight illuminance factors for each of the five cases described earlier are presented for a chosen building design. Using Fig 5.3 of Ref[6.1] as a design basis, a window design 7 metres wide and 2 metres high is considered. Using measured data for clear and overcast conditions, with the clear sky illuminance 73 klux and overcast sky illuminance 20 klux the following analysis was carried out.

Case 1: Overcast sky, window in shade[b=1.32]

$$\text{Sky Factor} = \frac{Lz}{0.5Lz(I_3 + I_4)}\left[\frac{I_1}{1+b} + \frac{bI_2}{1+b}\right] \qquad 6.22$$

where $I_3 = \pi$ 6.23

and $I_4 = [\pi(3+2*b)]/[3(1+b)]$ 6.24

These equations were obtained through further integration of equation 6.17 resulting in a Uniform and Non-Uniform sky section, I_3 and I_4 respectively. The transmissivity is incorporated in the integration of I1 and I2 using Rivero's formulae from ref[6.1].

Case 2: Overcast sky, sunfacing window[b=0]

$$\text{Sky Factor} = \frac{Lz}{0.5Lz(I_3 + I_4)}\left[\frac{I_1}{1+b}\right] \qquad 6.25$$

Case 3: Clear sky, window in shade[b=0]

$$\text{Sky Factor} = \frac{Lz\, I_1}{LG} \qquad 6.26$$

Case 4: Clear sky, diffusely illuminated sunfacing window[b= -0.69]

$$\text{Sky Factor} = \frac{Lz}{LG}\left[\frac{I_1}{1+b} + \frac{bI_2}{1+b}\right] \qquad 6.27$$

Case 5: Clear sky, directly illuminated sunfacing window[b= -0.69]

$$\text{Sky Factor} = \frac{Lz}{LG}\left[\frac{I_1}{1+b} + \frac{bI_2}{1+b} + \frac{\tau L_{BV}}{Lz}\right] \qquad 6.28$$

where τ is the glass transmissivity and L_{BV} is the beam component of the illuminance on the vertical window. For cases 3-5 Lz is calculated from the denominator of Case 1 where;

$$L_D = 0.5Lz(I_3 + I_4) \qquad 6.29$$

6.5 MODEL EVALUATION

The proposed luminance distributions perform well for real sky conditions. Figure 6.4.4b shows the fitted curves. A close correlation with the measured sky scanner data may be seen. An independent test of the proposed distributions was to predict pseudo zenith luminance from Eq.6.12. Figures 6.4.6 a & b are aids in evaluating this approach, the measured horizontal diffuse illuminance and zenith luminance data used being recorded at BRE using separate sensors. The simple model(Eq.6.4) appears to yield good results.

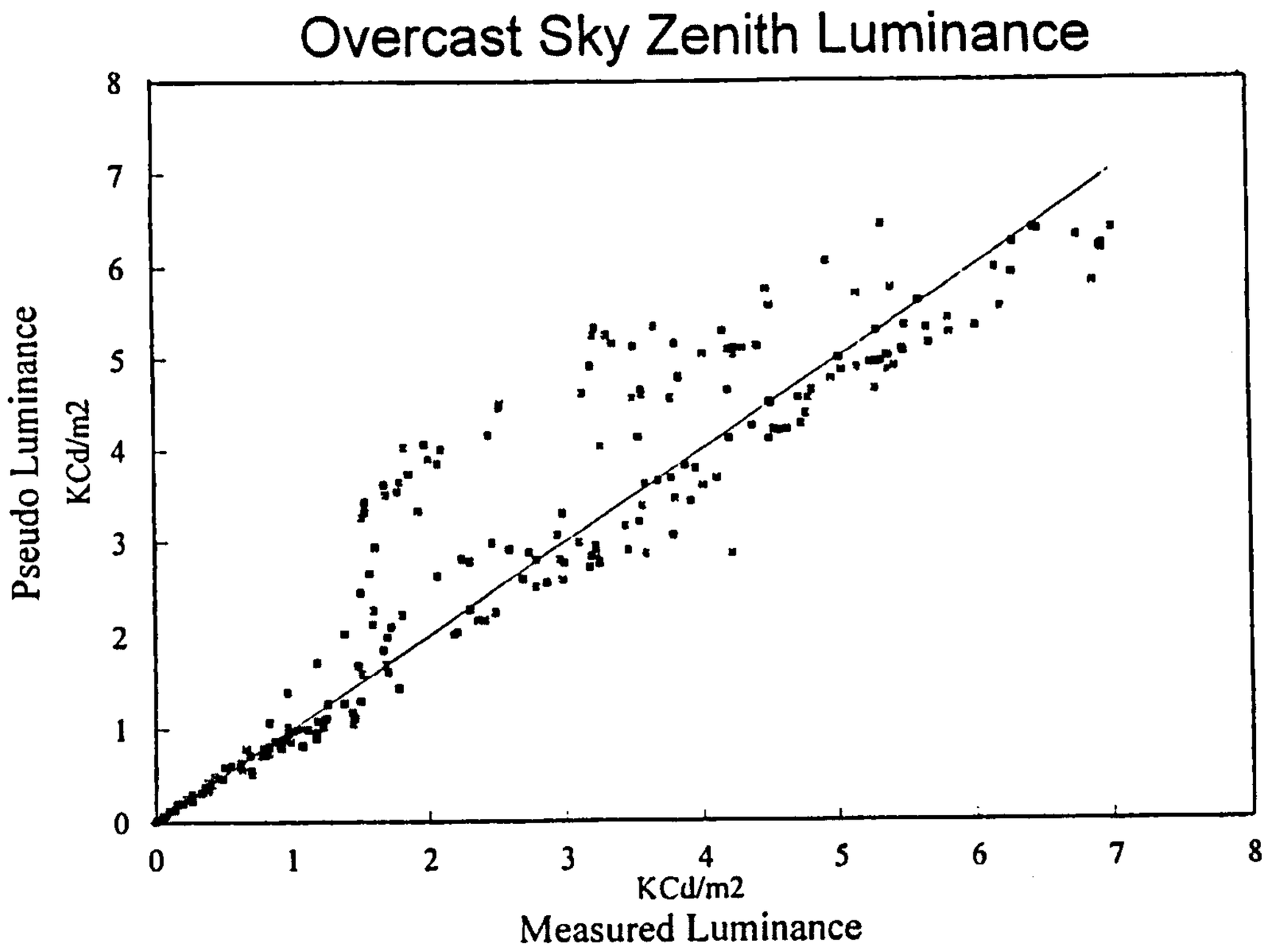

Figure 6.4.6a Prediction of zenith luminance for overcast skies

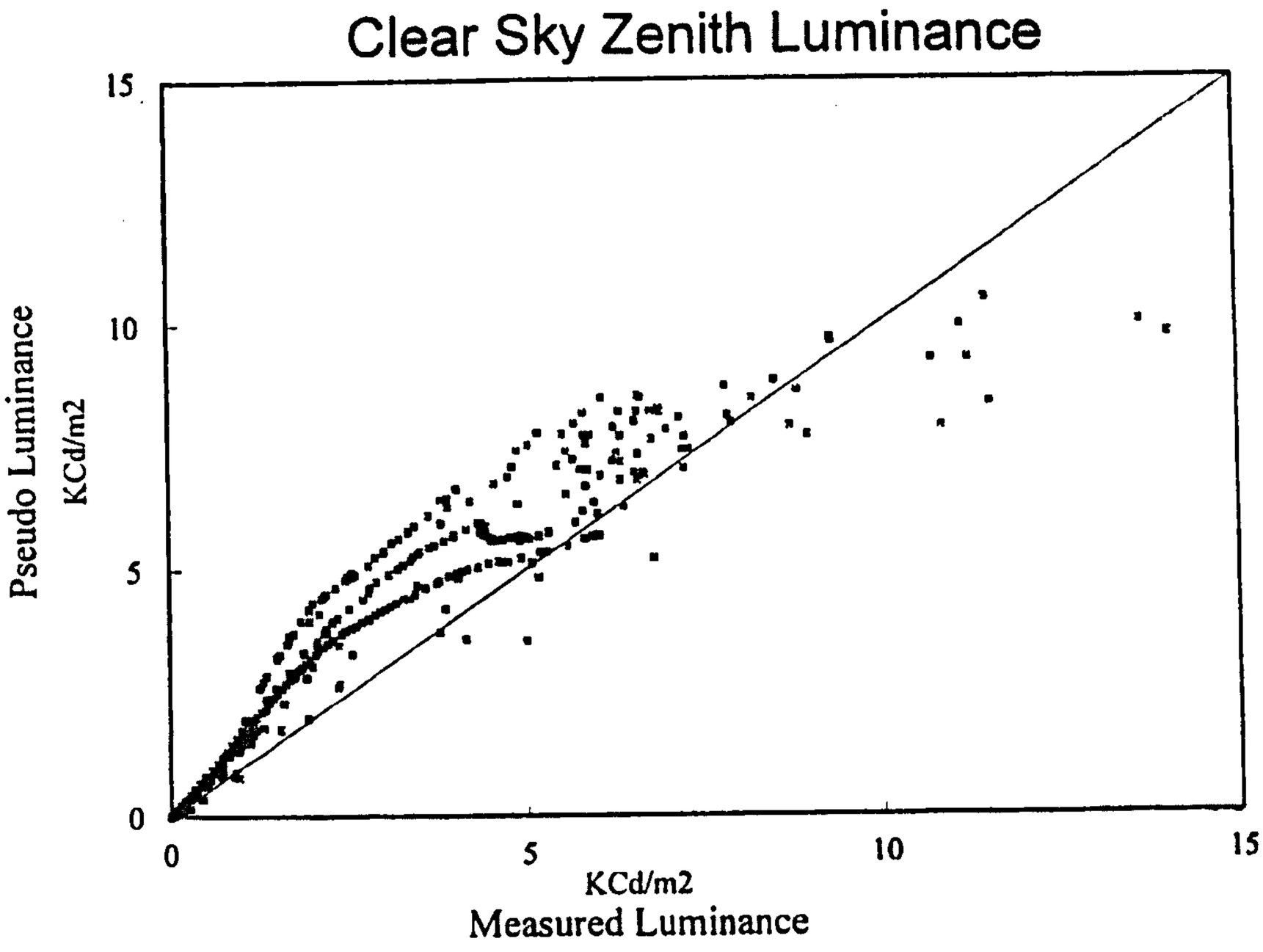

Figure 6.4.6b Prediction of zenith luminance for clear skies

By using an asymmetrical approach the large differences between different orientations are borne out. Moon and Spencer[6.9] developed their overcast sky distribution with out any regard for the sun's orientation. Figure 6.4.7a shows the results of the case study. With a sunfacing window under an overcast sky it is apparent that 38% more daylight is incident than that predicted by the CIE model. Tregenza[6.2] noted that daylight factors using the CIE overcast sky had a tendency to underpredict illuminance in some instances. Cases 3,4&5 shown in Figure 6.4.7b demonstrate the variation of sky factor with distance from the window. The most notable curve being that of case 5. It may be noted that after a recess of 1.3 metres from the window the sun's direct rays are no longer 'seen' in the room, hence from this point inwards case 5 resorts to case 4. These graphs are quite unique as neither Moon and Spencer nor CIE provide charts or tables for such conditions.

Taking an overall view of the use of the CIE and Uniform sky luminance distribution for daylight factor calculations, it is incorrect to assume an overcast sky as the norm for design purposes. Typical skies in the United Kingdom are partly cloudy with a small percentage of clear days in the year. The present author has estimated that the overcast sky is applicable for less than 30% of the year.

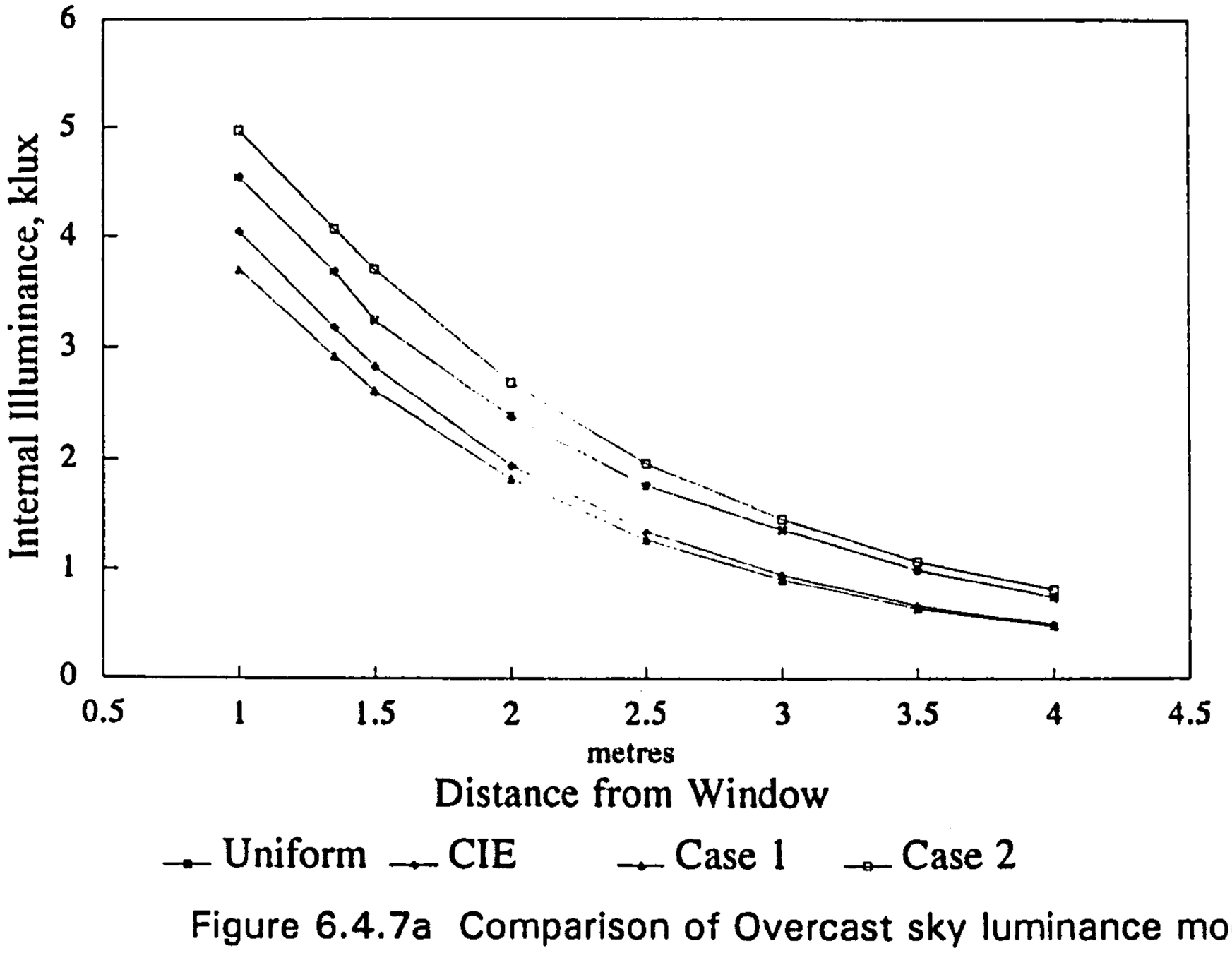

Figure 6.4.7a Comparison of Overcast sky luminance models

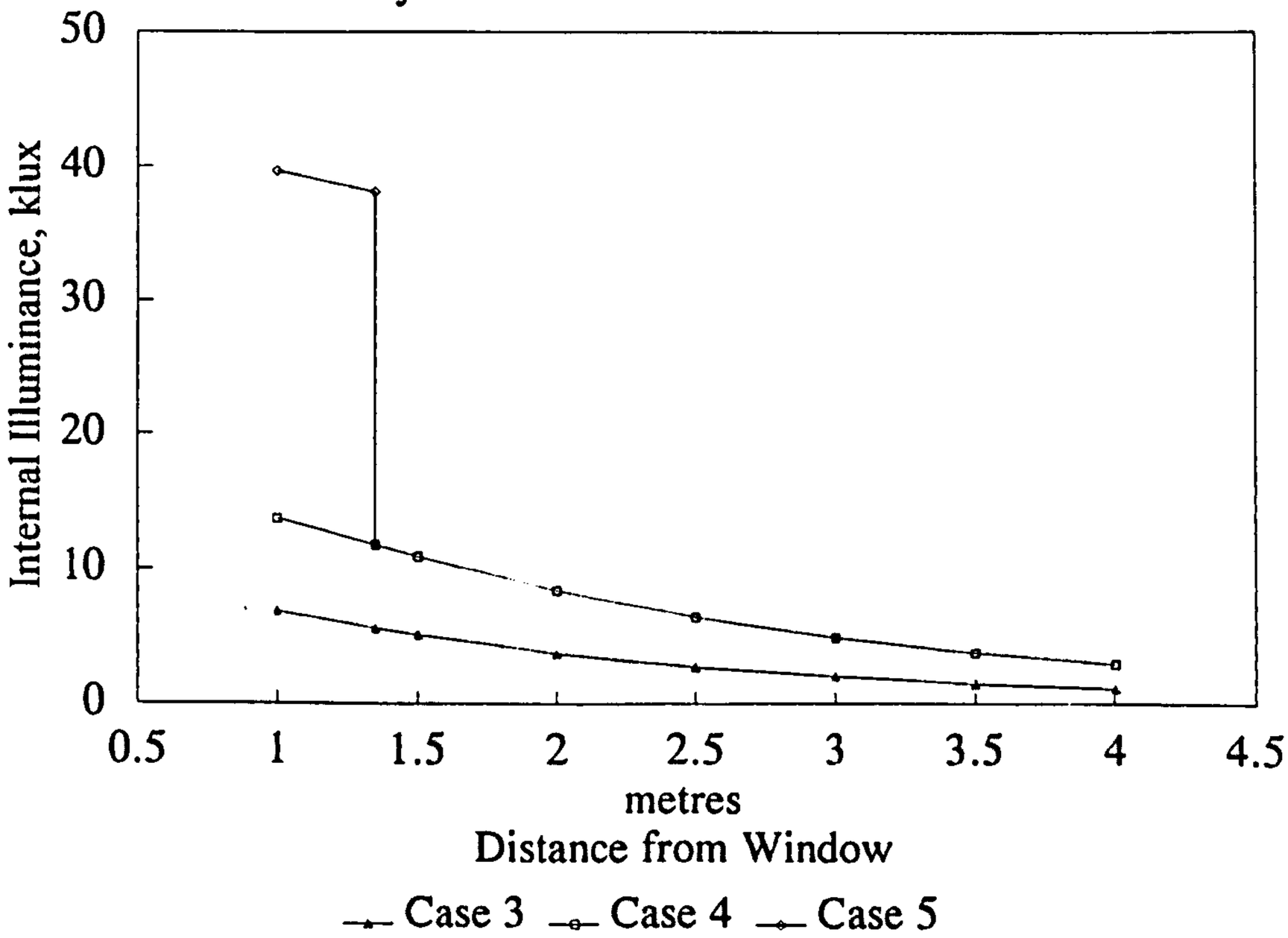

Figure 6.4.7b Comparison of Clear sky luminance models

Although the analysis and models presented herein have concentrated on the two extreme sky conditions it is possible to interpolate for all sky conditions by using the appropriate value of 'b' for shaded and sunfacing surfaces. This can be achieved by using a technique used by Muneer and Angus[6.27] which relates 'b' with 'F', the clearness index of the sky, so partly cloudy skies can be catered for. This linear correlation of what is effectively cloud cover, using 'F' as a weighting factor is similar to the quasi-clear/overcast model of Littlefair which used sunshine probability. 'F' is obtained from the ratio of horizontal beam to extraterrestrial illuminance[6.27]. Figure 6.4.8 shows the relationship of 'b' for varying degrees of clearness index, 'F'.

Other authors have also reported values of 'b' for varying sky conditions. Figure 6.4.9 shows this comparison and the influence of 'b' on the ratio of vertical incident to horizontal diffuse energy.

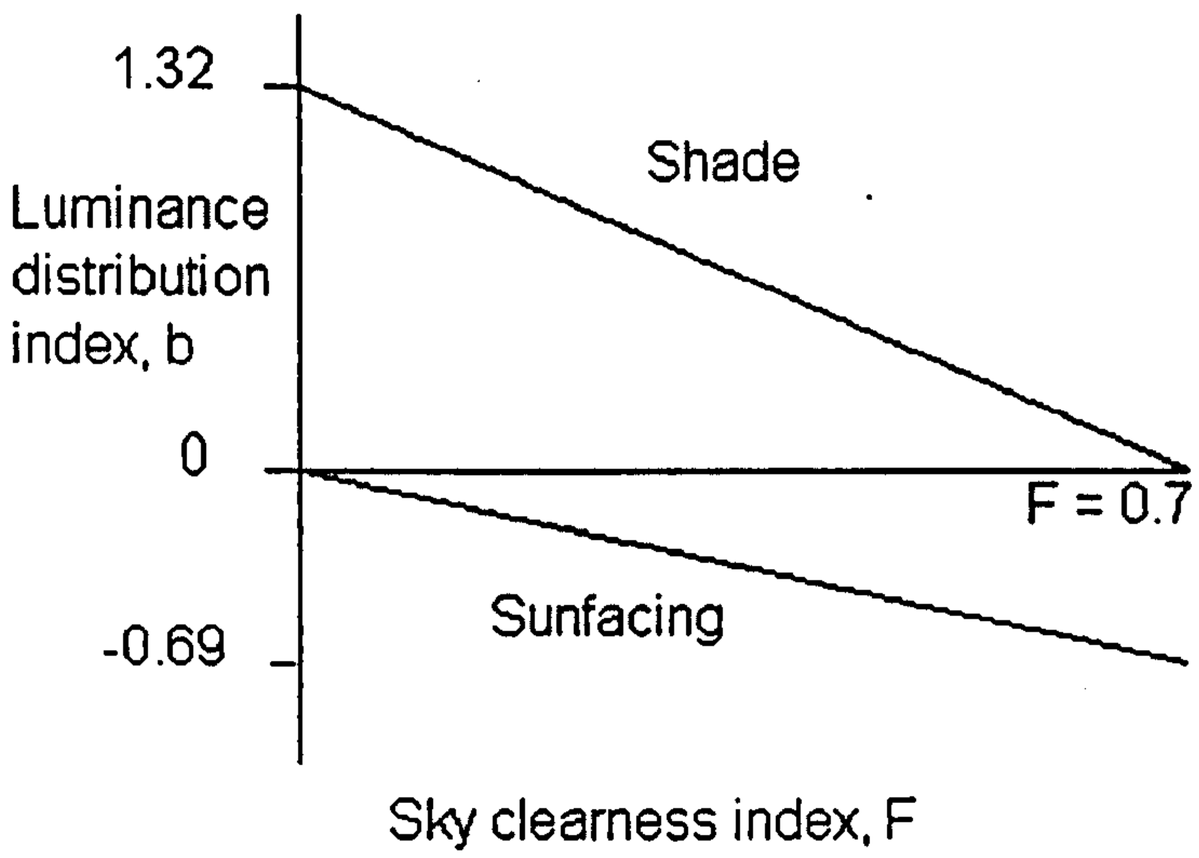

Figure 6.4.8 Variation of 'b' with F and orientation

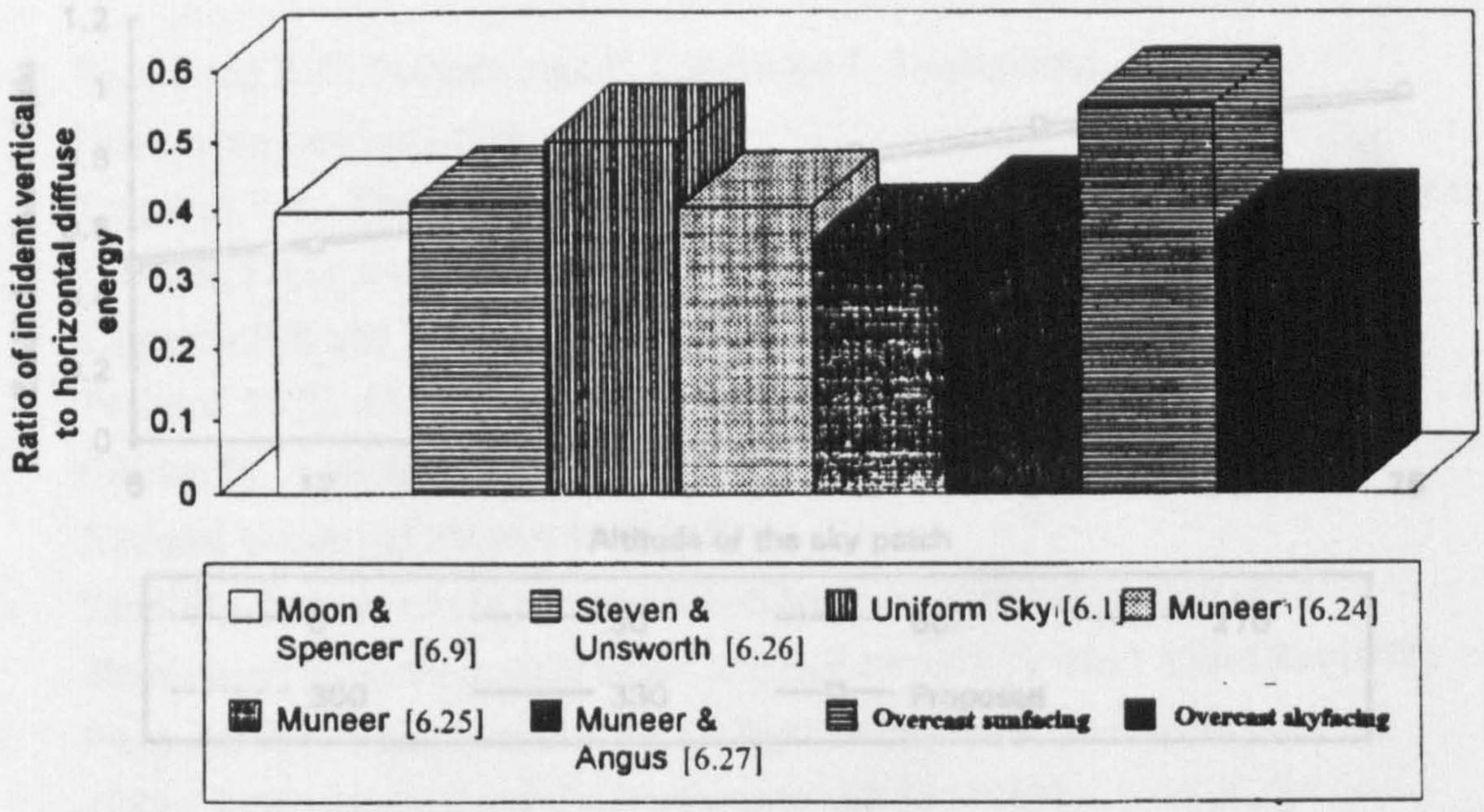

Figure 6.4.9 Comparison between published and proposed values of the ratio of incident vertical to horizontal diffuse energy

This approach uses a one-dimensional structure whereas other authors have reported a two-dimensional relationship with sky luminance distribution. In an independent test Littlefair's[6.15] work was compared with the proposed model. The results in Fig. 6.4.10 show that the presently proposed model compares favourable with Littlefair's two-dimensional model.

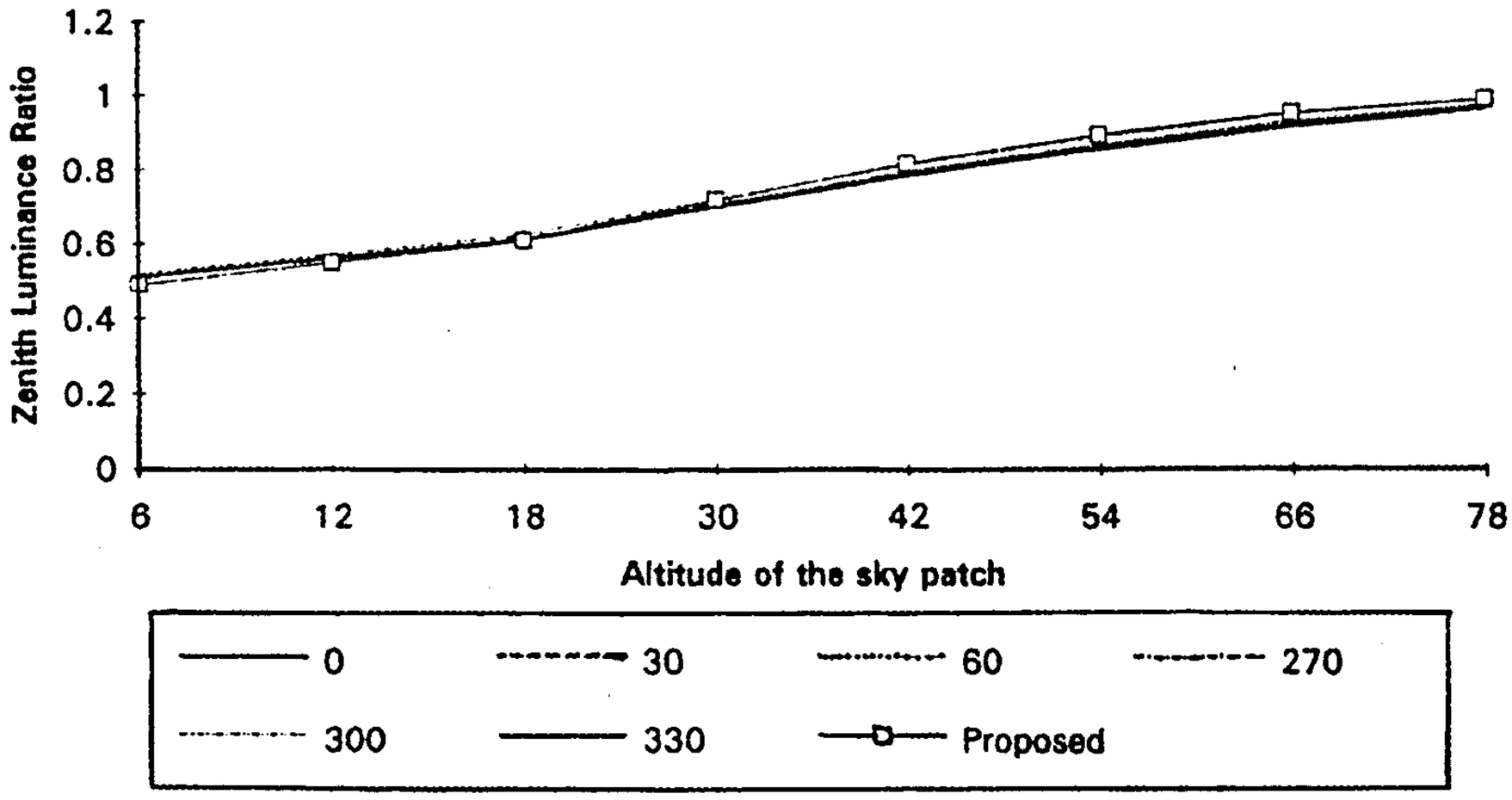

Figure 6.4.10 Comparison between Proposed and Littlefair's sky luminance distribution model for overcast skyfacing conditions

6.6 DISCUSSION

This investigation has shown that large variations exist between measured daylight illuminance conditions and presently used design tools. Two alternate and independent sets of measurements have been used to evaluate the proposed sky luminance distributions. It has been shown that the orientation of a window with respect to the sun has a bearing on the daylight illuminance factor. The most important finding arising from this investigation is the inadequacy of the CIE model for use in daylight factor calculations for real skies. The CIE and Uniform Sky factor tables are somewhat archaic design tools and it is recommended herein that they be replaced by design methods such as those proposed. One benefit of the daylight factor method is that it is simple to apply and gives a single internal illuminance value. The proposed distributions are both intricate in structure and yet simple in application yielding more precise results. It has to be stressed that the proposed method is primarily a computer orientated approach which with the current level of computational facilities available makes it attractive.

REFERENCES

6.1 Hopkinson R G, Petherbridge P, Longmore J Daylighting, Heinemann:London (1966)

6.2 Tregenza P R, The daylight factor and actual illuminance ratios Lighting Res. & Technol. 12(3) 64-68 (1980)

6.3 Tregenza P R and Waters I M, Daylight Coefficients Lighting Res. & Technol. 15(2) 65-71 (1983)

6.4 Gillette G, A daylight model for building energy simulation BSS-152 National Bureau of Standards (1983)

6.5 Farell R, The use of the perspective techniques in the calculation of illumination levels from clear skies Journal of the IES No.1 153-156 (1974)

6.6 Pierpoint W, A simple model for daylight calculations Proceedings of the 1983 International Daylight Conference 47-51 (1983)

6.7 El Diasty R, Shapiro M M and Fazio P, A time dependent concept for daylight calculation; Part 1: The direct component Journal of the IES 52-64 Summer (1989)

6.8 Kittler R, Standardisation of outdoor conditions for the calculation of daylight factor with clear skies Proceedings of the CIE conference: Sunlight in buildings 273-285 1967

6.9 Moon P and Spencer D E Illumination from a non-uniform sky, Trans. Illum. Eng. Soc. (London) 37, 707-725 (1945)

6.10 Krochmann J, The calculation of daylight factor for clear sky conditions Proceedings of the CIE conference: Sunlight in buildings 287-301 1967

6.11 Steven M D and Unsworth M H The angular distribution and interception of diffuse solar radiation below overcast skies. Quart.J.R.Met.Soc., 106, 57-61 (1980)

6.12 Standardisation of luminance distribution on clear skies Publication No 22, CIE, Paris (1973)

6.13 Karayel M, Navvab M, Ne'eman E and Selkowitz S Zenith and sky luminance distributions for daylighting calculations Energy and Buildings 6 283-291 (1984)

6.14 A comparison of sky luminance models with measured data submitted to Solar Energy P J Littlefair 1995

6.15 Littlefair P J The luminance distribution of clear and quasi-clear skies CIBSE Nat. Light. Conf. Cambridge 1994

6.16 Littlefair P J An assessment of overcast sky luminance models using measured data submitted to LR&T

6.17 Nakamura H, Oki M, Hayashi Y, Iwata T The mean sky composed depending on the absolute luminance values of the sky elements and its application to the daylighting prediction Proceedings of the International Daylighting Conference, Long Beach (1986)

6.18 Matsuura K Luminance distributions of various reference skies CIE Technical report (TC 3-09) draft (1988)

6.19 Perez R, Michalsky J, Seals R Modelling sky luminance angular distribution for real sky conditions: experimental evaluation of existing algorithms Journal of IES 21 84-92 (1992)

6.20 Kambezidis H D, Psiloglou B E, Muneer T and Angus R C, Comparison of solar irradiance models with measurements for two regions in Southern and Northern Europe NorthSun Int. Conf. Glasgow 177-182 (1994)

6.21 Perez R, Seals R, Michalsky J An all-weather model for sky luminance distribution Solar Energy 50 235-245 (1993)

6.22 Tregenza P R Guide to recommended practice of daylight measurement Supplement to CIE Journal 6(2) (1987)

6.23 Coulson K L Solar and terrestrial radiation (Academic Press, New York) (1975)

6.24 Muneer T Further refinement of an anisotropic model for inclined surface solar irradiation Proc. Inst. Mech. Eng. Part C Mech.Eng. Science 202, No.C1 pp67-71 (1988)

6.25 Muneer T Solar radiation model for Europe, BSER&T 11(4) 153-163 (1990)

6.26 Steven M D and Unsworth M H The diffuse solar irradiance of slopes under cloudless skies. Quart.J.R.Met.Soc., 105, 593-602 (1979)

6.27 Muneer T and Angus R C Illuminance models for the United Kingdom LR&T 25(3) 113-123 (1993)

7 ENERGY ANALYSIS OF DAYLIT BUILDINGS

Notation

θ = angle of the sky subtended at the centre of the window(°)
η = efficacy of the lamps (lumens/Watt)
ρ_{AV} = average reflectivity of surfaces (dimensionless)
τi = transmissivity of the glazing at incidence angle i
A_G = the area of glazing (m^2)
A_T = total area of room surfaces (m^2)
Awp = area of the working plane (m^2)
Ec = electrical consumption (kWh)
Es = electrical load of the lighting (kW)
Eskymax = the maximum sky illuminance (lux)
H = hours the lights were switched on (h)
Hmax = maximum number of hours during which the lighting can be on (h)
MF = maintenance factor (dimensionless)
UF = utilisation factor (dimensionless)

7.1 INTRODUCTION

Efficient use of energy in buildings is of increasing importance and may be addressed at the first stages of design. Through the utilisation of daylight and direct solar gains as substitutes for electrical lighting and space heating respectively, large energy savings are possible even under prevailing overcast conditions.

Traditional design methods are centred around the use of daylight sky factors which assume overcast sky conditions. It has been shown in the previous chapter that this crude approach although widely used, is inaccurate and is only applicable for a small percentage of real sky conditions. The daylight factor method excludes the contribution of direct sunlight to a building's internal illuminance and is insensitive to cloud cover. This is a particular weakness as partly cloudy skies are predominant in the UK. To this end the daylight illuminance factors are developed in chapter 6 were used in a passive energy design analysis.

In this chapter the impact of new design tools for precise estimation of internal illuminance and solar radiation, developed by the authors were examined in a

parametric design scenario on a model building possessing large glazed facades in each of the cardinal direction(i.e. N,E,S&W). The building was analysed to assess the internal lighting levels using a complete year's measured weather conditions. Each surface was taken in turn and using the illuminance factors the illuminance was calculated. Several glazing types were considered, namely single, double and triple glazing to provide further comparisons. The performance of each orientation and glazing type was ascertained by the amount of electrical lighting, space heating and cooling loads in each case. This was carried out by examining the reduction in electrical consumption using on/off and top-up controls for internal lighting and passive solar utilisation through a direct-gain design approach.

7.2 POTENTIAL FOR SAVINGS FROM DAYLIGHT

There are two ways in which daylight can be utilised to reduce electrical lighting consumption in buildings;

1. Reduction of lighting load through the use of better lighting controls.

2. Improved use of daylight in buildings through the implementation of light shelves and innovative daylight design features.

The latter method shall be dealt with in the following sections in this chapter.

7.2.1 LUMINAIRE SWITCHING PROBABILITIES

Photoelectric lighting controls provide the means of exploiting a large potential in electrical lighting savings. The implementation of these control systems is necessary as a result of the failure of building occupants to efficiently utilise artificial lighting alongside natural daylight. It is far too common an occurrence in office buildings to encounter electrical lighting left on in un-occupied areas. In a study of occupancy behaviour in artificially illuminated offices Hunt[7.1] found that lights tended to be completely on or off with little evidence of partial switching. The decision to switch lights on was taken on entry to an empty room and once they were switched on they were rarely switched off until the space became empty again. This work led to the development of a procedure for estimating the hours of lighting used by a manually switched installation in a later article[7.2]. Hunt[7.2] produced switching probability

curves using time of day and daylight factors as decision operators, the equation for which is given below;

$$p = a + c / \{1 + \exp[-b(x - m)]\} \qquad 7.1$$

where p is the probability of switching, a = -0.0175, b = -4.0835, c = 1.0361, m = 1.8223, x is $\log_{10}$(minimum daylight level in the working plane, lux), p =1.0 for $x \leq 0.843$, p = 0.0 for $x \geq 2.818$. A random number element is applied to this approach to simulate the switching habits of the occupants. This algorithm has been included in the SERI-RES building thermal analysis package to supplement its solar radiation component.

For analysis of the potential savings from photoelectric switching Littlefair[7.3] examined the distribution of daylight illuminances on working planes. Using experimental methods Littlefair physically modelled a daylit office with sensors positioned to provide various daylight factors. The external horizontal illuminance was then multiplied by the appropriate daylight factors and compared to the measured illuminance recorded by the sensors in a similar approach to Tregenza[7.4]. It was discovered that the daylight factor method severely underestimated the percentage of the year that a certain illuminance would have exceeded. This was most evident in the case of the southern rooms with the daylight factor underestimating by over 30%. This is not a surprising result as daylight factors have been shown in chapter 6 to be unreliable due to the lack of consideration given to orientation. To this end orientation factors were introduced and implemented to improve the previous method. The values for each orientation are given in Table 7.2.1 were multiplied by the daylight factors and horizontal diffuse illuminance to correct the predictions of internal illuminance.

Table 7.2.1 Orientation factors for daylight factor calculations

Orientation	Factor
North	0.77
East	1.04
South	1.20
West	1.00

Littlefair suggested that savings would still be underestimated as the light received is mainly from the horizon which the CIE sky predicts as a dark horizon. It is further suggested that a need exists for different orientation factors which can account for

the large variations that remain even after the implementation of the correction factors in Table 7.2.1. Littlefair proposed the use of total and diffuse orientation factors shown in Table 7.2.2.

Table 7.2.2 Total and diffuse orientation factors for daylight factor calculations

Orientation	Total	Diffuse
North	0.77	0.97
East	1.02	1.15
South	1.67	1.55
West	1.08	1.21

Littlefair noted that the total orientation factors when multiplied by the total horizontal illuminance and daylight factors produced precise results for the measured distributions but suggested that in actual rooms, with blinds and other shading devices, the diffuse orientation factors may be used.

Alternative methods such as using the Average sky[7.5] in place of the CIE overcast sky and a vertical illuminance approach were examined. The vertical illuminance method examined the role of measured vertical illuminance on the glazing aperture to the internal illuminance[7.6,7.7]. The findings of the study revealed that no generic solution was available and that each method was appropriate in different situations. The orientation factor was best suited to window geometry problems as it provides results of window orientation on internal daylighting. The average sky approach is ideal for use in computer analysis and simulation. The vertical illuminance method can be employed to calculate the cost-effectiveness of lighting controls.

In a study of solar heated and daylit offices by Muneer[7.8] a vertical illuminance approach using the calculated total incident illuminance and daylight factor to estimate the internal daylight illuminance was employed. It was then used to obtain the contribution of natural daylight to the internal illuminance. It was further shown that between 50 & 60% savings were achieved in the primary electrical consumption by exploiting daylight. In a comparison with the BRE digest[7.5] the daylight factors used in Muneer's study would predict enough internal illuminance such that there would be no need for artificial lighting for 69 - 83% of the working year. Both sets of results are comparable and more importantly demonstrate the large potential for savings with the introduction of daylight into buildings.

Wilkinson [7.9] developed algorithms to calculate the energy consumed by the electric lighting for top-up and on/off switching. The algorithms were dependent on several parameters.

On/Off controlled lighting;

$$Ec = \frac{H\ Es\ Awp}{UF\ MF\ \eta} \qquad 7.2$$

where Ec is the electrical consumption, H is the hours the lights were switched on, Es the load of the lighting, Awp the area of the working plane, UF the utilisation factor, MF the maintenance factor and η is the efficacy of the lamps.

And for top-up electric lighting;

$$Ec = \frac{Es^2\ K}{A_G \eta} \qquad 7.3$$

where A_G is the area of glazing and K is a constant given by equation 7.4.

$$K = \frac{Hmax\ Awp}{Eskymax UF\ MF\ C} \qquad 7.4$$

where Hmax is the maximum number of hours during which the lighting can be on, Eskymax is the maximum sky illuminance. C is constant given by equation 7.5;

$$C = \frac{\theta \tau i}{2A_T(1-\rho_{AV})x100} \qquad 7.5$$

where θ is the angle of the sky subtended at the centre of the window, τi is the transmissivity of the glazing at incidence angle i, A_T is the total area of room surfaces and ρ_{AV} is the average reflectivity of surfaces.

7.3 DAYLIGHT ANALYSIS USING DAYLIGHT ILLUMINANCE FACTORS

It has been demonstrated that various methods exist to calculate internal daylight illuminance frequencies for use in the estimation of the potential savings from photoelectric switching of luminaries. Furthermore it has been shown in case studies[7.8] that the implementation of such methods in actual building scenarios has been very successful.

The previous chapter saw the development of a new method for estimating internal illuminance. The next step is to employ the daylight illuminance factors in a design situation.

The development of new sky luminance distributions was necessary to properly assess the variation in daylight across the sky vault and hence the amount of daylight a window is exposed to. This was carried out using data from a sky scanner stationed at the Building Research Establishment(BRE) at Garston. The data were analysed to produce sky luminance distributions for several sky conditions and orientations. The scenarios are the same as presented in chapter 6;

Case 1: Overcast Sky, Skylit window (window in shade)
Case 2: Overcast Sky, Sunlit window (sunfacing window)
Case 3: Clear sky, Skylit window (window in shade)
Case 4: Clear sky, Sunlit window diffusely illuminated (sunfacing window)
Case 5: Clear sky, Sunlit window directly illuminated (sunfacing window)

In a comparative test the new daylight illuminance factors were analysed in a design scenario with an overcast and clear sky. Figures 6.4.7(a and b) show the results and demonstrate the levels of daylight calculated at different distances from a window of 7m width and 2m height. The versatility of the daylight illuminance factors for all types of cloud cover, is demonstrated.

Having established the calculation of internal illuminance from horizontal global and diffuse illuminance it was possible to complete the analysis on a full year's weather data to assess the daylight and passive solar performance of an office building.

The calculation of the electrical consumption in the office space assumes high efficiency luminaries (efficacy = 86 lm/W) and a lighting requirement of 500 lux at desk level, 2 metres away from the window.
If the estimated internal illuminance fails to meet the design threshold over a 5 minute period, then artificial lighting is assumed to be switched on until such time that 500 lux is exceeded. This may not be the switching decision time of lighting controls but was a convenient time scale in view of the data format. It is foreseen that this will not effect the results as it is a comparative study using the same database. The electrical consumption is then a simple calculation of time and energy.

Further analysis using top-up control was carried out, where the artificial lighting was used as a supplement to daylight. The calculation of top-up electricity consumption assumed once again an illuminance requirement level of 500 lux, whenever this threshold was breached, the difference between the required 500 lux and the calculated internal illuminance was assumed to be the electrical contribution of the luminaries. In practice the top-up control system would operate using a bandwidth approach to the internal illuminance, e.g. 50 or 100 lux levels at which the lighting was adjusted. In this study there was no rounding up or down of the illuminance difference and it was assumed that the lights could be adjusted exactly to compensate for the deficit. The results from this approach will hence be the best possible scenario but it is estimated that the differences between the practical application of top-up controls and this adaptation will not affect the overall conclusions.

7.4 RESULTS

7.4.1 Lighting loads

To aid the analysis of the results the two types of lighting controls were examined separately with each orientation and glazing type incorporated to provide a comprehensive comparison. Figure 7.4.1 demonstrates the electrical lighting consumption of the on/off control system. The south facade, as expected, performs best contributing to an estimated annual electricity consumption half that of the north surface. The east and west surfaces produce very similar results with their consumption figures lying between that of the north and south orientations. The glazing types considered were single, double and triple glazings with no low emissivity coatings or inert gas sections. The differences seen in Fig.7.4.1 are only slight, any difference being due to the transmissivity of the glass which does not vary significantly as the average incidence angle is relatively large. Figure 7.4.2 demonstrates the relationship between incidence angle and percentage transmittance for various glazings and also shows the modelled curves used in the calculations. The graph highlights the loss of light encountered when the number of panes of glass is increased.

Figure 7.4.3 displays the results of the top-up control system. Similar trends of the on/off controls are demonstrated once again with the south facade performing better than other orientations. There appears to be a greater difference between east and west surfaces with the east clearly consuming more electricity than the west. It is

possible that is due to the given site's weather pattern, i.e. overcast mornings clearing by afternoon.

Electrical energy consumption is just as insensitive to glazing type as in the case of on/off controls. The main difference between the two methods of lighting controls is evident in Fig.7.4.3 with the overall electrical consumption associated with the top-up system approximately 50% of the on/off controls. Although the calculation method used for the top-up controls is a 'best possible' scenario the difference between the two control methods seems reasonable. In a study of building performance using computer tools a Danish research team[7.10] found that top-up controls saved on average 45% more energy than an equivalent on/off control system. It is clear from the presented analysis and corroborating Danish results that top-up controlled lighting is far more effective in the reduction of electrical lighting consumption than straight forward on/off lighting controls. Further benefits result from savings in electrical lighting, the most significant being the reduction in air conditioning load due to reduced heat gains. In a recent study of air conditioned buildings by the BRE[7.11] it was estimated that introduction of lighting controls would reduce unnecessary internal heat gains by approximately 50% and hence minimise the need for air conditioning.

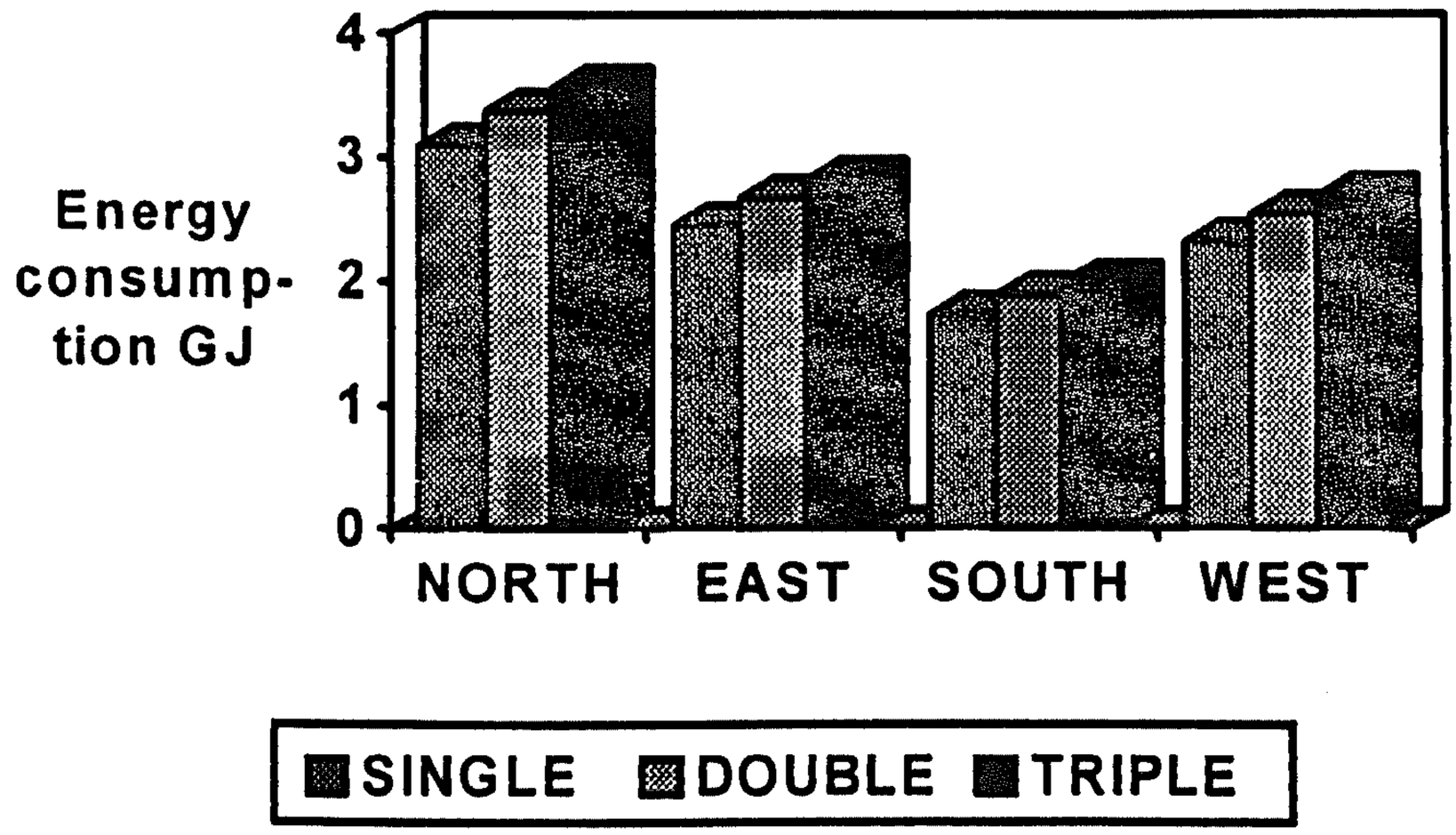

Figure 7.4.1 On/Off controls energy consumption analysis

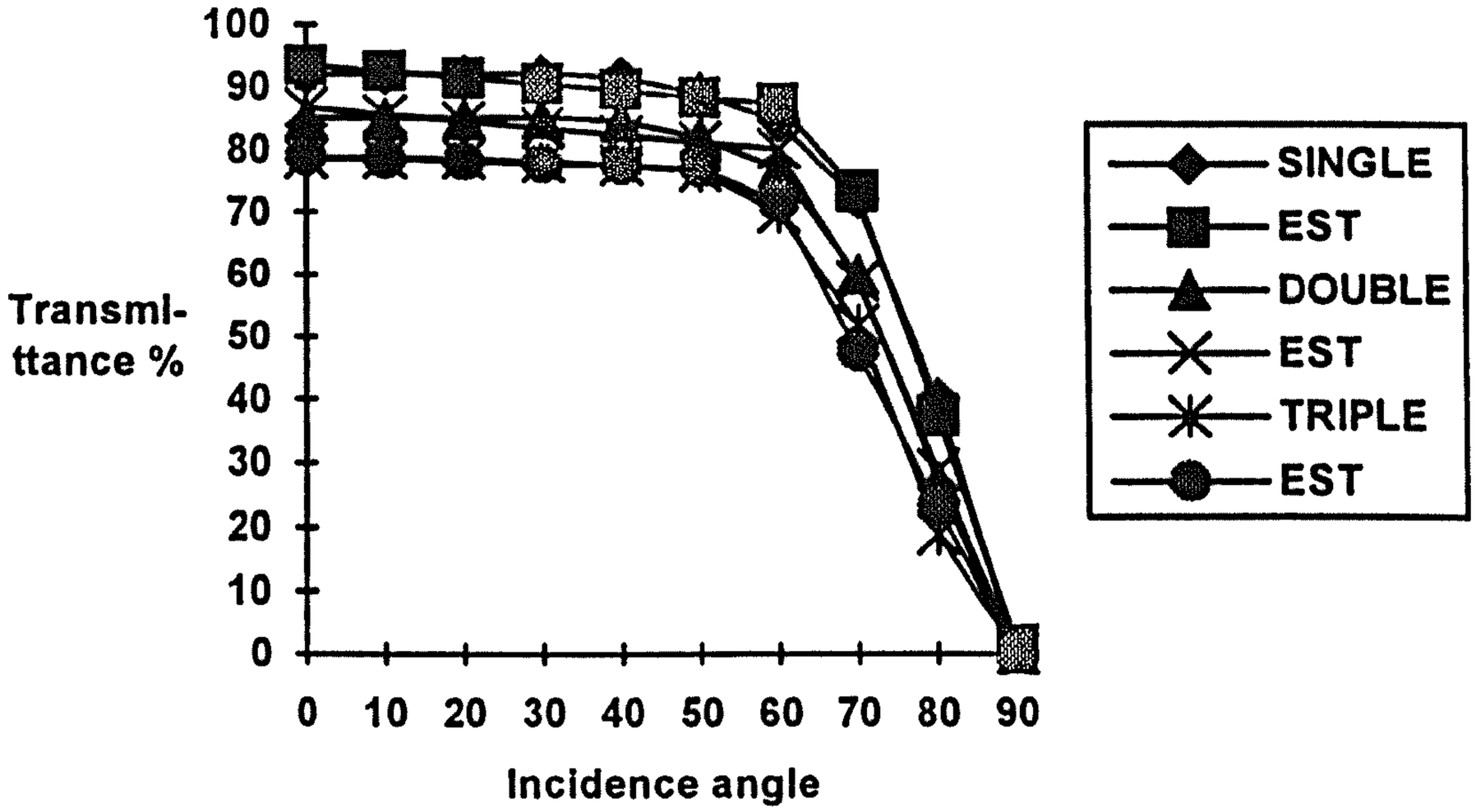

Figure 7.4.2 Transmission of glazing types with incidence angle

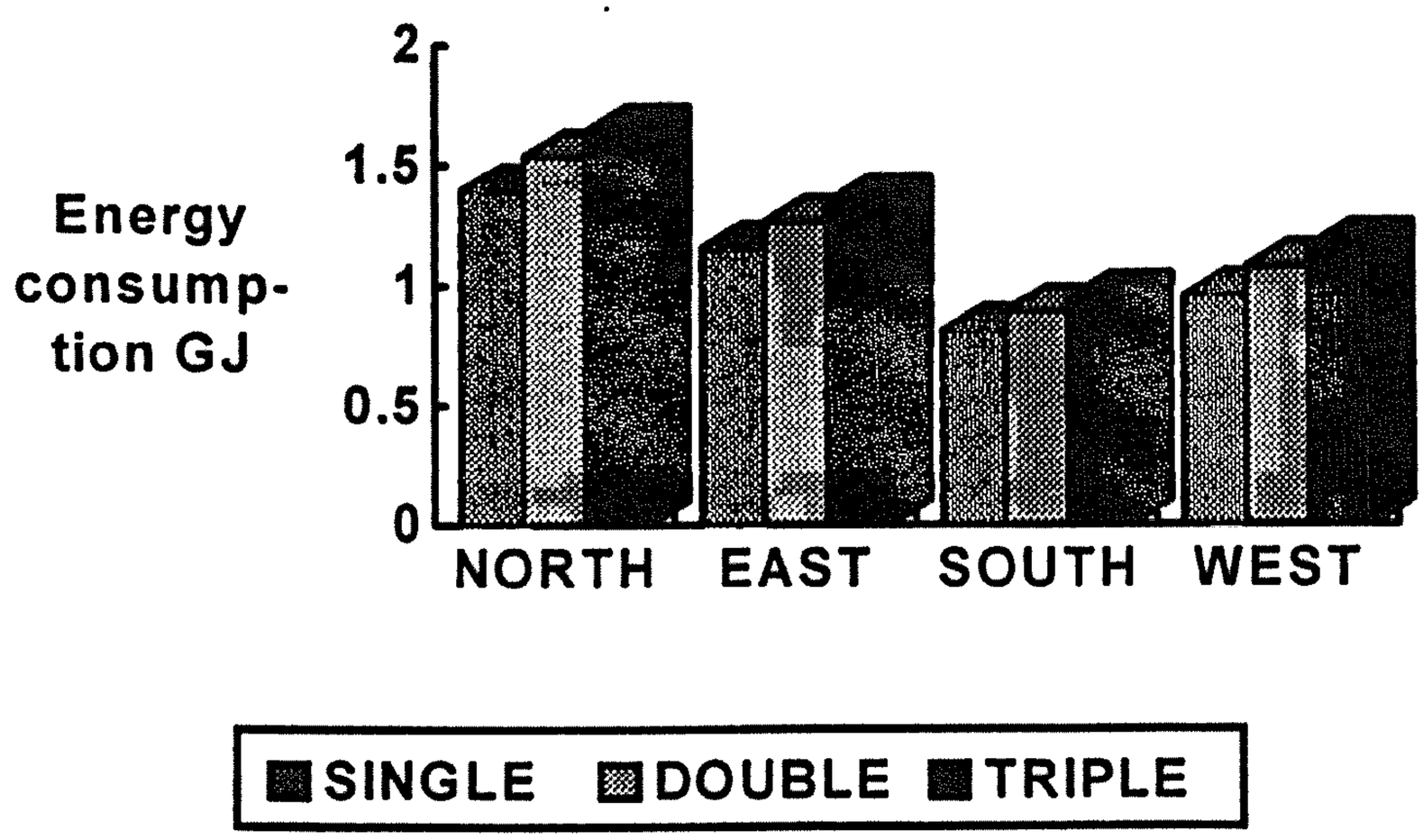

Figure 7.4.3 Top-up controls energy analysis

7.4.2 Heating and Cooling loads

In any design scenario it is vital to complete a full analysis to enable the development of an overall strategy for building design. Before any conclusions about the type, size or orientation of windows are made, it is necessary to examine the thermal aspects of this building due to the costs associated with heating. Using a comprehensive building design analysis software package(CYMAP [7.12]) the

building was subjected to a years' weather simulation comprising of solar gains and thermal transfer analysis. Each glazing type and orientation were taken in turn, the results of which are shown in Fig.7.4.4. The results in Fig.7.4.4 include heating and cooling loads and take into account solar gain through the large glass facade. As can be seen from the bar chart the triple glazing saves on average 10% more energy than the single glazed facades with double glazing saving approximately 7% energy. Larger savings might have been expected from the multiple glazed windows but since cooling as well as heating loads are considered, heat loss in the summer months may well favour the single glazed window.

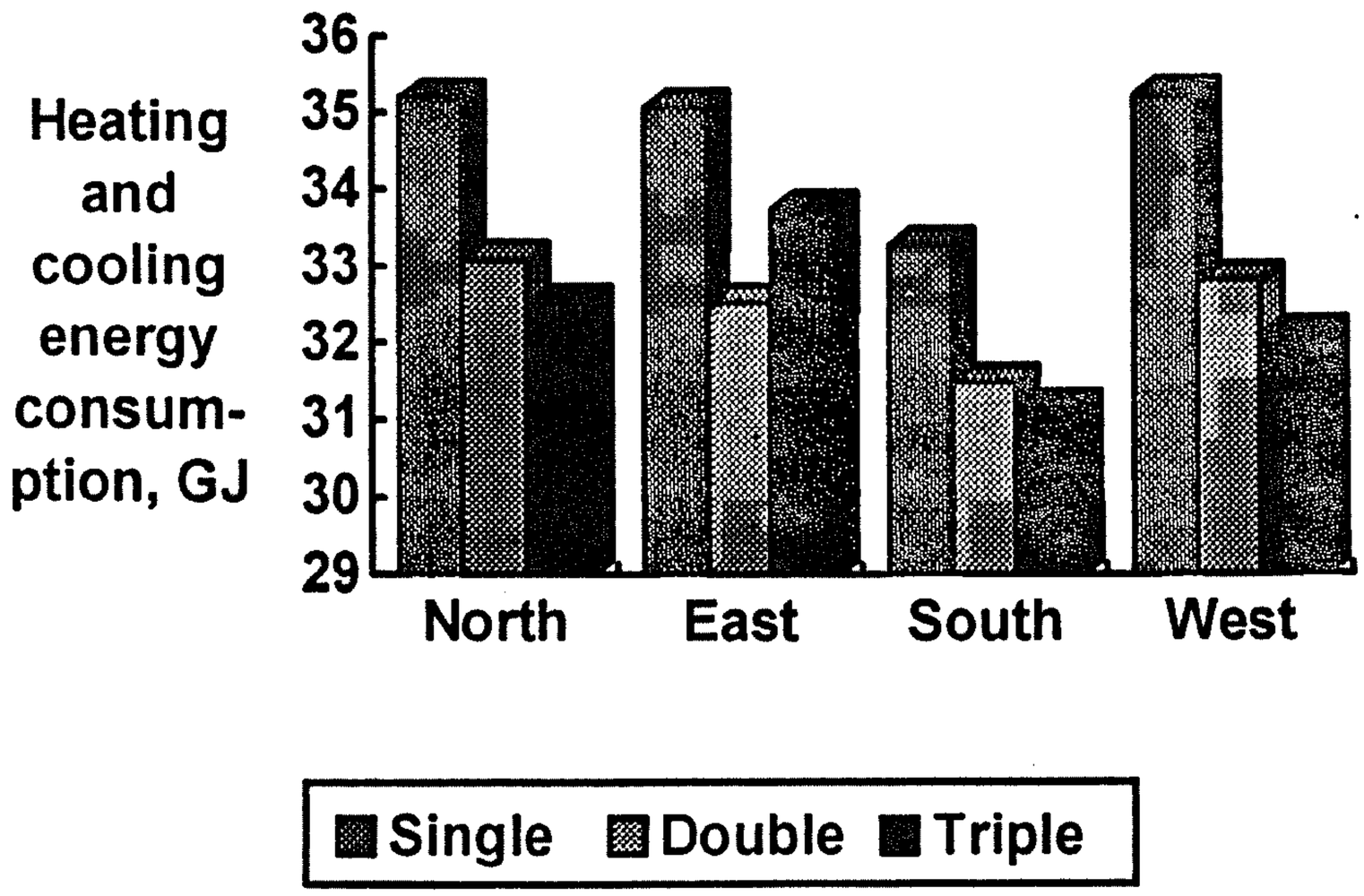

Figure 7.4.4 Heating and cooling energy analysis

Other considerations have to be made with regards to the energy consumption and expense of manufacturing double and triple glazed units. It has been demonstrated in this study that from a daylighting perspective multiple glazed units do not offer a significant penalty when compared to single glazings. However, from a thermal energy point of view, the potential savings to be made by employing multiple glazed units are significant. There still remains a fine balance between the energy consumed and potential savings once the full cost of a design strategy is examined, including embodied energy analysis.

7.5 EMBODIED ENERGY

To improve heat loss and maximise solar gain an increasing number of window manufacturers turn to the production of multiple glazing units which incorporate low emissivity coatings and special frames. The addition of these materials increase what is known as the embodied energy of the window unit, i.e. the energy consumed in the manufacturing process. It is therefore important to examine not only the energy that the window will save during its lifetime but the energy consumed to achieve these savings. To this end several glazing types have been compared to determine the optimal glazing type for energy conservation. Figure 7.5.1 shows the energy consumption of different glazing types over a period of 20 years[13]. As expected the single glazed window performs worst over the 20 years with the best overall performance due to the triple glazed unit. It is interesting to note that if the windows are to be installed for less than 18 months then single glazing may be a more attractive choice due to the higher embodied energy value of some of the multiple glazed units, namely the high performance double glazed aluminium window.

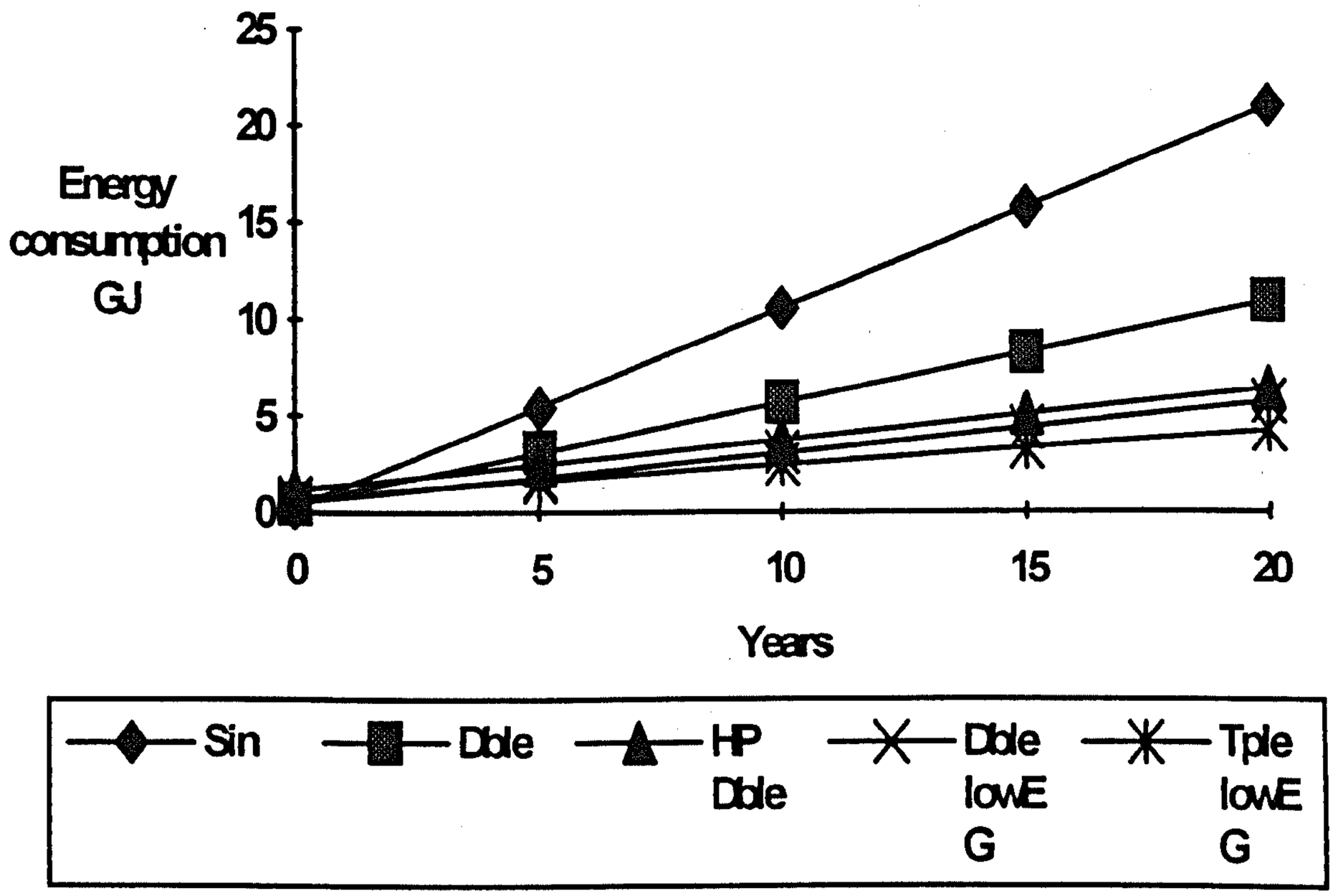

Figure 7.5.1 Embodied energy analysis for various glazing types

7.6 INNOVATIVE DAYLIGHTING DESIGN

An alternative method to using lighting controls to take advantage of natural daylight is the introduction of light shelves and prisms. These devices are generally passive design features attached to new or retrofit buildings with their purpose being to reflect light on to the ceilings and to the back of the room in order to improve the distribution of daylight the building receives. This can often be a more preferable option than sophisticated lighting controls due to the problems that they present. Occupants of offices that employ such systems complain of discomfort when switching occurs especially at illuminance levels around the bandwidth of the sensors. A common occurrence in such cases is to find the photosensors covered to ensure that the artificial lights remain on regardless of the contribution from daylight. This along with the expense of these lighting controls often excludes their implementation. To this end a passive lighting design is more favourable.

One such device which has been used successfully in office type environments is a fixed-angle prismatic panel[7.14]. Its construction is such that direct sunlight is rejected while zenith luminances are directed into the building. These devices have proved particularly useful in city centres where obstructions limit the amount of daylight. The prisms are typically mounted above windows allowing a normal outdoor view as shown in Fig.7.6.1.

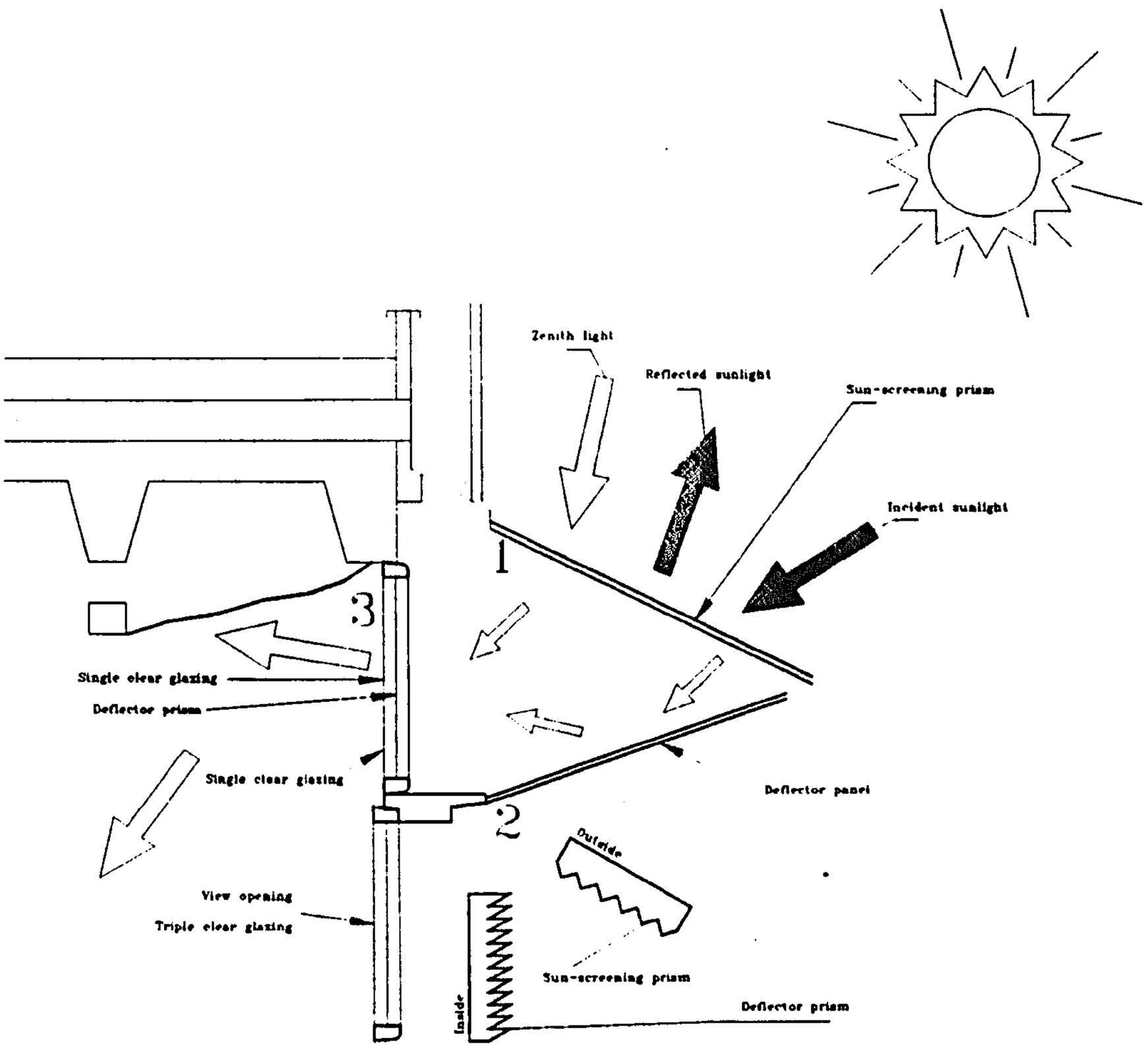

Figure 7.6.1 Innovative prismatic daylight design

One other type of dynamic daylight enhancement aid is the light pipe[7.15] which collects sunlight via a solar tracking mirror and transmits the light through a shaft into a 'solar chandelier' which scatters the light indoors. An example of this design is in operation at Manchester airport. As more and more designers become aware of the advantages of daylight and the development of innovative daylighting features then the potential energy savings from the use of daylight will be realised.

7.7 DISCUSSION

This chapter has shown how real sky distributions can be employed to calculate internal illuminances for office buildings and has presented the results of a daylight and passive solar analysis using one year's weather data. The results of this analysis suggest that window size, type and orientation play important roles in the energy consumption of buildings. The greatest benefits of energy conservation can be achieved through the use of large glass facades on the south of buildings and the restriction of windows on the north where a limited amount of solar gain is available. Furthermore careful consideration must be made towards the choice of window fitted, this will include energy and economic factors and this will depend on the specific requirements of the building and its owner/occupiers.

From a daylighting perspective it can be concluded that glazing type is not significant for internal lighting purposes, whereas orientation is of prime importance. Following these results it may be suggested that the window size is scaled in relation to orientation to optimise daylight utilisation and energy conservation.

Despite the overwhelming evidence to support the use of daylight in building design through lighting controls or innovative daylighting design there appears to be significant reluctance on the part of designers to implement daylight in design. In a relevant survey by Crisp et al[7.16], it was discovered that the reasons behind the lack of daylight exploitation in building design was the lack of available design tools. The information given in the preceding chapters should help provide the daylight design aids required by designers and increase awareness of daylight's potential in the United Kingdom from an energy consumption stand point.

REFERENCES

7.1 Hunt, D R G The use of artificial lighting in relation to daylight levels and occupancy Building Environment 14, 21-33 (1979)

7.2 Hunt, D R G Predicting lighting use -a method based upon observed patterns of behaviour Lighting Res. & Technol. 12, 7-14 (1980)

7.3 Littlefair P J Predicting annual lighting use in daylit buildings. Building & Environment 25, 1 43-54 (1990)

7.4 Tregenza P R, The daylight factor and actual illuminance ratios Lighting Res. & Technol. 12(3) 64-68 (1980)

7.5 Lighting Controls and Daylight Use BRE Digest 272, Garston (1985)

7.6 Lynes J A, Littlefair P J Predicting energy savings from daylight at the early design stage Proc. ISES/LEG Conference on Daylighting Buildings, London (1989)

7.7 Littlefair P J Modelling real sky daylight availability with the BRE Average Sky Proc. CIE, Amsterdam (1983)

7.8 Muneer T Solar heated and daylit offices: Design study Building Serv. Eng. Res. Technol. 11(4) 141-151 (1990)

7.9 Wilkinson M A The effect of glazing upon energy consumption within buildings Lighting Res.& Technol. 24(2) 99-101 (1992)

7.10 Christoffersen J, Johnsen K and Christensen J E Daylight analysis of an office using a daylight and energy analysis system

7.11 Willis S, The cool of the night Building Services, The CIBSE Journal, pp53-54, May 1995

7.12 CYMAP Software for building services, Users manual, Version 7, Bristol (1993)

7.13 Butler D and Howard N From the cradle to the grave Building Services pp49-51 Nov 1992

7.14 Swietzer G E Fixed-angle prismatic panel daylighting:Daylighting distribution in perimeter office and workshop areas CIBSE National Lighting Conference Manchester 275-282 (1992)

7.15 Littlefair P J New wave daylight Crown Copyright 1990- Building Research Establishment

7.16 Crisp V H C, Littlefair P J, Cooper I and McKennan G Daylighting as a passive solar energy option Crown Copyright 1987 Building Research Establishment

CONCLUSIONS

8.1 INTRODUCTION

This work has produced two new illuminance models which enable designers to obtain incident slope illuminance given the horizontal irradiance. The project involved the measurement and analysis of daylight and solar radiation which has provided detailed illuminance and irradiance data for Central Scotland which was previously not available.

A comprehensive study of luminous efficacy research was undertaken in chapter 3 which evaluated a complete range of models and commented on the results. Furthermore the luminous efficacy of various UK and international sites were compared to examine the climatic differences.

The development of a new slope illuminance model which more accurately predicts external illuminance for all sky conditions was shown to perform consistently better than previous models. This was due to the new model's treatment of the sky background diffuse component, which utilised an anisotropic form as opposed to the traditional assumption of an isotropic sky background diffuse component.

The availability of sky luminance distribution data obtained from sky scanners enabled innovative daylight illuminance factors to be developed. These factors model the distribution of the sky's hemisphere under all levels of cloud cover and calculate the internal illuminance taking into account window size, glazing type, orientation and time of day. The development of the daylight illuminance factors has been shown to significantly improve the energy efficient design of buildings in comparison to the current practice of employing the sky factor method.

The daylight illuminance factors were used in a modelled building design scenario to assess their performance and to examine the energy savings. Lighting controls and various glazing types were analysed to study their impact on a building's energy consumption. This study incorporated an embodied energy analysis which further considered the energy consumption of windows in manufacture and operation.

The conclusions of these main areas of work are given in greater detail in the remainder of this chapter.

The luminous efficacy chapter(4) provided beneficial comparison of UK wide luminous efficacy values including a microclimate analysis of the data from Edinburgh's two sites, urban and rural. Several luminous efficacy models were evaluated using the Edinburgh data to establish which, if any model was suitable for the conversion of irradiance to illuminance for Central Scotland. Luminous efficacy models were developed through the course of this work which on the whole performed well considering their simple nature. One observation arising from the luminous efficacy analysis was that the majority of UK sites had average luminous efficacy values that were very similar to each other. Some significant differences were observed with the Athens average diffuse luminous efficacy value which was far greater than the value for UK sites, this was attributed to its atmospheric conditions and air pollution problems. One interesting result from the analysis was the highly commendable performance of the average luminous efficacy values in each of the luminous efficacy models. The use of standard values, 104, 120 and 110 lm/W for direct, diffuse and global luminous efficacies respectively, yielded MBE and RMSE results on a par with much more complex models. The subject of luminous efficacy has been well researched and investigated by many authors to the extent that little scope exists for further development. The addition of atmospheric parameters into luminous efficacy models for increased accuracy unnecessarily complicates the subject and tends towards the law of diminishing returns. A solution which is simple to comprehend and implement yet sufficiently accurate will always be preferred to more complex alternatives.

The slope illuminance chapter highlighted the lack of work in this area especially in the UK. Previous work has centred around specific cloud cover conditions or were derived from non-British databases. The ability to estimate slope illuminance is essential for building designers and is the basis of many internal illuminance estimation tools. The resulting lack of models to adequately provide illuminance data to building designers led to the development of a new slope illuminance model. The model was designed to cater for all weather conditions from clear to heavily overcast skies. The proposed model took a fundamentally different approach to conventional models by incorporating an anisotropic background diffuse component which is more accurate at modelling the

variation in the skies luminance from zenith to horizon. The method utilises the radiance distribution index 'b' along with the sky clearness index F to account for all levels of cloud cover. The proposed model includes beam and circumsolar components and the introduction of an anisotropic background diffuse element to produce a comprehensive slope illuminance model. The proposed model was evaluated against current slope illuminance models using an independent dataset and performed better for the majority of cases. This was a significant achievement as the proposed model is less complex and easier to implement than many of the other contemporary models. The proposed model was further evaluated using data supplied from international and UK daylight stations, the results once again were very good. For the UK as a whole, the proposed model has proven to be an excellent performer in all types of weather and for all seasons, with one of its greatest attributes for designers being its simple structure.

The development of daylight illuminance factors to calculate internal illuminance was made possible through the use of real sky luminance distributions. Sky scanners have enabled accurate measurements of the sky's luminance and their wider application has increased the UK's database of sky luminance measurements for building design use.
Sky scanner data were analysed and used in order to model several sky conditions mathematically. Once typical skies were converted to formulae the luminance distributions were incorporated into daylight illuminance factors which provide a more accurate means of calculating internal illuminance than the current practice of employing the sky factor method. Five cases were derived to cater for shaded and non-shaded windows under various sky conditions. The model results were compared to that of the CIE and Uniform sky factor methods, where considerable underestimation was found to be demonstrated by the CIE approach. Overall the sky factor method was shown to be unsuitable for accurate prediction of internal illuminance and is limited to overcast skies. The newly developed daylight illuminance factors cater for all types of skies and are versatile in their ability to include direct sunlight. These factors provide designers and architects with a means of estimating a building's internal illuminance using measured or estimated data hence aiding energy efficient design.

Having established a comprehensive design tool for estimating internal illuminance that utilised measured data it was possible to carry out an energy analysis on a model building using a complete year's weather data. This analysis incorporated daylight and artificial

lighting through the use of on/off and top-up controls and paid due consideration to solar gain and heat loss. A sophisticated building software package allowed the simulated building to incorporate various glazing types in order to compare energy consumptions in each case. It was shown from a daylighting perspective that glazing type was not a major factor due to the rather small differences in the transmittance loss. South facades yielded better results for both on/off and top-up controls.

With the reduction in electrical energy consumption being paramount the use of top-up as opposed to on/off controls was shown to be far more advantageous. The building software package carried out heating and cooling load calculations for various glazing types and orientations. Once again the south facade performed better than the other orientations. As winter heating and summer cooling loads were taken into account the differences between single, double and triple glazings were less pronounced in terms of energy consumption. The building simulation package(CYMAP) did not, however, consider the reduction in heat gain achieved through the use of lighting controls. Reduction in air conditioning load creates significant energy savings due to the energy intensive nature of the air conditioning process.

The true impact of glazing type can only properly be assessed after undertaking an embodied energy analysis. This research takes into account the energy consumed during the manufacture stage of the glazings and the energy consumption during their lifetime. The results show that high performance glazings are overall better from an energy conservation view point.

8.2 FUTURE WORK

During the course of this research several areas of future work have been identified which stem directly from the findings presented herein.

The expansion of the sky luminance measurement database in the UK allows for a great deal of work in many areas and in particular sky luminance modelling. This is an area still in its infancy and possesses a large potential in respect of the implementation of the results into building energy analysis software.

The development of the daylight illuminance factors is an important step towards the implementation of innovative design tools into software packages. It would seem logical to evaluate these factors in a physical building simulation scenario to include all weather conditions. It is foreseen that as real sky luminance distributions are an integral part of the daylight illuminance factors, the physically modelled results would be of a similar order to the ones presented in chapter 6.

The Athens luminous efficacy, slope illuminance and irradiance results raised the possibility of using illuminance and irradiance measurements to investigate the severity of air pollution. The drooping irradiance plot of the background diffuse component versus sky clearness suggests atmospheric absorption of radiation while the equivalent illuminance plots display an increasing form. By employing a dual headed sky scanner that records simultaneous measurements of irradiance and illuminance, it may be possible to research this phenomenon in greater depth. The traffic related pollution problems are not restricted exclusively to Athens, as many other European and US cities are also affected. The sensitivity of the modelling work carried out in chapter 5 may well be used to produce an atmospheric pollution level indicator. In this context the differences between the illuminance curves for each location given in chapter 5 are accredited to climatic/atmospheric clarity.

With respect to the equipment employed in the project much time and effort would have been conserved if the quality of the control station's amplifiers were improved. Due to the budgeting constrictions of the project the amplifiers for both sites were built in-house from a simple design and whilst they proved satisfactory when operating they frequently broke down which resulted in a significant loss of data. A more satisfactory arrangement would be to employ high quality amplifiers and analogue to digital signal converters to reduce repair time and data loss.

Appendix 1

Appendix 1

LIST OF MEASUREMENT STATIONS FOR IDMP IN THE WORLD

Code	Pays	Ville	Latitude	Longitude	Altitude	Type	Date
J1	Japan	Fukuoka	33°31'03" N	130°28'45" E	69.250m	R	Nov-90
J2	Japan	Kyoto	35°01'30" N	135°47'10" E	62 m	R	Feb-91
J3	Japan	Sapporo	43°03' " N	141°20' " E	14 m	R	Apr-91
J4	Japan	Uozu	36°47'05" N	137°23'32" E	45 m	G	Jun-91
J5	Japan	Nagoya (Daido)	35°07'53" N	136°58'49" E	58 m	G	Jun-91
J6	Japan	Nagoya (Meijo)	35°04'37" N	136°54'49" E	21 m	G	Jun-91
J7	Japan	Toyota	35°10'48" N	137°06'58" E	189.570m	G	Jan-91
J8	Japan	Suita	34°50' " N	135°30' " E	60 m	S	Jun-91
J9	Japan	Ashikaga	36°20'56" N	139°23'58" E	68.800m	sR	Jul-91
J10	Japan	Tokyo	35°40'01" N	139°49'23" E	22 m	R	Mar-92
J11	Japan	Chofu	35°38'46" N	139°33'11" E	43	R	Jan-93
J12	Japan	Tsukuba	36°09' " N	140°03' " E	43 m	R	May-93
J13	Japan	Kiyose	35°46'55" N	139°32'30" E	44.200m	S	
J14	Japan	Osaka	34°35'11" N	135°30'30" E	31.200m	S	82
GB1	United Kingdom	Garston	51°42'36" N	0°22'12" W		R	Jul-92
GB2	United Kingdom	Edinburgh	55°57'00" N	3°13'12" W		G	92
GB3	United Kingdom	Manchester	53°30'00" N	2°15'00" W		R	92
GB4	United Kingdom	Sheffield	53°22'48" N	1°30'00" W		G	92
F1	France	Nantes	47°09'00" N	1°19'48" W	30 m	G	Sep-91
F2	France	Vaulx en Velin	45°46'48" N	4°55'48" E	170 m	G	Sep-91
F3	France	Strasbourg	48°34'48" N	7°45'00" E		S	
F4	France	Chanbery	45°34'12" N	5°55'48" E		S	93
F5	France	Grenoble	45°10'12" N	5°43'12" E		S	93
S1	Sweden	Norrkoping	58°36'00" N	16°10'48" E		R	92
S2	Sweden	Gavle	60°40'12" N	17°10'12" E		G	93
S3	Sweden	Kiruna	67°51'00" N	20°16'12" E		G	93
RFA1	Germany	Hamburg	53°33'00" N	9°58'48" E		G	91
RFA2	Germany	Freiburg	46°48'00" N	7°09'00" E		S	92
CH1	Switzland	Geneva	46°12'00" N	6°09'00" E		R	Sep-91
NL1	Netherland	Eidhoven	51°25'48" N	5°28'12" E		R	92
G1	Greece	Athens	37°58'12" N	23°43'12" E	107 m	G	Dec-91
P1	Portugal	Lisbon	38°45'36" N	9°08'24" W	106 m	G	Sep-91
IL1	Israel	Bet Dagan	32° ' " N	34°49'48" E		S	91
SU1	Russia	Voeikovo				G	
SU2	Russia	Moscow	55°45'00" N	37°34'48" E		S	
SU3	Ukraine	Karadag	40°16'12" N	49°34'48" E		S	
USA1	USA	Ann Arbor	42°16'12" N	83°43'12" W		R	90
USA2	USA	Albany	42°42'00" N	73°51'00" W	79 m	G	Oct-91
USA3	USA	Cape Canaveral	28°24'00" N	80°36'00" W		R	92
CDN1	Canada	Calgary	51°03'00" N	114°04'48" W		G	92
AUS1	Australia	Sydney	33°52'12" S	151°13'19" E		R	91
RC1	China	Chongquing				G	91
RC2	China	Beijing				R	91
RC3	China	Changchun				G	
SGP1	Singapore					R	
SGP2	Singapore					G	
IND1	India	Roorkee				R	
IND2	India					G	

R : Research Class, sR : Simplified Research Class, G : General Class, S : Simplified General Class

Appendix 2

Appendix 2.4 Horizontal global versus diffuse illuminance

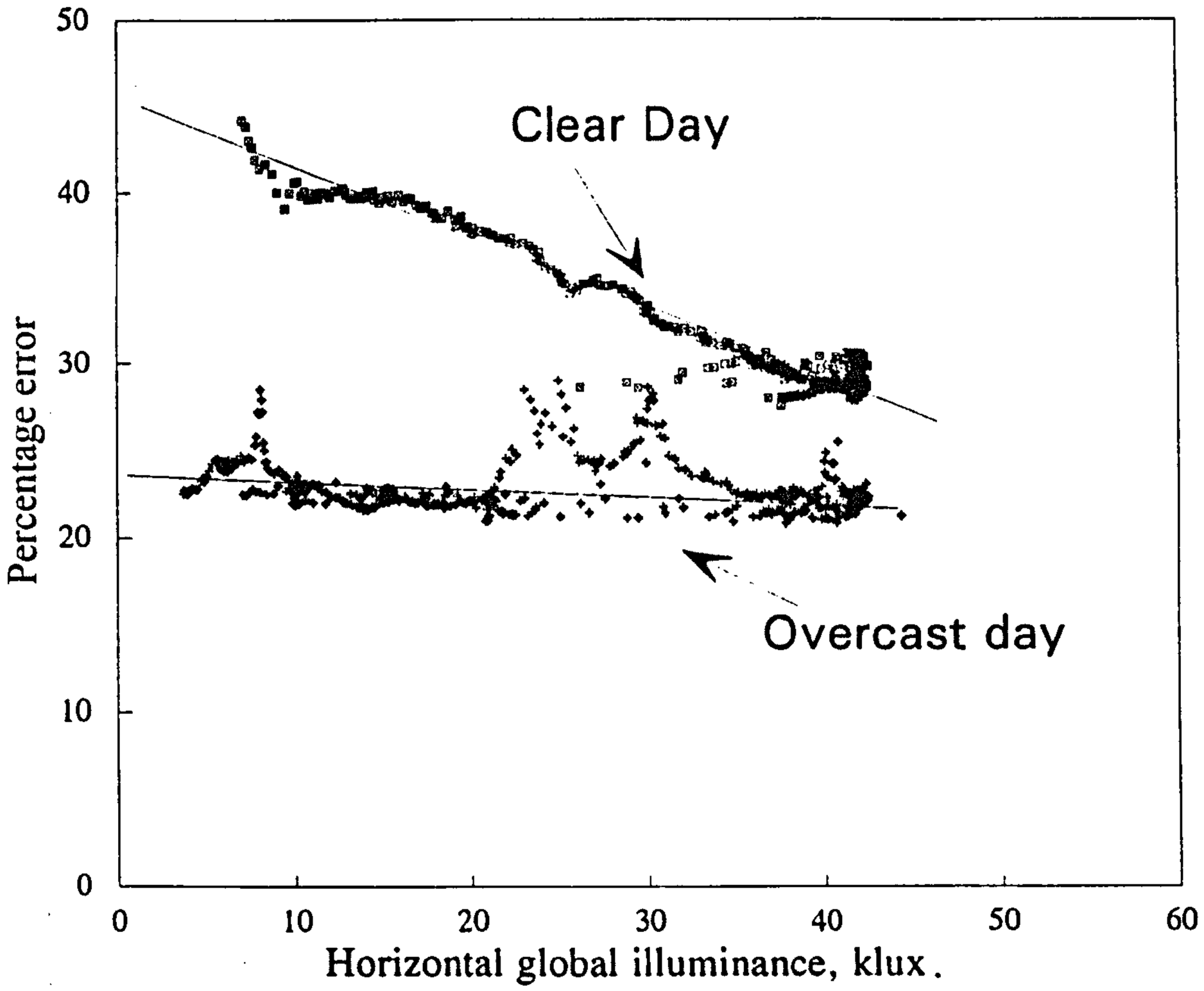

Appendix 2.5 Percentage error

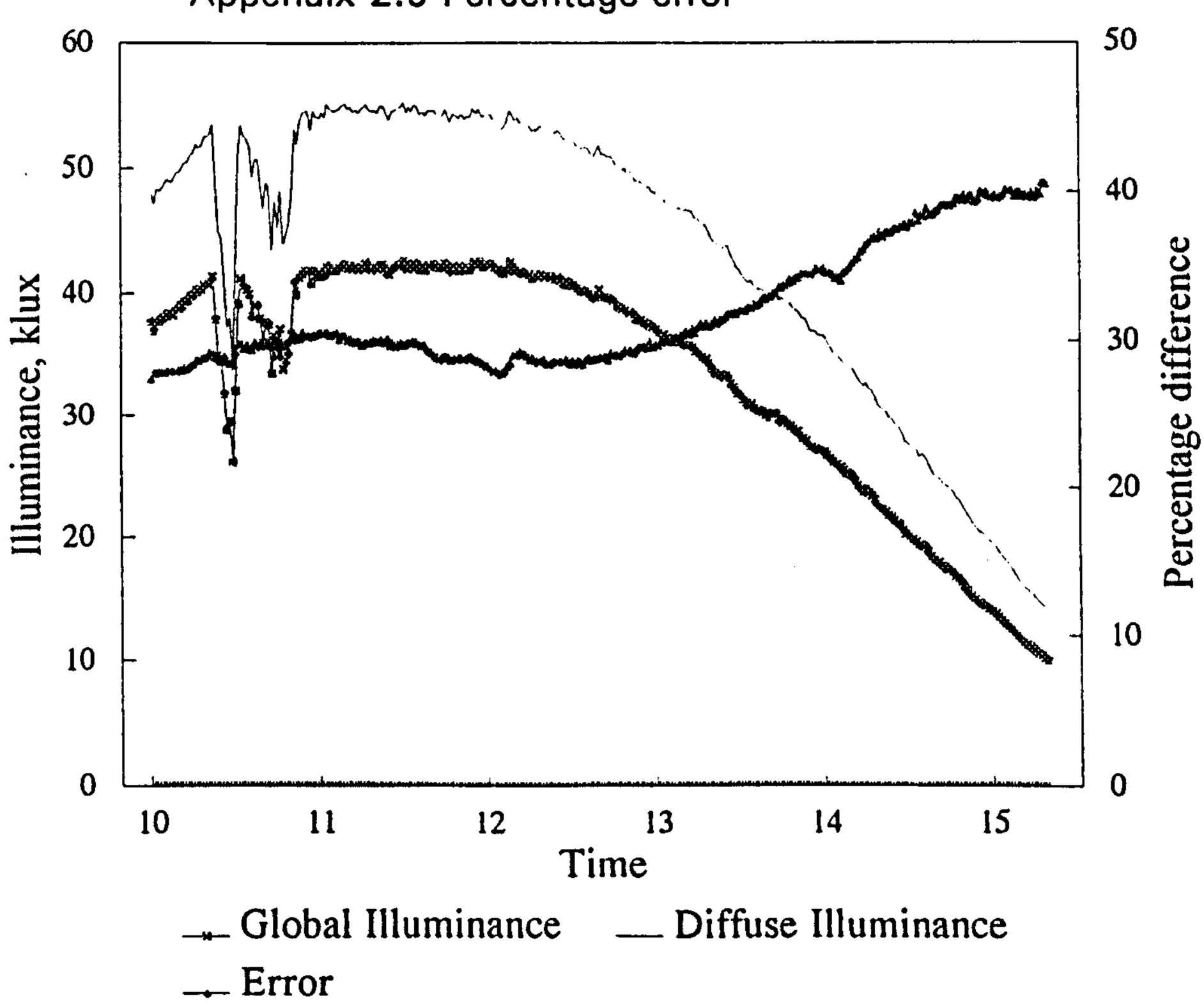

Pages Missing not Available

APP 2.5

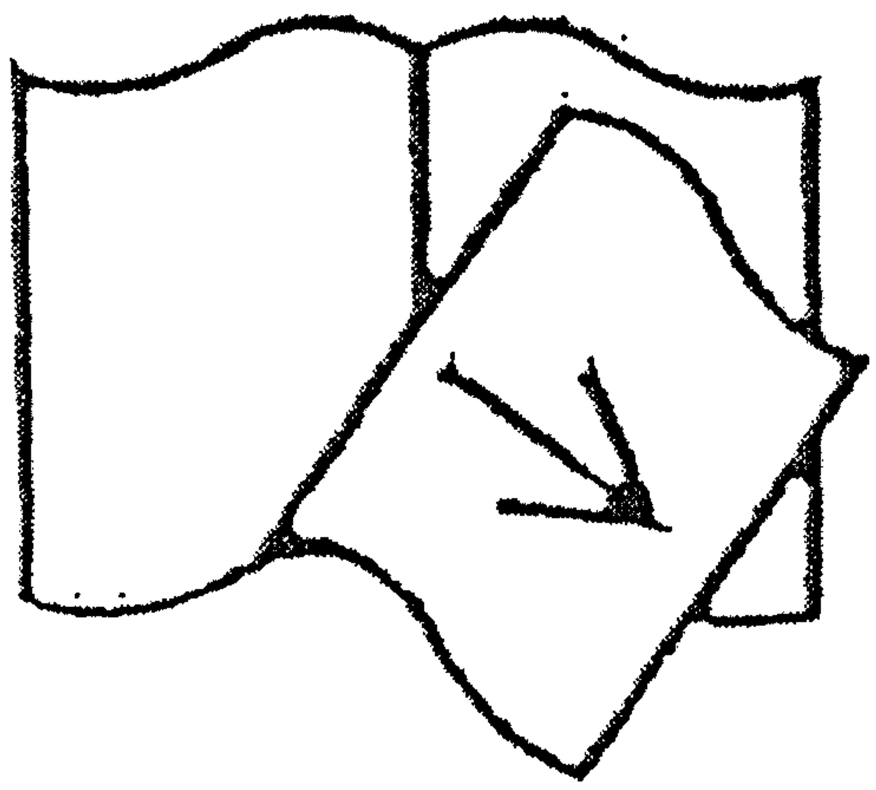

Appendix 2.6 Main station versus control station

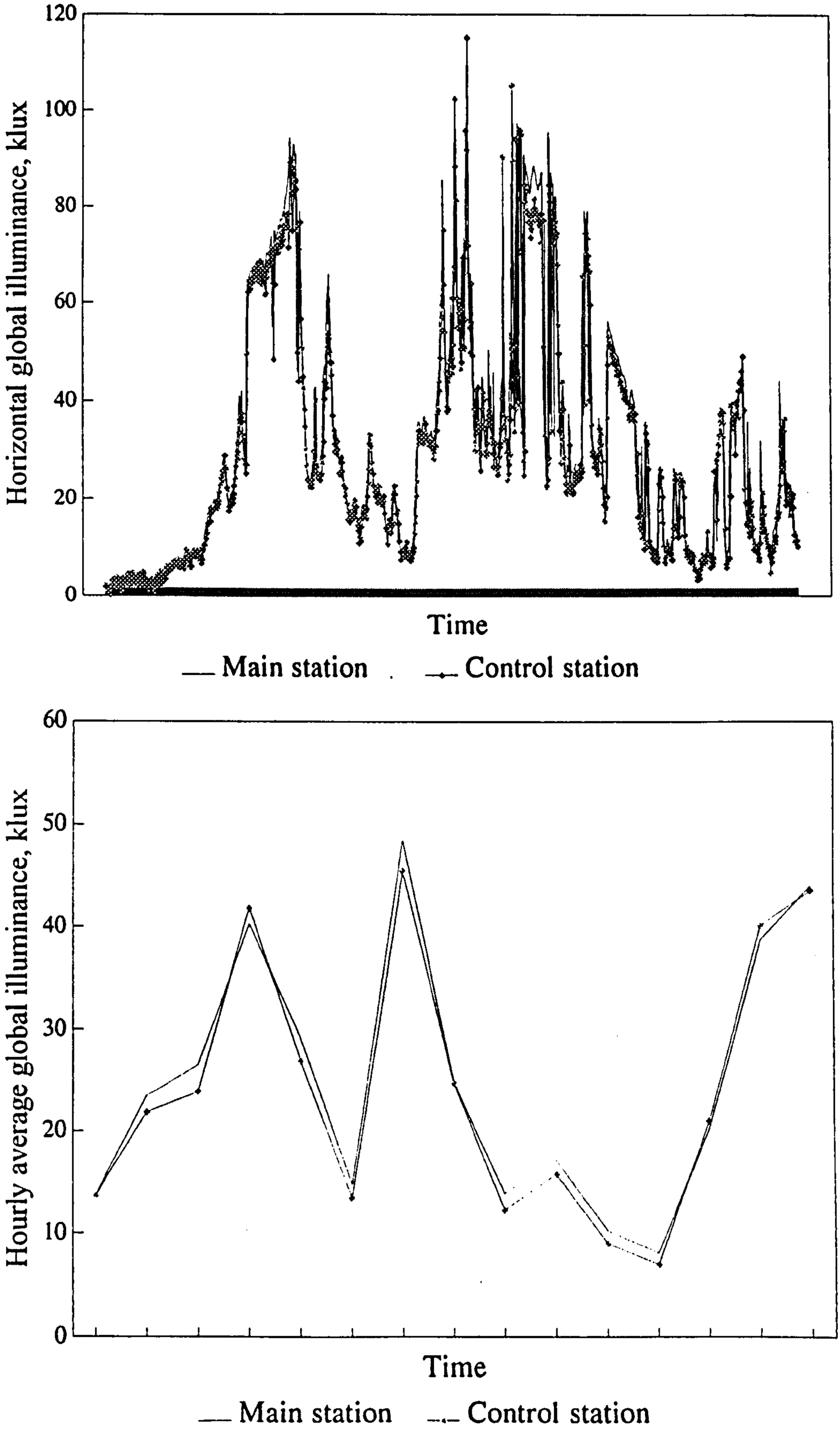

Appendix 2.7 Control station amplifier circuit

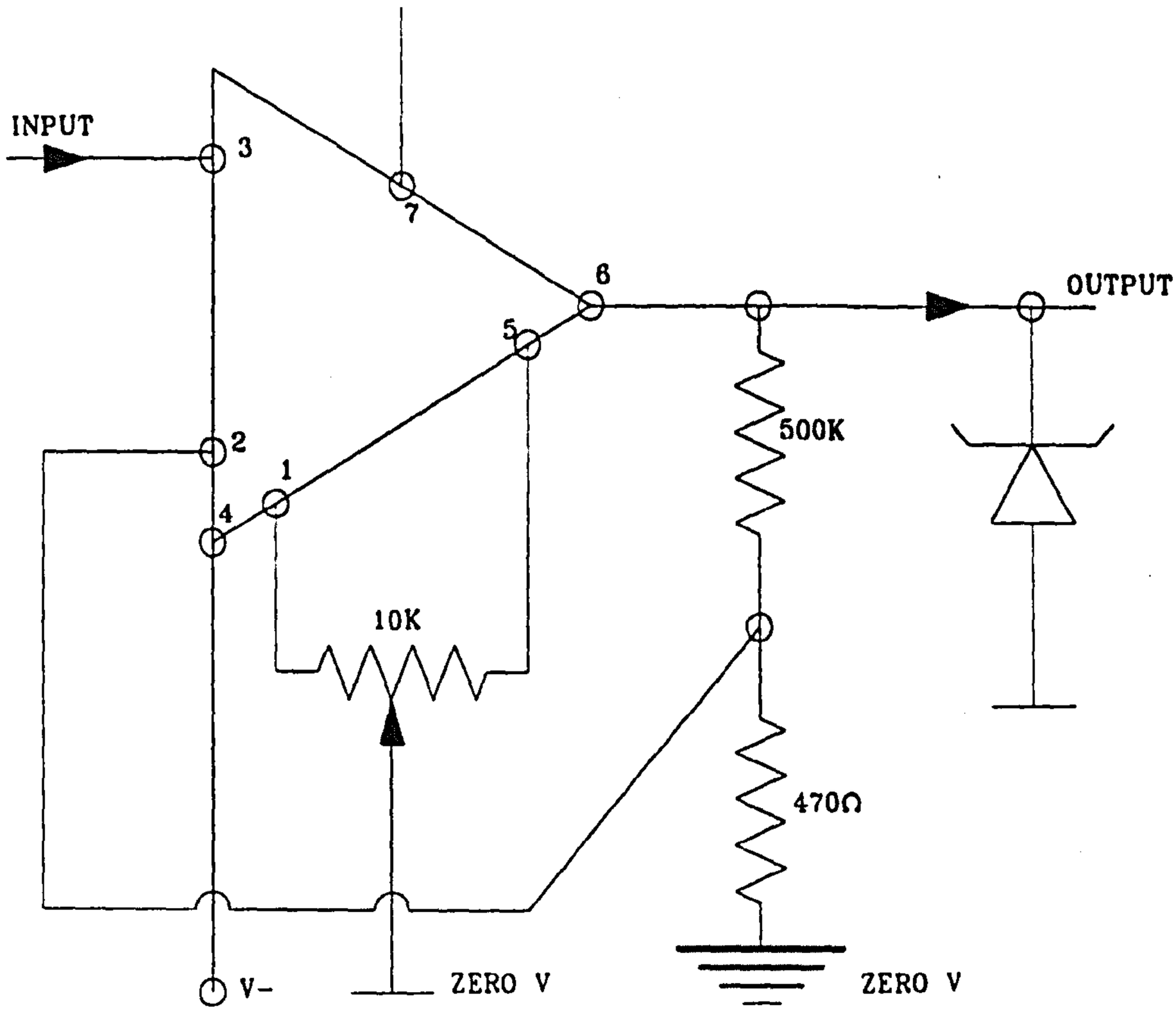

Appendix 2.8

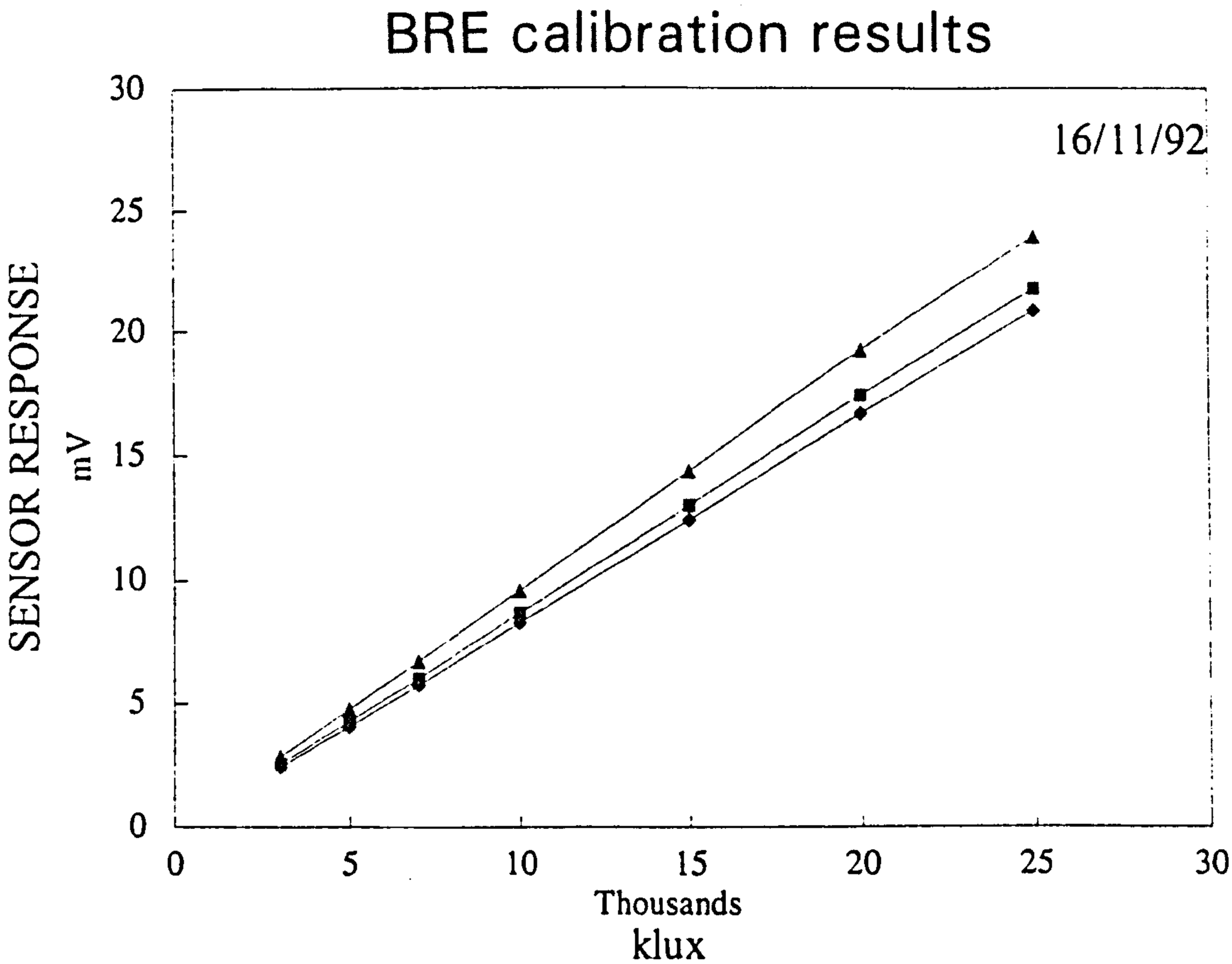

BRE CALIBRATION TEST RESULTS ON THREE BRE DAYLIGHT SENSORS
TEST DATE 16th OF NOVEMBER 1992

klux	No 25 mV	No 27 mV	No 30 mV
3000	2.45	2.565	2.86
5000	4.08	4.295	4.76
7000	5.73	6	6.67
10000	8.23	8.625	9.56
15000	12.45	13.01	14.37
20000	16.64	17.375	19.22
25000	20.9	21.81	24

CALIBRATION FACTOR = Sensor 25: 1.2128 klux/mV
= Sensor 27: 1.158589 klux/mV
= Sensor 30: 1.045852 klux/mV

Appendix 2.9

$$\int_{\varphi}^{\theta} \mathrm{d}\,\theta \mathrm{d}\,\varphi \cos\theta$$

The obstruction under investigation at Heriot Watt provided an altitude above the sensors eye line of 10° and an azimuth angle of 40° from edge to edge. The calculation therefore reads;

$$= \frac{10\pi}{180} . \frac{40\pi}{180} . \cos 10$$

$$= 0.1745 \times 0.698 \times 0.984$$

$$= 0.12 \text{ steradians}$$

The limits recommended by the CIE guide for an obstruction to the sensors is 0.13 steradians.

Appendix 2.10

IDMP STATION, GENERAL INFORMATION

Contacts:

Mr Roddy Angus
Napier University
Department of Mechanical Engineering
10 Colinton Road
Edinburgh
EH10 5DT
(44) 31 455 2535
Fax: (44) 31 447 8046

Station Location:

Edinburgh, Scotland, UK
Latitude: 55.95 N
Longitude: 3.2 E
Height above sea level: 110 m
Local Time: GMT

Type: General class.

Operation: Started in August 1992.

Topographic map showing the land within a 5 km radius of the station location

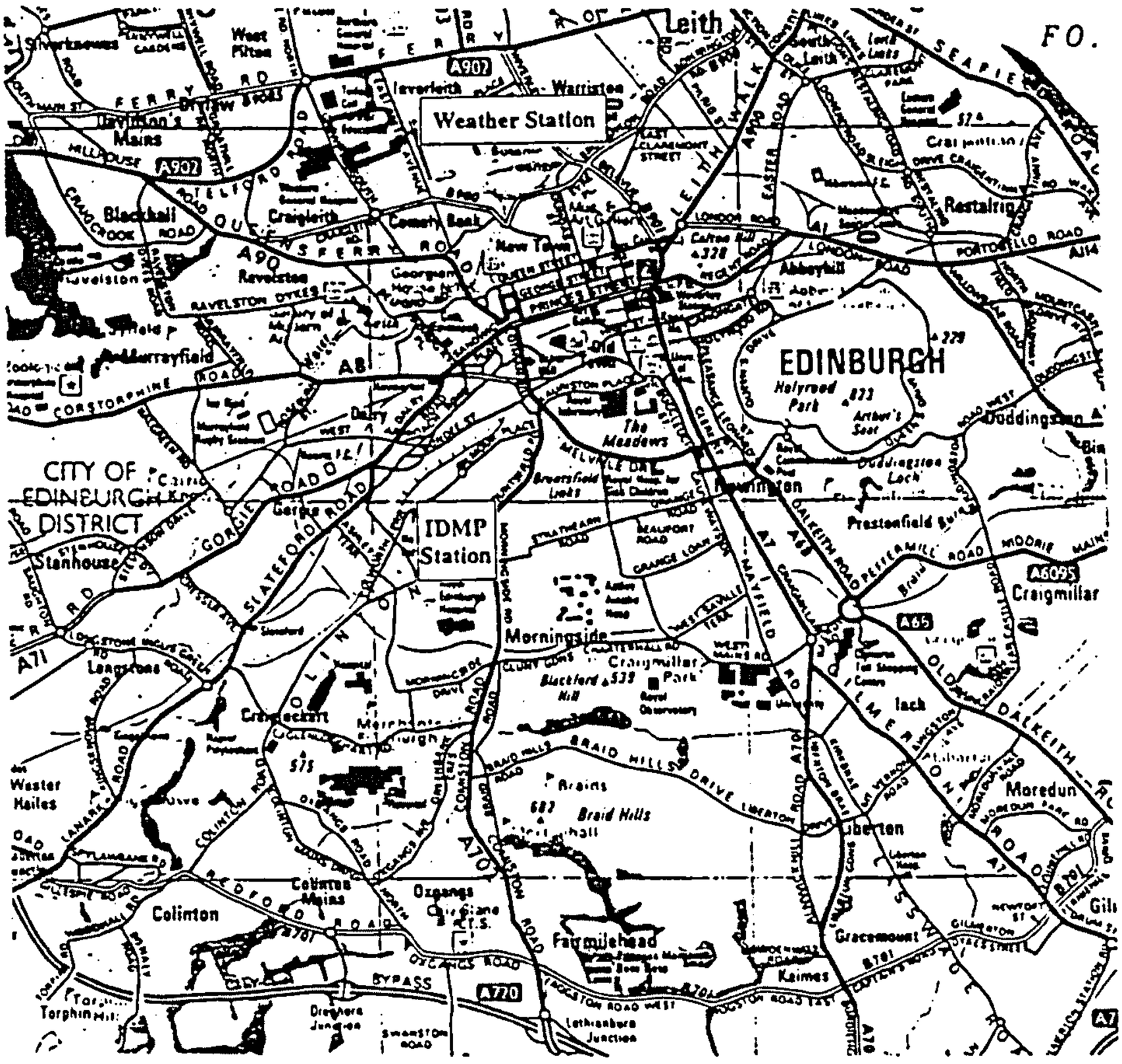

EDINBURGH, UNITED KINGDOM

1

D. Dumortier, P. Avouac-Bastie, LASH-ENTPE, February 23, 1994.

SITE DESCRIPTION

Site surroundings:

Napier University is located to the South-West of Edinburgh having a population of 400,000. The surrounding area within a 5 km radius is 80% urban and suburban housing and office accomodation and 20% farm land and natural features. The station is situated beside a main road 2 km from the city centre.

Climate characteristics:

The climate is temperate. Average temperature in January is 3°C and in July 15°C. Average sunshine duration is 1351 hours. The nearest weather station is located at the Royal Botanic Gardens Edinburgh.

Map showing the immediate surroundings of the station

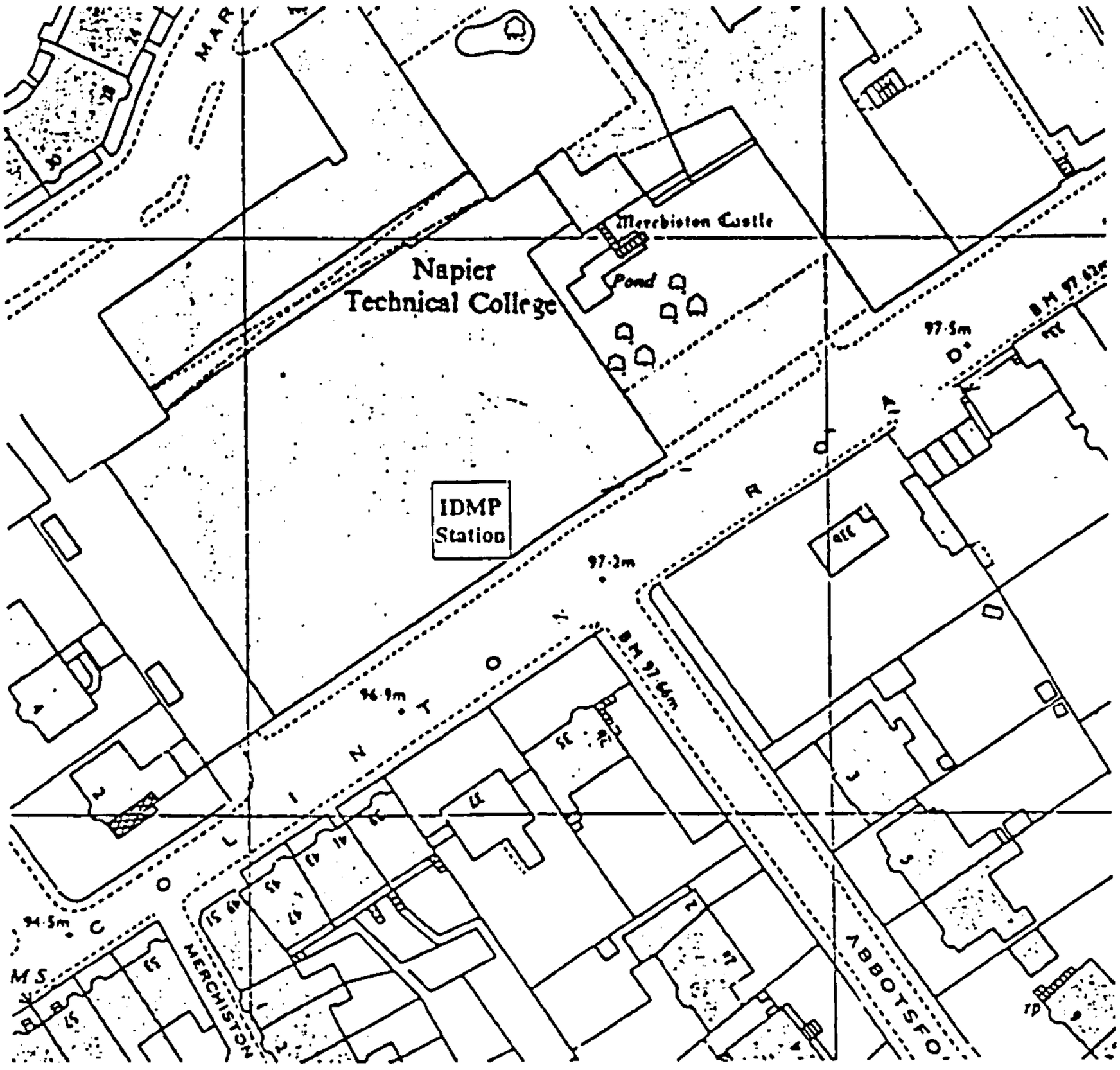

STATION DESCRIPTION

Recording Interval: 1 min.

Measured data:	**Sensor type:**
Illuminances:	
Global horizontal	PRC Krochmann 910GV
Diffuse horizontal	PRC Krochmann 910S
North vertical	PRC Krochmann 910GV
East vertical	PRC Krochmann 910GV
South vertical	PRC Krochmann 910GV
West vertical	PRC Krochmann 910GV
Irradiances:	
Global horizontal	Kipp & Zonen CM11-GV
Diffuse horizontal	Kipp & Zonen CM11/121
North vertical	Kipp & Zonen CM11-GV
East vertical	Kipp & Zonen CM11-GV
South vertical	Kipp & Zonen CM11-GV
West vertical	Kipp & Zonen CM11-GV

Shadow band specifications:

Diffuse illuminance	radius: 31 cm
	width: 5.5 cm
Diffuse irradiance	radius: 31 cm
	width: 5.5 cm

Station map

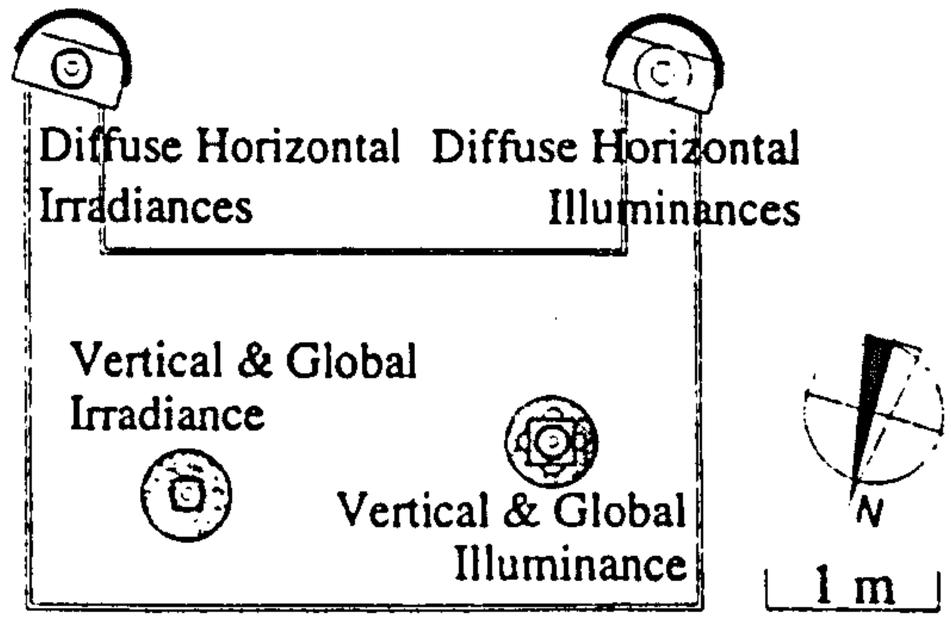

Obstruction for the global horizontal illuminance sensor

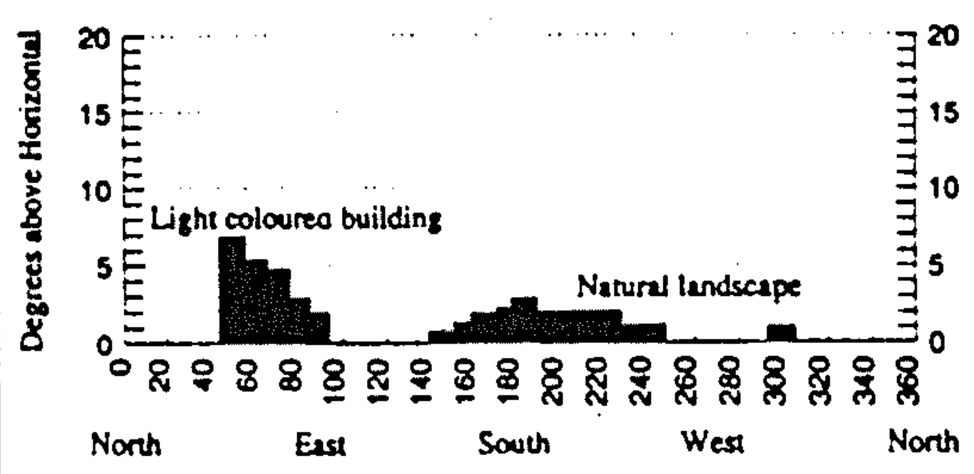

Comments

All sensors were calibrated against a reference photometer and solarimeter supplied by the Building Research Establishment, UK in August 1993.

STATION DESCRIPTION

View 1 of the station

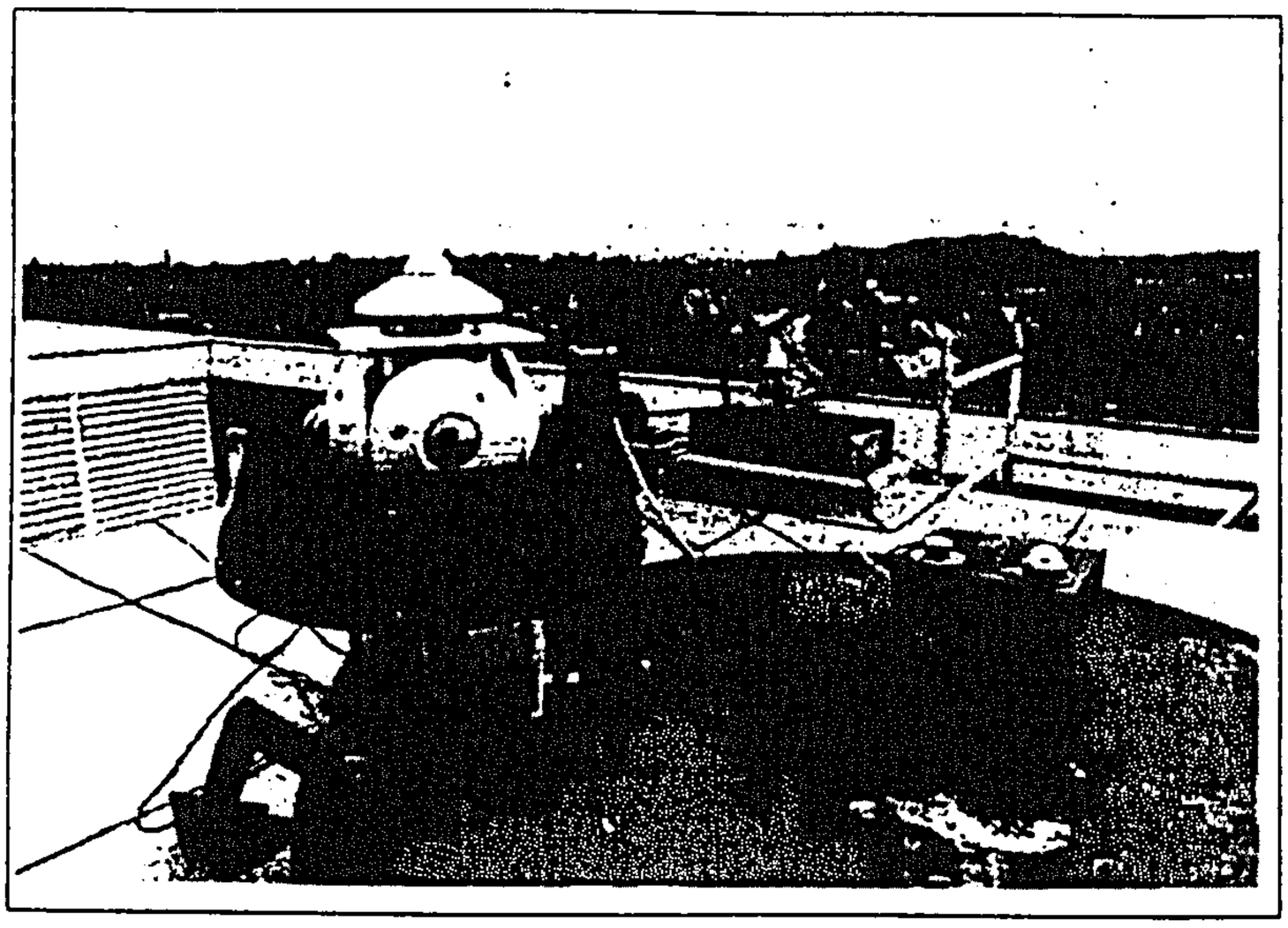

Comments

The view of the station is looking South-East. The vertical irradiance sensors can be seen in the foreground with the diffuse irradiance sensor in the back-ground.

View 2 of the station

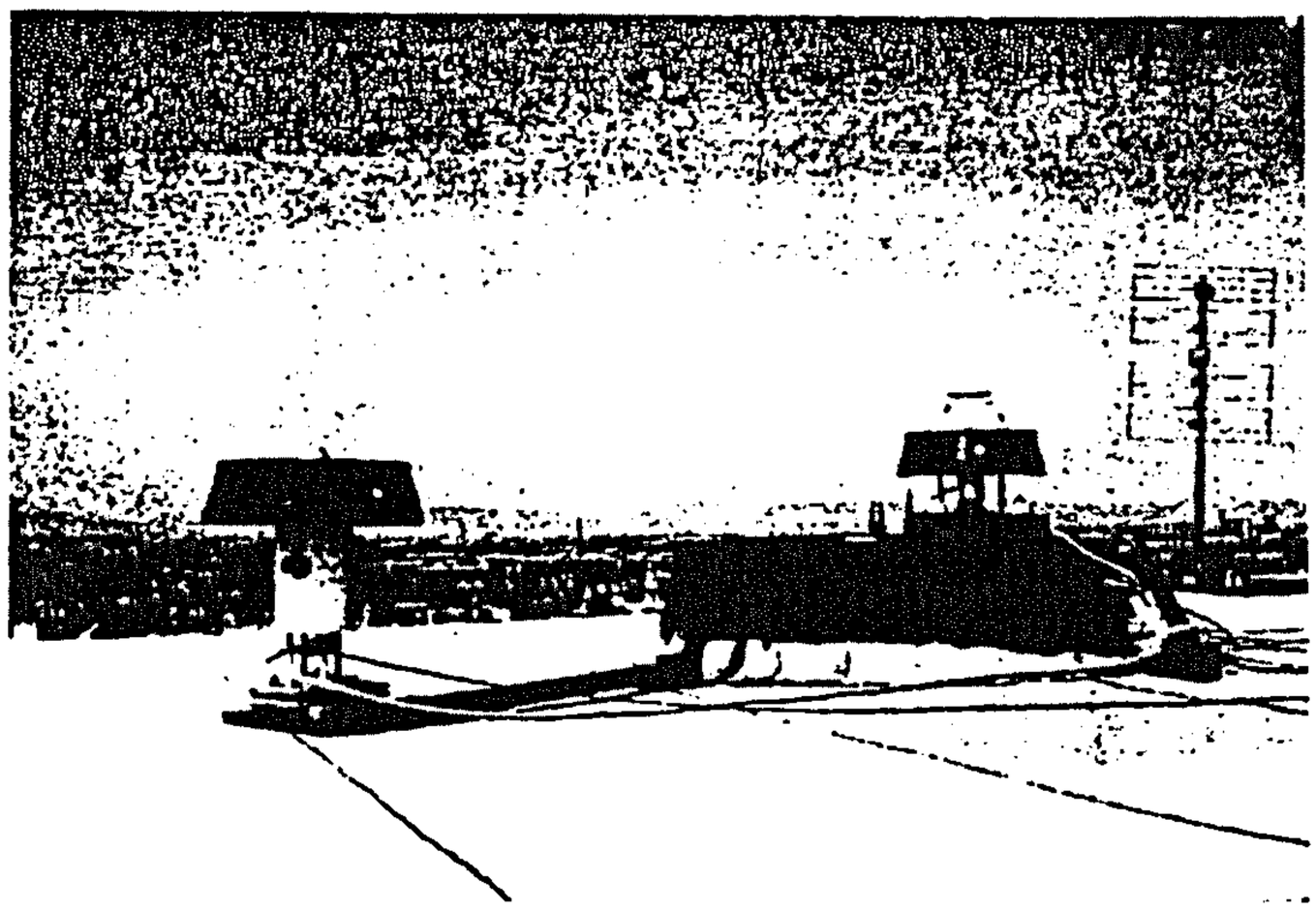

Comments

The view of the station is looking towards the North. The vertical illuminance sensors can be seen on the left with vertical irradiance sensors to the right.

D. Dumortier, P. Avouac-Bastie, LASH-ENTPE, February 23, 1994.

MAINTENANCE SHEET

Important modifications made to the acquisition system, recording interval modification, time during which the station was not operating...

Date	Comments
Dec 92 until Jan 93	Failure of diffuse illuminance thermostat and loss of sensors data.
Nov 93	Station is scheduled to move to a suburban site 7 km West out of the city (Heriot Watt University).

EDINBURGH, UNITED KINGDOM

D. Dumortier, P. Avouac-Bastie, LASH-ENTPE, February 23, 1994.

Appendix 3

Appendix 3.1a

SITE: Garston, UK, Lat : 51.71 N, Long : 0.37 W, Alt: 80 m
TIME: Winter local (GMT)
TYPE: 5mn averages of 1mn measurements
SOURCE: BRE, Garston, Watford, WD2 7JR, UK
Fax:(44) 923664782, Phone:(44) 923664874
COMMENTS: Values for diffuse illuminance and irradiance are corrected with shadowring correction factors calculated by BRE/CSTB methodology and presented in the associated extra data files.
For calibration details consult site description document.

Date	Time	Evg	Evd	Evgn	Evge	Evgs	Evgw	Eeg	Eed	Lvz
mm/dd/yy	hh/mm	Lux	Lux	Lux	Lux	Lux	Lux	W/m2	W/m2	Cd/m2
08/01/91	7:15	37020	16410	9117	70748	10408	5006	324	101	2337
08/01/91	7:20	38228	16771	9060	71270	11965	5025	333	103	2370
08/01/91	7:25	39885	17047	9035	72800	13239	5073	350	105	2408
08/01/91	7:30	41091	17113	8910	73416	14203	5096	363	105	2439
08/01/91	7:35	42446	17268	8809	74172	15240	5103	373	105	2495
08/01/91	7:40	43733	17503	8707	74507	16373	5111	382	106	2527
08/01/91	7:45	45121	17708	8593	74901	17679	5153	393	105	2588
08/01/91	7:50	46478	18086	8480	75045	19105	5196	403	107	2667
08/01/91	7:55	48647	18425	8369	76704	20845	5229	418	109	2751
08/01/91	8:00	50200	18786	8292	77110	22463	5252	429	108	2812
08/01/91	8:05	52001	19190	8237	77583	24059	5311	445	113	2949
08/01/91	8:10	52712	19561	8187	76317	25127	5403	455	114	3044
08/01/91	8:15	54571	20097	8203	76924	26636	5478	471	119	3135
08/01/91	8:20	55373	20252	8118	71186	27710	5527	479	122	3237
08/01/91	8:25	57016	20366	8231	76584	29444	5635	494	127	3316
08/01/91	8:30	58341	21151	8402	76203	30823	5733	505	132	3419
08/01/91	8:35	59654	21805	8461	75523	32289	5820	518	137	3516
08/01/91	8:40	60812	22674	8495	74452	33582	5991	529	144	3657
08/01/91	8:45	62065	23987	8840	73177	34794	6400	542	154	4018
08/01/91	8:50	63768	24987	8951	72923	36293	6675	556	162	4404
08/01/91	8:55	65212	24641	9059	73492	37618	6612	568	159	4094
08/01/91	9:00	67567	23660	9061	74055	39588	6699	587	151	4385
08/01/91	9:05	68167	24174	8848	72055	40653	7157	596	158	4967
08/01/91	9:10	68579	26162	9299	69178	41307	7948	604	174	4946
08/01/91	9:15	69792	26760	9386	68256	42828	8565	615	178	4847
08/01/91	9:20	73316	27224	9424	69387	45622	9430	642	182	4918
08/01/91	9:25	74544	28542	9473	67773	46925	10050	656	193	5126
08/01/91	9:30	73197	31299	10021	63045	46411	10796	653	217	5390
08/01/91	9:35	78007	34928	10508	63947	48759	11856	695	249	5997
08/01/91	9:40	83351	40951	11802	62916	50966	12955	747	306	8647

Appendix 3.1b

SITE: Garston, UK, Lat : 51.71 N, Long : 0.37 W, Alt: 80 m
TIME: Winter local (GMT)
TYPE: 5mn averages of 1mn measurements
SOURCE: BRE, Garston, Watford, WD2 7JR, UK
Fax:(44) 923664782, Phone:(44) 923664874
COMMENTS: Altitude and azimuth of the sun are computed using Walraven method.
Shadowring correction factors calculated by BRE/CSTB methodology.
For calibration details consult site description document.

Date	Time	Cvf&	Evs	Ees	Eegn	Eege	Eegs	Eegw	Rh	Dbt	Alt	Azi
mm/dd/yy	hh/mm	Cef %	Lux	W/m2	W/m2	W/m2	W/m2	W/m2	%	DgC	Dg	DgN
08/01/91	7:15	117.5	50310	543	61	627	80	36	92	18	24.5	91.9
08/01/91	7:20	117.5	50183	543	61	625	88	35	90	19	25.3	92.9
08/01/91	7:25	117.7	52651	560	62	638	96	35	89	19	26.0	93.9
08/01/91	7:30	117.8	53902	569	61	640	104	35	88	19	26.8	94.9
08/01/91	7:35	117.9	55244	576	62	646	112	35	87	19	27.6	95.9
08/01/91	7:40	118.0	56274	582	62	649	119	35	88	19	28.3	96.9
08/01/91	7:45	118.1	57731	593	62	649	127	35	88	19	29.1	98.0
08/01/91	7:50	118.1	58385	598	62	646	135	35	87	19	29.9	99.0
08/01/91	7:55	118.4	60874	615	61	652	146	34	85	20	30.6	100.1
08/01/91	8:00	118.5	61980	624	59	653	157	34	83	20	31.4	101.2
08/01/91	8:05	118.6	63529	634	57	653	170	35	81	21	32.2	102.2
08/01/91	8:10	118.5	62881	629	56	642	181	36	81	21	32.9	103.3
08/01/91	8:15	118.6	64201	637	56	644	194	37	80	21	33.7	104.4
08/01/91	8:20	118.5	63028	628	56	635	204	38	80	21	34.4	105.6
08/01/91	8:25	118.6	64247	636	57	634	217	39	80	21	35.2	106.7
08/01/91	8:30	118.6	63857	634	58	629	230	40	80	21	35.9	107.8
08/01/91	8:35	118.6	63628	635	59	624	244	41	78	22	36.6	109.0
08/01/91	8:40	118.4	62787	631	60	614	253	42	78	22	37.4	110.2
08/01/91	8:45	118.3	61779	621	64	603	263	47	79	22	38.1	111.4
08/01/91	8:50	118.3	61757	621	65	599	275	49	80	21	38.8	112.6
08/01/91	8:55	118.4	64073	636	66	601	288	49	78	22	39.5	113.8
08/01/91	9:00	118.8	68944	670	67	603	303	50	77	23	40.2	115.1
08/01/91	9:05	118.7	68132	665	65	589	314	54	75	23	40.9	116.4
08/01/91	9:10	118.3	64425	638	70	566	320	62	76	22	41.6	117.7
08/01/91	9:15	118.3	64202	636	72	558	333	67	77	22	42.3	119.0
08/01/91	9:20	118.6	68321	665	73	563	353	75	77	22	43.0	120.3
08/01/91	9:25	118.4	67150	657	74	554	369	81	75	22	43.7	121.7
08/01/91	9:30	117.7	58351	600	79	522	370	88	76	22	44.3	123.1
08/01/91	9:35	117.8	60202	614	84	526	390	97	76	22	45.0	124.5
08/01/91	9:40	117.6	58213	599	96	519	414	105	75	22	45.6	125.9

Appendix 3.2

SkyLog : V3.0 (c) Copyright Cambridge Consultants (SE) Ltd 1991

SL002_92.LUM
=-=-=-=-=-=-=-

Year : 1992
Julian Day : 2

Time Alt Azim Sky Luminance Distribution
---- --- ----- ----------

0 7 54 -2.4 125.1

8 6 6 4 8 6 6 4 6 6
4 4 2 2 4 2 2 6 4 4
6 2 6 4 4 8 6 4 6 6
11 8 6 6 8 8 8 8 8 6
6 6 6 6 4 6 4 6 6 6
6 6 6 6 6 8 8 6 11 8
6 6 11 6 8 8 11 11 6 6
8 6 6 11 6 8 6 11 6 11
6 11 8 8 8 8 11 11 11 11
11 11 8 6 8 8 6 8 8 11
8 11 6 11 11 11 8 11 11 11
13 11 13 11 8 11 4 8 11 11
11 8 8 8 11 8 8 11 11 11
8 11 8 8 11 8 6 8 8 11
8 8 11 8 8 11 11 8 11 11

0 8 00 -1.7 126.2

19 17 15 13 15 11 8 8 13 11
4 11 8 8 11 8 6 13 8 8
11 8 11 11 11 13 13 13 13 15
17 17 17 15 17 15 13 15 17 13
11 13 11 13 11 11 11 13 11 13
13 13 13 13 15 15 17 17 17 17
15 19 19 17 17 17 21 17 13 13
17 13 13 17 13 15 13 17 15 17
15 21 19 19 17 21 19 17 17 17
19 21 17 17 15 17 17 19 17 15
17 17 17 19 17 21 19 19 21 21
21 19 23 21 17 21 19 17 19 21
19 19 17 15 23 21 21 21 21 19
19 19 19 19 19 19 17 21 19 21
19 21 21 17 21 21 19 21 23 21

Appendix 3.3

These data validation are taken from an adaptation of the CIE guide to recommended practice of daylight measurement stations by Howard Porter and Paul Littlefair at the BRE Watford.

The first category of test involves the six base quantities of the Research class stations. The six quantities are: global irradiance and illuminance(Eeg and Evg), diffuse irradiance and illuminance(Eed and Evd) corrected for shadowband effect and direct irradiance and illuminance(Ees and Evs). These are rough absolute checks that ensure that no major problems exists.

Test 1.1: $0 < Eeg < 1.2$ E.T.R.
Test 1.2: $0 < Evg < 1.2$ E.T.I.
Test 1.3: $0 < Eed < 0.8$ E.T.R.
Test 1.4: $0 < Evd < 0.8$ E.T.I.
Test 1.5: $0 < Ees <$ E.T.R.
Test 1.6: $0 < Evs <$ E.T.I.

E.T.R. and E.T.I. are respectively the extraterrestrial irradiance and illuminance. These may be approximated to the solar constants to serve the current purpose: E.T.R. = 1367 Watt/m^2; E.T.I. = 127.5 klux.

The second category includes two consistency tests that utilise the redundancy existing between direct, diffuse and global components based on the knowledge of solar zenith angle z.

Test 2.1: $Eeg = (Ees \cos z + Eed) \pm 15\%$
Test 2.2: $Evg = (Evs \cos z + Evd) \pm 15\%$

The third category of tests makes use of the predictable relationship existing between the above base components and irradiance and illuminance values on vertical planes respectively(Eegi and Evgi).

Knowing the solar incidence angle I, it is possible to use the following tests to verify the coherence between measured direct irradiance/illuminance and each vertical measurement:

Test 3.1: Eegi = f(Ees, Eed, cosz, cosi) ± 150 W/m^2
Test 3.2: Evgi = f(Evs, Evd, cosz, cosi) ± 18 klux

The function f is a model that predicts the irradiance/illuminance impinging on a sloping plane from the knowledge of global and direct(or diffuse) irradiance/illuminance. The model has been extensively validated and is given in full in the appendix to the CIE guide to recommended practice(An alternative would be to employ the Perez or the proposed model). The model's governing equation is:

$$Eeng = Eed\{(1-F_1)/2 + F_1\,\sigma/cosz + F_2\} + \sigma\, Ees$$

or for illuminance prediction:

$$Evng = Evd\{(1-F_1)/2 + F_1\,\sigma/cosz + F_2\} + \sigma\, Evs,$$

where $\sigma = max(0,cosi)$.

The fourth category of tests involves intercomparisons between irradiance and illuminance components. The bench marks and thresholds in this series of tests are based on experimental measurements performed to date. The tests are:

Test 4.1: $Evg/Eeg = a_1 \pm b_1$
Test 4.2: $Evd/Eed = a_2 \pm b_2$
Test 4.3: $Evs/Ees = a_3 \pm b_3$
Test 4.4: $Evng/Eeng = a_4 \pm b_4$

The test limits are;
$a_1 = 120$ lumen/Watt, $b_1 = 30$
$a_2 = 140$ lumen/Watt, $b_2 = 40$
$a_3 = 51.8 + 1.646\gamma s - 0.01513\gamma s^2$ lumen/Watt
$b_3 = 30$

Here γs is solar altitude in degrees.
$a_4 = a_1$, $b_4 = b_1$

or if Ees> 100W/m^2;

$a_4 = a_3$, $b_4 = b_1$

or if i > 60°(and Ees> 100W/m^2)

$a_4 = a_1$, $b_4 = b_1$

or if i > 85°(and Ees> 100W/m^2)

$a_4 = a_2$, $b_4 = b_2$

Appendix 3.4

$$g = \frac{E_{HT}(g_{cl} - g_{ov}) + E_{HSMAX}}{E_{HSMAX} + E_{HDCELL}(g_{cl} - g_{ov})}$$

E_{HT} = Horizontal global illuminance

$$E_{HSMAX} = \frac{96 \sinh_s}{1 + \frac{0.2}{\sinh_s}}$$

E_{HDCELL} = Horizontal diffuse illuminance

$$g_{cl} = 1.104 + 0.101\delta - 0.165\delta^2 + 0.206h_s - 0.011\delta h_s - 0.375\delta^2 h_s - 0.161h_s^2 - 0.411\delta h_s^2 + 1.550\delta^2 h_s^2$$

$$g_{ov} = 1.054 + 0.139\delta + 0.018\delta^2$$

δ = declination angle, h_s = solar altitude angle both in radians

Appendix 4

APPENDIX

Appendix 4.1

γ_s	w	B=0,05				B=0,10				B=0,20			
		T_L	K_s	K_{cl}	K_g	T_L	K_s	K_{cl}	K_g	T_L	K_s	K_{cl}	K_g
10	0.5	2.4	68.3	124.9	88.3	3.1	53.5	122.4	86.2	4.4	30.9	116.0	86.1
10	1.0	2.6	74.0	127.3	93.6	3.3	58.6	125.5	91.4	4.6	34.4	119.7	91.3
10	2.0	2.8	80.1	129.9	99.1	3.5	63.9	128.9	96.8	4.9	38.0	123.9	96.5
10	3.0	3.0	84.4	131.7	102.8	3.7	67.7	131.2	100.4	5.1	40.7	126.6	100.1
10	4.0	3.1	87.7	132.9	105.6	3.8	70.7	132.8	103.2	5.2	42.9	128.6	102.8
20	0.5	2.6	89.1	123.8	96.7	3.2	80.2	126.4	94.1	4.6	63.1	125.9	90.8
20	1.0	2.8	94.3	125.2	101.3	3.5	85.3	128.3	98.7	4.9	68.0	128.5	95.4
20	2.0	3.0	100.7	127.1	106.9	3.8	91.7	130.8	104.3	5.2	73.9	131.7	100.9
20	3.0	3.2	104.6	128.3	110.2	3.9	95.5	132.4	107.6	5.4	77.4	133.8	104.2
20	4.0	3.3	107.4	129.1	112.7	4.1	98.3	133.6	110.1	5.6	80.0	135.3	106.6
30	0.5	2.7	95.4	120.8	99.5	3.4	85.4	125.0	97.3	4.7	77.2	127.4	94.0
30	1.0	2.9	99.6	121.8	103.3	3.6	93.7	126.4	101.2	5.0	81.5	129.2	97.9
30	2.0	3.2	105.5	123.2	108.5	3.9	99.6	128.4	106.5	5.4	87.4	131.8	103.2
30	3.0	3.4	109.3	124.2	111.9	4.1	103.4	129.7	109.8	5.6	91.2	133.5	106.5
30	4.0	3.5	112.0	124.9	114.3	4.2	106.2	130.7	112.2	5.7	93.9	134.8	108.9
40	0.5	2.8	98.0	118.6	100.7	3.5	93.5	123.6	99.0	4.8	84.2	127.1	96.0
40	1.0	3.0	101.6	119.3	104.0	3.7	97.2	124.7	102.3	5.2	87.9	128.6	99.4
40	2.0	3.3	106.9	120.5	108.8	4.0	102.5	126.3	107.1	5.5	93.4	130.7	104.2
40	3.0	3.5	110.5	121.4	112.0	4.2	106.2	127.5	110.4	5.7	97.1	132.3	107.5
40	4.0	3.6	113.1	122.0	114.4	4.4	108.9	128.3	112.8	5.9	99.8	133.5	109.9
50	0.5	2.8	99.3	117.1	101.3	3.5	95.7	122.4	99.9	4.9	88.0	126.6	97.2
50	1.0	3.1	102.5	117.7	104.2	3.8	98.9	123.3	102.8	5.2	91.3	127.9	100.2
50	2.0	3.4	107.3	118.7	108.7	4.1	103.8	124.8	107.3	5.6	96.3	129.7	104.7
50	3.0	3.5	110.8	119.5	111.8	4.3	107.3	125.8	110.4	5.8	99.9	131.1	107.9
50	4.0	3.7	113.3	120.1	114.2	4.4	110.0	126.6	112.8	6.0	102.6	132.2	110.3
60	0.5	2.9	100.1	116.0	101.7	3.6	96.9	121.6	100.4	5.0	90.3	126.2	98.0
60	1.0	3.1	103.0	116.6	104.4	3.9	99.8	122.4	103.1	5.3	93.3	127.3	100.7
60	2.0	3.4	107.4	117.6	108.5	4.2	104.4	123.7	107.2	5.7	98.0	129.0	104.9
60	3.0	3.6	110.7	118.3	111.5	4.4	107.8	124.7	110.3	5.9	101.4	130.2	108.0
60	4.0	3.7	113.3	118.8	113.9	4.5	110.4	125.5	112.7	6.0	104.1	131.3	110.4
70	0.5	2.9	100.5	115.4	101.9	3.6	97.6	121.1	100.7	5.0	91.6	125.9	98.4
70	1.0	3.2	103.2	115.9	104.4	3.9	100.4	121.8	103.2	5.4	94.4	126.8	101.0
70	2.0	3.5	107.4	116.8	108.4	4.2	104.7	123.0	107.2	5.7	98.9	128.4	105.1
70	3.0	3.6	110.6	117.5	111.3	4.4	108.0	124.0	110.2	5.9	102.2	129.6	108.2
70	4.0	3.8	113.1	118.0	113.6	4.5	110.5	124.7	112.5	6.1	104.8	130.6	110.4
80	0.5	2.9	100.7	115.1	102.0	3.6	98.0	120.8	100.8	5.0	92.3	125.7	98.7
80	1.0	3.2	103.3	115.6	104.4	3.9	100.6	121.5	103.3	5.4	95.0	126.6	101.2
80	2.0	3.5	107.4	116.4	108.3	4.2	104.8	122.6	107.2	5.7	99.3	128.1	105.2
80	3.0	3.7	110.6	117.0	111.2	4.4	108.0	123.5	110.1	6.0	102.6	129.3	108.1
80	4.0	3.8	113.0	117.6	113.4	4.6	110.5	124.3	112.4	6.1	105.2	130.3	110.3
90	0.5	2.9	100.8	114.9	102.0	3.6	98.1	120.7	100.9	5.0	92.5	125.6	98.6
90	1.0	3.2	103.3	115.4	104.4	3.9	100.7	121.4	103.3	5.4	95.2	126.5	101.2
90	2.0	3.5	107.4	116.3	108.2	4.2	104.9	122.5	107.2	5.7	99.5	128.0	105.1
90	3.0	3.7	110.5	116.9	111.1	4.4	108.1	123.4	110.1	6.0	102.7	129.2	108.1
90	4.0	3.8	113.0	117.4	113.4	4.6	110.5	124.1	112.4	6.1	105.3	130.1	110.4

Luminous efficacy values for Direct, clear sky and global radiation with various solar altitudes (γ_S), Linke turbidity(T_L), Schüepp (B) and water vapour content (w)

Appendix 4.2

Sky clearness categorisation

ε	Category	Lower limit	Upper limit
1	Overcast	1.00	1.07
2		1.07	1.23
3		1.23	1.50
4		1.50	1.95
5		1.95	2.80
6		2.80	4.50
7		4.50	6.20
8	Clear	6.20	----

Global Luminous efficacy coefficients

ε bin	a_i	b_i	c_i	d_i
1	96.6	-0.47	11.50	-9.16
2	108	0.79	1.79	-1.19
3	98.7	0.70	4.40	-6.95
4	92.7	0.56	8.36	-8.31
5	86.7	0.98	7.10	-10.94
6	88.3	1.39	6.06	-7.60
7	78.6	1.47	4.93	-11.37
8	99.7	1.86	-4.46	-3.15

Appendix 4.3

Diffuse luminous efficacy coefficients

ε bin	a_i	b_i	c_i	d_i
1	97	-0.46	12.00	-8.91
2	107	1.15	0.59	-3.95
3	105	2.96	-5.53	-8.77
4	102	5.59	-13.95	-13.90
5	101	5.94	-22.75	-23.74
6	106	3.83	-36.15	-28.83
7	142	1.90	-53.24	-14.03
8	152	0.35	-45.27	-7.98

Appendix 5

NUMBERING

AS ORIGINAL

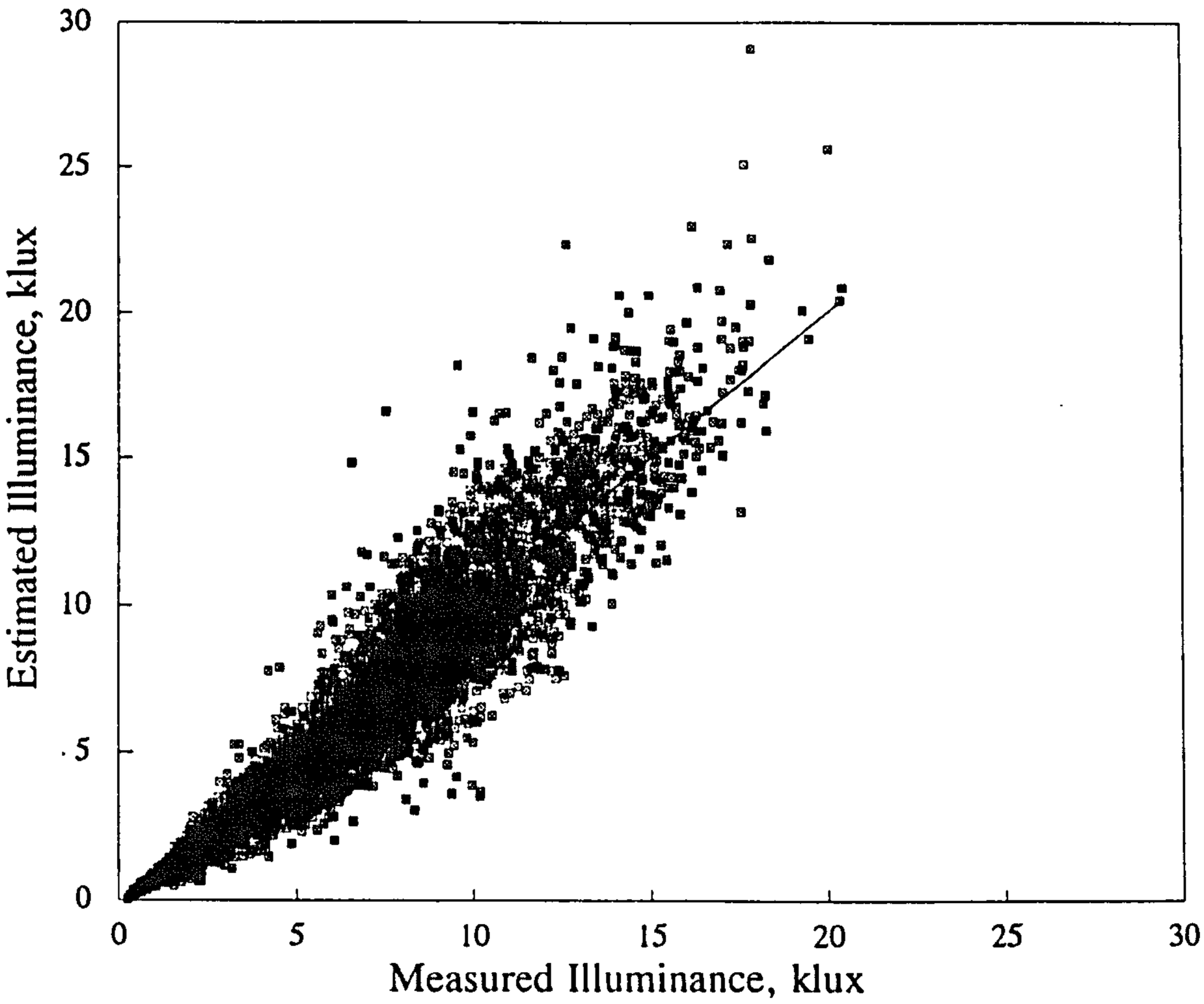

Figure 5.4.1a Autumn/spring: North surface illuminance

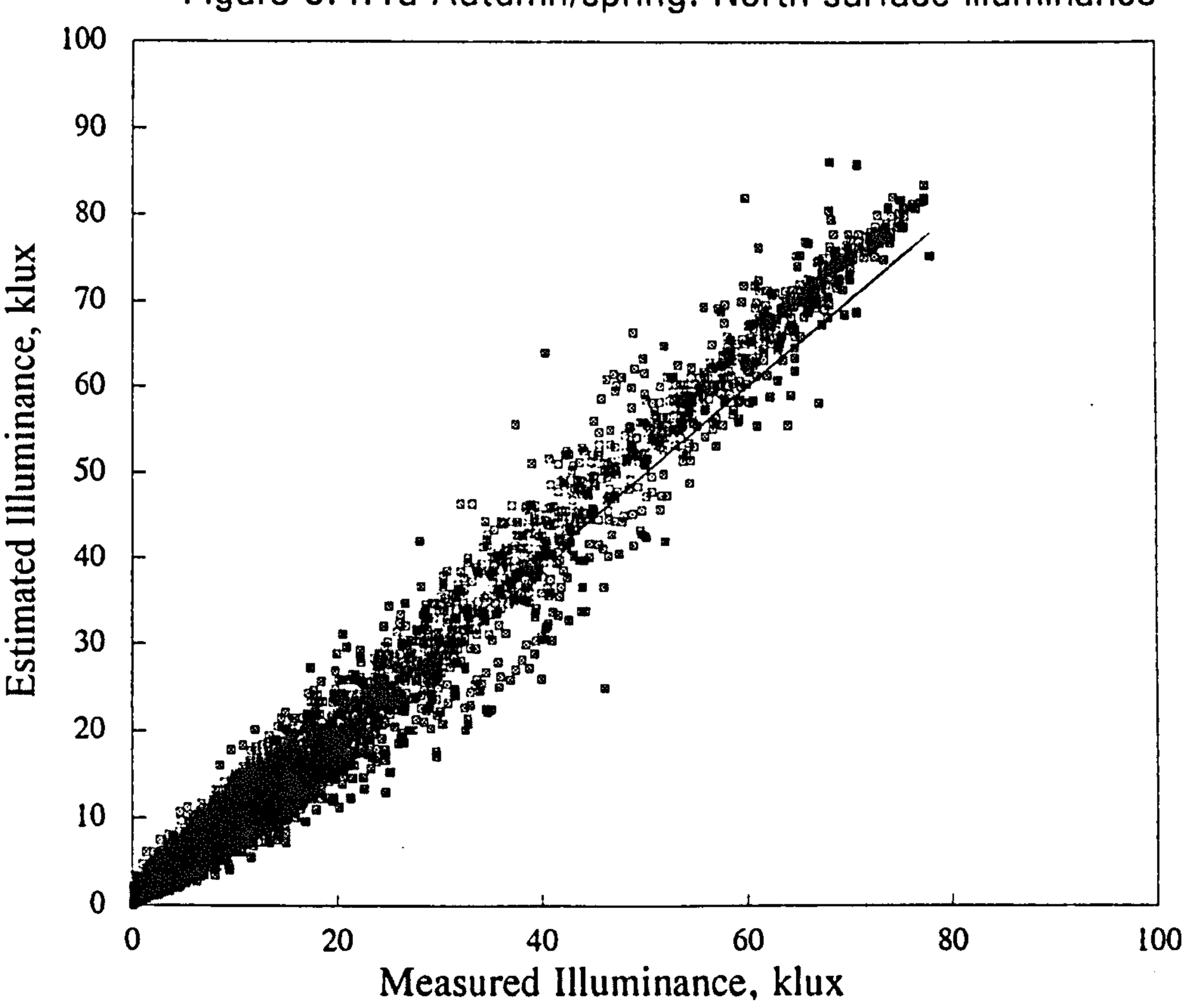

Figure 5.4.1b Autumn/spring: East surface illuminance

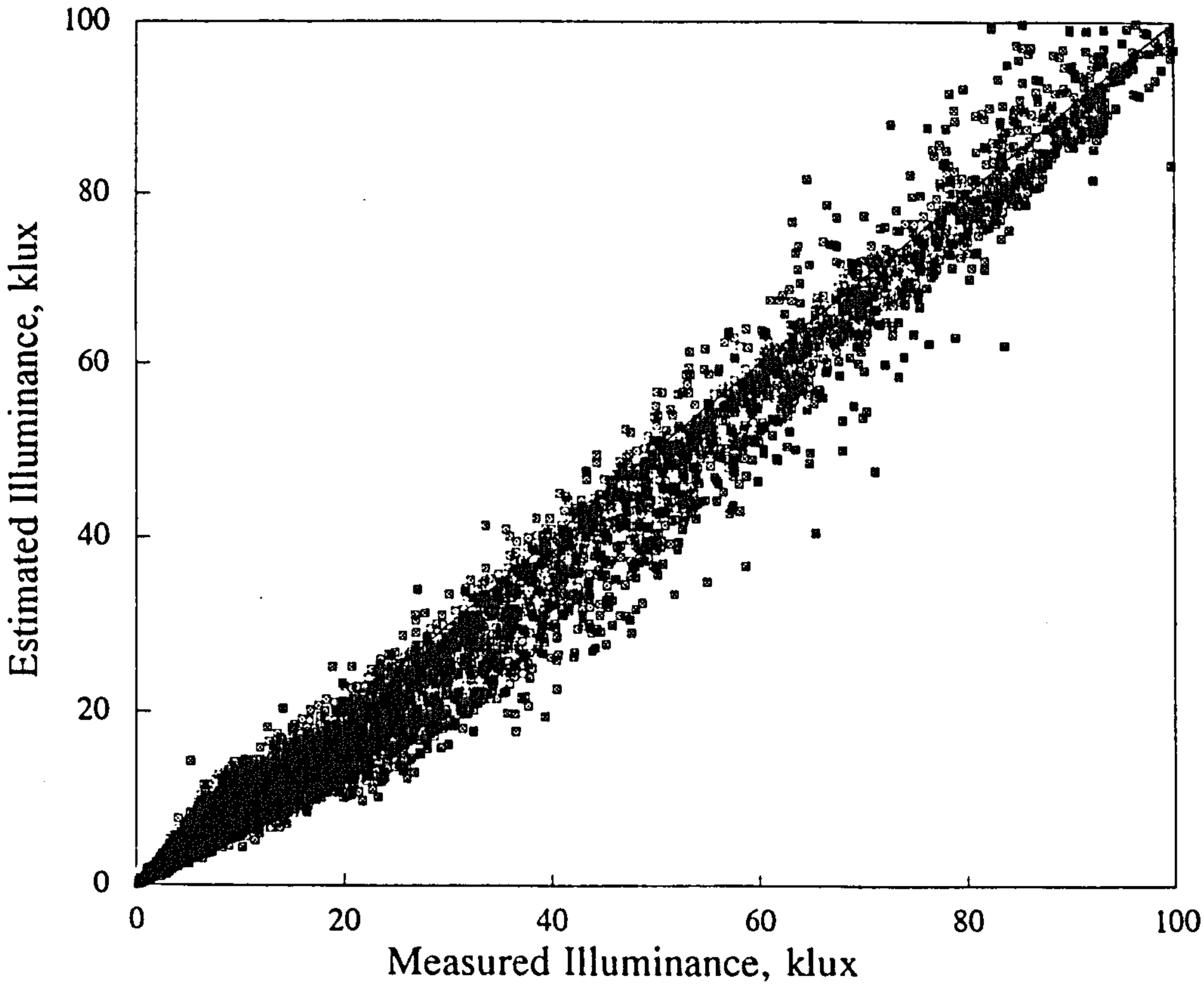

Figure 5.4.1c Autumn/spring: South surface illuminance

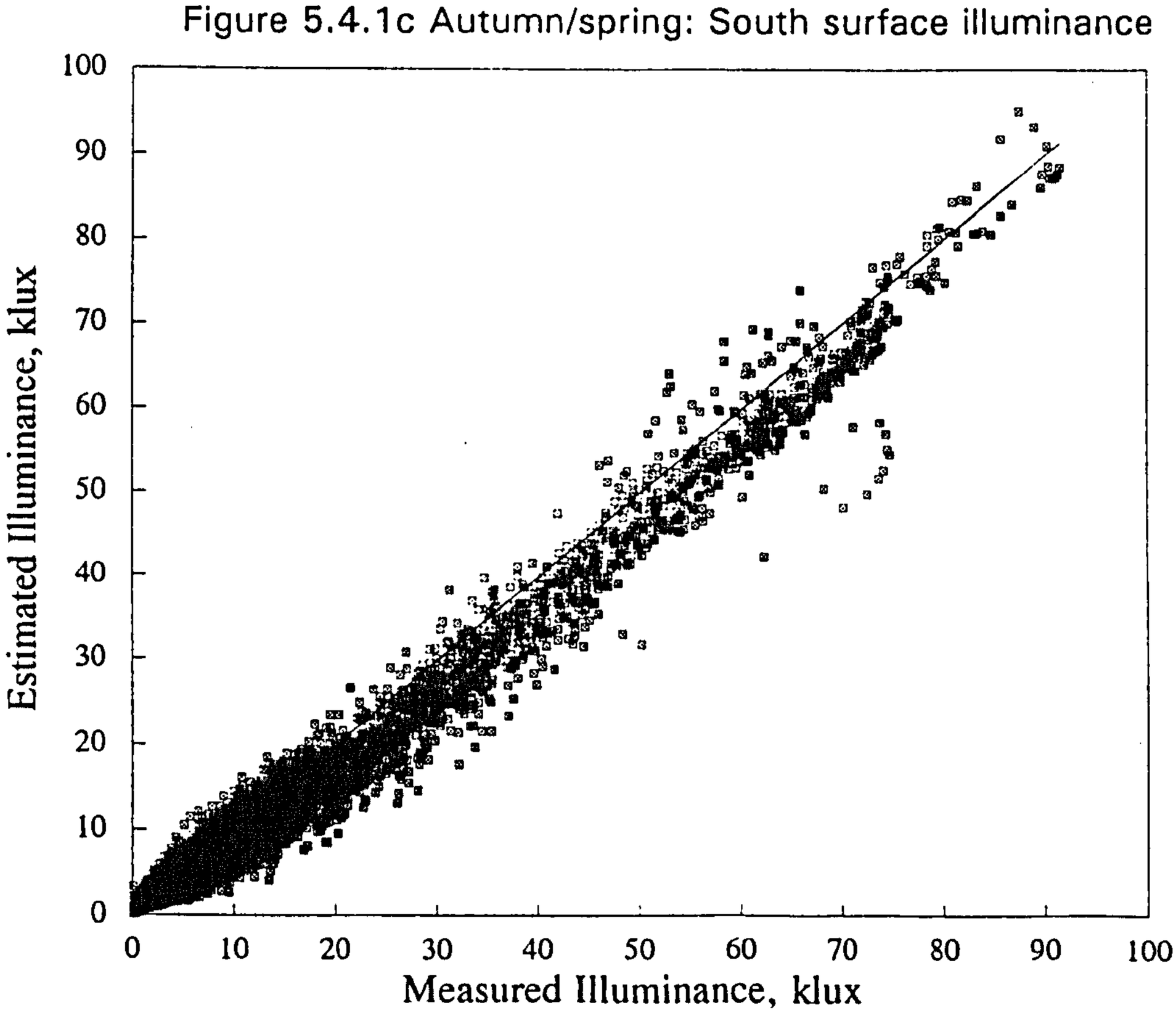

Figure 5.4.1d Autumn/spring: West surface illuminance

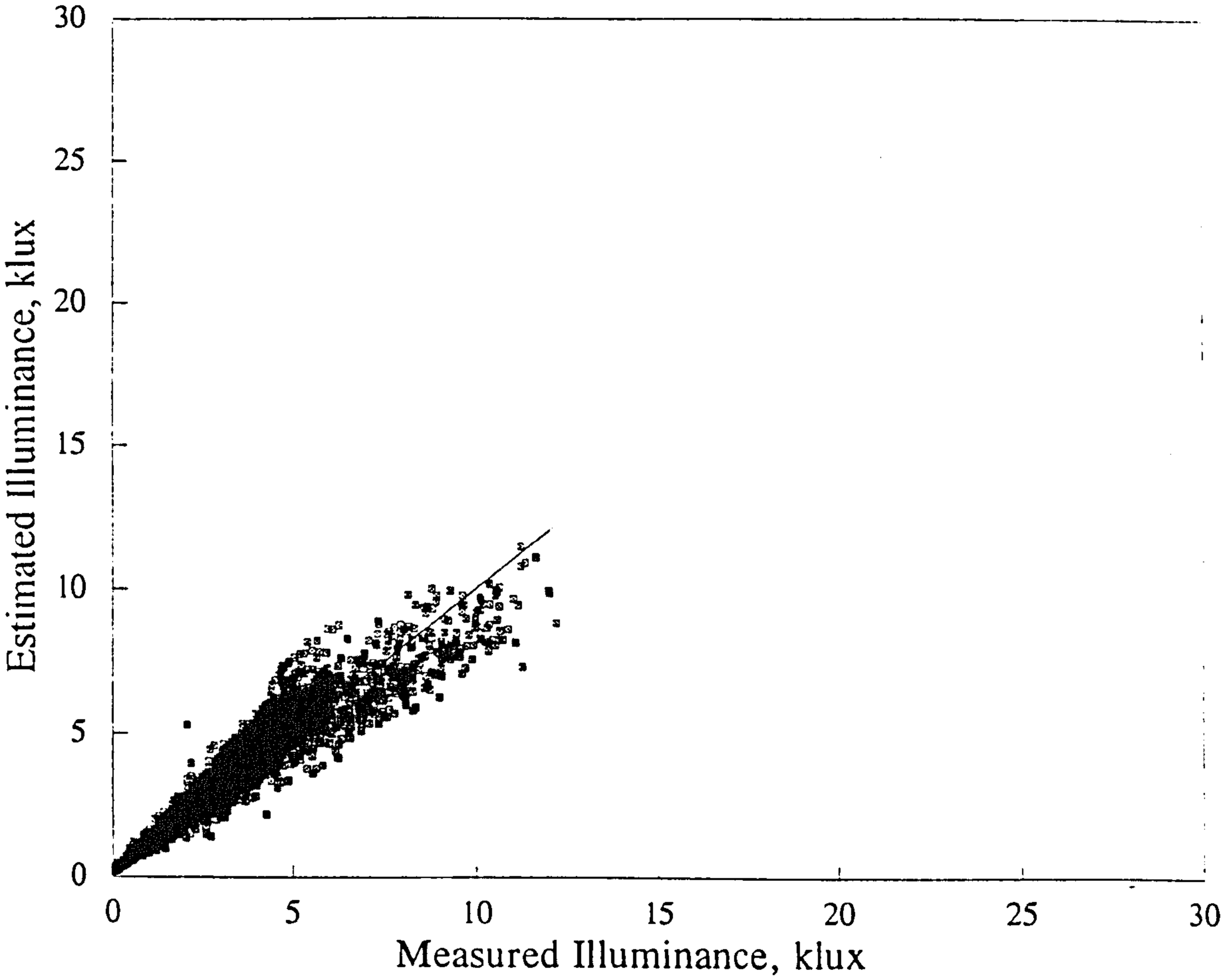

Figure 5.4.1e Winter: North surface illuminance

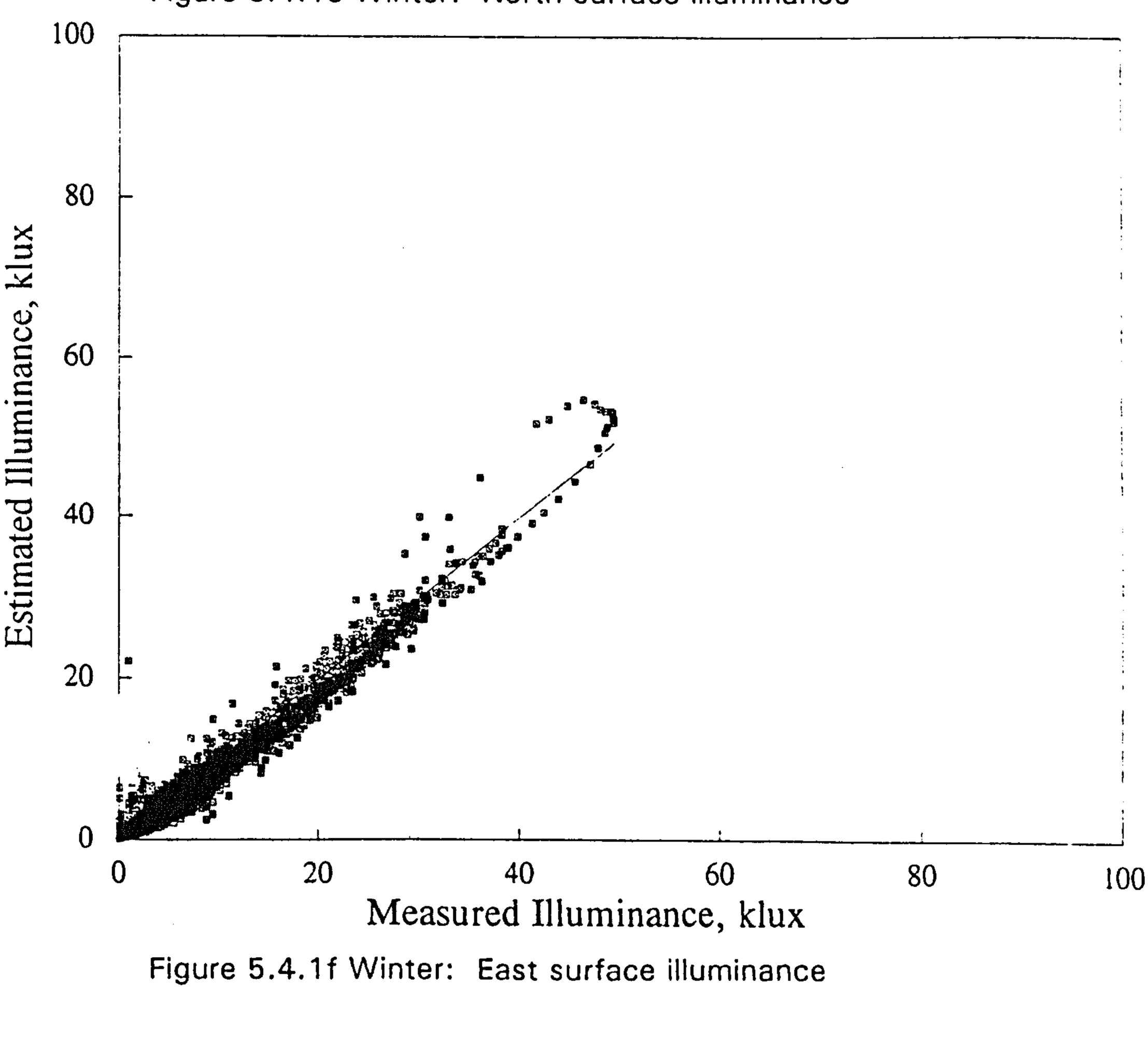

Figure 5.4.1f Winter: East surface illuminance

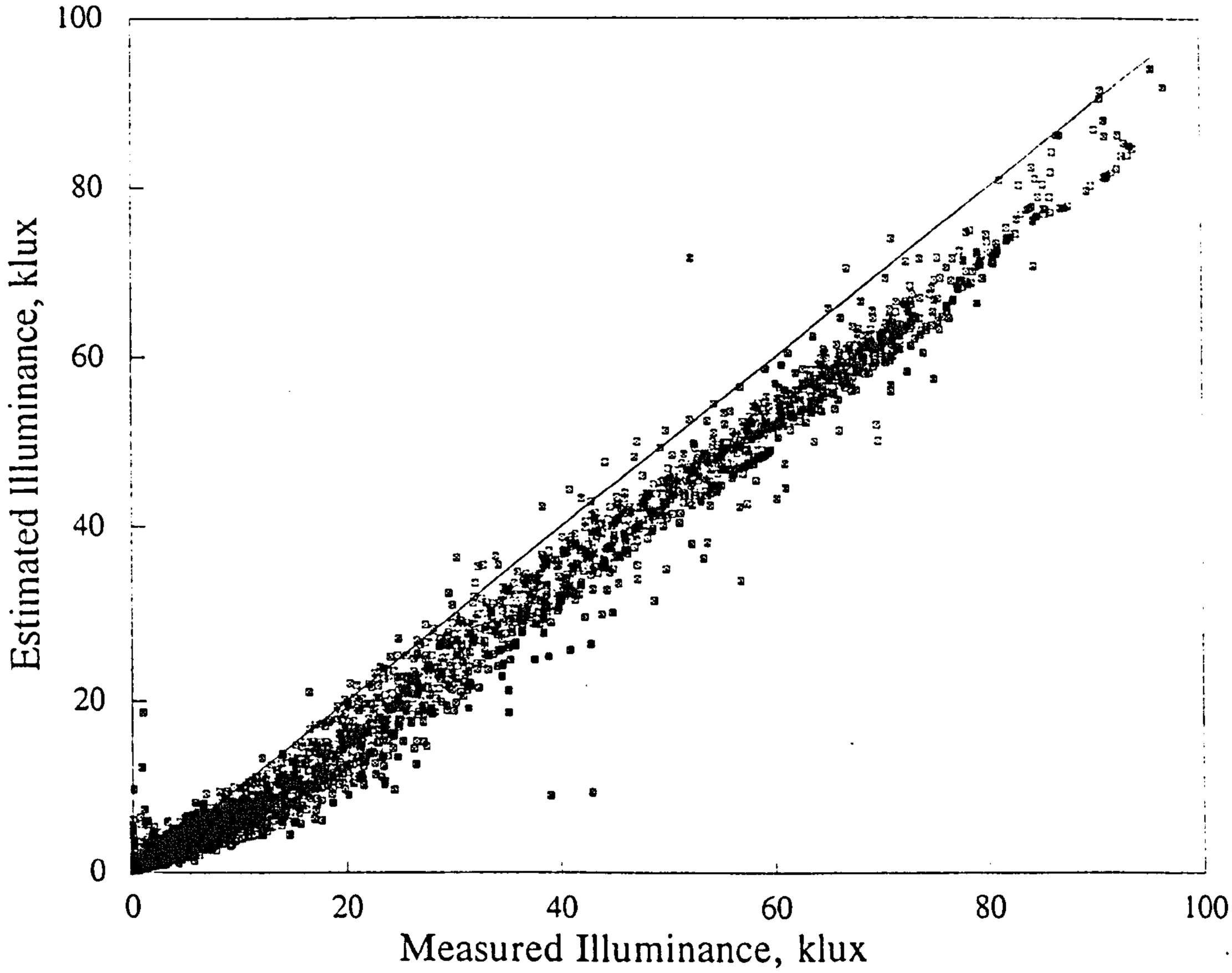

Figure 5.4.1g Winter: South surface illuminance

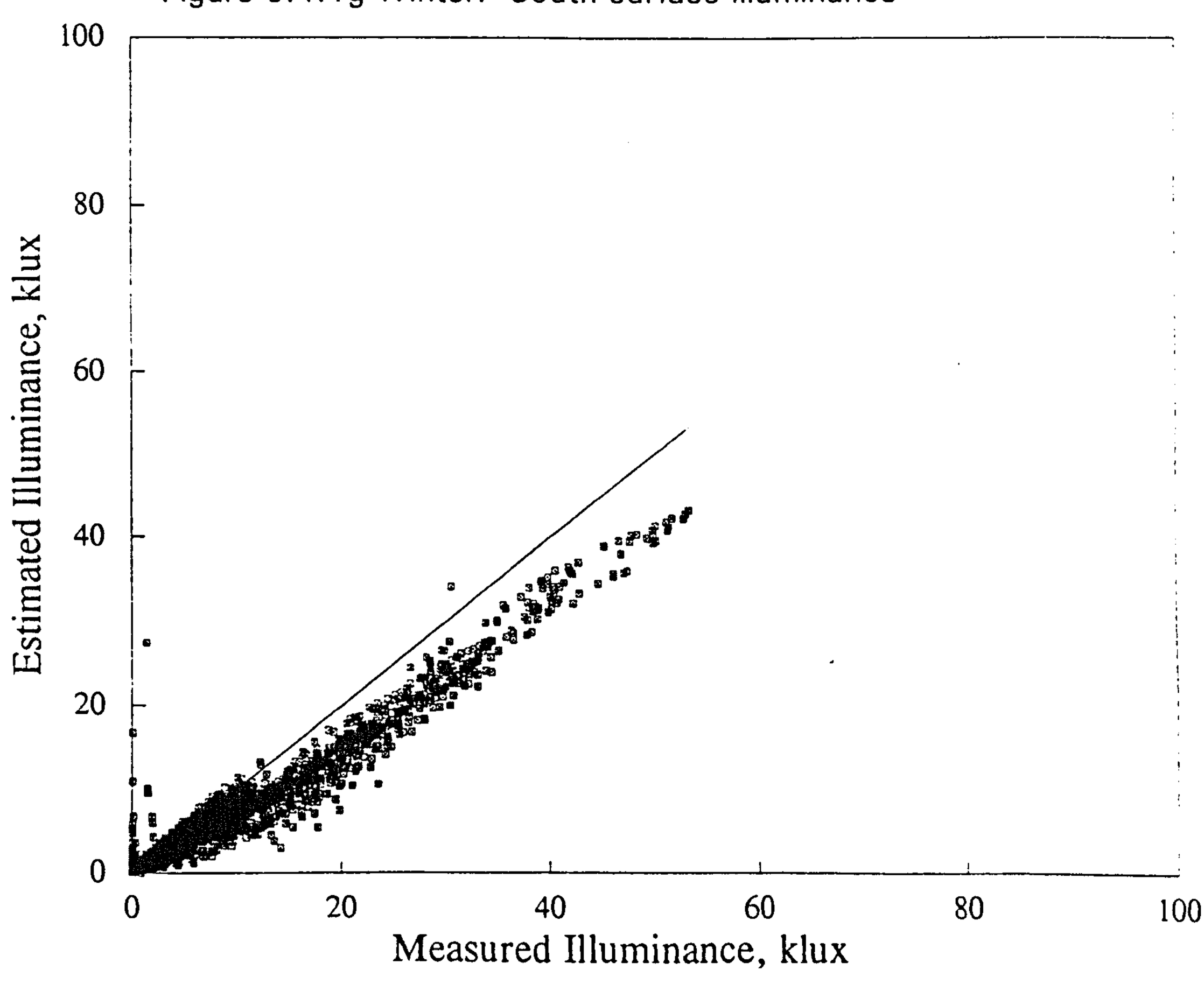

Figure 5.4.1h Winter: West surface illuminance

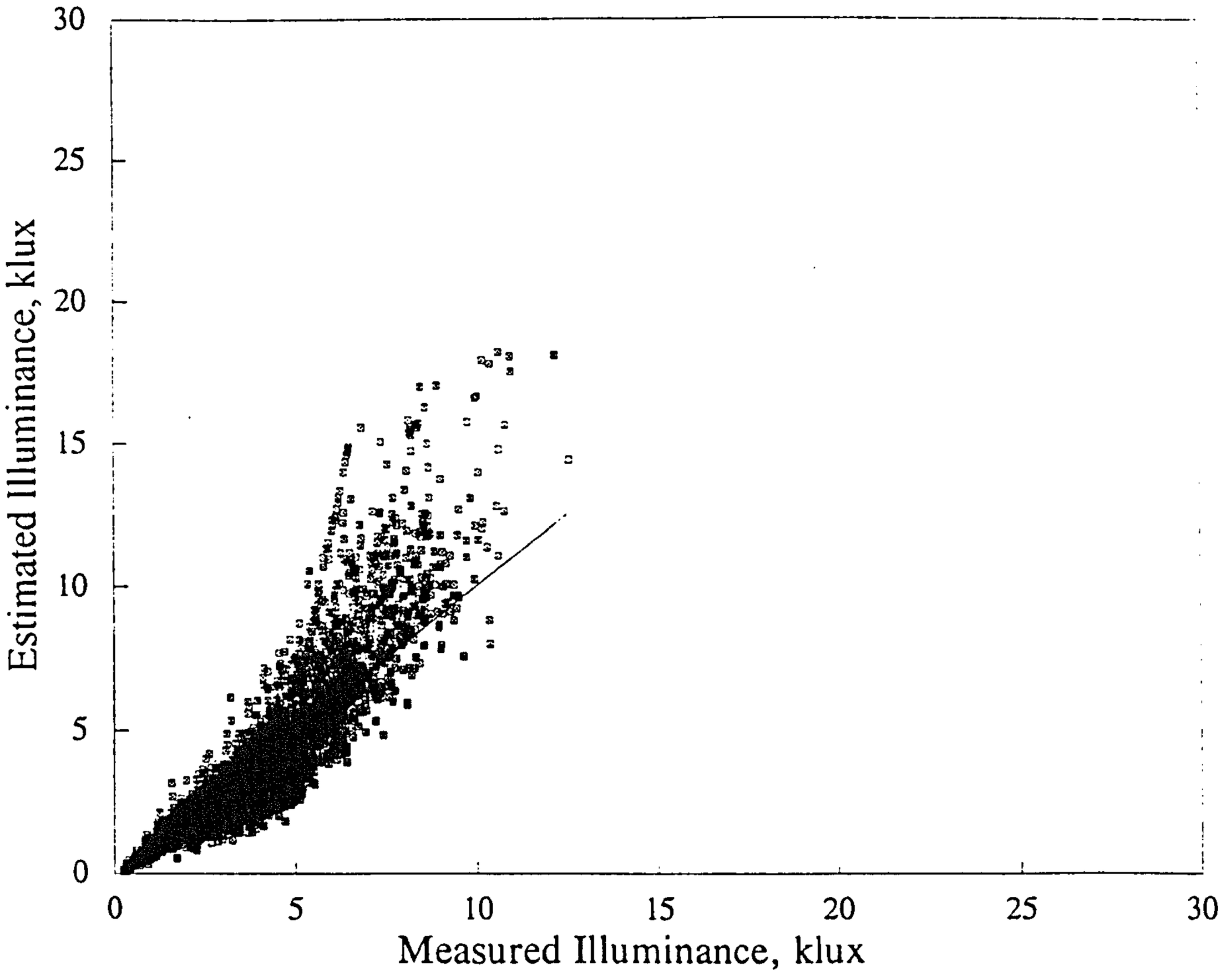

Figure 5.4.2a Winter: North surface illuminance

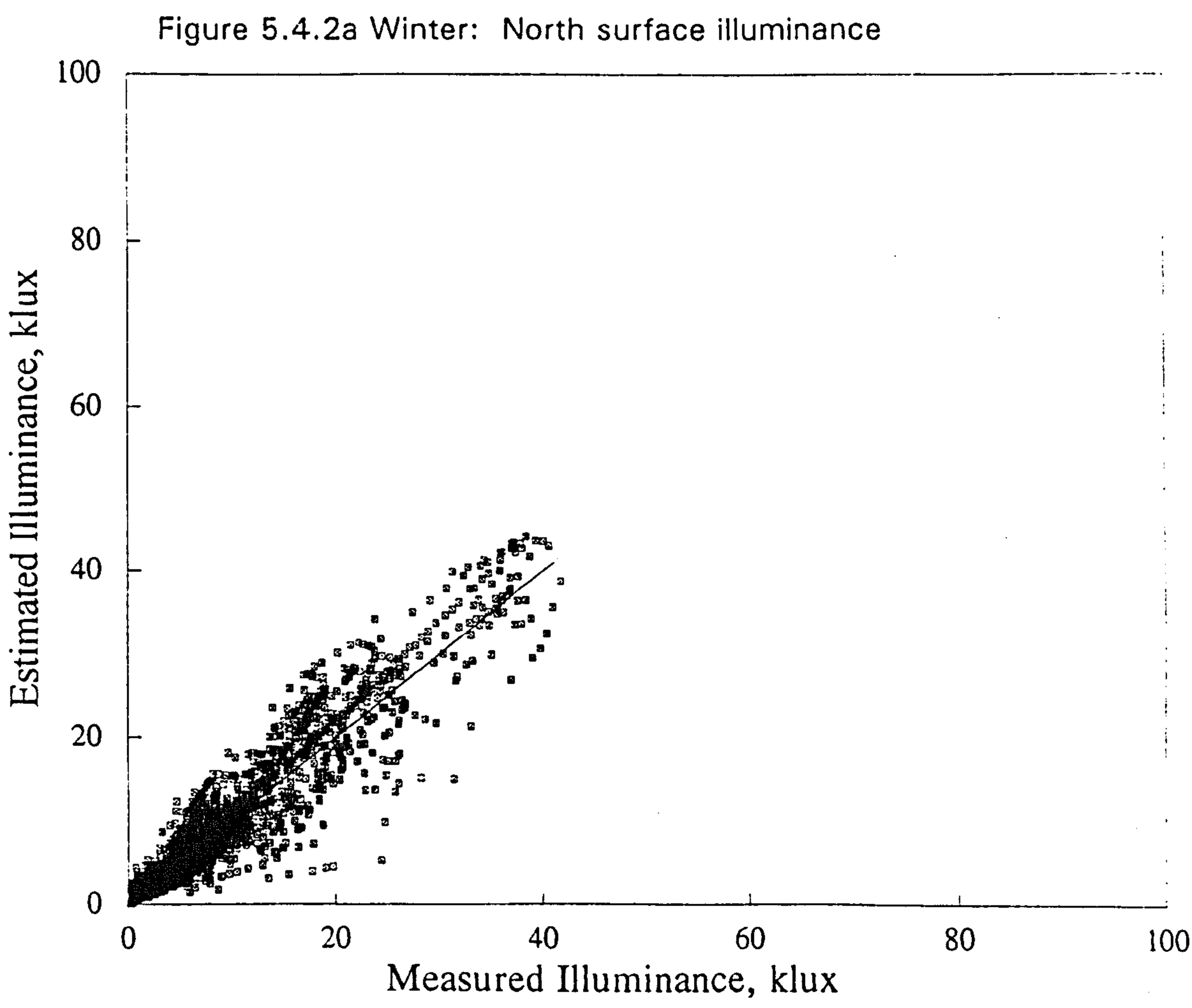

Figure 5.4.2b Winter: East surface illuminance

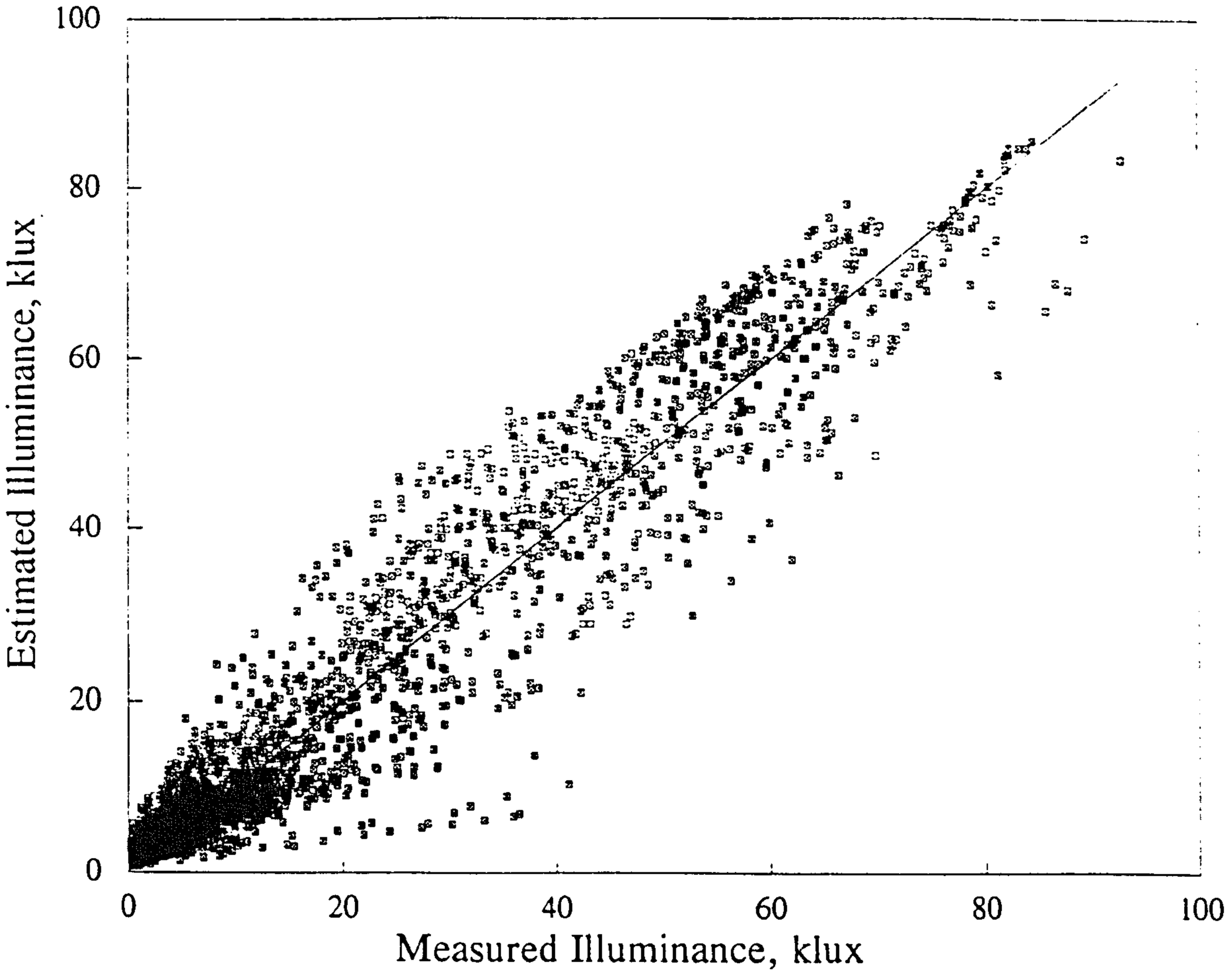

Figure 5.4.2c Winter: South surface illuminance

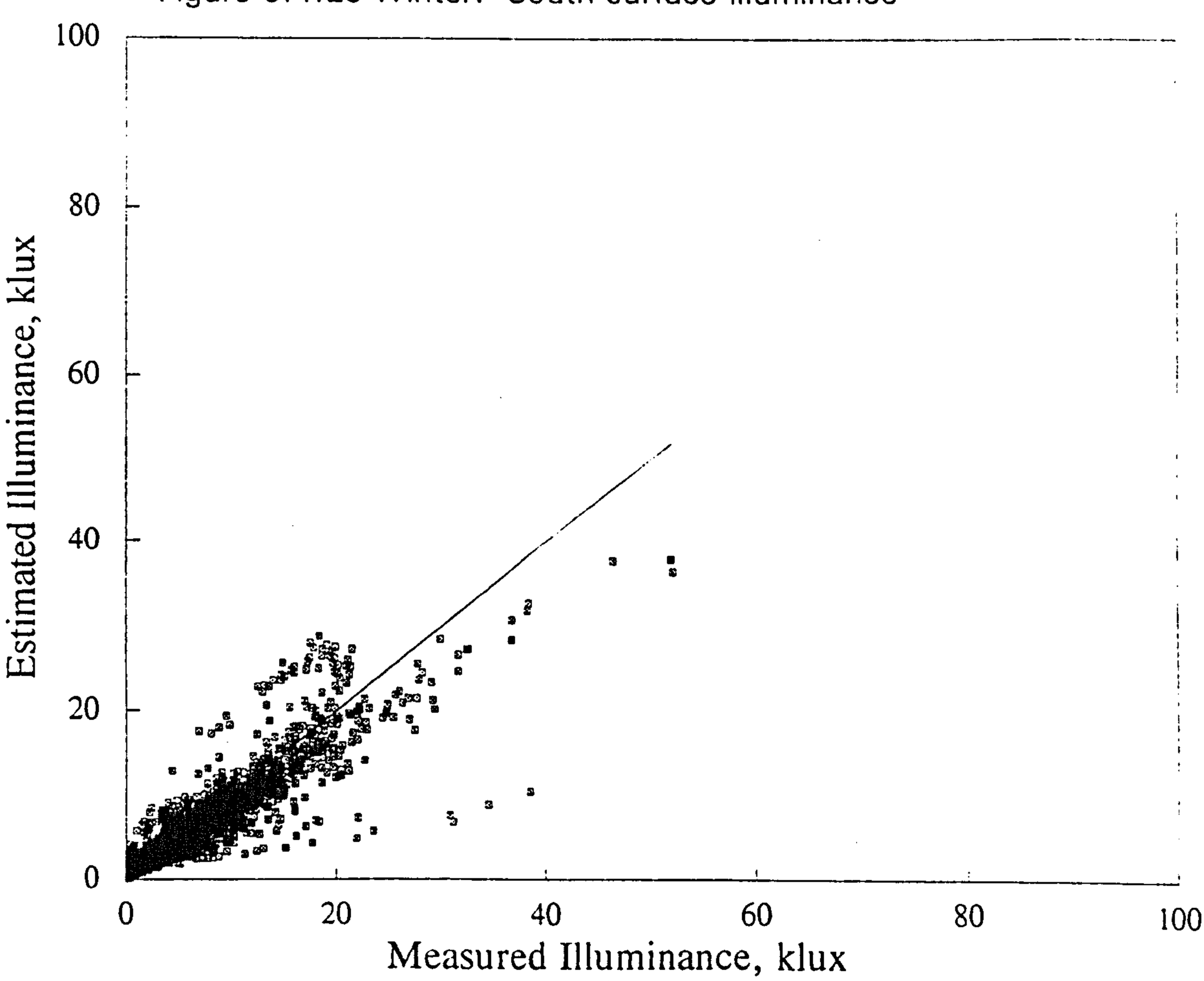

Figure 5.4.2d Winter: West surface illuminance

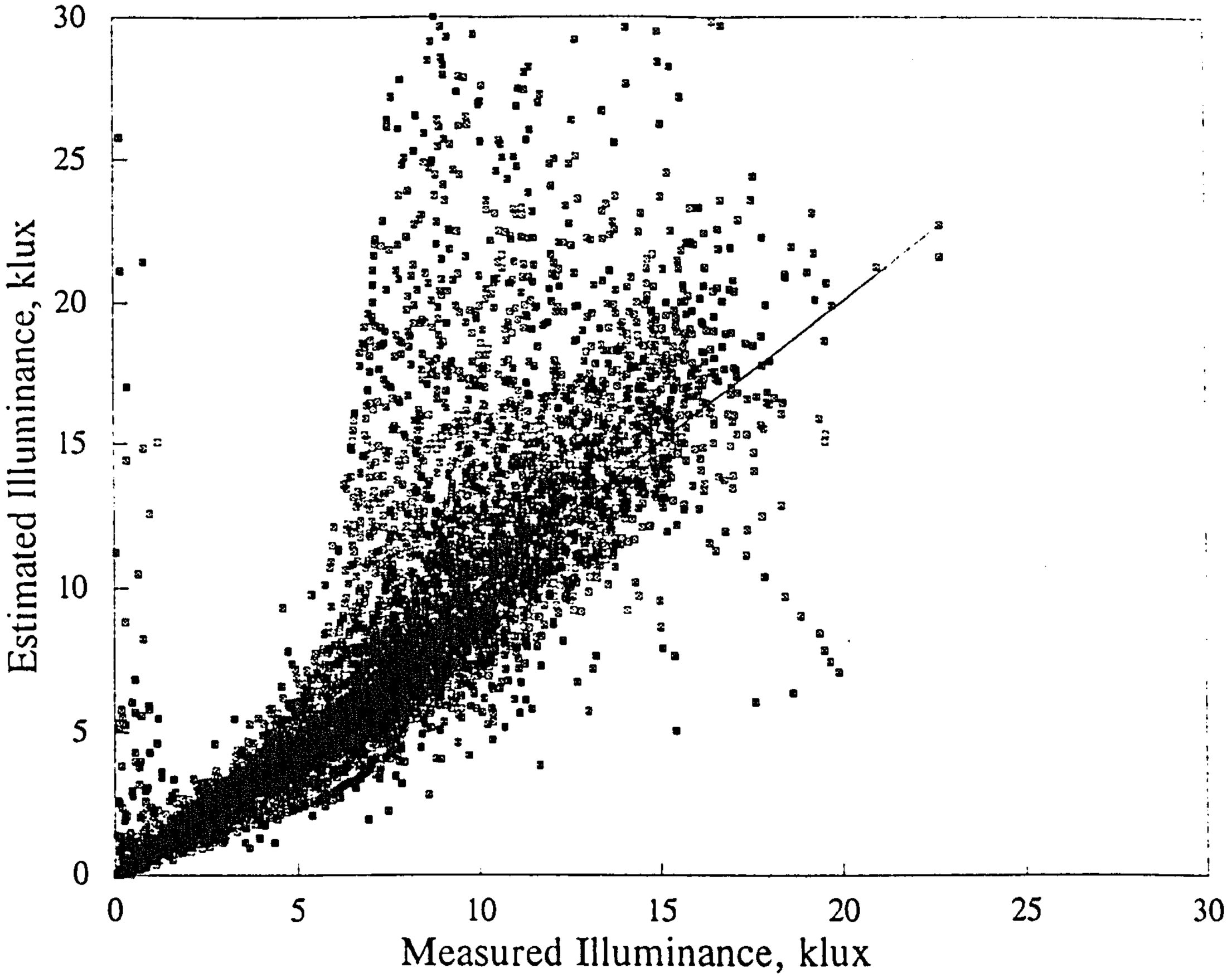

Figure 5.4.2e Autumn/spring: North surface illuminance

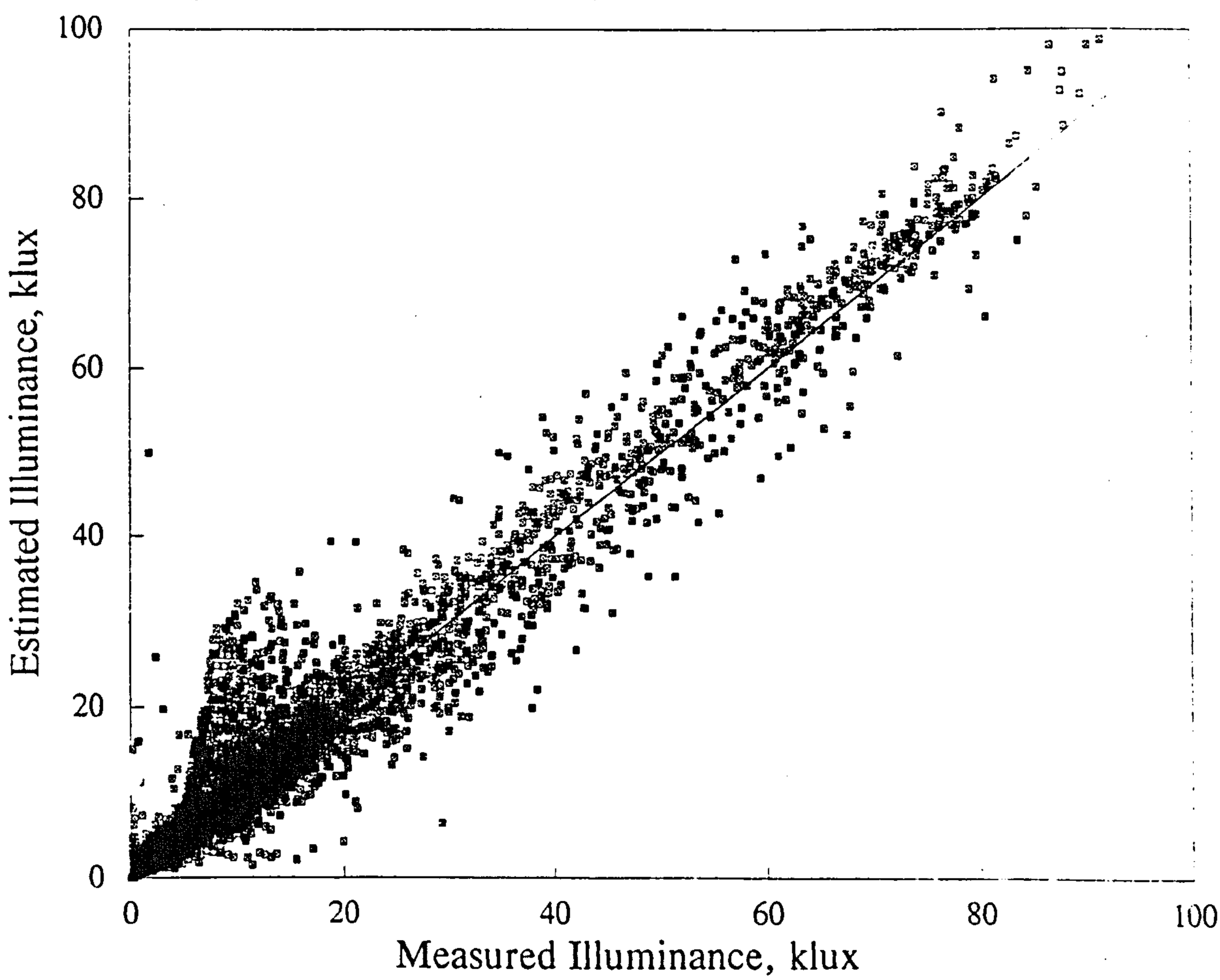

Figure 5.4.2f Autumn/spring: East surface illuminance

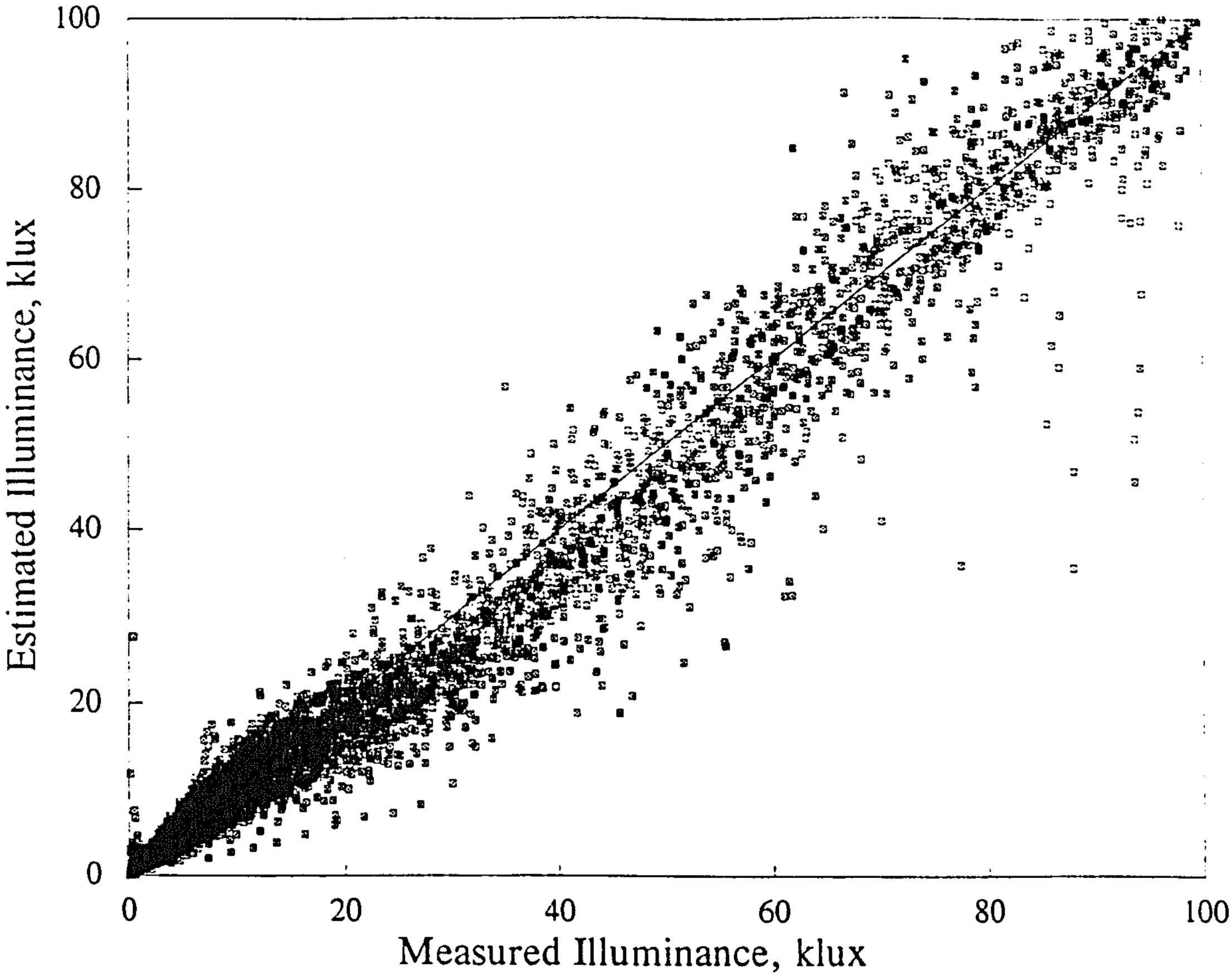

Figure 5.4.2g Autumn/spring: South surface illuminance

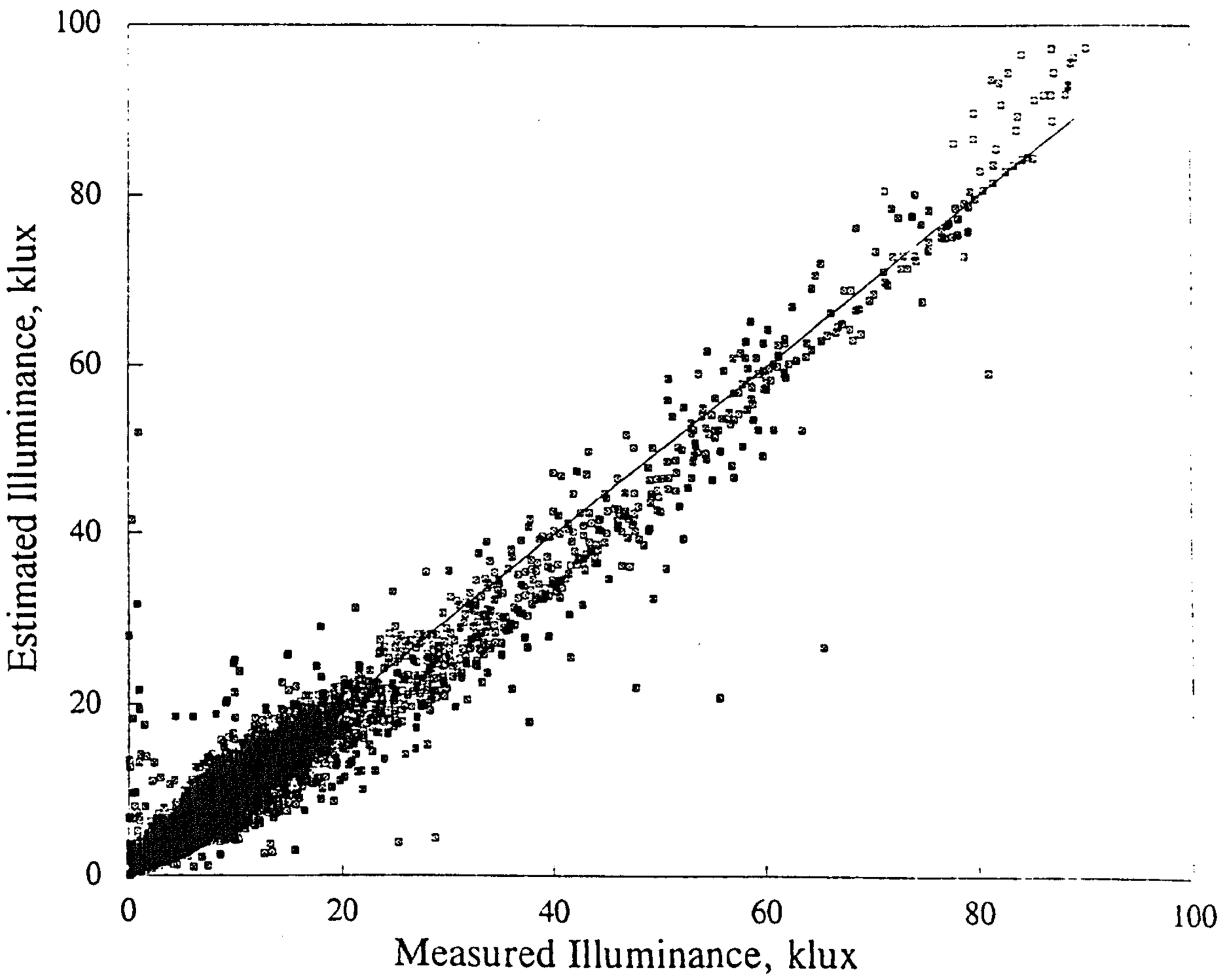

Figure 5.4.2h Autumn/spring: West surface illuminance

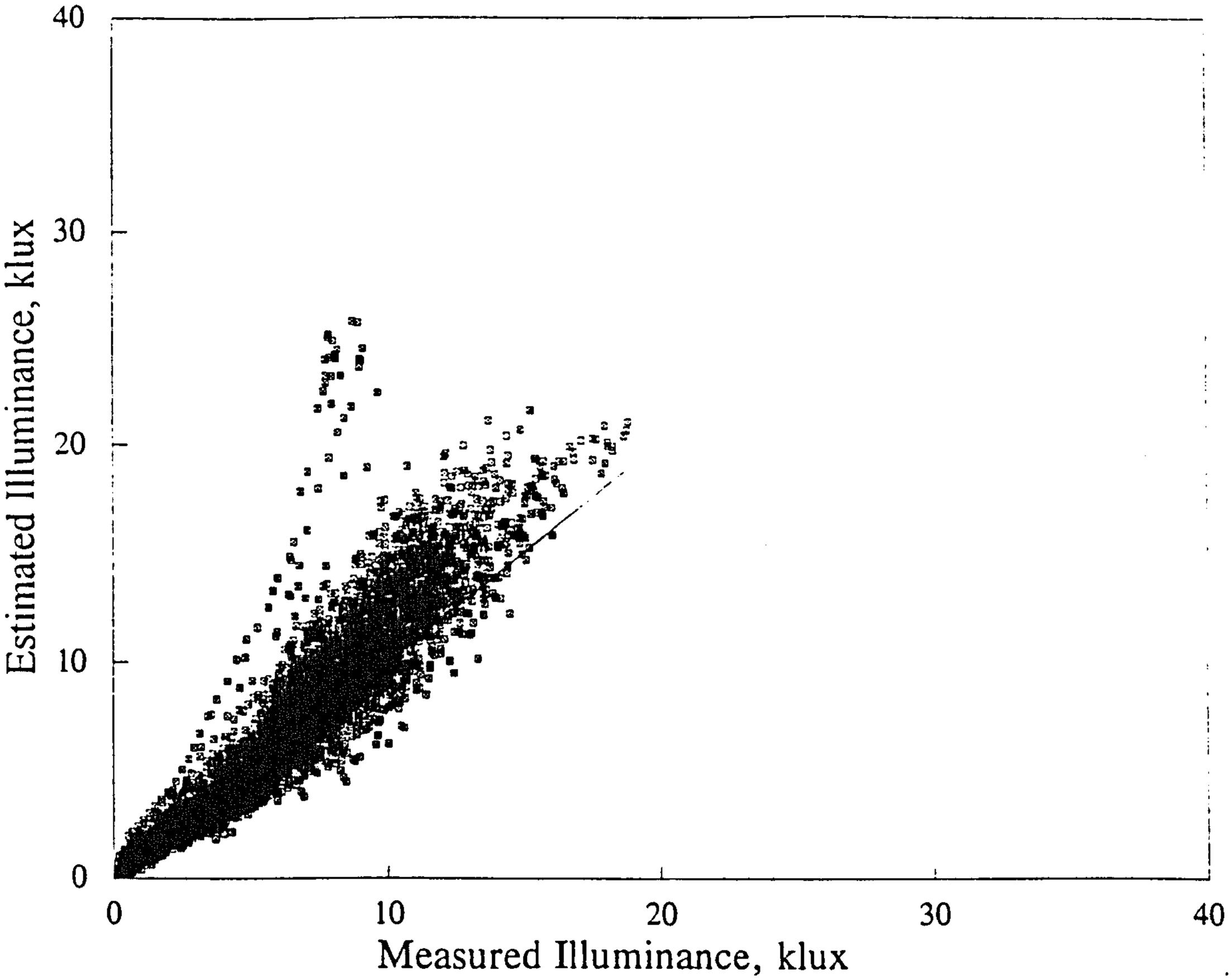

Figure 5.4.3a Autumn/spring: North surface illuminance

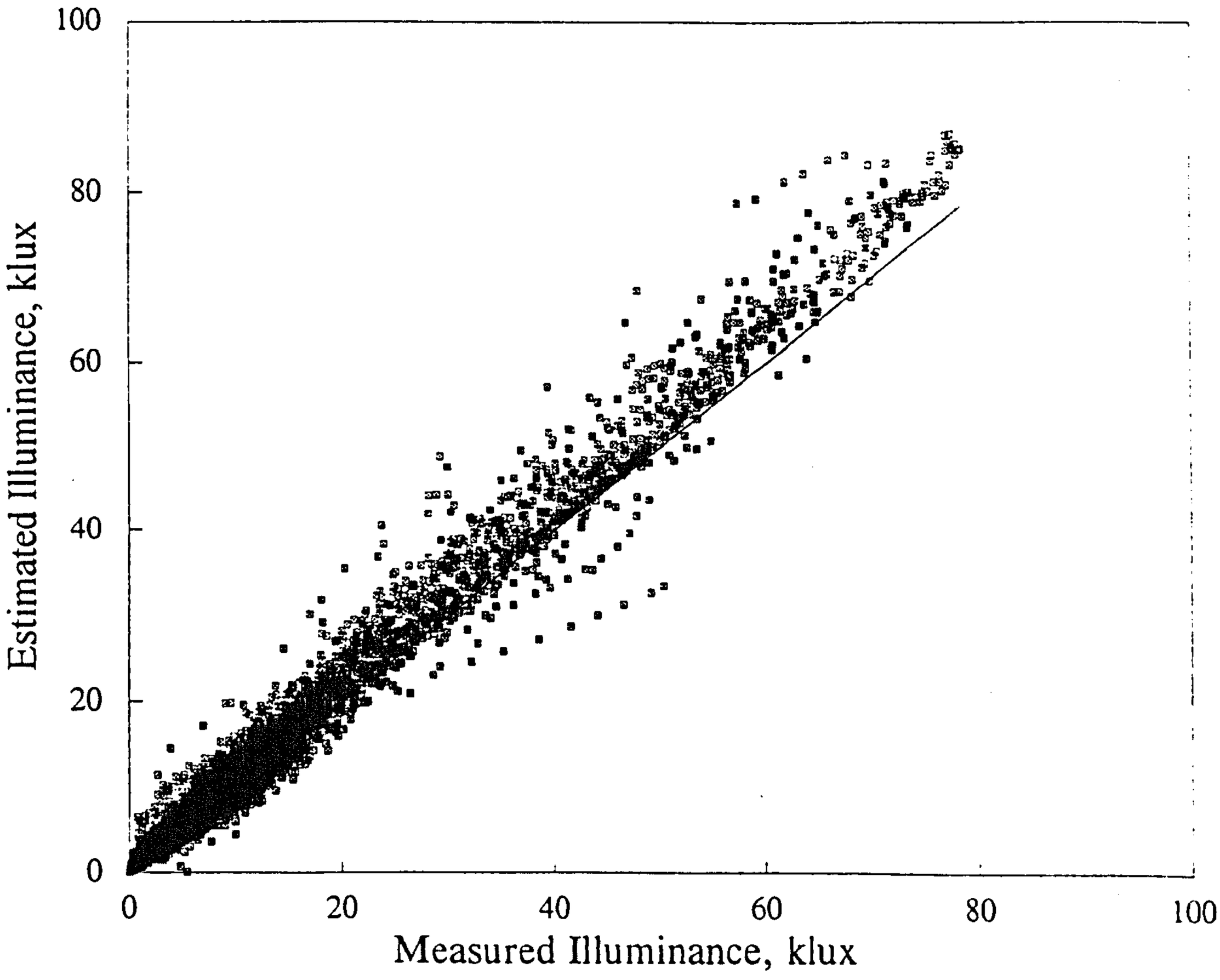

Figure 5.4.3b Autumn/spring: East surface illuminance

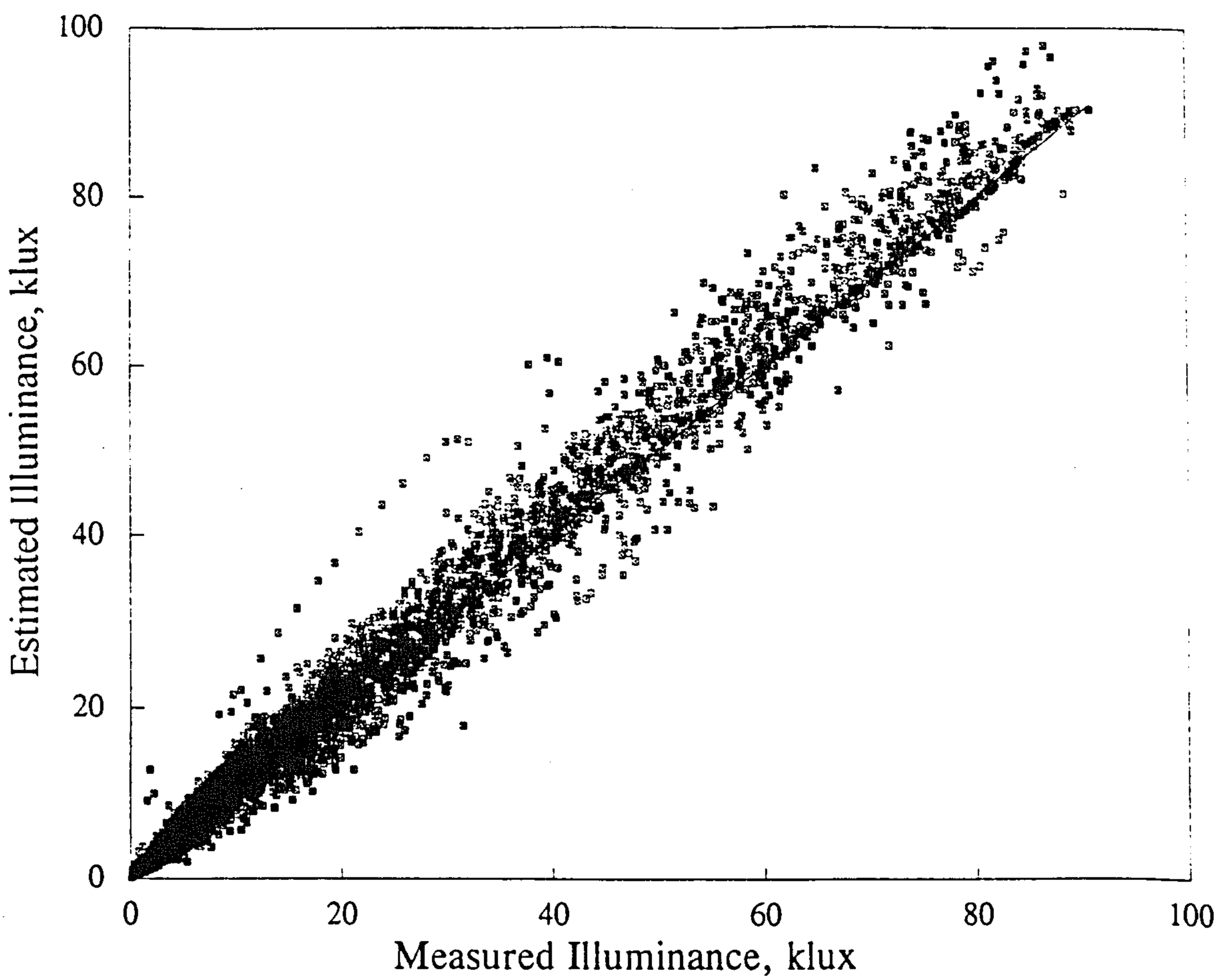

Figure 5.4.3c Autumn/spring: South surface illuminance

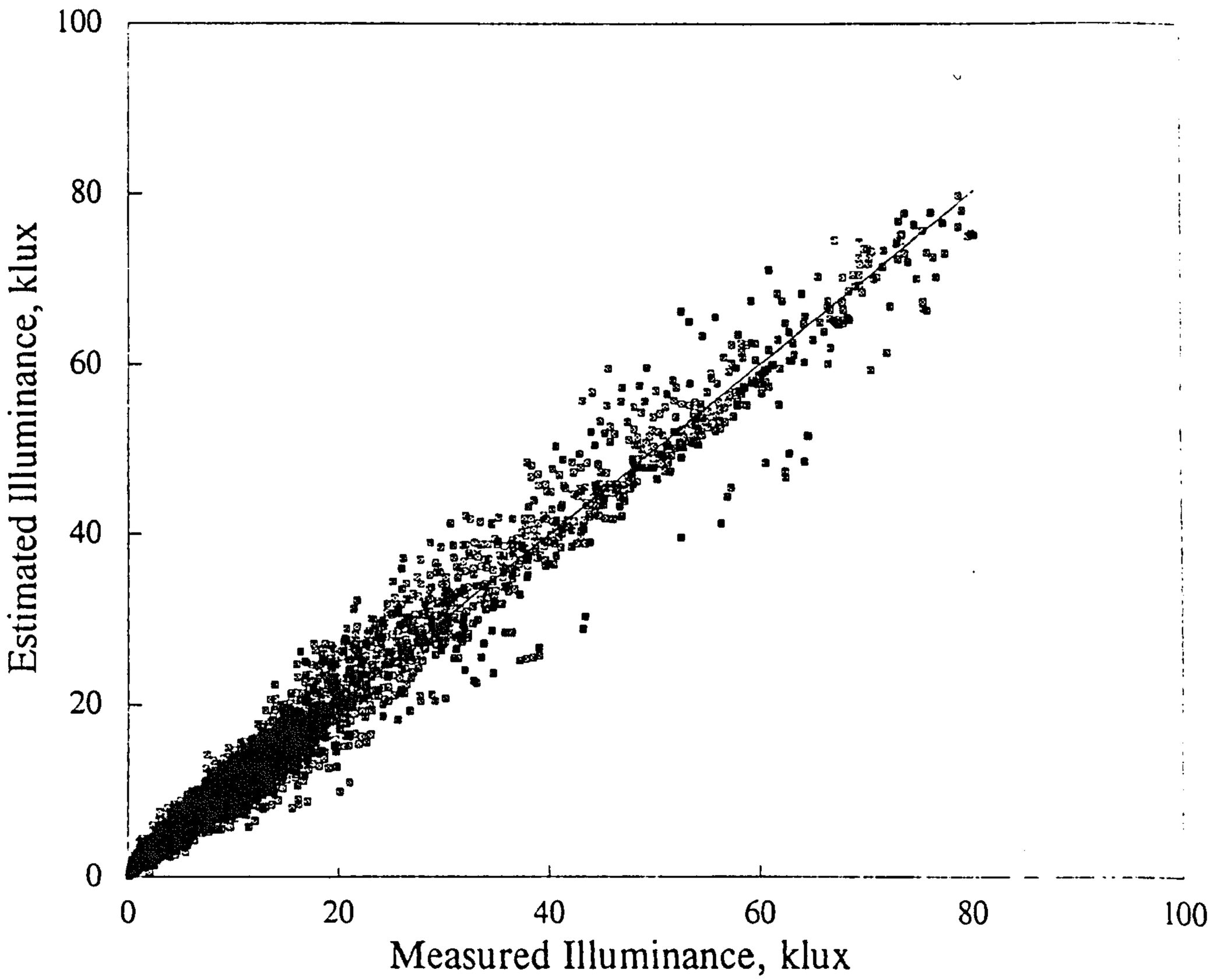

Figure 5.4.3d Autumn/spring: West surface illuminance

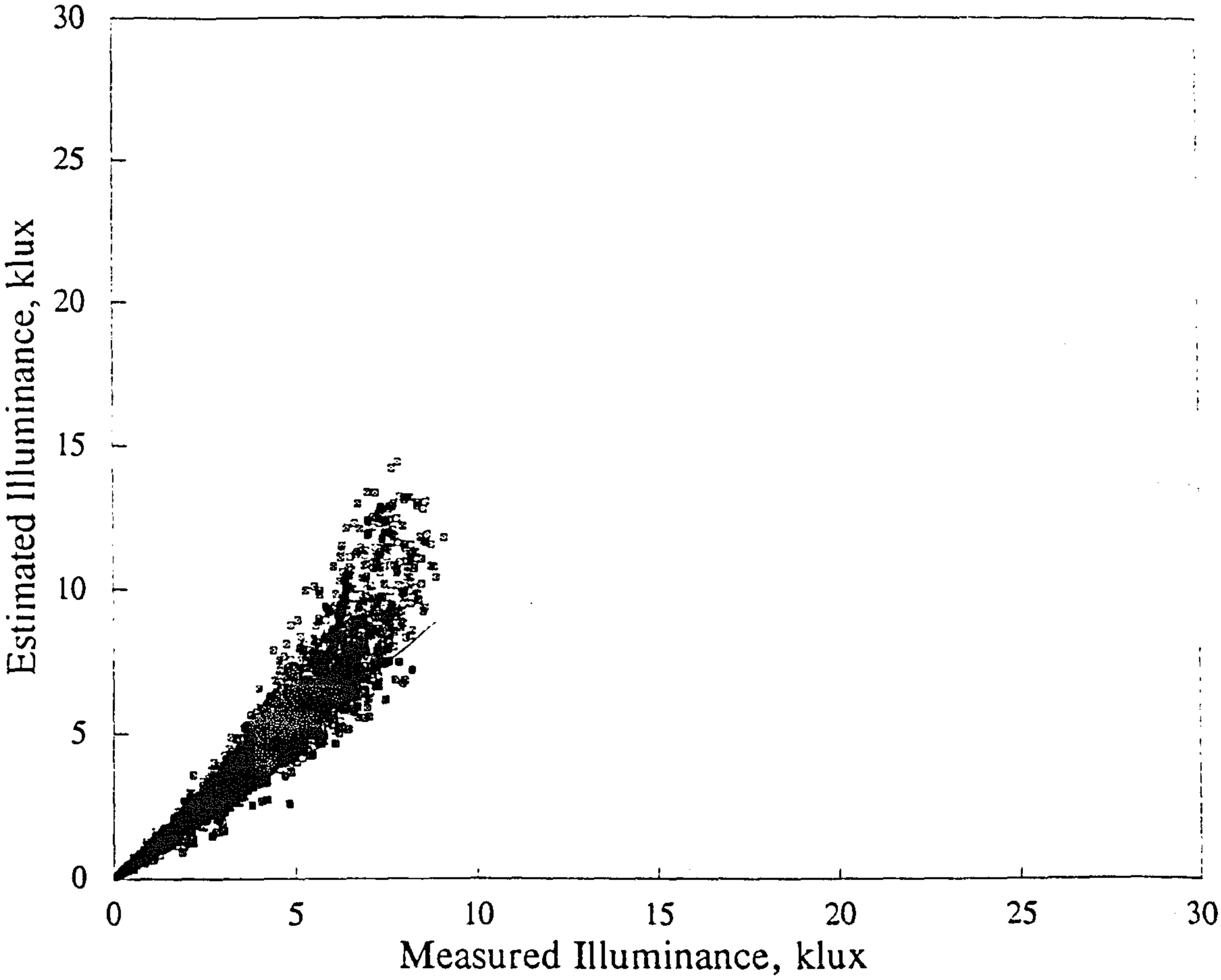

Figure 5.4.3e Winter: North surface illuminance

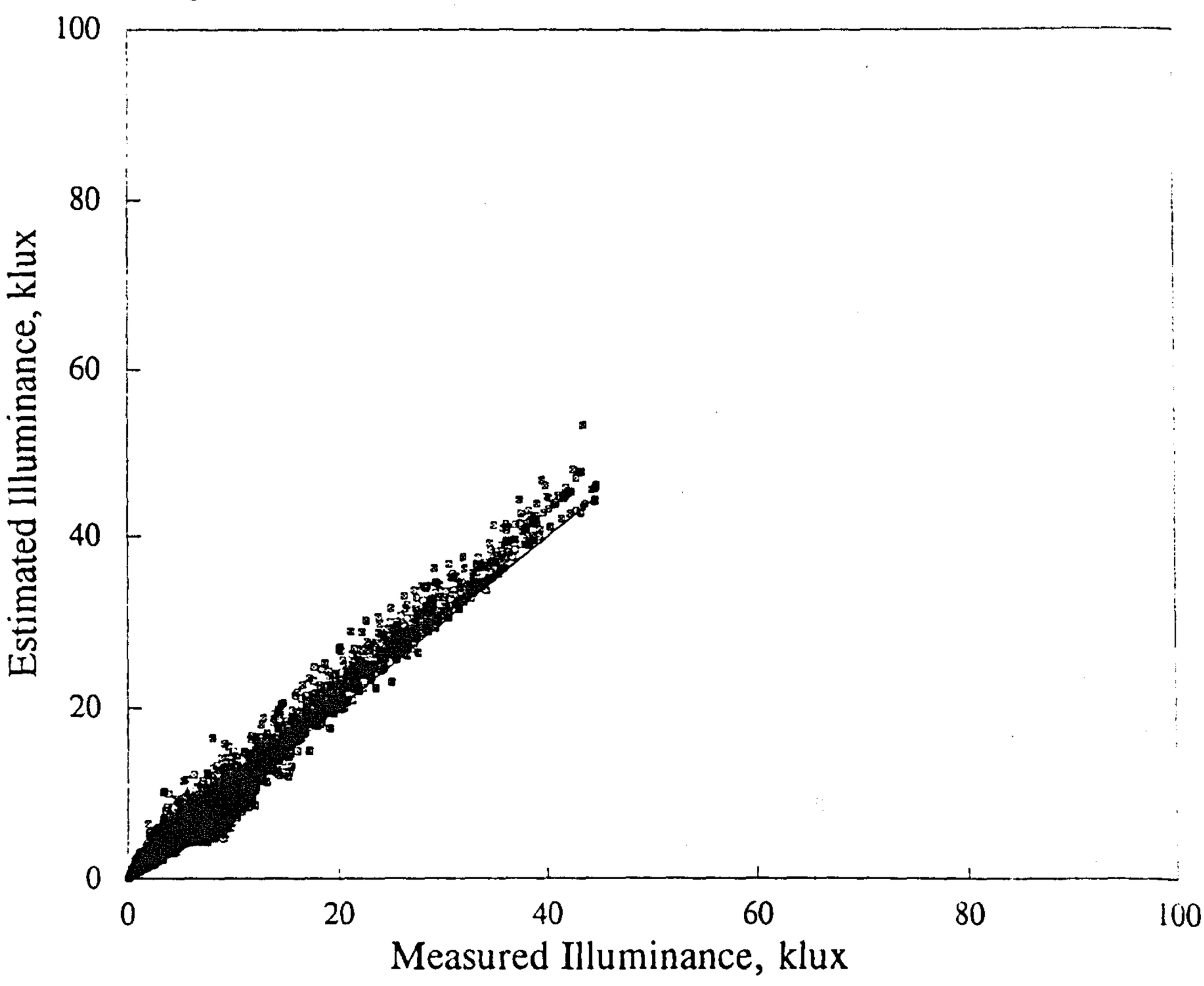

Figure 5.4.3f Winter: East surface illuminance

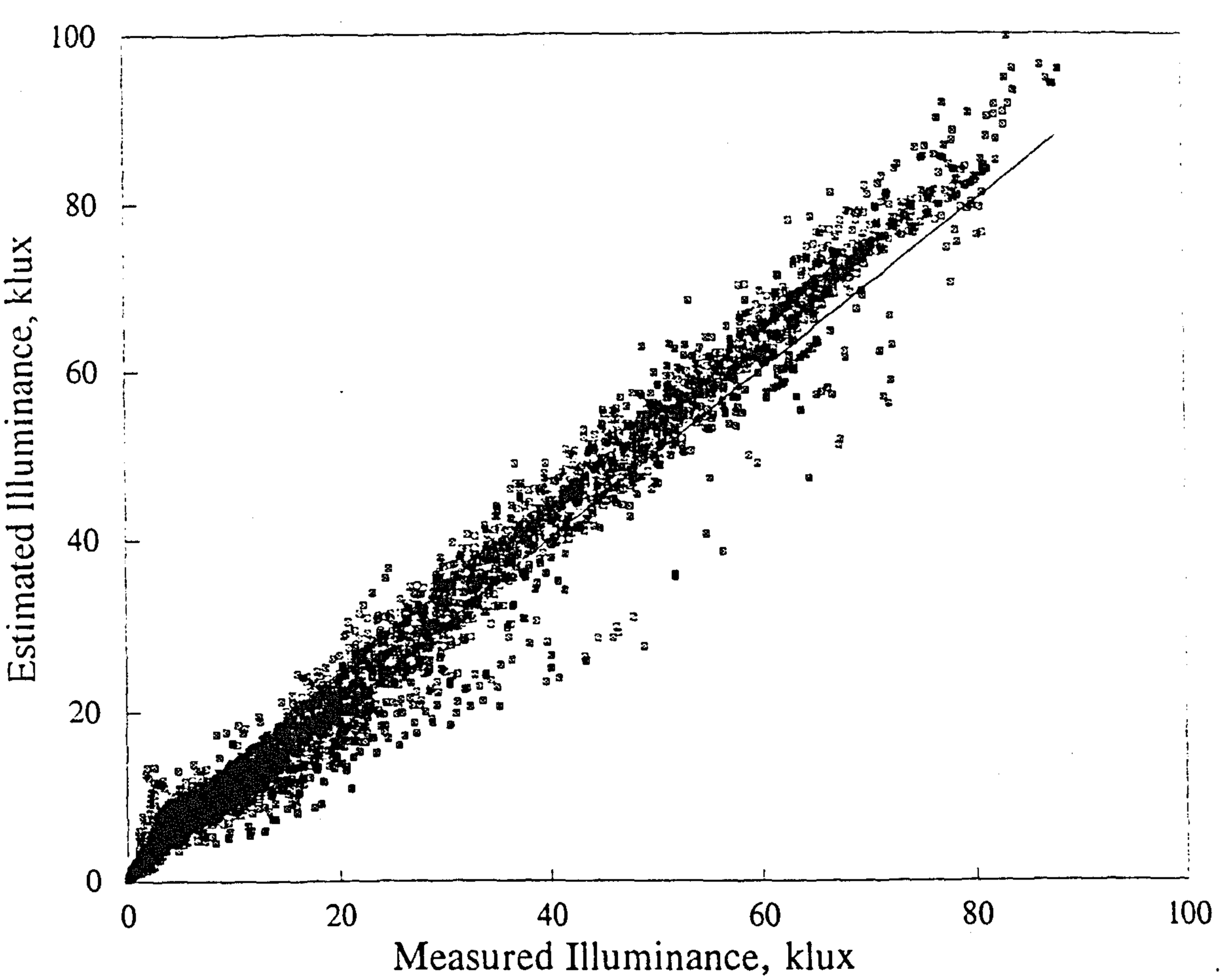

Figure 5.4.3g Winter: South surface illuminance

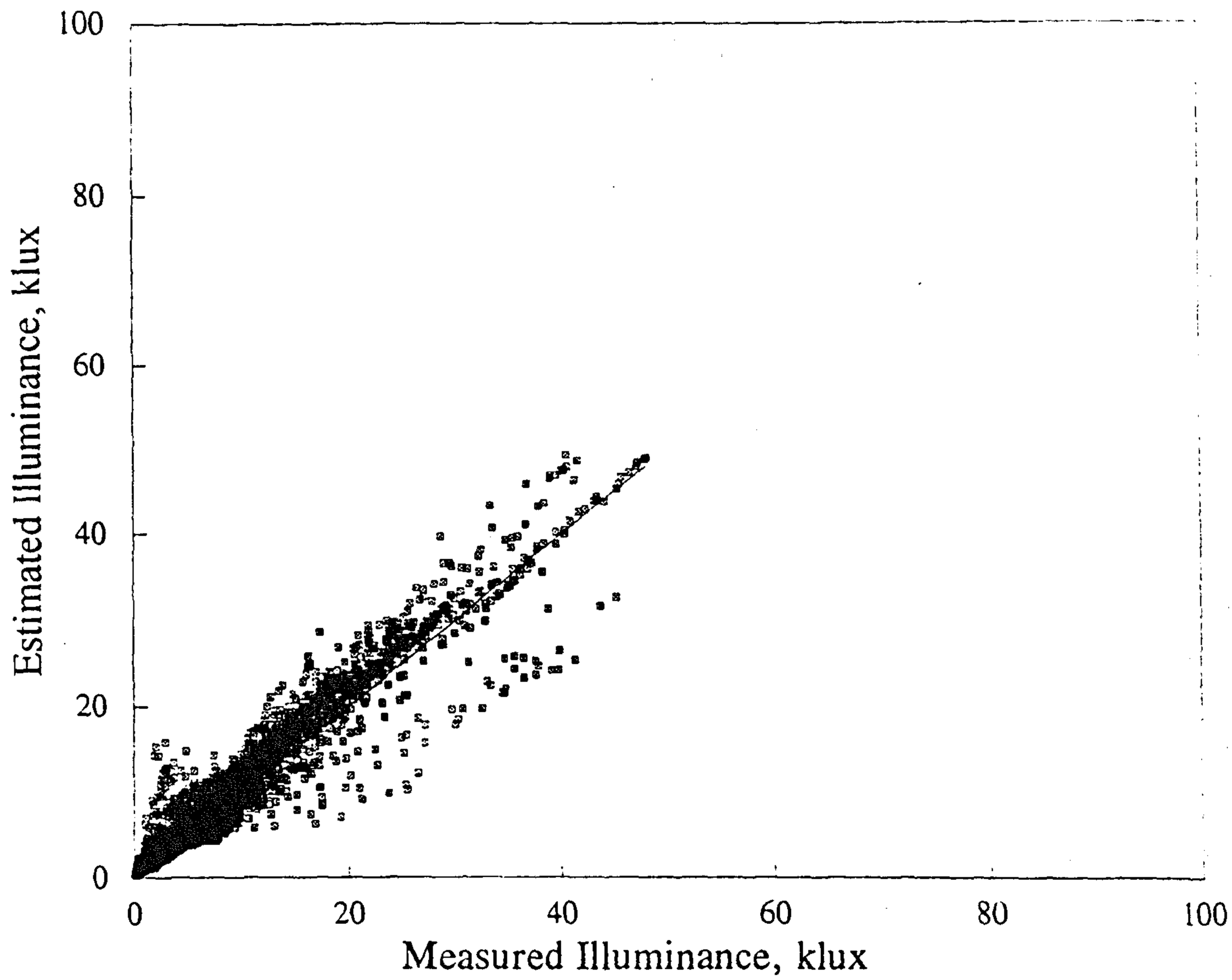

Figure 5.4.3h Winter: West surface illuminance

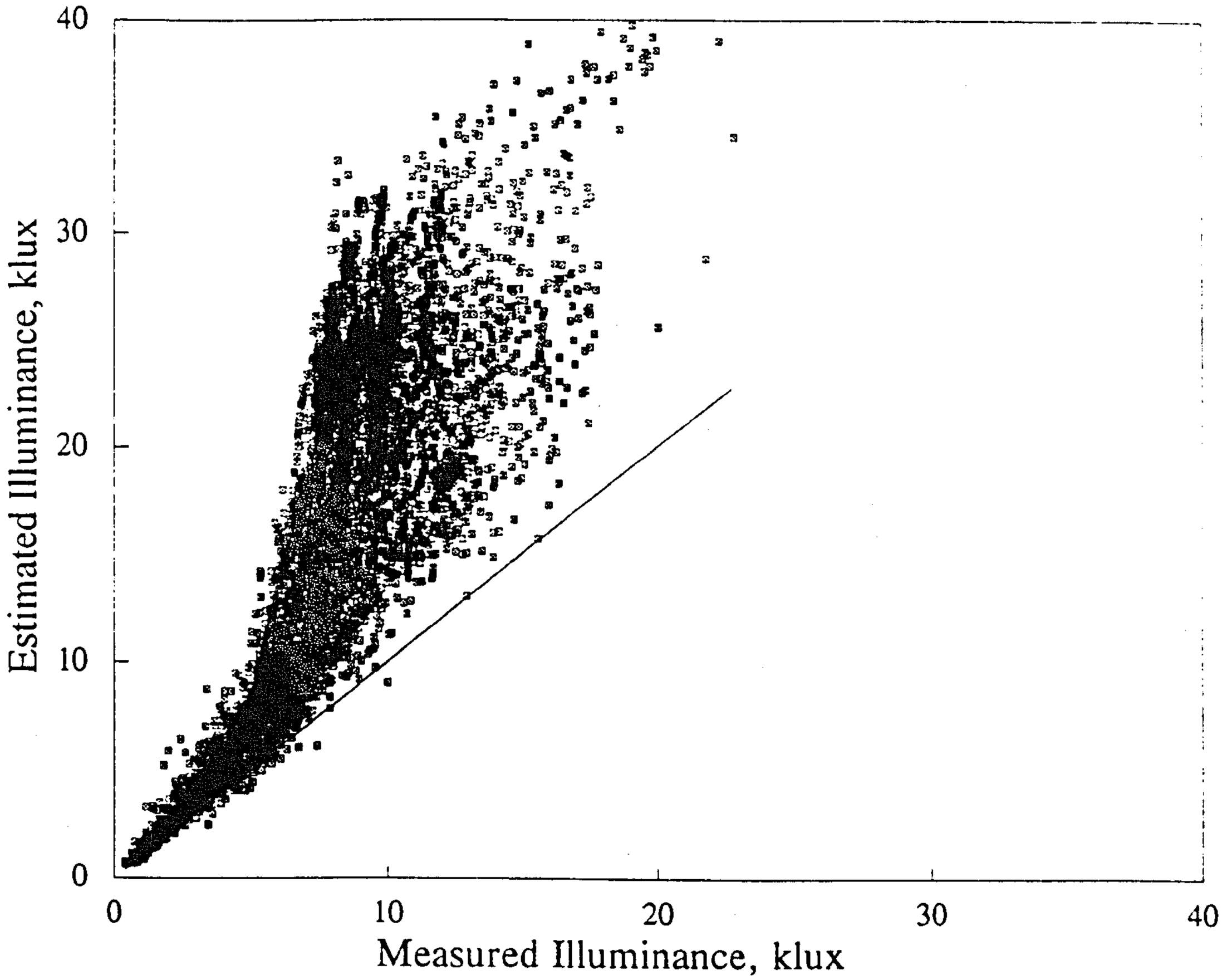

Figure 5.4.4a Autumn/spring: North surface illuminance

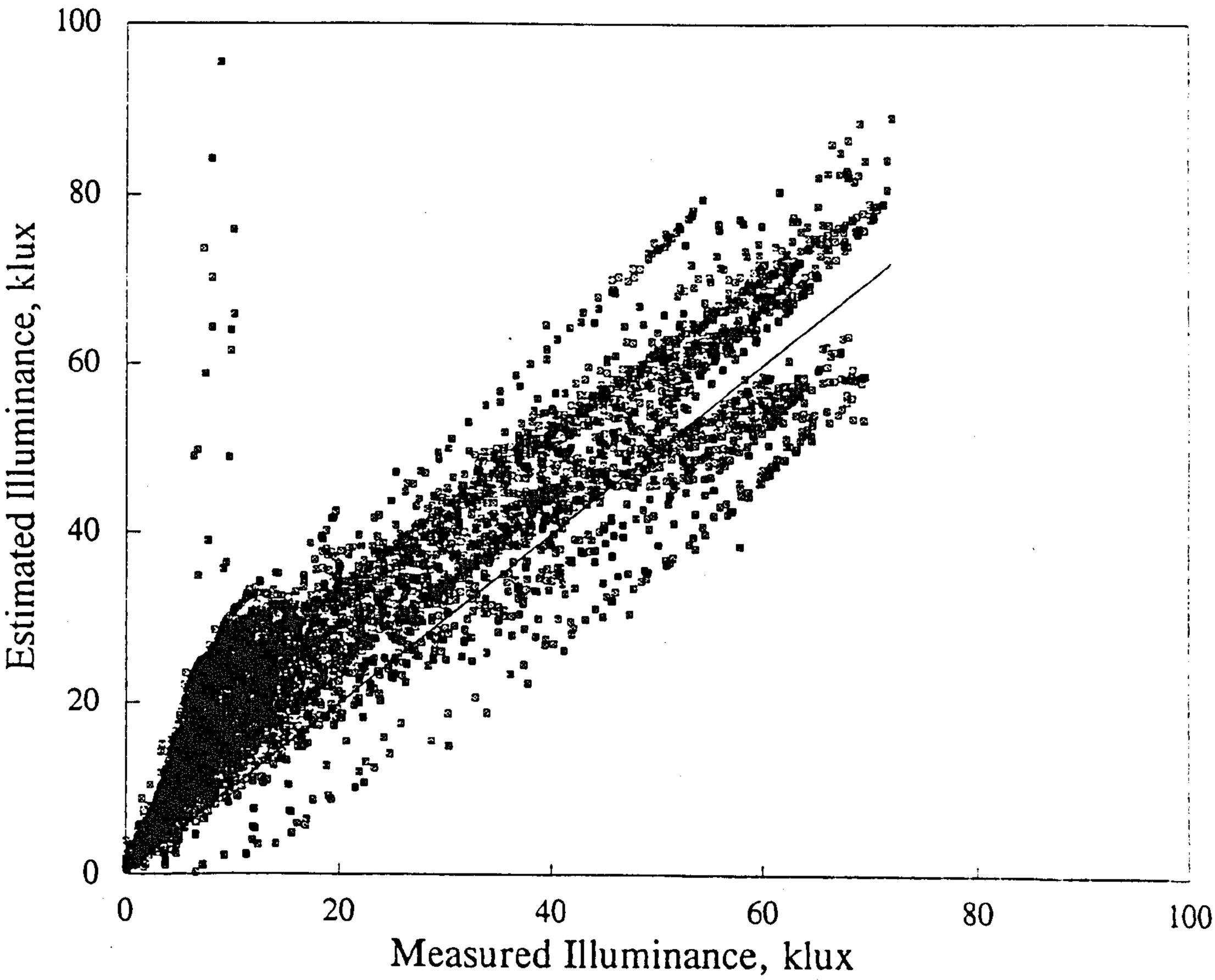

Figure 5.4.4b Autumn/spring: East surface illuminance

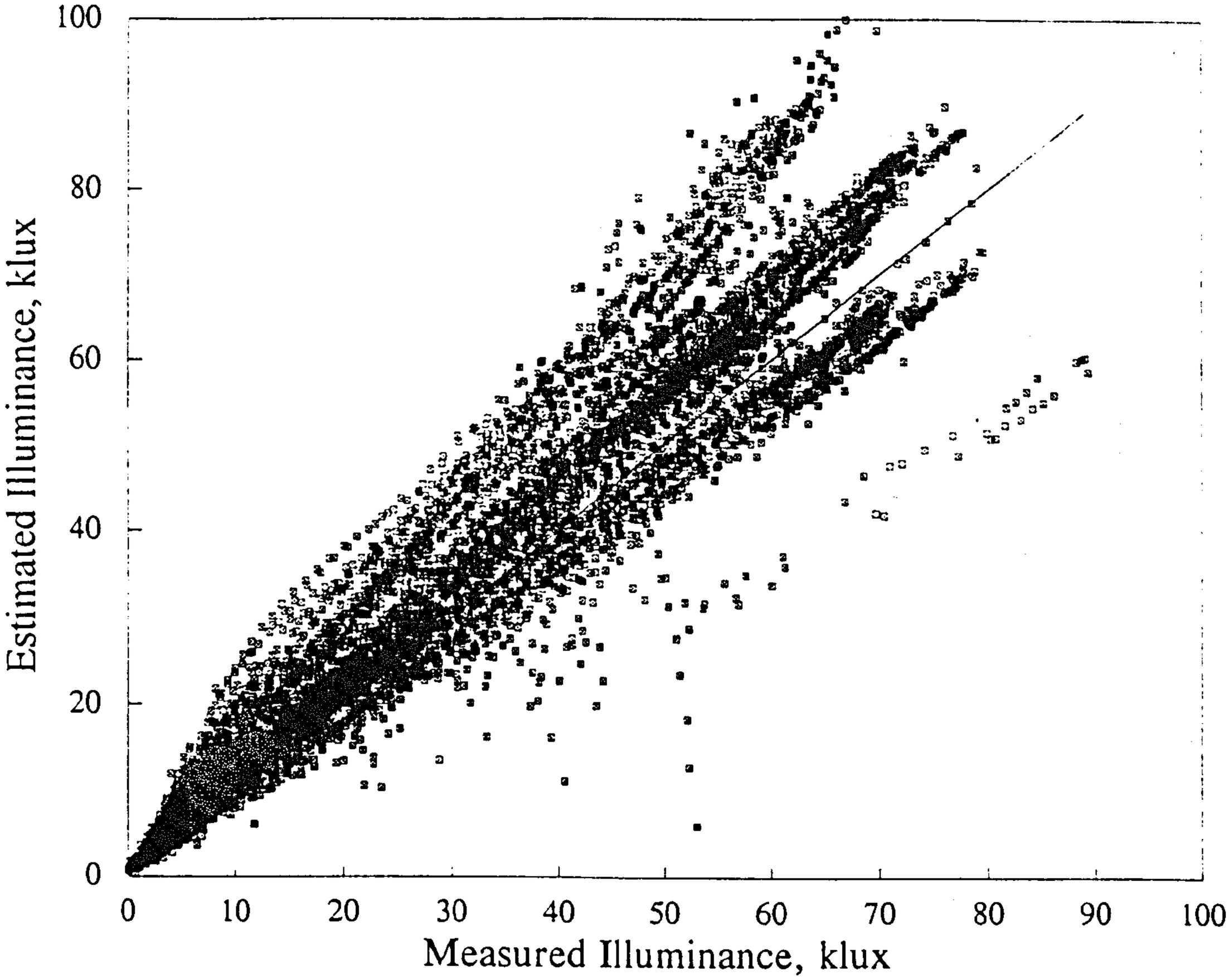

Figure 5.4.4c Autumn/spring: South surface illuminance

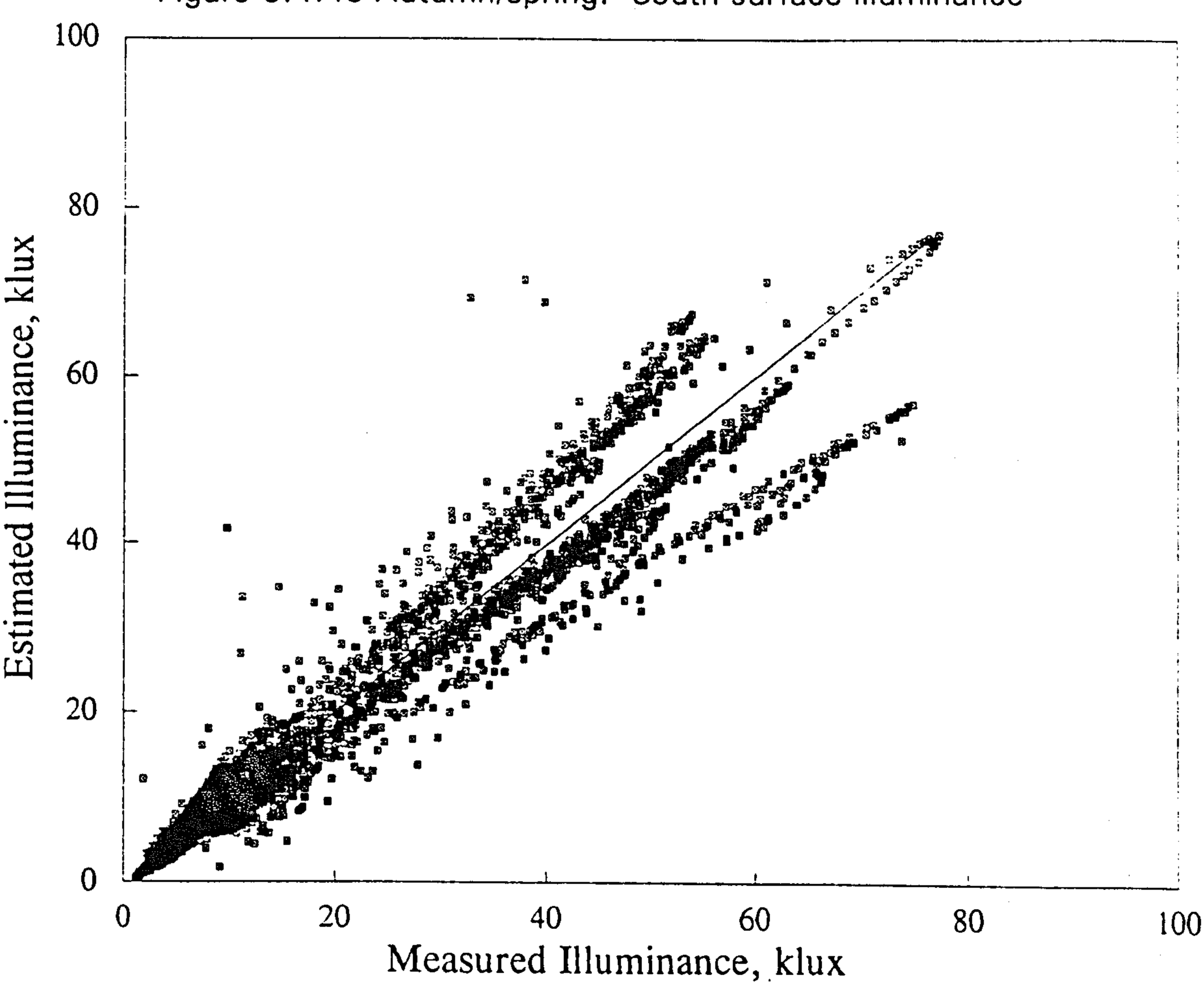

Figure 5.4.4d Autumn/spring: West surface illuminance

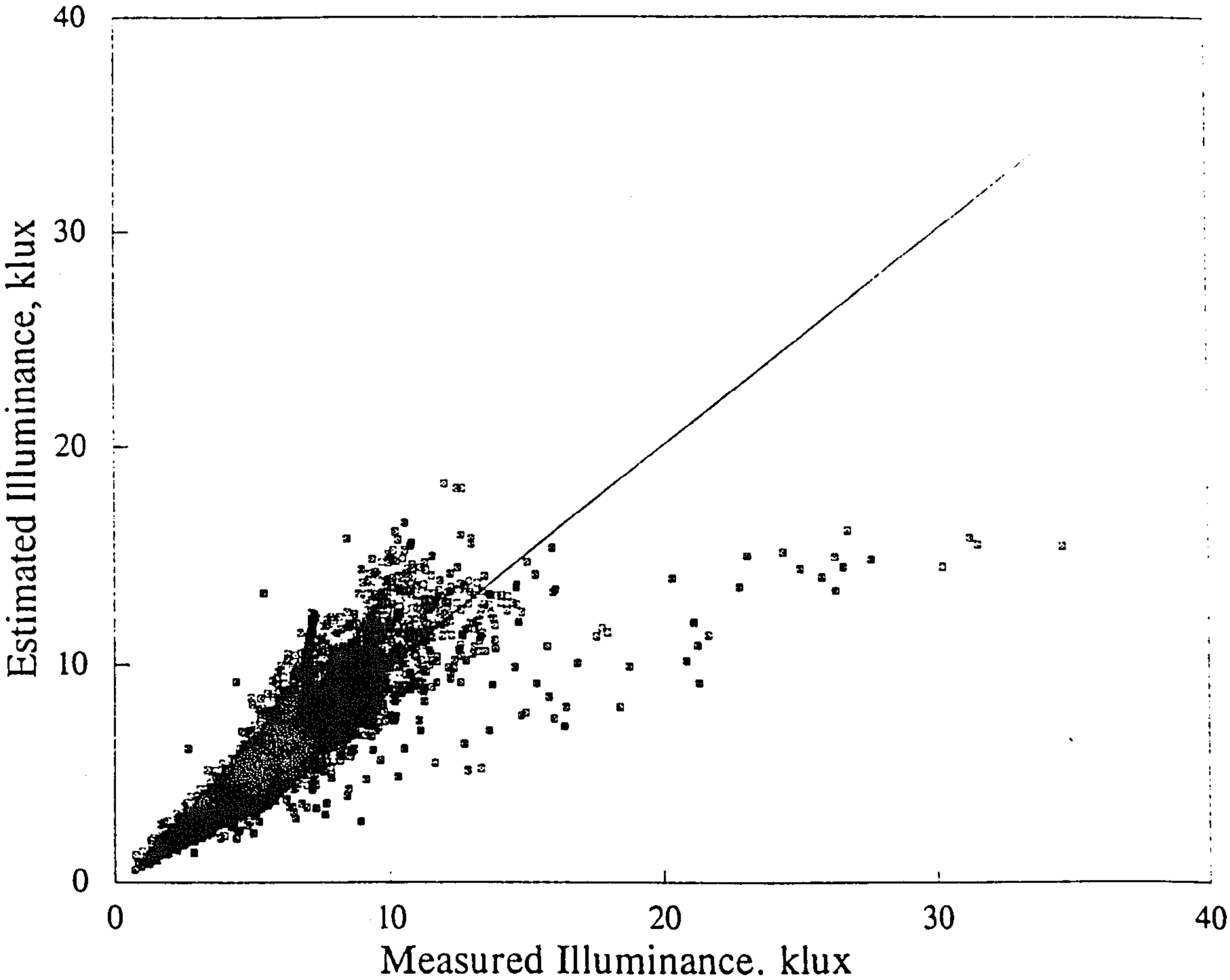

Figure 5.4.4e Winter: North surface illuminance

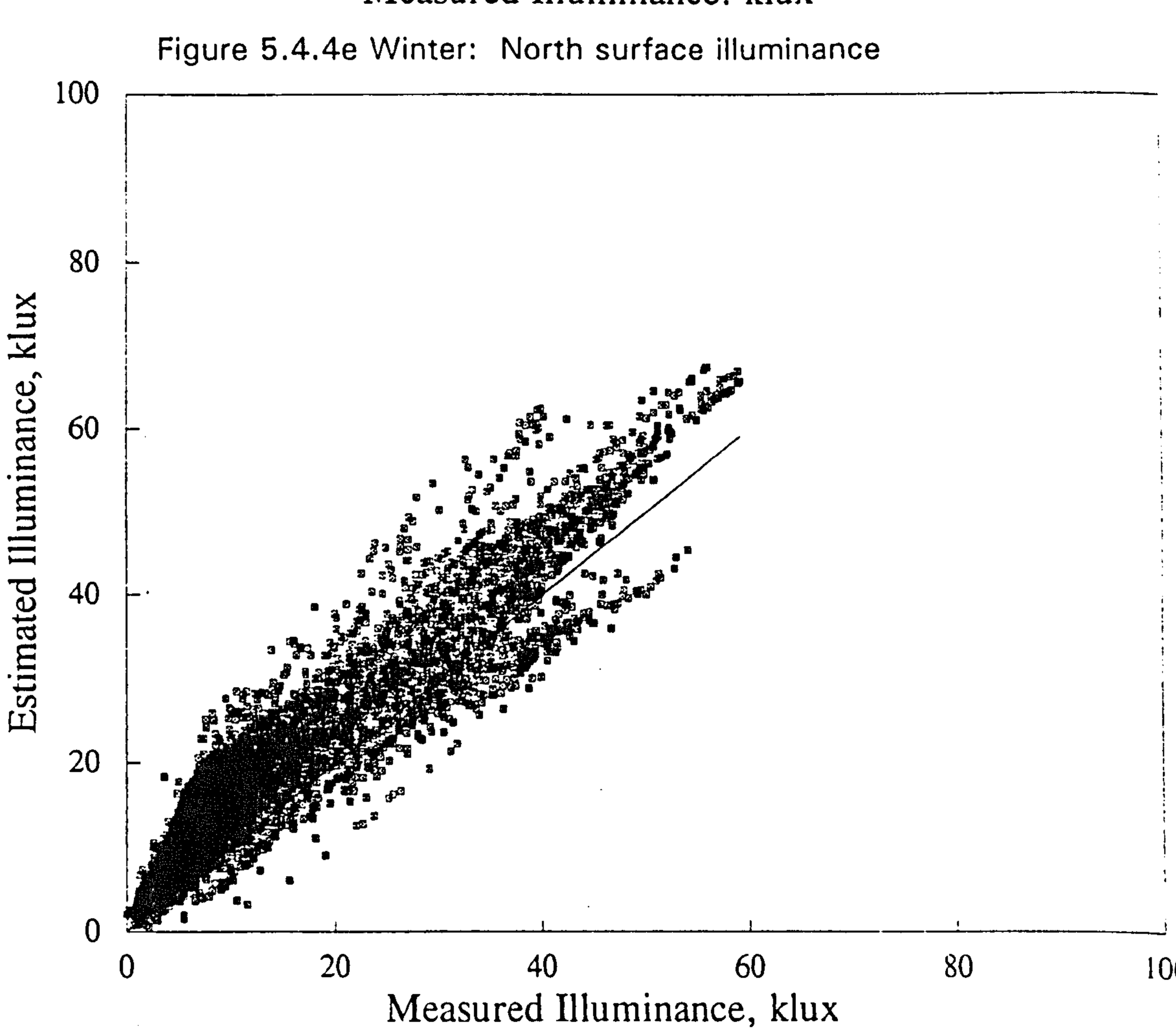

Figure 5.4.4f Winter: East surface illuminance

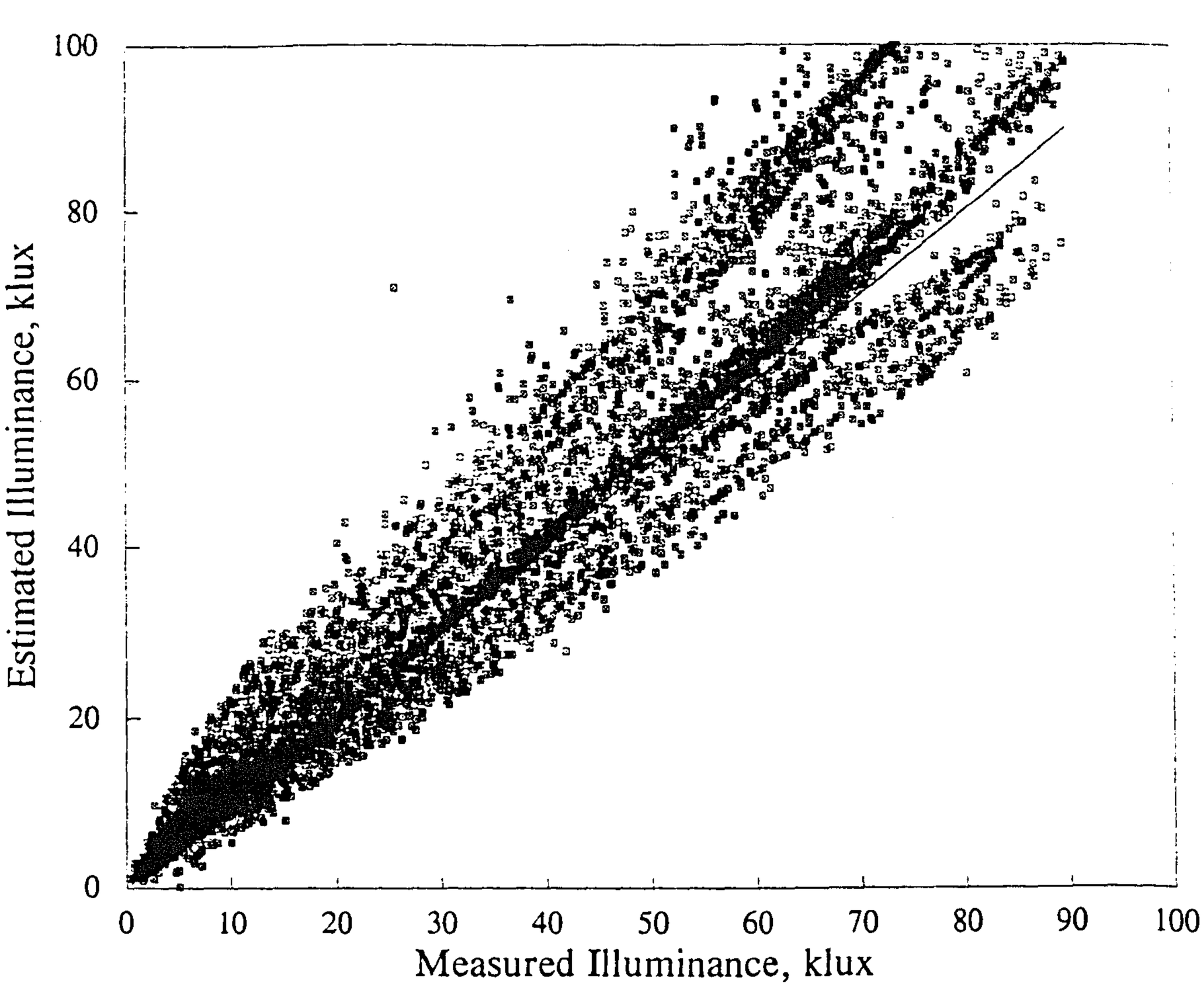

Figure 5.4.4g Winter: South surface illuminance

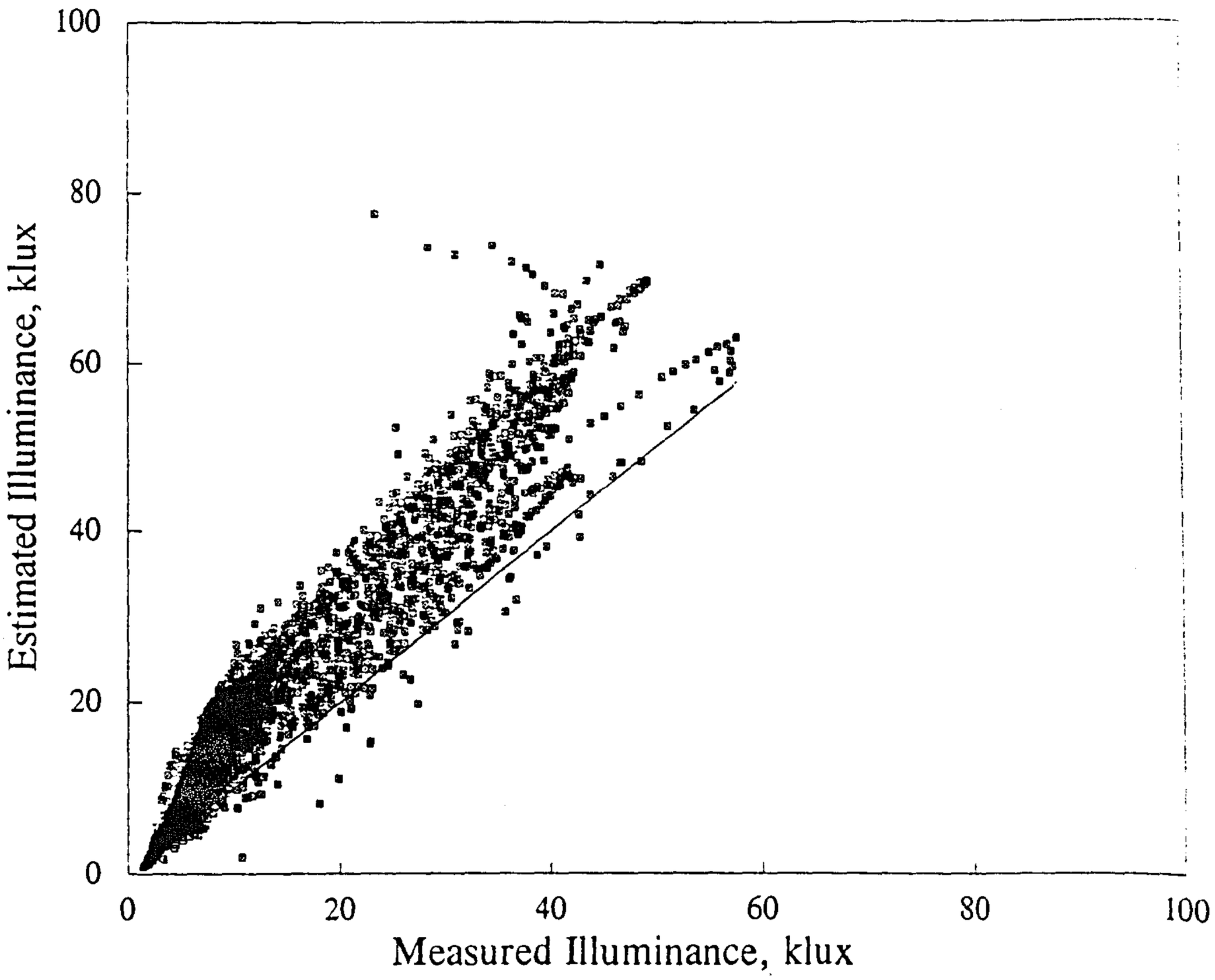

Figure 5.4.4h Winter: West surface illuminance

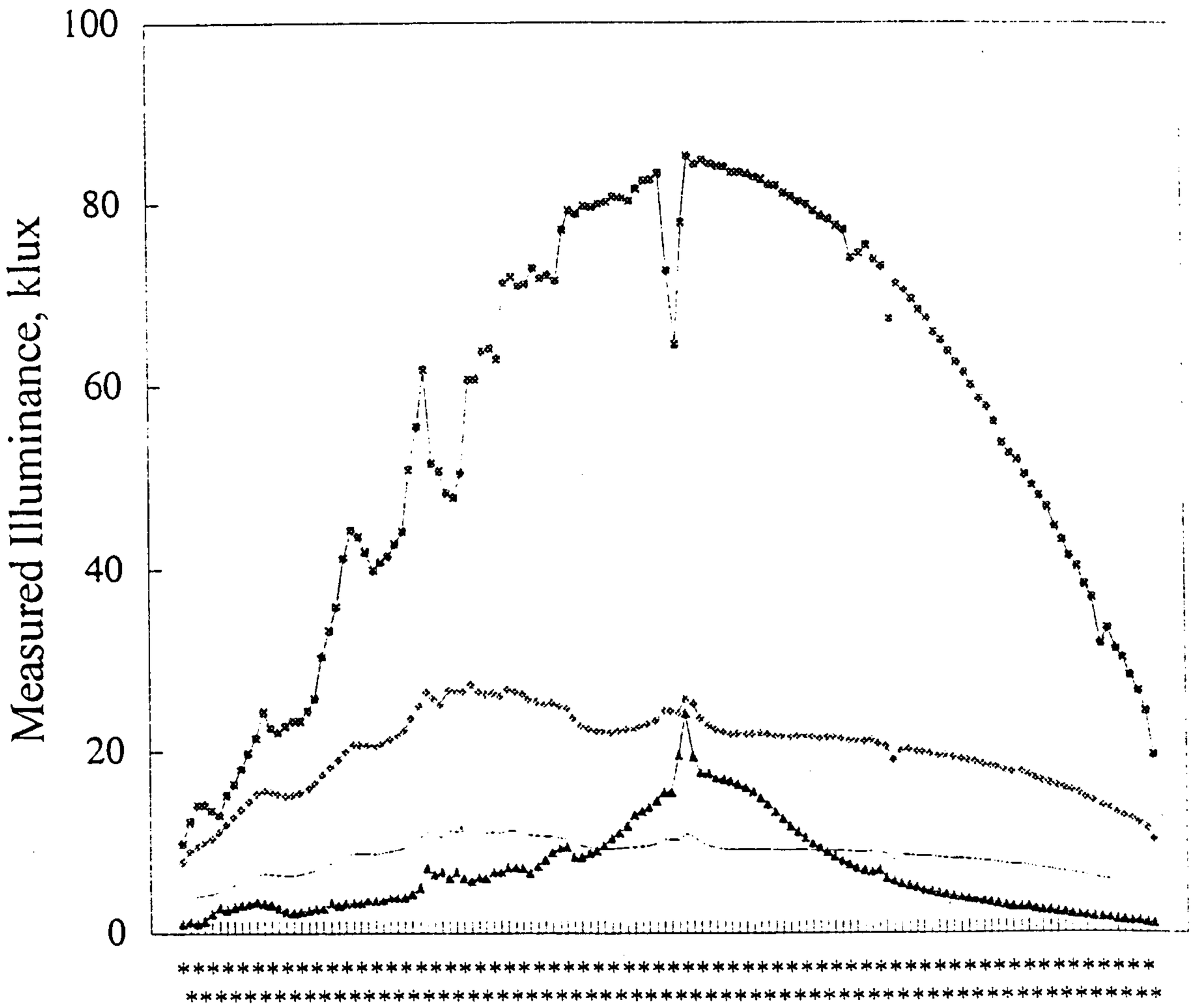

Figure 5.4.4i Athens: West surface data against Horizontal global and diffuse illuminance

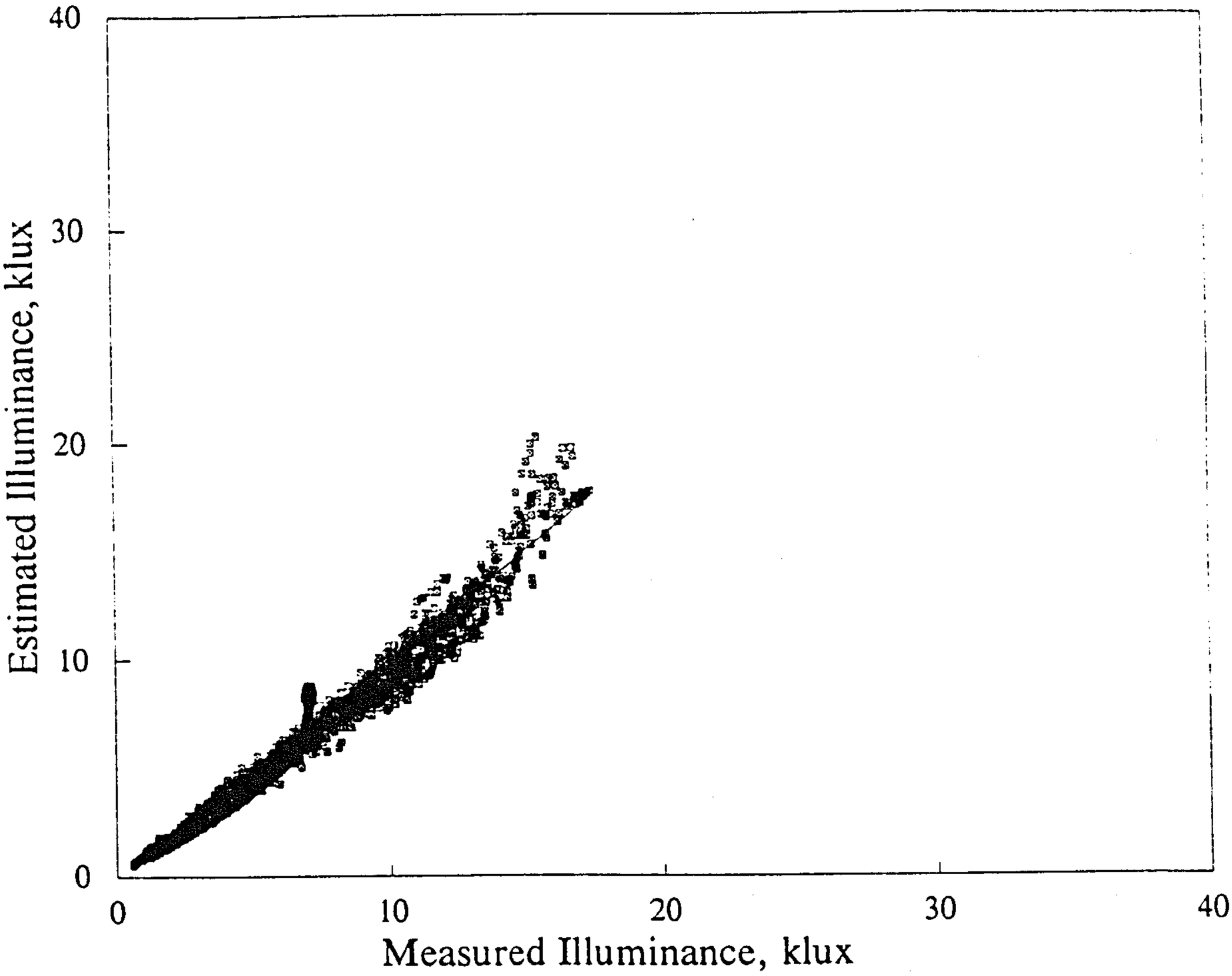

Figure 5.4.5a Autumn/spring: North surface illuminance

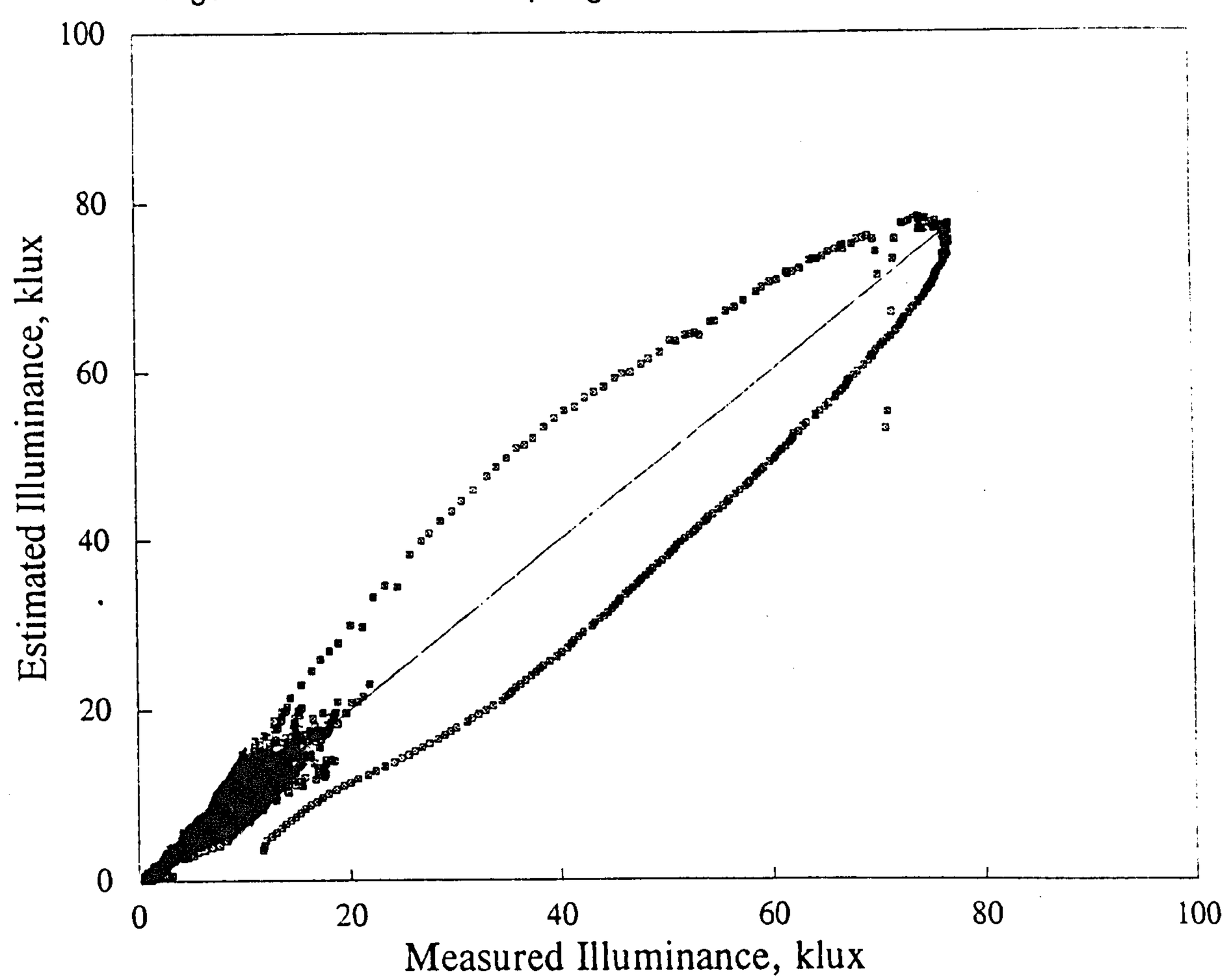

Figure 5.4.5b Autumn/spring: East surface illuminance

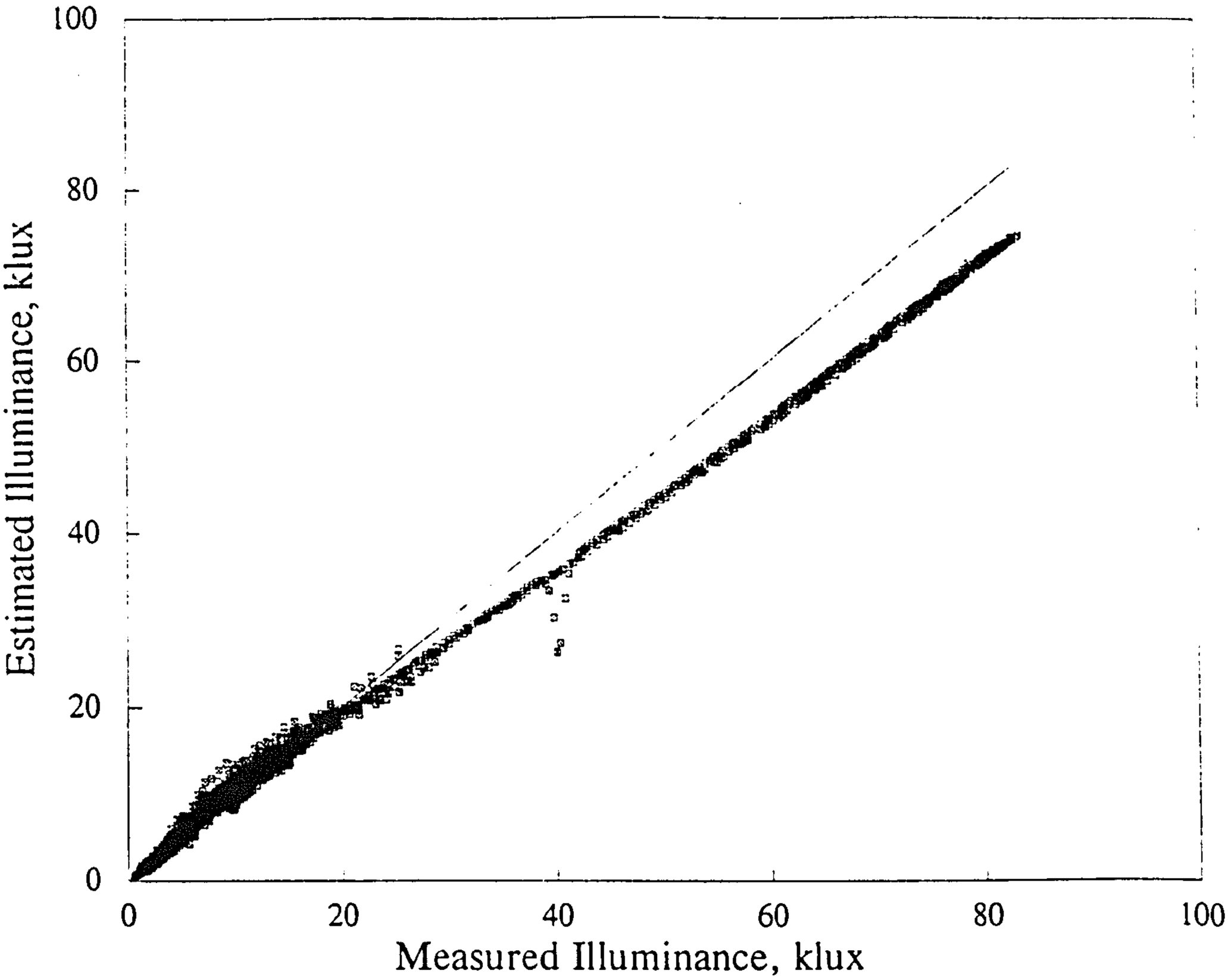

Figure 5.4.5c Autumn/spring: South surface illuminance

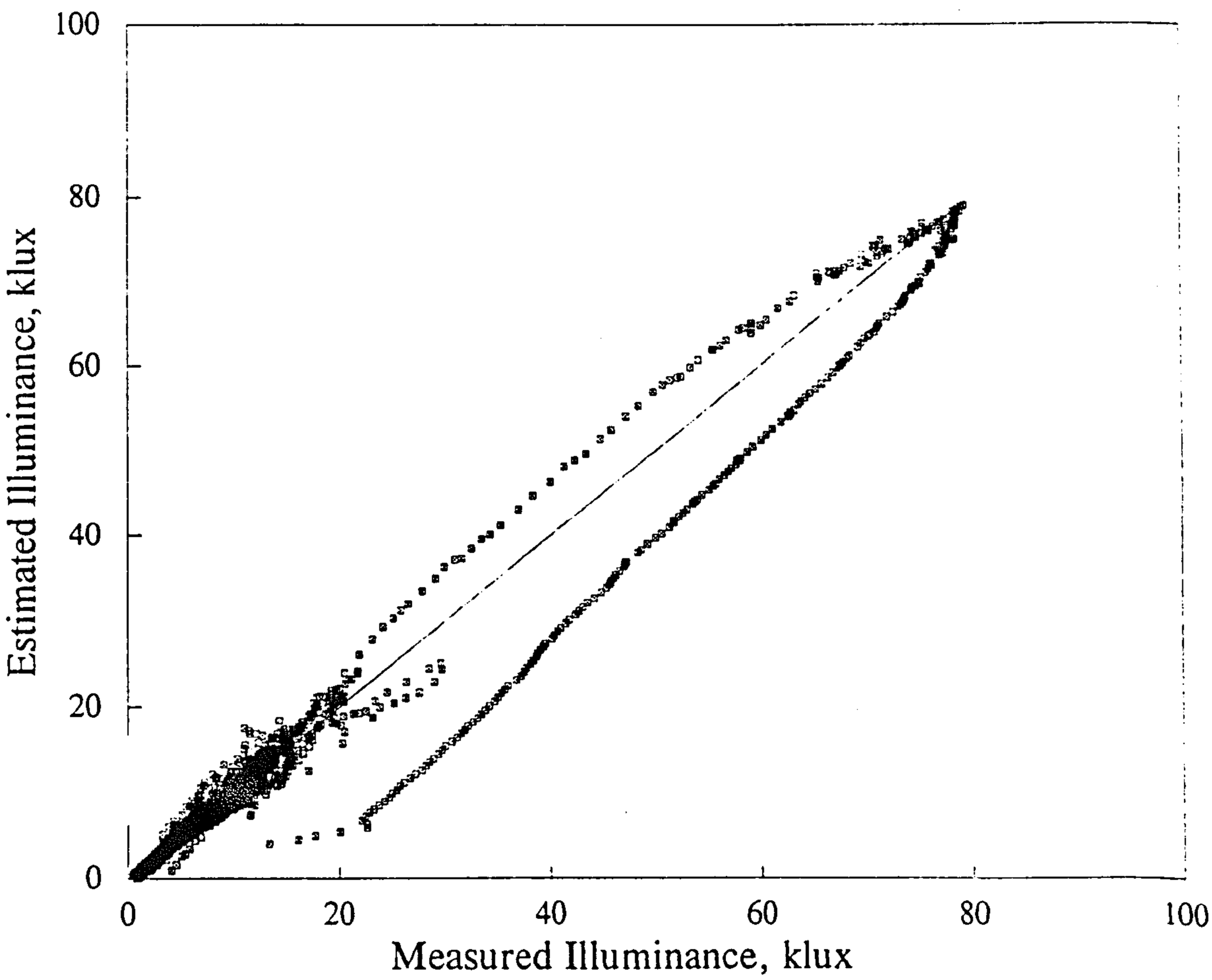

Figure 5.4.5d Autumn/spring: West surface illuminance

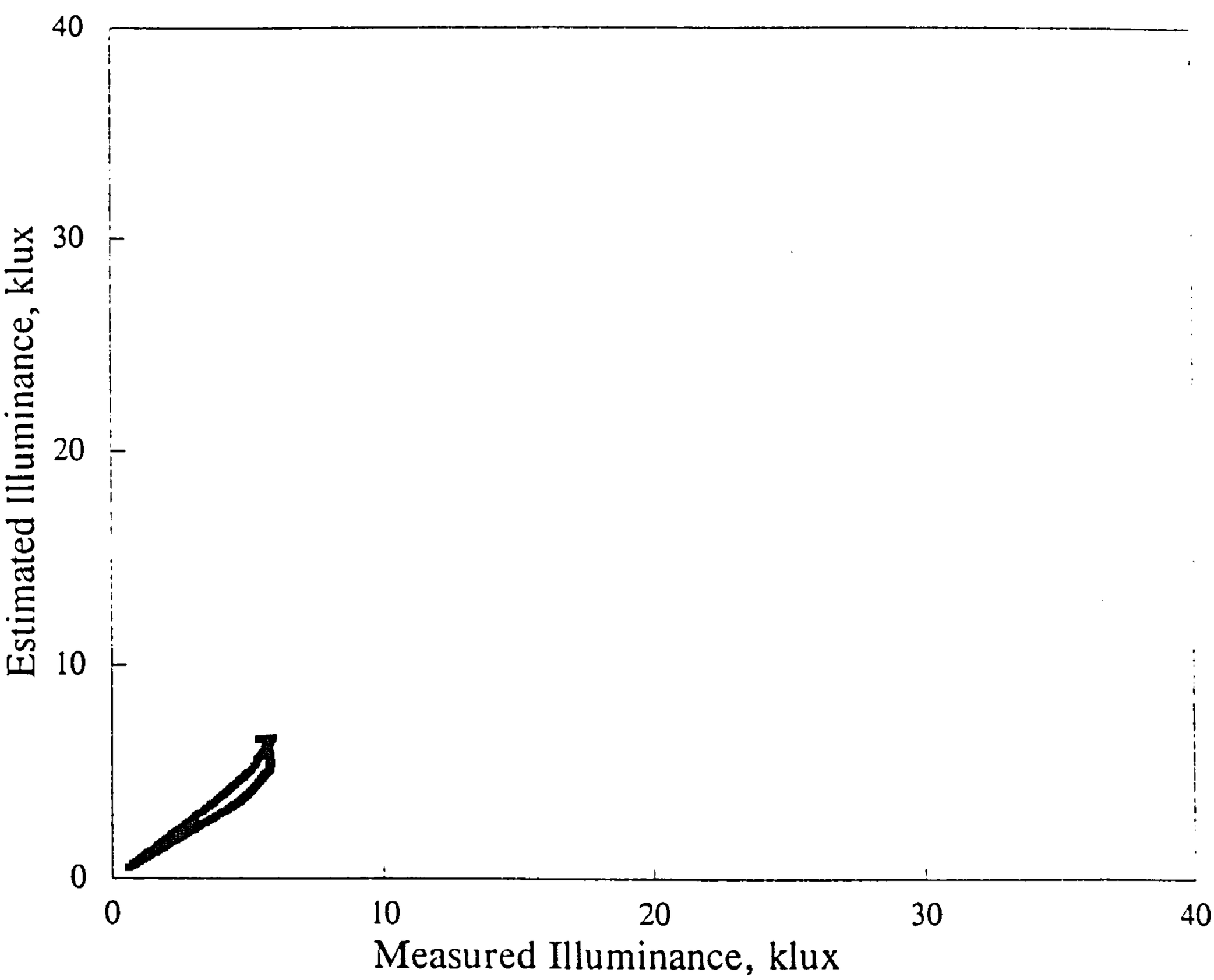

Figure 5.4.5e Winter: North surface illuminance

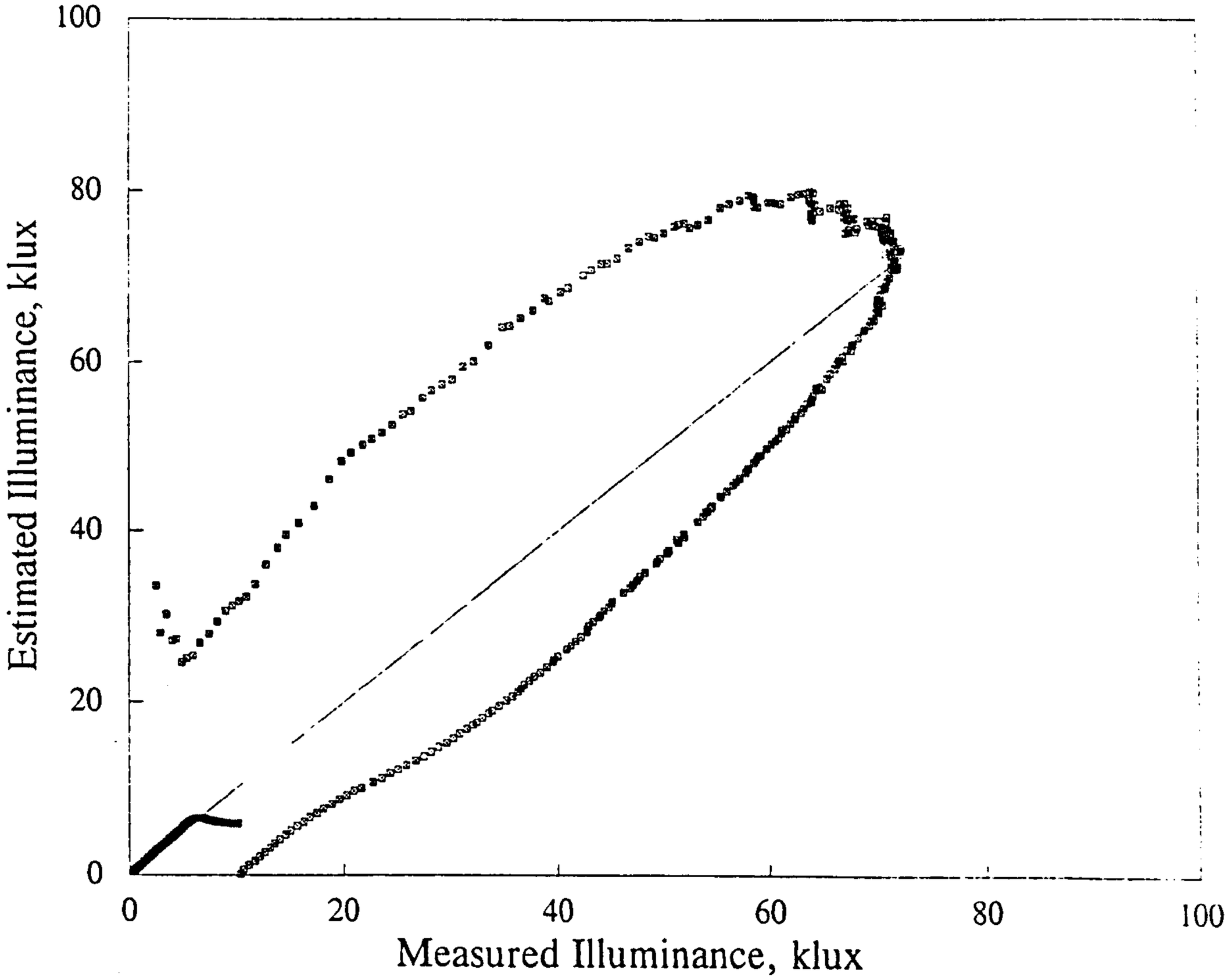

Figure 5.4.5f Winter: East surface illuminance

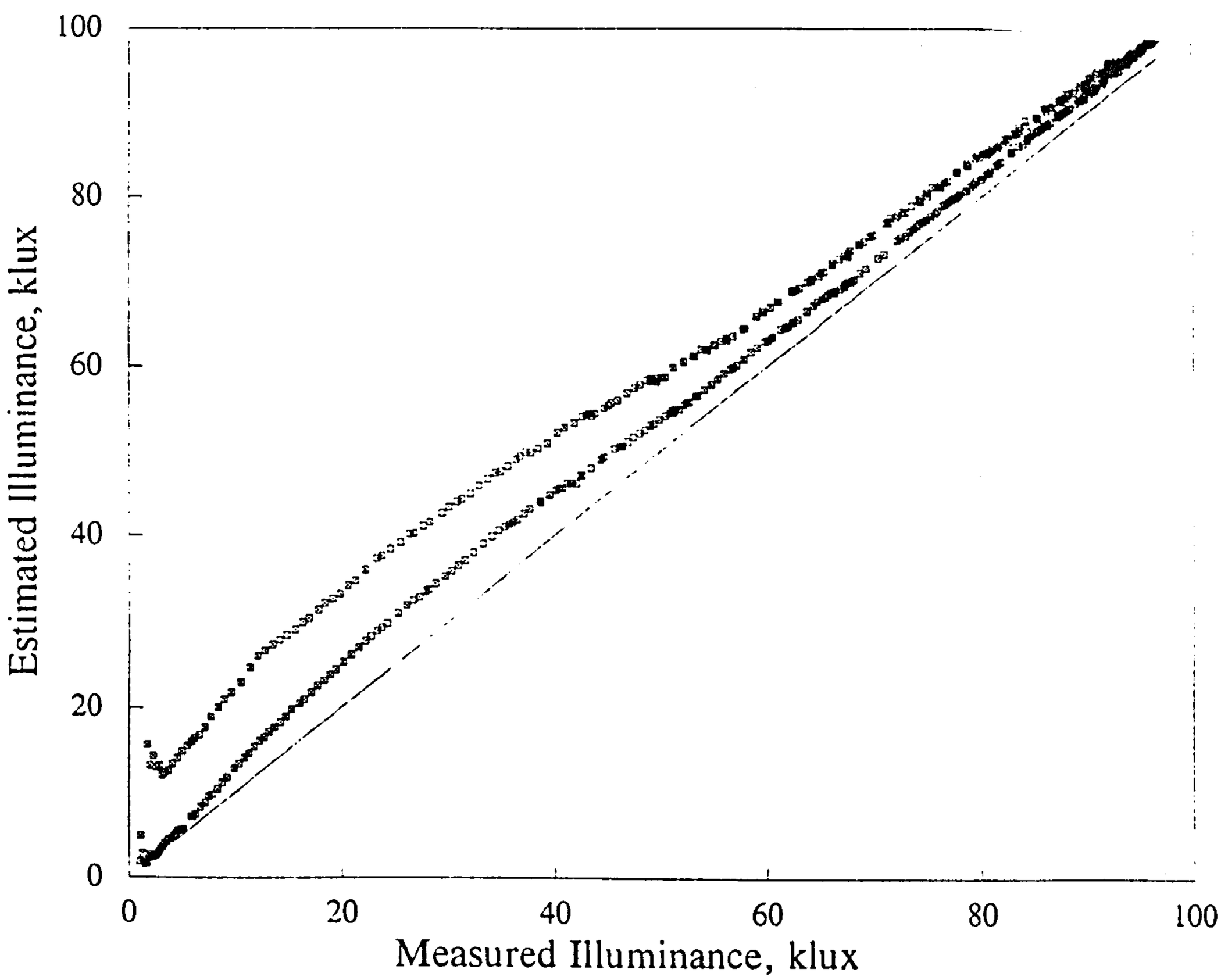

Figure 5.4.5g Winter: South surface illuminance

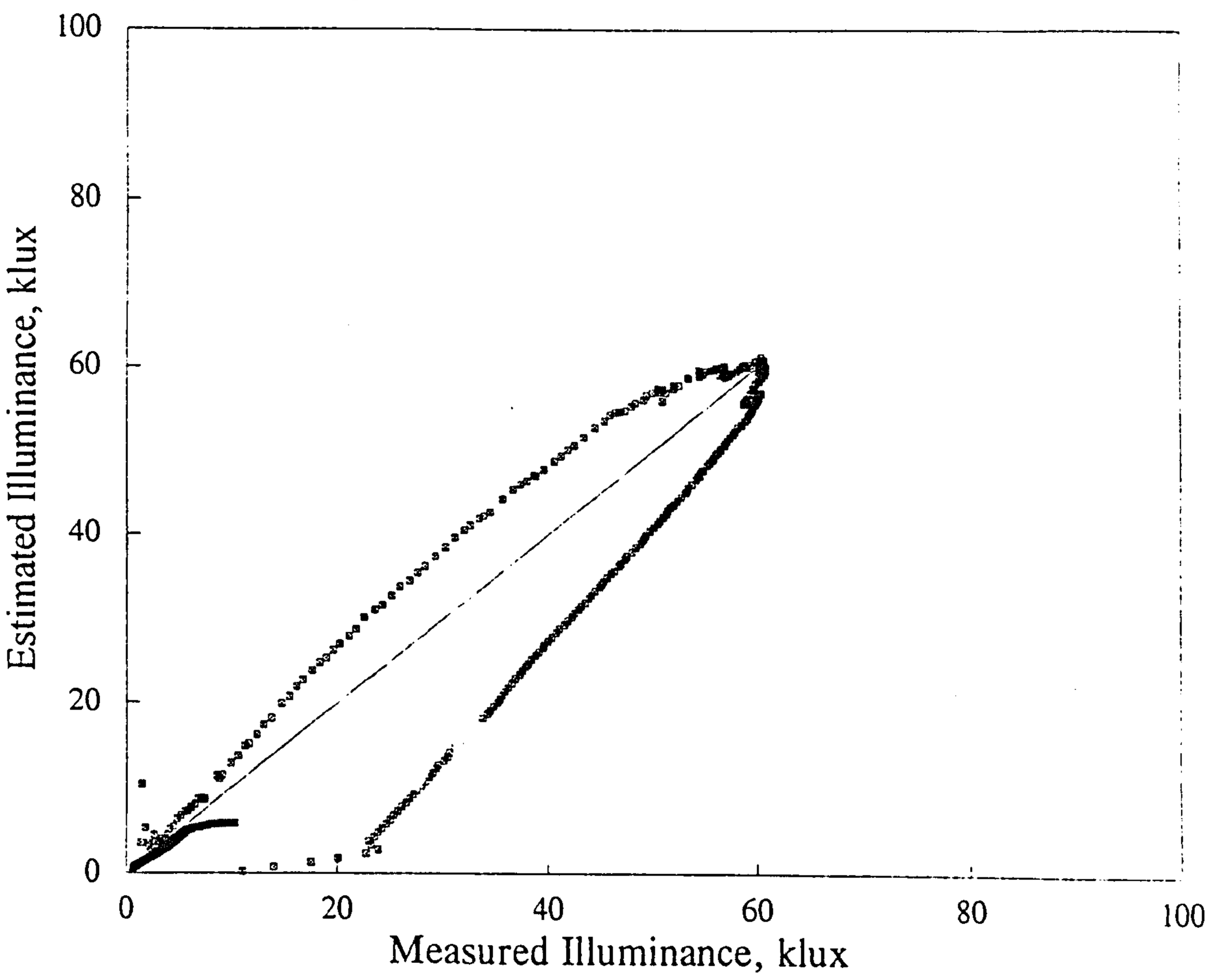

Figure 5.4.5h Winter: West surface illuminance

Appendix 5.5

ε bin	F_{11}	F_{12}	F_{13}	F_{21}	F_{22}	F_{23}
1	0.011	0.570	-0.081	-0.095	0.185	-0.018
2	0.429	0.363	-0.307	0.050	0.008	-0.065
3	0.809	-0.054	-0.442	0.181	-0.169	-0.092
4	1.014	-0.252	-0.531	0.275	-0.350	-0.096
5	1.282	-0.420	-0.689	0.380	-0.559	-0.114
6	1.426	-0.653	-0.779	0.425	-0.785	-0.097
7	1.485	-1.214	-0.784	0.411	-0.629	-0.082
8	1.170	-0.300	-0.615	0.518	-1.892	-0.055

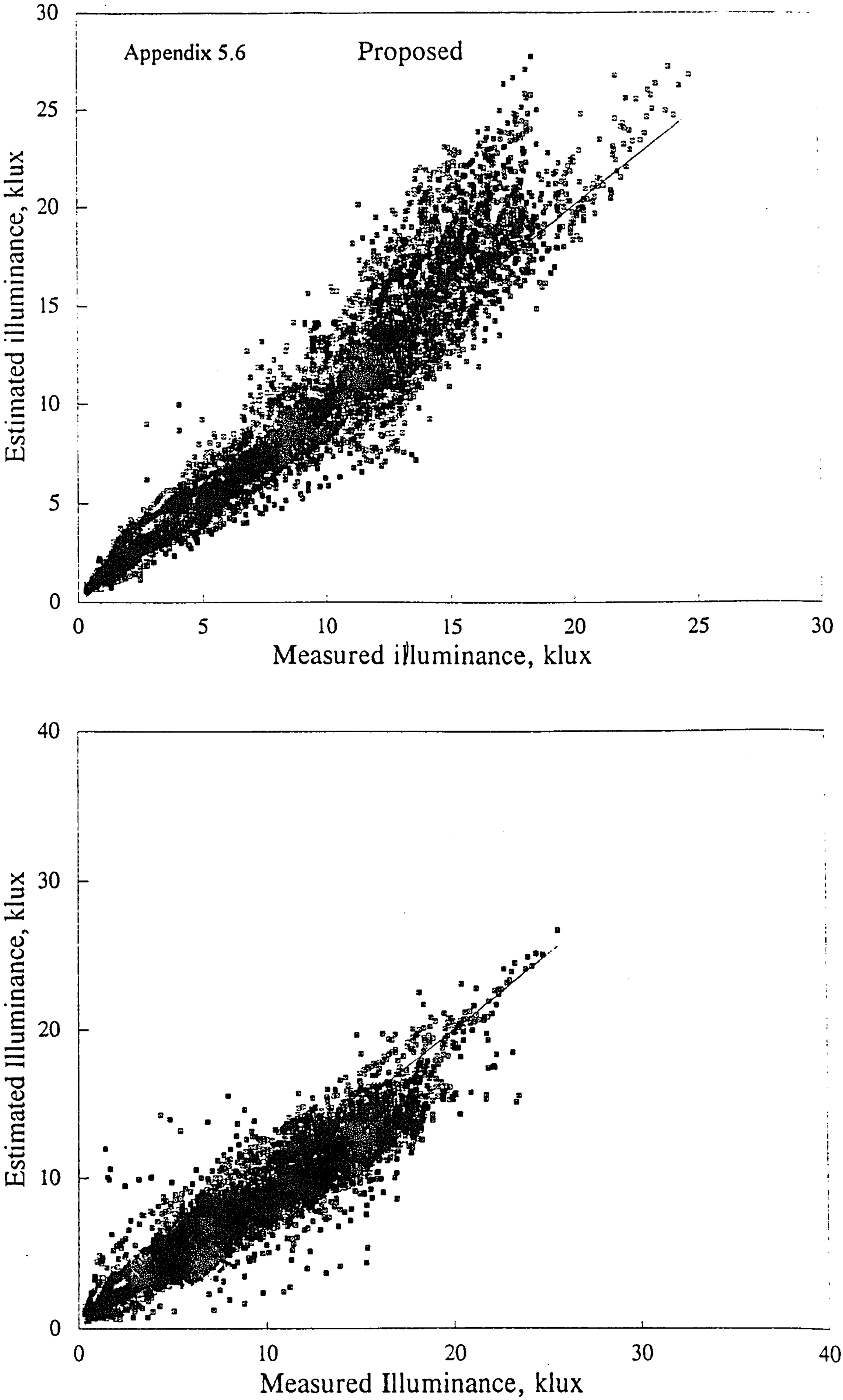

Figure 5.6.1 Summer: North surface Proposed against Perez model

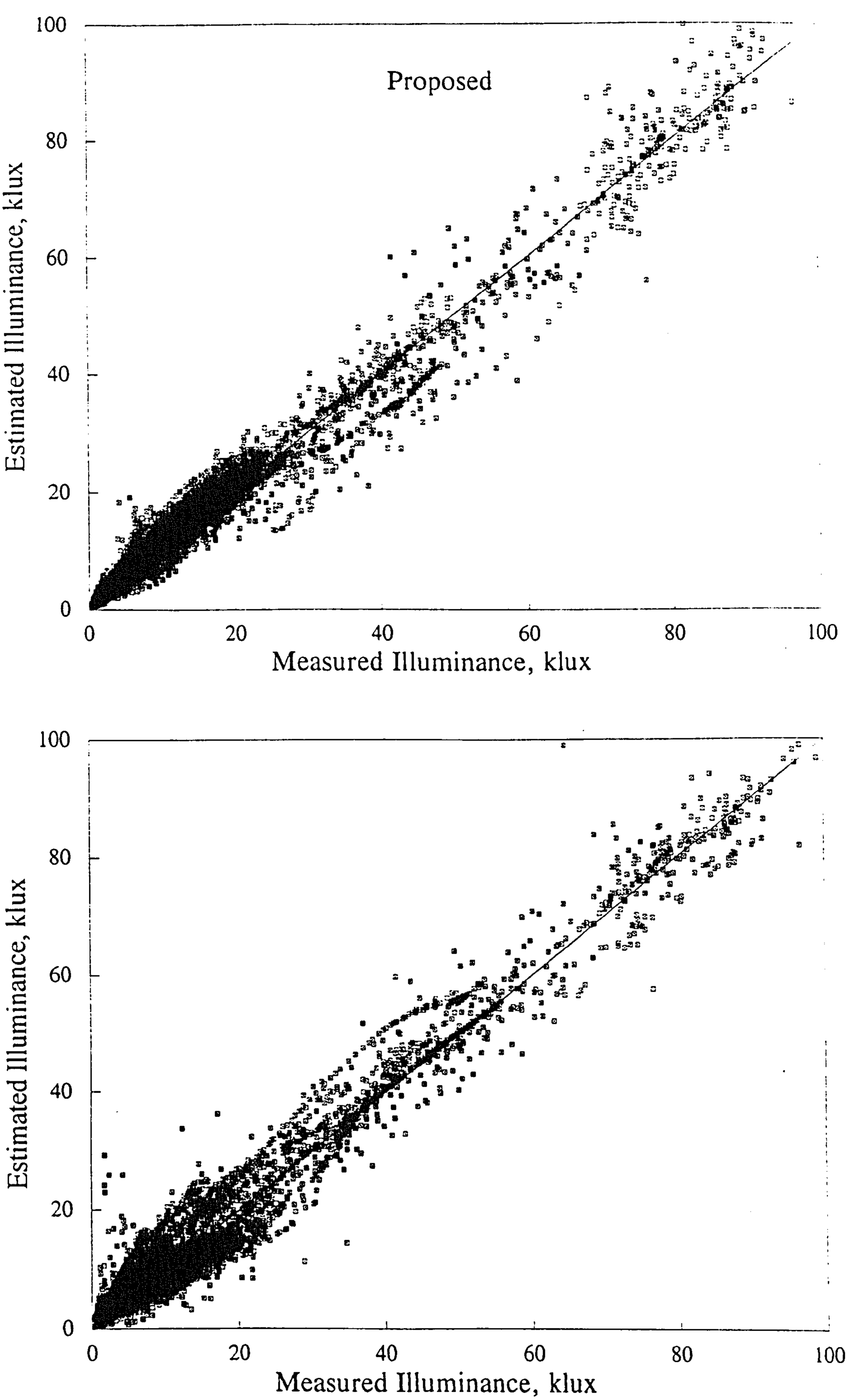

Figure 5.6.2 Summer: East surface Proposed against Perez model

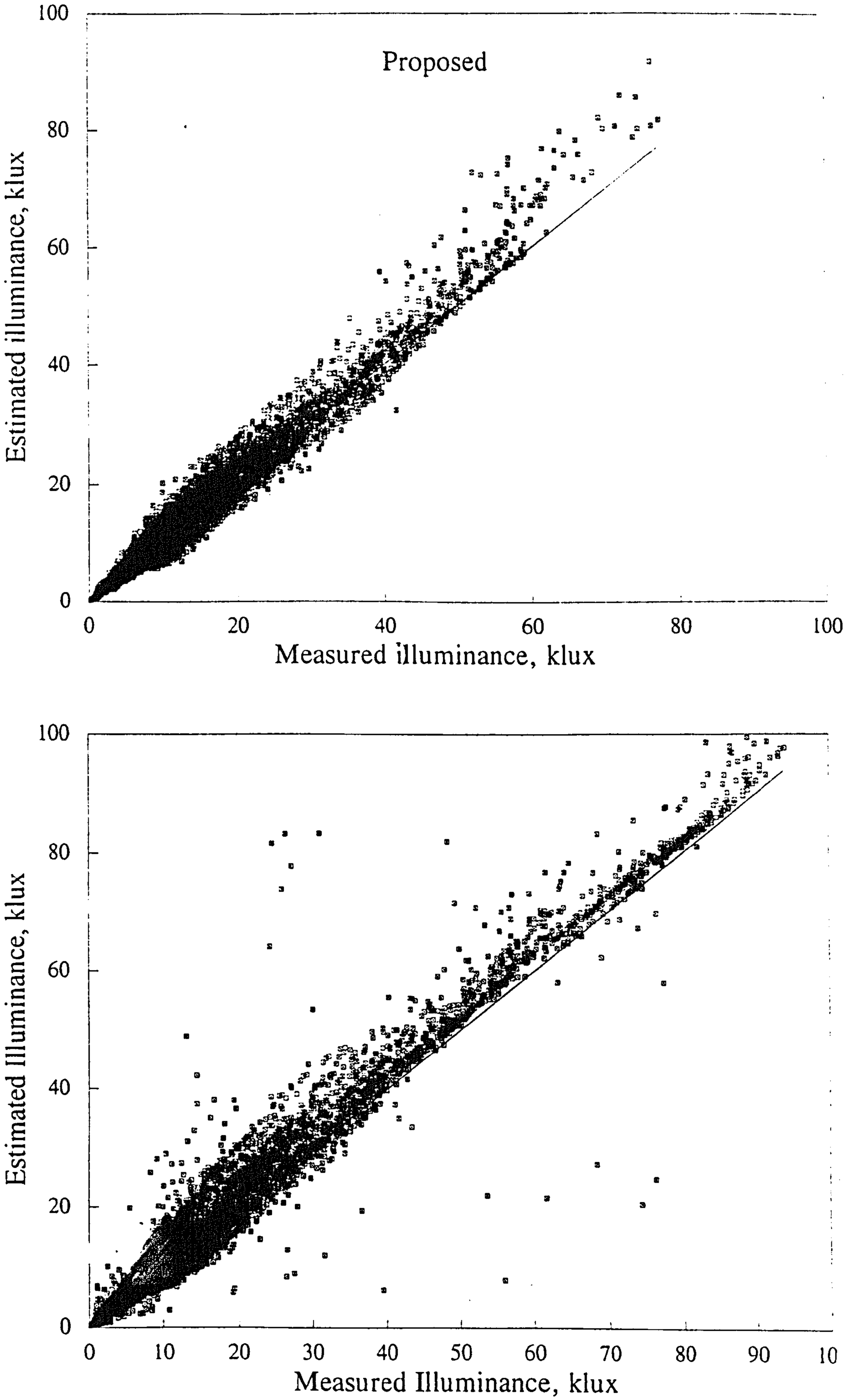

Figure 5.6.3 Summer: South surface Proposed against Perez model

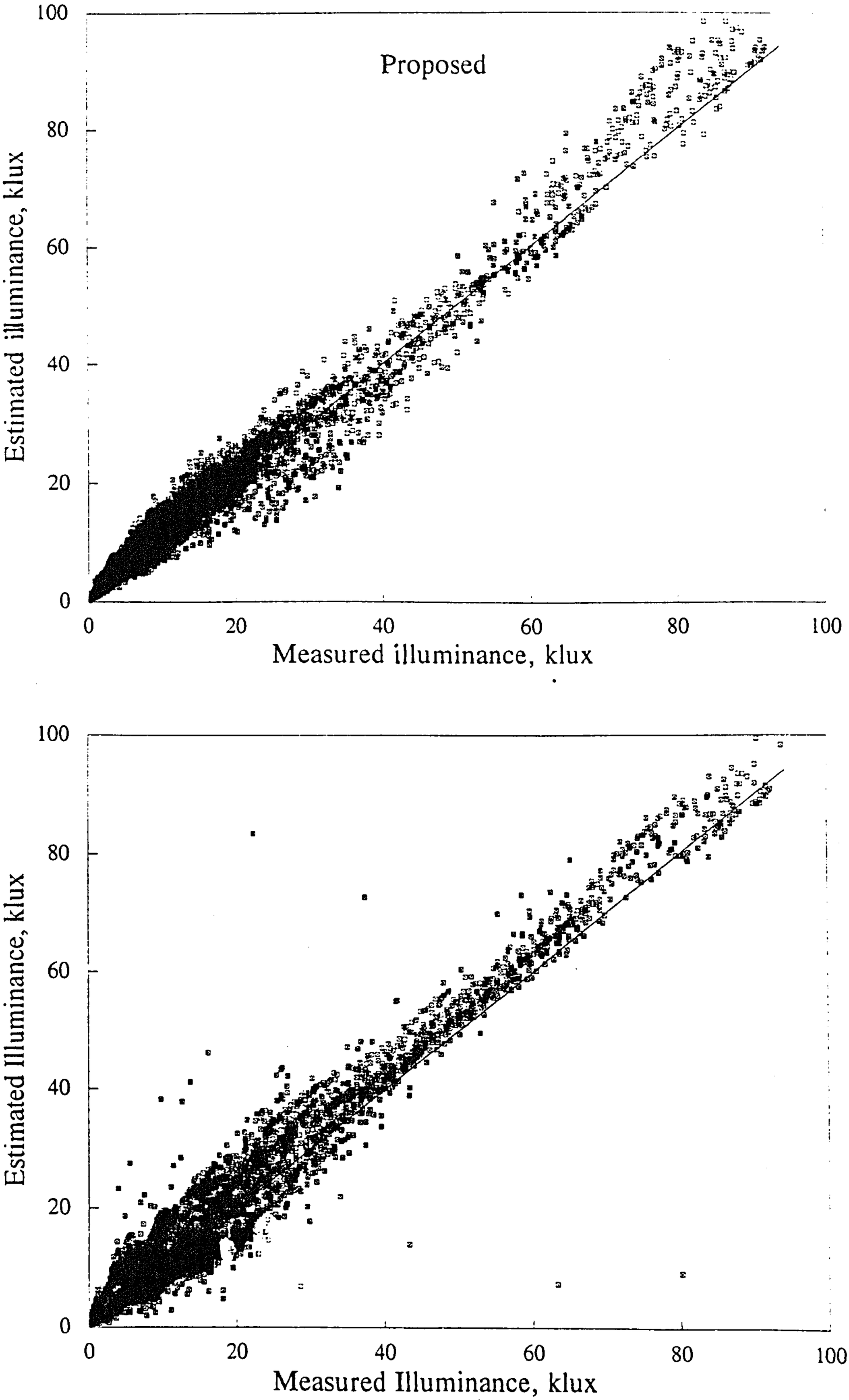

Figure 5.6.4 Summer: West surface Proposed against Perez model

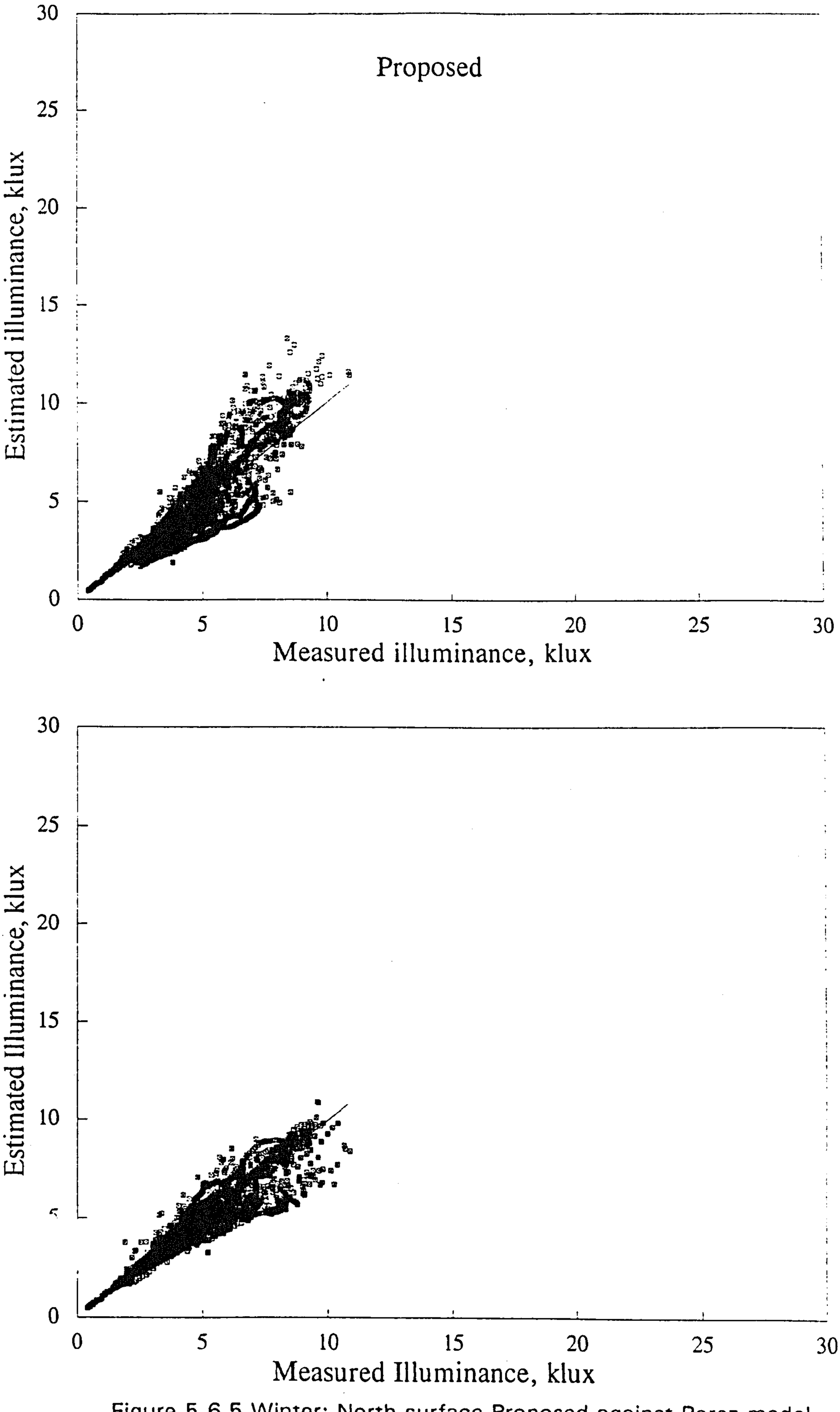

Figure 5.6.5 Winter: North surface Proposed against Perez model

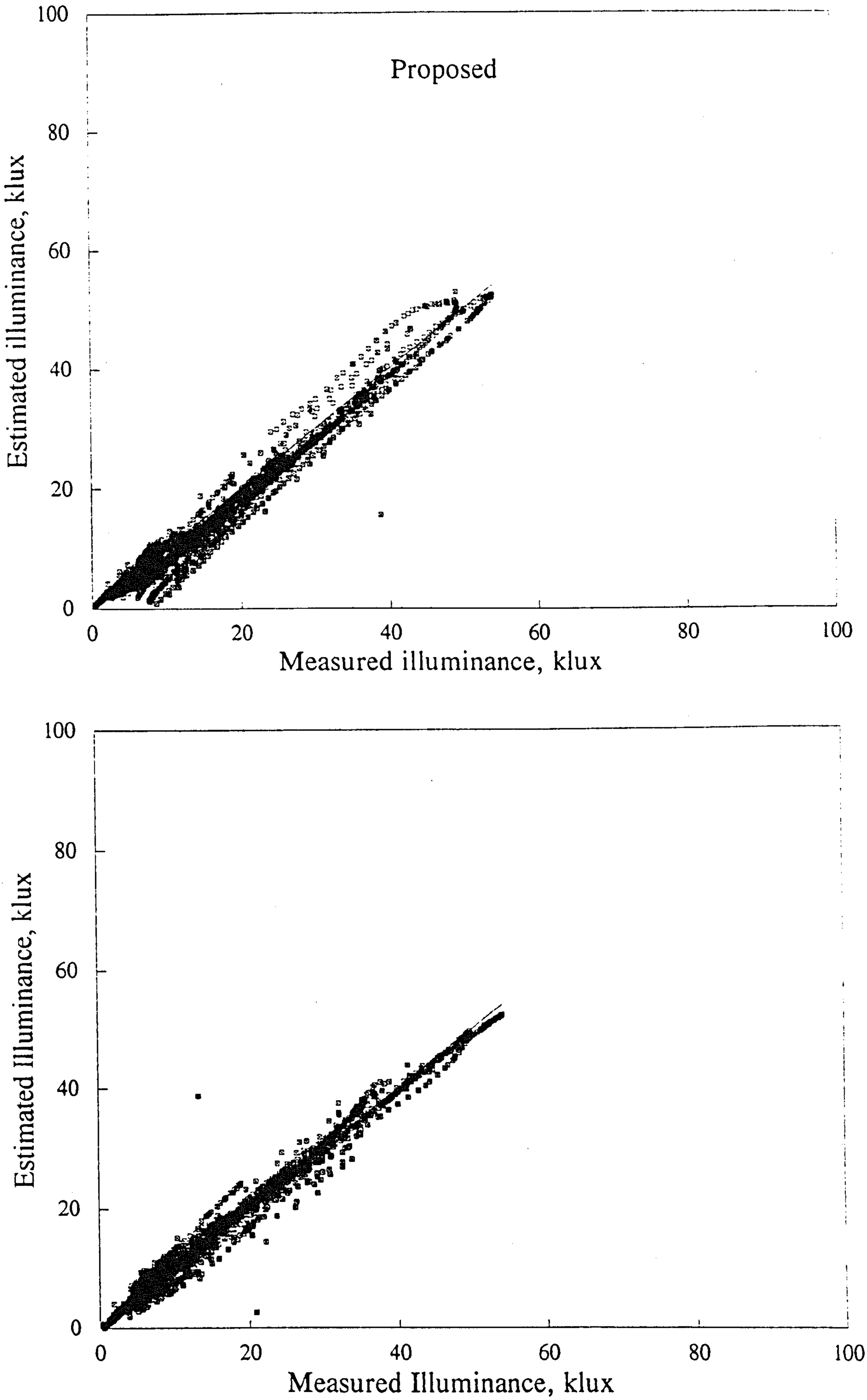

Figure 5.6.6 Winter: East surface Proposed against Perez model

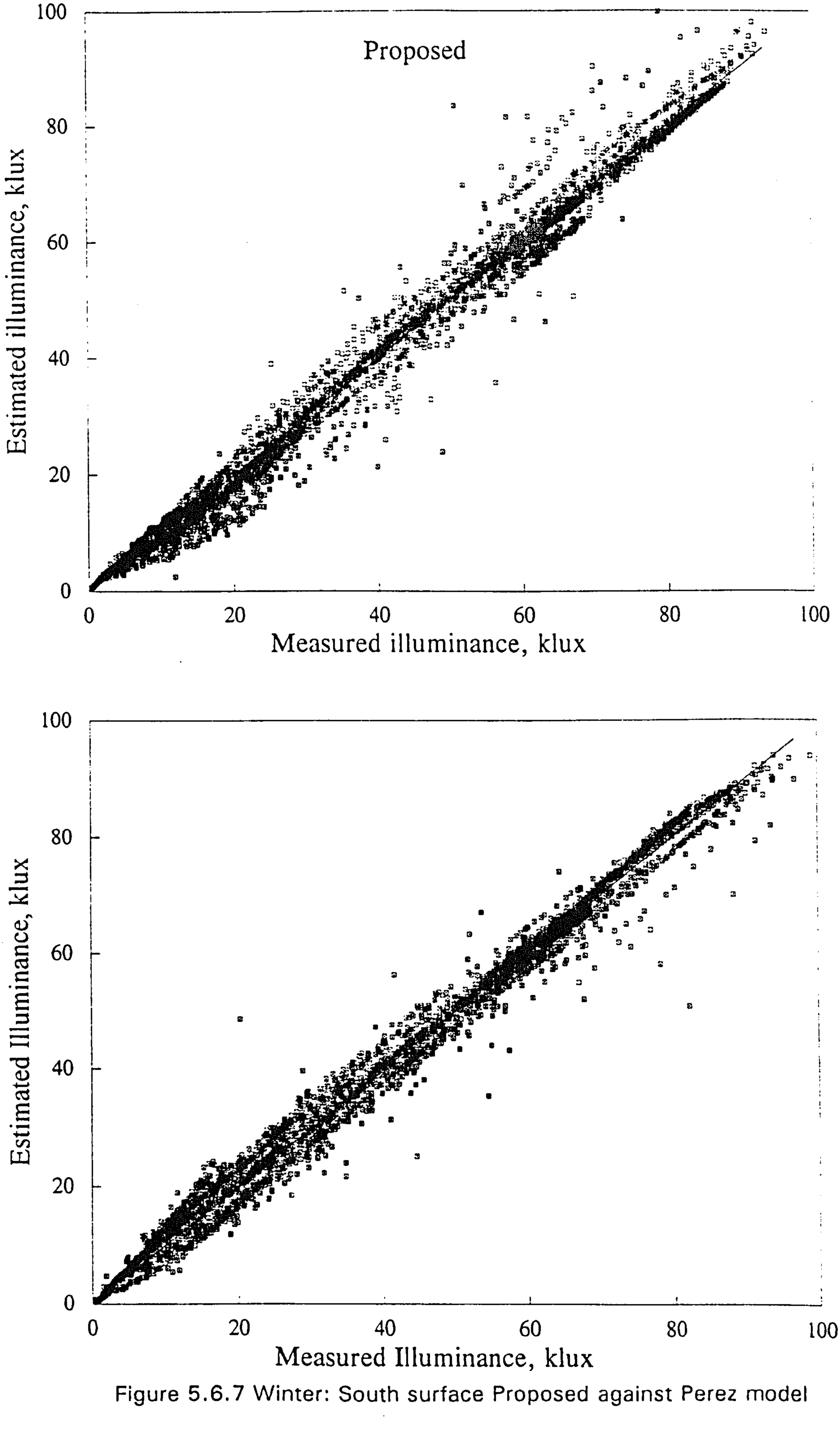

Figure 5.6.7 Winter: South surface Proposed against Perez model

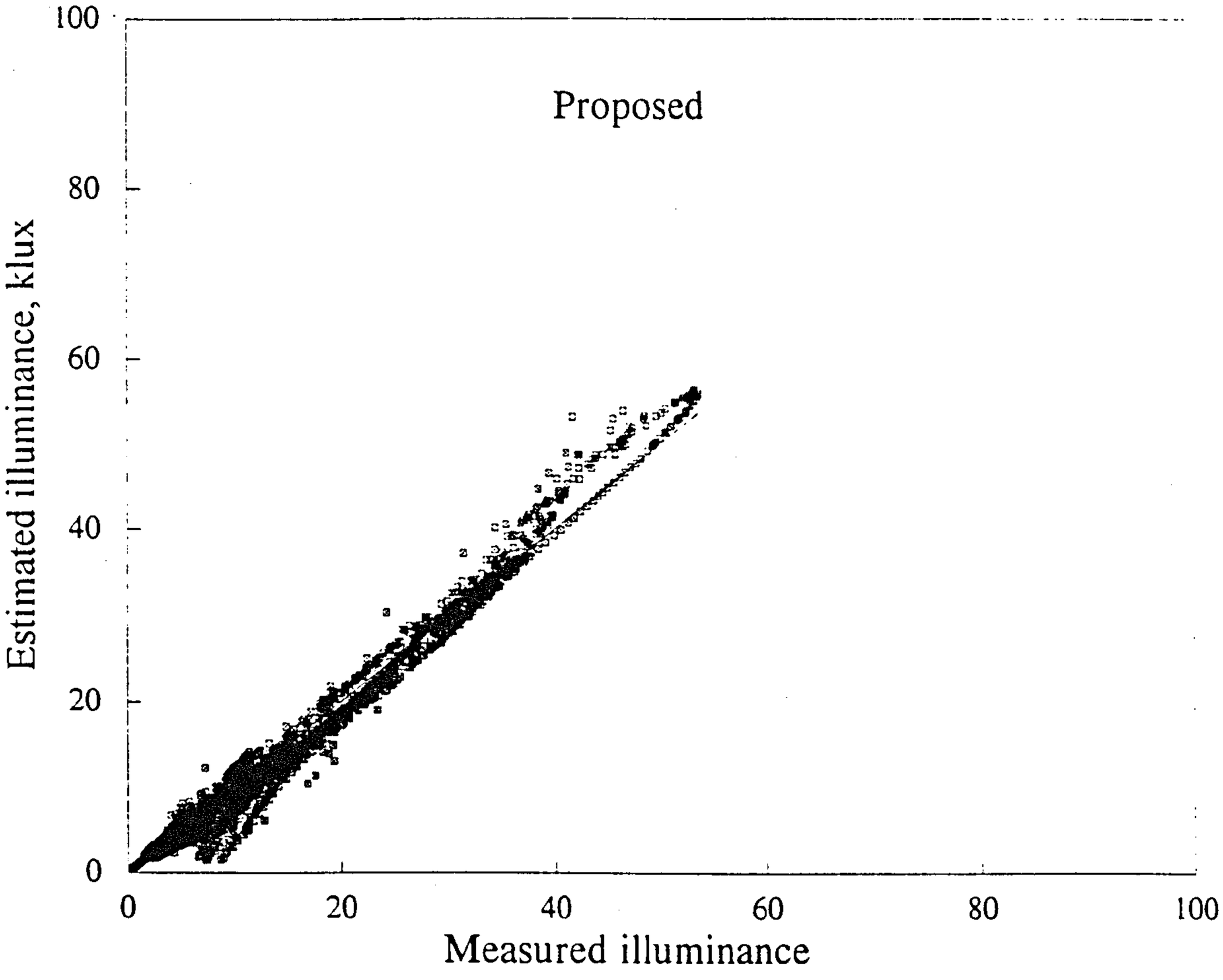

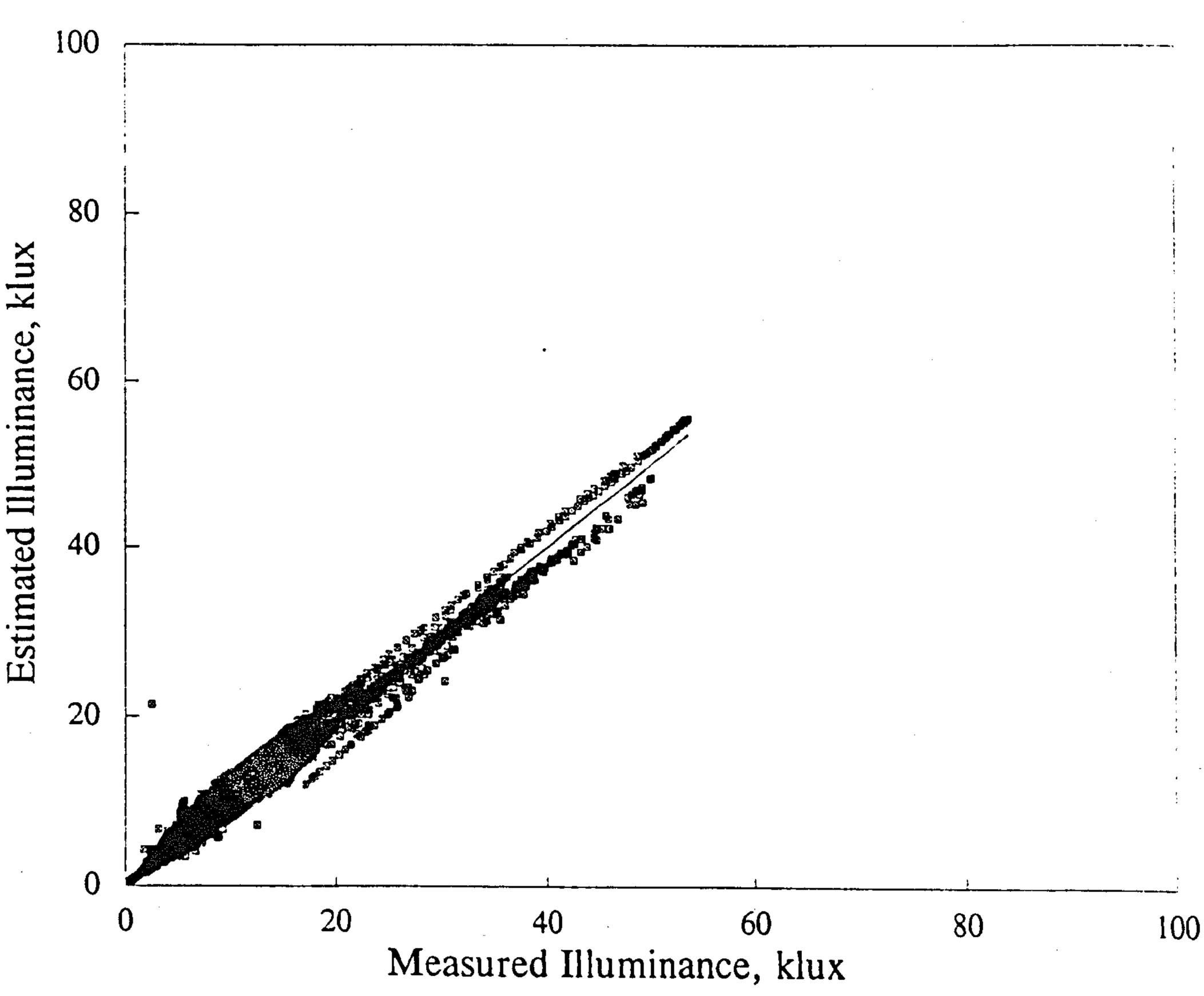

Figure 5.6.8 Winter: West surface Proposed against Perez model

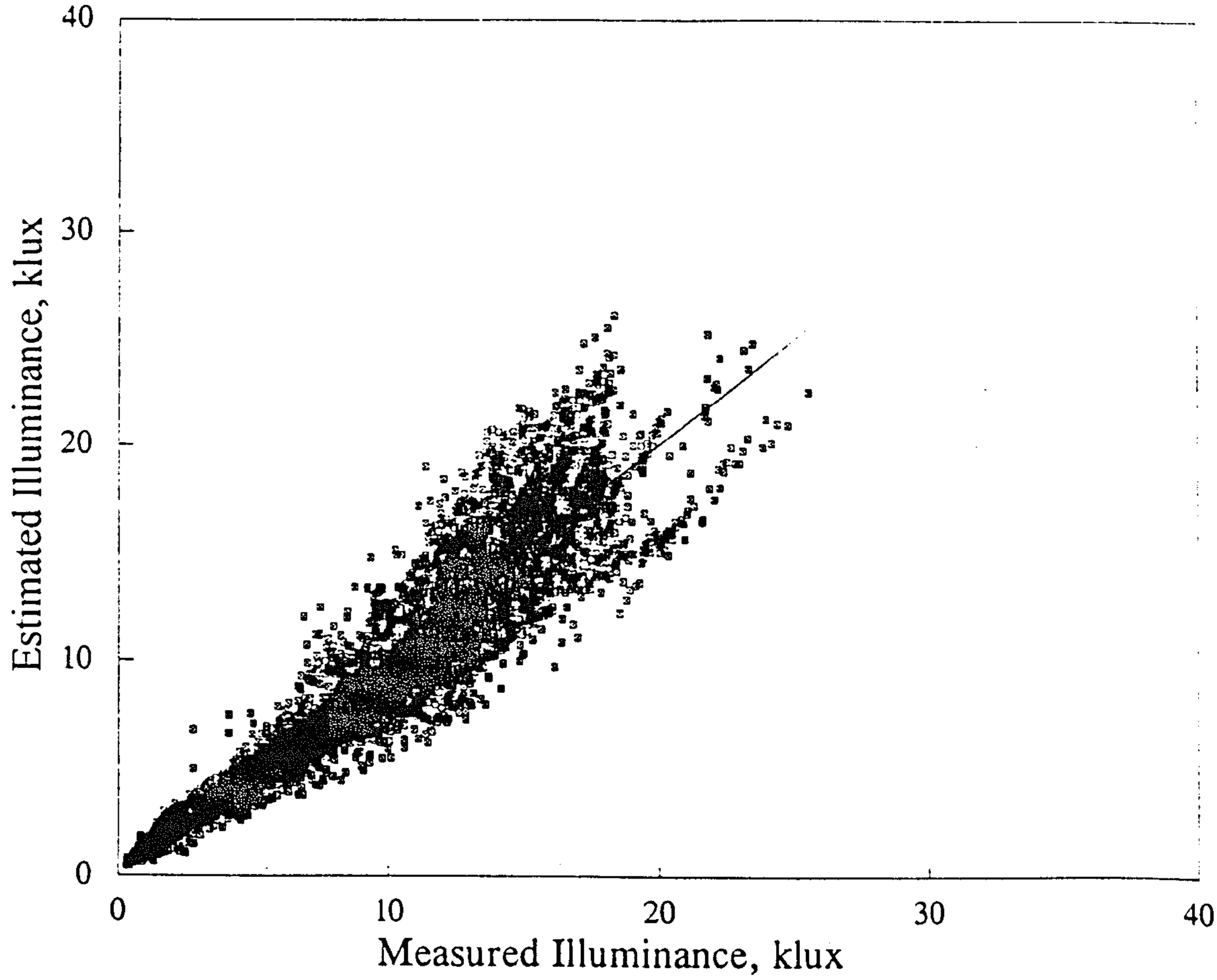

Figure 5.6.9 Summer: North surface Moon & Spencer model

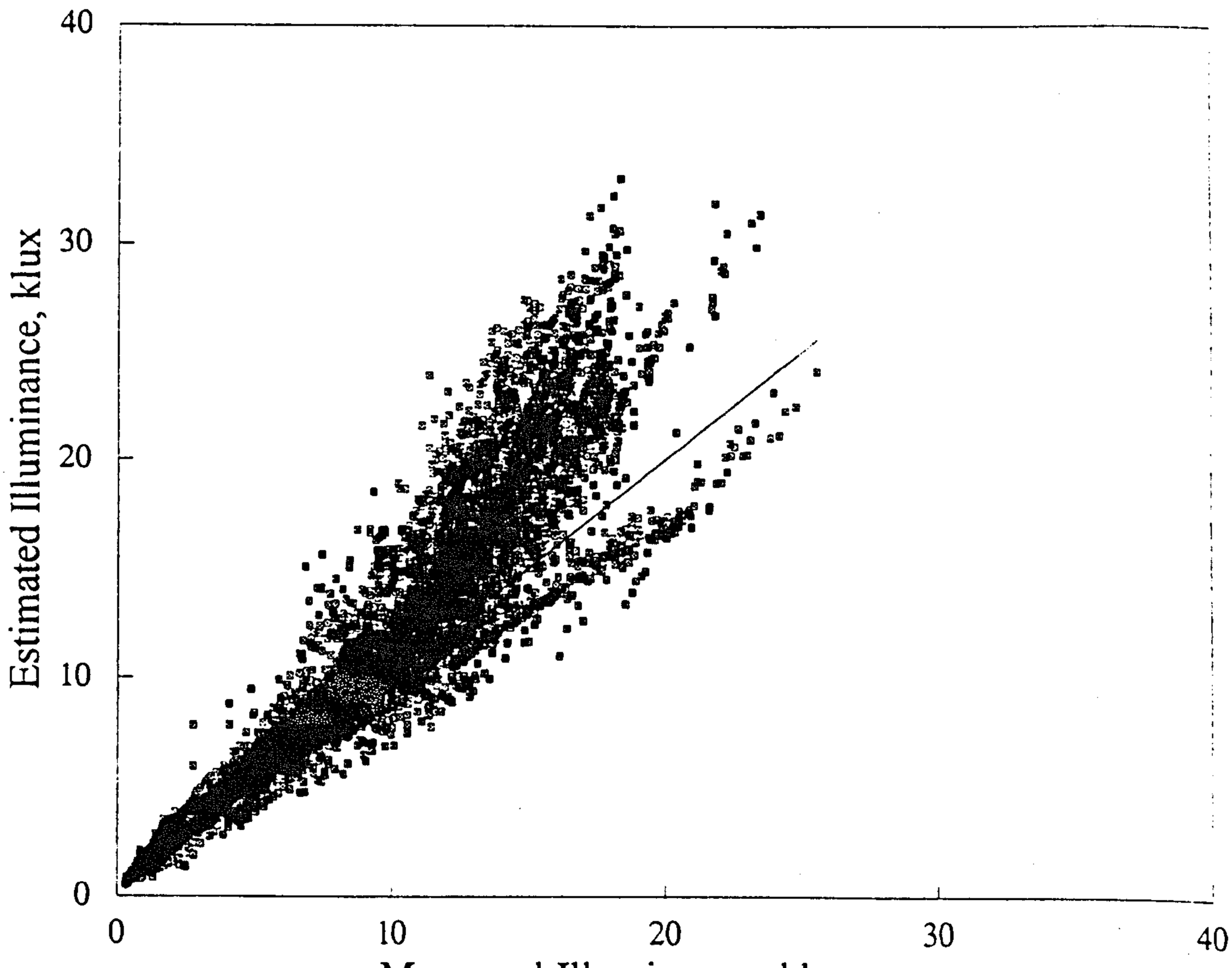

Figure 5.6.9 Summer: North surface Uniform model

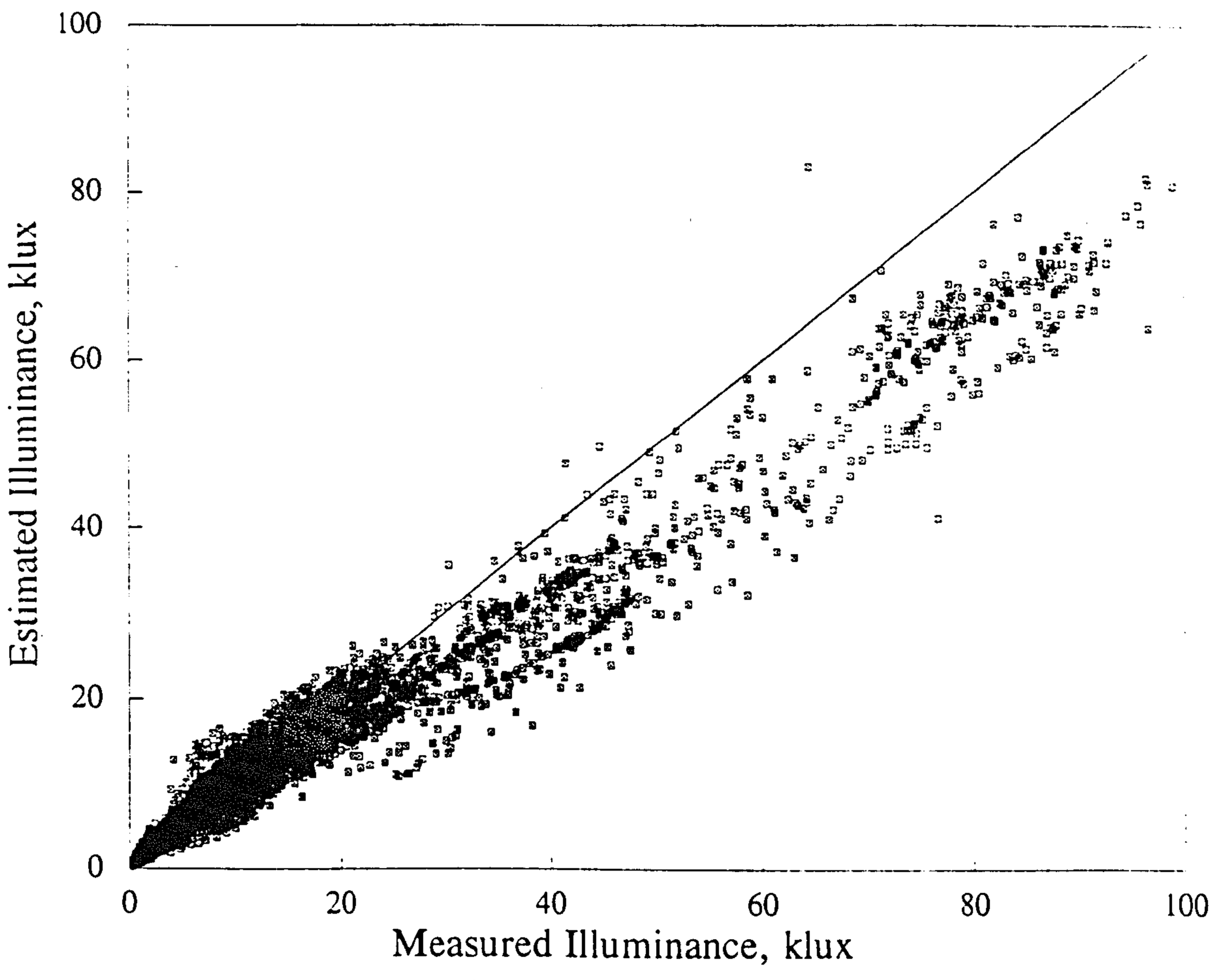

Figure 5.6.10 Summer: East surface Moon & Spencer model

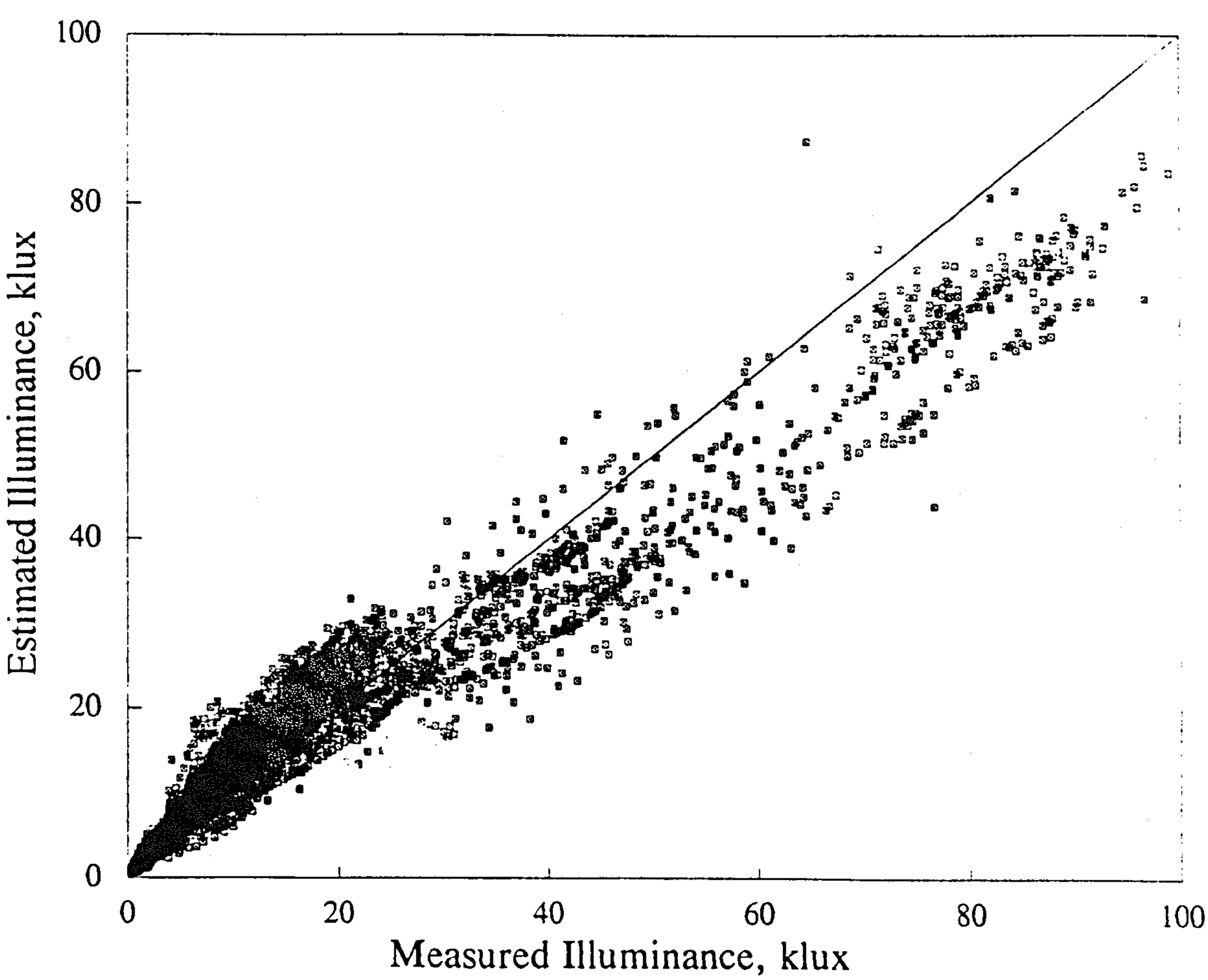

Figure 5.6.10 Summer: East surface Uniform model

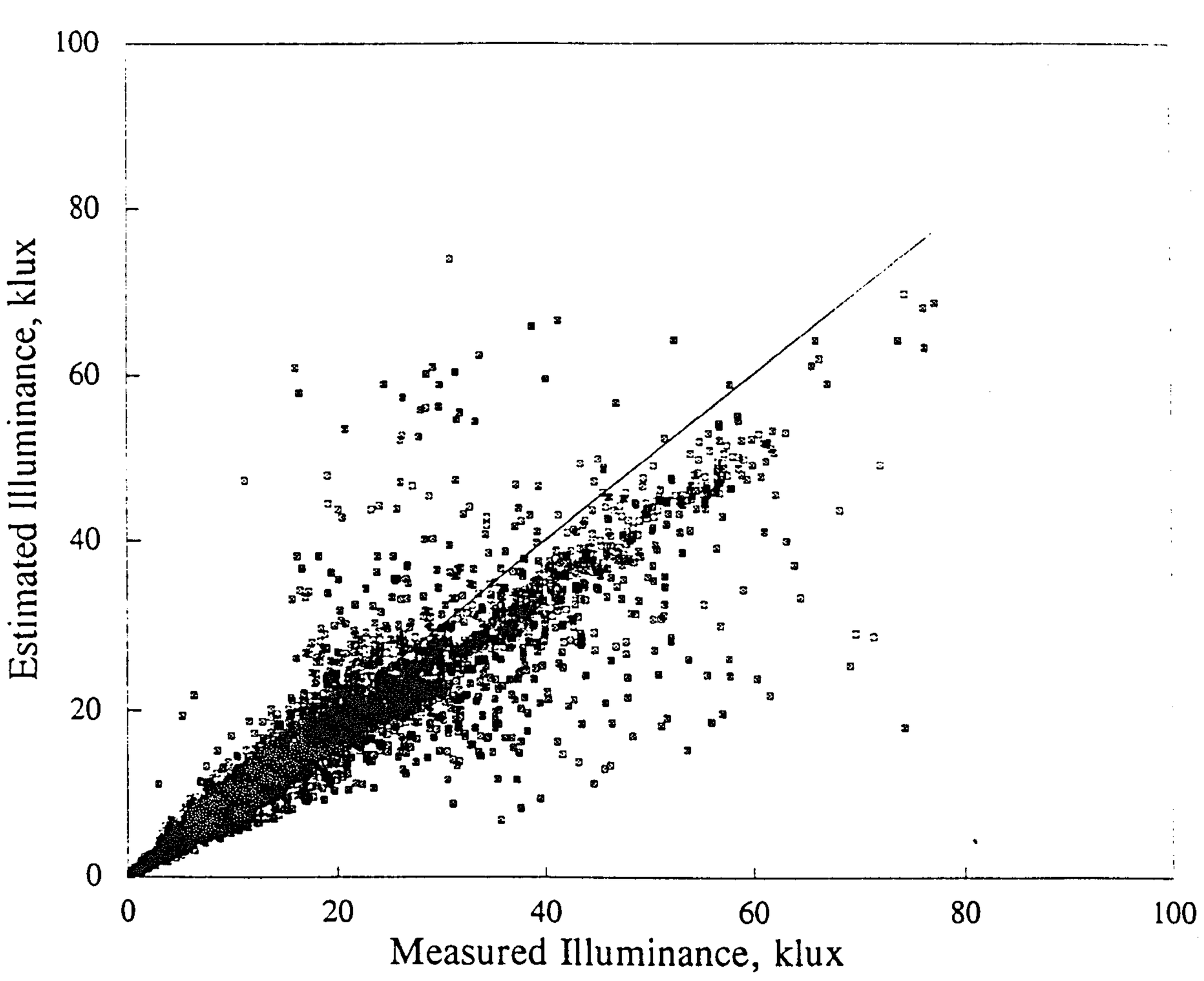

Figure 5.6.11 Summer: South surface Moon & Spencer model

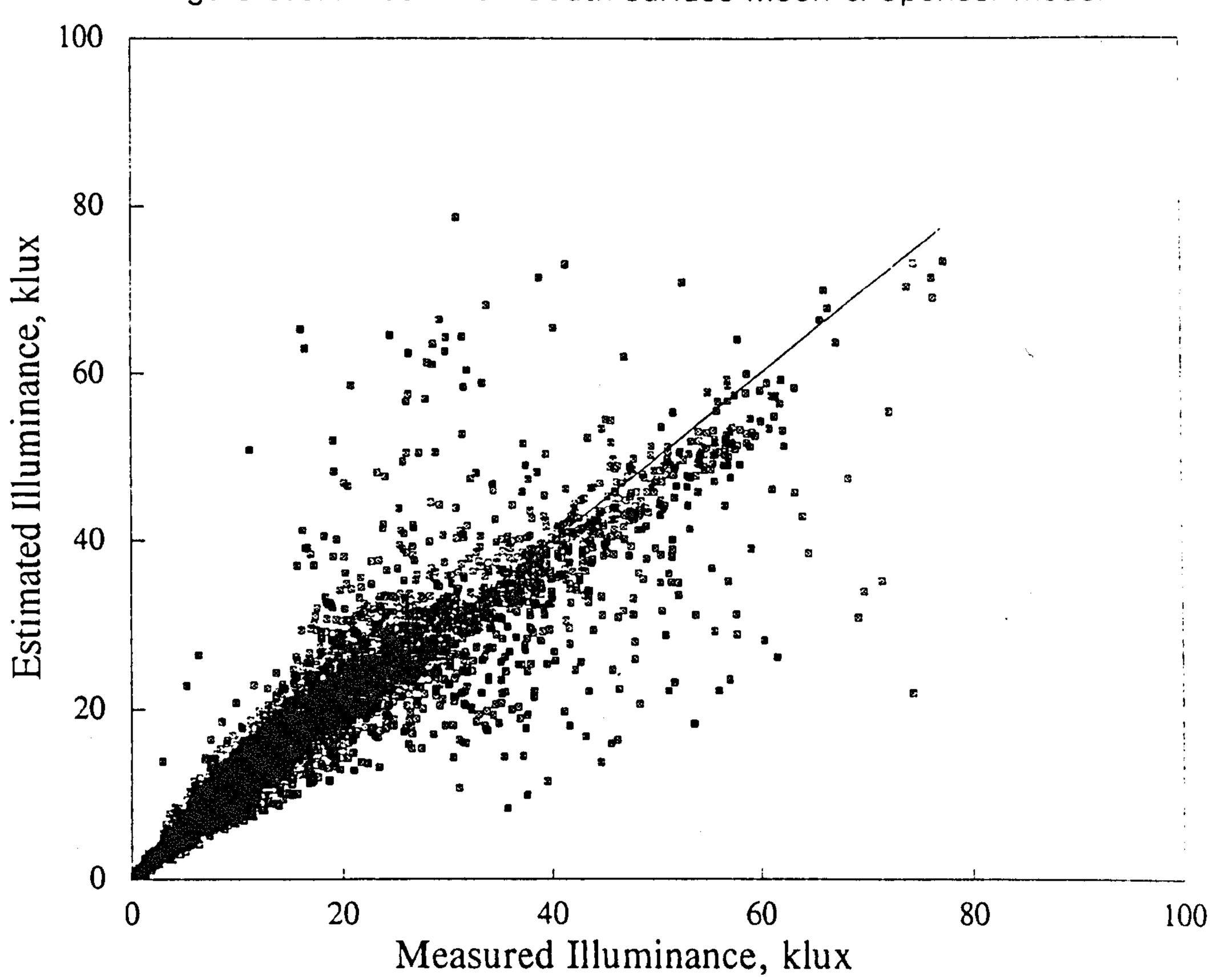

Figure 5.6.11 Summer: South surface Uniform model

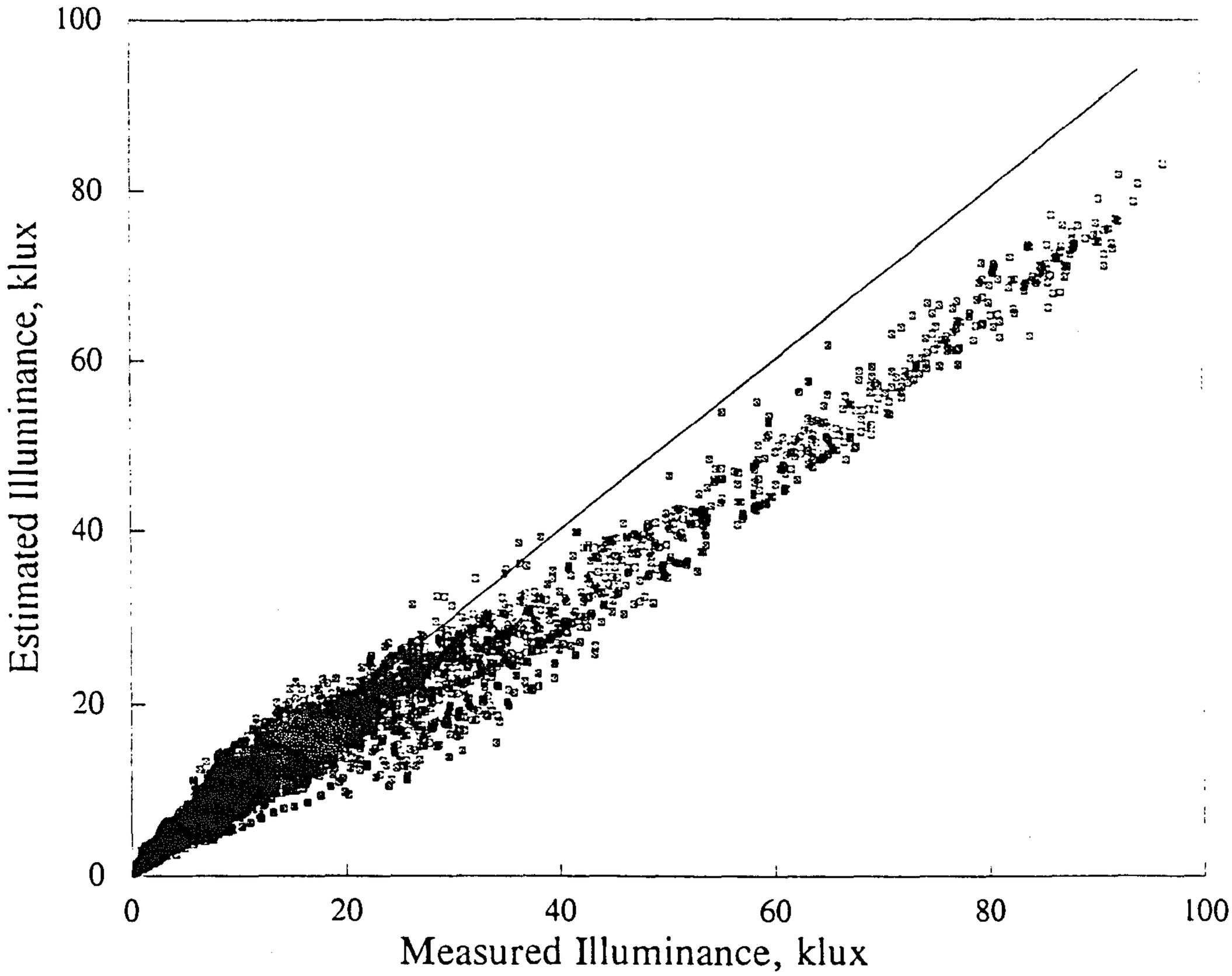

Figure 5.6.12 Summer: West surface Moon & Spencer model

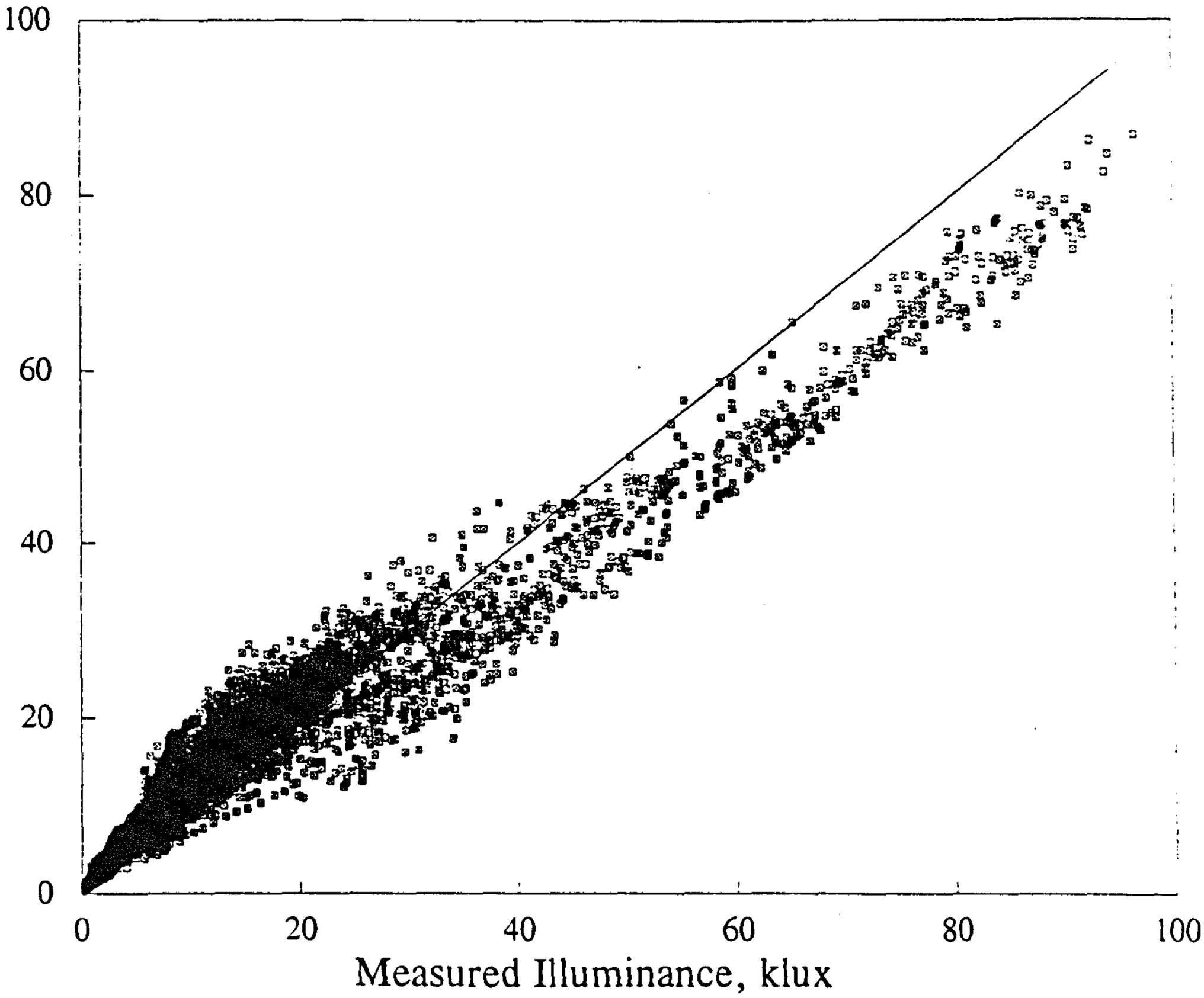

Figure 5.6.12 Summer: West surface Uniform model

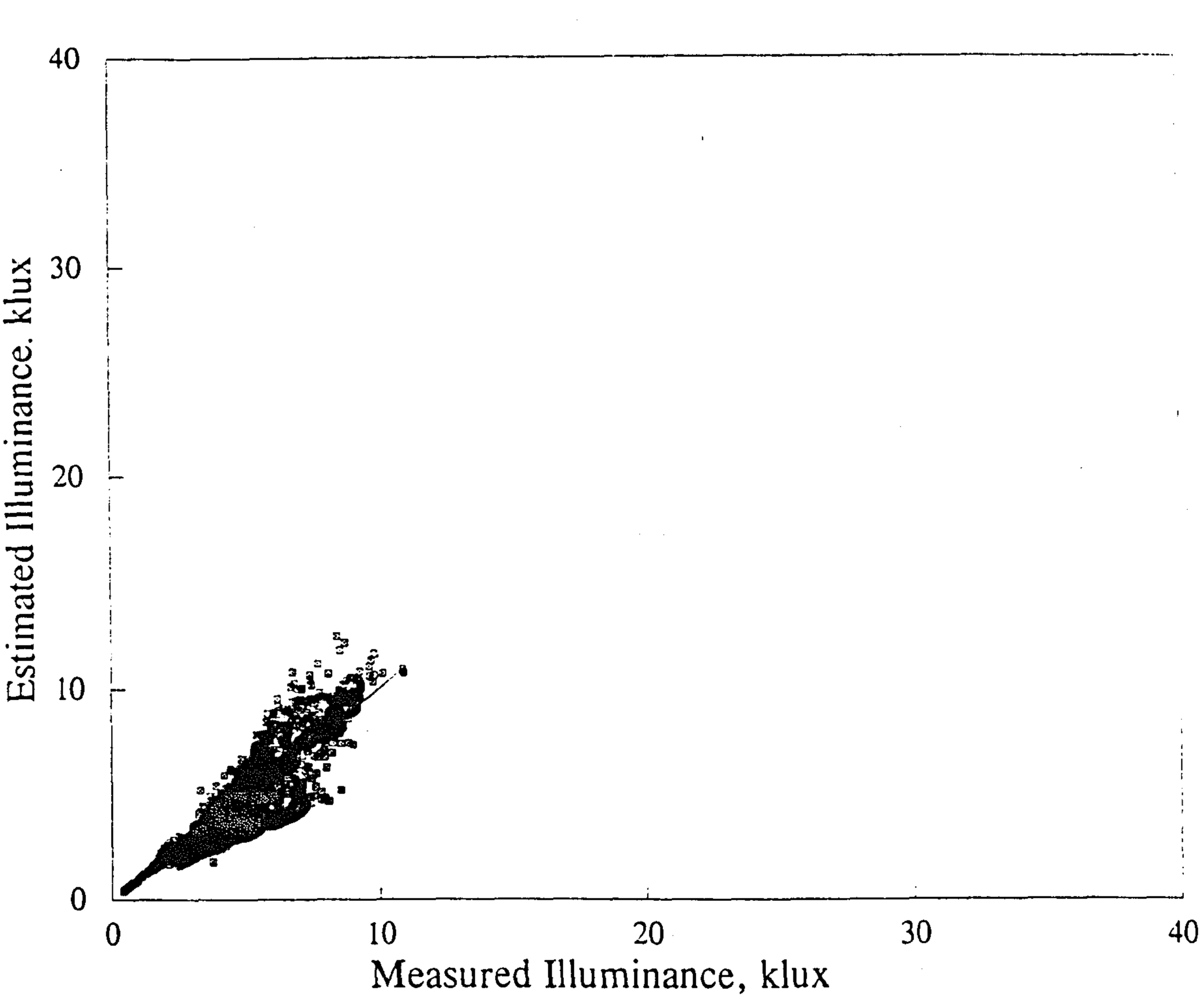

Figure 5.6.13 Winter: North surface Moon & Spencer model

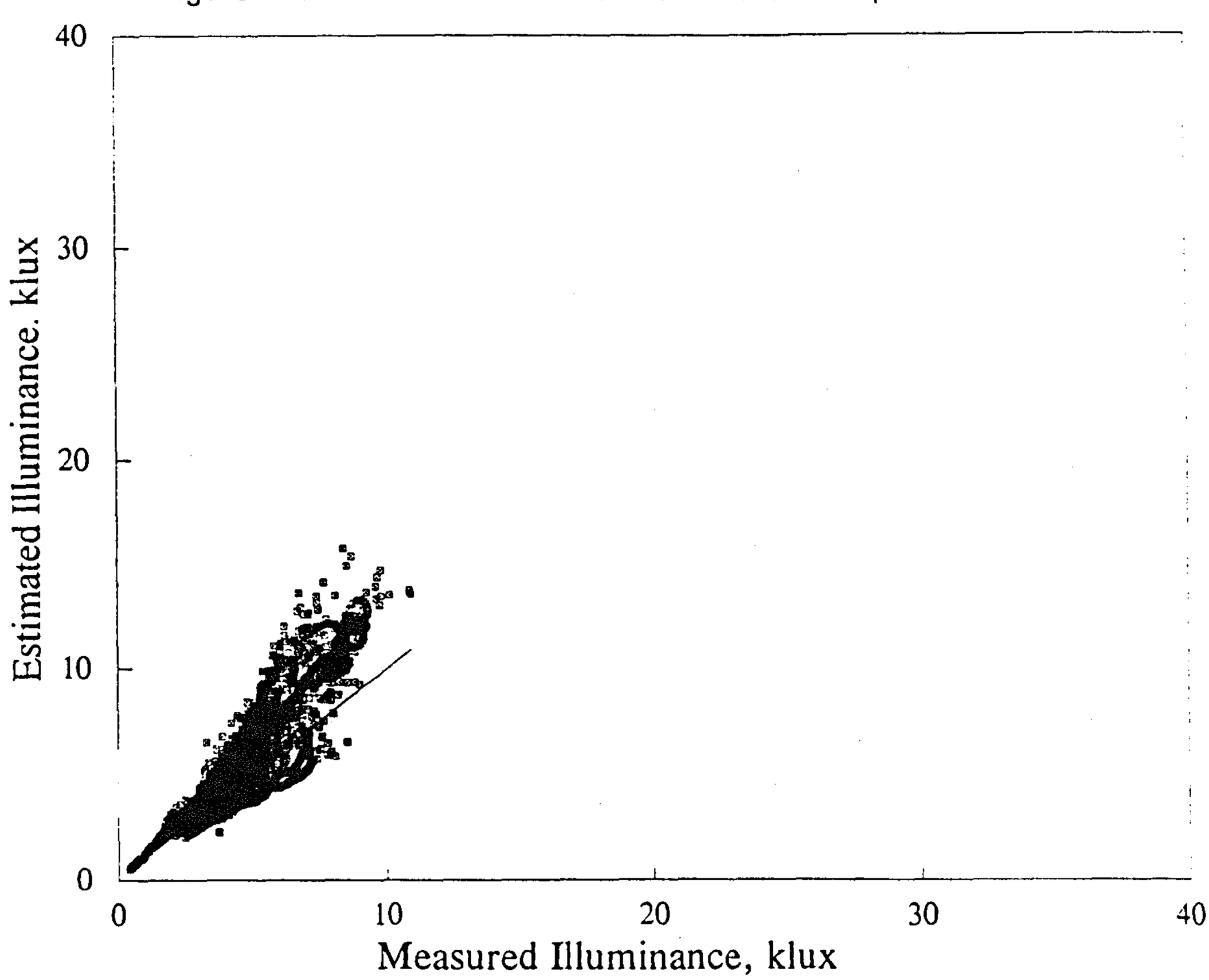

Figure 5.6.13 Winter: North surface Uniform model

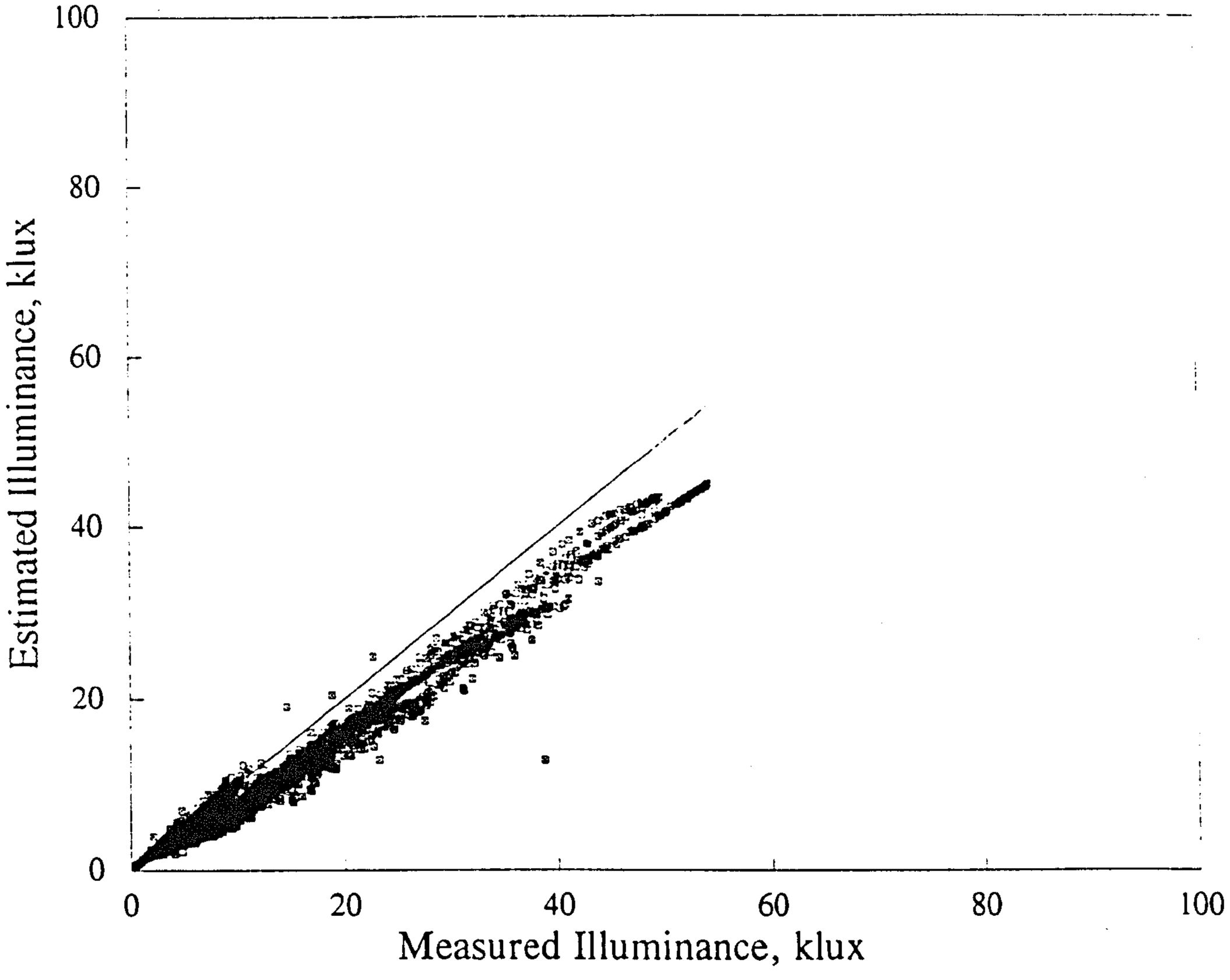

Figure 5.6.14 Winter: East surface Moon & Spencer model

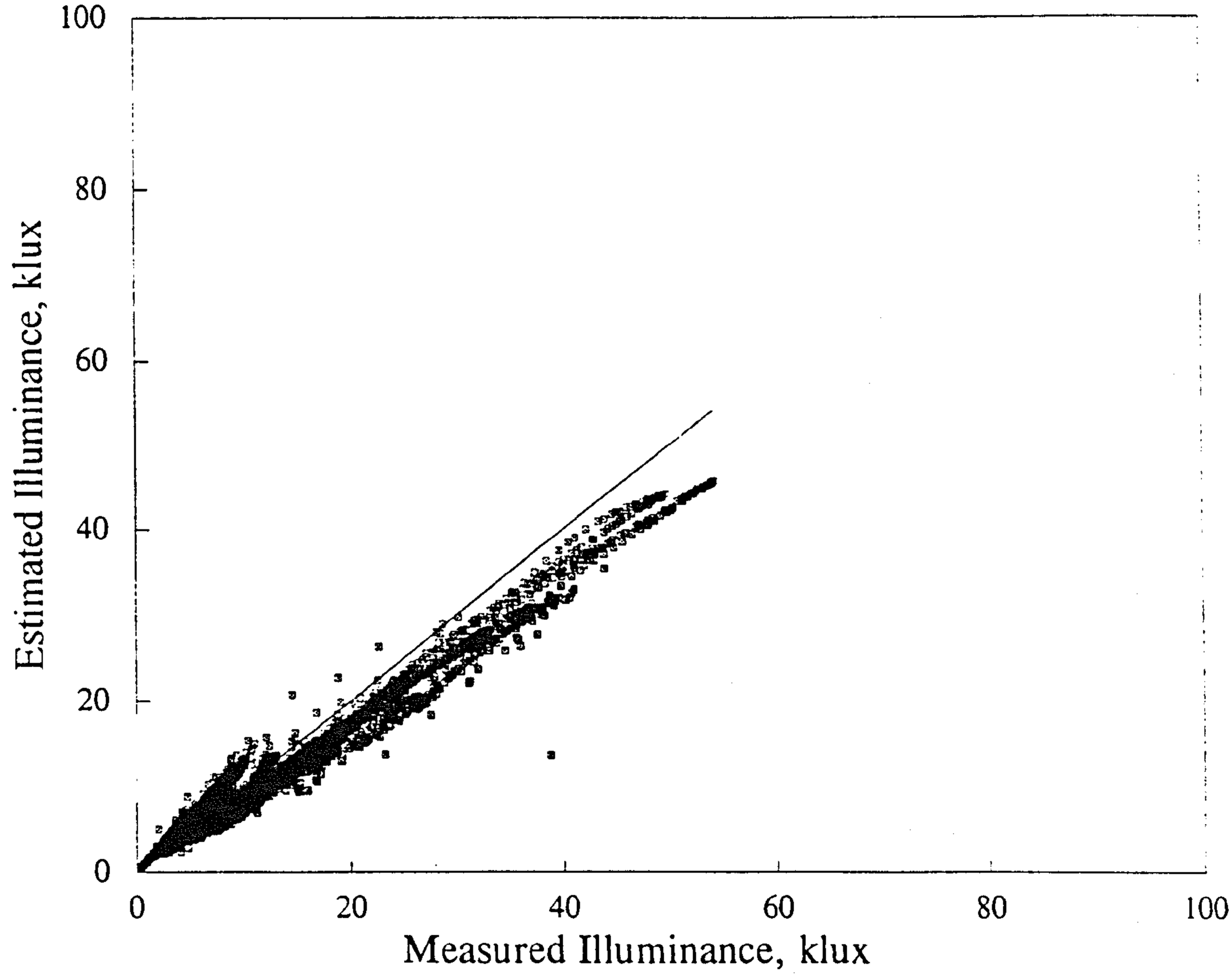

Figure 5.6.14 Winter: East surface Uniform model

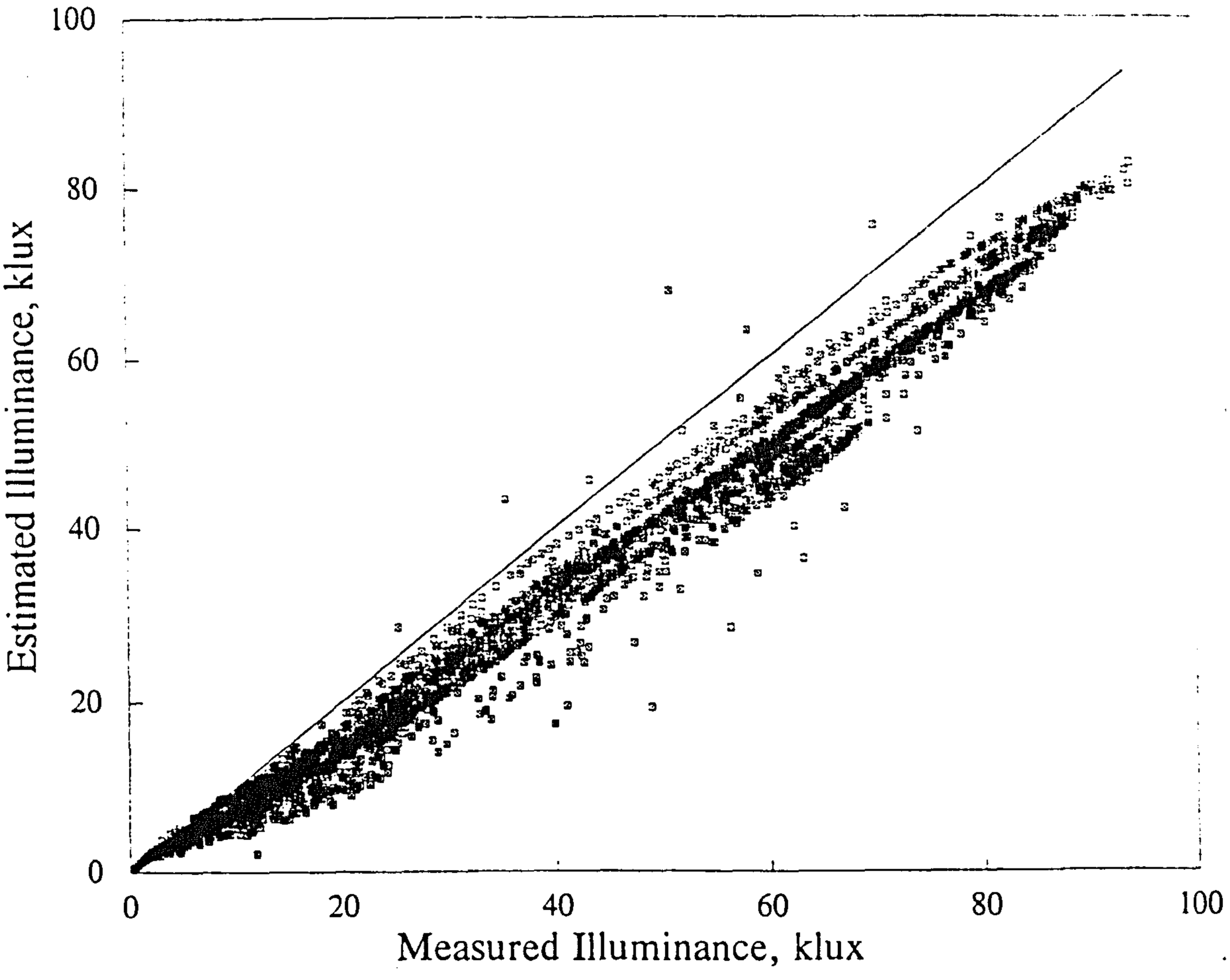

Figure 5.6.15 Winter: South surface Moon & Spencer model

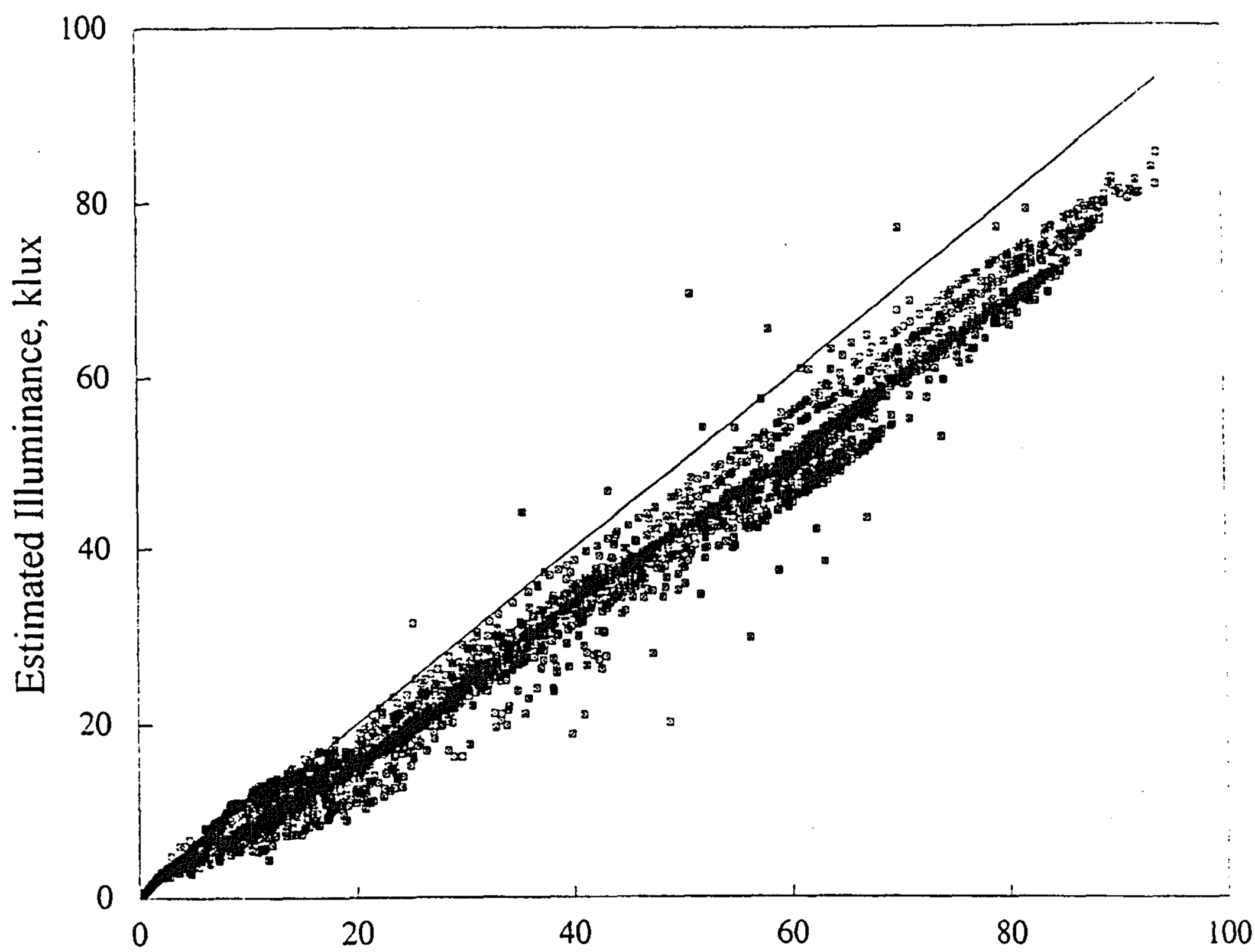

Figure 5.6.15 Winter: South surface Uniform model

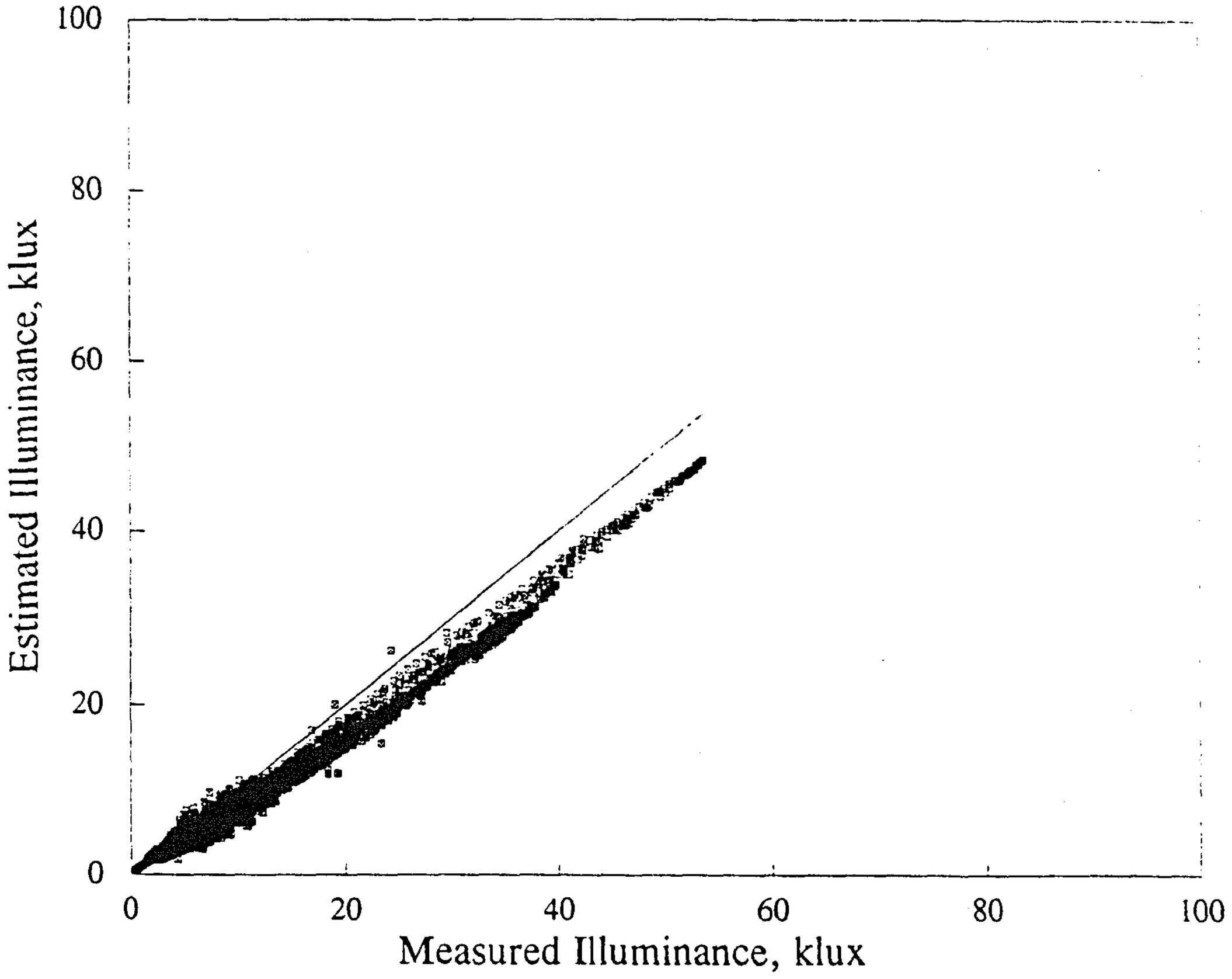

Figure 5.6.16 Winter: West surface Moon & Spencer model

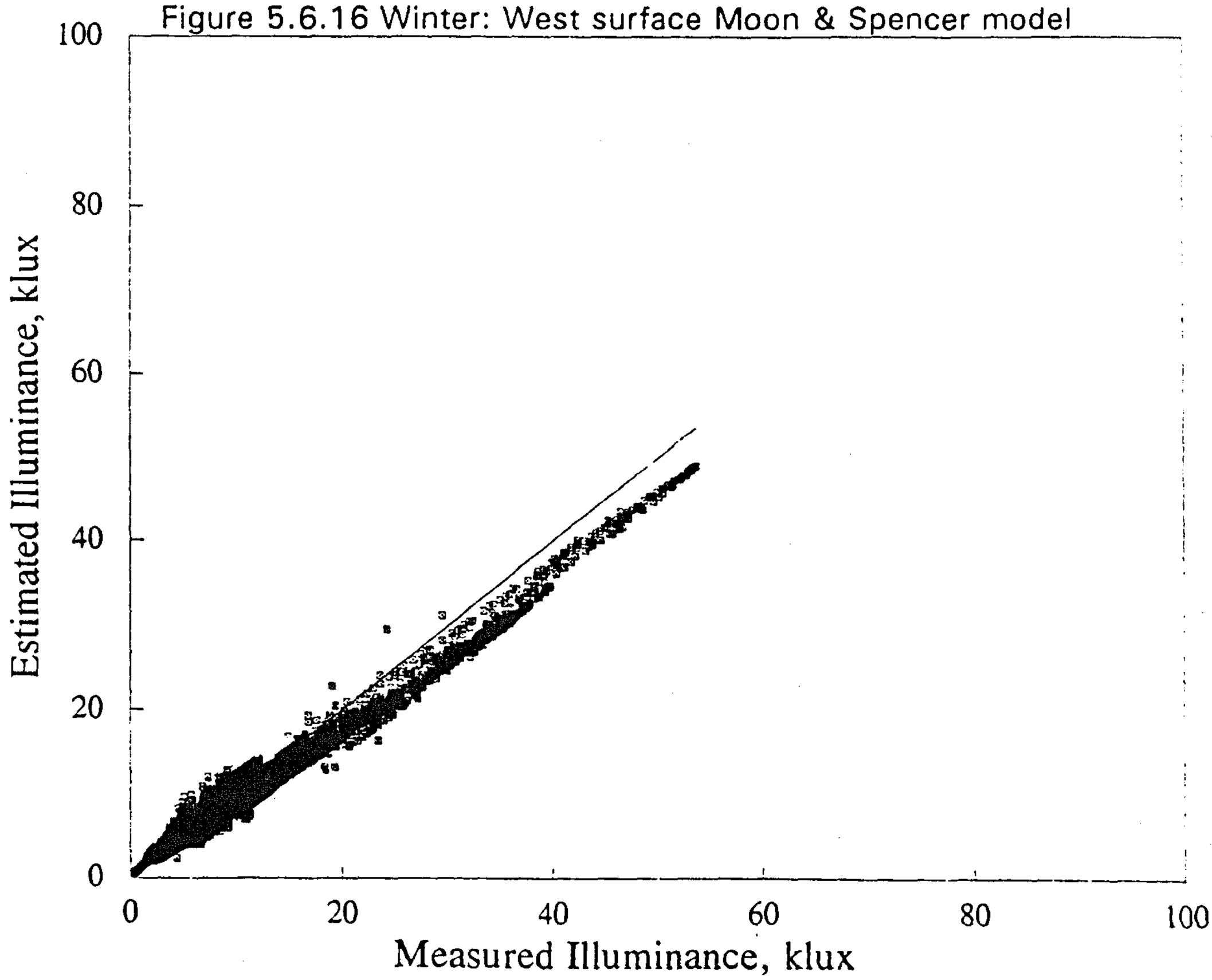

Figure 5.6.16 Winter: West surface Uniform model